SEISMIC BEHAVIOR AND DESIGN OF INTEGRAL ABUTMENT BRIDGES IN SOUTHERN ILLINOIS

BY

DEREK LORNE KOZAK

DISSERTATION

Submitted in partial fulfillment of the requirements
for the degree of Doctor of Philosophy in Civil Engineering
in the Graduate College of the
University of Illinois at Urbana-Champaign, 2018

Urbana, Illinois

Doctoral Committee:
Associate Professor Larry A. Fahnestock, Co-Chair
Professor James M. LaFave, Co-Chair
Associate Professor Scott M. Olson
Assistant Professor Eun Jeong Cha

ABSTRACT

The increased use of integral abutment bridges (IABs) throughout the United States has led to numerous studies concerning their behavior when subjected to a variety of loads. The seismic behavior of IABs is of particular interest to regions such as southern Illinois, where proximity to the New Madrid Seismic Zone may create significant ground motion accelerations during an earthquake. IABs are common in modern bridge design due to their lack of expansion joints between the superstructure and abutment, which can lead to decreased damage at the abutment seat when compared to stub abutment bridges because water, soil, and deicing chemicals are unable to penetrate through a compromised expansion joint in an IAB. However, elimination of expansion joints in IABs can also lead to the development of complex soil-structure-interaction limit states at the abutment and its foundation when an IAB is subjected to lateral loads. Despite this distinct behavior in IABs when subjected to lateral loading, such as seismic loads, there is a lack of comprehensive system-level studies investigating the behavior of IABs subjected to earthquakes.

This dissertation aims to determine the seismic behavior of typical IAB designs in southern Illinois and to develop feedback and recommendations that can improve Illinois IAB seismic designs. This is accomplished through modeling IABs as a whole bridge system, subjecting the IAB models to representative ground motions for southern Illinois, monitoring the behavior of key IAB components, using the monitored results to form a comprehensive view of IAB seismic behavior, and employing the developed knowledge to form recommendations for improving IAB seismic performance. The IAB models are developed in OpenSees through nonlinear modeling of multiple components within an IAB, as well as through connections between the components that allow for interactions between components to be observed. The models represent typical IAB designs for Illinois. They are subjected to 1000-year return period hazard ground motions

developed specifically for 10 sites within southern Illinois. Incremental dynamic analyses are also performed, by scaling the ground motion accelerations up and down.

IABs with varying superstructure materials, span configurations, bearing layouts, pier heights, and foundation soil conditions are dynamically analyzed using the 10 sets of developed ground motions. The results allow for observations and conclusions to be made concerning the overall seismic performance of current Illinois IAB designs, as well as concerning which components are the most vulnerable to damage during an earthquake. The abutment foundation piles and the pier columns are identified as most vulnerable and frequently encounter severe damage limit states under design-level shaking. Damage to pier columns is especially prominent in IABs with shorter piers and longer abutment-to-abutment spans, while abutment foundation damage, in terms of the yielding, local buckling, and rupture of the piles, frequently occurs in many IAB variants. Recommendations on design modifications to improve the seismic behavior of IABs by limiting the level of damage to these components are also investigated through modifying elastomeric bearing side retainer strength, fixed bearing strength, pier column size, and backfill contributions.

ACKNOWLEDGEMENTS

I would first like to thank my advisors, Dr. Larry Fahnestock and Dr. James LaFave, for providing me with the great opportunity to work on this project at the University of Illinois. Throughout my time as a student at the University of Illinois they have provided incredible amounts of support and advice towards my research, studies, and future ambitions. Without them I would not have been able to learn as much as I have concerning bridge and earthquake engineering over the past five years.

I would also like to thank the other members of the project team, both past and present, including Dr. Jie Luo and Dr. Evgueni Filipov. Jie was a fantastic colleague and office mate who helped me through many tough situations by bringing a fresh perspective to the problems and by always being patient with my inquiries. Although Evgueni was not a member of the project team during my tenure, his help was immeasurable as I was reviewing the Phase I documentation and code. I would also like to thank the members of the project Technical Review Panel, chaired by Mark Shaffer, for their valuable assistance with this project.

I would like to thank the faculty members who have agreed to serve on my doctoral committee for their feedback on my dissertation manuscript – Dr. Larry Fahnestock, Dr. James LaFave, Dr. Scott Olson, and Dr. Eun Jeong Cha.

I also had invaluable help from numerous students, staff, and faculty members throughout the Civil and Environmental Engineering department who helped in this project in more ways than they can imagine. Two people to note are Dr. Scott Olson and Darin Peetz. Dr. Scott Olson was instrumental in expanding my geotechnical engineering knowledge and in the development of soil profiles for southern Illinois. My friend and colleague Darin Peetz should be especially noted for

his ability, willingness, and patience in answering all my questions and helping me work through issues concerning supercomputer and linux operations.

Finally, I would like to thank my family and friends for all the support they have provided me throughout the years I have been working on this project and beyond. To my friends back home, in Champaign at the University of Illinois, and on the Flatlanders rugby football club, I appreciate your ability to make me relax and escape from the project periodically. To my parents, Maria and Mike Kozak, and my sister, Caylie. I would not be where I am today without them and without their hard work and support I would likely not be in a position to complete a Ph.D. in a subject I enjoy. To my girlfriend, Patricia Greene, for always being there and believing that I can accomplish anything. She has been invaluable in providing me with love and support and working with me through tough times.

This manuscript is based on the results of ICT R27-133, *Calibration and Refinement of Illinois' Earthquake Resisting System Bridge Design Methodology: Phase II*. ICT R27-133 was conducted in cooperation with the Illinois Center for Transportation (ICT); the Illinois Department of Transportation (IDOT), Division of Highways; and the U.S. Department of Transportation, Federal Highway Administration (FHWA). The contents of this paper reflect the view of the author, who is responsible for the facts and the accuracy of the data presented herein. The contents do not necessarily reflect the official views or policies of the ICT, IDOT, or FHWA.

TABLE OF CONTENTS

CHAPTER 1: INTRODUCTION

1.1 MOTIVATION

Highway bridges are an important component in the infrastructure network of the United States. The ability to transport goods and emergency services along these bridges is critical, especially after an extreme event such as an earthquake. Integral abutment bridges (IABs) in particular are important due to their popularity. Since the first construction of an IAB in the United States in 1920 (Paraschos and Amde, 2011) the amount of IABs in use in the U.S. has grown to over 9,000 as of 2011 (White, 2007). The state of Illinois has been constructing IABs since 1986 (Paraschos and Amde, 2011) and continues to refine their design procedures for this bridge type. The general desire to improve highway bridge seismic design and construction plus the popularity of IABs in Illinois combines to form an increased interest in the behavior of IABs. This is particularly the case in Illinois for IABs designed and constructed under the current design framework and subjected to the current bridge seismic hazard of a 1000-year return period event (5 percent probability of exceedance in 50 years, approximately equal to a 7 percent probability of exceedance in 75 years) (AASHTO, 2011).

1.1.1 Lack of Ground Motions for Southern Illinois

Many midwestern locations are not overly concerned with the seismic behavior of structures due to the small risk imposed by earthquakes, but southern Illinois is a midwestern region where this is not true. The proximity of southern Illinois to the New Madrid Seismic Zone (NMSZ) creates the potential for large ground motions in this region. The classification of seismic performance zones (SPZs) in Illinois, shown in Fig. 1.1, indicates that the most southern locations in Illinois could experience ground accelerations greater than 0.50g at a period of 1.0 s for a 1000-

year return period, indicated by SPZ 4. Nearly all of the southern half of Illinois could experience ground accelerations greater than 0.15g at a period of 1.0 s for a 1000-year return period, indicated by SPZ 2, 3, and 4 (IDOT, 2008). While many northern and central locations in Illinois, such as Chicago or Champaign, do not need to be especially concerned with the seismic behavior of bridges, it is important to know how bridges will behave in the southern portion of the state if and when they are subjected to relatively strong earthquake ground shaking.

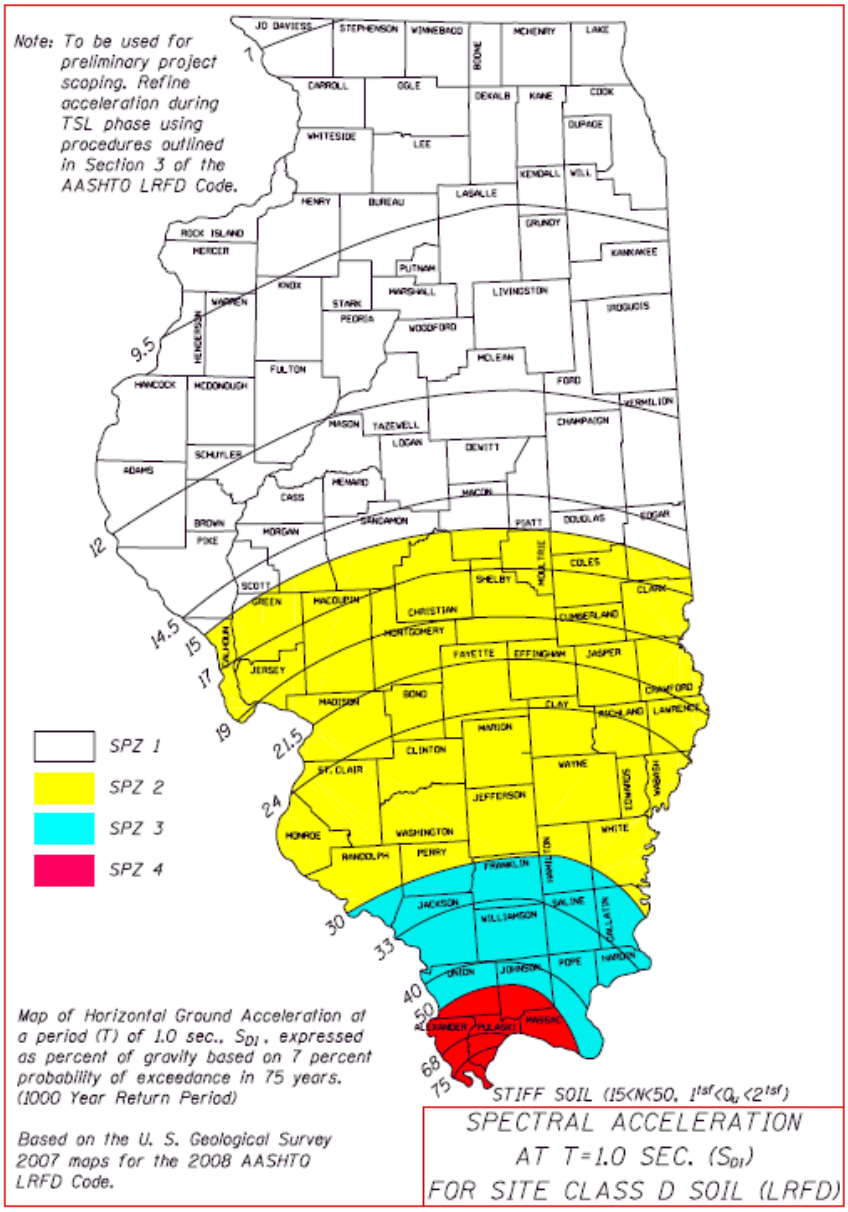

Figure 1.1: Map of Illinois Seismic Performance Zone (SPZ) classifications (IDOT, 2008).

Despite the importance of seismic design and assessment required in the areas surrounding the NMSZ, there is a lack of suitable ground motion recordings for Central North America (CNA), which stems from the low activity rate of the NMSZ (Wen and Wu, 2001; Fernandez and Rix, 2006). This poses challenges in determining the seismic behavior of structures in the area and necessitates the creation of synthetic ground motions or modification of existing ground motions to use in southern Illinois. Although there have been attempts to create synthetic ground motions in or surrounding southern Illinois (Wen and Wu, 2001; Fernandez and Rix, 2006), the produced ground motions are either not at the desired hazard level (*i.e.*, a 1000-year return period event) or not actually within the southern Illinois area. The lack of suitable ground motions for southern Illinois requires a new set of ground motions to be developed that account for the desired hazard of a 1000-year return period and the desired location of southern Illinois. In this study, the developed ground motions are desired to assess the seismic behavior of IABs within southern Illinois.

1.1.2 Unique Behavior of Integral Abutment Bridges

Beyond Illinois, there is even more broadly a lack of understanding about IAB overall seismic behavior in any location. Prior research has considered IAB behavior, but these studies have generally been limited by either IAB seismic models focusing on a single component and therefore simplifying the rest of the bridge model (*e.g.*, Teguh *et al.*, 2006; Frosch *et al.*, 2009; Kotsoglou and Pantazopoulou, 2009; Vasheghani-Farahani *et al.*, 2010; Itani and Pekcan, 2011; Zhao *et al.*, 2011; Franchin and Pinto, 2014) or due to detailed IAB models being mainly evaluated for thermal and/or live loads (*e.g.*, Olson *et al.*, 2013; LaFave *et al.*, 2016). This study investigates the seismic behavior of IABs by subjecting detailed IAB numerical models of entire bridge

systems to a suite of ground motions representative of southern Illinois at the design hazard level of a 1000-year return period event.

Integral abutment bridges (IABs) incorporate the superstructure and abutment in such a way that they displace together. This is achieved by placing the superstructure girder on a rocker plate or bearing pad on top of the abutment's pile cap, then pouring the concrete for the bridge deck and abutment at the same time. This single pour of concrete reduces costs in superstructure girder and abutment maintenance and repair by removing the possibility that exists in stub abutment bridges of water, dirt, and deicing chemicals dropping through an expansion joint in the deck to the pile cap. The presence of water, dirt, and deicing chemicals could lead to corrosion of the girders, bearings and pile caps (Kunin and Alampalli, 1999; Paraschos and Made, 2011).

While IABs reduce the maintenance costs when compared to stub abutment bridges, they also add complexity to the bridge behavior. The integral connection between the superstructure and abutment leads to the transfer of both moments and forces from the superstructure to the abutment and its foundations. In stub abutment bridges, only forces are transferred and the amount of bending in the abutment foundation piles is significantly less than in IABs. Additionally, the lack of an expansion joint and elastomeric bearing in the abutment means that any displacements in the superstructure are transferred into the backfill.

In general, there are four major differences between stub abutment bridges and IABs. The first major difference is the use of a rocker plate or bearing pad instead of an elastomeric bearing between the abutment and superstructure. The second major difference is the lack of an expansion joint, which is the fundamental integral nature of the superstructure and abutment. The third major difference is the lack of a separate backwall in IABs. In stub abutment bridges, where there is a gap between the girder ends and the abutments, the backwall provides longitudinal resistance

before the backfill fully engages. The fourth major difference is that IABs have only a single row of vertical piles as opposed to the multiple rows of vertical piles and batter piles found in stub abutment bridges (Olson *et al.*, 2009). The single row of vertical piles in IABs is an attempt to counteract the effects of the previous difference by making the abutment more flexible. These differences are also detailed in Fig. 1.2 on an integral abutment diagram.

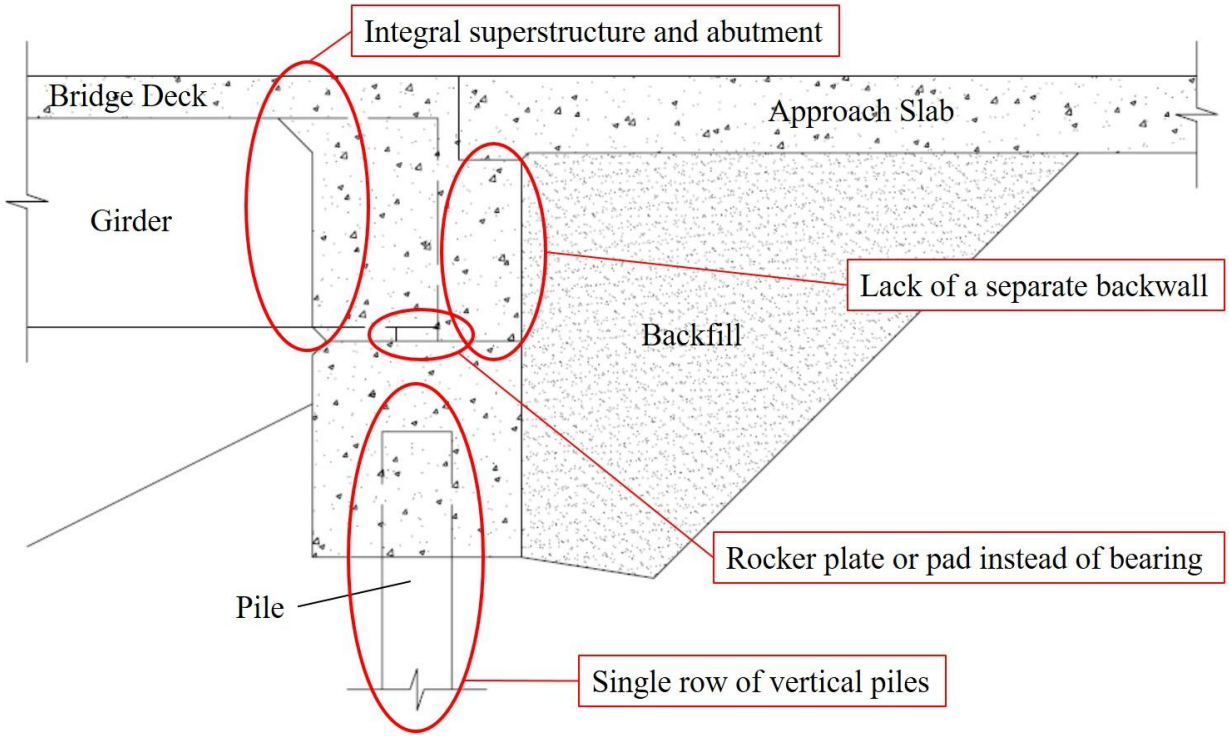

Figure 1.2: General diagram of an integral abutment showing the major differences from a stub abutment.

1.2 OVERVIEW OF RESEARCH

1.2.1 Background

In 2008 and 2009, the American Association of State Highway Transportation Officials (AASHTO) increased the design seismic hazard level from a 500-year return period event to a 1000-year return period event (AASHTO, 2011). This more intense seismic hazard level led to many structures in Illinois requiring seismic design which did not previously require it. The project

ICT-R27-070: *Calibration and Refinement of Illinois' Earthquake Resisting System Bridge Design Methodology* evaluated whether Illinois bridges can withstand the increased seismic hazard using the Illinois Department of Transportation's (IDOT) Earthquake Resisting System (ERS) concept. The ERS strategy generally keeps the superstructure and substructure elastic while allowing for the bearings between those two components to act as quasi-base isolators by fusing.

The study in this dissertation continues the research associated with the ICT-R27-133 project, *Calibration and Refinement of Illinois' Earthquake Resisting System Bridge Design Methodology: Phase II*. As such, there has already been extensive research into the seismic behavior of stub abutment bridges in Illinois during Phase I of the project (Filipov *et al.*, 2013a; Filipov *et al.*, 2013b; LaFave *et al.*, 2013a; LaFave *et al.*, 2013b; Steelman *et al.*, 2013; Steelman *et al.*, 2014; Steelman *et al.*, 2016; Steelman *et al.*, 2018). Phase II of the project also performed extensive research into the seismic behavior of stub abutment bridges in Illinois through the use of models refined further from Phase I and the inclusion of the ground motions developed in this study (Luo *et al.*, 2016; Luo *et al.*, 2017). Changes to the stub abutment model between Phase I and Phase II includes a more in-depth model of the abutments and foundations as well as the ability to consider bridge skew and ground motion incident angle.

Much of the focus in Phase I of the project concerned the behavior of elastomeric and fixed bearings commonly used in Illinois bridges. This led to extensive experimental studies to determine the force-displacement behavior of the bearings (LaFave *et al.*, 2013b; Steelman *et al.*, 2013; Steelman *et al.*, 2014; Steelman *et al.*, 2016; Steelman *et al.*, 2018). Bearing behavior models were then created to match the experimental results (Filipov *et al.*, 2013a; LaFave *et al.*, 2013a). These detailed bearing behavior models were essential in determining whether the desired quasi-isolated behavior will occur in the bridges using the bearings.

These bearing models were used in detailed stub abutment bridge models to assess the overall seismic behavior of the bridges (Filipov *et al.*, 2013b; LaFave *et al.*, 2013a). It was found that certain stub abutment bridges did achieve the IDOT ERS quasi-isolated behavior while others did not perform as well. The recommendations to achieve quasi-isolated behavior in the stub abutment bridges indicated that Type II elastomeric bearings should be limited to low seismic areas and that the fixed bearing anchor bolt size should be reduced to decrease potential damage in the pier beneath it (Filipov *et al.*, 2013b; LaFave *et al.*, 2013a).

The integral abutment in IABs removes the expansion joint and bearing between the abutment elements and superstructure that is present in stub abutment bridges. This leads to a much stiffer bridge that behaves differently due to its lack of individual movement of the superstructure and substructure. Given this, the conclusions found in the Phase I studies may not apply to IABs due to the inability for quasi-isolated behavior to occur. Further elaboration on previous Illinois seismic bridge behavior research from this project (Phase I) is presented in Chapter 2 of this dissertation.

The lack of quasi-isolated behavior in IABs leads to the interest in Phase II of the project to study IABs. While there is no information concerning the seismic behavior of IABs in Illinois, there have been numerous studies, outside of this project, which focused on the behavior of IABs when subjected to thermal and live loads (Olson *et al.*, 2013; LaFave *et al.*, 2016). The thermal and live loads are of interest due to their applicability to a larger set of regions (*i.e.*, not just in high seismicity regions like for this study) and because the lack of an expansion joint leads to larger stresses in the abutment foundations (Olson *et al*., 2013). These projects have also analyzed IABs using numerical models, leading them to be useful resources for seismic IAB modeling.

Another portion of the seismic project that required refinement in Phase II involved the ground motions used in the dynamic analyses of Phase I. As mentioned, earthquake time histories are difficult to acquire for Illinois and the modification of existing ground motions is often necessary. However, the ground motions used in Phase I, presented in Fig. 1.3, used ground motions from two sites (Cape Girardeau, MO and Paducah, KY) from Fernandez and Rix (2006) with simple linear scaling of the ground motions to better match the AASHTO design spectrum for Cairo, IL (Filipov *et al.*, 2013b). Both the source ground motions and the modification process gave the researchers in Phase I reason to believe that changes to the ground motion development procedure were necessary in the future.

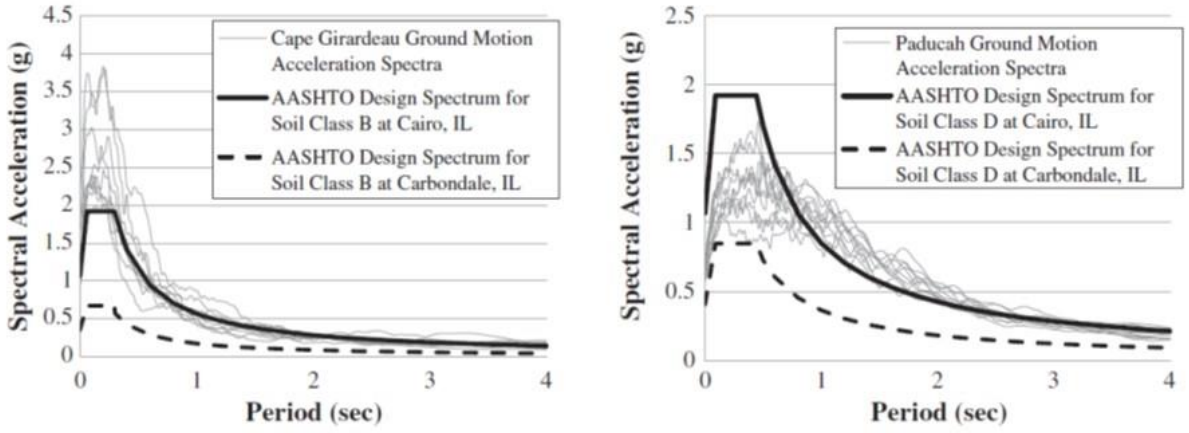

(a) Acceleration spectra for Cape Girardeau normalized to Cairo Soil Class B Hazard (rock)

(b) Acceleration spectra for Paducah normalized to Cairo Soil Class D Hazard (stiff soil)

Figure 1.3: Phase I ground motion spectra (Filipov *et al.*, 2013b).

1.2.2 Research Objectives

Based on the motivations described and the past research conducted in previous phases of this project, the following research objectives were set:

1. Develop horizontal ground motion records with appropriate hazard and site conditions for highway bridge dynamic analyses in southern Illinois.

2. Develop models of entire Illinois IABs in the Open System for Earthquake Engineering Simulation (*OpenSees*) program (McKenna *et al.*, 2006). The models will be developed using numerous individual detailed component models combined into an overall bridge model.
3. Identify and monitor critical components in IABs, which may differ from stub abutment bridges.
4. Develop a more comprehensive and complete view of IAB behavior with seismic design using IAB model results and previous knowledge from existing projects and literature.
5. Provide IDOT with feedback and recommendations which can be used to modify their IAB design procedures with respect to seismic design.

1.2.3 Research Tasks

To achieve the stated research objectives, a set of six research tasks was developed. The research tasks are as follows:

- Task I: Develop appropriate ground motions

  Existing ground motions are used and modified to develop horizontal ground motions appropriate for southern Illinois at a 1000-year return period hazard level. These developed ground motions use state-of-the-art techniques such as employing the conditional mean spectrum (CMS) (Baker, 2011) and region-specific soil properties. These ground motions will be extremely useful for the seismic assessment of both integral and stub abutment bridges in southern Illinois. Note that only horizontal ground motions are considered in this study for simplicity and due to a lack of information concerning developing vertical ground motions for sites and propagating them though soil profiles.

- Task II: Create nonlinear integral abutment bridge models

  IAB models will be developed in *OpenSees*. These models will take into account specific element models for components such as the elastomeric bearings, fixed bearings, and backfill response, as was done for stub abutment bridges in earlier phases of this project (LaFave *et al.*, 2013a). These component models are based on experimental behavior found in the literature. Unlike previous phases of the project, the IAB models must account for the monolithic nature of the integral abutments as opposed to including bearings and expansion gaps as found in stub abutments. Based on previous studies of IABs subjected to thermal loading (LaFave *et al.*, 2016) and specific IAB components subjected to seismic loads. Components such as the backfill soil (Kotsoglou and Pantazopoulou, 2009; Olson *et al.*, 2009), the abutment piles (Frosch *et al.*, 2009), and the soil-pile interaction (Vasheghani-Farahani *et al.*, 2010; Zhao *et al.*, 2011) are very important seismic components in IABs. The specific modeling of these important seismic components allows for the definition of key IAB limit states to be performed within Task II. The overall IAB model is validated against qualitative results from the post-earthquake condition of IABs.

- Task III: Perform static pushover analyses

  A static pushover analysis of IABs in both the bridge longitudinal and transverse directions will be performed on the IAB models. The results from this analysis will allow for the identification of critical limit states that the bridge reaches before failure.

- Task IV: Perform dynamic analyses

  Dynamic analyses of the IAB models will be conducted using the developed ground motions in both the bridge longitudinal and transverse directions. The results from the dynamic analyses allow for a better understanding of how the bridge will behave and what

limit states will be reached under design level ground motions, as well as the excitation levels at which certain damage occurs.

- Task V: Process results

  Post-processing of the data from the analyses allows for specific limit states to be identified. Trends can then be found in the results to identify critical components in the bridges. The results can then be compared to ideal failure sequences and limit states to determine which components require modification.

- Task VI: Form recommended seismic design guidelines of IABs

  The processed results and conclusions concerning specific component and overall bridge behavior are reviewed. Specific enhancements to component designs shown to be useful in seismic design can be used to form recommended changes to IAB design in Illinois to enhance IAB seismic behavior. The proposed enhancements are implemented and analyzed on a limited basis to evaluate and ensure that the desired behavior is obtained from the enhancements.

1.3 ORGANIZATION OF THE DISSERTATION

This dissertation describes the procedures for developing ground motions and IAB models suitable for southern Illinois. The results from the IAB models being subjected to the ground motions are also discussed to determine their potential design implications. This dissertation contains ten chapters:

- Chapter 1: Introduction

  A summary is provided of the motivation behind this project, along with background information on previous bridge studies (both seismic and non-seismic) in Illinois. Knowledge of the previous bridge studies is then used to detail specific research objectives

to be achieved in this study. Six research tasks are outlined, which allow for the research objectives to be achieved. These research tasks were used to develop the in-depth study presented in this dissertation. Finally, the overall organization of the dissertation is presented, with each chapter being briefly described.

- Chapter 2: Literature Review

  Research from previous studies is presented in three categories. (1) Ground motion selection and development techniques are described in order to assess which method is most appropriate for CNA. (2) Previous Illinois seismic bridge behavior research from this project (Phase I) is presented. The bridges analyzed did not contain any IABs. (3) IAB modeling research is presented. These studies typically focus on thermal effects or do not consider overall bridge seismic behavior.

- Chapter 3: Ground Motion Development

  Ground motions are developed for ten sites around southern Illinois. The 20 ground motions at each site are developed by modifying existing ground motions to the hazard and spectral shape expected at the sites and then propagating the motions through a soil profile representative of each site. Existing ground motions are modified through wavelets in the time domain to closer match the desired conditional mean spectra at each site. The soil profiles for each site are developed using existing boring data from Illinois bridge construction details. The soil profiles at the ten sites were split into two representative categories: alluvial and non-alluvial. The resulting ground motion time histories developed in this chapter are further described in Kozak *et al.* (2017a) along with a report containing the location of the developed time histories in Kozak *et al.*, (2017b).

- Chapter 4: Integral Abutment Bridge Model Development

  The description of an IAB and how it differs from stub abutment bridges is explored. The IAB models for this study and each of their numerous components are then detailed. Each component is modeled using existing literature and/or experimental study results. Many of the elements from Phase I of the study, which examined stub abutment bridges only, are used in the IAB models, while other components are new to this portion of the study and were not considered in the previous phase of the work. Finally, limit states are presented which use the individual component models to help determine the overall bridge behavior.

- Chapter 5: Parametric Study of Southern Illinois IABs

  The parametric study of IABs is described. The parametric study observes the behavior of 51 IAB variants subjected to the Cairo ground motions at the design and other hazard levels. The 51 bridge variants include realistic Illinois IAB variations to the superstructure material, span configuration, pier height, bearing layout, and foundation soil type.

- Chapter 6: Parametric Study Pushover Analysis Results

  The static pushover results of all 51 IAB variants detailed in Chapter 5 is presented. The occurrence of limit states is observed throughout the pushover analysis, allowing for a sequence of damage to be assessed up to failure of the IAB. Observations are made from the results of the pushover curves and are compared to each other to recognize trends in IAB behavior. Trends are observed across all bridges as the foundation soil, bearing layout, and other design factors are varied.

- Chapter 7: Parametric Study Dynamic Analysis Results

  Similar to Chapter 6, this chapter evaluates the seismic behavior of all 51 IAB variants, except this chapter evaluates them using dynamic analyses. The dynamic analyses are

performed with the 20 ground motions for Cairo at the design hazard level, as well as at different hazard levels by scaling the design level ground motions by factors from 0.5 – 1.75. The results allow for the behavior at the design hazard level to be assessed across various design factors. The inclusion of multiple hazard levels allows for incremental dynamic analyses to be conducted and fragility functions of the damage limit states to be observed.

- Chapter 8: Effect of Ground Motion Intensity on IAB Behavior

  The initial parametric study includes only the Cairo ground motions, so this chapter varies the ground motions across the 9 other sites selected in southern Illinois which had ground motions developed in Chapter 3. This varies the seismic hazard and intensity of shaking that the IABs are subjected to in the analyses. The bridges at the 9 other sites also use the appropriate soil conditions for the site and are conducted at the design hazard level. The results allow for observations to be made concerning which sites do not require seismic consideration in design. The results are related to seismic performance zone designations within Illinois.

- Chapter 9: Proposed Enhancements to Illinois IAB Seismic Design

  The observations from Chapters 6, 7, and 8 are used to form conclusions and potential design enhancements for the seismic design of IABs in Illinois. The proposed enhancements affect the bearing size, retainer anchor bolt size, fixed bearing anchor bolt size, pier column size, and abutment-backfill contact area size. The design enhancements are implemented on a limited basis and IABs with the enhancements are analyzed at Cairo to assess the induced effects on the seismic behavior of the bridges. Based on the analyses of enhanced IABs, recommendations are formed concerning improving the seismic

behavior of IABs in southern Illinois While these recommendations are specifically for IABs within the state of Illinois, the more general conclusions will be useful for those studying IAB seismic behavior in other locations.

- Chapter 10: Conclusions and Future Work

  Conclusions and recommendations concerning the seismic behavior and design of IABs in different sites around southern Illinois are reviewed. Using these conclusions and recommendations, future work is proposed to address concerns with the models that could be improved in the future. Future work is also presented which expands the IAB seismic study to include other factors such as more earthquake excitation directions, including bridge skew, and including semi-integral abutment bridges.

CHAPTER 2: LITERATURE REVIEW

2.1 GROUND MOTIONS IN CENTRAL NORTH AMERICA

2.1.1 Existing Ground Motions

The low activity rate of the NMSZ and other sources of seismicity in CNA poses a major hurdle in performing seismic structural analyses within the region. Focusing on the state of Illinois and for a specific hazard level further narrows the search parameters and limits the amount of suitable recorded ground motions. In the past, synthetic ground motions have been produced for southern Illinois and areas directly surrounding it, however their suitability for use in southern Illinois analyses may not be fully acceptable. The issues concerning the suitability of existing synthetic and recorded ground motions include the lack of ground motions within the specific region of interest, the lack of ground motions with the appropriate hazard level, and the limited amount of strong ground motions within CNA.

The first two issues are exemplified by the ground motions used in Phase I of the project, provided in Fig. 1.3. The source ground motions (*i.e.*, ones that have not yet been modified) are synthetic motions from Wen and Wu (2001) and Fernandez and Rix (2006) (Filipov *et al.*, 2013b). Wen and Wu (2001) developed 20 ground motions each for three Midwest locations at two hazard levels. The locations were Memphis, TN, Carbondale, IL, and St. Louis, MO, and the hazard levels were at 2% and 10% probability of exceedance (PE) in 50 years (about a 2500- and 500-year return period event, respectively). While Carbondale is within southern Illinois and St. Louis is extremely close, Memphis is much further south within the NMSZ and produces motions with much larger intensities than expected in Illinois. Furthermore, the hazard levels differ from the 5% PE in 50

years (1000-year return period) AASHTO design-level hazard for highway bridges, making the Wen and Wu (2001) motions not suitable for this project.

The Fernandez and Rix (2006) motions have been produced for a 5% PE in 50 years. However, their locations are not within the state of Illinois. The motions were developed for Cape Girardeau, MO and Paducah, KY, which are across the Mississippi and Ohio Rivers, respectively, from Illinois. Although they are close to southern Illinois, there is a strong possibility that the site conditions are different outside of the state.

The final concern for existing CNA ground motions is the lack of recorded ground motions for the region. This is exemplified by the two main ground motion databases which contain CNA recorded ground motions – the U.S. Nuclear Regulatory Commission's central and eastern United States database (NUREG/CR-6728) (McGuire *et al.*, 2001), and the Pacific Earthquake Engineering Research Center's (PEER) NGA-East database (Goulet *et al.*, 2014). The NUREG/CR-6728 database provides 138 intraplate ground motion records at rock sites, with some recordings coming from central and eastern North American (CENA) earthquakes, but it mostly comprises motions from California or Japan that have been modified to appropriately represent the seismic source and crustal properties of CENA (McGuire *et al.*, 2001). The California and Japan motions are included to fill out the database due to the lack of CENA recordings (McGuire *et al.*, 2001). The PEER NGA-East database comprises 89 events which occurred in CENA. As shown in Fig. 2.1, the 89 PEER NGA-East events occur within CENA, but they mainly stay below a magnitude of 6 (Goulet *et al.*, 2014), making them typically not strong enough for 1000-year return period events in southern Illinois. The ground motions from these two databases often overlap, such as with the 1988 Saguenay earthquake in Quebec, leading to a limited amount of suitable ground motions for a 1000-year return period hazard in southern Illinois.

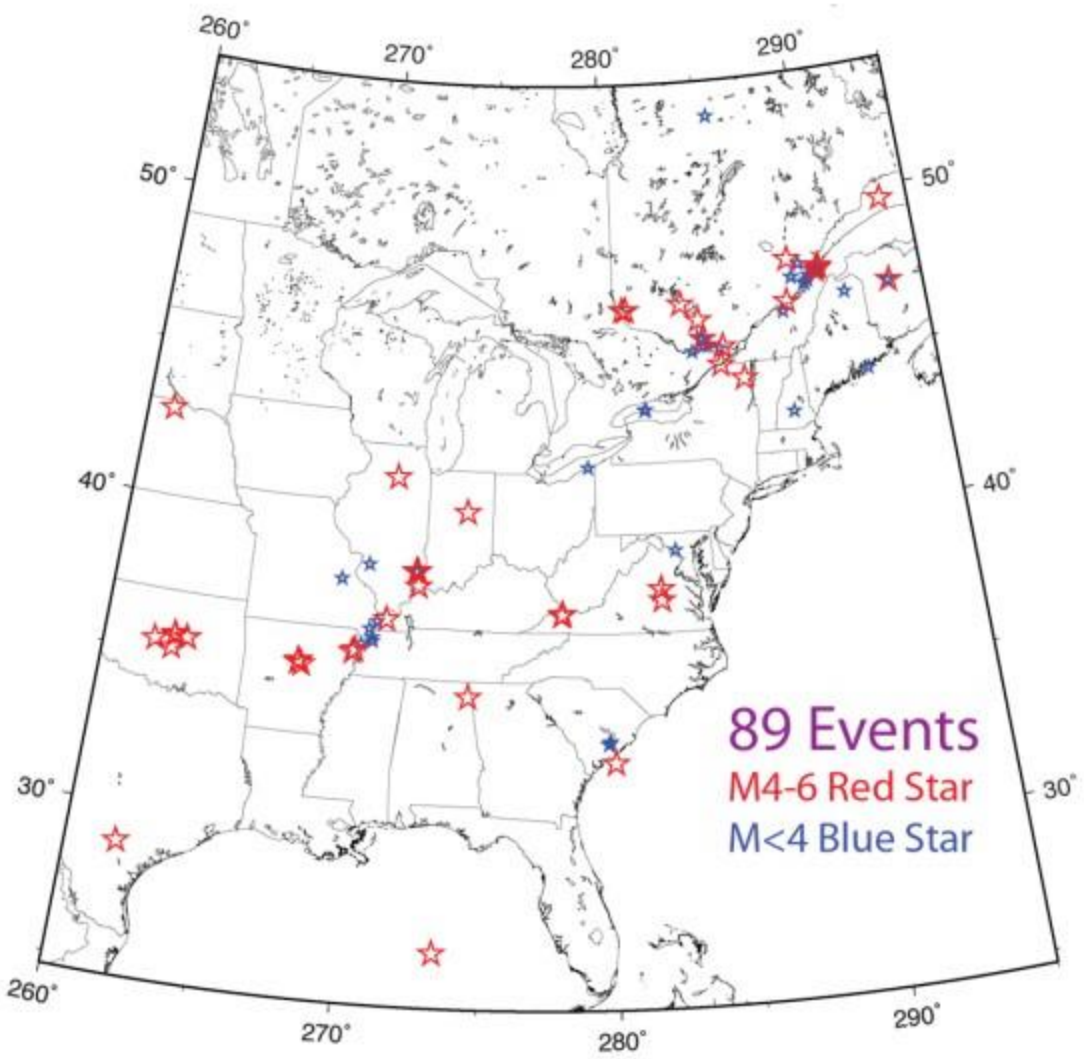

Figure 2.1: Epicenter location and magnitude of the earthquakes included in the PEER NGA-East database, not including the 1929 Grand Banks (Newfoundland, Canada) and 1985 Nahanni (Northwest Territories, Canada) earthquakes which are outside the region of this map (Goulet *et al.*, 2014).

2.1.2 Modification and Development of Ground Motions

In the past, the lack of ground motion recordings led to the modification of existing ground motion recordings or the development of ground motions to be suitable for the region and hazard level of interest. The development of synthetic ground motions is typically performed by using ground motion prediction equations (GMPEs). The GMPEs (also known as attenuation relationships) account for the epistemic and aleatory uncertainties in the ground motion

development process. Region-specific GMPEs may be developed, but the more common method involves using established GMPEs from literature. Examples of these GMPEs include the Atkinson and Boore (2006) and Toro *et al.* (1997) GMPEs. These two GMPEs along with six other GMPEs were used to develop the 2008 National Seismic Hazard Map for the central and eastern United States (CEUS) (Petersen *et al.*, 2008). GMPEs are used in conjunction with stochastic point-source or finite-fault methods to create ground motions for use in a region (Atkinson and Boore, 2006).

The modification of existing ground motions is another common process for acquiring suitable ground motions for a specific region and hazard level. The source ground motions are typically modified such that their spectra match a target spectrum for the bedrock level which is appropriate for the site and hazard level of interest. Three common target spectra are the uniform hazard response spectrum (UHS) (Baker, 2011), the design spectrum (Filipov *et al*., 2013b), and the conditional mean spectrum (CMS) (Baker, 2011). Examples of these three target spectra are shown in Fig. 2.2 where the Median + 2σ spectrum in Fig. 2.2b is the CMS.

Initial source ground motions are typically selected from a database of existing bedrock ground motion records. The motions are selected based on their similarity in spectral shape and similarity to certain variables expected at the desired site and hazard level. These variables include moment magnitude, fault mechanism, and source-to-site distance; however, other factors such as the code-based site class and strong motion duration may also be considered (Katsanos *et al.*, 2010).

The similar ground motions are then modified to better match the target spectrum. Spectral matching can be accomplished through various methods such as the linear scaling of the ground motion to match the target spectrum at a single period or a range of periods (Somerville *et al*.,

1997; Hancock *et al*., 2008), the addition of wavelets in the time domain to modify the spectral shape (Hancock *et al*., 2008), or even through modification using a genetic algorithm (Naeim *et al*., 2004). There also exists methods which have less emphasis on spectral matching to a target spectrum (Watson-Lamprey and Abrahamson, 2006).

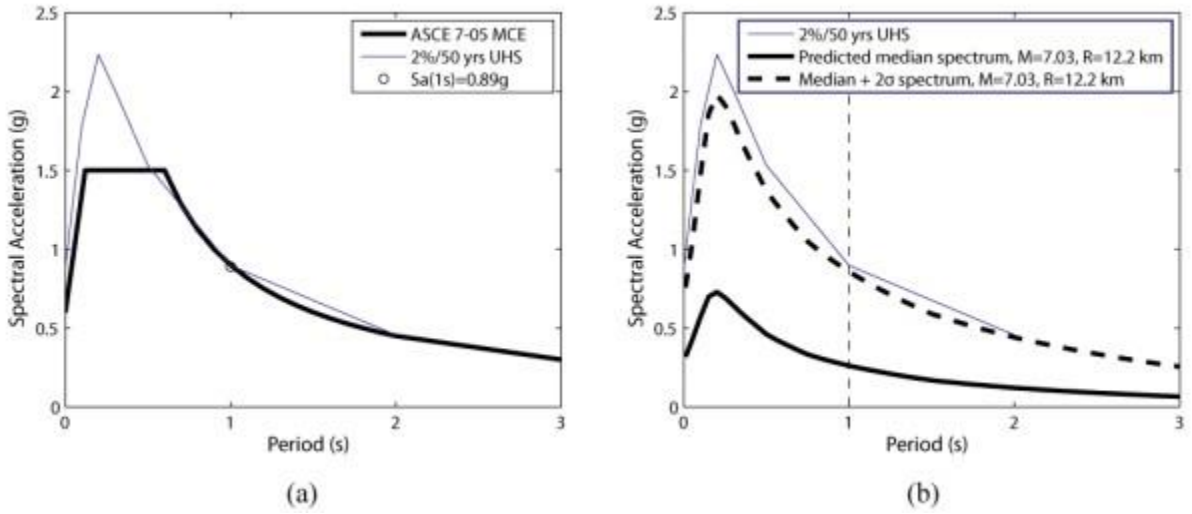

Figure 2.2: Typical target spectra to match modified ground motions to: (a) the UHS (2%/50yrs UHS) and design spectrum (ASCE 7-05 MCE); (b) the UHS (2%/50yrs UHS) and CMS (Median + 2σ spectrum) (Baker, 2011).

As mentioned, the target spectrum can be a variety of existing spectra such as the UHS, the design spectrum, or the CMS, with the UHS being the generally accepted method. However, there is growing use of the CMS as a target spectrum. The motivation of the CMS is that the UHS provides unrealistically large spectral accelerations across all periods and would therefore produce some unrealistic ground motions (Baker and Cornell. 2006). This is exemplified by acknowledging that the UHS is developed by incorporating both small magnitude near-field earthquakes and large magnitude far-field earthquakes which dominate the short period and long period behavior of the spectrum, respectively, in the midwestern United States. Due to the development of the UHS incorporating multiple sources, an earthquake would need to have large spectral accelerations in

both the short and long period range to match the UHS, which is unrealistic (Baker and Cornell, 2006).

It is instead proposed that the UHS value at a certain period is better suited as an intensity measure to match the CMS to at that particular period (Baker and Jayaram, 2008). This is achieved by following the procedure laid out in Baker (2011) to develop the CMS based on expected magnitude, expected source-to-site distance, and the epsilon parameter (describing the number of standard deviations between the UHS and the median spectrum at a specific period) from hazard deaggregation. A median spectrum can be developed with the deaggregation results using an appropriate GMPE, and the CMS can then be created using the median spectrum and the UHS (Baker, 2011). In general, the CMS matched to the UHS at the conditional period will then have smaller spectral accelerations at any other periods. Given this formulation, the UHS typically represents an envelope of maximum spectral acceleration for the CMS to match at a conditional period, as shown in Fig. 2.3.

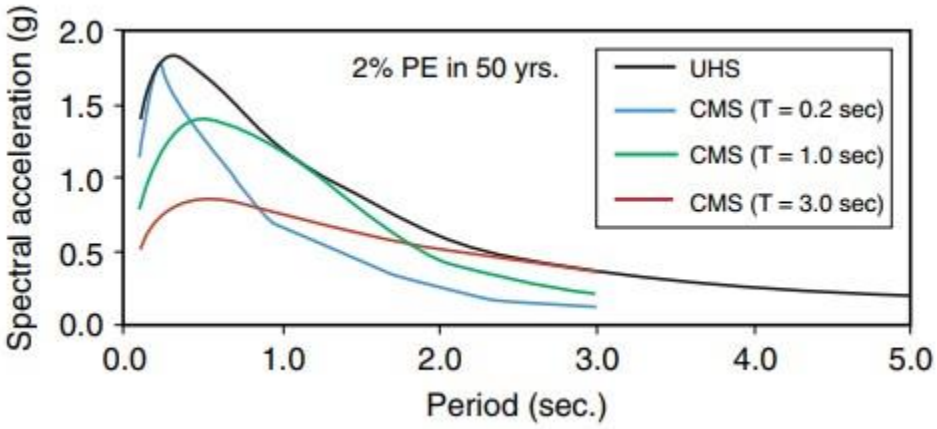

Figure 2.3: Example CMS enveloped by the UHS (Roy *et al*., 2014).

The CMS has begun to be studied for use as the target spectrum more frequently in various locations. These studies include the applicability of the CMS as a target spectrum in Romania (Vacareanu *et al.*, 2014) and the development of the epsilon parameter for use with the CMS in

Europe (Cimellaro, 2013). The CMS has also been used to develop ground motions for use in the investigation of building seismic behavior in eastern Canada (Daneshvar *et al.*, 2014), in Los Angeles (Roy *et al.*, 2014), and in the design of a bridge crossing the Mississippi River (Hashash *et al.*, 2015a). The CMS has not been thoroughly studied for use in Illinois in the past. Two advantages found in using the CMS as a target spectrum in dynamic analyses are that the CMS has been shown to produce ground motions more realistic than those matched to the UHS (Banerjee *et al.*, 2016), and fewer CMS-matched motions are required to achieve similar results found from UHS-matched motions (Roy *et al.*, 2014).

2.1.3 Soil Effects

Once the source ground motions are matched to a target spectrum, there is still a need to translate these ground motions from the bedrock level to the level of the surface (or another depth of interest) by accounting for the soil's effects. The site-specific soil conditions are typically accounted for in GMPEs using code-based amplification factors. These amplification factors are usually a function of the site class and the ground motion amplitude. They are initially developed through calibration with measured seismic data, and then parametric studies of various site classes and ground motions are used to extrapolate the data to create amplification factors for a variety of scenarios (FEMA, 2003).

An alternative to developing amplification factors is to incorporate the soil effects directly into the GMPE. This is done in GMPEs such as the Atkinson and Boore (2006) GMPE, which was developed directly for soil sites instead of bedrock sites and therefore already incorporates the soil's effects (Fernandez and Rix, 2006).

Another common method of accounting for local soil conditions is to propagate the ground motions through site-specific soil columns. This method is more involved than the previously

mentioned methods. A soil column representing the soil properties of the site is used in an equivalent linear or nonlinear ground response analysis to achieve the ground motion time history at various depths. A set of soil columns for a site or region may be either analyzed deterministically or using another method to include the potential uncertainties within the soil profiles (Silva and Costantino, 2002).

2.2 STUB ABUTMENT BRIDGE SEISMIC BEHAVIOR STUDIES

In the past there have been studies concerning the seismic behavior of bridges in southern Illinois, the majority of which came from Phases I and II of this project. The modeling of the stub abutment bridges and their seismic analysis can be explained in three parts – the physical experiments of highway bridge components, the modeling of the stub abutment bridges, and the evaluation of the bridges and the conclusions drawn.

2.2.1 Bridge Component Experiments

Bearings commonly used in Illinois bridge design were studied by Steelman *et al.* (2013; 2014; 2016; 2018) to determine their monotonic and cyclic behavior. The three main types of bearings investigated and tested were Type I elastomeric, Type II elastomeric, and low-profile fixed bearings. The side retainers, which accompany the elastomeric bearings in bridges, were also studied. The Type I elastomeric bearings are fabricated using a steel shim reinforced elastomer block which is fused on top to a steel plate and in contact with the concrete on the bottom to allow for movement. The Type II elastomeric bearings differ from the Type I bearings by being vulcanized to a steel plate at the bottom and allowing for movement at the top between a steel plate vulcanized to the elastomer with a polytetrafluoroethylene (PTFE) top surface contacting a polished stainless steel top plate. The low-profile fixed bearings are comprised of two steel plates held in place by pintles (IDOT, 2012a).

The results from the physical experiments demonstrated clear behavior in all four components. The Type I and Type II bearings showed an initial static friction force followed by a bearing slip and reduced kinetic friction resistance under monotonic loading, as shown in Fig. 2.4a. Under cyclic loading the behavior slightly differed in that the Type I bearings needed to reach a post-slip static friction force before sliding again (Fig. 2.4b) while Type II bearings only needed to reach the kinetic friction resistance on reloading (Fig. 2.4c). The Type II bearings also have significantly less friction due to the smaller coefficient of friction between a PTFE surface and steel than the friction between an elastomer and concrete (LaFave *et al.*, 2013b).

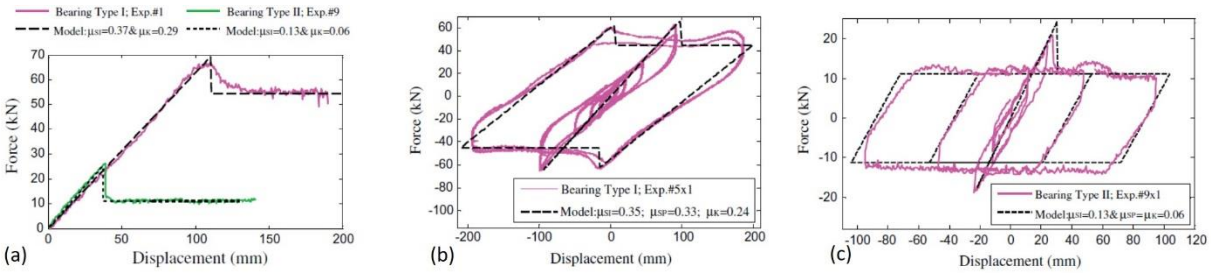

Figure 2.4: Experimental and modeled behavior for: (a) monotonic Type I and II elastomeric bearing behavior; (b) cyclic Type I elastomeric bearing behavior; and (c) cyclic Type II elastomeric bearing behavior (Filipov *et al.*, 2013a).

The behavior of the side retainers and low-profile fixed bearings are found to behave similarly in that the anchor bolts are the weak point of both components. This means that the yielding and fracture of the bolts dictates their behavior (LaFave *et al.*, 2013b).

2.2.2 Stub Abutment Bridge Models

The experimental data for the elastomeric bearings, side retainers, and low-profile fixed bearings was used to create simplified behavior models which can be used in analysis. The corresponding behavior models for the elastomeric bearings are shown in Fig. 2.4. The experimental data, which only examined a limited amount of bearing and retainer specimens, is

further extrapolated such that the behavior of all potential IDOT bearings and retainers can be predicted (Filipov *et al.*, 2013a; Filipov *et al.*, 2013b; LaFave *et al.*, 2013a).

Bearings and side retainers are just a few components within the complete stub abutment bridge model. The behavior of the numerous other components not experimented on by Steelman *et al.* (2013; 2014; 2016; 2018) were developed based on existing literature. These components include the piers, the foundations at the abutment and pier locations, the abutment backwall, and the backfill (Filipov *et al.*, 2013a). These models were combined with other elements such as elastic superstructure elements to form the complete stub abutment bridge model.

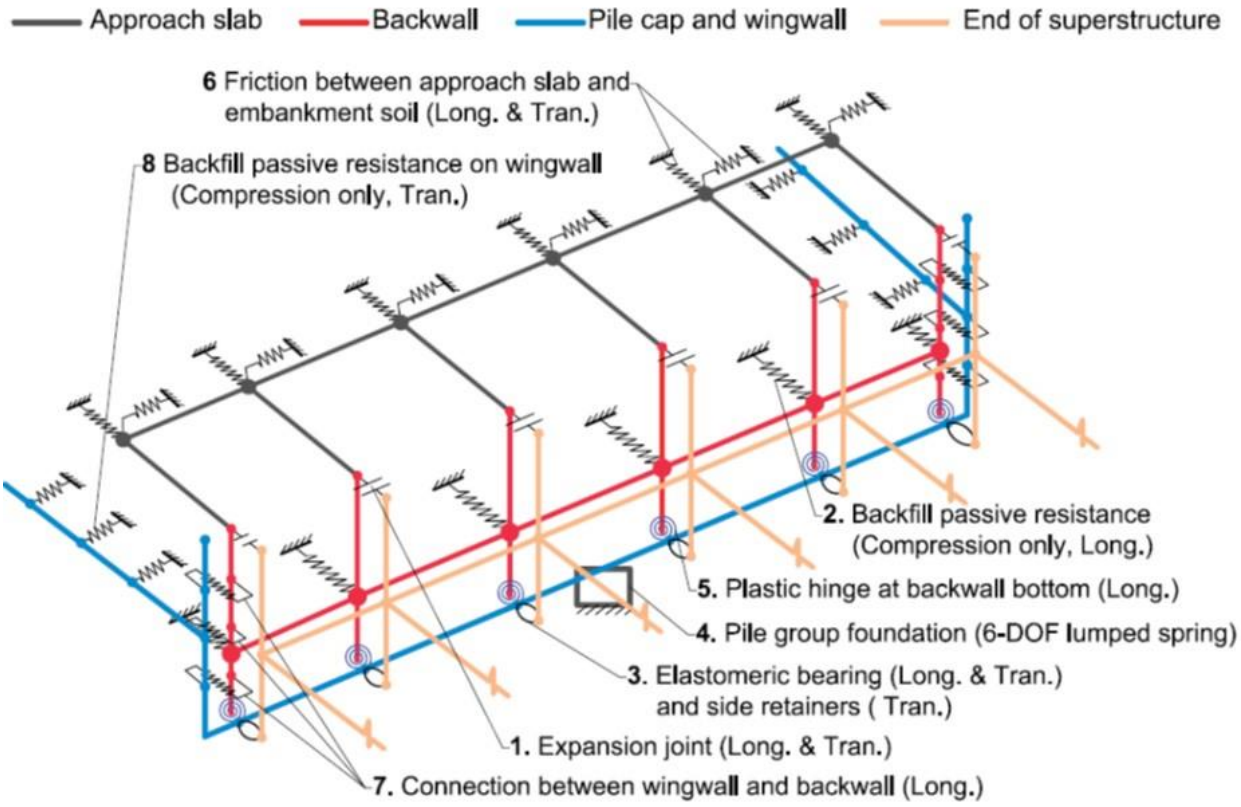

Figure 2.5: Detailed stub abutment model from Luo *et al.* (2016).

The models in Phase I of the project were adequate to obtain many useful conclusions, however an improvement was desired to the abutment modeling. Luo *et al.* (2016) developed a much more detailed abutment model for use in stub abutment bridges in Illinois. This detailed

abutment model, shown in Fig. 2.5, expands on the simpler stub abutment model by providing enhanced details on the expansion joint, backfill, foundation, and backwall behavior. In addition, the backfill's effect on the wingwalls, the wingwall connection, and the approach slab friction are all explicitly modeled (Luo *et al.*, 2016).

2.2.3 Analysis of Stub Abutment Bridges in Illinois

The combination of all the individual components into a complete bridge model for Illinois allowed for previous studies to monitor and evaluate the behavior of each component individually during a global bridge analysis (Filipov *et al.*, 2013a; Filipov *et al.*, 2013b; LaFave *et al.*, 2013a). Key limit states within the bridges are evaluated based on the component behavior during the analysis. These limit states include elastomeric bearing sliding and unseating, side retainer fracture in the transverse bridge direction (perpendicular to the direction of traffic), fixed bearing anchorage fracture, abutment backwall hinging, and pier yielding (Filipov *et al.*, 2013b). These limit states were used to determine the sequence of damage in a bridge as the ground motions become stronger. The sequence of damage in the stub abutment bridges allows for observations and conclusions to be made concerning the vulnerability of certain components and whether the desired quasi-isolated behavior is achieved in the bridge (Filipov *et al.*, 2013b; LaFave *et al.*, 2013a).

The results from the Illinois stub abutment bridge seismic analyses indicated a few observations which can be used to form recommendations for future design. The main observation dealt with the behavior of bridges which use Type II elastomeric bearings. It was found that unseating is very common in these bridges leading to the recommendation that Type II elastomeric bearings should be limited to use in lower seismic areas (LaFave *et al.*, 2013a). This observation can be seen in Fig. 2.6 where there is bearing unseating at the abutment (UA) in SsC15T2S when

subjected to ground motions 1.25 times the design hazard level (as seen in Fig. 2.6a and c). This bridge uses Type II elastomeric bearings at the abutment location. Conversely, neither SsC40T1F, which uses Type I elastomeric bearings, nor the defined acceptable sequence of damage, experiences bearing unseating (as seen in Fig. 2.6b and c) under any scale factor (Filipov *et al.*, 2013b).

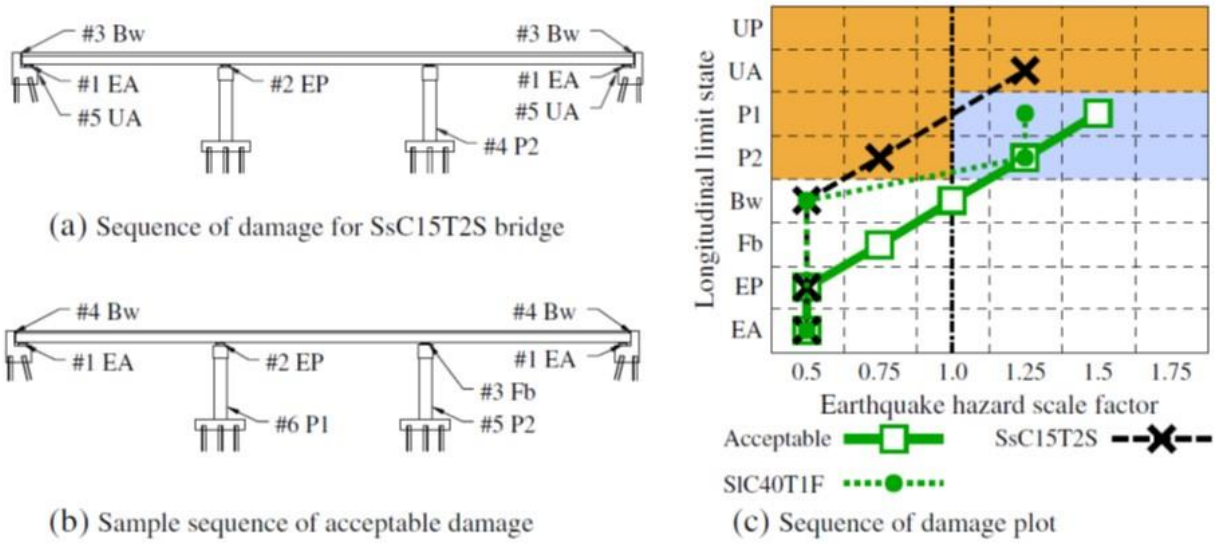

Figure 2.6: An acceptable sequence of damage along with the sequence of damage for a bridge using a Type I elastomeric bearing (SsC40T1F) and a Type II elastomeric bearing (SsC15T2S) (Filipov *et al.*,2013b).

Another observation is the occurrence of yielding of the piers under the fixed bearings. In some bridges, like SsC15T2S, the piers yield under much smaller ground motions than anticipated in the acceptable sequence of damage, as seen in Fig. 2.6c (Filipov *et al.*, 2013b). This led to a recommendation that the fixed bearing anchor bolt size be revised (LaFave *et al.*, 2013a).

2.3 INTEGRAL ABUTMENT BRIDGE STUDIES

2.3.1 Advantages and Limitations of Integral Abutment Bridges

Conventional stub abutment bridges traditionally account for movement of the superstructure caused by thermal, creep, or shrinkage strains by employing expansion joints and

elastomeric bearings at the abutments (Kunin and Alampalli, 1999), as seen in Fig. 2.7a. While this method is effective in accommodating the superstructure movement, expansion joints are expensive to buy, install, maintain, and repair. Expansion joints may also cause larger issues if they leak, allowing water, dirt, and deicing chemicals to reach the abutment seat, which is undesirable due to the difficulty in cleaning this location and the increased potential for corrosion of the girders (Kunin and Alampalli, 1999; Paraschos and Amde, 2011). The use of elastomeric bearings in stub abutments also creates issues due to their cost to purchase and install (Paraschos and Amde, 2011).

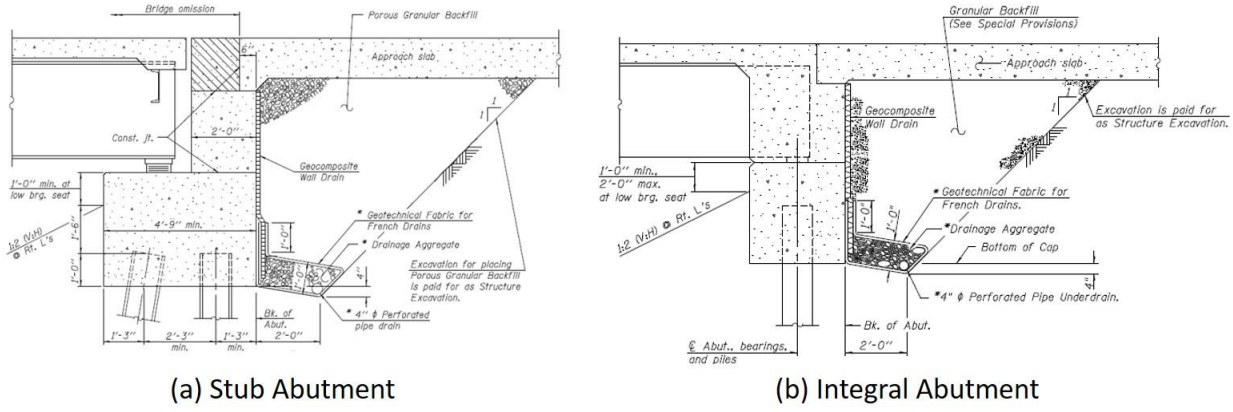

(a) Stub Abutment (b) Integral Abutment

Figure 2.7: Representative diagram of (a) a stub abutment (IDOT, 2012a); (b) an integral abutment (IDOT, 2012b).

The advantage of an integral abutment is in the elimination of the issues presented above for stub abutments. Integral abutments remove the expansion joint and abutment elastomeric bearing components in favor of creating a superstructure-substructure system which moves together at the abutments. This monolithic design is achieved by embedding the single row of piles (if a pile foundation is used) into the pile cap, resting the superstructure girders on the pile cap, and then pouring the deck and abutment concrete at the same time. By pouring the deck and abutment at the same time, the girders end up being embedded approximately 1 ft or more into the abutment (Olson *et al.*, 2009). A diagram of an integral abutment is presented in Fig. 2.7b, and as

can be observed this abutment style eliminates the use of expansion joints and bearings as well as the expensive costs associated with their installation and maintenance.

While integral abutments provide advantages in the form of reducing potential maintenance costs to the girders and abutment seat, there are also some disadvantages and limitations that present themselves. The major issue with integral abutments stems from the fact that, due to the superstructure and abutment being rigidly connected, both forces and moments are transferred from the superstructure to the abutment and piles, as opposed to just forces in the case of stub abutments. This interaction between the girders and abutments, as well as between the abutment, piles, and the soil surrounding the piles, creates a complex soil-foundation-structure interaction problem (Olson *et al.*, 2009). The unknown effects from this soil-structure interaction (SSI) problem and the uncertainties they lead to in terms of pile flexural stresses has led to limitations on IAB span lengths and skew angles (Itani and Pekcan, 2011).

Despite these limitations IABs are commonly constructed in the United States, with the first being constructed in 1905 in Colorado and over 9,000 constructed IABs in service in the United States and Canada as of 1996 (Kunin and Alampalli, 1999). The state of Illinois is no different from the rest of the country, with IAB construction beginning in 1983 and having around 350 constructed IABs in 1996. Additionally, IAB use is not limited to non-seismic regions, with thousands of IABs being constructed in the western states of California and Washington since the 1950s (Kunin and Alampalli, 1999).

2.3.2 Past IAB Studies

The use of IABs in Illinois has led to studies that assess the behavior of IABs under thermal loads, in order to modify IDOT's IAB design process, as necessary. Studies have included both the 2-D and 3-D modeling of IABs (Olson *et al*., 2013; LaFave *et al.*, 2016) as well as the

monitoring of IABs in the field (Olson *et al.*, 2009; Olson *et al.*, 2013; LaFave *et al.*, 2017) to determine their behavior when subjected to normal degrees of thermal and live loads. These studies observe how IABs deal with expansion and contraction of the superstructure without the use of expansion joints or elastomeric bearings at the abutments.

In addition to the studies of entire IAB behavior that have been performed in Illinois, a variety of studies have also examined the behavior of individual components of IABs. The increased bending moments in the piles and increased forces transferred to the soil surrounding the abutment piles has led to an abundance of studies focused primarily on the SSI at the abutment (Vasheghani-Farahani *et al*., 2010; Zhao *et al.*, 2011; Franchin and Pinto, 2014). The SSI manifests in two situations at the abutments – between the abutment and the backfill, and between the piles and the surrounding soil. The SSI at the backfill was shown to contribute significant hardening in the post-elastic range of the overall IAB model behavior in Kotsoglou and Pantazopoulou (2009), demonstrating the importance of the backfill to overall response. The SSI between the piles and the surrounding soil has been studied much more extensively than the backfill SSI. Vasheghani-Farahani *et al.* (2010) and Zhao *et al.* (2011) determined that the SSI at the piles effects the IAB behavior by dictating the amount of pile deflection that occurs. It was also found that although the maximum moment in the piles occurs at the pile-abutment interface, the magnitude of the bending is also dependent on the soil surrounding the piles. The SSI at the piles has also been found to be extremely important under transverse excitation due to the lack of significant backfill resistance in the transverse direction (Spyrakos and Loannidis, 2003).

Other key components that have been studied include the pile-pile cap connection, which undergoes larger moments than experienced in stub abutment bridges. It was found that the piles should be embedded at least 2 ft in order to not experience any significant reduction in lateral

resistance (Frosch *et al.*, 2009). It has also been indicated that due to the extreme difficulty in inspecting and replacing abutment piles, they should ideally remain elastic during thermal events (Teguh *et al.*, 2006). Due to the large moments at the interface, the girder-abutment connection has also been studied (Itani and Pekcan, 2011).

2.3.3 Observed IAB Damage

Damage to IABs has also been assessed after earthquakes to determine which components tend to fail the most. One location where damage may occur is at the superstructure-abutment interface, due to the large moments present during seismic shaking (Itani and Pekcan, 2011). Two other common damage locations are at the abutment-pile interface and in the pier columns (Waldin *et al*., 2012; Wood, 2015).

Figure 2.8: Examples of IAB damage from (a) abutment rotation, and (b) pile plastic hinging (Waldin *et al.*, 2012).

In the abutments, damage is typically caused in the connecting components due to the overall rotation of the abutments. The rotation of the abutments has been found to be related to the liquefaction-induced lateral spreading caused by earthquakes (Waldin *et al*., 2012). It has been found in observations of New Zealand and California IABs after earthquakes that this abutment

rotation has also led to the plastic hinging of the abutment piles at the abutment-pile interface, cracking of the superstructure-abutment joints (Waldin *et al.*, 2012), and other failures of the connections to the superstructure (Wood, 2015). An example of abutment rotation and damage to the concrete piles is presented in Fig. 2.8a and b, respectively.

The frequent pile damage brings about suspicion that the piles may have yielded or formed plastic hinges before the occurrence of the earthquake. The reasoning behind this would be that the thermal, shrinkage, and creep strains on the IAB superstructure would be sufficient to cause enough movement in the piles to cause plastic hinging. However, this theory does not seem to be plausible as there have been studies on existing IABs which show that under thermal loads it is not expected for the abutment piles to yield or form plastic hinges (Kim *et al*., 2012; Kong *et al*., 2015).

Figure 2.9: Damage to an IAB pier column following an earthquake in New Zealand (Waldin *et al.*, 2012).

Failure of the pier columns is another common damage state observed in IABs during past New Zealand earthquakes (Waldin *et al*., 2012). Damage of the pier columns is commonly found

to be caused by the inertial forces during earthquakes stemming from heavy superstructures. The inertial forces have caused shear failure of the pier columns as well as localized buckling of the vertical reinforcing bars, as shown in Fig. 2.9 (Waldin *et al.*, 2012). This type of damage compromises the vertical load capacity of the piers and makes the bridge unable to accommodate traffic after an earthquake. A potential solution utilized when pier damage has occurred in New Zealand is to rigidly brace the piers at the damaged locations to restore vertical load capacity (Waldin *et al*., 2012).

2.3.4 Integral Abutment Bridge Modeling

The majority of IAB studies involve the modeling of IABs to assess the behavior of such bridges. While some models attempt to account for all the components in an IAB, the focus has generally been put on the SSI elements. In these models the soil behavior is accounted for using springs attached to elastic abutment and foundation elements. The superstructure is represented by elastic shell or beam elements which rigidly attach to the abutment and is modeled mostly to account for the mass of the system (Spyrakos and Loannidis, 2003; Kotsoglou and Pantazopoulou, 2009; Vasheghani-Farahani *et al.*, 2010; Zhao *et al.*, 2011; Franchin and Pinto, 2014).

Additional IAB models attempt to determine the bridge behavior by also modeling the abutment piles as nonlinear elements attached to spring elements representing the surrounding soil. While the superstructure is once again modeled as elastic, there is more detail in the abutment components. These models also typically include multi-span IABs, which require the consideration of pier effects. Multiple methods are used to account for the piers, with the two most common being to model the pier-superstructure connection as a roller (Olson *et al.*, 2009; Olson *et al.*, 2013) or to explicitly model a pier that can experience damage and provide realistic lateral resistance to the superstructure (LaFave *et al.*, 2016). The IAB model from LaFave *et al.* (2016), which

considers the detailed abutment and pile model as well as an explicitly modeled pier column bent in SAP2000, is presented in Fig. 2.10.

There are also IAB models which ignore the effects of SSI in favor of exploring the behavior of another component. An example of this model is from Itani and Pekcan (2011), whose study focuses on the superstructure-abutment connection and therefore models that connection in much more detail than the rest of the bridge.

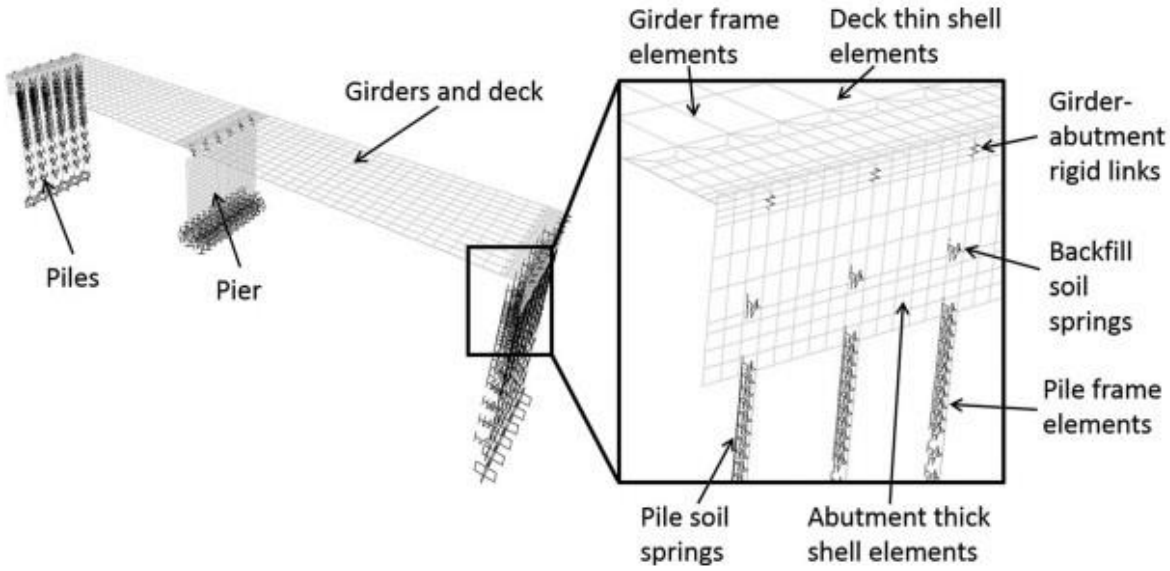

Figure 2.10: IAB model in SAP2000 considering detailed abutment and pile models as well as a modeled pier column bent (LaFave *et al.*, 2016).

Although there have been numerous studies of IABs using detailed models in the past, there are typically shortcomings when considering studies of overall seismic behavior for IABs. The three main shortcomings of these IAB models concerns the overly simplistic approach to overall bridge modeling, the focus on individual components, and/or the use of the detailed components for thermal and live load studies only.

Neglecting important behavior in components such as the piles, bearings, and piers to focus on a specific component in the IAB leaves the models too simplistic and unable to capture overall bridge behavior (Spyrakos and Loannidis, 2003; Itani and Pekcan, 2011; Franchin and Pinto,

2014). Others model the component of interest only to study their specific effects. Component-specific models have been developed for the embankment (Shasabadi *et al.*, 2005; Shasabadi *et al.*, 2007; Kotsoglou and Pantazopoulou, 2009) and the pile-pile cap connection (Teguh *et al.*, 2006; Frosch *et al.*, 2009). Models do exist which include the components known to experience significant nonlinear behavior during earthquakes, however these models have only been used for thermal behavior assessments in the past (Olson *et al.*, 2009; Olson *et al.*, 2013; LaFave *et al.*, 2016). The presented shortcomings of the previous models to seismic IAB analysis justifies the work in this project to develop detailed IAB models for assessing seismic behavior.

CHAPTER 3: GROUND MOTION DEVELOPMENT

The lack of suitable ground motions for a 1000-year return period event in southern Illinois necessitates the development of ground motions for this specific purpose. This chapter describes the process used to modify existing ground motion records to ground motions which can be used for seismic bridge assessments in southern Illinois. The process involved the creation and matching of existing ground motions to conditional mean spectra (CMS) for 10 sites around southern Illinois which were then propagated through site-appropriate soil profiles to acquire surface ground motions. These surface ground motions are the motions used in the seismic analysis of IAB models in later chapters.

3.1 FORMATION OF SOIL PROFILES IN SOUTHERN ILLINOIS

3.1.1 Southern Illinois Sites

Ten sites were selected in southern Illinois to represent the different combinations of seismic risk and geologic setting that could be encountered in the region. The ten sites are: Anna, Benton, Cairo, Carbondale, East St. Louis, Eldorado, Elizabethtown, Mt. Carmel, Salem, and Sparta. The latitude and longitude of the sites, along with their approximate depth to bedrock (Herzog *et al.*, 1994) are presented in Table 3.1. The sites were selected based on their general geologic setting, their location relative to each other, and the availability of nearby soil boring data.

Table 3.1: Location of sites in southern Illinois.

Site Name	Latitude (º)	Longitude (º)	Approximate Depth to Bedrock (m) (Herzog *et al.*, 1994)
Anna	37.461	-89.239	30
Benton	38.004	-88.916	15
Cairo	37.013	-89.180	60
Carbondale	37.726	-89.220	20
East St. Louis	38.617	-90.133	40
Eldorado	37.814	-88.441	20
Elizabethtown	37.449	-88.304	35
Mt. Carmel	38.415	-87.769	40
Salem	38.268	-88.948	10
Sparta	38.133	-89.700	20

The general geologic setting was based on the different quaternary deposits found throughout southern Illinois. A variety of geologic settings were considered when selecting the sites, as shown by their location on the quaternary (ice age) deposits map (ISGS, 2005) in Fig. 3.1. Their geographic location was also important to consider ensuring that sites from across southern Illinois were included. A variety of geographic locations allows for different levels of ground motion shaking to be experienced due to the different hazard sources that affect different locations. Finally, the availability of soil boring data was important to account for site-specific soil effects through representative soil profiles. The representative soil profiles were used to propagate the developed bedrock ground motions to the surface, as well as for considering soil behavior in the IAB models. The soil boring data was acquired using information found in boring logs from IDOT bridge projects (IDOT, 2014).

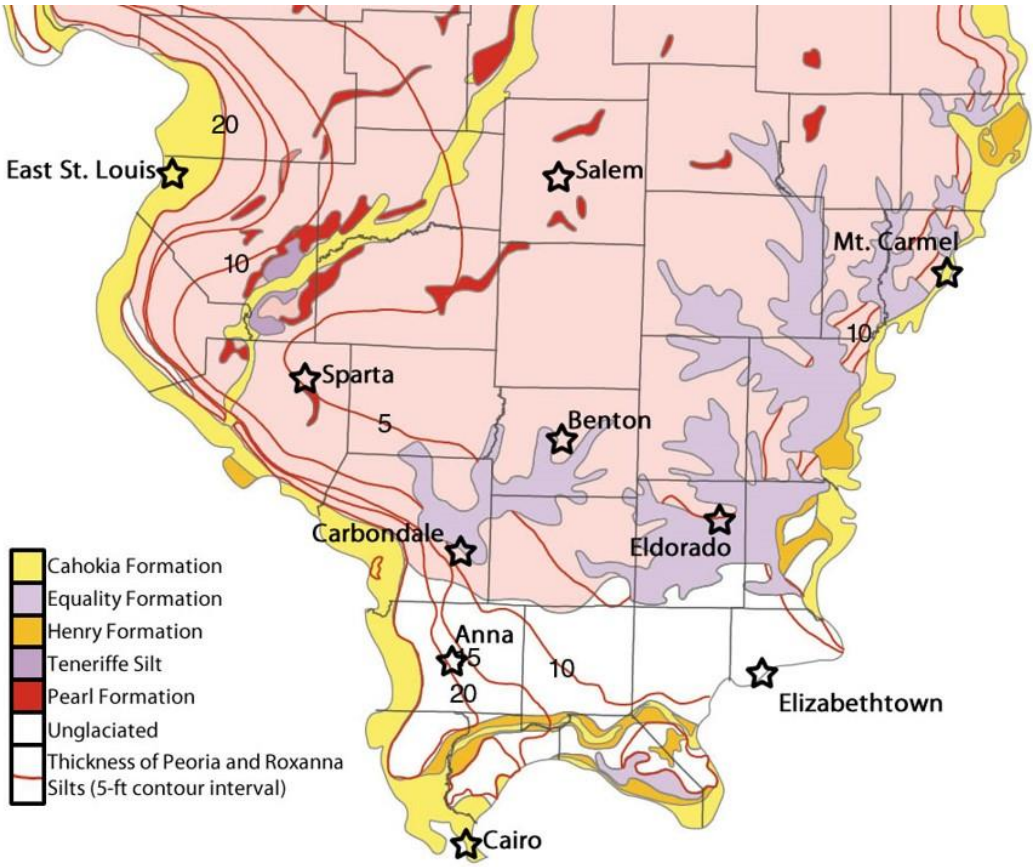

Figure 3.1: Location of sites in southern Illinois overlaid on the Quaternary (ice age) deposits map for the region (ISGS, 2005).

3.1.2 Soil Profiles

The site-specific soil effects in the developed ground motions were accounted for by using site-representative soil profiles. The soil profiles were developed using 140 boring logs from bridge construction projects across southern Illinois (IDOT, 2014). The data acquired from the boring logs included the bore location, surface elevation, bedrock elevation, water table elevation, soil type for each soil layer, and standard penetration test (SPT) results for each soil layer. The soil type is described in terms of the AASHTO soil classification system, which is in turn used to estimate other key soil properties including liquid limit and median particle size. Some boring logs lack AASHTO soil classifications but do include soil descriptions. In these cases, an AASHTO soil classification is assigned based on the description. The data from the boring log and soil

classification was used to create shear wave velocity (V_s) and coefficient of at-rest earth pressure (K_0) profiles for the 10 sites, which are necessary to propagate the ground motions from the bedrock to the surface.

As mentioned, the AASHTO soil classifications were used to make assumptions for soil properties such as the median particle size (D_{50}, in mm), the percent of soil passing a #200 sieve (P_{200}), the clay fraction (CF), and the liquid limit (w_L). These assumptions were made by placing the values within the limits described in each AASHTO class, which can be found in many geotechnical engineering books, such as in Coduto *et al.* (2011).

To develop the V_s and K_0 profiles, the corrected SPT blow count (N_{60}), the effective vertical stress, and the effective friction angle (ϕ') must all be calculated using the boring and soil classification data. The N_{60} value was determined to be 1.25N, where N is the SPT blow count results from the boring logs (Coduto *et al.*, 2011; IDOT, 2014). The soil layer's unit weight (γ) and the effective vertical stress (σ'_z) in the layer could then be calculated using Eqs. (3.1)-(3.4). Eq. (3.1) describes the calculation of the SPT N-value corrected for field procedures and overburden stress, $N_{1,60}$ (Coduto *et al.*, 2011); Eq. (3.2) describes the relative density, D_r (Coduto *et al.*, 2011); Eq. (3.3) describes the unit weight, γ (Peck *et al.*, 1974); and Eq. (3.4) describes the effective vertical stress, σ'_z, where H is the height of each layer (Coduto *et al.*, 2011). As mentioned, these equations were used to solve iteratively, beginning with an assumption of σ'_z = 2000 psf and continuing until D_r converges.

$$N_{1,60} = N_{60}\sqrt{\frac{2000psf}{\sigma'_z}} \tag{3.1}$$

$$D_r = \sqrt{\frac{N_{1,60}}{C_p C_A C_{OCR}}} \; where \; C_p = 60 + 25\log(D_{50}),\; C_A \approx 1.2, C_{OCR} \approx 1.1329 \tag{3.2}$$

$$\gamma = \left\{ \begin{array}{c} 124\ pcf\ for\ loose\ (D_r \leq 0.35) AASHTO\ Class\ A-1, A-3 \\ 135\ pcf\ for\ dense\ (D_r > 0.35) AASHTO\ Class\ A-1, A-3 \\ 145\ pcf\ for\ AASHTO\ Class\ A-2 \\ 110\ pcf\ for\ soft\ (D_r \leq 0.35) AASHTO\ Class\ A-4, A-5, A-6, A-7 \\ 129\ pcf\ for\ stiff\ (D_r > 0.35) AASHTO\ Class\ A-4, A-5, A-6, A-7 \end{array} \right\} \quad (3.3)$$

$$\sigma_z' = \sum \gamma H - (62.4pcf)(depth\ from\ top\ of\ water\ table) \quad (3.4)$$

The V_s and K_0 values for each individual soil layer from each boring profile were then calculated using the corrected SPT blow count (N_{60}), effective vertical stress (σ'_v), and effective friction angle (ϕ') in each layer. In coarse-grained soils, ϕ' can be calculated from Eq. (3.5) below (Wolff, 1989; Hettiarachchi and Brown, 2009). The calculation of ϕ' in fine-grained soils is slightly more complex by first determining the residual friction angle (ϕ'_r) from the clay fraction and liquid limit of the soil, and then relating ϕ'_r to ϕ'. Both of these relationships involving ϕ'_r are described in plots in Terzaghi *et al.* (1996). Eq. (3.6) and (3.7) was then used to calculate the shear wave velocity (in m/s with the effective vertical stress, σ'_v, in in kPa) of coarse- and fine-grained soils, respectively, for Quaternary-age deposits (Wair *et al.*, 2012). The coefficient of at-rest earth pressure for each soil layer can be calculated from Eq. (3.8) with OCR estimated to be 2.0 (Coduto *et al.*, 2011).

$$\emptyset' = 27.1 + 0.3N_{60} - 0.00054N_{60}^2 \quad (3.5)$$

$$V_{s,coarse} = 30.0N_{60}^{0.23}\sigma_v'^{0.25} \quad (3.6)$$

$$V_{s,fine} = 26.0N_{60}^{0.17}\sigma_v'^{0.32} \quad (3.7)$$

$$K_0 = 1 - \sin(\emptyset')OCR^{\sin(\emptyset')} \quad (3.8)$$

The calculated shear wave velocity profiles were found to follow two trends and therefore provided two distinct geologies to consider: alluvial and non-alluvial. The alluvial sites consist of Benton, Cairo, East St. Louis, Mt. Carmel, Salem, and Sparta. The non-alluvial sites consist of Anna, Carbondale, Eldorado, and Elizabethtown. The calculated shear wave velocity profiles from

each bore associated with the sites and their respective geology were combined to create the average shear wave velocity profiles for the alluvial and non-alluvial geologies. The individual shear wave velocity profiles from the bores and the average shear wave velocity profile for the upper 30 m of each geology is presented in Fig. 3.2. It was found that the southern Illinois region does not have extremely large variations in shear wave velocity with respect to depth when considering the individual geologies. This is demonstrated by the relatively small dispersion found in the individual bore shear wave velocity profiles, shown in Fig. 3.2 using the bounds formed by being one standard deviation from the average profile. These small variations allowed for the assumption that single shear wave velocity profiles are appropriate for representing each of the two geologies – the alluvial and non-alluvial.

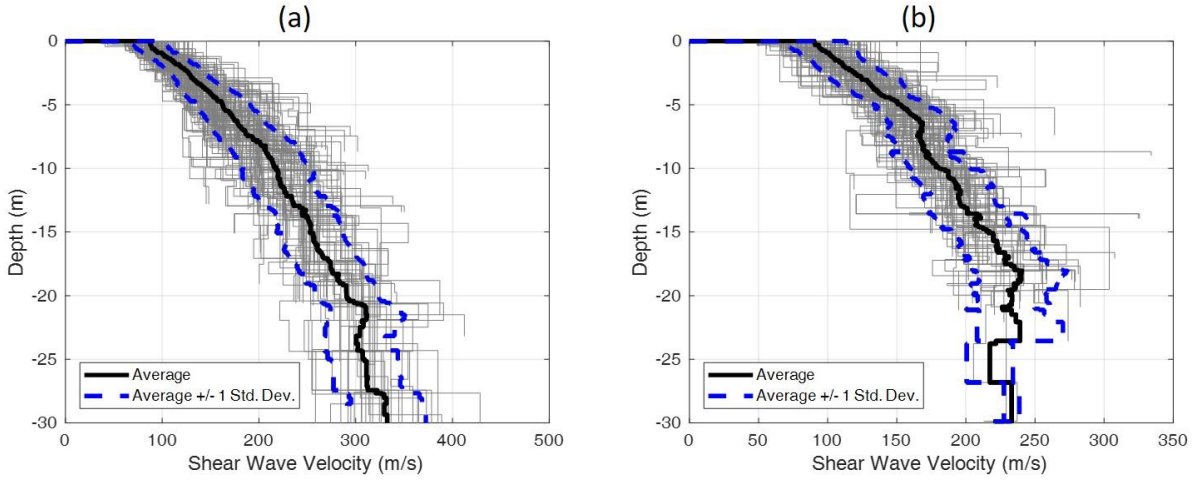

Figure 3.2: Individual shear wave velocity profiles, average shear wave velocity profiles, and the bounds formed by being one standard deviation from the average for the upper 30 m of (a) the alluvial geology, and (b) the non-alluvial geology.

Many of the sites considered have a depth to bedrock deeper than the depths of the individual bores. This required a method of extending the average velocity profile to deeper depths. This was accomplished by using established Site Class D upland and lowland V_s reference profiles from Hashash and Moon (2011). The calculated shear wave velocity profiles were used for the upper 30 m of soil while the reference profiles were used for deeper depths. The upland and

lowland V_s profiles were compared to the alluvial and non-alluvial V_s profiles to determine good matches based on minimizing any jumps in the profile at the 30 m depth. It was found that the alluvial and lowland profiles were comparable as well as the non-alluvial and upland profiles. These updated alluvial and non-alluvial profiles allow for site response to be dominated by the local geology condition while still maintaining a reasonable V_s profile to bedrock deeper than 30 m. Examples of the alluvial and non-alluvial profiles which contain both the calculated and reference profiles are presented in Fig. 3.3a for Cairo (alluvial) and Fig. 3.3b for Anna (non-alluvial).

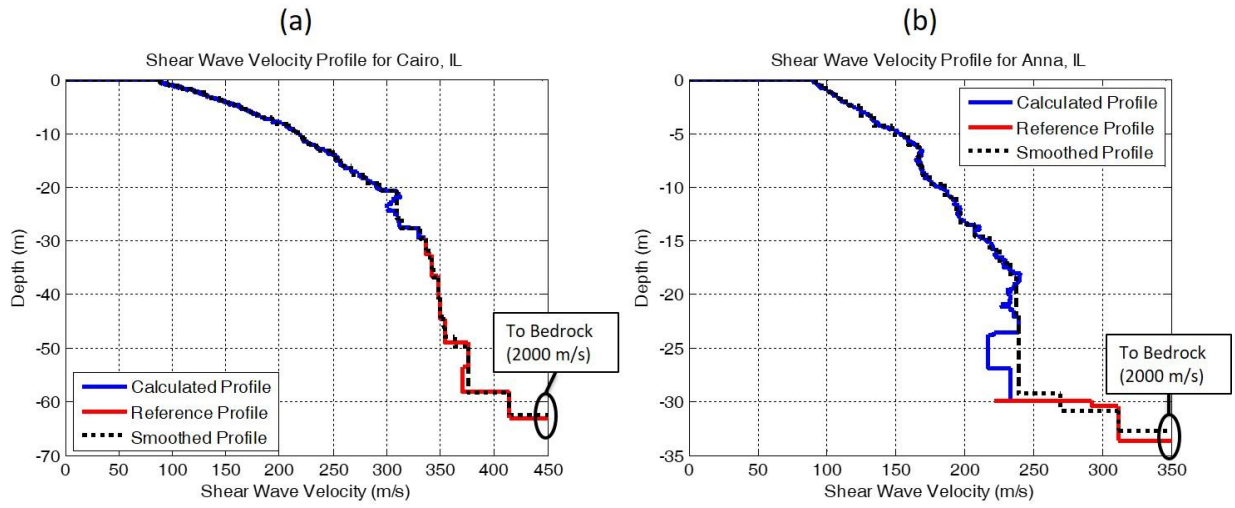

Figure 3.3: Shear wave velocity profiles for (a) Cairo, which uses the alluvial profile for the top 30 m and the lowland profile for deeper than 30 m; and (b) Anna, which uses the non-alluvial profile for the top 30 m and the upland profile for deeper than 30 m.

Fig. 3.3 also shows a smoothed profile for each geology along with the calculated and reference profile. These smoothed profiles were developed to allow for a more reasonable number of thicker soil layers as opposed to a larger number of thin layers in analysis. The smoothed profile also avoids any large impedance contrasts (particularly V_s inversions) within the profile. Another element to note from Fig. 3.3 is that once the profile reaches the site's depth to bedrock (approximately 60 m for Cairo and 30 m for Anna, see Table 3.1) the V_s value increases to the

bedrock V_s value of 2000 m/s and no longer follows the alluvial or non-alluvial profiles. The final V_s profiles used in the development of ground motions for each site use this smoothed profile and account for the V_s jump at bedrock, as demonstrated in Fig. 3.4. Note that due to all sites within the same geology (alluvial or non-alluvial) using the same calculated and reference (and therefore smoothed) V_s profiles, the only difference is the depth at which bedrock is encountered. The unit weight (γ) and effective friction angle (ϕ') profiles, which were used to calculate the coefficient of at-rest earth pressure (K_0), are similarly combined for the alluvial and non-alluvial geologies and smoothed to create thicker soil layers.

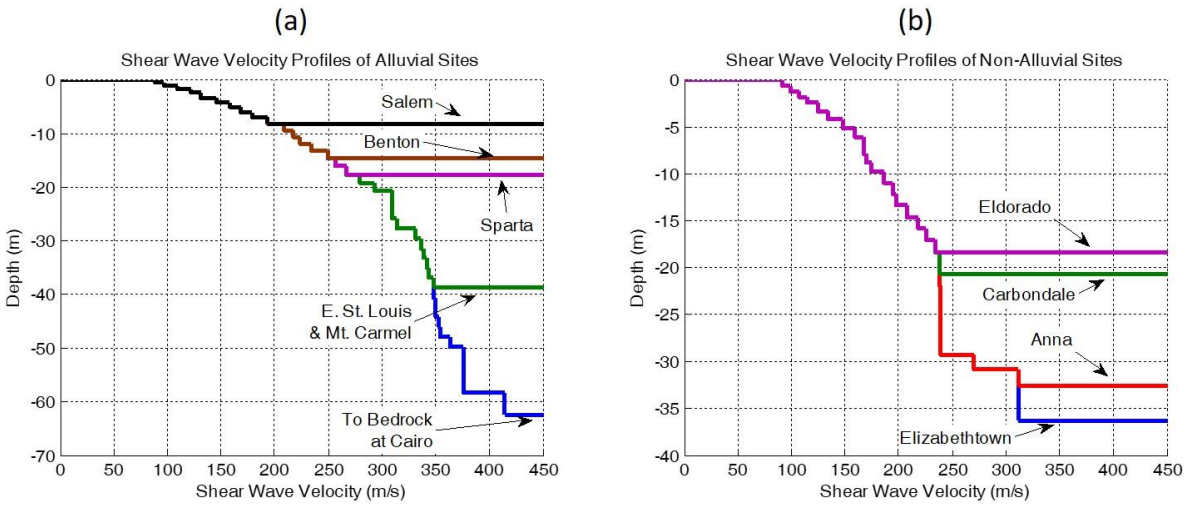

Figure 3.4: Smoothed shear wave velocity profiles for (a) alluvial sites and (b) non-alluvial sites.

3.2 CONDITIONAL MEAN SPECTRUM DEVELOPMENT

3.2.1 Conditional Mean Spectrum and Uniform Hazard Spectrum Comparison

At the bedrock level existing ground motions are often modified such that their spectrum matches a target spectrum which accounts for the seismic hazard at a specific location. The target spectrum that has typically been used in the past is the uniform hazard spectrum (UHS) (Hancock *et al.*, 2008), which can be obtained from sources such as the United States Geological Survey (USGS) (2014). However, the conditional mean spectrum (CMS), originally developed by Baker

and Cornell (2006), has been gaining popularity in its use as a target spectrum and is used in this project.

The motivation for using the CMS as opposed to the UHS lies with the unrealistic ground motion spectrum produced by matching to the UHS. The UHS is deemed unrealistic due to its large spectral acceleration values across all periods (Baker and Cornell, 2006). The UHS commonly integrates multiple earthquake sources at the same time, leading to the UHS being developed while considering both small magnitude, near-field earthquakes (which dominate short period behavior) and large magnitude, far-field earthquakes (which dominate long period behavior). Realistic ground motions would only consider one source, meaning that the UHS will be accurate around the period range dominated by the one source, but the UHS will be unrealistically large for any period outside this range (Baker and Cornell, 2006). This leads to the conclusion that the UHS would better serve as an intensity measure at a specific period during the ground motion development process (Baker and Cornell, 2006).

Deaggregated magnitude and source-to-site distance pairs (M, R) were acquired for each site and used to develop a median spectrum using an appropriate ground motion prediction equation (GMPE). The median spectrum and the UHS were then used to develop the CMS for the site (Baker, 2011). The shape of the CMS and its position between the median spectrum and UHS is based on empirical data and such that the CMS matches the UHS at a specific period of interest called the conditional period, T^* (Baker and Jayaram, 2008). In general, the CMS and UHS are distinct from each other. However, in some cases where the seismic hazard is overwhelmingly dominated by a single source, the CMS and UHS tend to be similar. This is due to the UHS considering only one hazard source in its development, similar to how the CMS is meant to be developed. While there is a negligible advantage of the CMS in these situations, it is still not a

disadvantage to use the CMS. These single source situations are rare, although they can occur in southern Illinois.

3.2.2 Conditional Mean Spectrum Creation

The conditional period, *T**, is typically taken as the fundamental period of the structure when developing a CMS. However, it is indicated that this approach is not always appropriate and if a range of periods is under investigation then a set of multiple *T** periods should be selected to induce different responses in structures by exciting different structural components (Baker, 2011). Selecting multiple *T** periods, and therefore making multiple CMS, was performed for the Illinois highway bridges studies in this project due to the variety of bridges under investigation. It was found that the initial fundamental period of Illinois highway bridges varies between 0.2-1.5 s (Revell, 2013). Additionally, damage to the bridges and their components could change the fundamental period of the bridge during dynamic or pushover analyses (Filipov *et al.*, 2013b). A variety of *T** periods will allow the developed ground motions to be applicable to all the different bridges in the project throughout the analyses. For these reasons, the periods of 0.2, 0.3, 0.5, 1.0, and 2.0 s were selected as the five *T** periods for which to create CMS.

Four ground motions were developed for each of the five CMS at each site. This leads to 20 ground motions at each site and 200 ground motions for the entire southern Illinois region. All 20 ground motions will be applied to each bridge dynamic analysis for each site in this study. However, a main advantage of the CMS is its targeted nature, which means that if a fundamental period for a structure or component is known, then the use of fewer ground motions matched to CMS with a *T** matching that fundamental period is sufficient to obtain accurate seismic behavior (Baker, 2011). Unfortunately, as explained above, the varying fundamental period of the bridges during analysis in this study somewhat limits the use of this advantage of the CMS.

The hazard deaggregation results for each of the five T^* periods at each of the sites were then determined using the USGS Interactive Deaggregation application (USGS, 2008). The resulting mean (M, R) pairs for each of the sites and T^* periods were acquired at a 5% in 50-year probability of exceedance at a site class A rock boundary. The site class A rock boundary was used due to the CMS being developed for the bedrock level, with a shear wave velocity of 2000 m/s in the southern Illinois region (Hashash *et al.*, 2014), which corresponds to a site class A (hard rock) boundary (ASCE, 2016). Examples of the results for Cairo and East St. Louis at a period of 0.5 s are provided in Fig. 3.5a and b, respectively. The results indicate that the mean (M, R) pair for Cairo is (7.65, 11.6 km) while it is (7.20, 152.1 km) for East St. Louis. These results are logical given that East St. Louis is much further north than Cairo and the NMSZ, resulting in its mean source-to-site distance being much further than Cairo's.

Fig. 3.5 also demonstrates the difference between single- and multi-source hazard sites that was mentioned earlier. Fig. 3.5a shows that in Cairo the hazard is largely dominated by a single source (the NMSZ). In Fig. 3.5b, it is shown that at East St. Louis the hazard does have a large contribution by a source around 200 km away (the NMSZ), but it also has many additional smaller contributions from much closer sources (less than 50 km). This is the reason why some southern Illinois sites, such as Cairo, do not benefit as much from using the CMS over the UHS, as they both end up only accounting for the single source. However, at multi-source sites such as East St. Louis, the UHS is developed using both the close sources and far sources while the CMS only considers one of the sources at a time.

Additionally, Fig. 3.5a provides a mean epsilon parameter, ε_0, of -0.30. The epsilon parameter describes the number of standard deviations between the median spectrum and the UHS at a specific period (0.5 s for the cases in Fig. 3.5). By being negative, Fig.3.5 is indicating that the

median spectrum will be larger than the UHS at a period of 0.5 s for Cairo. This result is rare, with only Cairo and Anna experiencing negative epsilon values due to their single-source hazard characteristics.

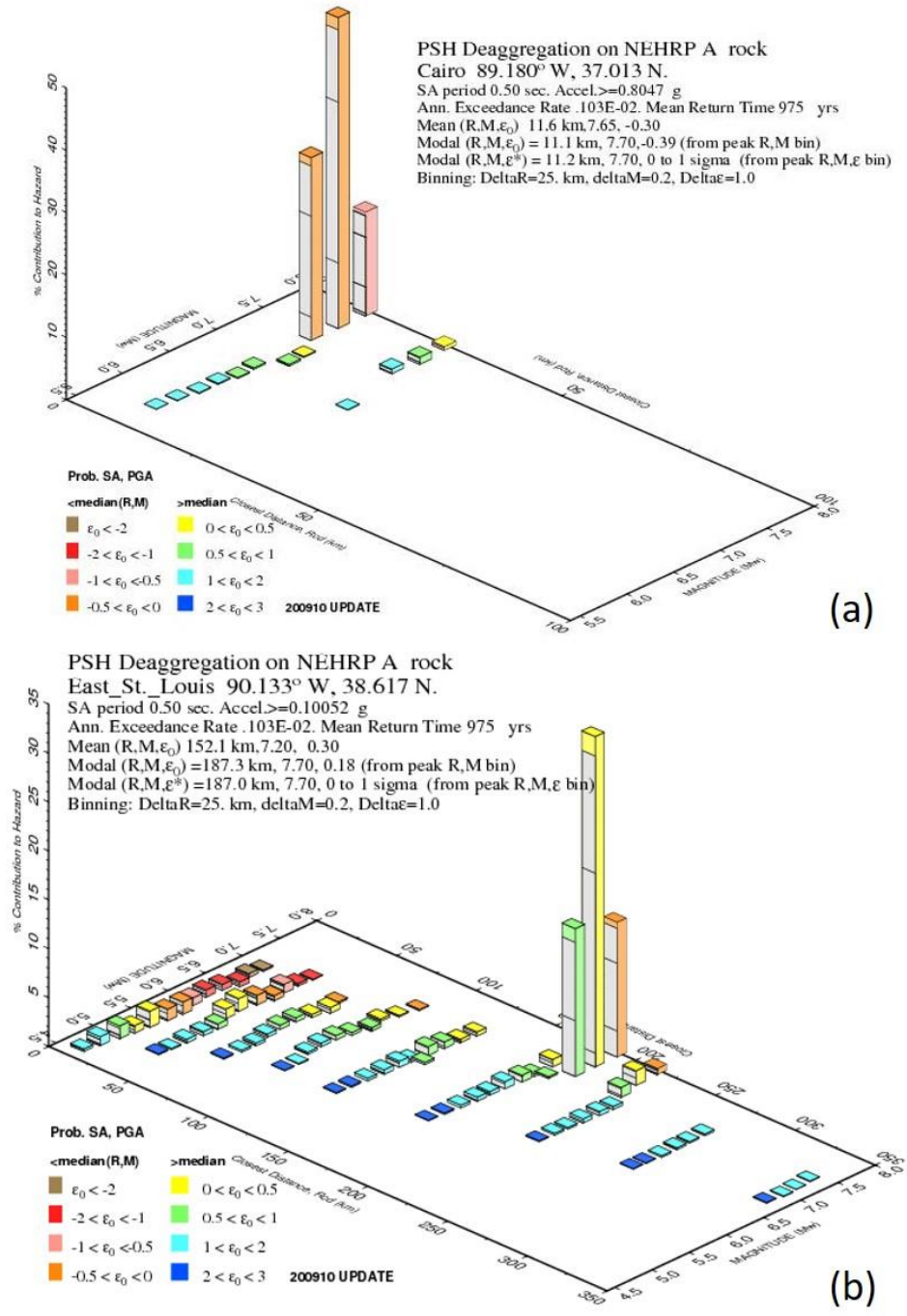

Figure 3.5: Hazard deaggregation results for (a) Cairo, and (b) East St. Louis (USGS, 2008).

The hazard deaggregation results are used to develop median response spectra for each of the T^* periods. The median response spectrum, S_a, was determined using the Toro *et al.* (1997) GMPE. This GMPE was selected due to its use in the development of the USGS's UHS and hazard deaggregation results for central and eastern North America (Petersen *et al.*, 2008). To better match the USGS procedure, spectral acceleration caps were applied to the Toro *et al.* (1997) GMPE as was performed by the USGS (Petersen *et al.*, 2008). The predicted mean and standard deviation of the natural logarithm of the median response spectrum $\ln(S_a)$ ($\mu_{\ln(Sa)}(M, R, T)$ and $\sigma_{\ln(Sa)}(T)$ respectively), are required for the calculation of the CMS. These values were determined by noting that in lognormal distributions the exponential of the mean of $\ln(S_a)$, $\mu_{\ln(Sa)}(M, R, T)$, is the same as the median response spectrum calculated using the GMPE (Baker, 2011). Examples of the CMS, UHS, and median spectrum are provided in Fig. 3.6 for Cairo and East St. Louis with a T^* of 0.5 s. As discussed earlier, note that the Cairo median spectrum is larger than the UHS, as indicated by its negative epsilon value, while the East St. Louis median spectrum is smaller than the UHS.

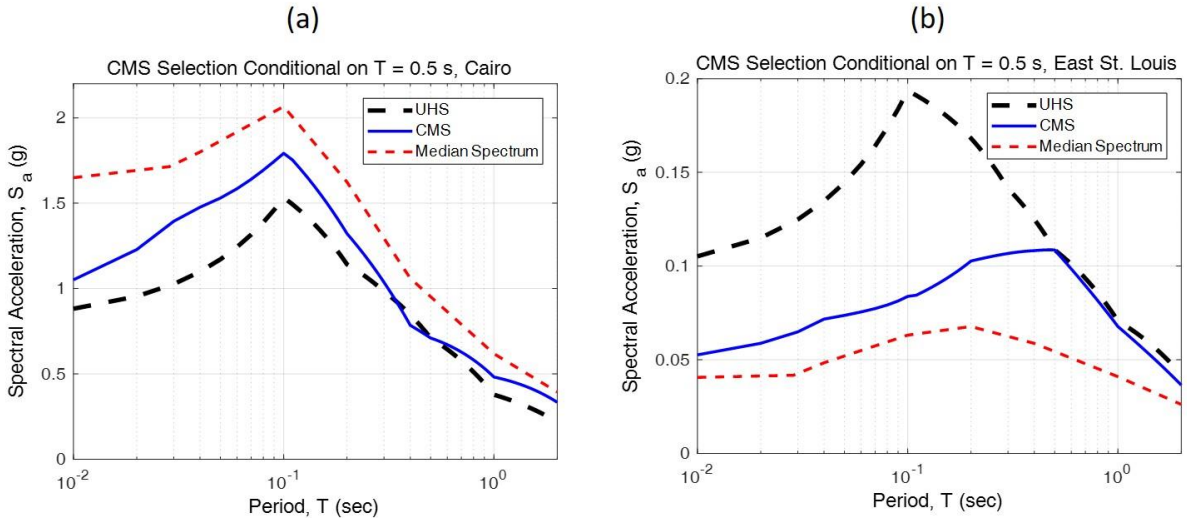

Figure 3.6: UHS, CMS, and median spectra for a conditional period of 0.5 s at (a) Cairo, and (b) East St. Louis.

The procedure for developing the CMS using the predicted mean and standard deviation of ln(S_a) is provided in Baker (2011). The concept is to determine $\varepsilon(T^*)$ (the number of standard deviations between the ln($S_{a,CMS}$) and the $\mu_{\ln(Sa)}(M, R, T^*)$ curves at the conditional period T^*) such that the UHS and CMS match at T^*. The definition of $\varepsilon(T^*)$ is provided in Eq. (3.9); note that at the conditional period, T^*, $S_{a,CMS}(T^*) = S_{a,UHS}(T^*)$. Eq. (3.9) is specific to the conditional period, however once $\varepsilon(T^*)$ is determined the equation is rearranged into Eq. (3.10), which determines the natural logarithm of the CMS at all spectra ($S_{a,CMS}(T)$) using a correlation coefficient, $\rho(T, T^*)$, based on empirical data from Baker and Jayaram (2008).

$$\varepsilon(T^*) = \frac{\ln(S_{a,CMS}(T^*)) - \mu_{\ln(Sa)}(M,R,T^*)}{\sigma_{\ln(Sa)}(T^*)} \tag{3.9}$$

$$\ln\left(S_{a,CMS}(T)\right) = \mu_{\ln(Sa)}(M,R,T) + \rho(T,T^*)\varepsilon(T^*)\sigma_{\ln(Sa)}(T) \tag{3.10}$$

The CMS, $S_{a,CMS}$, was then simply calculated as a function of the period. These CMS were then used as the target spectra for the development of bedrock level ground motions. The developed CMS for all five T^* periods along with the UHS are provided for all ten sites in southern Illinois in Fig. 3.7 and Fig. 3.8. Fig. 3.7 provides the CMS for the alluvial sites, Fig. 3.8 provides the CMS for the non-alluvial sites. Note that many look similar, however the scale of the y-axis (spectral acceleration) varies considerably from site to site depending on their location within southern Illinois.

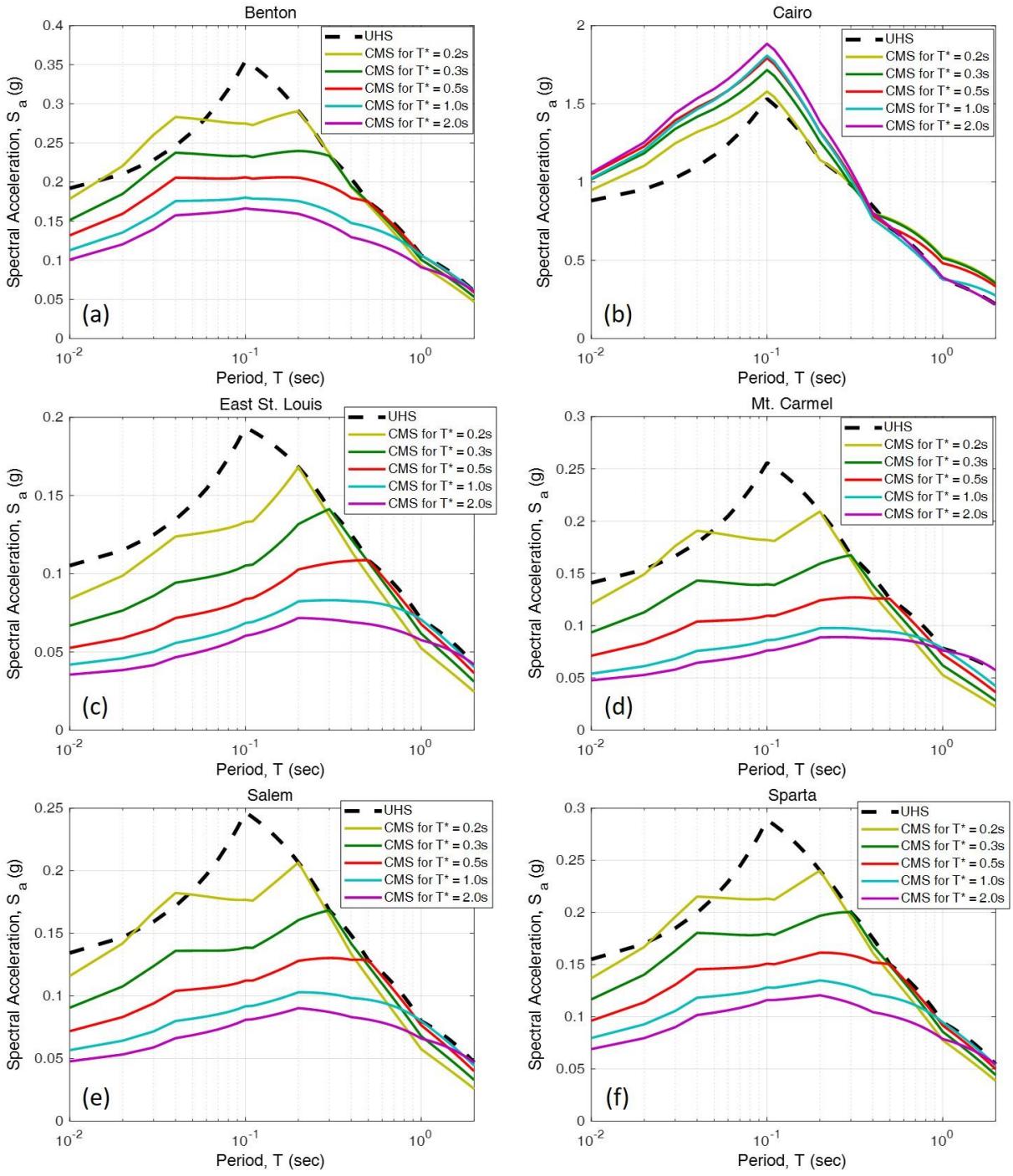

Figure 3.7: CMS and UHS for alluvial sites (a) Benton, (b) Cairo, (c) East St. Louis, (d) Mt. Carmel, (e) Salem, and (f) Sparta.

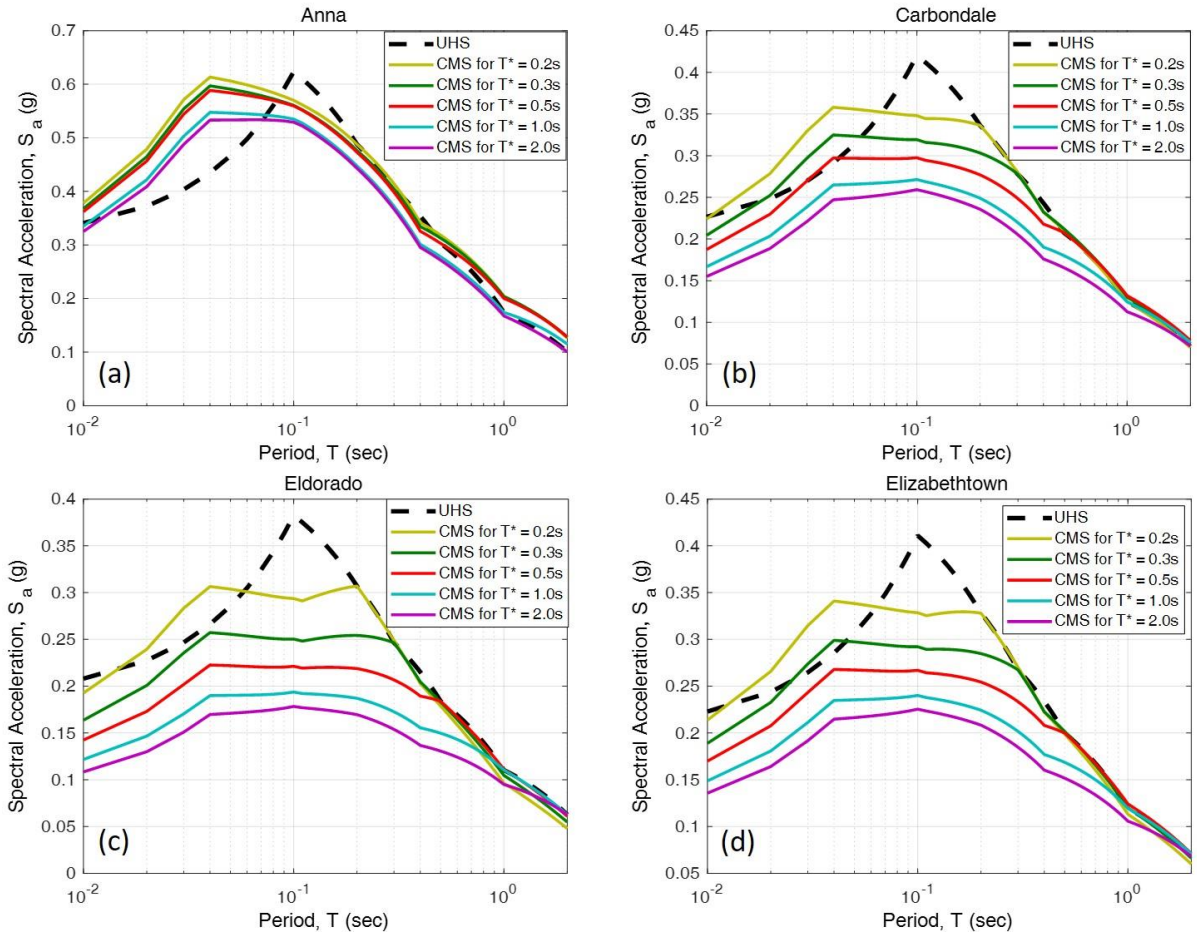

Figure 3.8: CMS and UHS for non-alluvial sites (a) Anna, (b) Carbondale, (c) Eldorado, and (d) Elizabethtown

3.3 MATCHING EXISTING GROUND MOTIONS TO THE CMS

3.3.1 Existing Ground Motions at the Bedrock Level

Existing ground motions for central and eastern North America (CENA) at the bedrock level were modified to match the CMS determined in section 3.2 for the 10 southern Illinois sites. The existing ground motions are for the desired 1000-year return period event prescribed for AASHTO seismic design (AASHTO, 2011). Two main databases were used to act as the source ground motions that will be heavily modified in the following procedure: the NUREG/CR-6728 database (McGuire *et al.*, 2001), and the PEER NGA-East database (Goulet *et al.*, 2014).

The NUREG/CR-6728 database comprises 138 ground motion records for rock sites that are appropriate for use in CNA (McGuire *et al.,* 2001). The records originate from events worldwide and include many records from events in intraplate regions similar to CNA. The database is also supplemented with records from California and Japan which are modified to account for the seismic source and crustal properties of CNA (McGuire *et al.,* 2001).

The PEER NGA-East database contains ground motion records from 89 events within CENA (Goulet *et al.*, 2014). All of the records have magnitudes less than 6.0, limiting their use in the ground motion development, however they are considered in the process. This database contains many CENA ground motions not included in the NUREG/CR-6728 database, such as the 2008 Illinois earthquake whose epicenter was near Mt. Carmel, IL (Goulet *et al.*, 2014). However, many of the records, such as the records from the 1988 Saguenay earthquake in Quebec, are contained in both databases.

Both databases provide magnitude (M) and source-to-site distance (R) information for all the records. This information is important in determining which ground motions to use in matching to the CMS. Both databases also provide records for the combined 227 records in two orthogonal directions. Due to the limited amount of ground motion records in CNA the recordings in the two orthogonal directions are considered as individual records. This does present a bias in the overall set of ground motion records due to some records being related to others, however this bias is acknowledged and accepted. The acceptance of this bias can be justified by acknowledging that these source records are seed ground motions which will be heavily modified in the following procedure, so even minor differences in the bedrock source records allows for different surface ground motions to be developed. Additionally, there have been past studies which have determined that ground motion records from the same event at the same site but in orthogonal directions have

sufficiently different spectral characteristics (Somerville *et al.*, 1997). The inclusion of both orthogonal directions allows for selection from among 454 individual records.

3.3.2 Selection of Source Records for Modification

Four source records were selected from the ground motion record databases provided above to match each of the five CMS developed for each southern Illinois site, leading to a suite of 20 ground motions for each site. The first step in selecting source records to match the CMS is to allocate the records into bins appropriate for each CMS based on magnitude and source-to-site distance. A source record was included in the bin of a CMS if the magnitude was within ±0.5 and the source-to-site distance was within ±30 km of the mean hazard deaggregation results for the appropriate site and period.

The source records within the bins were then evaluated for spectral similarity to the CMS. Similarity in spectral shape was assessed through the root-mean-squared values of the difference between the shape of the two spectra in terms of their ratio to the peak ground acceleration (Ambraseys *et al.*, 2004; Hancock *et al.*, 2008; Katsanos *et al.*, 2010). The root-mean-squared difference, D_{rms}, is calculated in Eq. (3.11), where *PSA* represents the pseudo-spectral acceleration at a period, *PGA* represents the peak ground acceleration, N_p represents the number of sampling periods, T_i represents the sampling period, and the subscripts *0* and *S* represent the record and target spectrum, respectively. The sampling points used to determine the spectral shape similarity were taken in a pseudo-logarithmic manner by sampling periods of 0.01, 0.02, 0.03, 0.04, 0.05, 0.06, 0.07, 0.08, 0.09, 0.1, 0.2, 0.3, 0.4, 0.5, 0.6, 0.7, 0.8, 0.9, 1.0, 2.0, 3.0, 4.0, and 5.0 s. The four source records with the smallest D_{rms} values which are within an average scale factor of 0.5-2.0 were then selected for modification to match to the CMS.

$$D_{rms} = \sqrt{\frac{1}{N_p}\sum_{i=1}^{N_p}\left(\frac{PSA_0(T_i)}{PGA_0} - \frac{PSA_S(T_i)}{PGA_S}\right)^2} \quad (3.11)$$

3.3.3 Modification of Source Records to Match the CMS

The four source records determined to be the best fit for spectral matching to a CMS were further modified through the software *RspMatch09* (Al Atik and Abrahamson, 2010). *RspMatch09* modifies the time history records by performing time-domain spectral matching between an input ground motion (the source records in this case) and a target spectrum (the CMS in this case) through the inclusion of improved tapered cosine wavelets to the time history. The improved tapered cosine wavelet is an improvement over other time-domain spectral matching software using other wavelets (like the reverse acceleration impulse response wavelet or the tapered cosine wavelet) due to its lack of velocity and displacement drift, and because it is more numerically efficient (Al Atik and Abrahamson, 2010).

The period range modified by *RspMatch09* is the 0.01-2.0 s period range. This range is too large for *RspMatch09* to modify in one pass, so modifications were made incrementally in 10-40 passes. The minimum period of every matching range is 0.01 s, however the maximum period considered in each pass varies. The maximum period in the initial pass was between 0.02125-0.055 s depending on if convergence is achieved, then the maximum period gradually increased with each subsequent pass until the entire 0.01-2.0 s range was included in the final pass.

The limited amount of source records that were included in many of the CMS bins unfortunately sometimes leads to poor spectral shape matches which cannot be completely corrected by *RspMatch09*. This often leads to poor spectral matches at the extremely short period range (periods less than or equal to 0.02s), as shown in Fig. 3.9 which presents the initial (source) and unfiltered records compared to the CMS. This issue could be alleviated by more passes at the

short period range in *RspMatch09*; however, this was deemed too computationally expensive, especially considering that it is extremely rare for a structure to be so stiff that the fundamental period is less than 0.02 s. The alternative solution, which was performed, was to filter the results such that none of the erroneous results in this extremely stiff period range affects the final ground motions. The filtering is performed using a fourth-order, low-pass Butterworth filter, which filters contributions from periods less than 0.02 s (frequencies greater than 50 Hz) after the wavelet modification has been completed.

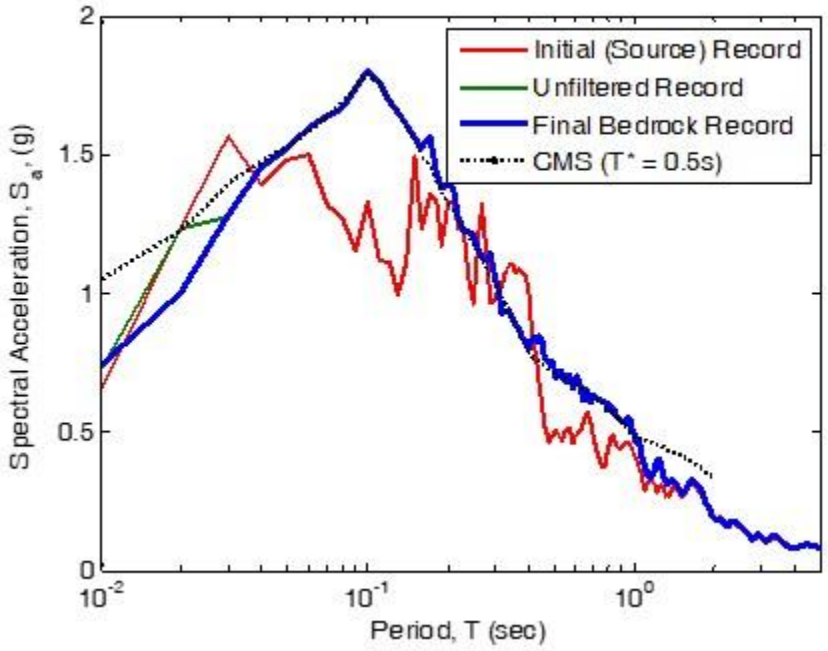

Figure 3.9: Sample spectra for matching the TCU-089-W source record from the NUREG/CR6728 database (McGuire *et al.*, 2001) to the T^* = 0.5 s CMS for Cairo.

Additionally, the poor spectral matches may also cause velocity and displacement drifts in the time histories. The program *DEEPSOIL* (Hashash *et al.*, 2015b) was used to baseline correct the time histories such that there is not any velocity or displacement drift. This process is performed by truncating the initial time history at the first and last zero-crossings, padding the ends with zeroes, applying a high-pass Butterworth filter (0.1 Hz cut-off frequency), and truncating

the new time history at the first and last zero-crossings (Hashash *et al.*, 2015b). The resulting time history has been spectrally matched, filtered, and baseline corrected. This time history represents the final bedrock ground motions which were used in the remaining ground motion development procedure. An example of the final bedrock ground motion record is also presented in Fig. 3.9, in order to demonstrate the changes made throughout section 3.3 to match the source records to the CMS.

As indicated previously, four ground motions are matched to each CMS at each site. Fig. 3.10 presents the results for the five CMS developed at Cairo. While there is some variation of the individual ground motion spectra around the CMS they are matched to, the average of the four developed bedrock ground motion spectra tend to agree well with the CMS. The ground motions presented in Fig. 3.10 are combined into a single plot for Cairo and presented alongside the final bedrock level ground motion spectra for the alluvial sites in Fig. 3.11 and for the non-alluvial sites in Fig. 3.12. Note how in single-source hazard sites, such as Cairo and Anna, the ground motion spectra from all the CMS are very close together, while in multi-source hazard sites such as East St. Louis there is a clear distinction between the bedrock level ground motions for each CMS, indicating the targeted nature of the CMS.

The suite size of 20 ground motions per site allows for each suite to be classified as large (FEMA, 2012). However, having only 4 ground motions matched to each CMS is below the industry standard of matching 7 ground motions to a target spectra to effectively account for the variability of the ground motions. In sites with single hazard sources (such as Cairo) this is not a large concern due to the CMS for all conditional periods being very similar leading to essentially 20 ground motions matched to a single target spectrum. Multiple hazard sites (such as East St. Louis), on the other hand, do have distinct CMS leading to the 4 ground motions matched to each

CMS being insufficient in reaching the 7 ground motion per target spectra goal. This limitation is recognized and acknowledged.

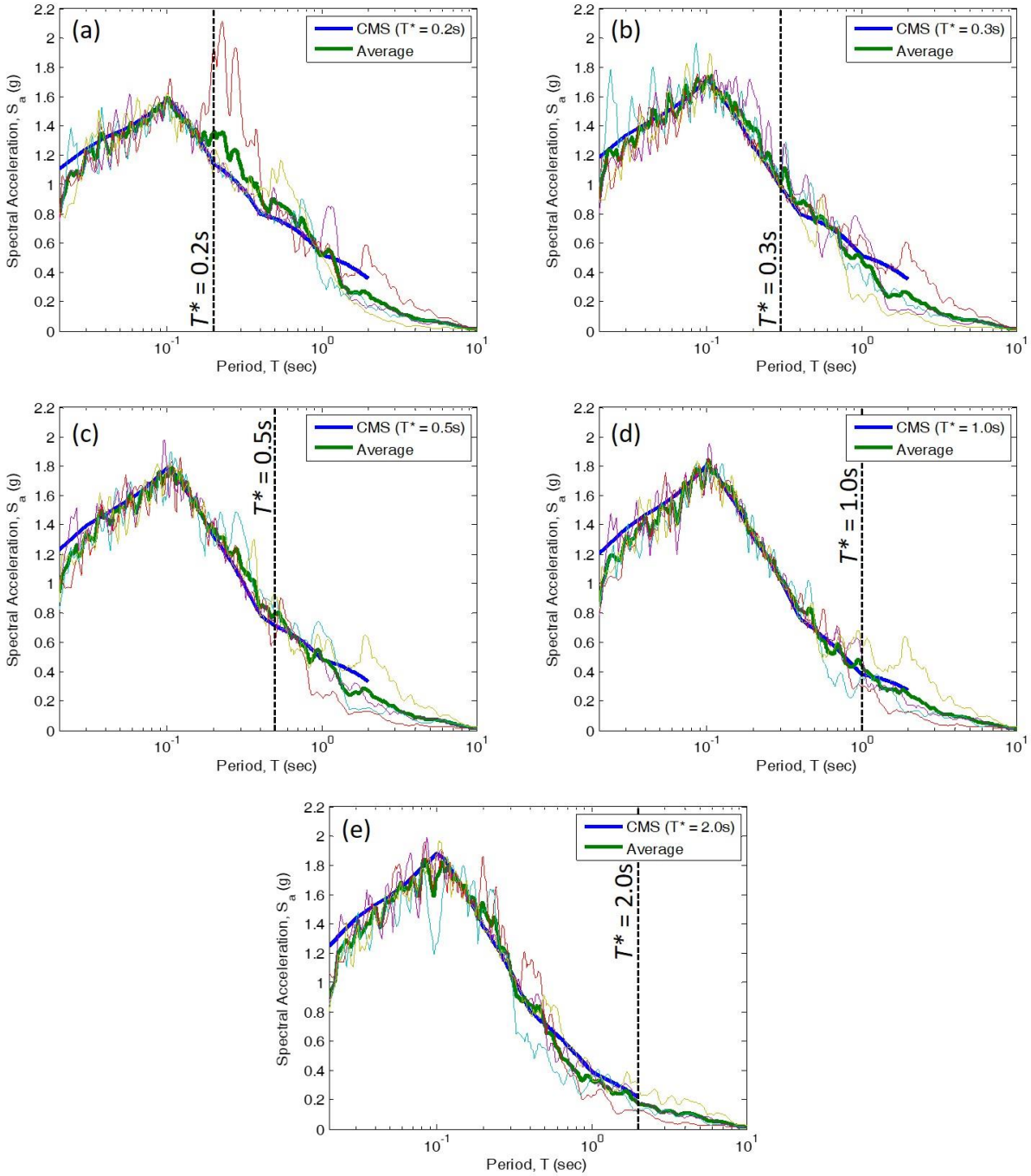

Figure 3.10: Bedrock ground motion spectra for Cairo matched to the (a) T^* = 0.2 s CMS, (b) T^* = 0.3 s CMS, (c) T^* = 0.5 s CMS, (d) T^* = 1.0 s CMS, and (e) T^* = 2.0 s CMS.

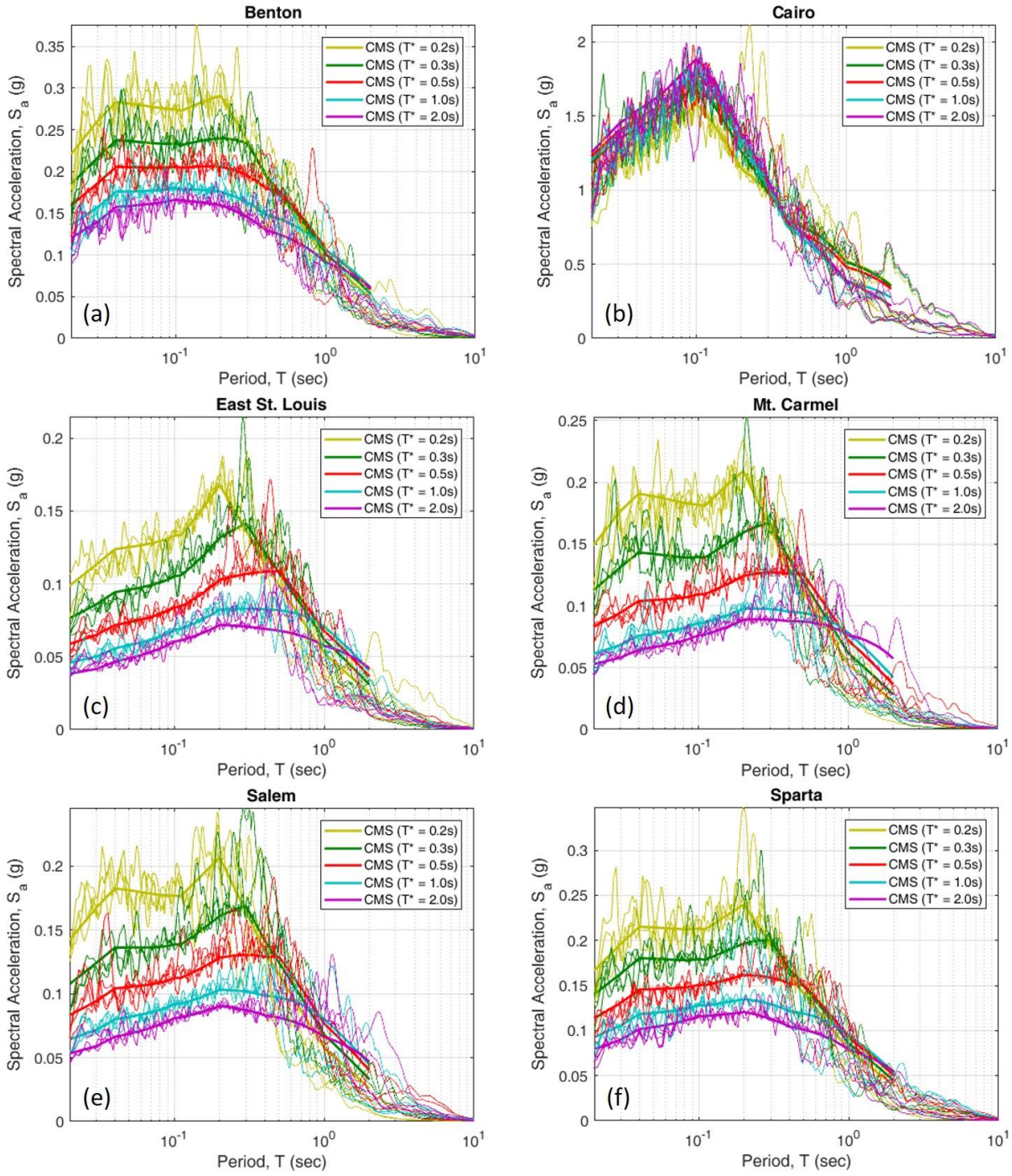

Figure 3.11: Bedrock ground motion spectra for the alluvial sites (a) Benton, (b) Cairo, (c) East St. Louis, (d) Mt. Carmel, (e) Salem, and (f) Sparta.

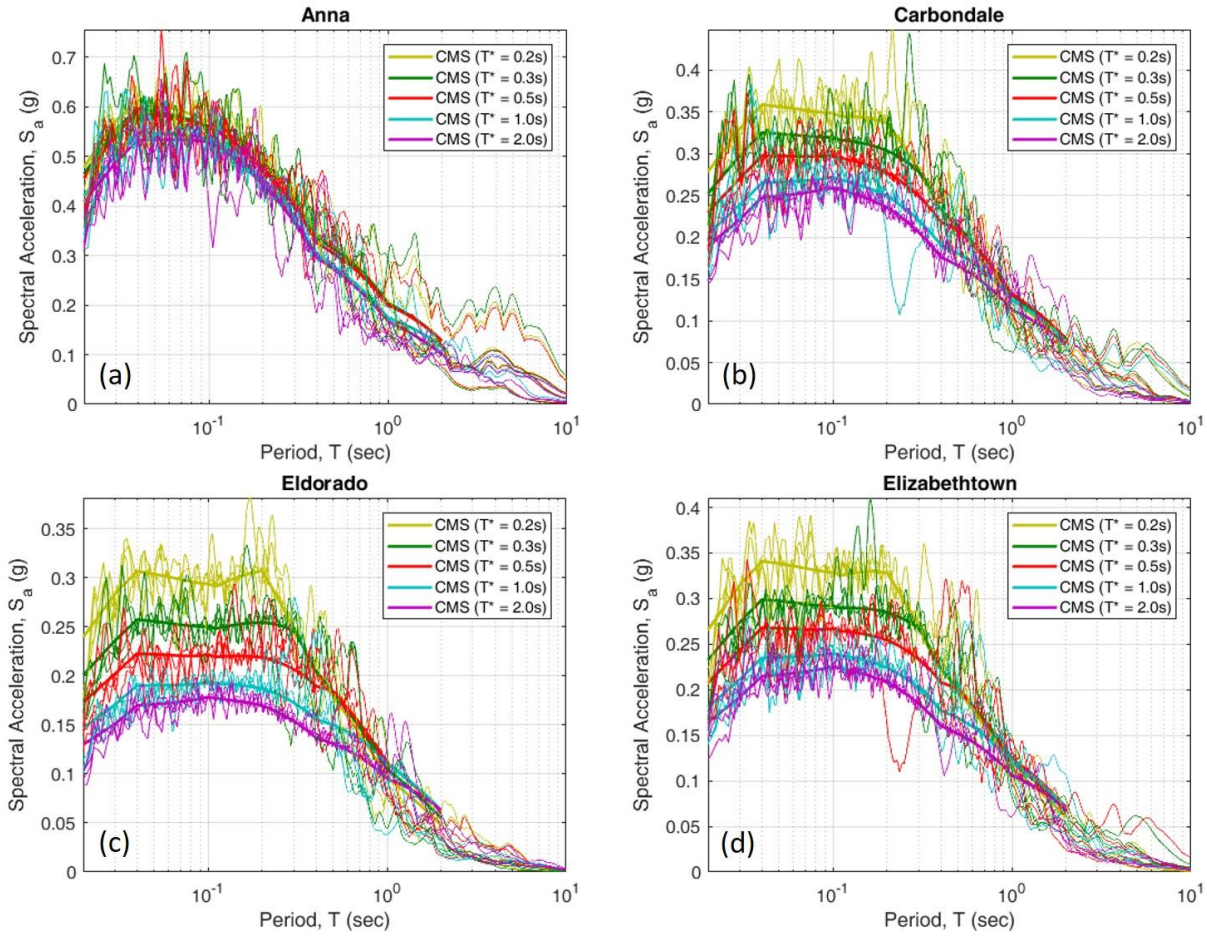

Figure 3.12: Bedrock ground motion spectra for the non-alluvial sites (a) Anna, (b) Carbondale, (c) Eldorado, and (d) Elizabethtown.

3.4 SURFACE LEVEL GROUND MOTIONS

3.4.1 Propagation of Ground Motions from the Bedrock to the Surface

The soil property profiles developed in section 3.1 were used to propagate the bedrock ground motions developed in section 3.3 to the ground surface. The bedrock ground motions were propagated through each site's soil profile using the one-dimensional equivalent-linear frequency domain and nonlinear time domain analysis program *DEEPSOIL* (Hashash *et al.*, 2015b). The nonlinear time domain analysis was used in this study, which uses the Newmark β method to solve the equations of motion in the time domain and accounts for the nonlinear properties of the soil.

Equivalent-linear analyses were also performed for comparison to the nonlinear analyses in order to ensure that the soil is behaving reasonably in the nonlinear analyses.

As discussed earlier, soil property profiles were developed for the shear wave velocity, unit weight, and coefficient of at-rest earth pressure for all ten sites. In addition to this information, the layer thickness and ground water depth, as well as the modulus reduction ($G/G_{max} - \gamma$) and damping ratio ($D - \gamma$) curves (where γ is shear strain), were also required at each soil layer in *DEEPSOIL*. *DEEPSOIL* provides a selection of soil models for use to describe the modulus reduction and damping ratio curves for both sand and clay soils. For this study the Darendeli (2001) models are used for both the sand and clay soil layers. The general Quadratic/Hyperbolic (GQ/H) (Groholski *et al.*, 2016) stress-strain constitutive model, which provides a small-strain shear modulus equal to the measured maximum shear modulus and a large-strain shear strength which asymptotically approaches the target shear strength, is used in this study through *DEEPSOIL*. The target shear strengths were defined as $\sigma'_{vo}tan(\phi')$ for coarse-grained soils and the undrained shear strength, s_u, for fine-grained soils. The effective friction angle, ϕ', was defined using the SPT results (as described earlier) and the undrained shear strength, s_u, was based on the soil layer description. The selected soil hysteretic behavior in *DEEPSOIL* was the non-Masing model described in Phillips and Hashash (2009).

Bedrock properties were also required in *DEEPSOIL* – the shear wave velocity and whether an elastic or rigid half-space is used. The shear wave velocity for bedrock in southern Illinois was taken as 2000 m/s (Hashash *et al.*, 2014), which is consistent with the site class A (hard rock) designation used in the creation of the CMS. The half-space of the bedrock describes whether an outcrop motion is being used in the analysis (elastic half-space) or a within motion is being used

(rigid half-space). An elastic half-space was used in this study to represent that the ground motions were originating from the bedrock and not within the soil column.

The characteristics of the ground motion changes in both the time and spectral domains when propagated through the soil profile. An example demonstrating some of the changes that occur to a Cairo ground motion is presented in Fig. 3.13. The differences in the time history and spectra at the bedrock and surface levels are clearly seen.

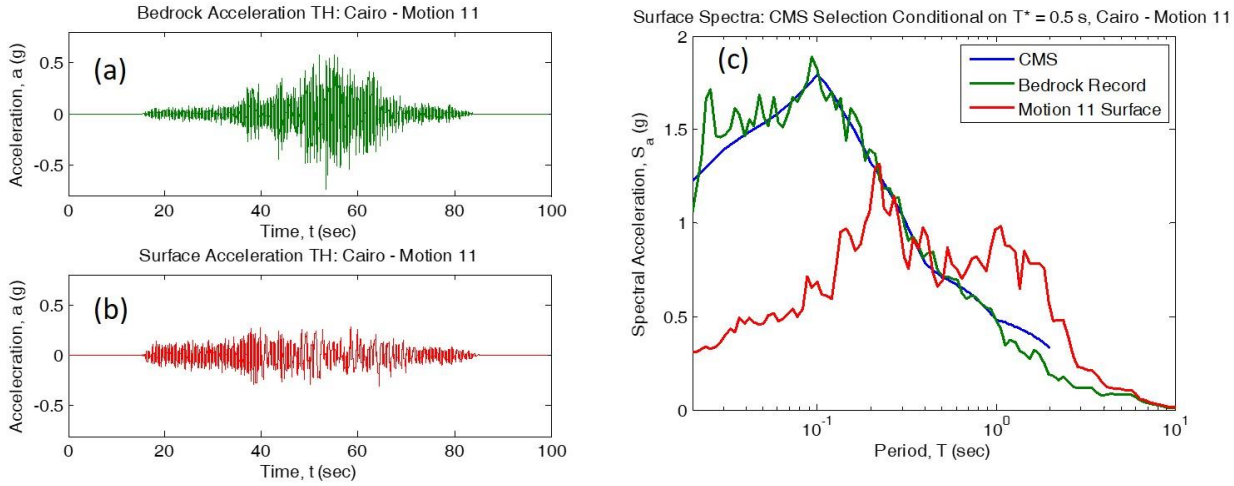

Figure 3.13: Comparison of acceleration time histories of a ground motion developed for Cairo at the (a) bedrock level and (b) surface level. (c) The effect of ground motions propagation through the soil in the spectral domain.

3.4.2 Final Ground Motions

The surface ground motions acquired from the propagation of the bedrock ground motions through the soil property profiles in *DEEPSOIL* are the final ground motions for use in the study of seismic bridge behavior in Illinois. The final surface ground motion spectra are provided in Fig. 3.14 for the alluvial sites and Fig. 3.15 for the non-alluvial sites.

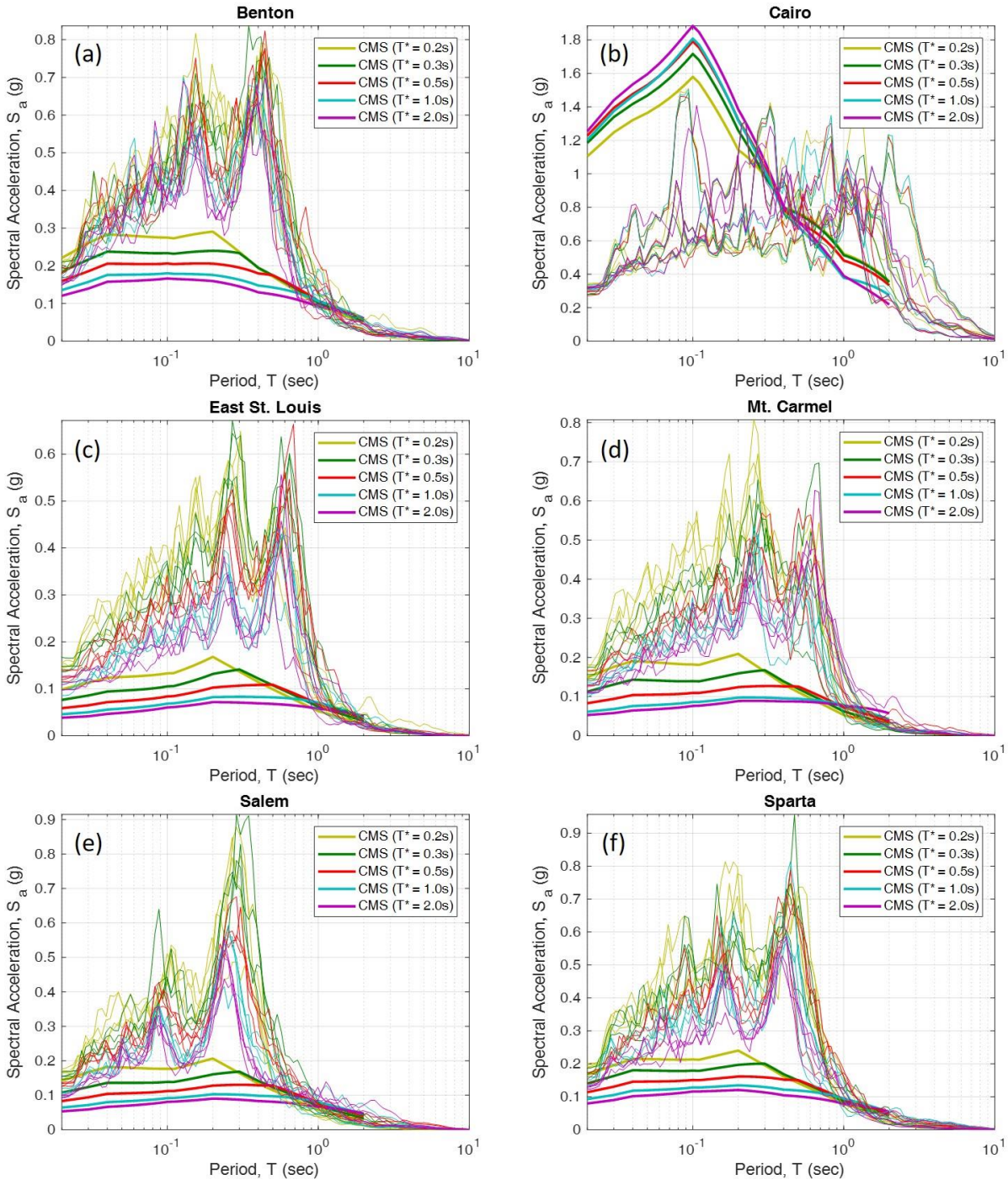

Figure 3.14: Final ground motion spectra for the alluvial sites (a) Benton, (b) Cairo, (c) East St. Louis, (d) Mt. Carmel, (e) Salem, and (f) Sparta.

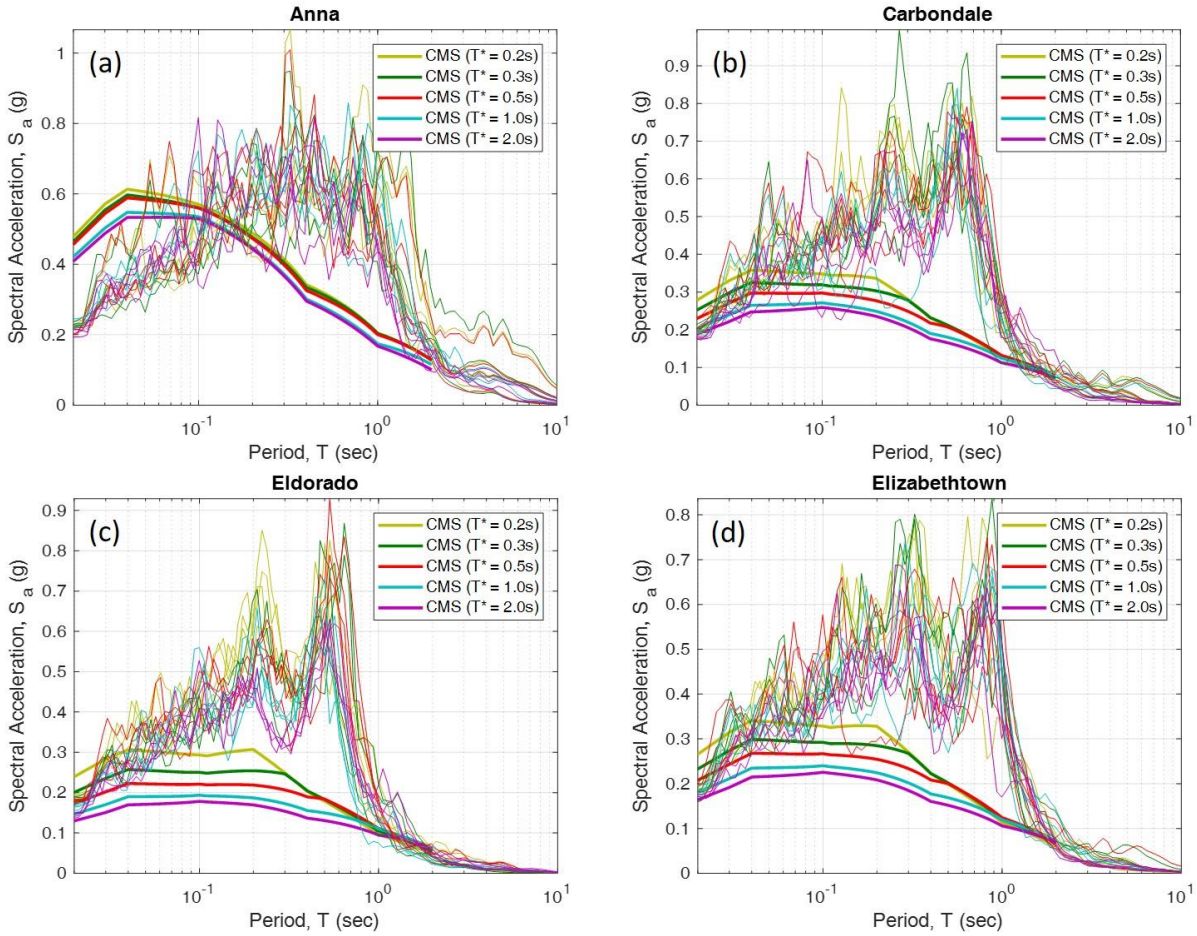

Figure 3.15: Final ground motion spectra for the non-alluvial sites (a) Anna, (b) Carbondale, (c) Eldorado, and (d) Elizabethtown.

It can be noted in Fig. 3.14 and Fig. 3.15 that the soil properties tend to increase the spectral accelerations of some sites (as can be observed from their comparison to the CMS), such as at East St. Louis and Eldorado, while the spectra decrease in size at sites such as Cairo and Anna for some periods. Additionally, it can once again be observed that there are clear differences between the ground motion spectra produced at single- and multi-source hazard sites. Sites with a single hazard source, such as Cairo which is solely affected by the NMSZ, demonstrate that the spectra of the final ground motions produced when matching to all five CMS at the bedrock level are similar, as seen in Fig. 3.14b. Sites with multiple hazard sources, such as East St. Louis which is affected by more than just the NMSZ, produce final ground motions that are separate from each other

depending on the CMS they were matched to at the bedrock level. This is demonstrated in Fig. 3.14c where clear distinctions in the color of the individual ground motions (which indicate which CMS they are matched to) are still discernable at the surface level. This difference is also made clear in Fig. 3.16 where the average of the surface ground motions which were matched to the same CMS are plotted for Cairo and East St. Louis. As expected due to the difference in hazard sources, the average of Cairo's motions are all similar while East St. Louis' have a discernable difference, especially at short periods.

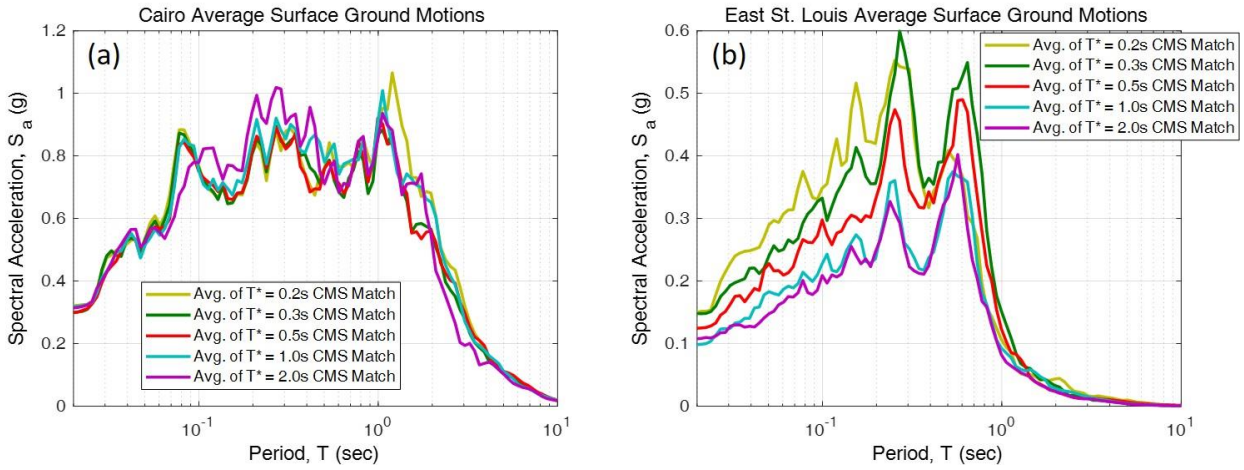

Figure 3.16: Average of the surface level ground motions that were matched to each CMS at the bedrock level for (a) Cairo, and (b) East St. Louis.

It is important to acknowledge that this difference in surface ground motion spectral behavior between single- and multi-source hazard sites demonstrates how the CMS is less useful for a single-source hazard site. However, it is still just as useful as matching to the UHS in this case, which is essentially all that was performed for the Cairo site due to the similarity between the UHS and CMS. Advantages of the CMS are present in multi-source hazard sites such as East St. Louis, where a variety of fundamental periods are considered in analyses using these ground motions due to the multiple T^* periods considered in the development of the ground motions. As discussed earlier, the ability to consider multiple fundamental periods is important in this study

due to the wide range of bridges investigated with these ground motions that have various fundamental periods which may change throughout analyses due to damage.

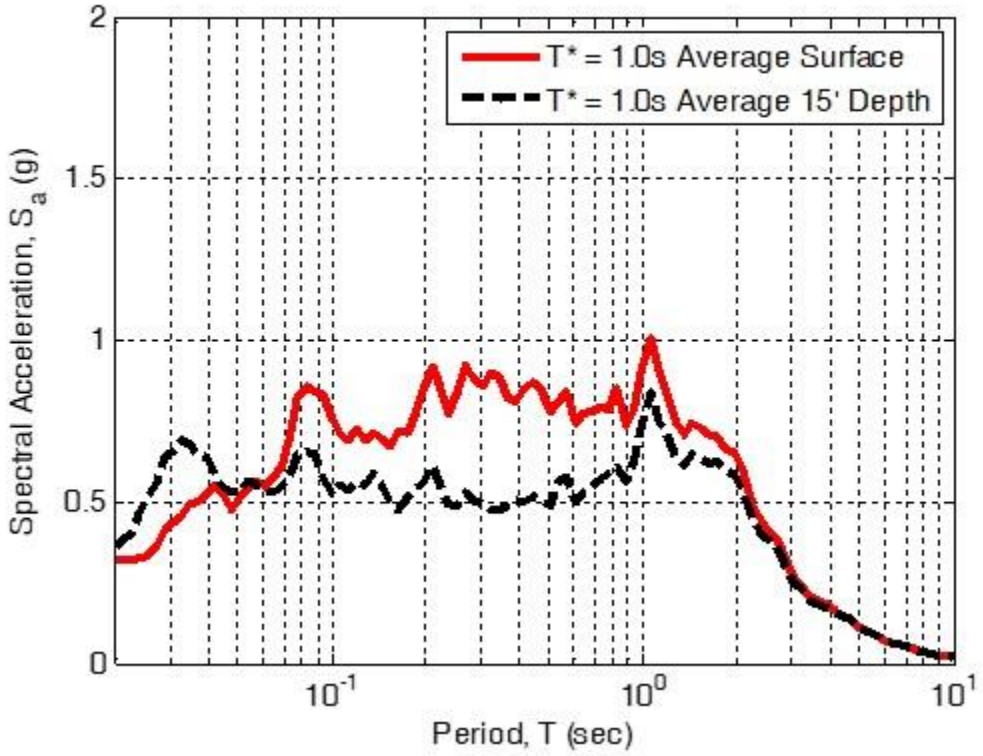

Figure 3.17: Comparison of the average surface and 15-ft depth spectra for the ground motions matched to the *T** = 1.0 s CMS at Cairo.

As stated, the ground motions are developed for the ground surface level. For the sake of simplicity in the procedure, these results at the surface were assumed to be near enough to the results at the assumed point of fixity of the foundation piles of 15-ft deep. Fig. 3.17 compares the average surface and 15-ft depth spectra for the ground motions matched to the *T** = 1.0 s spectra at Cairo. As can be observed, there are some differences, but the moderate differences are deemed acceptably similar for this study. A main point in accepting these ground motions is that the surface motions are generally larger than the 15-ft-deep ground motions, indicating that the surface ground motions will not underestimate the seismic loads on the bridges. As noted in Fig. 3.14 and 3.16, the average spectra for the ground motions matched to all the CMS in Cairo are very similar, so

the observations made from Fig. 3.17 would hold true for all other ground motions matched to other CMS. Given these observations, it was decided that the use of the surface ground motions in the dynamic analyses of bridges in this study is acceptable

These developed ground motions are unique to southern Illinois in that they utilize the CMS, which has not previously been used for ground motion development in the region. The ground motions are also unique in their applicability to the study of highway bridges in Illinois due to the period range covered by the developed CMS. The ground motions for Cairo are generally used in the dynamic analyses of the studies in this project due to that site producing the most intense ground motions in the state. While the developed ground motions are used in this study to observe the seismic behavior of IABs, the Cairo ground motions have already also been used in published studies of the seismic behavior of stub abutment bridges in Luo *et al.* (2016; 2017) demonstrating their applicability and adequacy for use in the studies of this project. The ground motion time histories described in this chapter are also discussed in Kozak *et al.* (2017a) and a database containing the developed ground motion time histories can be accessed through Kozak *et al*. (2017b).

CHAPTER 4: INTEGRAL ABUTMENT BRIDGE MODEL DEVELOPMENT

4.1 INTEGRAL ABUTMENT BRIDGE MODEL DESCRIPTION

The goal of the development of the IAB model is to accurately represent the IAB's seismic behavior while still accounting for computational efficiency. This goal is achieved by using experimental data and literature to develop models for individual components, ensuring accurate masses are appropriately placed, and by ensuring the model captures the damage found in actual IABs after earthquakes. The model must also account for the bridge parameters of interest which are varied throughout the parametric study described in Chapter 5. These parameters include the span configuration, superstructure girder material, bearings used at piers, foundation details. A sample three-span steel IAB is presented alongside its *OpenSees* model in Fig. 4.1 to show the similarity in component placement.

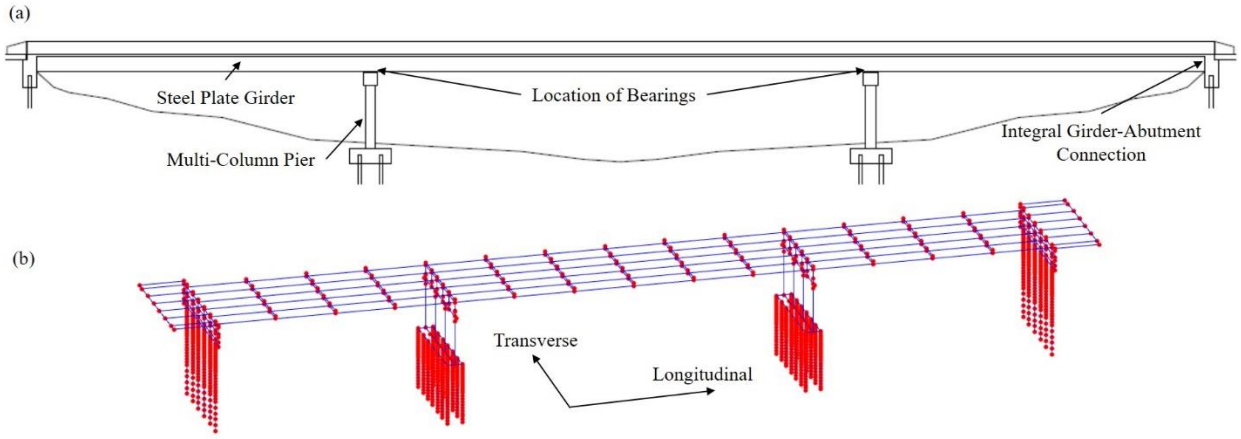

Figure 4.1: (a) Diagram of a typical three-span steel IAB and (b) The representative *OpenSees* model for the three-span IAB.

The IAB model developed for this study is similar to the models developed to study stub abutment bridge seismic behavior in Illinois (Filipov *et al.*, 2013a; Filipov *et al.*, 2013b; Luo *et al.*, 2016; Luo *et al.*, 2017) and developed in the Open System for Earthquake Engineering

Simulation program (*OpenSees*) (McKenna *et al.*, 2006). The prior work that developed stub abutment bridge models established useful component numerical models for simulating seismic response of highway bridges in Illinois. Full-scale testing was used to validate elastomeric bearing, side retainer, and low-profile fixed bearing models that were implemented in *OpenSees* (Filipov *et al.*, 2013a).

The overall IAB model is not validated with experimental data. However, qualitative validation is conducted through comparison of the IAB model behavior to damage found in post-earthquake IAB observation studies. Waldin *et al.* (2012) and Wood (2015) found large amounts of damage to the abutments, abutment piles, and piers in IABs after earthquakes in New Zealand. Significant damage in these components is also found in the IAB models developed in this study, generally validating the overall behavior of the model to actual bridge behavior. The damage in the IAB models is assessed through component behavior and is discussed in more detail in section 4.4, which provides the component limit states monitored in the IABs.

4.2 INTEGRAL ABUTMENT COMPONENT MODELS

The integral abutment model comprises ten primary components whose models are described in the following subsections. A diagram presenting the integral abutment and its components is presented in Fig. 4.2. The representation of the model which is used in *OpenSees* to describe the abutment presented in Fig. 4.2 is provided in Fig. 4.3.

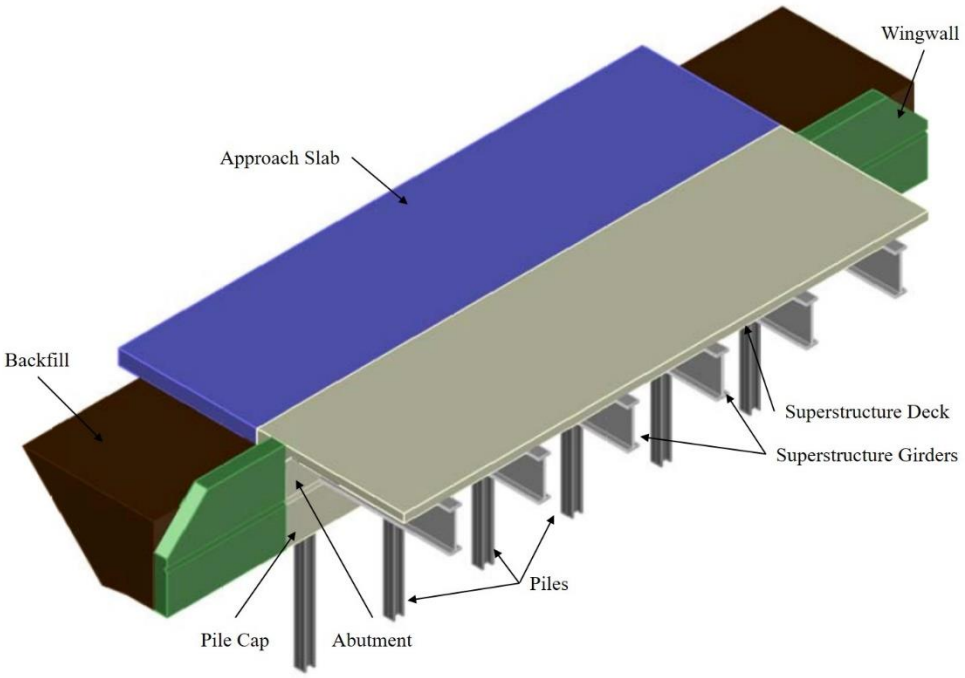

Figure 4.2: Diagram of an integral abutment and the components within the abutment.

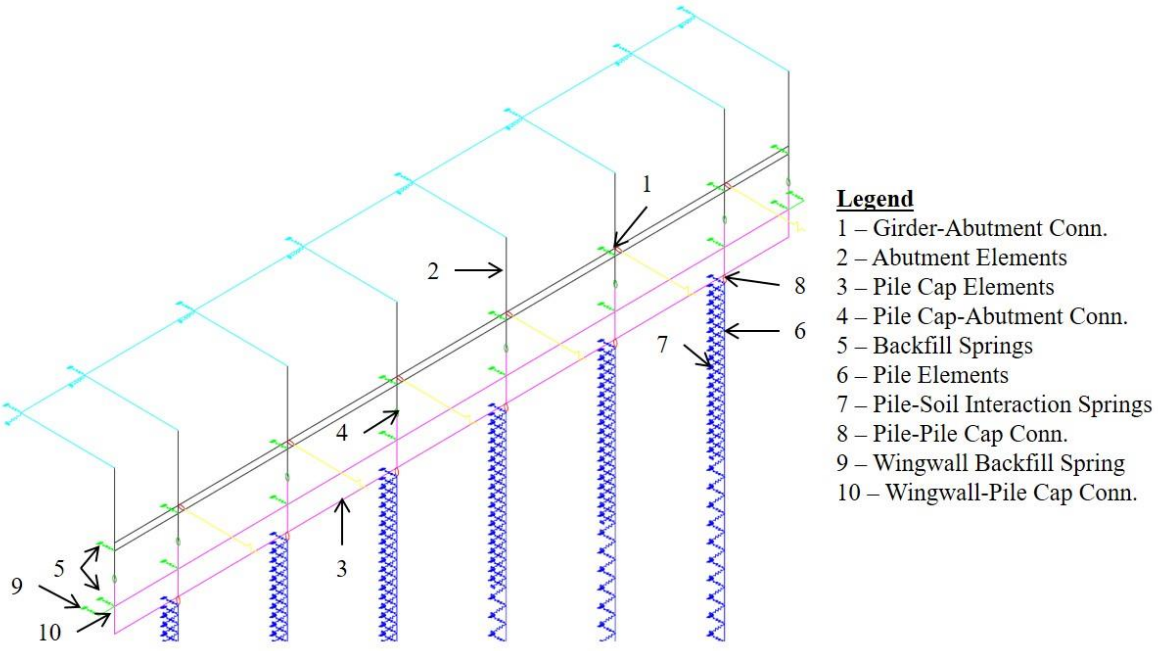

Figure 4.3: Model representation of an integral abutment.

4.2.1 Girder-Abutment Connections

The girder-abutment connection (component 1 in Fig. 4.3) consists of two primary elements:

1. Direct bearing of the superstructure girder on either a 2-in thick rocker plate or a 1-in thick bearing pad. A rocker plate is used if the girders are steel plate girders and the bearing pad is used if the girders are prestresed concrete beams (IDOT, 2012b).
2. Concrete poured such that the girders are cast directly into the abutment and the deck and abutment are a single monolithic piece of concrete. While the concrete is wet, the girder may still rotate on the rocker plate or bearing pad to accommodate the weight of the concrete deck. However, once the concrete hardens, rotation of the girders do not generally occur due to the large section of concrete encasing them in the abutment with a sufficient embedment length. The monolithic cast of the deck and abutment, which confines the girder, can be observed in Fig. 4.4.

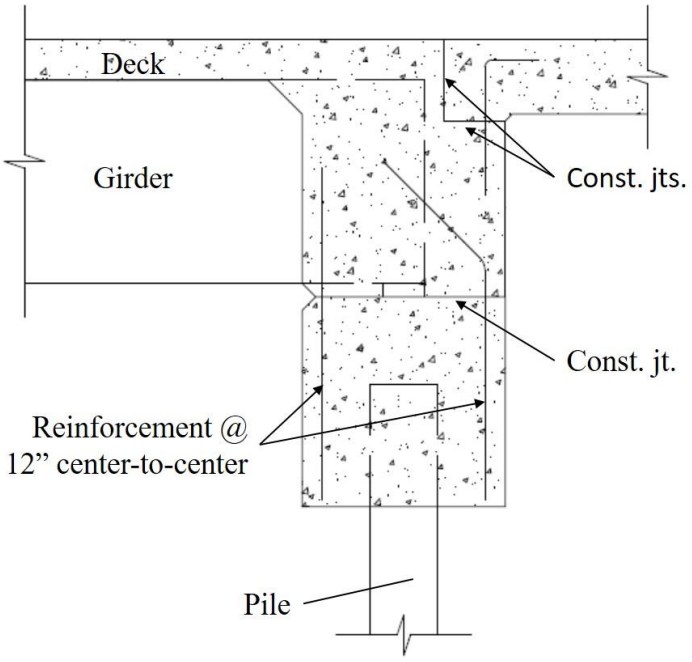

Figure 4.4: Diagram of the connections in an integral abutment.

The connection between the superstructure girders and the abutment allows for large force and moment transfers to occur at this point. While they are large, it is unlikely that the connection will reach its capacity and allow for large rotations despite some cracking which can be found when exposed to large moments (Itani and Pekcan, 2011). Prior research indicates that, although the connection is unlikely to allow large rotations, it is not completely rigid, it is semi-rigid (Itani and Pekcan, 2011). The degree of semi-rigidity has not been extensively studied although it is thought to be more rigid than not, so a small assumption was made by modeling the connection as a rigid connection.

In the model, the connection is only set to rigid after the dead load application. To simulate the wet concrete allowing for rotation and because the wet concrete does not transfer moments from the superstructure to the abutment during the application of the dead load, the connection is first modeled to allow for free rotation. The connection model is set to rigid during the dynamic analysis to simulate the hardened concrete which does transfer moments and rotation. This approach is the same that has been taken in previous Illinois IAB studies for thermal behavior (Holloway, 2012).

4.2.2 Abutment and Pile Cap

The abutments and pile caps (components 2 and 3, respectively, in Fig. 4.3) are both individually poured sections of concrete which are connected through a construction joint, as shown in Fig. 4.4. The components themselves are much stronger and stiffer than any of the other components attached to them. Per standard IDOT details, for steel girders both components are 3-ft 4-in wide and for prestressed concrete girders they are 3-ft 8-in wide. The pile cap is a minimum of 3-ft 6-in tall, and the height of the abutment varies depending on the girder height and deck

thickness (IDOT, 2012b). Given these large sections the abutment and pile cap elements are modeled as rigid elements.

The construction joint between the pile cap and abutment (component 4 in Fig. 4.3) is composed of #8 steel dowels at the front and back of the abutment with a 12-in center-to-center spacing (IDOT, 2012b), as shown in Fig. 4.4. This construction joint is represented by a connection in *OpenSees* which considers both the dowels and the friction between the two concrete surfaces. The behavior of the dowels and friction are combined together into a single constitutive model which is used in *OpenSees*. Sample cyclic behavior models for the dowel, the friction, and the overall connection are provided in Fig. 4.5.

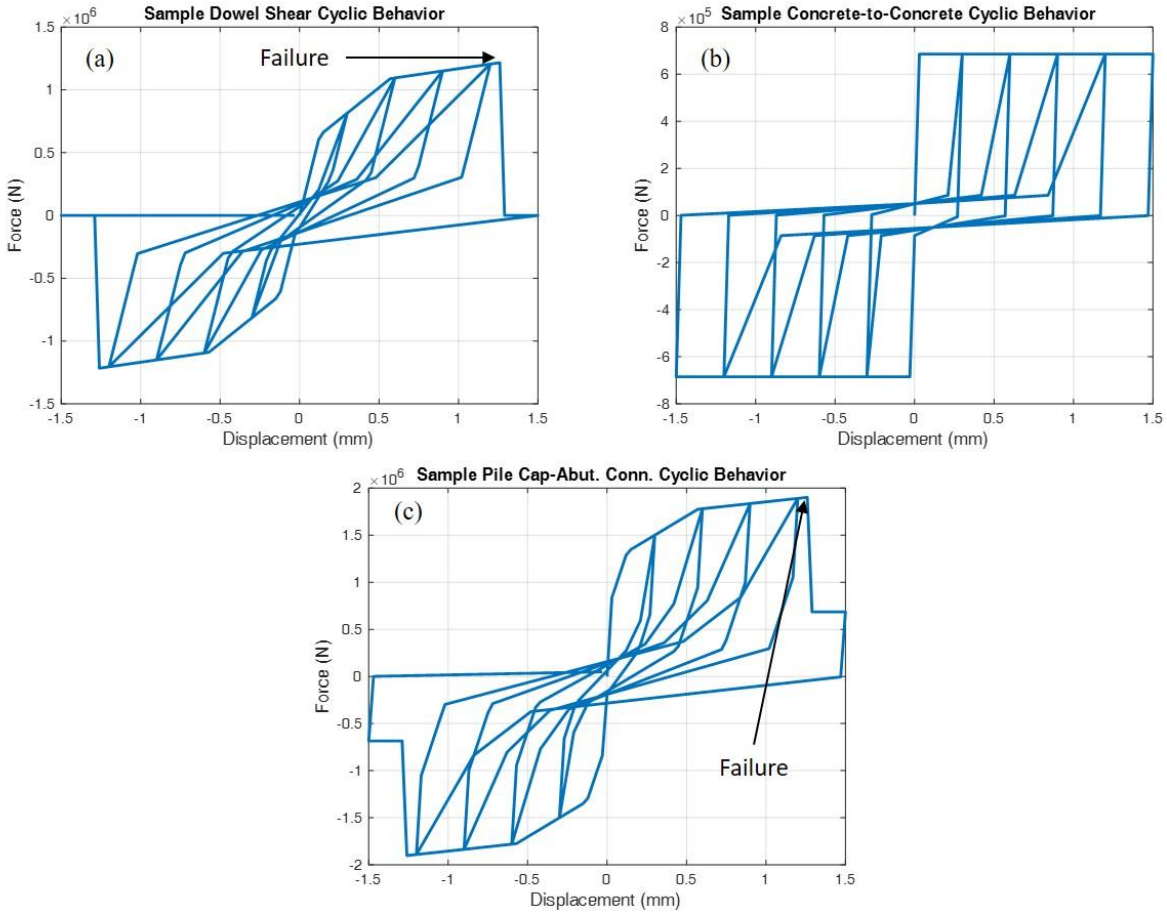

Figure 4.5: Sample cyclic behavior for (a) shear in the dowel rod through the pile cap-abutment interface, (b) the concrete-to-concrete friction at the pile cap-abutment interface, and (c) the overall behavior at the pile cap-abutment interface.

Dowel shear behavior is determined through the use of a model based on experimental data by Vintzeleou and Tassios (1986). The ultimate shear resistance of a single dowel bar (D_u) is calculated using Eq. (4.1) where d_b is the bar diameter, f_c' is the unconfined concrete strength (3.5 ksi), and f_y is the bar yield strength (60 ksi). The force-displacement behavior shown in Fig. 4.5a is based on the ultimate shear strength and a relationship from Vintzeleou and Tassios (1986) and demonstrates the failure of the dowel bars in shear after which the dowels provide no lateral resistance.

$$D_u = d_b^2\sqrt{1.7f'_c f_y} \tag{4.1}$$

The concrete-to-concrete friction model is based on equations from Tassios (1983) which can be used to determine the coefficient of friction on the interface (μ_0 using Eq. (4.2)) as well as the relative displacement to reach maximum shear resistance (s_0 using Eq. (4.3)). Both equations require the normal stress applied to the interface (σ) which is taken as the weight of the abutment section in addition to the weight of half the exterior superstructure span divided over the pile cap-abutment interface area. The force-displacement relationship shown in Fig. 4.5b is developed using the μ_0 and s_0 values in a pinching concrete-to-concrete friction model presented in Tassios (1983).

$$\mu_0 = 0.8\sigma^{-0.7} \tag{4.2}$$

$$s_0 = 0.27\sigma \tag{4.3}$$

As discussed, the two individual constitutive models for dowel and friction behavior are combined to form an overall model for the interface. Due to the lack of failure in the friction model aside from reaching sliding, the failure of the overall interface is considered when dowel shear failure occurs, as indicated in Fig. 4.5c.

4.2.3 Abutment Backfill

Prior numerical studies have shown that the abutment backfill (component 5 in Fig. 4.3) is a key component of stub abutment bridge seismic behavior (Luo *et al.*, 2016). The lack of a gap between the superstructure and abutment in IABs means that the backfill is immediately engaged and therefore contributes a large amount of longitudinal horizontal load resistance. The model simulates the passive backfill pressure against the abutment and pile cap using the force-displacement relationship provided in Shamsabadi *et al.* (2005) and Shamsabadi *et al.* (2007).This relationship is based on soil mobilizing in a logarithmic spiral failure surface and also considers a hyperbolic stress-strain behavior of the soil. This model, also known as the LSH model, is validated in laboratory and numerical experiments to reliably predict the force-displacement relationship required for the backfill soil.

In *OpenSees*, the *HyperbolicGapMaterial* material may be used to describe the LSH model, though there are still some minor differences. The major difference consists of the resistance asymptotically approaching the backfill's ultimate resistance in the LSH model while the *HyperbolicGapMaterial* material allows for the ultimate resistance to be exceeded. A modified *HyperbolicGapMaterial* material was developed for Luo *et al.* (2016) which accounts for the asymptotic approach to the ultimate resistance. This modified material was used in the IAB model to represent the backfill at various points, two of which are presented in Fig. 4.6. It can be noted from Fig. 4.6 that resistance is only experienced when the abutment is compressed into the backfill. When the abutment pulls away from the backfill there is no resistance from the backfill.

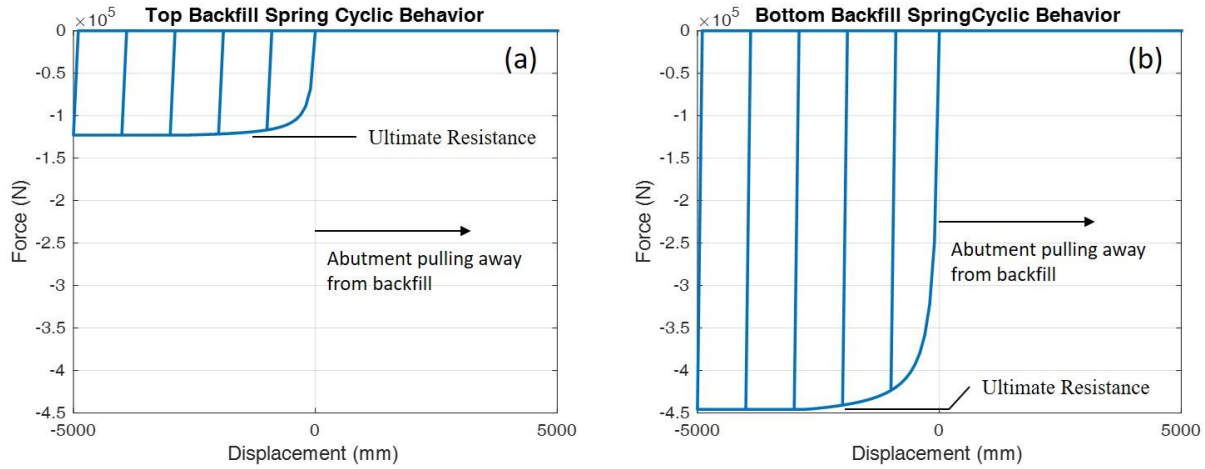

Figure 4.6: Sample backfill soil cyclic behavior at two locations.

The properties of the backfill soil used in the equations from Shamsabadi *et al.* (2007) to determine the ultimate resistance and other LSH model parameters were provided by IDOT. The backfill soil properties were based on typical values used for the backfill material in Illinois. The backfill soil properties are provided in Table 4.1.

Table 4.1: Backfill soil properties

Property	**Symbol**	**Value**
Unit Weight	γ	16.2 kN/m^3 (0.103 kcf)
Effective Friction Angle	ϕ'	39^o
Mobilized Cohesion of the Embankment Soil	c	0
Wall-to-Soil Interface Friction Angle	δ	39^o
Poisson's Ratio	v	0.35
Failure Ratio	R_f	0.97
Strain at 50% of Failure Strength	ε_{50}	0.03

Fig. 34 shows that the backfill springs are only applied in the bridge longitudinal direction and are applied at two points vertically along the abutment and pile cap. The backfill springs are applied in the longitudinal direction and not in the transverse direction due to the minimal resistance (only soil-concrete friction) they offer in the transverse direction (Spyrakos and Ioannidis, 2003). The backfill is modeled at two locations vertically to account for the potential failure of the pile cap-abutment connection and any relative displacements that may occur between

the abutment and pile cap. The two spring components are developed by dividing the stiffness and ultimate resistance of the entire backfill (pile cap and abutment) into the two components. The properties are split, as shown in Fig. 4.7, by dividing the triangular backfill pressure into triangular and trapezoidal regions. The location of the backfill springs are also determined through these assumptions and taken at the centroids of the triangle and trapezoid. The ultimate resistance and stiffness of the backfill springs against the pile cap tends to be larger than the ultimate resistance and stiffness against the abutment. This is shown using the equations in Fig. 4.7 and the comparison of the behavior in Fig. 4.6.

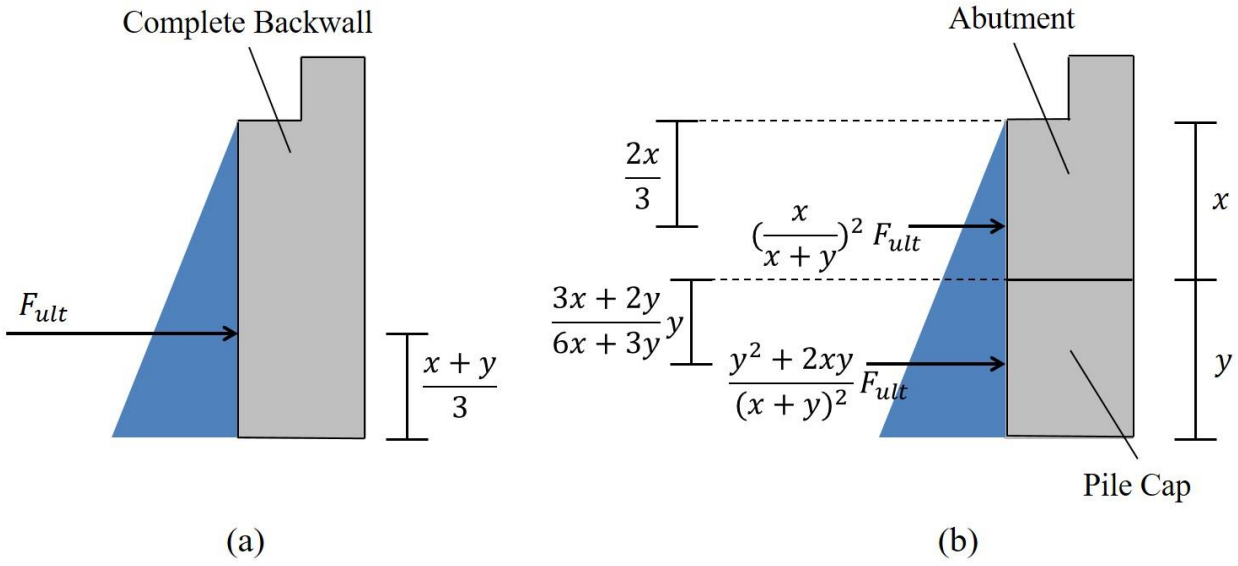

Figure 4.7: Separation of backfill forces for the abutment and pile cap.

4.2.4 Abutment Foundations

The foundations of the abutments are composed of piles attached to pile caps. The abutment foundations are modeled to account for the pile element behavior (component 6 in Fig. 4.3), the behavior of the soil surrounding the piles (component 7 in Fig. 4.3) and the behavior of the connection between the piles and the pile cap (component 8 in Fig. 4.3). The pile elements are represented in *OpenSees* by nonlinear beam-columns, the soil surrounding the piles is represented

by zero-length element springs, known as p-y and t-z springs, in the horizontal and vertical direction, respectively, and the pile-pile cap connection is represented by a zero-length element spring as well. These components are detailed in Fig. 4.8 which demonstrate how the elements are represented.

As discussed, the piles are modeled as nonlinear beam-column elements. These elements account for both the nonlinear steel material in the piles as well as the HP-shape of the piles using fiber sections. The piles are oriented such that weak-axis bending occurs when forces are applied in the bridge longitudinal direction (IDOT, 2012b). This orientation is used to allow for the integral abutments to be more flexible in the longitudinal direction to accommodate thermal loads. The sizes of the HP-shapes used for the piles are dictated by pile sizing charts provided by IDOT (2012b). These sizing charts relate the effective expansion length (the length of half of the total bridge span for IABs) and the bridge skew angle to determine adequate pile sections.

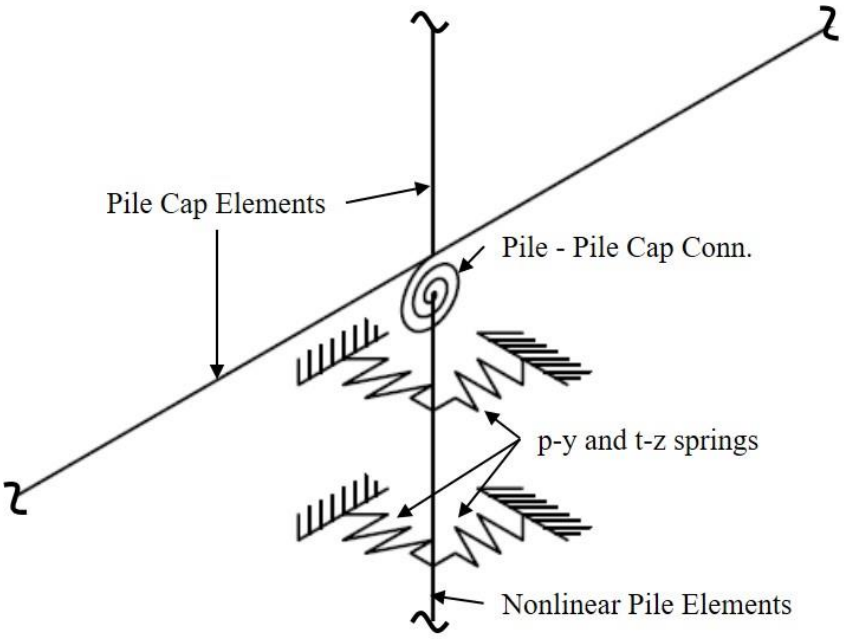

Figure 4.8: Model representation of the components comprised in the abutment foundations.

The HP-shape cross-sections are divided into multiple fibers, each with a defined material behavior. Due to the significant potential nonlinear behavior in the piles, caused by both axial

forces and bending moments, the pile section is discretized into 120 fibers. The 120 fibers are arranged such that each flange and the web contains 20x2 fibers, as shown in Fig. 4.9a. The steel material used in each fiber follows the Giuffré-Menegotto-Pinto Model with isotropic strain hardening model (*Steel02* in *OpenSees*). The steel parameters used in this study are defined by a Young's modulus of 29000 ksi, an actual yield strength of 55 ksi (1.1 x 50 ksi), and an actual ultimate strength of 71.5 ksi (1.1 x 65 ksi) based on A572 Gr. 50 steel (AISC, 2017). The strain hardening ratio was determined as 0.48% using the A572 Gr. 50 steel data and assuming the ultimate strain occurs at 0.12 similar to A706 steel. The remaining parameters were based on comparisons to experimental data (Sizemore, 2017). The monotonic static behavior of the steel model used in the piles is presented in Fig. 4.9b. Yielding is clearly observed in Fig. 4.9b, however other limit states beyond yielding are also accounted for and described in section 4.4.

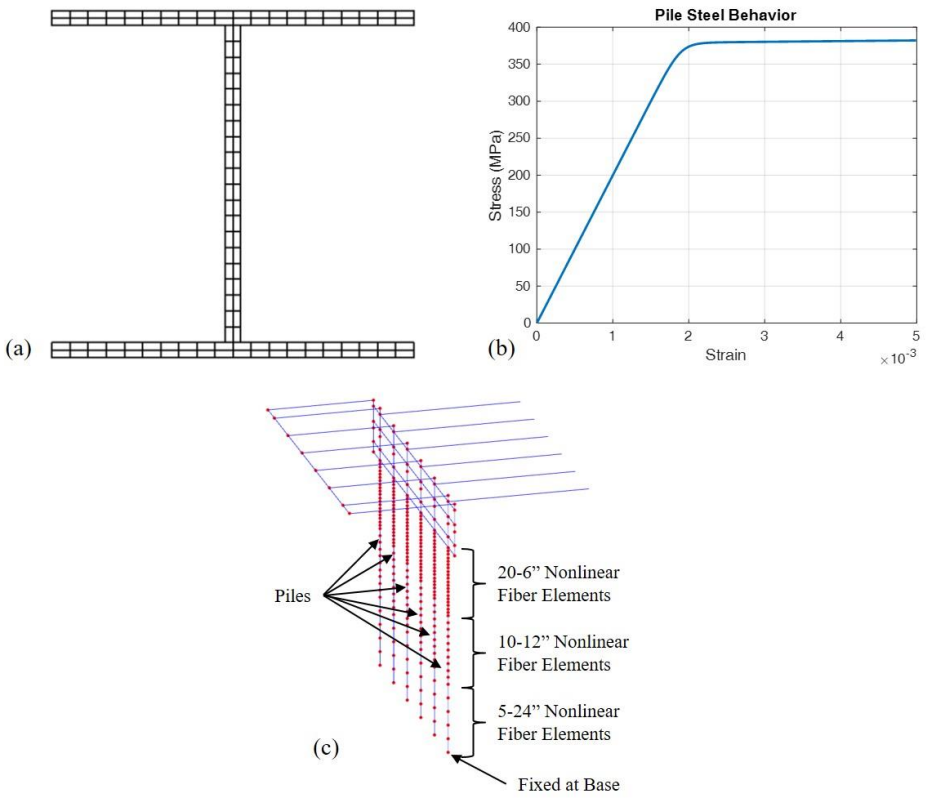

Figure 4.9: (a) Discretization of the pile cross-section. (b) Monotonic static behavior of the pile steel material model. (c) Discretization of the pile elements along their length.

The pile elements are discretized along the length of the pile to account for the larger moments that will be experienced near the abutments. It is indicated that the critical pile depth is taken to be the top 10 ft of the soil (IDOT, 2012b), so the soil closest to the top will contain shorter elements to better capture the behavior. As shown in Fig. 4.9c, the top 10 ft of the piles are discretized into (20) 6-in sections, the following 10 ft are discretized into (10) 12-in sections, and the deepest 10 ft are discretized into (5) 24-in long sections. At a depth of 30 ft the pile elements are fixed.

Attached to the ends of each of the nonlinear pile elements are zero-length elements representing the soil surrounding the piles at that specific depth through p-y and t-z springs. The *OpenSees* built-in material model *PySimple1* is used for the p-y springs in both horizontal directions. This material is based on the models from Boulanger *et al.* (1999) and requires the ultimate capacity of the soil, p_{ult}, the displacement at which 50% of p_{ult} is mobilized, y_{50}, and the drag coefficient, C_d, be defined. C_d can be assumed to be 0.3 based on centrifuge experiments from Wilson (1998), however the two other properties are based on data from Illinois soil profiles. Four Illinois soil conditions with accompanying soil profiles are considered; alluvial, non-alluvial, stiff, and soft. The alluvial and non-alluvial profiles are based on the soil boring data described in Chapter 3 and Kozak *et al.* (2017). The stiff and soft soil profiles were developed in Luo *et al.* (2016) to describe realistic bounds for soft and stiff soil conditions in southern Illinois. The soil properties required for the calculation of the p-y spring parameters are the undrained shear strength for clay, s_u, and the effective friction angle for sand, ϕ'. These properties are provided in Fig. 4.10.

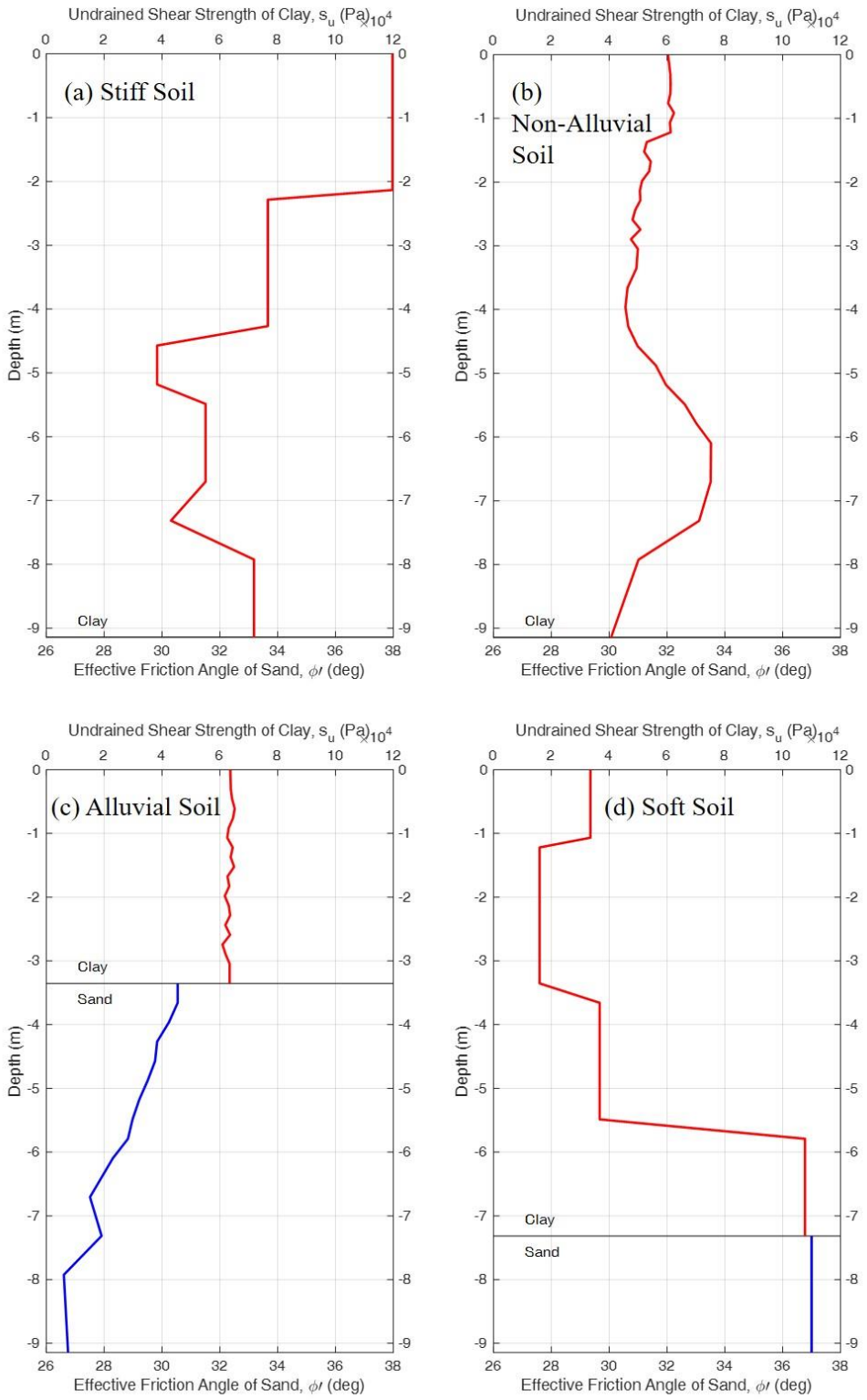

Figure 4.10: Undrained shear strength of clay and effective friction angle of sand profiles for (a) stiff soil conditions, (b) non-alluvial soil conditions, (c) alluvial soil conditions, and (d) soft soil conditions.

For p-y springs in a clay layer, the p_{ult} parameter is calculated from equations in Matlock (1970) and Terzaghi *et al.* (1996) using the soil's undrained shear strength (c in the equations, s_u in Fig. 4.10) and unit weight (γ), as shown in Eq. (4.4) and Eq. (4.5). The undrained shear strength was determined through the standard penetration test results and a table in Terzaghi *et al.* (1996) for each layer. The remaining variables in the equations represent an empirical constant, J, (0.5 based on Matlock's recommendations), the pile diameter, D, the depth below the surface, X, and the depth to the bottom of the reduced resistance zone, X_R. Matlock (1970) also describes the value for y_{50} as $2.5\varepsilon_{50}D$ where ε_{50} can be taken as 0.005 (based on laboratory data from Boulanger *et al.* (1999)).

$$X_R = \frac{6D}{\frac{\gamma D}{c} + J} \tag{4.4}$$

$$p_{ult} = \begin{cases} 3c + \gamma X + J\frac{cX}{D} \; for \; X < X_R \\ 9c \; for \; X \geq X_R \end{cases} \tag{4.5}$$

Sand p-y behavior is based on equations and figures from the American Petroleum Institute (API) (2002). p_{ult} can be calculated using Eq. (4.6) and coefficients C_1, C_2, and C_3 which are determined graphically and based on the effective friction angle of the soil and the depth of the layer, H. Eq. (4.7) can be used to calculate y_{50} by setting the P value to $p_{ult}/2$ and solving for y. In these equations, D and γ are as described for the clay equations, k is based on a plot relating it to the effective friction angle, and A is taken as 0.9.

$$p_{ult} = \min \begin{cases} (C_1 H + C_2 D)\gamma H \\ C_3 D \gamma H \end{cases} \tag{4.6}$$

$$P = A p_{ult} \tanh\left(\frac{kH}{A p_{ult}} y\right) \tag{4.7}$$

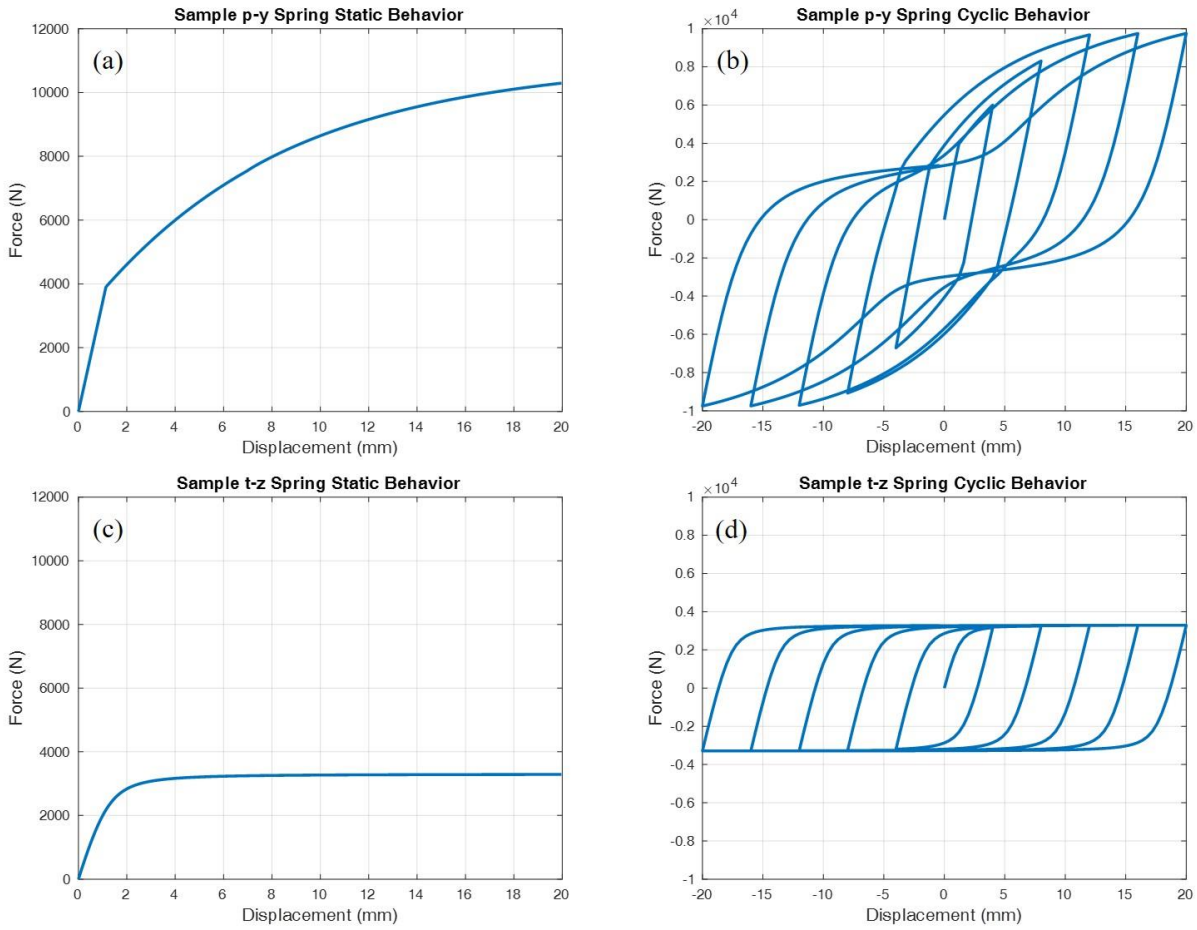

Figure 4.11: Example zero-length spring behavior for (a) monotonic static p-y springs, (b) cyclic p-y springs, (c) monotonic static t-z springs, and (d) cyclic t-z springs.

The t-z springs account for the vertical resistance applied to the piles from the soil and also use soil parameters from the four soil conditions discussed above. Similar to the p-y springs, the t-z springs require t_{ult} and z_{50} values in the *OpenSees* model. The API (2002) provides equations and suggested values for modeling these springs. Eq. (4.8) through (4.10) are used to define the t_{ult} values for both sand and clay where c, and D are as described above, ψ is the ratio of the undrained shear strength to the effective overburden pressure, K is the coefficient of lateral earth pressure, p_o is the effective overburden pressure, and δ is the friction angle between the soil and the pile wall for sand (assumed to be 25º). The z_{50} values are determined using recommended values from API (2002) of $0.0031D$ for clay and $0.05D$ for sand.

$$\alpha = \begin{cases} 0.5\psi^{-0.5} \; for \; \psi \leq 1.0 \\ 0.5\psi^{-0.25} \; for \; \psi > 1.0 \end{cases} \tag{4.8}$$

$$t_{ult,clay} = \alpha c \tag{4.9}$$

$$t_{ult,sand} = Kp_o \tan \delta \tag{4.10}$$

Examples of the p-y and t-z spring behavior under both cyclic and monotonic static loading conditions are shown in Fig. 4.11. The t-z spring resistance is from friction only, leading to a lower capacity at the plateau. In the p-y springs, the effects of drag and re-engagement with soil can be observed through the pinching behavior in the cyclic response.

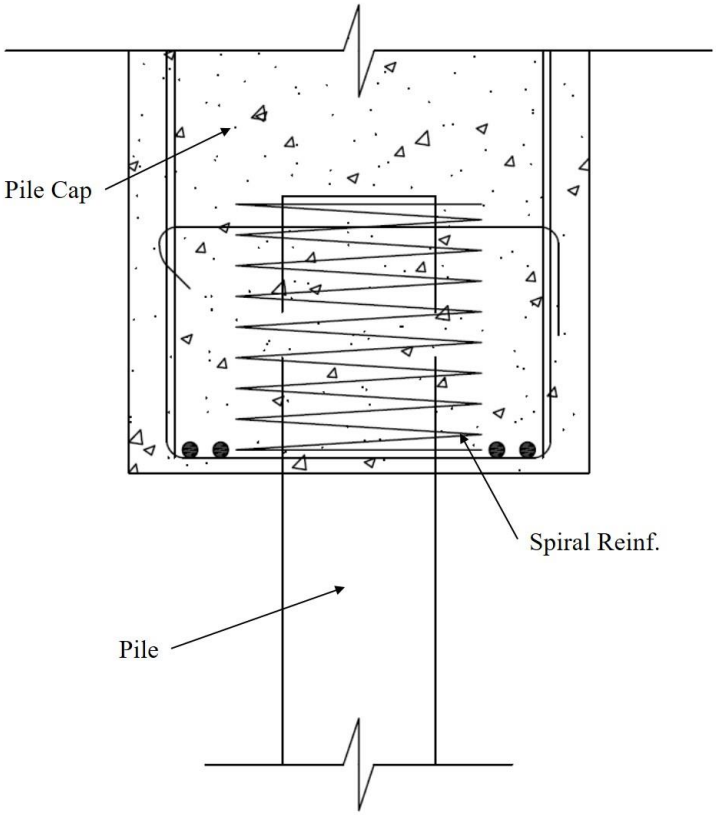

Figure 4.12: Diagram of the pile-pile cap connection.

The final modeled component of the abutment foundations are the pile-pile cap connections. As shown in Fig. 4.12, these connections are meant to represent the embedment of the pile in the pile cap and account for the spiral reinforcement present. The piles are embedded

24 in into the pile cap (IDOT, 2012b) which is sufficient to model this connection as rigid. This assumption is further verified through past studies which observed that there is no decrease in the lateral load capacity of the connection if the piles are embedded 24 in or more (Frosch *et al.*, 2009). While some slight cracking was observed in the pile cap in these experiments, it should be noted that the pile cap in the experiment was much less robust and did not include spiral reinforcement. While the connection is rigid, significant damage at this interface is still expected. This damage is accounted for through the nonlinear pile element adjacent to the interface which will turn into a plastic hinge under significant stress.

4.2.5 Wingwall Connections and Backfill

IDOT (2012b) indicates that the wingwall in an integral abutment should be parallel to the centerline of the abutment and have a length between 4 and 10 ft and be 1 ft thick. Given a 10-ft by 1-ft wingwall dimension and assuming the wingwall is the same height as the abutment, the backfill resistance applied to the wingwall will be calculated using the method applied to the abutment and pile cap. However, it is assumed that there will be no potential separation in the wingwall as there may be at the construction joint between the pile cap and abutment. Due to this the effects of the backfill on the wingwall are applied in one spring (component 9 in Fig. 4.3, also shown in Fig. 4.13).

The wingwall is assumed to be rigid and to not sustain any damage, so to be computationally efficient, the wingwall backfill spring is applied directly next to the abutment and the wingwall is not explicitly modeled. This can be seen in Fig. 4.13 where the wingwall backfill spring is connected directly to the abutment through a wingwall-pile cap connection spring (component 10 in Fig. 4.3). The wingwall-pile cap connection consists of the dowel connections similar to those described for the pile cap-abutment connection. IDOT designs identified the

dowels in the connections as (10) #7 bars for single-span bridges, (16) #5 bars for three-span bridges, and (14) #5 bars for four-span bridges. Friction between the abutment and wingwall is not considered, so failure of this connection is governed by the failure of the dowels.

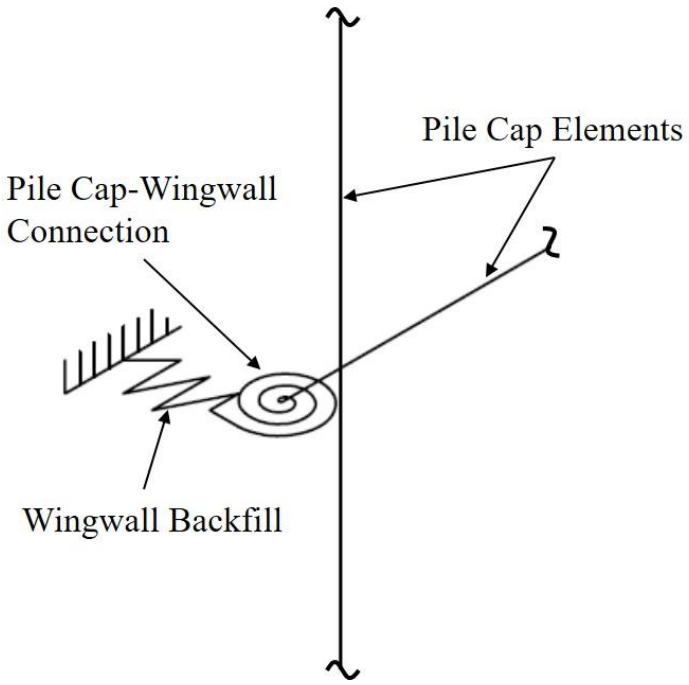

Figure 4.13: Schematic for modeling the wingwall and its components in the IAB model.

4.3 NON-ABUTMENT COMPONENTS

Outside the abutment, the IAB model includes the superstructure longitudinal and transverse elements, the approach slab, the fixed and elastomeric bearings found between the piers and superstructure, the pier columns, and the pier foundations. The location of these components within the IAB model is presented in Fig. 4.14. Many of the non-abutment components, such as the bearings and pier columns are similar to those developed in Filipov *et al.* (2013a; 2013b) for use in stub abutment bridges, so the constitutive models are unchanged. Refinements have been made to components such as the pier columns and superstructure to better represent the IAB.

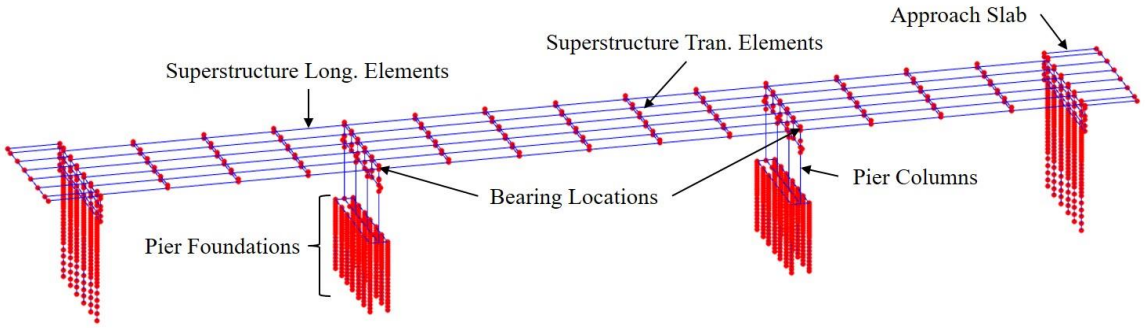

Figure 4.14: Location of non-integral abutment components modeled in the overall IAB model.

4.3.1 Superstructure

The bridge superstructure is modeled using the grillage method, which represents the girders, deck, parapets, and transverse diaphragms as beam-column elements in the longitudinal and transverse directions. These elements are illustrated in Fig. 4.14. The longitudinal elements represent the composite girder-deck section and are located at the elevation of the centroid of the composite section. The longitudinal elements are spaced according to the girder spacing used in the bridge design.

Two transverse elements are defined at different elevations in the superstructure, as presented in Fig. 4.15 for the deck and model cross-section. The lower transverse elements are located at the girder-deck composite centroid elevation and represent the diaphragms connecting the girders when steel girders are used and either the permanent bracing (at non-pier and non-abutment locations) or concrete diaphragms (at pier and abutment locations) when prestressed concrete girders are used. The steel girder diaphragms are composed of either a single C-section or angle cross-bracing (IDOT, 2012a). The prestressed concrete girder permanent bracing is a single MC-section and the concrete diaphragms at the piers are 2-ft 6-in wide concrete members (IDOT, 2012a). The upper transverse elements are located at the deck centroid's elevation and represents the deck. The transverse elements are spaced according to the diaphragm and permanent bracing spacing limits provided in the IDOT Bridge Design Manual (IDOT, 2012a).

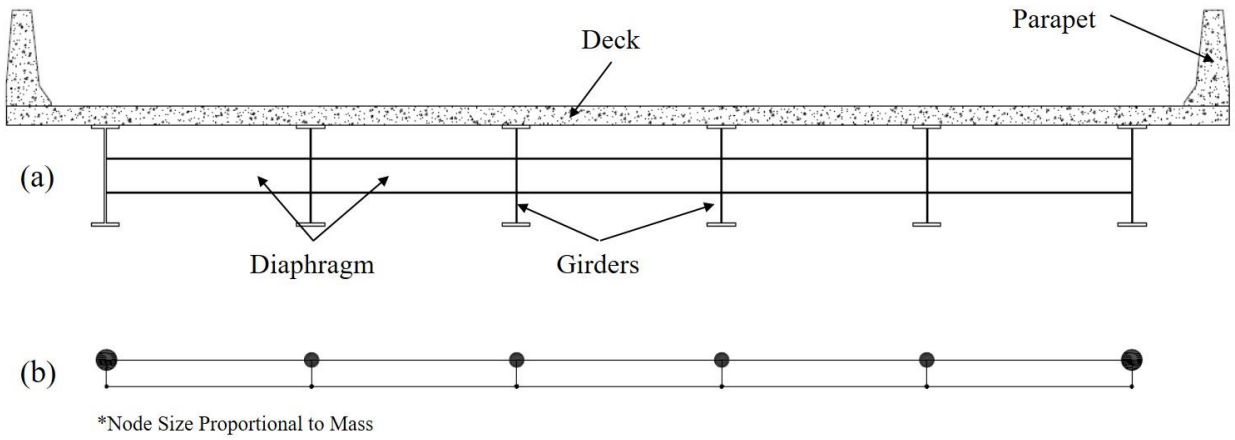

Figure 4.15: (a) Diagram of the superstructure cross-section. (b) Representative model of the superstructure cross-section with masses.

The mass of the superstructure is also accounted for in the model, as indicated by the circles at the nodes in Fig. 4.15b. The masses along the upper transverse element represent the deck and the parapets (only in the exterior nodes, as indicated by the larger circles in those locations). The masses along the lower transverse element represents the mass of the girders. Fig. 4.15 is demonstrating the masses and arrangement for a superstructure with steel girders whose relative masses are much less than those found in prestressed concrete girders. This is the reason for the relatively small masses at the lower nodes of Fig. 4.15b.

The beam-column elements used to represent the superstructure are modeled as elastic and do not consider nonlinearities caused by material or geometry since there is no evidence of significant damage in IAB superstructures after earthquakes. Additionally, IAB superstructures in Illinois are specifically designed to remain in the elastic range. These points validate the assumption that they will remain elastic and should be modeled as elastic, like previous Illinois IAB studies (Filipov *et al.*, 2013b; LaFave *et al.*, 2013a). Elastic grillage elements also improve the computational efficiency of the IAB model.

The assumption that the beam-column elements for the superstructure can be represented as elastic is also partially validated through pushover analyses following the procedure in Chapter 6. Superstructure elements were analyzed and it was found that the girders remain in the elastic range. However, there were large stresses found in the concrete deck of some IABs which exceeded the elastic stress limit of the deck concrete. Stresses exceeding the elastic limit were found in some diaphragm elements as well. The elastic behavior of the superstructure is discussed in more detail in section 6.4.

4.3.2 Approach Slabs

The approach slabs are not modeled in detail due to their lack of observed damage in past earthquakes. The important contribution from the approach slabs in the model is the mass of the 30-ft long concrete slabs, which may have significant inertial contributions during dynamic events. Also, as shown in Fig. 4.4, the connection between the approach slab and abutment consists of only dowels running through the construction joint (IDOT, 2012b). As such the approach slab is represented by rigid elements with appropriate masses and is attached to the abutment through a pinned connection. At the end opposite to the abutment, a roller condition is assumed due to the approach slab resting on the approach slab-transition slab foundation and resisted only by friction. Friction between the approach slab and the soil beneath it is not modeled due to the assumption that the soil has settled and there is negligible contact with the slab (Luo *et al.*, 2016).

4.3.3 Elastomeric Bearings and Side Retainers

IDOT employs two elastomeric expansion bearing types, Type I and Type II, with Type I the most commonly used. Although Type II elastomeric bearings, which include a low-friction sliding interface and accommodate larger thermal movements, these bearings are being used in new Illinois bridges less frequently. Nonlinear dynamic analyses have shown that Type II bearings

are more vulnerable to unseating during seismic response than Type I bearings (LaFave *et al.*, 2013a), so Type II bearings are not considered in this study. Type I elastomeric bearings, shown in Fig. 4.16, comprise an elastomer block with steel shims vulcanized to a steel plate at the top. The bottom of the elastomer rests directly on the pier cap concrete surface (IDOT, 2012a). Adjacent in the transverse direction, though not initially in contact with the bearings, are the side retainers that prevent excessive transverse displacement of the bearings. The side retainers are designed to be 0.425 in from the transverse faces of the bearing to allow for minor bearing movement prior to engagement with the retainers. The retainers do not have any influence in the longitudinal direction.

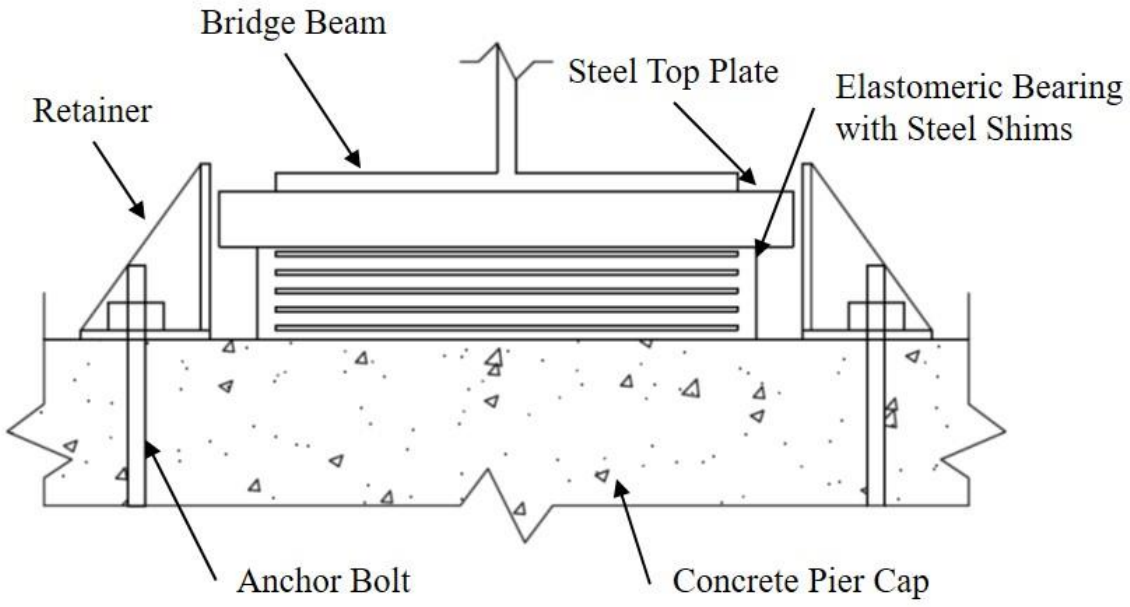

Figure 4.16: Diagram of a Type I elastomeric bearing and its side retainers.

Type I elastomeric bearings have been experimentally studied in the past (LaFave *et al.*, 2013b; Steelman *et al.*, 2013; Steelman *et al.*, 2018) and numerical models for use in bridge response analysis have been developed based on the experimentally-observed behavior (Filipov *et al.*, 2013b; LaFave *et al.*, 2013a). These previously-developed numerical models are used to represent Type I bearing behavior in the IAB model as well. The experimental results from

Steelman *et al.* (2013) were used to determine the monotonic static and cyclic behavior for the Type I bearings as well as the coefficient of friction and stiffness values appropriate for the bearings. The bearing stiffness was determined to be calculated as 85 psi multiplied by the plan area of the bearing and divided by the bearing height. It was determined that three coefficients of friction were required – the initial slip coefficient of friction (μ_I), the kinematic/sliding coefficient of friction (μ_K), and the post-slip coefficient of friction (μ_{PS}). The initial slip coefficient of friction is used to determine the force at which the initial slip begins to occur and was determined to be μ_I = 0.6. The kinematic/sliding coefficient is used to describe the resistance experienced during the bearing sliding and was determined to be μ_K = 0.45. The post-slip coefficient of friction is used to determine the resistance occurring before sliding occurs during reloading after the initial sliding has occurred. It was determined to be μ_{PS} = 0.5 (Filipov *et al.*, 2013a). Sample monotonic static and cyclic responses of a Type I elastomeric bearing under a constant normal load are presented in Fig. 4.17. Note that the friction forces in the bearings are dependent on the normal force in the bearing, which may vary during a dynamic analysis and lead to a force-displacement behavior different from those shown in Fig. 4.17.

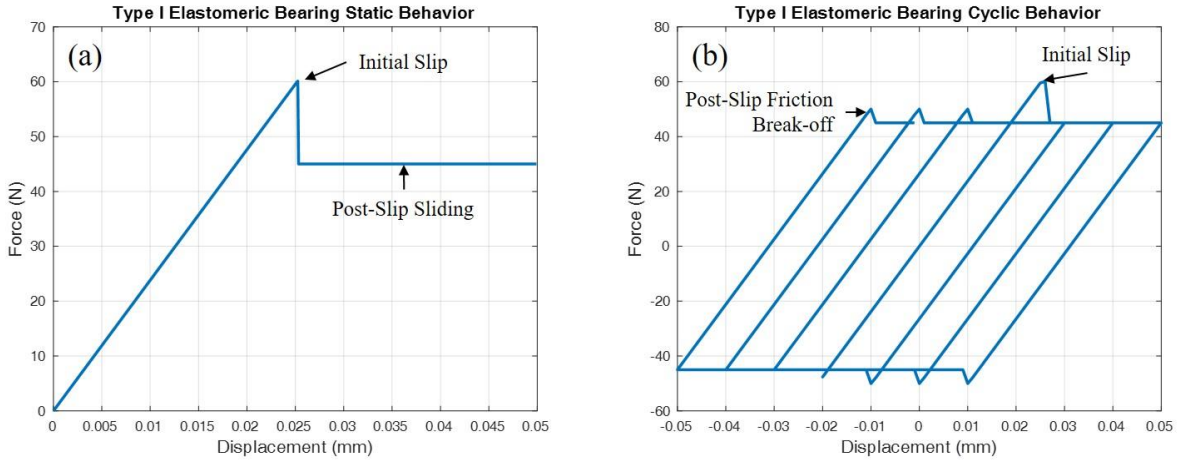

Figure 4.17: Example (a) monotonic static and (b) cyclic behavior for a 15-a Type I elastomeric bearing under a constant normal load.

The side retainers accompanying the Type I elastomeric bearings have also been experimentally studied (LaFave *et al.*, 2013b; Steelman *et al.*, 2013) and have had numerical models developed to represent their behavior (Filipov *et al.*, 2013b; LaFave *et al.*, 2013a). The behavior of the side retainers is dominated by the behavior of the anchor bolts, as indicated by the IDOT design equation for retainer strength provided in Eq. (4.11). Eq. (4.11) provides the value for the retainer ultimate capacity where A_b is the nominal anchor bolt area, F_u is the ultimate strength, and ϕ = 1.

$$P_{ret,ult} = \phi 0.8 A_b F_u \tag{4.11}$$

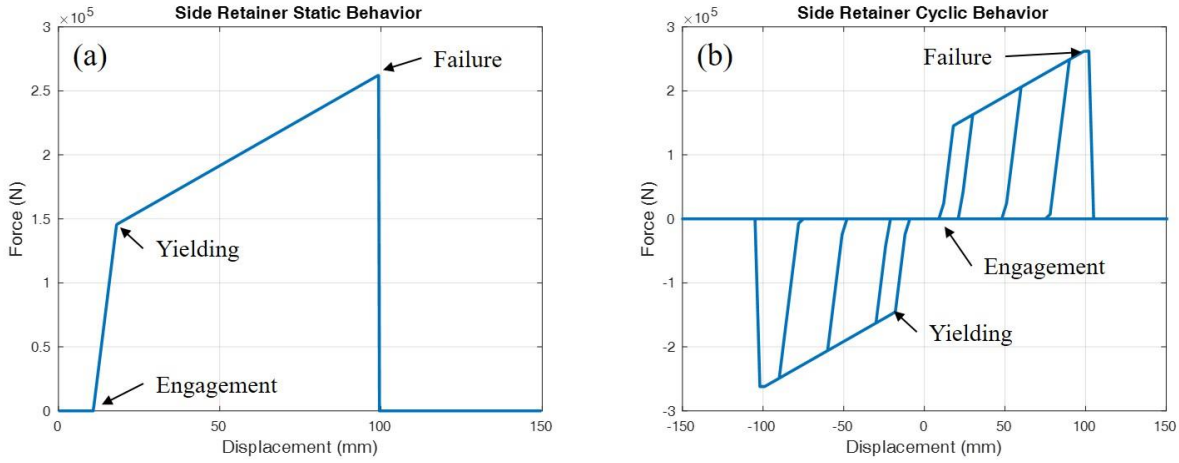

Figure 4.18: Sample (a) monotonic static and (b) cyclic side retainer behavior for a retainer using 1.25-in diameter steel anchor bolts.

Steelman *et al.* (2013) found the retainers to exhibit roughly elasto-plastic behavior, as shown in Fig. 4.18. The observed experimental data and the model developed from the data (Filipov *et al.*, 2013a) follow this behavior and account for limit states such as retainer engagement (when the bearing contacts the retainer), yielding of the retainer anchor bolts, and fracture of the retainer anchor bolts after which the retainers can resist no force (Filipov *et al.*, 2013a). As discussed above, the ultimate capacity of the retainer, $P_{ret,ult}$, representing retainer fracture is described through Eq. (4.11). The yielding of the retainer bolts is expressed as $P_{ret,ult}$ / *1.80* based

on experimental results. Experimental results also provided values for the ultimate anchor bolt strength (F_u) of 60 ksi. Sample monotonic static and cyclic behavior for a retainer with 1.25-in diameter steel anchor bolts is provided in Fig. 4.18.

Within the IAB model, the elastomeric bearings and side retainers are modeled at each location where the pier cap and superstructure girders meet. The bearings and retainers are modeled considering the lateral resistance from both the bearing friction and the retainer anchor bolts. The model also accounts for the height of the bearing such that the pier cap-superstructure connection geometry is accurate. Fig. 4.19 provides a schematic of the overall bearing model including zero-length elements for the bearings and retainers, a rigid zero-length element for recording the bearing friction behavior, and two rigid elements to represent the bearing height.

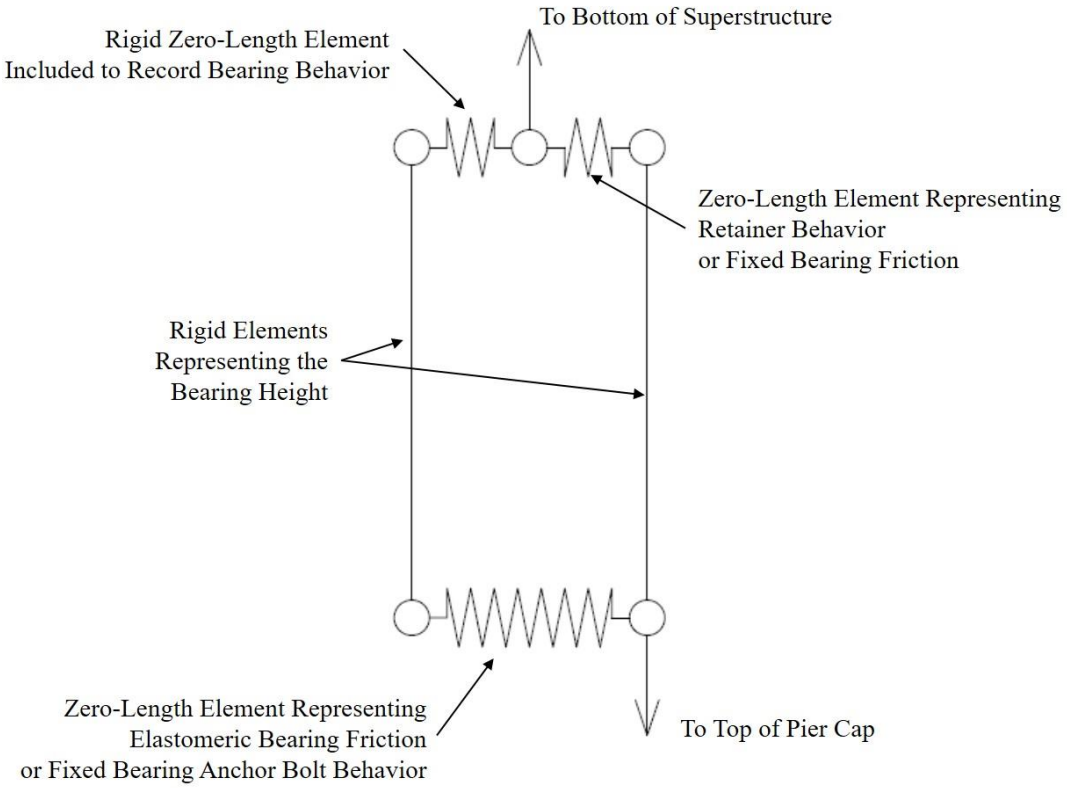

Figure 4.19: Arrangement of the bearing components and their related components used to connect the superstructure and pier cap.

4.3.4 Fixed Bearings

Low-profile fixed bearings restrain horizontal movement and are composed of two steel plates connected by pintles, as shown in Fig. 4.20. The bottom steel plate is connected to the pier cap using anchor bolts and the top steel plate is connected to a superstructure girder (IDOT, 2012a).

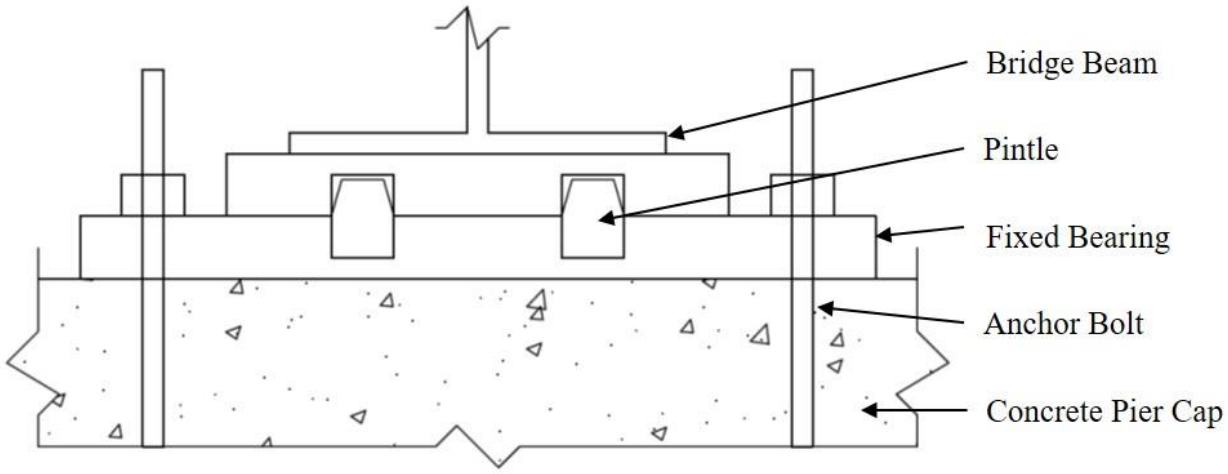

Figure 4.20: Diagram of a low-profile fixed bearing.

Low-profile fixed bearings have been experimentally studied to determine their monotonic static and cyclic loading behavior (LaFave *et al.*, 2013b; Steelman *et al.*, 2014). The experiments demonstrated that the primary fuse in the fixed bearing (the component that will fail first) is the anchor bolts (LaFave *et al.*, 2013b). Given this, the bearing model accounts for the shear behavior of the steel anchor bolts and the friction occurring between the plate and concrete after the anchor bolts fracture. The behavior of the steel anchor bolts, shown in Fig. 4.21, is similar to the behavior of the side retainers shown in Fig. 4.18 in that they both exhibit an elasto-plastic response. The yielding and ultimate capacity of each bolt is accounted for using Eq. (4.12) where ϕ = 1, 0.6 is based on the von Mises failure criterion for shear failure, 0.8 accounts for the reduction in the bolt area due to the threads, A_b is the nominal bolt diameter, and $F_{u\ or\ y}$ is the ultimate or yielding strength of the bolts (60 ksi and 36 ksi, respectively based on LaFave *et al.* (2013b)). Note that

Fig. 4.21a differs from Fig. 4.18a in that the fixed bearing engages immediately, whereas there is a gap before the retainer engages. The lack of a gap in the fixed bearing is also reflected in the cyclic behavior of Fig. 4.21b.

$$P_{fix,u\ or\ y} = \phi 0.6 * 0.8 A_b F_{u\ or\ y} \tag{4.12}$$

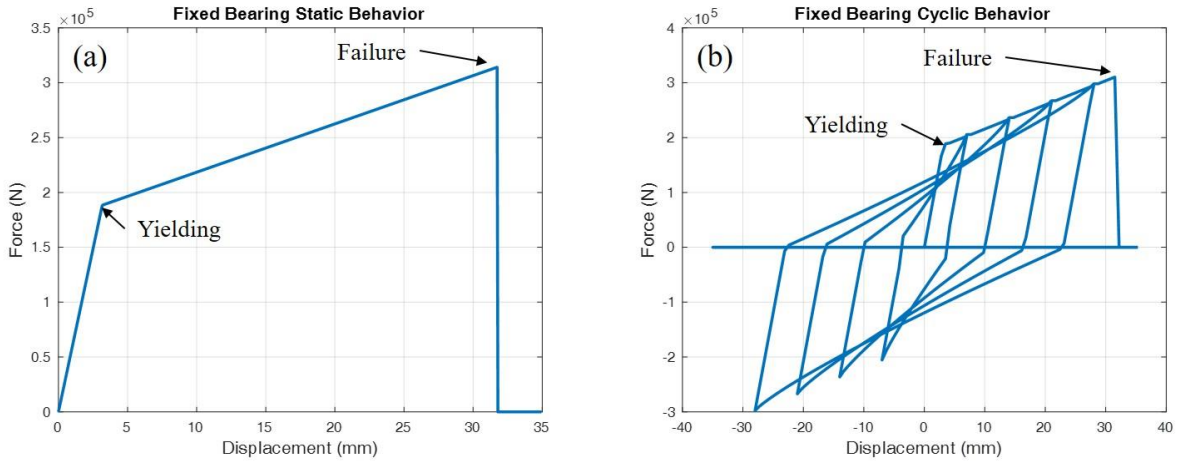

Figure 4.21: Sample (a) monotonic static and (b) cyclic low-profile fixed bearing behavior for a bearing using 1.25-in diameter steel anchor bolts.

Fig. 4.21 demonstrates that the low-profile fixed bearings are unable to resist lateral loads once fracture of the anchor bolts occurs. Upon fracture of the anchor bolts, the fixed bearings slide and are resisted by friction between a very thin elastomer pad attached to the bottom steel plate and the pier cap concrete. This friction is represented using the same model as the elastomeric bearings, presented in Fig. 4.17, but with different coefficients of friction. For the low-profile fixed bearings, the stiffness is 40 kip/in, the initial slip coefficient of friction is μ_I = 0.31, the kinematic/sliding coefficient of friction is μ_K = 0.3, and the post-slip coefficient of friction is μ_{PS} = 0.305 based on results from LaFave *et al.* (2013b).

The low-profile fixed bearing is arranged in a similar fashion to the elastomeric bearings and side retainers are in the IAB model. As indicated in Fig. 4.19, the elastomeric bearing friction behavior is replaced by the fixed bearing behavior caused by the anchor bolt while the retainer

behavior is replaced by the fixed bearing friction behavior. The arrangement of these elements in the model once again accounts for the height of the bearing such that the distance between the pier cap and superstructure girders is accurately represented.

4.3.5 Pier Columns

There is evidence of significant damage to pier columns during earthquake events (Waldin *et al.*, 2012). As such, the four circular pier columns of the IABs are explicitly modeled between the pier cap and pile cap at each pier. The pile caps and pier caps are modeled as rigid since they are much stiffer and stronger than the columns. While the pile and pier caps are modeled as rigid, their masses, along with the column masses, are still accounted for in the IAB model. As indicated in Fig. 4.22, the pier columns are modeled using distributed plasticity column elements and span between the top of the pile cap and the bottom of the pier cap. The rigid pile cap elements account for the appropriate dimension of the section with four smaller vertical rigid elements attaching the columns to the main horizontal pile cap element. A similar procedure is used in the pier cap, which accounts for the pier cap dimensions though four vertical rigid elements attached to the top of the pier columns and six, seven, or eight (depending on the bridge) vertical rigid elements attaching the pier cap to the bottom of the bearing elements.

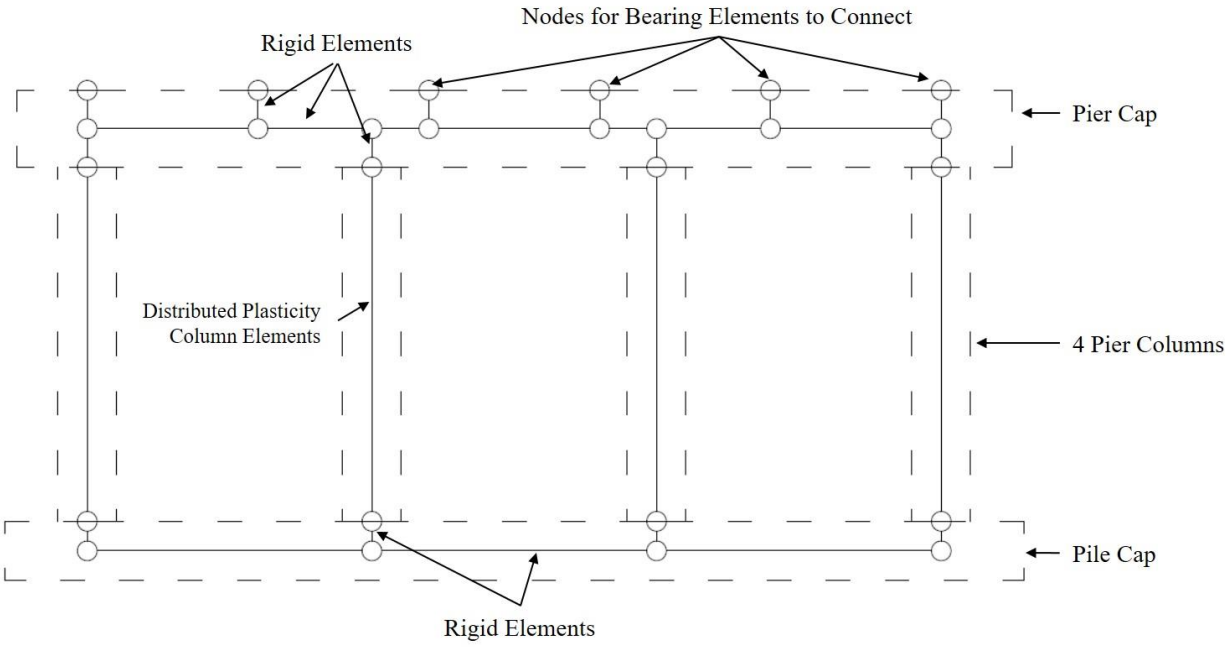

Figure 4.22: Schematic of the pier model illustrating element placement in relation to real geometry.

The distributed plasticity column elements used to represent the pier columns are force-based beam-column elements developed by Scott and Fenves (2006). This element models the columns by dividing them into three regions: two plastic hinge regions surrounding a center linear elastic region. This discretization of the column is demonstrated in Fig. 4.23a where the plastic hinge region length, l_p, is defined by Eq. (4.13) where L is the distance from the critical section to the point of contraflexure, f_y is the reinforcing steel yield strength (60 ksi), d_b is the diameter of the reinforcing steel bars, and f_c' is the concrete compressive strength (3.5 ksi) (Berry *et al.*, 2008).

$$l_p = 0.05L + \frac{0.1 f_y d_b}{\sqrt{f'_c}} \tag{4.13}$$

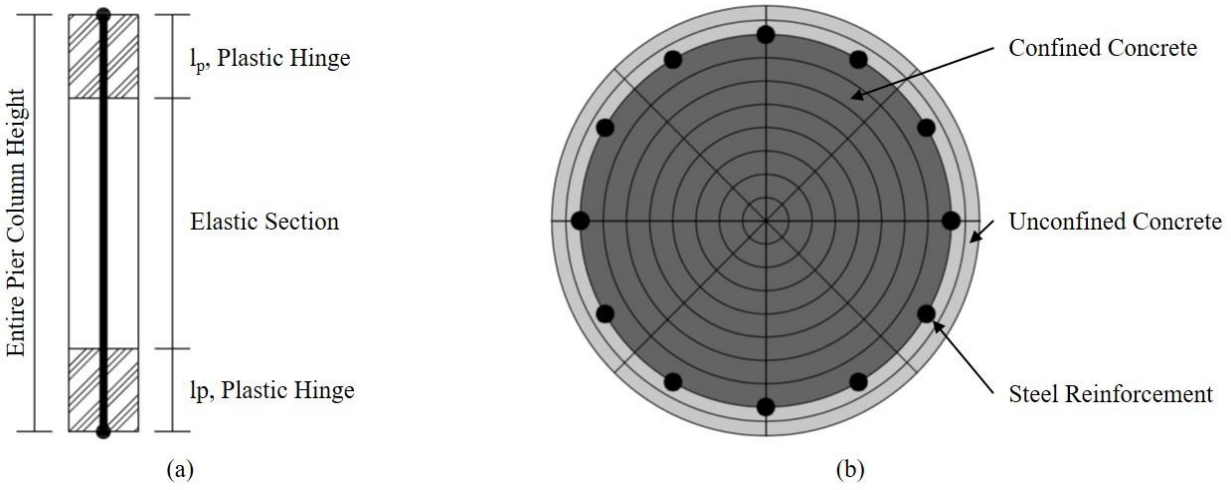

Figure 4.23: (a) Pier column model regions. (b) Plastic hinge region section.

The nonlinear behavior in the plastic hinge region is accounted for using a fiber model of the column cross section, as provided in Fig. 4.23b. The section is modeled with 8 wedges split into 10 rings. The 2 exterior rings represent the unconfined concrete, which has a compressive strength of f_c' = 3.5 ksi, a tensile capacity of $0.12f_c'$, a modulus of elasticity of $4730\sqrt{f_c'}$, and is modeled in *OpenSees* using the *Concrete02* material (linear tension softening). The inner 8 rings represent the confined concrete in the column, also modeled using the *Concrete02* material but with a compressive strength of $1.23f_c'$ and appropriate tensile capacity and modulus of elasticity values based on the confined compressive strength. The steel reinforcing bars in the column are found between the confined and unconfined concrete and are modeled in *OpenSees* with the *Steel02* material (Giuffré-Menegotto-Pinto model with steel isotropic hardening). The parameters and modeling methods described for the pier columns have been validated in Filipov *et al.* (2013b) against experiments by Kowalsky *et al.* (1999).

4.3.6 Pier Foundations

The pier foundation model is similar to the abutment foundation model. In both cases, the pile caps are modeled as rigid while the individual piles are explicitly modeled along with p-y and

t-z springs to represent the effects of the soil surrounding the piles. Unlike the abutment foundations, the pier foundations experience relatively smaller bending stresses and comprise more than one row of piles. The multiple rows of piles in the pier foundations are arranged according to IDOT design accounting for potential lateral and vertical loads applied to the IABs. The piles are typically arranged in two to three rows of 6 to 8 piles. The orientation of the piles also differs from the abutments in that strong axis bending is experienced when forces are applied in the bridge longitudinal direction.

The relatively lower bending stresses in the pier piles when compared to the abutment piles leads to some changes in the model of the pier piles as well. The discretization of the pier piles in terms of both the element and the cross section varies from the abutment piles. The pile elements are discretized such that they only extend 20 ft below the pile where they are assumed to be fixed. The bottom 10 ft of piles are discretized into (10) 12-in elastic beam-columns while the top 10 ft are discretized in (20) 6-in long nonlinear beam-columns, as seen in Fig. 4.24a. For computational efficiency, the bottom 10 elements are elastic beam-columns. A sensitivity study comparing linear elastic and nonlinear elements demonstrated negligible differences in behavior. Additionally, the nonlinear beam-column elements in the top 10 ft have sections composed of only 30 fibers, as seen in Fig. 4.24b, as opposed to the 120 fibers used in the abutment piles.

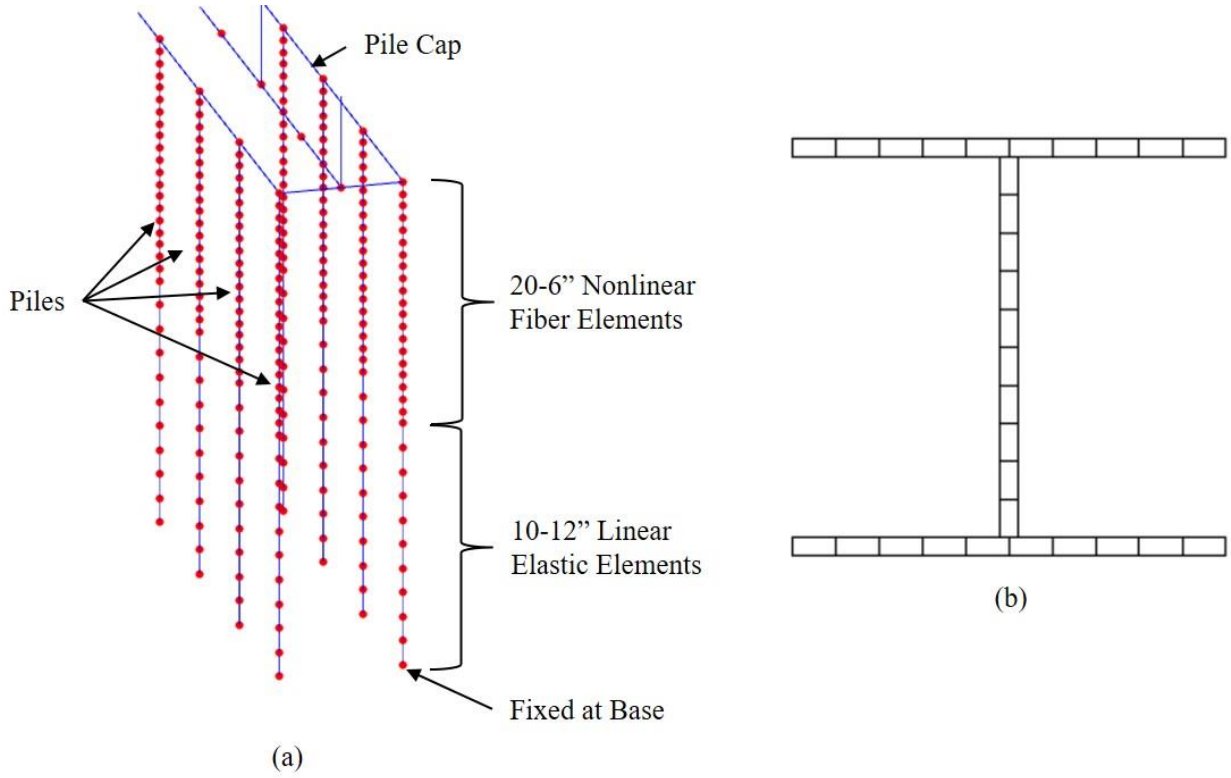

Figure 4.24: (a) Discretization of the pile elements. (b) Discretization of the nonlinear fiber elements.

The p-y and t-z springs used in the pier foundations are calculated using the same method described for the abutment foundations. Once again, the four different soil conditions shown in Fig. 4.10 are available for use. There are slight changes between the p-y and t-z curves in the pier and abutment foundations due to the potential differences in pile size (depending on design) and due to the different pile orientations used between the two abutments.

4.4 LIMIT STATES

The seismic damage limit states that track inelastic bridge behavior are divided into three categories based on their desirability – ideal, acceptable, and unacceptable. Ideal limit states act as fuses and protect more critical bridge components. The ideal limit states typically cause minimal damage or damage components that are easily replaceable or repairable, so the bridge remains functional immediately after an earthquake. Acceptable limit states do not involve severe damage,

but the damage occurs in components that are difficult to inspect or replace. Damage from acceptable limit states still allows for immediate use of the bridge after an earthquake for emergency services. Unacceptable limit states are those involving severe damage and renders the bridge unusable for emergency services immediately after a seismic event. A list of the potential limit states in the IAB model and their abbreviations are presented in Table 4.2. The limit states of all three categories are defined in more detail below

Table 4.2: Limit states of the IAB model.

Ideal Limit States	Acceptable Limit States	Unacceptable Limit States
Backfill Mobilization – BF	Abut. Pile Yielding – APY	Bearing Unseating – BU
Retainer Engagement – RE	Abut. Pile Local Buckling – APB	Severe Steel Pier Damage – SS
Retainer Yielding – RY	Abut. Pile Soil Mobilization – APS	Severe Concrete Pier Damage - CS
Retainer Fusing – RF	Pile Cap-Abut. Interface Failure – PA	Abut. Pile Rupture – APR
Fixed Bearing Yielding – FY	Pier Pile Yielding – PPY	
Fixed Bearing Fusing – FF	Pier Pile Soil Mobilization– PPS	
Bearing Sliding – BS	Moderate Steel Pier Damage – SM	
Light Steel Pier Damage - SL	Moderate Concrete Pier Damage - CM	
Light Concrete Pier Damage - CL		

4.4.1 Ideal Limit States

Nine limit states are classified as ideal limit states. The mobilization of the backfill soil at the abutments (BF) is a product of the complex SSI at the integral abutments. BF is indicated to have occurred when one of the backfill springs achieves its ultimate capacity, as shown in Fig. 4.6. Three retainer limit states are included: engagement (RE), yielding (RY), and fusing (which occurs

at anchor bolt fracture) (RF), as shown in Fig. 4.18. Retainers are ideal fuse elements (Filipov *et al.*, 2013a; LaFave *et al.*, 2013b), along with fixed bearings, which experience yielding (FY) followed by fusing (again, occurring when anchor bolt fracture occurs) (FF), as shown in Fig. 4.21. Damage to the retainers or fixed bearings leads to the onset of sliding. The bearing sliding limit state (BS) occurs if a bearing reaches the kinetic/sliding portion of the bearing friction behavior.

Light damage to the reinforcing steel (SL) and the unconfined concrete (CL) of the column piers is also classified as ideal. These are not fuse limit states, but indications of minor damage to the pier columns, which can be related to observed damage in the piers during past earthquakes (Waldin *et al.*, 2012; Wood, 2015). The light pier column damage limit states are based on the strains within the reinforcement and unconfined concrete and are determined from Kowalsky (2000) and Revell (2013). The limit states for light pier column damage as well as for moderate and severe damage are presented in Table 4.3. Steel damage corresponds to the beginning of yielding for light damage, the end of yielding for moderate damage, and rupture for severe damage. Concrete damage is represented by concrete cracking and concrete spalling for light and moderate damage, respectively. Severe concrete damage is defined as strains beyond the limit where the concrete is still repairable (Kowalsky, 2000).

Table 4.3: Corresponding strain values for pier column limit states.

Limit State	Concrete (compression)	Reinforcing Steel (Tension)
Light Damage	$-0.005 < \varepsilon_{conc} \leq -0.002$	$0.0021 \leq \varepsilon_{rebar} < 0.015$
Moderate Damage	$-0.018 < \varepsilon_{conc} \leq -0.005$	$0.015 \leq \varepsilon_{rebar} < 0.06$
Severe Damage	$\varepsilon_{conc} \leq -0.018$	$0.06 \leq \varepsilon_{rebar}$

4.4.2 Acceptable Limit States

Eight limit states are classified as acceptable. Moderate damage to the reinforcing steel (SM) and unconfined concrete (CM) of the pier columns indicates that there is a significant amount

of damage in the columns, yet not enough to cause collapse. The strain limits for moderate pier column damage are indicated in Table 4.3.

Contained damage in foundation components is acceptable since it is not expected to severely inhibit post-earthquake functionality. Yielding of the piles at the abutment (APY) and pier (PPY) foundations is indicated by the yielding of the material of any of the fibers in the steel pile cross-section. Local buckling of the abutment piles (APB) is also considered and estimated to occur when the strain in any pile fiber reaches 20 times the strain at expected yield (yield strain). This value of 20 times the yield strain is identified as the onset of local buckling through a combination of cyclic pile loading experiments and analyses (Frosch *et* al., 2009). Local buckling of the pier piles is not considered due to the significantly lower strains experienced in those when compared to the abutment piles. The difference between the strains in the abutment and pier piles is discussed further in Chapter 7. The soil surrounding the piles may also be mobilized by reaching their capacity in the abutment (APS) and pier (PPS) foundations. The APS and PPS limit states occur when the resistance in any of the p-y or t-z springs reaching the p_{ult} or t_{ult} forces. The failure of the pile cap-abutment interface (PA) is also classified in the acceptable limit state due to its occurrence not leading to a severe loss of bridge capacity. The onset of the PA limit state occurs when the failure of the dowels occurs, as seen in Fig. 4.5a and 4.5c.

4.4.3 Unacceptable Limit States

Four limit states are classified as unacceptable due to the likelihood of a loss of bridge span should any of them occur. The first limit state is bearing unseating (BU), which occurs if the bearing displaces an amount, *N*, which is the distance from the centroid of the bearing to the edge of the pier cap as shown in Fig. 4.25. Per the IDOT Bridge Manual (IDOT, 2012a), *N* (in) is calculated using Eq. (4.14). In Eq. (4.14), *L* is the length between the expansion joints (ft), *B* is the

width of the superstructure (ft), H is the height of the tallest pier (ft), α is the skew angle of the bridge (degrees), F_vS_1 is the 1 sec period spectral response coefficient, and B/L is a that which must not exceed 3/8.

$$N = \left[3.94 + 0.0204L + 0.084H + 1.087\sqrt{H}\sqrt{1 + \left(2\frac{B}{L}\right)^2}\right]\frac{1+1.25F_vS_1}{\cos\alpha} \qquad (4.14)$$

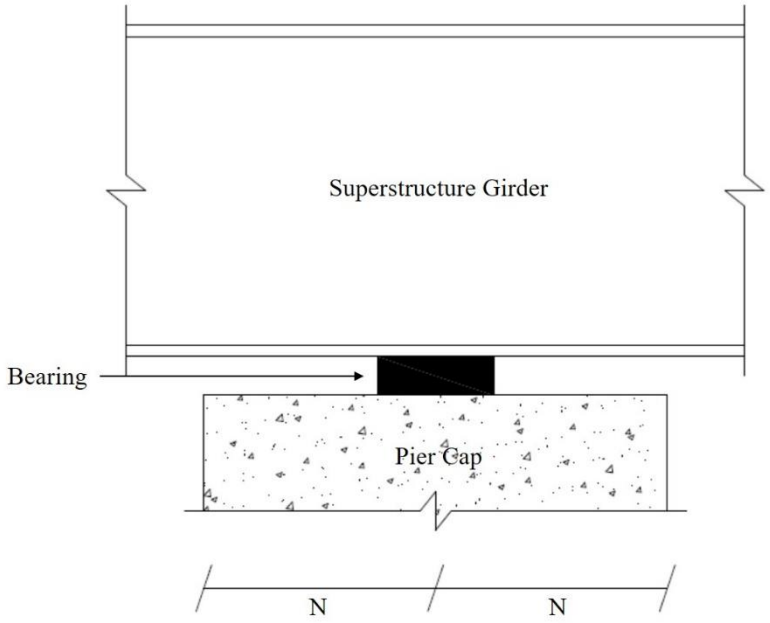

Figure 4.25: Unseating distance for the bearings.

A loss of span may also occur if there is severe damage to the pier columns. Severe damage to the reinforcing steel (SS) or unconfined concrete (CS) of the pier columns, indicated by strains in Table 4.3, could compromise the vertical load-carrying capacity of the column and make travel on the bridge dangerous immediately after an earthquake. The occurrence of any of the three unacceptable limit states during an earthquake would result in a dangerous bridge that could not be crossed and would significantly hinder emergency response.

Rupture of the abutment piles (APR) is also identified as an unacceptable limit state due to a bridge becoming dangerous to use once piles have cracked and ruptured. The APR limit state

identified in this study is based on judgement and is estimated to occur when the strain in any pile fiber reaches a value of 40 times the yield strain of the steel. This value may be slightly conservative when compared to monotonic static analyses of steel pile behavior, however it is anticipated that the cyclic behavior of the loading will decrease the values of these monotonic static results.

Most of the ideal and acceptable limit states directly correspond with a change in behavior occurring in the component models. Unlike those limit states, the unacceptable limit states do not correspond to any changes in behavior but instead only identify when certain strain or displacement limits are reached. Given this, the bridge continues to behave normally once these limit states occur despite severe adverse effects occurring in actual bridges should these strains or displacements be achieved. Any behavior beyond the occurrence of the first unacceptable limit state is not meaningful and discarded in analyses such as the pushover analyses of Chapter 6.

CHAPTER 5: PARAMETRIC STUDY OF SOUTHERN ILLINOIS IABS

The IAB models developed in Chapter 4 are used in a parametric study of IAB seismic behavior. The parametric study includes a range of IABs that have typically been designed and constructed in Illinois in the past. The parametric study also includes IABs designed for use in the near future, which incorporate newer design properties such as longer spans than previously constructed for IABs. The bridges in the parametric study are designed using the IDOT Bridge Manual (IDOT, 2012a) and other IDOT references which provided updated information not found in the Bridge Manual. The IABs in the parametric study are designed for the city of Cairo due to its proximity to the NMSZ, which is responsible for the high seismic hazard in southern Illinois

5.1 BRIDGES IN THE PARAMETRIC STUDY

The parametric study matrix represents the most common IABs in Illinois based on discussion with IDOT and study of the IAB inventory in southern Illinois. The 51 scenarios, described further in Table 5.1, are developed by varying the bridge's superstructure material and span configuration, the height of the piers, the layout of the bearings at the pier locations, and the foundation soil condition. Additionally, variations in seismic hazard are also investigated through varying the site of the bridge throughout southern Illinois. These variations are explored using the bridge analyses described in Chapters 6, 7, and 8, with naming convention provided in Fig. 5.1. For this study, no skew is considered. Although many IABs in Illinois include skew, a fundamental study of IAB seismic behavior without skew is imperative before adding the complexity of skew.

Table 5.1: Matrix of IABs analyzed in the parametric study.

Parameter	Alternatives	IAB Type 1 1-Span Steel	IAB Type 2 3-Span Steel				IAB Type 3 4-Span Steel				IAB Type 4 3-Span Concrete				IAB Type 5 4-Span Concrete			
		1	2	3	4	5	6	7	8	9	10	11	12	13	14	15	16	17
Span Configuration	145' - 160' - 160' - 145'						*	*	*	*					*	*	*	*
	80' - 120' - 80'		*	*	*	*					*	*	*	*				
	160'	*																
Pier Type	Multi-Column	N/A	*	*	*	*	*	*	*	*	*	*	*	*	*	*	*	*
Pier Height	Short - 15'		*	*			*	*			*	*			*	*		
	Tall - 40'				*	*			*	*			*	*			*	*
Bearing Layout	All Fixed		*		*		*		*		*		*		*		*	
	All Type I Elastomeric			*		*		*		*		*		*		*		*
Foundation Soil Condition	Stiff	The above (17) bridges are modeled with all three foundation soil conditions (Stiff, Soft, and Alluvial/Non-Alluvial)																
	Soft																	
	Alluvial/Non-Alluvial																	

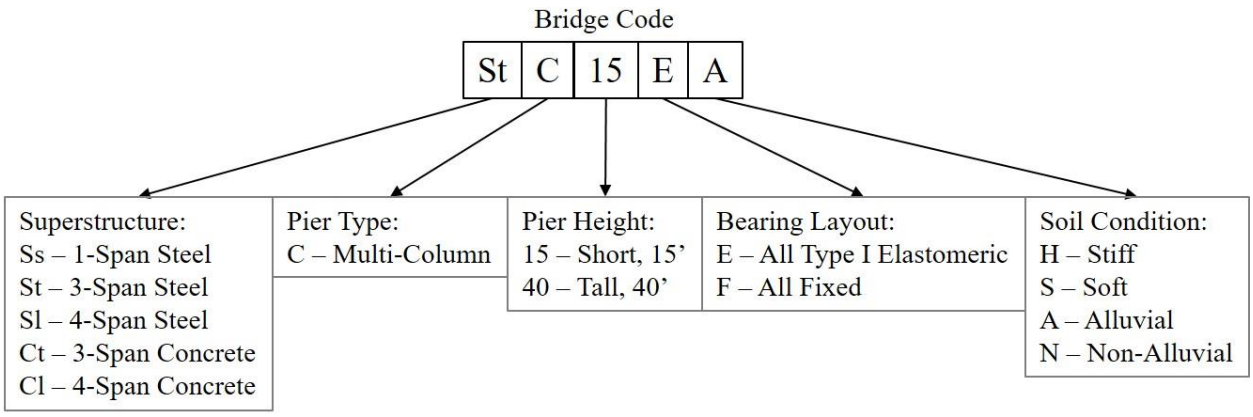

Figure 5.1: Bridge model naming convention.

5.1.1 IAB Superstructure Material and Span Configuration

The parametric study considers five IAB superstructures, and this set contain two superstructure girder materials and three span configurations. The two superstructure girder types are steel plate girders and precast prestressed concrete (PPC) girders. The steel girders are based on typical designs while the PPC girder properties are taken from the IDOT All Bridge Designers Memorandum 15.2 concerning PPC IL-shapes (IDOT 2015a). This Memorandum contains information on updated PPC shapes used by IDOT to design for longer spans than previously constructed. The designs of the girders for each of the five superstructures is discussed in a later subsection.

The three span configurations investigated in the parametric study include single-span (1-span), 3-span, and 4 span IABs. The single-span bridge is only considered with steel girders (Ss in the naming convention of Fig. 5.1) while the 3- and 4-span IABs are considered for both steel girders (St and Sl in the naming convention of Fig. 5.1 for 3- and 4-span, respectively) and concrete girders (Ct and Cl in the naming convention of Fig. 5.1 for 3- and 4-span, respectively). Only steel girders are considered for single-span bridges since the superstructures are modeled as elastic and differences in response between concrete and steel single-span bridges are minimal. The single-

span bridges span 160-ft between the abutments. The three-span IABs represent typical spans for southern Illinois. These bridges consist of exterior spans of 80-ft between the abutments and piers and a central span of 120-ft between the piers. The four-span IABs consist of exterior spans of 145-ft between the abutments and the piers and two interior spans between piers of 160-f. The four-span bridges are included in the study as a maximum span that could be encountered with IDOT design since the overall span of 610-ft is the maximum allowed in the abutment pile selection charts (IDOT, 2012b). The individual 160-ft span is one of the longest possible span lengths for design with the PPC IL-shapes (IDOT, 2015a). Diagrams of the three span configurations are provided in Fig. 5.2 along with their model representations in Fig. 5.3.

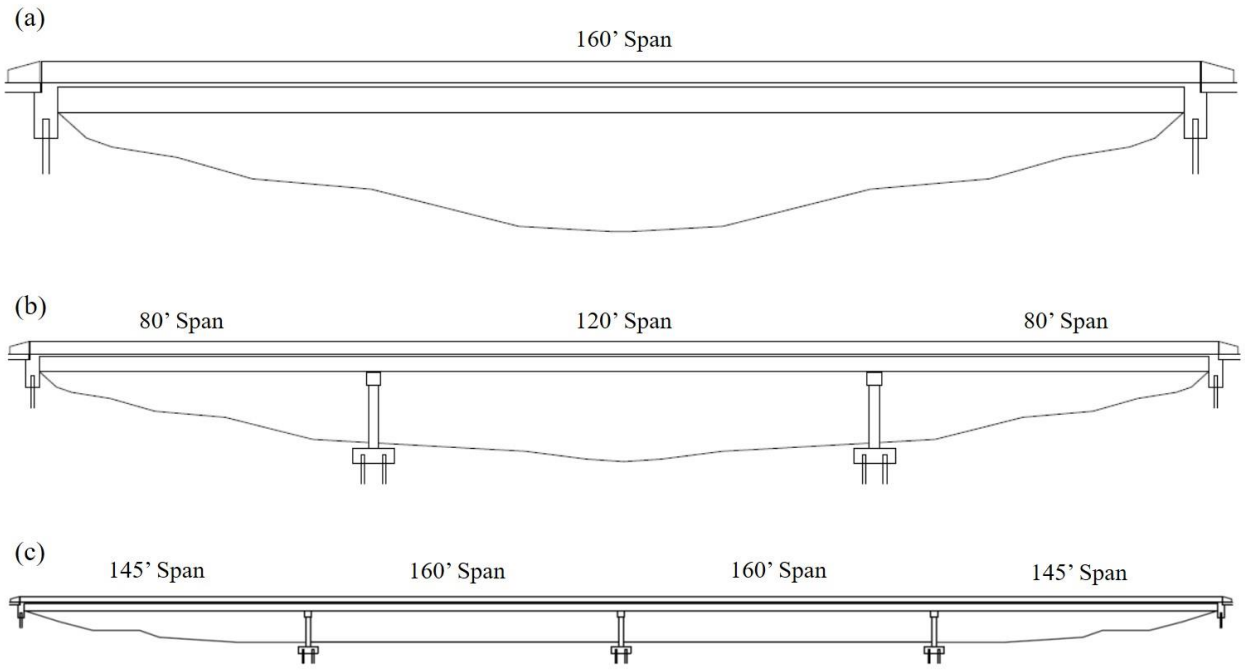

Figure 5.2: Diagrams of the three span configurations considered in the parametric study: (a) 1-span, (b) 3-span, (c) 4-span.

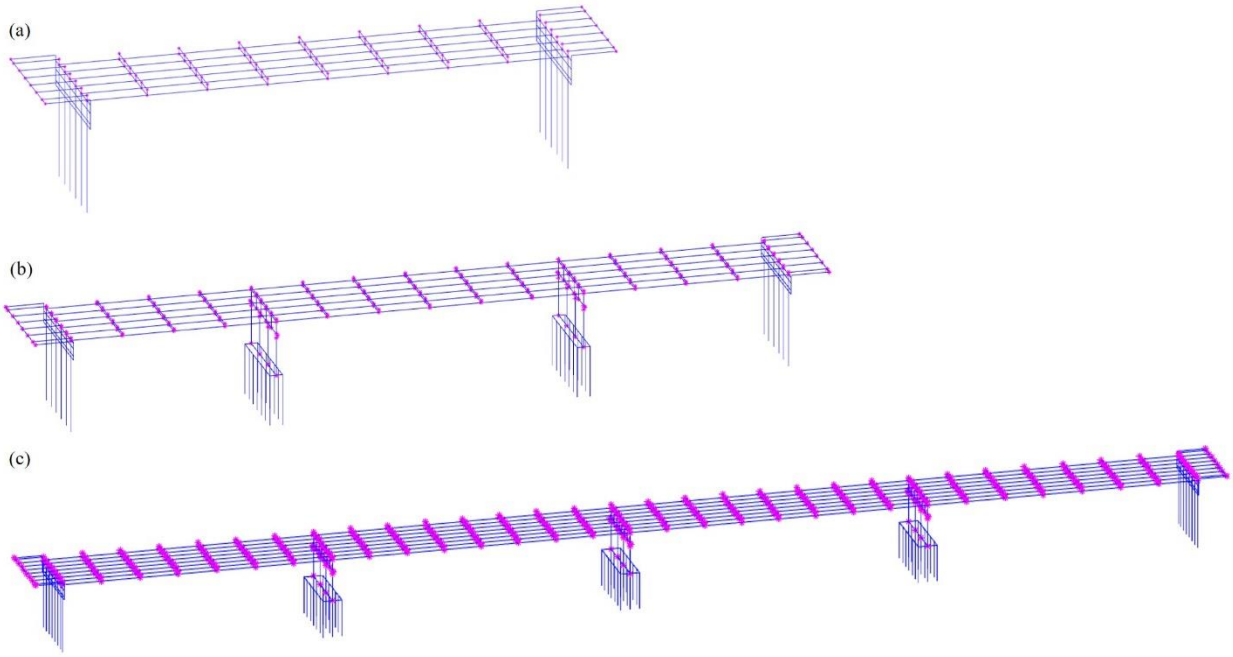

Figure 5.3: Model representations of bridges with the three span configurations considered in the parametric study: (a) 1-span, (b) 3-span, (c) 4-span.

5.1.2 Multi-Column Piers

Illinois bridges are typically designed to have either wall piers or multi-column piers, as shown in Fig. 5.4. Both of these options have been studied in past Illinois bridge seismic studies, but it has been found that there is a negligible difference between the use of walls or columns at the piers in terms of seismic response (LaFave *et al.*, 2013a). For this reason, and to reduce the computational expense of the parametric study, only multi-column piers with four columns (C in the naming convention of Fig. 5.1) are considered in the IABs of the parametric study.

Although past seismic Illinois bridge studies have indicated that the type of pier does not have a significant effect on the seismic behavior of the bridge, they have indicated that the clear height of the piers does have a significant influence on seismic behavior (LaFave *et al.*, 2013a). The clear height of the piers, the height between the top of the pile cap and the bottom of the pier cap as indicated in Fig. 5.4, is varied in the parametric study between a relatively short pier and a taller pier. The short pier clear height is 15 ft (15 in the naming convention of Fig. 5.1) while the

tall pier is represented by a clear height of 40 ft (40 in the naming convention of Fig. 5.1). The designs of the pier columns vary depending on the IAB, as discussed in a later subsection.

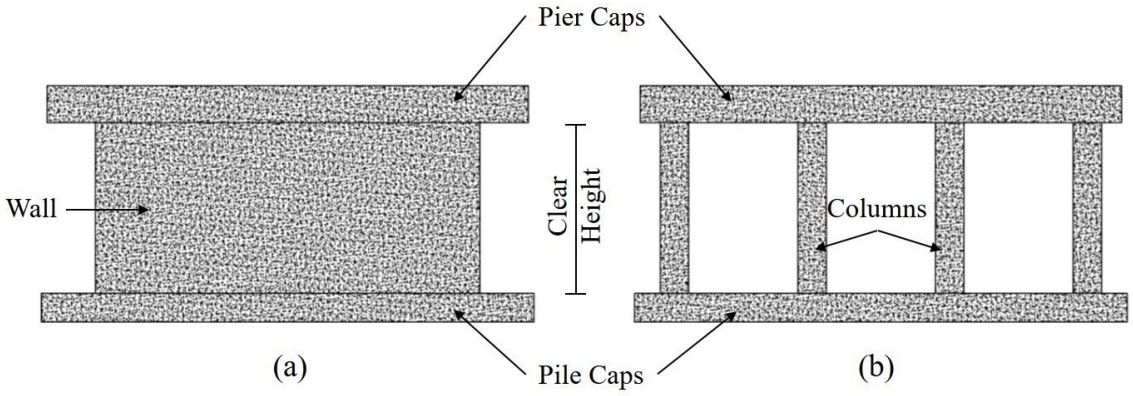

Figure 5.4: Two of the most common pier types used in Illinois: (a) wall pier; (b) multi-column pier.

5.1.3 Bearing Layout

Type I elastomeric bearings and low-profile fixed bearings are considered in the parametric study. While stub abutment bridges typically have bearings at both the abutments and piers, bearings are not needed at the abutments in IABs. Whereas stub abutment bridges require fixed bearings at one pier, IABs are restrained at the ends and may employ elastomeric bearings at all piers. Although uncommon in practice, the case of fixed bearings at all piers is also considered based on IDOT interest in a very stiff bridge scenario.

The elastomeric bearings considered in the parametric study are all Type I elastomeric bearings (E in the naming convention of Fig. 5.1). As indicated in Chapter 4, Type II elastomeric bearings were found to have detrimental effects on the seismic behavior of stub abutment bridges (LaFave *et al.*, 2013a) and are being used less in seismic design, so they are not considered in this study. Each Type I elastomeric bearing is accompanied by side retainers in the bridge transverse direction. The fixed bearings considered in the parametric study are low-profile fixed bearings (F

in the naming convention of Fig. 5.1). The size of the elastomeric bearings and the anchor bolts for the retainers and fixed bearings are discussed in a later subsection.

5.1.4 Foundation Soil Conditions

Four foundation soil conditions are considered in the parametric study; stiff soil (H in the naming convention of Fig. 5.1), soft soil (S in the naming convention of Fig. 5.1), alluvial soil (A in the naming convention of Fig. 5.1) and non-alluvial soil (N in the naming convention of Fig. 5.1). The soil conditions are used to define the p-y and t-z springs of the pier and abutment foundations, as explained in Chapter 4. As discussed earlier, the stiff and soft soil conditions are based on the realistic bounds of soil for southern Illinois (Luo *et al.*, 2016) and the alluvial and non-alluvial soil conditions are based on actual soil data for southern Illinois (Kozak *et al.*, 2017a).

The stiff and soft soil conditions are considered for all sites to represent the realistic bounds. However, only one of the alluvial and non-alluvial soil conditions are considered for each site, leading to a total of three soil conditions for each site. The use of either alluvial or non-alluvial soil conditions at a site is based on the local geology of the site described in Chapter 3 with Benton, Cairo, East St. Louis, Mt. Carmel, Salem, and Sparta having alluvial soil conditions and Anna, Carbondale, Eldorado, and Elizabethtown having non-alluvial soil conditions. In summary, the three soil conditions considered in the majority of the parametric study for Cairo are the stiff, soft, and alluvial soil conditions.

5.1.5 Ground Motion Intensity Variations from Different Site Locations

The majority of the parametric study considers only the soil conditions and seismic hazard for Cairo. This is due to Cairo being the closest location in Illinois to the New Madrid Seismic Zone and therefore experiences the largest intensity of ground motion shaking and increased seismic hazard. The parametric study also investigates changes to the seismic hazard and intensity

of ground motions shaking by varying the location of the site being investigated. In general, sites further north in Illinois typically have less intense ground motions in terms of spectral acceleration. This is demonstrated in Fig. 1.1 through the seismic performance zone designation of sites further north in the state are related to smaller design spectral accelerations at the 1.0 s period than at sites further south. 10 sites are considered which span seismic performance zones 2, 3, and 4. These sites correspond to the 10 sites described in Chapter 3 and the ground motion intensity is varied in the study by using the appropriate ground motions developed for each site.

This portion of the parametric study is reported in Chapter 8 and differs from the parametric study in terms of the bridges it considers. The bridges considered in this portion of the parametric study include the IABs with 15-ft tall piers, elastomeric bearings, and either the alluvial or non-alluvial soil conditions only. The soil condition is determined based on the local geology of the site described in Chapter 3. This leads to the consideration of 5 IABs for each site: Ss____A or Ss____N, StC15EA or StC15EN, SlC15EA or SlC15EN, CtC15EA or CtC15EN, and ClC15EA or ClC15EN.

5.2 BRIDGE DESIGN DETAILS

The bridge parameters considered in the parametric study includes IAB designs for each of the 51 different variations. The IAB designs are based on the IDOT Bridge Manual (IDOT, 2012a), IDOT All Bridge Designers Memorandum 12.3 concerning IABs (IDOT, 2012b), and input from IDOT to ensure the designs are typical for the state. The IABs designed for the parametric study represent typical designs of existing single-span and 3-span bridges as well as designs for the long 4-span IAB which are beginning to be designed for future use.

5.2.1 Superstructure Details

The girders and diaphragms/permanent bracing are designed for each of the five main bridge types (single-span steel, 3-span steel, 4-span steel, 3-span concrete, and 4-span concrete). The design details of the girders used in the IABs are described first, followed by the design details of the diaphragms/permanent bracing. The decks of all the bridges are 43-ft 2-in width and have an 8-in thickness. This common deck width is used for consistency across all bridges. Table 5.2 provides general information about the bridge superstructures, and Tables 5.3 and 5.4 provide more detailed superstructure information concerning the superstructure weight and shape properties, which are used in modeling.

The girder designs, per IDOT standard practice are described in Table 5.2 and shown to-scale against each other in Fig. 5.5. They are: 70-in deep plate girders for the single-span steel IAB, 40-in deep plate girders for the 3-span steel IAB, 60-in deep plate girders for the 4-span steel IAB, 54-in deep IL54-2438 PPC shapes for the 3-span concrete IAB, and 72-in deep IL72-3838 PPC shapes for the 4-span concrete IAB. The number of girders and the spacing of these girders are based on the girder properties and span loads for each bridge. The IL72-3838 PPC shape used in the 4-span concrete IAB is the largest IL-shape available in order to span the 160-ft center-spans.

Table 5.2: General superstructure details.

	1-Span Steel	**3-Span Steel**	**4-Span Steel**	**3-Span Concrete**	**4-Span Concrete**
Girder	70" Plate Girder: 5/8"x70" Web, 1-5/8"x16" Flanges	40" Plate Girder: 1/2"x40" Web, 1-1/2"x12" Flanges	60" Plate Girder: 5/8"x60" Web, 1"x24" Flanges	IL54-2438 PPC Girder, 44B-2T-8db-4d Strand Pattern	IL72-3838 PPC Girder, 58B-2T-8db-6d Strand Pattern
Girder Count	6	6	8	6	7
Girder Spacing	7'-0"	7'-3"	5'-6"	7'-3"	6'-2"
Deck Width	43'-2"	43'-2"	43'-2"	43'-2"	43'-2"
Deck Thickness	8"	8"	8"	8"	8"
Diaphragm	IDOT Cross-Frame (see Fig. 5.6)	C15x40	IDOT Cross-Frame (see Fig. 5.6)	2'-6" Wide Concrete at Piers, MC12x31 Permanent Bracing at Non-Piers	2'-6" Wide Concrete at Piers, MC18x42.7 Permanent Bracing at Non-Piers

Table 5.3: Detailed steel superstructure information used for bridge modeling.

Basic Deck Properties	**Bridge Type**		
	1-Span Steel	**3-Span Steel**	**4-Span Steel**
Deck width - m (ft)	13.1572 (43.1667)	13.1572 (43.1667)	13.1572 (43.1667)
Deck thickness - cm (in)	20 (8)	20 (8)	20 (8)
Girder type	177.8cm PL Girder (70" PL Girder)	101.6cm PL Girder (40" PL Girder)	152.4cm PL Girder (60" PL Girder)
Span lengths - m (ft)	49 (160)	24-37-24 (80-120-80)	44-49-49-44 (145-160-160-145)
Shortest Span - m (ft)	49 (160)	24 (80)	44 (145)
Longest Span - m (ft)	49 (160)	37 (120)	49 (160)
Girder spacing - m (ft)	2.1 (7.0)	2.2 (7.25)	1.7 (5.5)
Girder Depth - cm (in)	186 (73.25)	109 (43)	157 (62)
Girder Area - cm^2 (in^2)	618 (95.75)	361 (56)	552 (85.5)
Girder I_{xx} - cm^4 (in^4)	3519986 (84568)	756459 (18174)	2326983 (55906)
Girder I_{yy} - cm^4 (in^4)	46235 (1110.8)	17998 (432.4)	95950 (2305.2)
Total Girder Weight - kN/m (kips/ft)	29 (1.9549)	17 (1.1433)	34 (2.3275)
Concrete Deck Weight - kN/m (kips/ft)	63 (4.3167)	63 (4.3167)	63 (4.3167)
Asphalt Topping Weight (1.5") - kN/m (kips/ft)	12 (0.8094)	12 (0.8094)	12 (0.8094)
Parapets Weight - kN/m (kips/ft)	11 (0.75)	11 (0.75)	11 (0.75)
Total deck weight - kN/m (kips/ft)	114 (7.8309)	102 (7.0194)	120 (8.2035)
Deck Modeling Properties (Based on concrete stiffness of 23.2 MPa / 3370 ksi)			
Transverse composite modulus I_{yy} - m^4 (ft^4)	81 (9374.8)	65 (7546.0)	95 (10963.6)
Vertical composite modulus I_{xx} - m^4 (ft^4)	3.37 (390.9)	0.86 (99.7)	2.85 (330.2)
Composite area - m^4 (ft^2)	0.54 (63.1)	0.42 (48.8)	0.60 (69.6)

Table 5.4: Detailed concrete superstructure information used for bridge modeling.

Basic Deck Properties	**Bridge Type**	
	3-Span Concrete	**4-Span Concrete**
Deck width - m (ft)	(13.1572) (43.1667)	13.1572 (43.1667)
Deck thickness - cm (in)	20 (8)	20 (8)
Girder type	IL54-2438: 44B-2T-8db-4d Strand Pattern	IL72-3838: 58B-2T-8db-6d Strand Pattern
Span lengths - m (ft)	24-37-24 (80-120-80)	44-49-49-44 (145-160-160-145)
Shortest Span - m (ft)	24 (80)	44 (145)
Longest Span - m (ft)	37 (120)	49 (160)
Girder spacing - m (ft)	2.2 (7.25)	1.9 (6.1667)
Girder Depth - cm (in)	137 (54)	183 (72)
Girder Area - cm^2 (in^2)	5510 (854)	6822 (1057.4)
Girder I_{xx} - cm^4 (in^4)	12296600 (295427)	30727702 (738236)
Girder I_{yy} - cm^4 (in^4)	2139554 (51403)	2936887 (70559)
Total Girder Weight - kN/m (kips/ft)	78 (5.34)	113 (7.714)
Concrete Deck Weight - kN/m (kips/ft)	63 (4.3167)	63 (4.3167)
Asphalt Topping Weight (1.5") - kN/m (kips/ft)	12 (0.8094)	12 (0.8094)
Parapets Weight - kN/m (kips/ft)	11 (0.75)	11 (0.75)
Total deck weight - kN/m (kips/ft)	164 (11.2160)	198 (13.5900)
Deck Modeling Properties (Based on concrete stiffness of 23.2 MPa / 3370 ksi)		
Transverse composite modulus I_{yy} - m^4 (ft^4)	100 (11630.6)	127 (14736.9)
Vertical composite modulus I_{xx} - m^4 (ft^4)	2.00 (231.7)	4.76 (551.3)
Composite area - m^4 (ft^2)	0.65 (75.4)	0.83 (96.1)

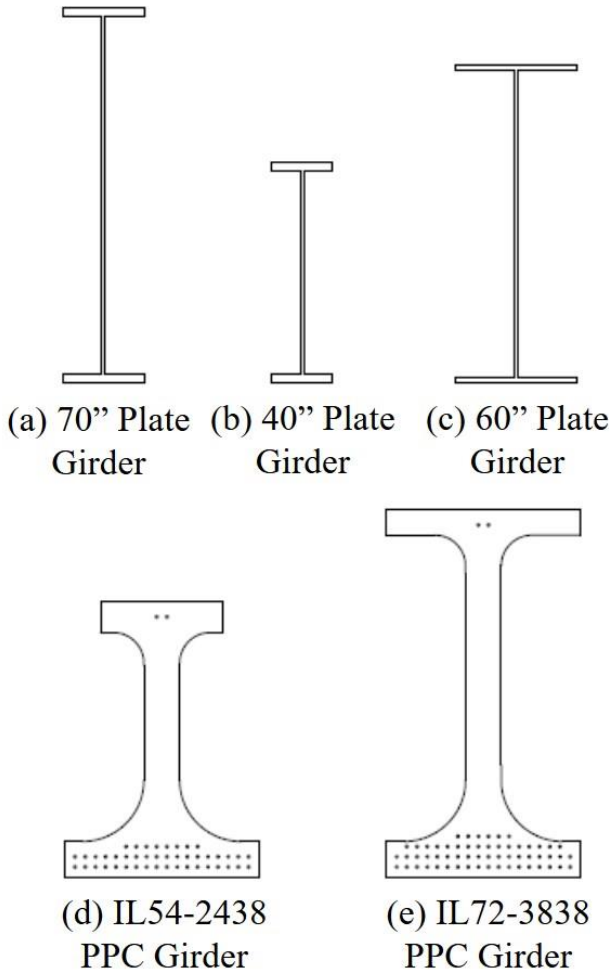

Figure 5.5: The girders used in the (a) single-span steel IAB, (b) 3-span steel IAB, (c) 4-span steel IAB, (d) 3-span concrete IAB, and (e) 4-span concrete IAB.

The steel diaphragms between the steel girders and the permanent bracing between the PPC girders are also designed using the IDOT Bridge Manual (IDOT, 2012a). As stated in Table 5.2, the single-span and 4-span steel IABs use a cross-frame between the girders. The cross-frame, whose details are provided in Fig. 5.6, consists of two L4x4x3/8 sections forming an X along with another L4x4x3/8 section parallel to the horizontal along the bottom of the cross-frame. This cross-frame was modeled by accounting for the area, the moment of inertia in both plane directions, and the polar moment of inertia through a representative single element. This single element is also used to represent the C15x40 section used as a diaphragm for the 3-span steel IAB, and the

MC12x31 and MC 18x42.7 sections used as permanent bracing in the 3-span and 4-span concrete IABs, respectively (IDOT, 2012a). At the pier locations of concrete IABs there are no permanent bracing members, instead having a 2-ft 6-in wide concrete section at that location (IDOT, 2012a).

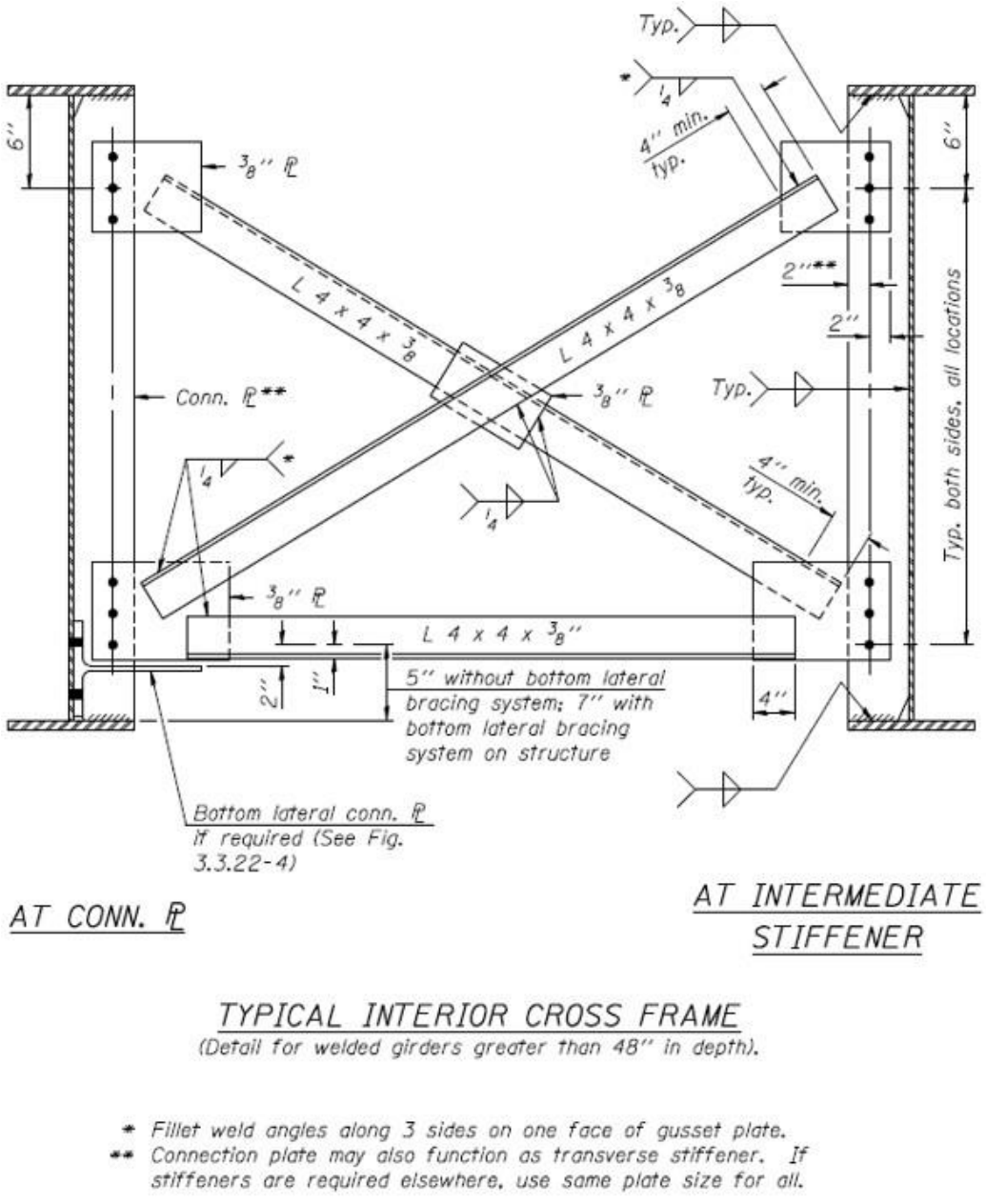

Figure 5.6: Cross-frame used as the diaphragm element for single-span and 4-span steel IABs (IDOT, 2012a).

5.2.2 Bearing Details

The Type I elastomeric bearings, their accompanying side retainers, and the low-profile fixed bearings are designed with input from IDOT and IDOT bearings tables to ensure they meet typical bearing sizes for four of the five main bridge types (the single-span IAB does not have piers and therefore does not require bearings). The number of bearings at each pier is equal to the number of girders. The design for the Type I elastomeric bearings involves determining which pre-existing bearing size should be used. The design for the side retainers involves designing the diameter of the anchor bolts used. Similar to the side retainers, the low-profile fixed bearings are also designed by specifying the diameter of the anchor bolts. The design parameters are used to calibrate the modeled bearings against experimental results.

Table 5.5: Details of Type I elastomeric bearings used in the parametric study.

Parameter	15-a (3-Span Steel)	20-d (4-Span Steel)	13-b (3-Span Concrete)	18-d (4-Span Concrete)
Width in Long. Dir. (in.)	15	20	13	18
Length in Tran. Dir. (in.)	24	24	20	24
Elastomer Height (in.)	2.25	5.69	2.50	5.25
Number of Shims	2	6	3	6
Spacing of Shims (in.)	0.75	0.8125	0.625	0.75
Steel Shim Thickness (in.)	0.1875	0.1875	0.1875	0.1875

Existing Type I elastomeric bearings are used for design per the IDOT All Bridge Designers Memorandum 15.6 (IDOT, 2015b) concerning elastomeric bearing sizes. The main details for the elastomeric bearing designs are the elastomer width in the bridge longitudinal direction, the elastomer length in the bridge transverse direction, and the elastomer height, as well as the number, spacing, and thickness of the steel shims within the elastomer. The Type I elastomeric bearings used in the bridge designs are 15-a bearings for the three-span steel IAB, 20-d bearings for the four-span steel IAB, 13-b bearings for the three-span concrete IAB, and 18-d

bearings for the four-span concrete IAB. Details for these four Type I elastomeric bearings are provided in Table 5.5.

The side retainers that accompany the Type I elastomeric bearings in the transverse direction and the low-profile fixed bearings are both controlled by their anchor bolts since these are the weak links that cause fusing. Through discussion with IDOT, it was determined that the sizes of the anchor bolts for both the retainers and fixed bearings are the same for each bridge. A summary of the anchor bolt diameters used for each IAB is presented in Table 5.6.

Table 5.6: Side retainer and low-profile fixed bearing anchor bolt sizes for the IABs of the parametric study.

IAB	3-Span Steel	4-Span Steel	3-Span Concrete	4-Span Concrete
Retainer and Fixed Bearing Anchor Bolt Diameter (in.)	1.25	2.00	1.00	1.50

5.2.3 Pier Column Details

The columns at each pier are designed to accommodate the axial and lateral forces potentially encountered in the bridge. For simplicity the design of the columns remained consistent depending on the clear height of the columns. The single-span IAB does not require pier columns due to its lack of piers, but the three-span and four-span IABs each use both the short (15-ft clear height) and tall (40-ft clear height) piers. The piers for each bridge were designed to use four circular pier concrete columns, as shown in Fig. 5.4. The design for the short pier columns involved a 2-ft 6-in diameter column reinforced with (12) #10 reinforcing bars. The tall pier columns were designed as 3-ft diameter concrete columns reinforced with (14) #11 reinforcing bars. Cross-sections of the two columns are presented in Fig. 5.7.

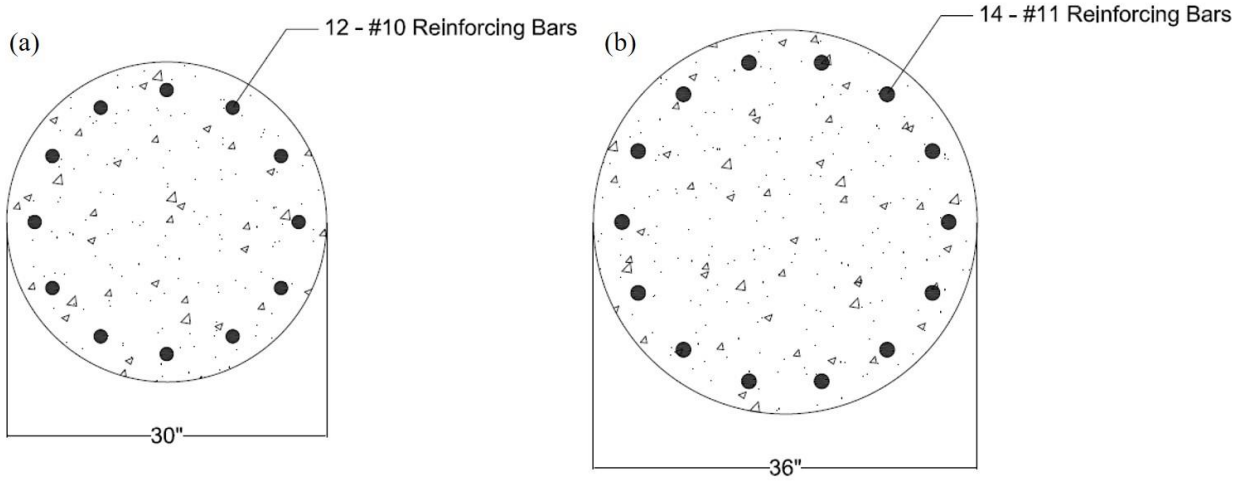

Figure 5.7: Cross-sections of the pier columns used in (a) the 15-ft clear height short piers, and (b) the 40-ft clear height tall piers.

5.2.4 Pier Foundation Details

The pier foundation details comprise the number, size, and arrangement of the piles. Although a 2-ft 6-in thick pile cap is used in the pier foundations, it is modeled with rigid elements because it is overdesigned and extremely stiff. The amount of piles, their size, and the arrangement within the pile cap depends on not only the vertical (axial) forces expected on the piles, but also on lateral bridge forces which cause bending. The lateral bridge forces considered in the design of the foundations were wind on the bridge superstructure and the traffic braking forces applied on the bridge deck. For each of the four IABs with piers and the two pier clear heights, a pile configuration was designed such that stresses in all of the piles does not exceed 12 ksi. The distance between the pile rows (longitudinal direction) is also variable and represents the distance between the centerlines of any two adjacent pile rows, as indicated in Fig. 5.8. The piles are distributed evenly along the width (transverse direction) of the pile cap. The resulting pile configurations included 2-3 rows of 6-8 HP10x42 or HP12x74 piles, arranged for strong axis bending when longitudinal loads are applied, in each row. A summary of the arrangement for each of the situations is described in Table 5.7.

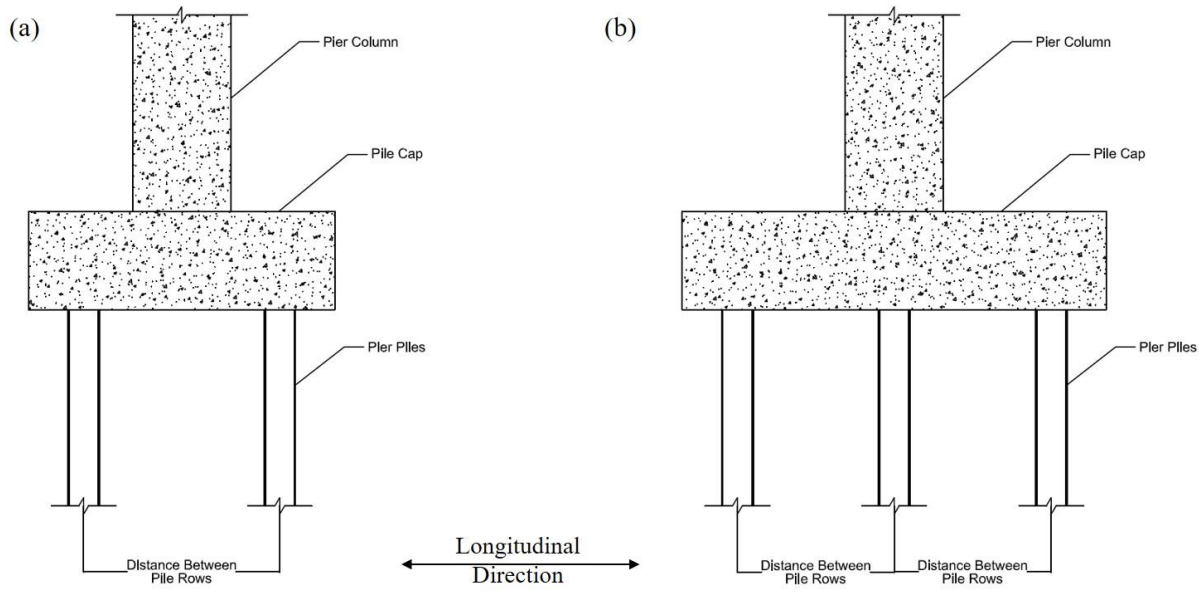

Figure 5.8: Diagram illustrating the arrangement of a pier foundation with (a) two rows of piles, and (b) three rows of piles.

Table 5.7: Pier pile arrangement details.

Bridge	**3-Span Steel**		**4-Span Steel**		**3-Span Concrete**		**4-Span Concrete**	
Column Clear Height	**15'**	**40'**	**15'**	**40'**	**15'**	**40'**	**15'**	**40'**
Pile Section	HP10x42		HP10x42		HP10x42		HP12x74	
Number of Pile Rows	2	2	3	3	3	3	3	3
Piles per Pile Row	7	8	7	8	7	7	6	7
Distance Between Pile Rows	5'-0"	5'-0"	5'-0"	5'-0"	4'-0"	4'-0"	4'-0"	4'-0"

5.2.5 Abutment Foundation Details

As previously discussed, there is a single row of piles in the abutment, which is oriented such that weak-axis bending occurs when longitudinal bridge forces are applied. This pile orientation increases flexibility in the IAB. The pile shape and number of piles are chosen using the IDOT IAB pile charts (IDOT, 2012b). The pile shapes vary between HP10x42, HP12x74, and HP14x117 (Table 5.8).

Table 5.8: Abutment pile details.

	1-Span Steel	3-Span Steel	4-Span Steel	3-Span Concrete	4-Span Concrete
Number of Piles	6	6	8	6	7
Pile Section	HP12x74	HP10x42	HP14x117	HP10x42	HP14x117

5.2.6 Abutment Details

Owing to rigid modeling of the abutment and abutment pile caps, the abutment-wingwall connection and the pile cap-abutment connections are the primary locations where deformation can occur above the piles in the abutments. The wingwall is a 10-ft long by 1-ft deep concrete element (modeled as rigid) with a height equal to the abutment and pile cap combined. The wingwall is connected to the main abutment through a construction joint that has steel reinforcement crossing the interface. The reinforcement for the single-span IAB is (10) #7 bars, the three-span IABs (both steel and concrete) use (16) #5 bars, and the four-span IABs (both steel and concrete) use (14) #5 bars. The wingwall connection details were determined in consultation with IDOT.

The pile cap-abutment connection is described in detail in Chapter 4 as a construction joint within the abutment. Connecting the two sides of this construction joint are #8 bars spaced at 12-in center-to-center along the back and front of the abutment. These bars can be observed in the details provided in Fig. 4.4 and are proportioned per IDOT All Bridge Designers Memorandum 12.3 concerning IAB design (IDOT, 2012b).

CHAPTER 6: PARAMETRIC STUDY PUSHOVER ANALYSIS RESULTS

6.1 PROCEDURE

The 51 IAB variants produced for the parametric study were subjected to static pushover analyses in both the bridge longitudinal and transverse directions. The pushover analysis is performed by inducing a displacement on a control node within the IAB and determining the magnitude of the loads, applied in a predetermined pattern, which would allow for the control node displacement to be achieved.

The load pattern utilized in this study corresponds to the size and location of the masses assigned to the nodes in the bridge. An example of the location of masses in a three-span IAB is provided in Fig. 6.1 where the magenta stars indicate mass locations. Using this load pattern for the pushover analyses is justified because the inertial forces on the structure caused by the earthquake shaking in dynamic analyses are also applied at node mass locations and proportioned relative to the magnitude of the mass at the node.

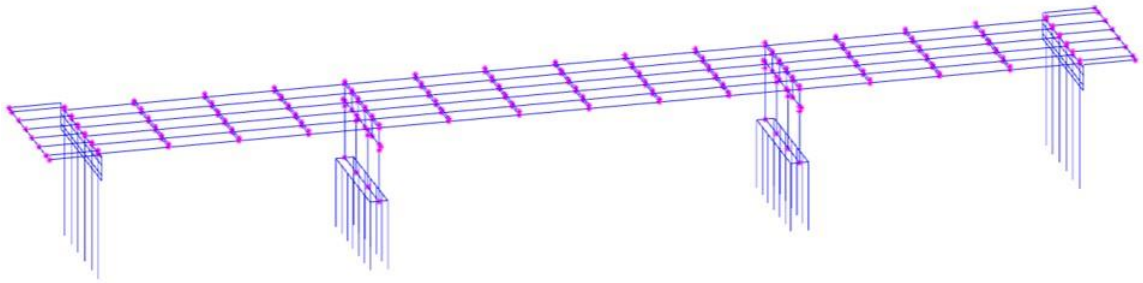

Figure 6.1: Example three-span IAB model showing the location of node masses, represented by magenta stars.

The control node used in the pushover analyses corresponds to the center-most node in the IAB at the composite girder-deck centroid level. The control node is described as the center-most because an even number of girders is used in four of the five main IAB types (only the four-span

concrete IAB uses an odd number of girders with seven) meaning that there is no node at the center of the deck with respect to the deck width. In this case, one of the two nodes closest to the center are selected instead. Another point to note concerning the control node is that although for single- and three-span IABs the control node is at the center of a span, the control node for the four-span IABs is at an intermediate pier location. This last point is important to recall when comparing pushover results between the single- or three-span IABs and the four-span IABs.

6.2 GENERAL RESULTS

The pushover results for the 51 IAB variants provided valuable information concerning the nonlinear behavior of the IABs given different design parameters. While the variations and trends based on design parameters are detailed in a later subsection, this subsection is concerned with the more general results that were seen across the IAB pushover results. The general observations presented are typically concerned with the shape of the pushover curve, the force resistance contributions from the piers and abutments, and the sequence of limit states.

6.2.1 General Observations from Basic IABs

Of the 51 total IAB variants 9 are selected to represent the basic IAB designs. These 9 IABs include the single-span IAB with alluvial foundation soil conditions as well as the three- and four-span steel and concrete IABs with elastomeric bearings, alluvial foundation soil conditions, and both short and tall piers. The pushover results of the 9 basic IABs are presented in Fig. 6.2 through Fig. 6.4 for pushover analyses in both the longitudinal and transverse directions.

Fig. 6.2 provides the pushover analysis results for the single-span steel IAB with alluvial foundation soil conditions. Only six limit states are possible in the single-span IABs. The yielding of the abutment piles (APY) and mobilization of the soil surrounding the piles (APS) occurs in both directions within a reasonable amount of control node displacement and the local buckling of

the abutment piles (APB) occurs at larger displacements. The important observation to make in these results is the contributions from the abutments. In the longitudinal direction (Fig. 6.2a) the contributions from the two abutments differ due to one abutment pulling away from the backfill while the other compresses into it. Compressing into the backfill allows for more force resistance contribution from that abutment (dashed line), while the other abutment (solid line) resists the load using only the piles and no backfill contribution. In the transverse direction the contributions are the same from both abutments due to the lack of any engagement with the backfill in that direction leading to all the force being resisted by the abutment piles and their surrounding soil. The effect of backfill engagement allows for the longitudinal force capacity to be nearly twice the transverse force capacity in the IAB.

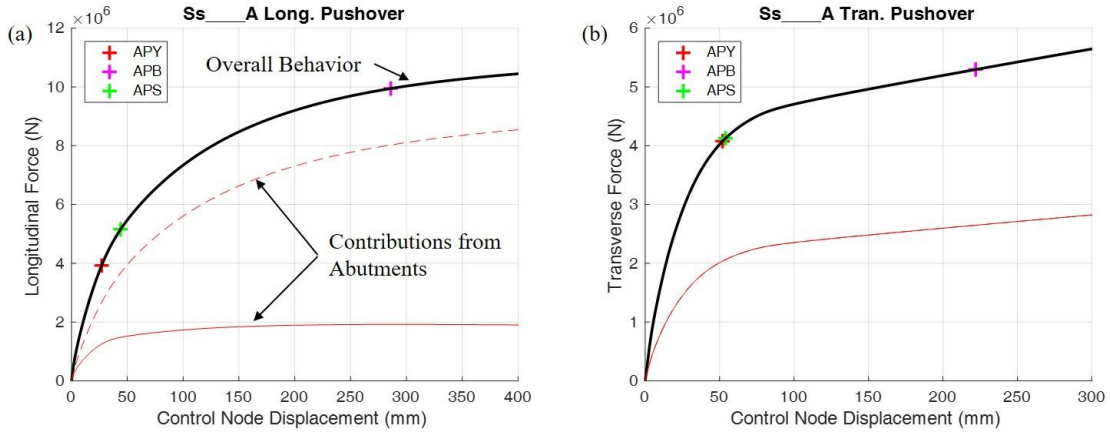

Figure 6.2: Pushover analysis results for the single-span steel IAB with alluvial foundation soil conditions in the (a) longitudinal, and (b) transverse bridge directions.

The effect from the backfill engagement can also be observed in Fig. 6.3, which provides the pushover curve results for three- and four-span steel and concrete IABs with elastomeric bearings, alluvial foundation soil conditions, and short piers. In addition to the contributions from the abutments, the contributions from the piers are also presented which demonstrate that an individual abutment typically contributes more to the lateral resistance in the IAB than any individual pier.

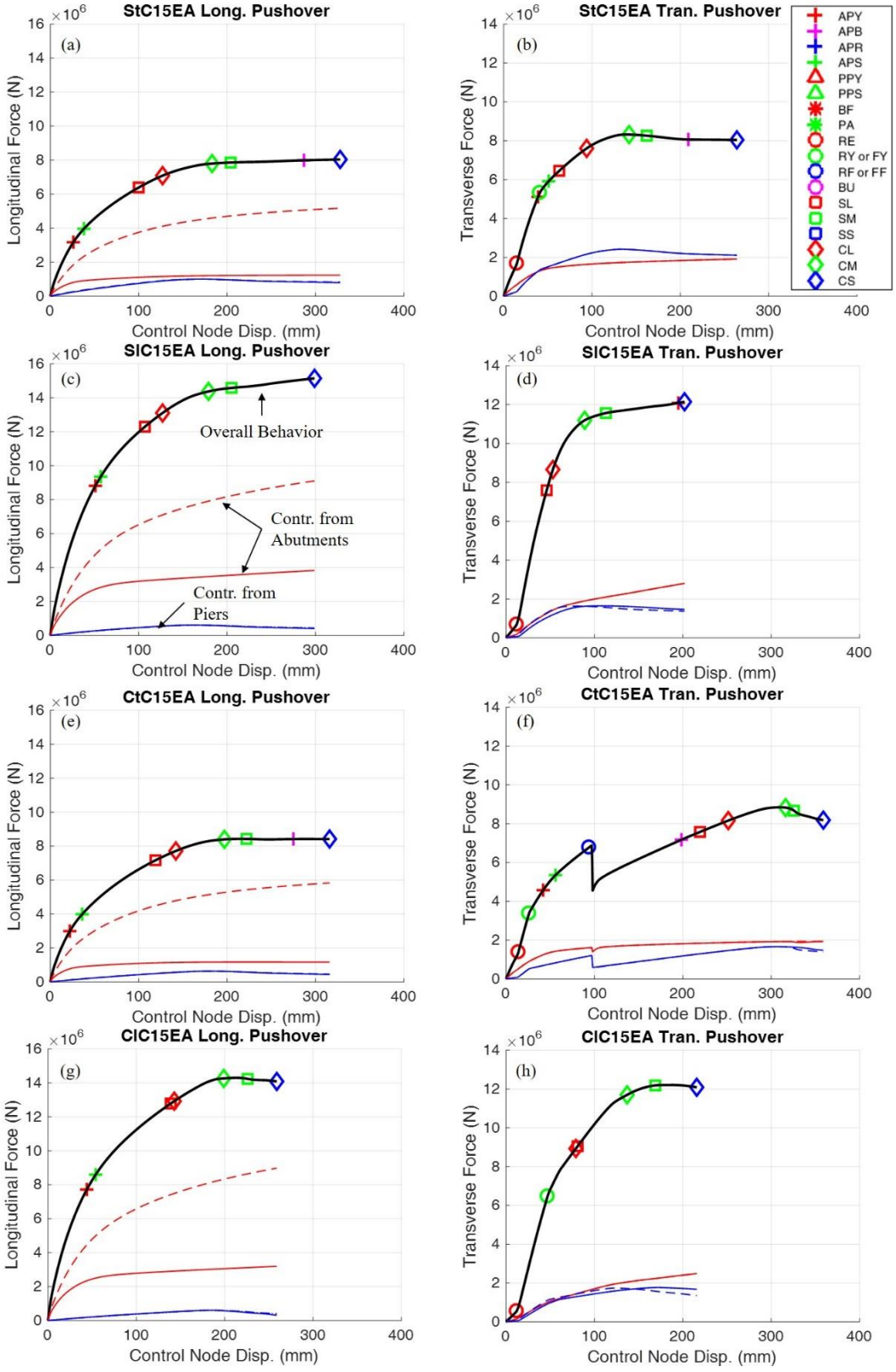

Figure 6.3: Pushover analysis results in the longitudinal and transverse bridge directions for (a) (b) StC15EA, (c) (d) SlC15EA, (e) (f) CtC15EA, and (g) (h) ClC15EA.

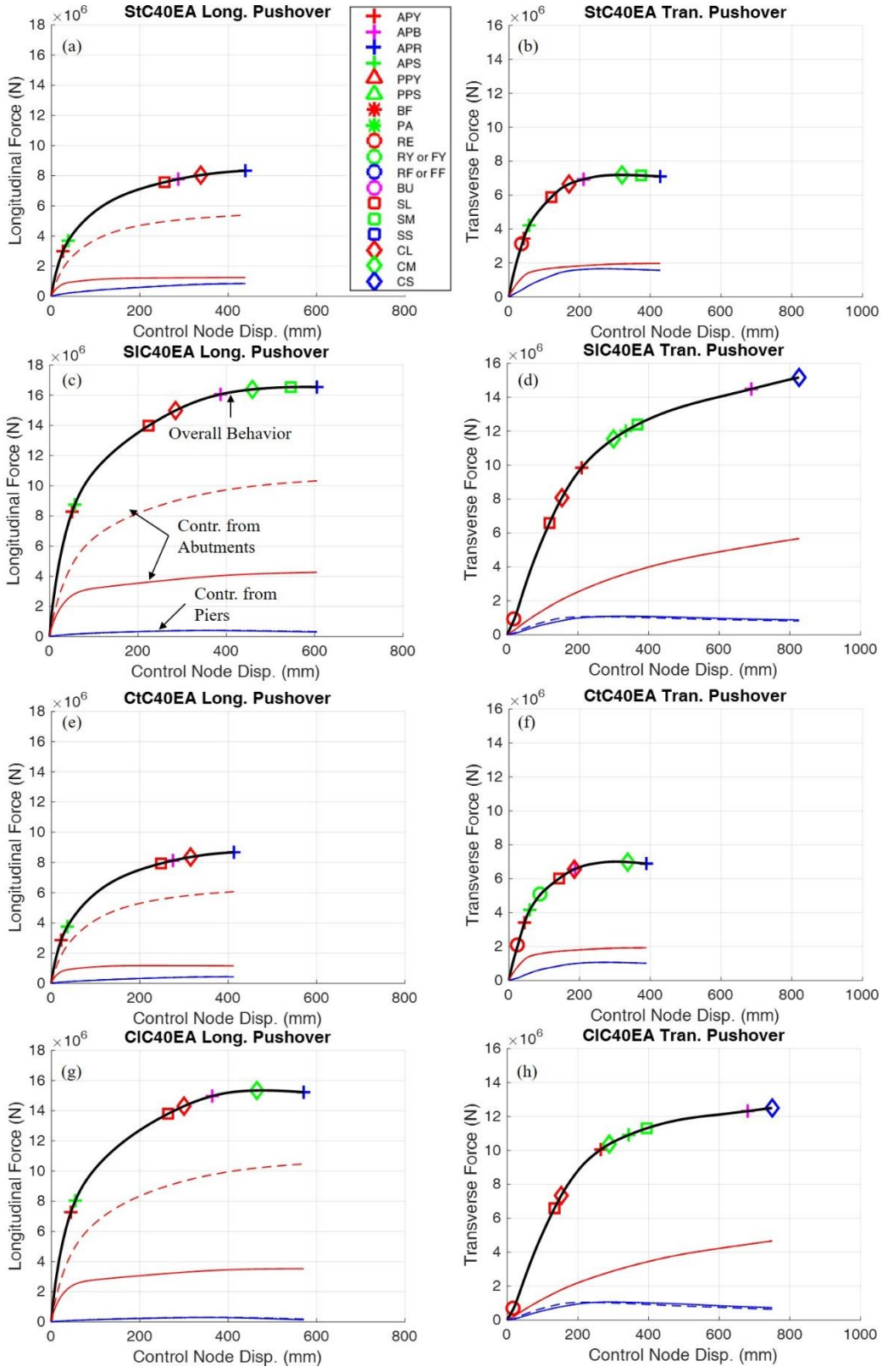

Figure 6.4: Pushover analysis results in the longitudinal and transverse bridge directions for (a) (b) StC40EA, (c) (d) SlC40EA, (e) (f) CtC40EA, and (g) (h) ClC40EA.

In the longitudinal direction pushover results from Fig. 6.3 (the left column of plots) a few general trends can be observed. The first being that the shape tends to have some consistent characteristics across the IABs. The yielding of the abutment piles (APY) and mobilization of the soil surrounding the abutment piles (APS) occurs early on and creates a change in the slope of the pushover curve and therefore a change in the overall IAB stiffness. This change in stiffness is subtler in the longer bridges (Fig. 6.3c and 6.3g), however it still exists and can be accounted for by the change in slope of one of the abutment contribution curves due to pile yielding. The next major change in the stiffness of the pushover curves occurs when moderate pier damage occurs (SM and CM). Note that light pier damage (SL and CL) has little effect on IAB stiffness. The onset of moderate pier damage tends to create a peak in the pier contributions due to damage beyond the moderate level leading to a loss of strength in the pier columns. In the concrete IABs (Fig. 6.3e and 6.3g), moderate pier damage tends to indicate the peak lateral force capacity of the bridge due to the rapid deterioration of the pier columns caused by the heavy concrete superstructure. The steel IABs (Fig. 6.3a and 6.3c) continue to take on load due to the steel superstructures being lighter, so the increase in force from the backfill contribution is larger than the decrease in pier column force capacity. The steel IABs do reach a peak around the onset of severe pier damage (SS and CS). Three-span IABs also tend to encounter more abutment pile strain, as indicated by the occurrence of abutment pile local buckling (APB) before CS.

Many of the observations for the longitudinal direction pushover results also hold in the transverse direction, however the inclusion of retainer engagement does cause differences in the behavior. The retainer engagement (RE) is the first limit state encountered in all the IABs and causes an immediate increase in bridge stiffness. The behavior after this depends on the IAB, while all of them reach another change in stiffness with the onset of moderate pier damage (SM and

CM), the behavior varies in between the two points. StC15EA (Fig. 6.3b) encounters abutment pile yielding (APY) and retainer yielding (RY) at roughly the same time leading to a decrease in stiffness. SlC15EA (Fig. 6.3d) only encounters a change in stiffness at a larger displacement due to the four-span bridges allowing for abutment pile yielding to occur much later. This also allows for the force capacity to continue to increase at large displacements CtC15EA (Fig. 6.3f) experiences both a change in stiffness due to the retainer yielding (RY) and a sharp change in force capacity due to retainer fusing (RF). ClC15EA (Fig. 6.3h) is also a four-span bridge, so the abutment pile yielding does not occur before severe pier column damage. However, unlike SlC15EA, ClC15EA does experience retainer yielding (RY) causing a decrease in bridge stiffness.

The pushover results of the basic IABs with taller piers are presented in Fig. 6.4. Many of the observations from the shorter pier IABs observed in Fig. 6.3 are consistent with the tall pier IABs, although there are some changes. In general, there is less contribution from the piers due to their tall heights leading to damage occurring earlier. This allows the pushover curves to be smoother and resemble the single-span results in Fig. 6.2. The general observations of a decrease in stiffness due to abutment pile yielding (APY) and the peak force capacity tending to occur around the onset of moderate pier damage (SM and CM) still hold in analyses where SM and CM are reached. However, changes in stiffness caused by retainer engagement (RE) and yielding (RY) tend to be less pronounced. Retainer yielding even occurs less in the IABs with taller piers due to the damage to the piers limiting the amount of force being transferred through the bearings and retainers on the pier caps. A major difference is the occurrence of abutment pile rupture (APR) as the first unacceptable limit state encountered in most analyses. The only IABs where CS occurs before APR is in the transverse four-span bridges which tend to make the abutment piles yield

(APY) later than usual causing Fig. 6.4d and 6.4h to have pushover curves which seem to continue to increase in force capacity despite large displacements.

6.2.2 Limit State Occurrence Sequence

The sequence of limit state occurrence within the pushover analysis results also yields interesting observations useful in assessing IAB lateral behavior. Tables 6.1 through 6.5 present the sequence of limit state occurrences for all 51 IABs in the parametric study. Observations on the sequences and their differences between each other is described below. The presented sequences consist of all the limit states encountered up until the first unacceptable limit state (bearing unseating, severe pier column damage, or abutment pile rupture) occurs.

6.2.2.1 *Single-Span Steel IABs*

Table 6.1 provides the sequence of limit state occurrences for the single-span steel IAB pushovers. Recall that these IABs do not vary significantly with only the foundation soil condition changing. Also recall that there are only six limit states possible in the single-span bridge due to its lack of piers – abutment pile yielding, local buckling, and rupture (APY, APB, and APR, respectively), mobilization of the soil surrounding the abutment pile (APS), backfill failure (BF), and pile cap-abutment interface failure (PA). In both the longitudinal and transverse direction it can be shown that abutment pile yielding, mobilization of the soil surrounding the piles, and local buckling of the piles occurs in every IAB, though the sequence varies. The general trend is that the soft soil condition (Ss____S) has the soil mobilization occurring first while in stiffer soil conditions (Ss____A and Ss____H) the pile yields before the soil mobilizes. This makes sense due to the stiffer soils being stronger making the weaker component the HP12x74 piles. APB always occurs after APY and APS. It can also be noted that in stiffer soils there is more strain in the piles

at similar center node displacements, as indicated by the occurrence of APR in the Ss____H sequences.

Table 6.1: Sequence of limit state occurrences for single-span steel IABs.

Bridge	Sequence of Limit State Occurrences	
	Longitudinal Direction	**Transverse Direction**
Ss____S	APS-APY-APB	APS-APY-APB
Ss____A	APY-APS-APB	APY-APS-APB
Ss____H	APY-APS-APB-APR	APY-APS-APB-APR

6.2.2.2 *Three-Span Steel IABs*

The sequence of limit state occurrences from the pushover analyses of three-span steel IABs in the parametric study is presented in Table 6.2. In the longitudinal direction it can be seen that the limit states encountered are only abutment pile yielding, local buckling, and rupture (APY, APB, APR), mobilization of the soil surrounding the abutment piles (APS), and light (SL and CL), moderate (SM and CM), and severe (CS) pier column damage. The sequence of limit state occurrences always progresses such that damage to the abutment piles and the surrounding soil occurs first followed by progressive pier damage and local buckling of the abutment piles until the first unacceptable limit state of either severe pier column concrete damage (CS) or abutment pile rupture (APR). The main variations between the bridges is the order of abutment pile yielding and mobilization of the soil surrounding the abutment piles and the location of APB occurrence. Similar to the behavior of the single-span steel IABs, the soft soil condition has the soil mobilize first while the alluvial and stiff soil conditions allow the piles to yield before the soil mobilizes. Also similar to the single-span steel IABs, there tends to be more pile damage in models with stiffer soils as APB and APR occur earlier in the IABs with stiff soil conditions.

Table 6.2: Sequence of limit state occurrences for three-span steel IABs.

Bridge	Sequence of Limit State Occurrences	
	Longitudinal Direction	**Transverse Direction**
StC15ES	APS-APY-SL-CL-CM-SM-CS	RE-APS-RY-APY-SL-PPS-PPY-CL-CM-SM-APB-CS
StC15EA	APY-APS-SL-CL-CM-SM-APB-CS	RE-APY-RY-APS-SL-CL-CM-SM-APB-CS
StC15EH	APY-APS-SL-CL-CM-SM-APB-CS	RE-APY-RY-SL-APS-CL-CM-SM-APB-CS
StC40ES	APS-APY-SL-CL-APB-CM-SM-APR	RE-APS-APY-SL-CL-RY-APB-CM-SM-APR
StC40EA	APY-APS-SL-APB-CL-APR	RE-APY-APS-SL-CL-APB-CM-SM-APR
StC40EH	APY-APS-SL-APB-CL-APR	APY-RE-APS-SL-APB-CL-APR
StC15FS	APS-APY-SL-CL-CM-SM-APB-CS	FY-APS-SL-APY-PPS-PPY-CL-CM-SM-APB-CS
StC15FA	APY-APS-SL-CL-CM-SM-CS	FY-APY-SL-APS-CL-CM-SM-APB-CS
StC15FH	APY-APS-SL-CL-CM-SM-APB-CS	FY-APY-SL-CL-APS-CM-SM-APB-CS
StC40FS	APS-APY-SL-CL-APB-CM-SM-APR	APS-APY-SL-CL-FY-APB-CM-SM-APR
StC40FA	APY-APS-SL-APB-CL-APR	APY-APS-SL-CL-APB-CM-SM-APR
StC40FH	APY-APS-SL-APB-CL-APR	APY-APS-SL-CL-APB-APR

The sequence of limit state occurrences in the transverse direction for three-span steel IABs also includes abutment pile yielding, local buckling, and rupture, mobilization of the soil surrounding the abutment piles, and pier column damage in every bridge. However, the occurrence of retainer and bearing limit states is also very common with retainer engagement (RE) always occurring in IABs with elastomeric bearings. Retainer or fixed bearing yielding (RY and FY, respectively) occurs in bridges with 15-ft tall piers and soft soil conditions. Damage to the pier foundation piles (PPY) and soil (PPS) also occurs in bridges with 15-ft tall piers and soft soil conditions due to the shorter, stiffer columns transferring more force to the foundations. Despite the occurrence of retainer and fixed bearing yielding, neither the retainers nor the fixed bearings fuse in the three-span steel bridges. In terms of the limit state occurrence sequence, the onset of

abutment pile yielding (APY) and mobilization of the soil surrounding the abutment piles (APS) once again occurs early in the transverse direction and the order of the two depends on the soil conditions. However, APY and APS begin to occur further apart from each other in stiffer soils allowing for other limit states to occur between them. This can be observed in StC15E_ bridges which always have RY occurring between APY and APS, but with stiff soil conditions light steel pier column damage (SL) also occurs between APY and APS. In general, once again the sequence involves initial damage to the abutment foundation (APY and APS), with bearing and retainer damage mixed in, followed by pier column damage, ending with the first unacceptable limit state of severe concrete pier column damage (CS) in IABs with 15-ft tall piers and abutment pile rupture (APR) in IABs with 40-ft tall piers.

6.2.2.3 *Four-Span Steel IABs*

The sequence of limit state occurrences from longitudinal pushover analyses of four-span steel IABs, shown in Table 6.3, is similar to the longitudinal three-span steel IAB sequence discussed above. This is meant in the manner that the sequence involves initial abutment foundation damage followed by pier column damage and the order of the abutment pile yielding and mobilization of the soil surrounding the abutment pile and the occurrence of APB and APR depends on the soil condition specified. However, the four-span steel IAB with 15-ft tall pier columns and fixed bearings does not exactly follow this trend as it allows for light pier column damage (SL and CL) to occur between the APY and APS limit states.

Table 6.3: Sequence of limit state occurrences for four-span steel IABs.

Bridge	Sequence of Limit State Occurrences	
	Longitudinal Direction	**Transverse Direction**
SlC15ES	APS-APY-SL-CL-CM-SM-CS	RE-SL-CL-PPS-CM-SM-APY-CS
SlC15EA	APY-APS-SL-CL-CM-SM-CS	RE-SL-CL-CM-SM-APY-CS
SlC15EH	APY-APS-SL-CL-CM-SM-APB-CS	RE-SL-CL-CM-SM-APY-CS
SlC40ES	APS-APY-SL-CL-APB-CM-SM-APR	RE-SL-CL-APY-APS-CM-SM-APB-CS
SlC40EA	APY-APS-SL-CL-APB-CM-SM-APR	RE-SL-CL-APY-CM-APS-SM-APB-CS
SlC40EH	APY-APS-SL-CL-APB-APR-CM-SM-CS	RE-SL-CL-APY-CM-SM-APS-APB-CS
SlC15FS	APS-SL-CL-APY-CM-SM-CS	SL-CL-PPS-CM-SM-CS
SlC15FA	APY-SL-APS-CL-CM-SM-CS	SL-CL-CM-SM-CS
SlC15FH	APY-SL-APS-CL-CM-SM-CS	SL-CL-CM-SM-APY-CS
SlC40FS	APS-APY-SL-CL-APB-CM-SM-APR	SL-CL-APY-APS-CM-SM-APB-CS
SlC40FA	APY-APS-SL-CL-APB-CM-SM-APR	SL-CL-APY-CM-APS-SM-APB-CS
SlC40FH	APY-APS-SL-CL-APB-CM-APR	SL-CL-APY-CM-SM-APS-CS

The limit states which occur in the transverse pushover analyses of four-span steel IABs, also shown in Table 6.3, do vary from the results for the three-span steel IABs discussed earlier. The main difference is that the abutment pile yielding and mobilization of the soil surrounding the abutment piles mobilizes much later in the sequence than previously observed with other IABs. This also leads to APB occurring later and APR never occurring. The earliest occurrence of APY is found in the IABs with 40-ft tall piers and elastomeric bearings where they occur only after light pier column damage (SL and CL) occurs. In some instances, such as the SlC15__ IABs, APS does not occur before the first unacceptable limit state. However, as observed in other IABs, as stiffer soils are considered the gap between APY and APS does tend to increase. The results also differ from previous bridges in that although there is some contribution from the side retainers in their

engagement (RE) always occurring, there is no yielding or fusing and no limit states involving the fixed bearings at all. This lack of limit states from retainers and fixed bearings leads to the observations that the only difference in the sequence between the IABs with fixed and elastomeric bearings is the occurrence of RE at the beginning. This leads to the observation that SlC15FA only has damage to the pier columns. SlC15FS is close to having only pier column damage, however the softer soil allows for pier pile yielding to occur in the IABs with 15-ft tall piers and soft soil conditions.

6.2.2.4 *Three-Span Concrete IABs*

The observations concerning the sequence of limit state occurrences during the pushover analyses of three-span IABs with prestressed precast concrete superstructure girders is presented in Table 6.4. The longitudinal results provide the same observations found for the three-span steel IABs. Those observations being that the sequence consists of initial damage to the abutment foundation followed by damage to the pier columns. Once again, the order of occurrence for the yielding of the abutment piles and soil surrounding the abutment piles as well as the occurrence of abutment pile local buckling varies depending on the soil conditions with the soil mobilizing later under stiffer soil conditions. It is also shown that APR only occurs in IABs with taller piers.

The first observation made concerning the transverse direction results relates to the occurrence of retainer engagement (RE) always occurring first for bridges with retainers. Shortly after the retainer engagement, retainer yielding occurs (RY). While the yielding may not occur directly after engagement in the 40-ft pier IABs, it does still occur fairly shortly after, being separated only by initial abutment foundation damage (APY and APS). This observation of the retainer yielding (RY) before APY and APS for the IABs with 15-ft tall piers and after APY and APS occur for the IABs with 40-ft tall piers also holds true when replacing retainer yielding with

fixed bearing yielding (FY). The fusing of the retainers (RF) and fixed bearings (FF) also only occur in the bridges with 15-ft tall piers due to the increased stiffness of the pier columns leading the bearings to account for more of the superstructure/control node displacement. The taller piers also increase the strain in the piles, as indicated by the occurrence of APR instead of CS.

Table 6.4: Sequence of limit state occurrences for three-span concrete IABs.

Bridge	Sequence of Limit State Occurrences	
	Longitudinal Direction	**Transverse Direction**
CtC15ES	APS-APY-SL-CL-CM-SM-CS	RE-RY-APS-APY-RF-SL-APB-CL-CM-SM-CS
CtC15EA	APY-APS-SL-CL-CM-SM-APB-CS	RE-RY-APY-APS-RF-APB-SL-CL-CM-SM-CS
CtC15EH	APY-APS-SL-CL-CM-SM-APB-CS	RE-RY-APY-APS-RF-APB-SL-CL-APR
CtC40ES	APS-APY-SL-CL-APB-CM-SM-APR	RE-APS-APY-RY-SL-CL-APB-CM-SM-APR
CtC40EA	APY-APS-SL-APB-CL-APR	RE-APY-APS-RY-SL-CL-APB-CM-APR
CtC40EH	APY-APS-SL-CL-APB-CM-SM-APR	RE-APY-APS-RY-SL-CL-APB-CM-SM-APR
CtC15FS	APS-APY-SL-CL-CM-SM-CS	FY-APS-APY-SL-CL-FF-APB-BU
CtC15FA	APY-APS-SL-CL-CM-SM-CS	FY-APY-SL-APS-CL-FF-APB-APR
CtC15FH	APY-APS-SL-CL-CM-SM-APB-CS	FY-APY-SL-CL-APS-FF-CM-SM-APB-CS
CtC40FS	APS-APY-SL-CL-APB-CM-SM-APR	APS-APY-FY-SL-CL-APB-CM-SM-APR
CtC40FA	APY-APS-SL-APB-CL-APR	APY-APS-FY-SL-CL-APB-CM-SM-APR
CtC40FH	APY-APS-SL-APB-CL-APR	APY-APS-FY-SL-CL-APB-APR

The fusing of the fixed bearing in the transverse direction of CtC15FS leads to unique cases where neither severe pier column damage nor abutment pile rupture are the first unacceptable limit state achieved. Instead, the low friction between the fixed bearing steel and pier cap concrete allows the fixed bearing to slide off the pier cap and cause bearing unseating (BU). This IAB is

the only multi-span IAB in the parametric study not to experience severe pier column damage or abutment pile rupture. In fact it does not even reach moderate pier column damage due to the fixed bearing acting as a fuse and displacing instead of transferring more force to the piers. Note that every other IAB in the transverse direction tends to follow the sequence of mixed retainer or fixed bearing and abutment foundation damage followed by pier column and abutment pile damage to failure. Even when retainer fusing occurs, the friction between the elastomeric bearing and pier cap is strong enough to not slide excessively and pier column damage continues.

6.2.2.5 *Four-Span Concrete IABs*

The longitudinal sequence of limit state occurrences from pushover analyses on four-span concrete IABs is generally the same as the sequences determined for three-span steel and concrete IABs. This is in terms of abutment foundation damage through pile yielding (APY) and soil mobilization (APS) occurring first followed by pier column damage until the first unacceptable limit state of severe pier column concrete damage (CS) in IABs with 15-ft tall piers and abutment pile rupture in IABs with 40-ft tall piers occurs. Note that APB and APR only occur in IABs with taller piers. The observation that under soft soil conditions the soil surrounding the pile mobilizes before the piles yield but the order switches for the two stiffer soil conditions also holds true for four-span concrete IABs.

Table 6.5: Sequence of limit state occurrences for four-span concrete IABs.

Bridge	Sequence of Limit State Occurrences	
	Longitudinal Direction	**Transverse Direction**
ClC15ES	APS-APY-SL-CL-CM-SM-CS	RE-RY-CL-SL-CM-SM-CS
ClC15EA	APY-APS-SL-CL-CM-SM-CS	RE-RY-CL-SL-CM-SM-CS
ClC15EH	APY-APS-SL-CL-CM-SM-CS	RE-RY-CL-SL-CM-SM-CS
ClC40ES	APS-APY-SL-CL-APB-CM-SM-APR	RE-SL-CL-APY-APS-CM-SM-APB-CS
ClC40EA	APY-APS-SL-CL-APB-CM-APR	RE-SL-CL-APY-CM-APS-SM-APB-CS
ClC40EH	APY-APS-SL-APB-CL-APR	RE-SL-CL-APY-CM-SM-APS-CS
ClC15FS	APS-APY-CL-SL-CM-SM-CS	FY-SL-CL-CM-SM-CS
ClC15FA	APY-APS-CL-SL-CM-SM-CS	FY-SL-CL-CM-SM-CS
ClC15FH	APY-APS-CL-SL-CM-SM-CS	FY-SL-CL-CM-SM-CS
ClC40FS	APS-APY-SL-CL-APB-CM-SM-APR	SL-CL-APY-APS-CM-SM-APB-CS
ClC40FA	APY-APS-SL-CL-APB-CM-APR	SL-CL-APY-CM-APS-SM-APB-CS
ClC40FH	APY-APS-SL-APB-CL-APR	SL-CL-APY-CM-SM-APS-CS

In the transverse direction, it can once again be observed that when retainers are present the first limit state reached is the retainer engagement (RE). When 15-ft tall piers are present either retainer yielding (RY) or fixed bearing yielding (FY) occurs very early on before any pier damage as well. While these components yield, they do not fuse in the four-span concrete IABs. The damage to the retainers and fixed bearings is caused by the short, stiff piers being able to accommodate large lateral forces. For both the IABs utilizing 15-ft and 40-ft piers, the only difference in the sequence when comparing those with elastomeric and fixed bearings occurs from the presence of the retainer engagement (RE) limit state and the replacement of the retainer yielding (RY) limit state with the fixed bearing yielding (FY) limit state. Aside from those changes the sequences remain the same for their respective pier heights. For IABs using the 15-ft tall piers this sequence involves only damage to the piers and is one of the few cases where abutment foundation damage does not occur. The IABs using 40-ft tall piers are less stiff due to their height leading to the abutments needing to accommodate some of the force and therefore damage to both

the pier columns and abutment foundations occur. However, unlike other sequences which have APS and APY occur before any pier column damage limit states, these sequences have APS and APY occur after light pier column damage (SL and CL) which occurs early due to the slenderness of the piers. The order of the APS and APY limit states do not change with APY always occurring before APS. The two limit states do become more separated under stiffer soil conditions allowing other limit states, such as moderate concrete (CM) and steel (SM) damage in the pier columns to occur after APY but before APS. The IABs with 40-ft tall piers also experiences more abutment pile damage before the occurrence of an unacceptable limit state, as indicated by the occurrence of APB

6.2.2.6 *Overall Observations*

Given the data presented above, a few general observations can be made concerning the sequence of IAB limit state occurrences achieved from pushover analyses. The first major observation concerns the longitudinal behavior which tends to be consistent across almost all of the IABs in the parametric study. The observed sequence shows that limit states in the abutment foundation occur first then progressively worse damage limit states occur in the pier columns until the severe damage to pier column concrete or abutment pile rupture limit state is reached as the first unacceptable limit state. The sequence of the abutment foundation damage is also consistent with mobilization of the soil surrounding the abutment piles occurring first under soft soil conditions and abutment pile yielding occurring first under the stiffer two soil conditions.

The only major observation in the transverse direction results which is mostly consistent across all the IABs is that pier damage almost always occurs. The only exception to this is if the fixed bearing fusing allowing for it to act as a fuse and limit the forces transferred to the piers. Many of the IABs which have pier damage also experience abutment foundation damage, however

an exception to this is in the transverse direction if the IAB is a four-span bridge with 15-ft tall piers. The presence of 3 short pier bents provides the majority of the stiffness in the bridge, leading to the damage in the piers to occur before significant damage in the abutment piles are experienced. This does not translate to when taller piers are used as their decreased stiffness requires contributions from the abutments to resist the lateral forces and the strains in the abutment piles to increase.

As mentioned, in the transverse direction damage to the abutment foundations in the form of abutment pile yielding, local buckling, and rupture (APY, APB, APR), and mobilization of the soil surrounding the piles (APS) often accompanies pier damage as the major damage locations. Similar to the longitudinal direction, the order of these limit states does change and often in stiffer soils the APY and APS will occur at different times allowing other limit states to occur between the two.

Another main characteristic of the sequences of limit state occurrence in the transverse direction includes retainer and fixed bearing behavior. While retainer engagement (RE) and yielding (RY) as well as fixed bearing yielding (FY) are fairly common, the fusing of the retainers (RF) and fixed bearings (FF) are much less common. RF and FF only occur in three-span concrete IABs with 15-ft piers. This is due to the large mass of the concrete superstructure inducing large normal forces in the bearings which leads to greater frictional forces being transferred. The short, stiff piers also help to resist the lateral forces causing large shear forces within the bearings leading to the fusing of the retainers and fixed bearings. This behavior leads to the only pushover which does not encounter severe pier column concrete damage as the first unacceptable limit state due to the fusing and subsequent sliding and unseating of the fixed bearings.

6.3 PUSHOVER CURVE TRENDS IN THE PARAMETRIC STUDY

It is important to understand how various design parameters affects the seismic behavior of the 51 IABs analyzed. To accomplish this, the pushover curves for the basic IABs presented earlier are compared against the pushover curves for similar IABs that vary one parameter. The variations include superstructure material, span configuration, pier height, bearing layout, and foundation soil conditions. These comparisons allow for vulnerable components to be identified and potential solutions to the vulnerabilities to be made.

6.3.1 Superstructure Material

The use of steel plate girders and precast prestressed concrete girders in the superstructure allows for comparisons between the two different superstructure girder materials. The comparisons of the pushover curves for IABs with both steel and concrete girders are provided in Fig. 6.5 for both the longitudinal and transverse directions. In general, it can be seen that the initial stiffness of the bridges tend to be very similar regardless of the superstructure material and the IABs with steel girders are usually stronger than the concrete IABs. However, this is not always the case as seen in the longitudinal pushover curves for the three-span IABs (Fig. 6.5a and 6.5c). The change in behavior for this scenario is due to the plate girders in the three-span steel IABs being the smallest girders in the parametric study leading to a reduced axial force when compared to the three-span concrete girders.

The occurrence of limit states under both superstructure materials tends to occur under similar control node displacements for nearly all the comparisons in Fig. 6.5. The sequence in the longitudinal direction typically indicates that there is abutment pile yielding followed by soil mobilization surrounding the piles, then pier column damage to severe pier column damage in IABs with 15-ft tall piers or abutment pile rupture in IABs with 40-ft tall piers. In the transverse

direction the sequence changes slightly due to the inclusion of retainer and fixed bearing limit states as well as from four-span bridges only experiencing abutment damage after pier column damage. However, the location of the limit states in terms of control node displacement within each comparison is generally close.

The only comparison where there is a major change in pushover behavior is in the transverse results for _tC15EA bridges (Fig. 6.5b). The concrete IAB in this comparison is the only bridge in this figure to experience retainer fusing (RF). The retainer fusing is caused by weaker anchor bolts (1-in diameter for concrete, 1.25-in diameter for steel) as well as a heavier superstructure causing more shear force to be transferred through the bearings and retainers. The fusing of the retainer allows for shear deformation of the elastomeric bearing to occur, however the friction between the elastomeric bearing and the concrete pier cap is strong enough to keep the bearing from sliding. The large friction resistance allows for the lateral force to be transferred to the pier columns and damage to be experienced in the columns. The fusing of the retainers proves to be beneficial to the behavior of the IAB as it allows for column damage to occur at larger control node displacements adding to the deformation and force resistance capacity of the IAB.

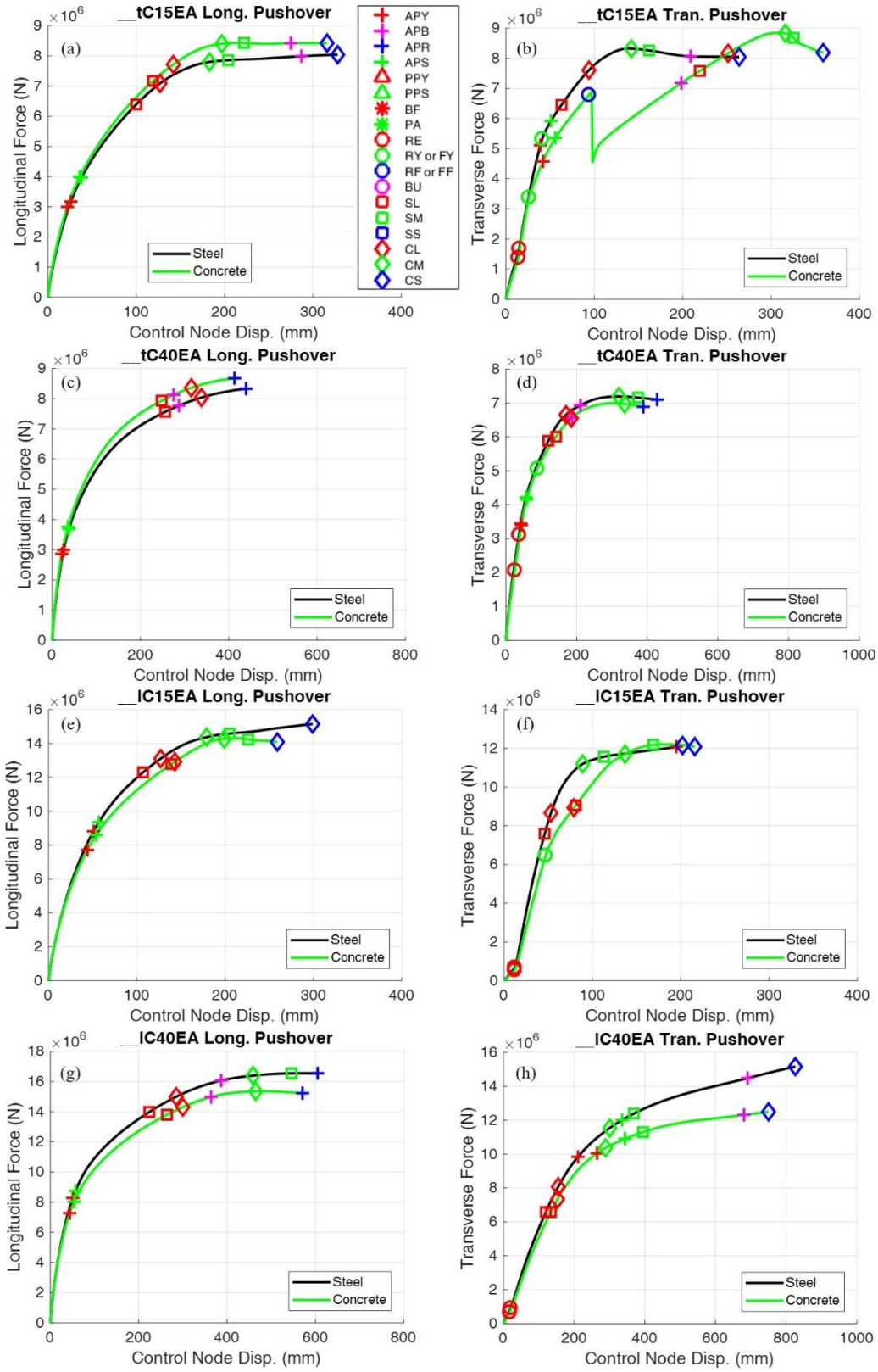

Figure 6.5: Comparison of IAB pushover curves in the longitudinal (left column) and transverse (right column) directions with varying superstructure girder materials.

Other observations concerning the different superstructure materials includes how IABs using concrete superstructures tend to decrease in strength after moderate pier column damage (CM and SM) at a faster rate than observed in IABs using steel plate girders. This trend is caused by the much heavier concrete girders adding substantial axial forces as well as increased second order effects which accelerate the deterioration process in the pier columns. Another observation is the occurrence of retainer yielding (RY) in the transverse pushover results. Concrete bridges tend to have more retainer yielding than steel IABs due to the heavier girders in the superstructure allowing for large shear forces across the bearings. The occurrence of retainer yielding allows the concrete IABs to achieve lateral resistance peaks at larger control node displacements and allows for moderate pier column damage to also occur at larger displacements, as seen in Fig. 6.5b and 6.5f. This trend is important to note as it allows the bridges to remain serviceable under larger deformations.

6.3.2 Span Configuration

Three potential span configurations were considered and compared against each other in Fig. 6.6 – single-span, three-span, and four-span. Note that the single-span IAB only uses a steel superstructure and is therefore not compared against concrete IAB pushover results. The single-span pushover results also do not experience control node displacements as large as those imposed on the multi-span bridges due to the lack of large displacements occurring during the dynamic analyses. The general trend among pushover results is that an increasing number of spans increases the force capacity of the bridge. The exception to this trend is when the single-span IAB is considered in the longitudinal direction. The reason the trend in these situations differs is due to the single-span steel IAB using a 70-in deep plate girder, the three-span steel IAB using a 40-in plate girder, and the four-span IAB using a 60-in plate girder. The much smaller girder used in the

three-span steel reduces the axial force capacity in the longitudinal direction leading it to be weaker than the single-span results. This combination of weak girder and long span seems to be unique to the three-span steel bridge as the four-span steel bridge is much stronger than the single-span despite also having smaller girders.

The limit states which occur in the longitudinal direction occur in the same sequence and at similar control node displacements regardless of the span configuration of the IAB. An exception to this trend is the lack of pier column damage in the single-span IAB due to the lack of piers. The pushover curves in the transverse direction tend to produce limit states which occur in different sequences and at different control node displacements. The first interesting observation concerning the transverse pushover curve comparisons is that the initial stiffness of the single-span IABs tend to be stiffer than the multi-span IABs due to the lack of piers and therefore the lack of the retainer engagement (RE) limit state. Once the retainer engagement occurs, the multi-span IABs do end up being stiffer than the single-span IAB. Another common trend in the transverse pushover curves is that initial damage to the abutment foundations (APY and APS) tends to occur at larger control node displacements in the four-span IAB than in the three-span IAB. This is also shown by three-span IABs tending to have abutment pile rupture (APR) be the first encountered unacceptable limit state while it is severe pier column concrete damage (CS) in four-span IABs. This can be attributed to longer overall span between the abutments causing a more flexible bridge where it is more difficult to transfer forces to the abutments. The only occurrence of retainer yielding (RY) in the steel IABs and the only occurrence of retainer fusing (RF) in the concrete IABs occurs when there are 3-spans and 15-ft tall piers due to the increased shear force across the bearings. The occurrence of these limit states allows the peak force capacity to be achieved at larger displacements, which may be beneficial during earthquakes.

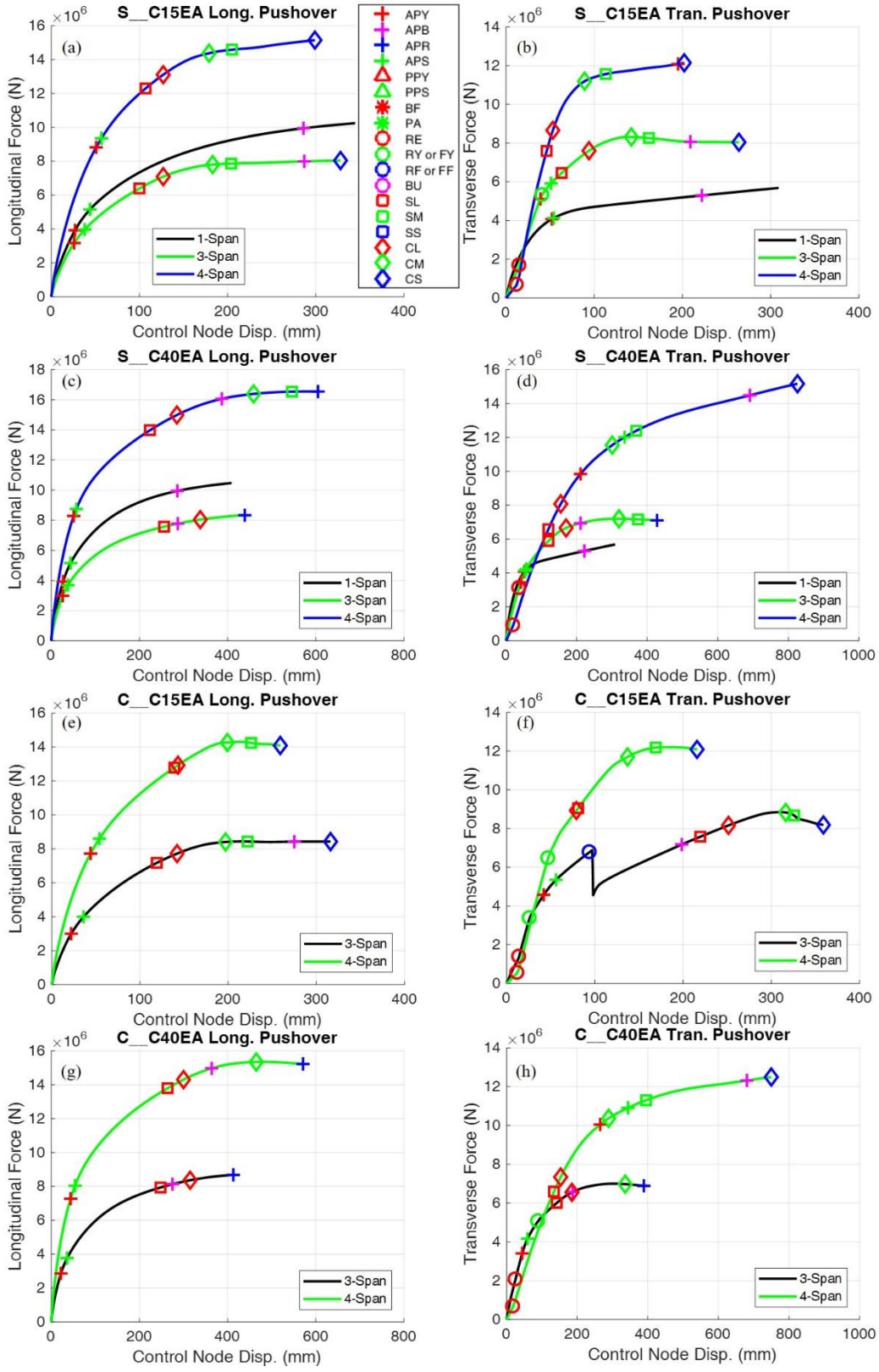

Figure 6.6: Comparison of IAB pushover curves in the longitudinal (left column) and transverse (right column) directions with varying span configurations.

Peaks in the force capacity can be clearly observed in nearly all the pushover curves presented. The exceptions to this trend are the four-span IABs with 40-ft piers due to the late abutment damage in the limit state occurrence sequence. The peak force resistance points always tend to correspond well with moderate pier column damage (CM and SM). As observed earlier, the decrease in capacity occurs much faster in the concrete IABs than the steel IABs due to the heavy superstructures speeding up the column deterioration.

6.3.3 Pier Height

Pier height is varied between short 15-ft piers and tall 40-ft piers in the parametric study. Comparisons of pushover curves between the two pier height options is presented in Fig. 6.7. In the longitudinal direction, the 40-ft piers produce IABs with larger force capacities, though the force capacities of both bridges with both pier types are relatively similar to each other. Initially the stiffness of the two bridges in each longitudinal situation is identical, however after abutment foundation initial damage (APY and APS) occurs the pushover curves diverge. The stiffness of the bridges with 40-ft piers is lower than the stiffness of the 15-ft pier bridges. This leads to the IABs with 40-ft piers reaching their peak force capacity at larger control node displacements. Again, the peak force capacities tend to be tied closely to the moderate pier column damage (SM and CM) limit states. The occurrence of moderate pier column damage in IABs with 15-ft piers also tends to create a more severe change in stiffness than in the IABs with 40-ft piers. IABs with 40-ft piers also experience more abutment pile strain as indicated by the consistent occurrence of APR in IABs with taller piers and no APR in IABs with shorter piers.

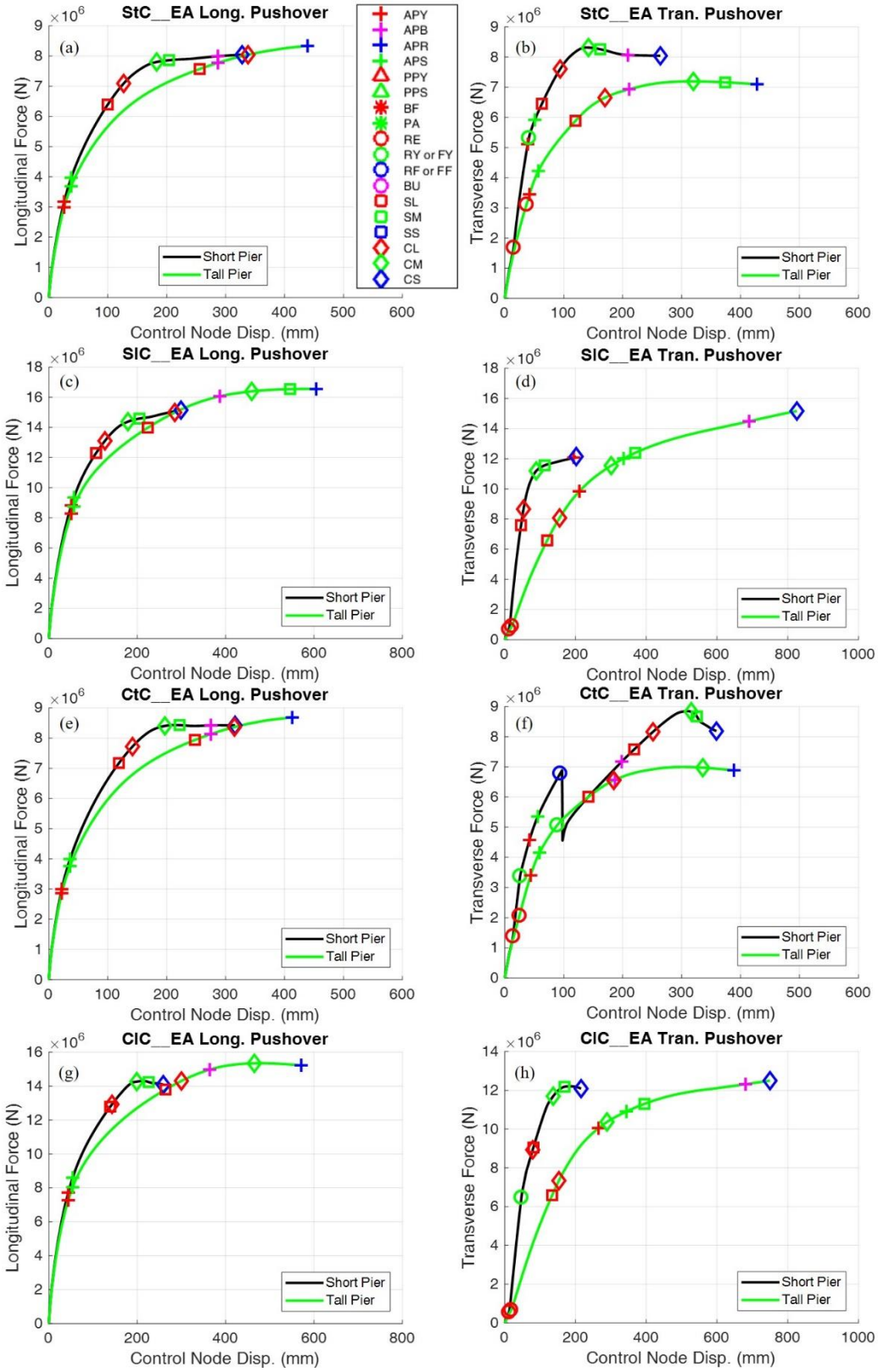

Figure 6.7: Comparison of IAB pushover curves in the longitudinal (left column) and transverse (right column) directions with varying pier heights.

The more severe stiffness change during moderate pier damage in IABs with shorter piers is also present in the transverse direction pushover results. This is once again due to the stiffer short piers contributing more stiffness to the overall IAB and when they begin to fail the overall IAB behavior also suffers. Contrarily, because a lot of the tall pier IAB stiffness is coming from the abutments, a drop in stiffness of the already flexible 40-ft piers leads to less of a dramatic overall IAB stiffness change.

The transverse pushover results also indicate that the tall pier IABs achieve less force capacity than the short pier IABs. This differs from the longitudinal direction observations, however the observation that damage, especially severe pier column damage (CS or SS), occurs at larger control node displacements still holds in the transverse direction. When observing the three-span IAB transverse results (Fig. 6.7b and 6.7f) there is more retainer damage in the IABs with shorter piers than in those with taller piers. This is seen by retainer yielding (RY) occurring in StC15EA but not StC40EA (in Fig. 6.7b) and retainer fusing (RF) occurring in CtC15EA but not CtC40EA (in Fig. 6.7f). This occurs due to the stiffer 15-ft tall piers resisting more lateral forces than the 40-ft tall piers under similar lateral forces applied to the superstructure. This leads to larger shear forces transferred from the superstructure to the piers through the bearings and retainers of the 15-ft pier IABs. The increased shear force leads to more retainer damage. In previous pushover curves it has been noted that IABs with more retainer damage typically produces stronger and more ductile IABs. However, this does not hold true in these situations due to the decreased stiffness of the 40-ft piers providing more ductility than retainer yielding or fusing could provide.

6.3.4 Bearing Layout

The bearings used at the pier cap-superstructure connection of the basic IABs are varied between using low-profile fixed bearings and Type I elastomeric bearings at all the locations. The resulting comparisons for the two bearing layouts in the basic steel IABs are provided in Fig. 6.8. The comparisons for the bearing layouts in the basic concrete IABs are provided in Fig. 6.9.

The pushover curves of the steel IABs presented in Fig. 6.8 demonstrate how the behavior of the IAB does not vary significantly depending on the type of bearing used. In general, there is more difference in the pushover curves when 15-ft piers are used. This difference is caused by 40-ft piers being less stiff than the 15-ft piers which in turn allows the IABs with taller piers to have limited force demands in the piers and bearings. The limited forces in the piers and bearings causes the behavior to be closely tied to the abutment behavior, which is the same in bridges with fixed and elastomeric bearings. The slight difference in the longitudinal pushover curves for IABs with 15-ft tall piers can be attributed to the increased stiffness of the piers after abutment foundation damage (APY and APS) when fixed bearings are used as compared to elastomeric bearings. The same limit states tend to occur in the same sequence, however they occur at slightly larger control node displacements when elastomeric bearings are used.

Differences in the transverse pushover curves for steel IABs with 15-ft tall piers can be observed due to the different limit states reached concerning elastomeric bearing side retainers and fixed bearings. The gap between the elastomeric bearing and the retainer allows for a small amount of bearing shear deformation to occur before retainer engagement (RE). After the retainer is engaged, the behavior of the fixed and elastomeric bearing IABs are extremely similar. Another difference occurs due to retainer yielding (RY) which changes the stiffness of the IAB in a slightly different manner than fixed bearing yielding (FY).

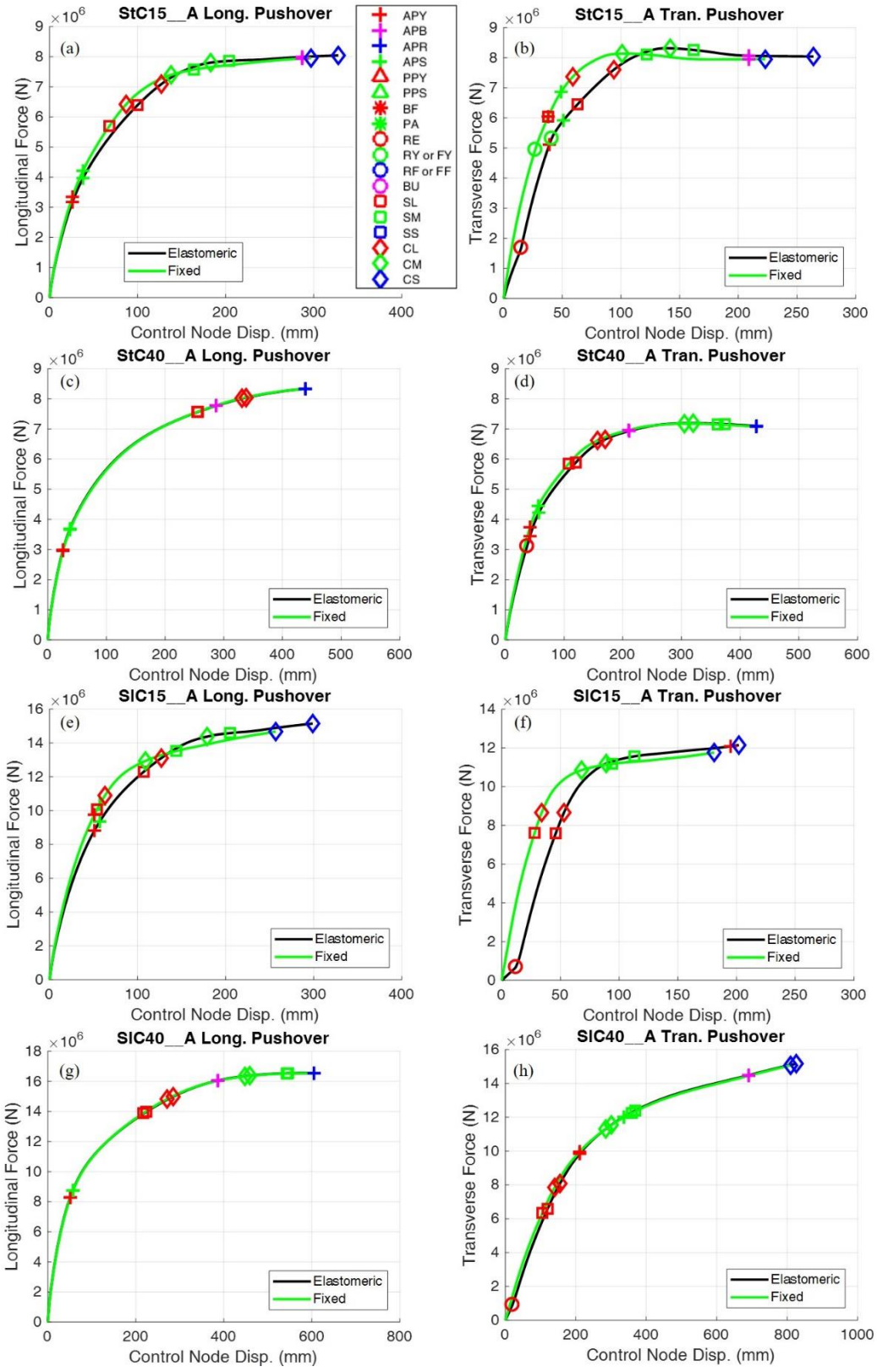

Figure 6.8: Comparison of steel IAB pushover curves in the longitudinal (left column) and transverse (right column) directions with varying bearing layouts.

The pushover curves for the concrete IABs presented in Fig. 6.9 also follow some of the same trends observed in the steel IABs. The concrete IABs with 40-ft piers have little difference depending on the bearing type used due to the decreased stiffness of the piers leading to an increased importance of abutment behavior. The longitudinal pushover curves for IABs with 15-ft tall piers differ depending on bearing type after initial abutment foundation damage (APY and APS) due to the fixed bearing IABs being stiffer in the longitudinal direction. Also, a major difference in one of the transverse pushover curves for a concrete IAB with 15-ft tall piers (ClC15_A, Fig. 6.9f) is attributed to the occurrence of retainer engagement causing an offset.

A major observation from the pushover curves of concrete IABs presented in Fig. 6.9 is the comparison of behavior between CtC15EA and CtC15FA in the transverse direction in Fig. 6.9b. Both bridges behave similarly up to the fusing of the retainer (RF) and fixed bearing (FF), although, as expected, the pushover curves do indicate that the fixed bearing IAB is stiffer. After fusing of the retainer and fixed bearings allow the bearings to be free to slide and deform. There is still enough friction between the elastomeric bearing and the concrete pier cap such that only shear deformations occur in the bearing which allow a significant amount of force to be transferred to the piers. This allows the damage to the pier columns to continue. However, the friction between the steel plate of the fixed bearing and the concrete pier cap is significantly less, allowing the fixed bearing to slide. This fixed bearing sliding acts as a fuse and limits the amount of force transferred to the piers. The sliding also allows for bearing unseating to take place when the bearing slides off the pier cap. The bearing unseating limit state is only observed in 2 of the 51 IAB pushover analyses, both of which use fixed bearings.

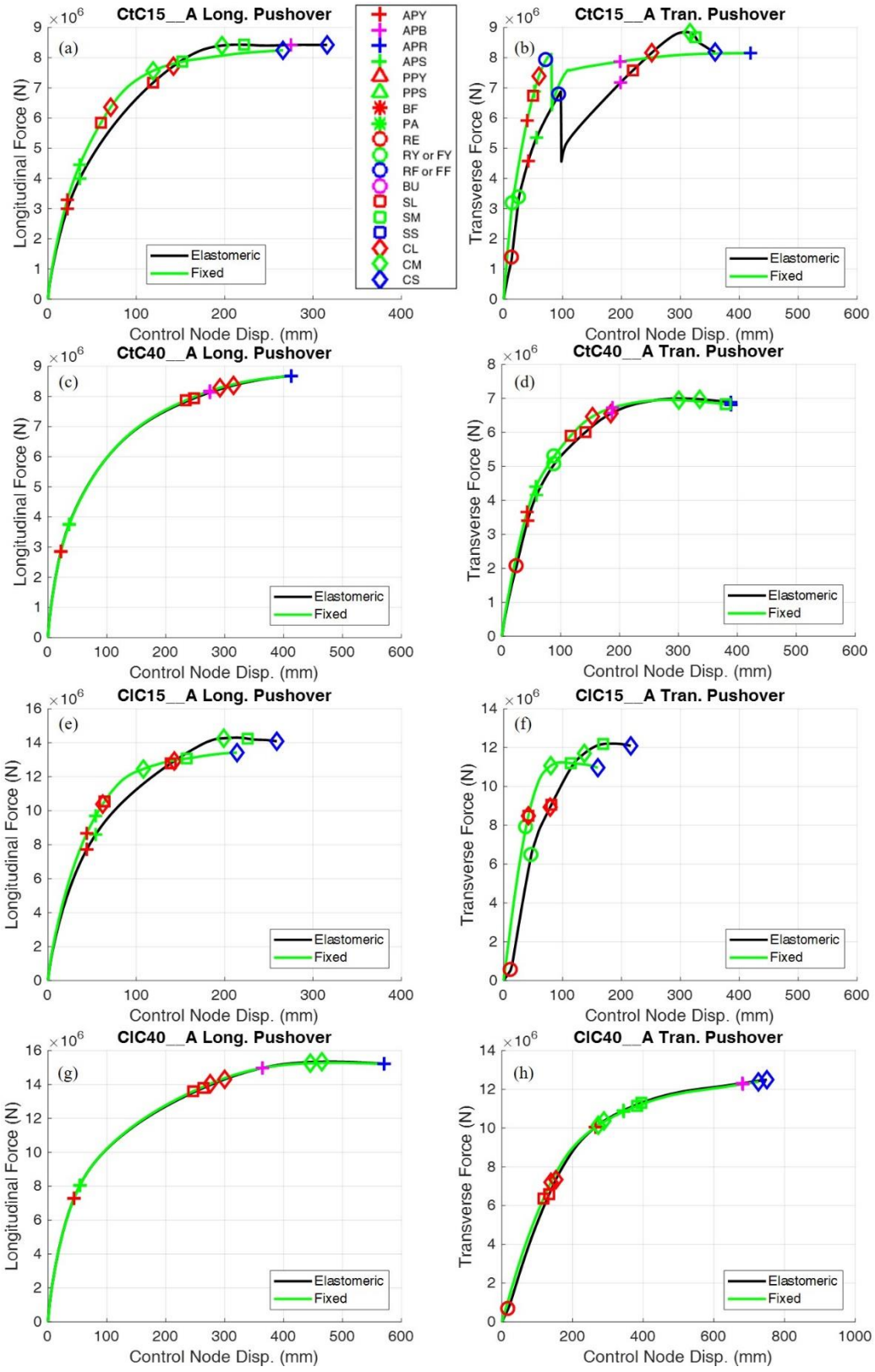

Figure 6.9: Comparison of concrete IAB pushover curves in the longitudinal (left column) and transverse (right column) directions with varying bearing layouts.

6.3.5 Soil Conditions

The foundation soil conditions are varied in the basic IABs to observe differences in behavior during the pushover analyses. The comparison of pushover analyses with the soft, alluvial, and stiff soil conditions are provided in Fig. 6.10 through Fig. 6.12. Fig. 6.10 provides the comparison of the pushover curves for the single-span steel IABs, Fig. 6.11 compares the results of the multi-span steel IABs, and Fig. 6.12 provides the results for the multi-span concrete IABs.

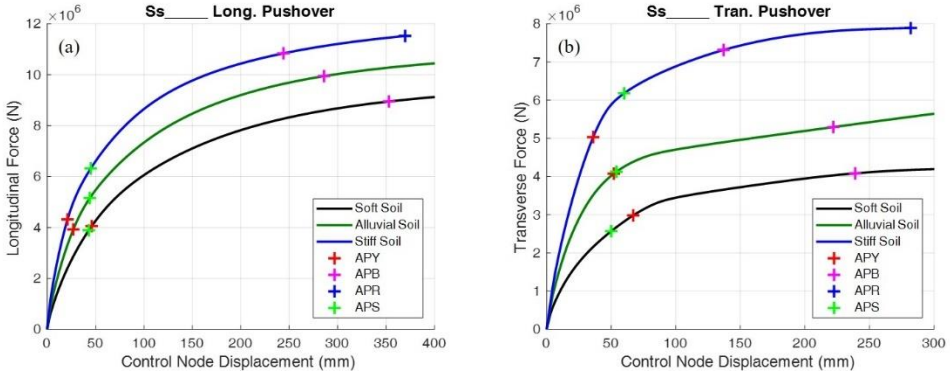

Figure 6.10: Comparison of single-span steel IAB pushover curves in the (a) longitudinal and (b) transverse directions with varying soil conditions.

The effects of the foundation soil conditions are simple to identify across all the IABs. This trend reveals that under stiffer soil conditions the bridges have a larger force capacity and the bridge in general is stiffer. This is logical given the large influence abutment behavior has on the overall IAB behavior. The sequence and position of the limit states which occur in the pushover analyses tend to always occur in the same order and at roughly the same control node displacement. A few exceptions to this include the occurrence of pier foundation damage (PPY and PPS) in StC15ES (Fig. 6.12b) and the abutment pile yielding (APY) and abutment soil mobilization (APS) changing order depending on the soil conditions. The changing in order of APY and APS has been discussed earlier. Through the APB and APR limit states it can also be shown that there is more stress and strain in the piles in IABs with stiffer soil conditions. The shape of the pushover curves are also extremely similar, varying only in force magnitude as the soil conditions change.

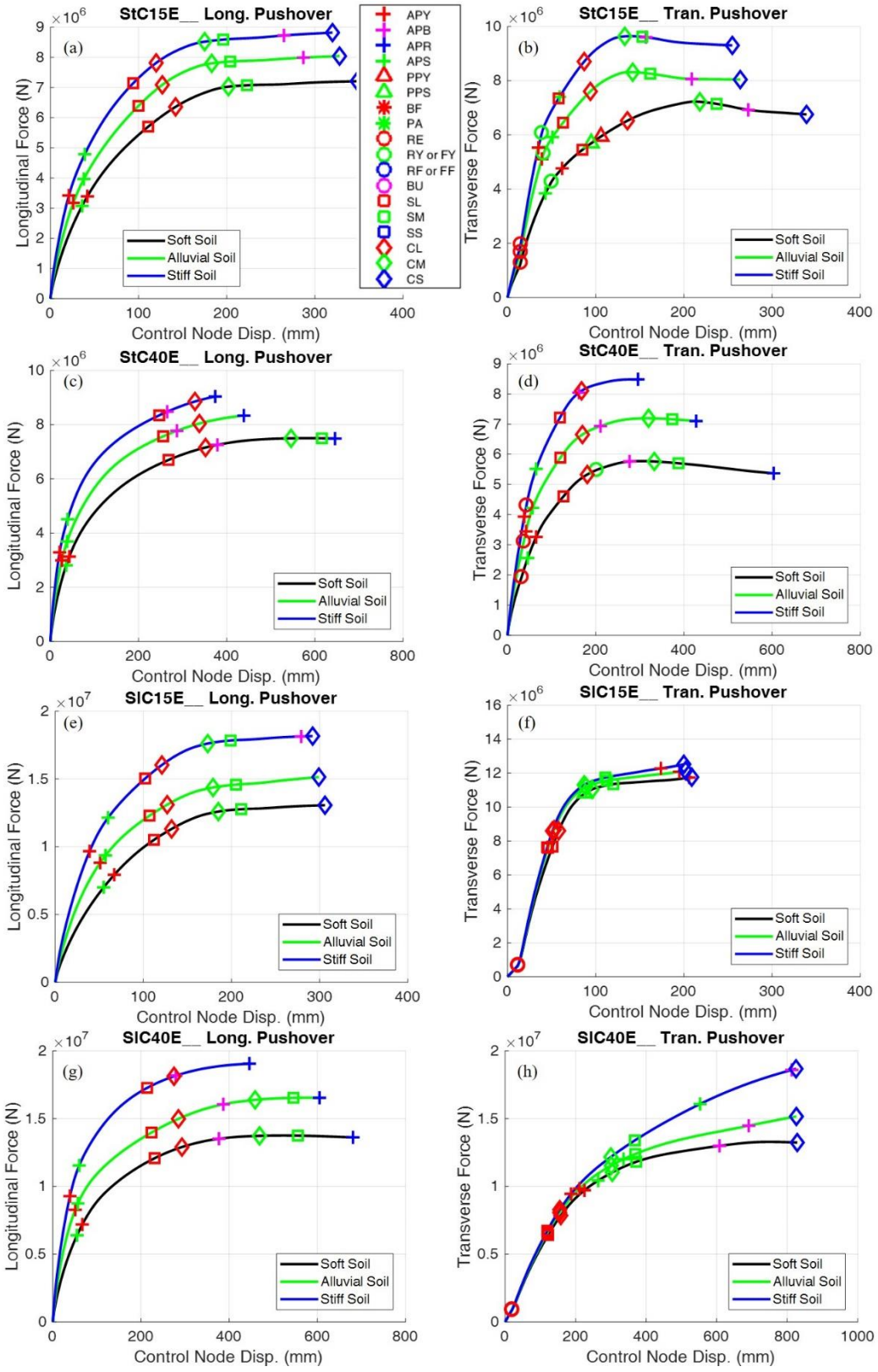

Figure 6.11: Comparison of steel IAB pushover curves in the longitudinal (left column) and transverse (right column) directions with varying soil conditions.

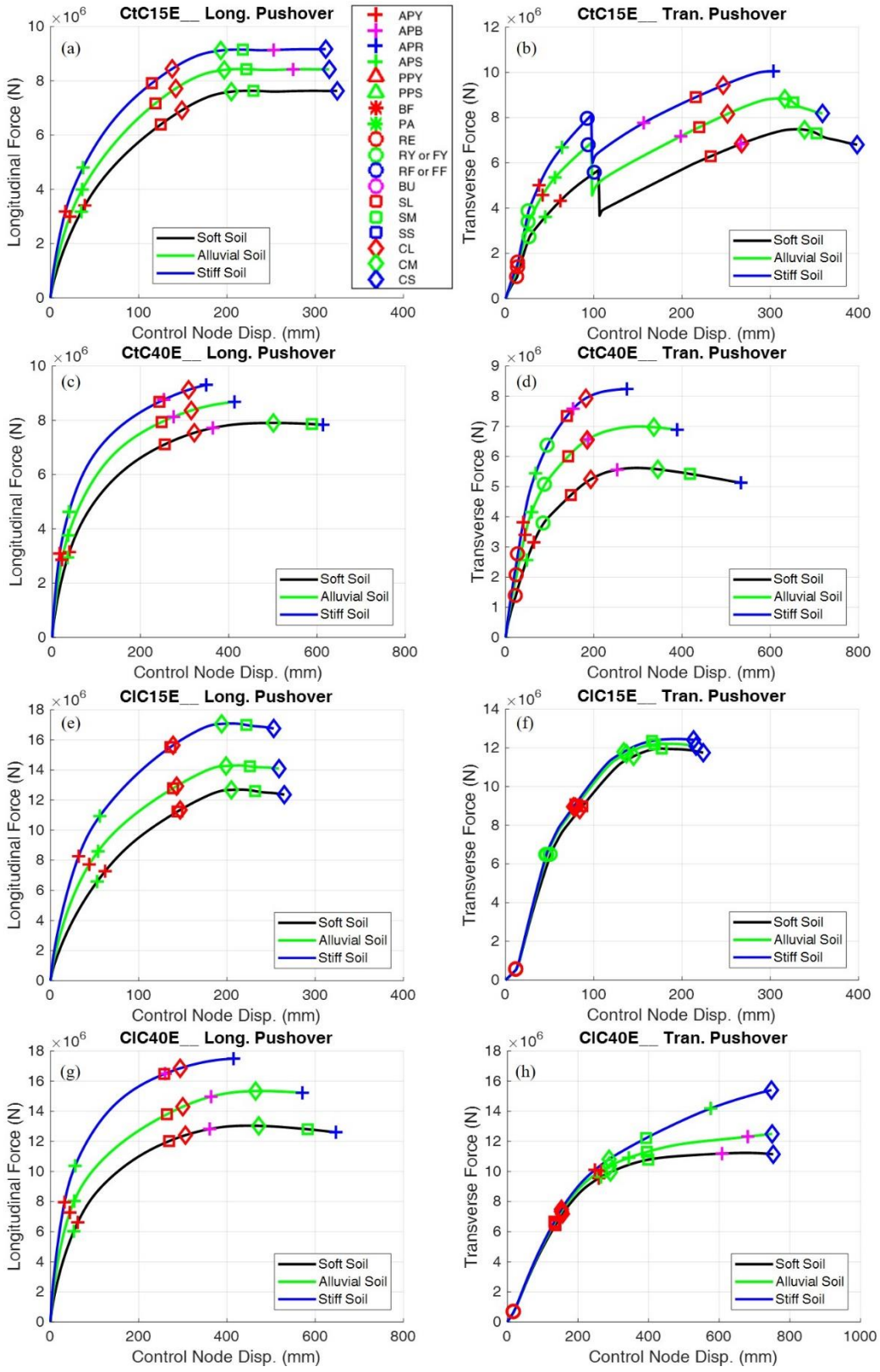

Figure 6.12: Comparison of concrete IAB pushover curves in the longitudinal (left column) and transverse (right column) directions with varying soil conditions.

6.4 CONCLUSIONS FROM PUSHOVER ANALYSES

Observing the sequences of limit state occurrence and trends from IABs submitted to the pushover analyses allows for some general conclusions to be made concerning the lateral behavior of IABs. The first major conclusions concerns the vulnerable components within the IABs. Given that nearly every IAB analyzed shows damage to the pier columns and abutment foundations through the occurrence of the moderate and severe pier column damage, abutment pile yielding, and mobilization of the soil surrounding the abutment pile limit states, these components are found to be the most vulnerable in the IABs. This conclusion agrees with damage observed in abutment foundations and pier columns after large earthquakes (Waldin *et al.*, 2012). It was found that the occurrence of abutment pile yielding largely affects the stiffness of the IAB in the pushover analysis. Further damage to the abutment piles through larger strains and the occurrence of APB and APR are also encountered more frequently in IABs with taller piers, stiffer soil conditions, and shorter spans. It was also found that moderate damage to the concrete or reinforcing steel of the pier columns tends to correspond with the peak force capacity of the IAB. Also, the first unacceptable limit state achieved in all but 2 of the 51 IABs is either severe damage to the pier column concrete or rupture of the abutment piles. These observations lead to the conclusion that pile strength, pier column strength, and soil condition play a large part in IAB behavior.

The trends observed through the design variations in the parametric study allowed for conclusions to be drawn concerning the effects on the limit state occurrences in the IAB. In general, it was observed that there was less retainer and fixed bearing damage to IABs with a steel superstructure. This is largely due to the much heavier concrete superstructures causing more force to be transferred through the bearings to the piers. Less retainer and fixed bearing damage is also encountered in bridges with taller piers. This is due to the less stiff pier columns limiting the

amount of force transferred through the bearings and therefore limiting the force applied to the retainers and fixed bearing anchor bolts. Span configuration was also found to affect the occurrence of limit states as the four-span bridges placed more demand on piers in the transverse direction, allowing the abutment piles to yield and the abutment soil to mobilize at much larger control node displacements than typically encountered. The order of limit state occurrence of abutment pile yielding and mobilization of the abutment soil also relies heavily on the soil conditions which generally has the soil mobilize before pile yielding in soft soil conditions, but the opposite occurring under stiffer soil conditions.

In terms of the shape and force capacities of the IAB pushover curves, it is found that having more spans and stiffer soils surrounding the piles of the abutments and piers allows for stiffer, stronger IABs. Taller piers in IABs do not necessarily allow for a larger force capacity, however they do decrease the stiffness of the IAB and allow for much more displacement before an unacceptable limit state is reached. Variations in the bearing layout between using elastomeric and fixed bearings has relatively small effects on the IAB pushover behavior, especially in four-span IABs. However, the use of fixed bearings does increase the chance of bearing unseating occurring due to the low friction between the fixed bearing steel and pier cap concrete.

In addition to the components which have modeled nonlinear behavior, the behavior of the superstructure elements were also monitored during the Ss____A, StC15EA, StC40EA, SlC15EA, SlC40EA, CtC15EA, CtC40EA, ClC15EA, and ClC40EA pushover analyses. The longitudinal superstructure elements tend to stay within the elastic range for most IABs, however 4-span IABs subjected to transverse loads do encounter stresses beyond the elastic limit in the concrete decks of SlC15EA, SlC40EA, ClC15EA, and ClC40EA. The girders of the IABs remain elastic, as is intended in the design of the superstructure. The increased stresses in the deck during transverse

loading indicates that the deck is particularly susceptible to cracking in that situation. The transverse diaphragm elements only encounter stresses beyond the elastic limit in IABs with concrete girders due to the increased lateral forces in the bridge. While it is not expected to significantly affect the results of this study, the inclusion of nonlinear behavior of the superstructure would be a prudent step in future analyses.

CHAPTER 7: PARAMETRIC STUDY DYNAMIC ANALYSIS RESULTS

7.1 PROCEDURE

Dynamic analyses are performed on the IABs of the parametric study in order to obtain information concerning the behavior of IABs during design-level seismic events and the sequence of damage occurring during seismic events of varying intensities. The sequence determined through seismic analyses may be different from the sequence determined through static pushover analyses in Chapter 6. Modal analyses are also performed on the bridges before the dynamic analyses to obtain overall stiffness and mode shape properties.

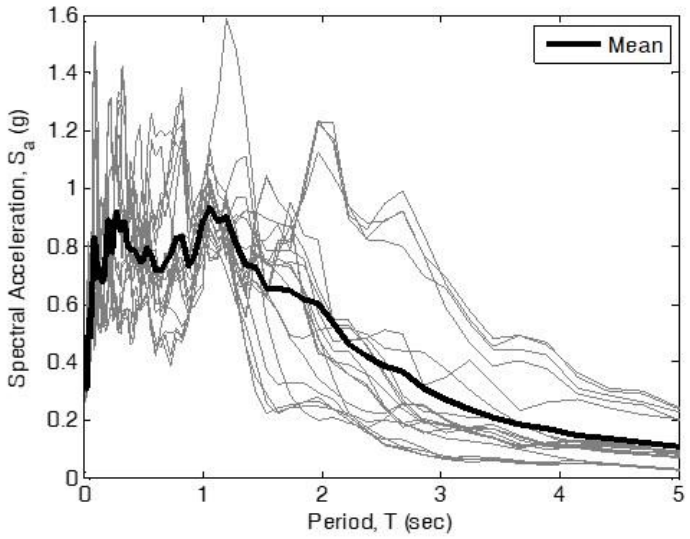

Figure 7.1: Spectra for the 20 ground motions at Cairo at the 1000-year return period hazard level.

The dynamic analyses are performed through the application of the 20 ground motions developed in Chapter 3 for Cairo, IL. Recall that the five CMS used to develop the ground motion at Cairo were very similar allowing for the suite of 20 ground motions to be matched for essentially the same target spectra (*i.e.* CMS). This satisfies the industry standard of having 7 ground motions

matched to a target spectra to account for the variability in the ground motions. These ground motions, whose spectra are presented in Fig. 7.1 and properties are described in Table 7.1, represent a 1000-year return period hazard for the site. The ground motions range in duration from 78.37 s to 99.41 s and have maximum ground accelerations between 0.260g and 0.343g. All 51 IAB variations were analyzed using the 20 ground motions. As indicated in earlier chapters, the soil properties in Cairo correspond to the alluvial soil condition, so that is used in the analyses as the realistic foundation soil condition. Analyses for the three-span and four-span concrete IABs with 15-ft tall piers and fixed bearings were not able to converge with any soil condition through numerous attempts, therefore there are only design-level dynamic analysis results for 45 of the 51 IABs.

Table 7.1: Ground motion characteristics for the 20 motions at Cairo, IL at the design-level.

Ground Motion	Maximum Acceleration, a_{max} (g)	Record Duration (s)	Time Steps	Time Step Size, dt (s)
Cro01	0.2819	98.330	19666	0.005
Cro02	0.2910	78.455	15691	0.005
Cro03	0.2670	94.120	18824	0.005
Cro04	0.3429	95.650	19130	0.005
Cro05	0.2737	99.050	19810	0.005
Cro06	0.2685	78.640	15728	0.005
Cro07	0.2761	94.205	18841	0.005
Cro08	0.2992	94.280	18856	0.005
Cro09	0.3064	94.710	18942	0.005
Cro10	0.2601	94.190	18838	0.005
Cro11	0.2885	78.730	15746	0.005
Cro12	0.2860	99.410	19882	0.005
Cro13	0.2953	94.880	18976	0.005
Cro14	0.2916	78.370	15674	0.005
Cro15	0.2971	78.670	15734	0.005
Cro16	0.2971	99.360	19872	0.005
Cro17	0.2870	94.245	18849	0.005
Cro18	0.2802	78.930	15786	0.005
Cro19	0.3202	78.595	15719	0.005
Cro20	0.3105	99.370	19874	0.005

Incremental dynamic analyses (IDA) are also performed on the 17 IABs which have alluvial foundation soil conditions using ground motion scale factor as an intensity measure. These dynamic analyses expose the IAB models to the design-level ground motions scaled up and down to varying degrees. The ground motions are linearly scaled between a scale factor (SF) of 0.5 to 1.75 in 0.25 increments where a scale factor of 1.00 corresponds to the design-level hazard of a 1000-year return period. Through comparison of the UHS for the design-level 1000-year return period hazard and the maximum considered earthquake (MCE)-level 2500-year return period hazard, it was determined that a scale factor of 1.75 is a suitable approximation for the MCE across southern Illinois. Similar to how the three-and four-span concrete IABs with 15-ft tall piers and fixed bearings did not yield any analysis results at the design-level, they were also unable to converge during the IDA. The four-span concrete IAB with 40-ft tall piers and fixed bearings was also unable to converge at larger scale factors leading to its exclusion from the IDA as well.

The acceleration time history of each ground motion, regardless of site or scale factor, is applied to the model as a uniform horizontal base excitation at all boundary nodes. This means that any potential spatial variation of the ground motion along the length of the bridge is not considered. The spatial variation is not accounted for due to the variability of conditions which may be present between the abutments. These variabilities include whether the bridge is crossing a deep river, a shallow river, or another road, as well as any slight differences between the embankment soil at each abutment. To account for the most general case in this study, these variations are not considered, and the ground motion is assumed to be identical along the length of the bridge.

7.2 MODAL ANALYSIS

Complementing the dynamic analyses is the modal analysis of the IABs which explores the dynamic properties of the bridges. The modal analysis accounts for the location and magnitude of mass in the bridge as well as the interaction of the connected bridge components to give insight into the overall bridge stiffness in different directions. This analysis is useful in providing an initial idea of which directions of excitation the bridges are vulnerable and what bridge property changes have significant effects on bridge stiffness and dynamic behavior. The first two modes of each of the bridges are observed and their corresponding natural periods are recorded along with the mode shape type. Tables 7.2 through 7.6 provide the natural period and corresponding mode shape data while Figs. 7.2 through 7.4 provide examples of the observed mode shapes.

7.2.1 Single-Span IABs

The single-span steel IABs, provided in Table 7.2, are relatively stiff with a first natural period not exceeding 0.6 s. The first mode is always the vertical mode (shown in Fig. 7.2a) due to the 160-ft span bridge being confined between the abutments and therefore being extremely stiff in the longitudinal and transverse directions. The second mode typically corresponds to the longitudinal mode shape (Fig. 7.2b). However, the longitudinal mode becomes significantly stiffer (shorter period) as the foundation soil condition becomes stiffer up to the point where the longitudinal mode becomes stiffer than the transverse mode (Fig. 7.2c).

Table 7.2: Modal analysis data for single-span steel IABs.

Bridge	1st Mode		2nd Mode	
	T_1 (s)	Shape	T_2 (s)	Shape
Ss____S	0.5967	Vert.	0.4231	Long.
Ss____A	0.5666	Vert.	0.3434	Long.
Ss____H	0.5389	Vert.	0.3091	Tran.

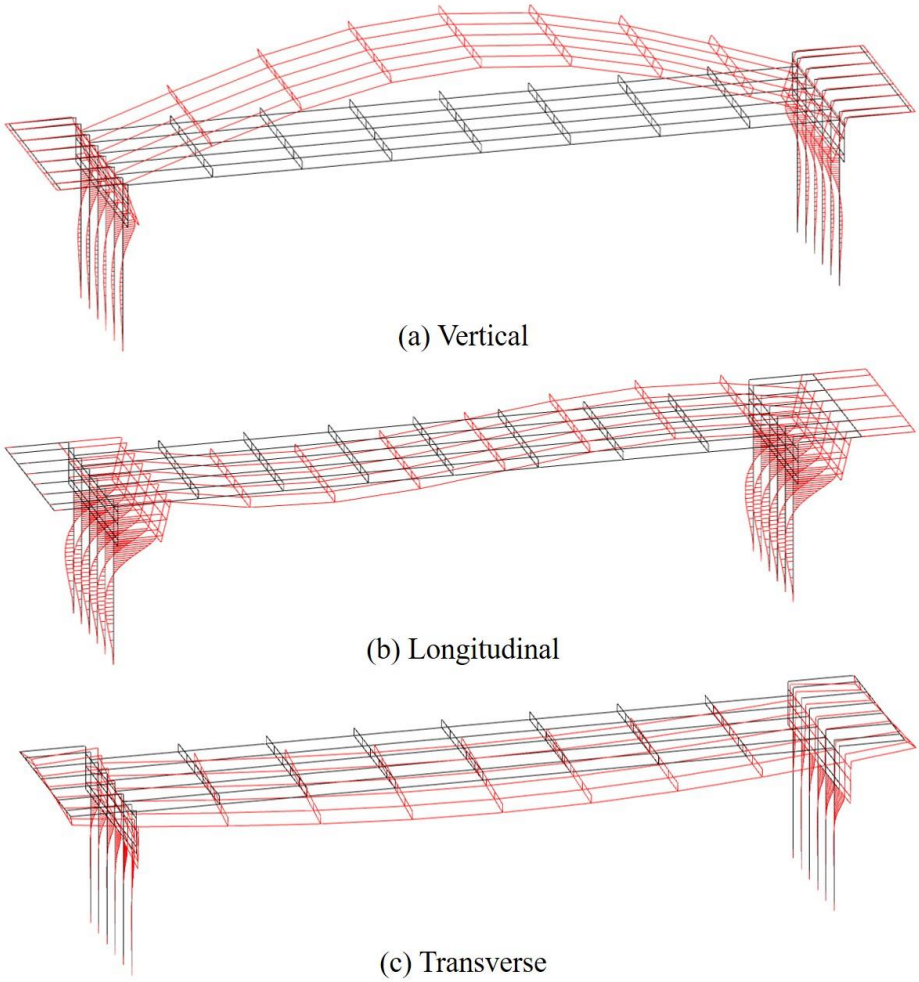

Figure 7.2: Mode shapes present in the first two modes of the single-span steel IABs.

7.2.2 Three-Span IABs

The three-span steel IABs provide a range of first mode periods between 0.5 and 0.6 s, as shown in Table 7.3, indicating that they too are relatively stiff. It can be noted that the first mode for each of the bridges with soft soil conditions is longitudinal (Fig 7.3a) due to the soil being weak to a point where movement in the longitudinal direction is much easier. When stiffer soil conditions are present the longitudinal mode is typically the second or higher mode. With 40-ft tall piers, as the soil becomes stiffer the longitudinal mode changes from the first to second mode, then to a mode greater than the second under the stiffest soil conditions. As this occurs the transverse mode (Fig. 7.3b) becomes more prominent due to the flexible nature of the tall piers. The modal periods

can also demonstrate conclusions concerning pier height similar to those found in the pushover analyses with shorter piers being associated with stiffer IABs (have shorter first periods). The vertical mode shape (Fig. 7.3c) is also prominent in these bridges due to the relative stiffness of the IAB in the longitudinal and transverse direction leading to movement of the deck only.

Table 7.3: Modal analysis data for three-span steel IABs.

Bridge	1st Mode		2nd Mode	
	T_1 (s)	Shape	T_2 (s)	Shape
StC15ES	0.5780	Long.	0.5707	Tran.
StC15EA	0.5275	Tran.	0.4989	Vert.
StC15EH	0.5028	Tran.	0.4956	Vert.
StC40ES	0.6346	Long.	0.6203	Tran.
StC40EA	0.5716	Tran.	0.5454	Long.
StC40EH	0.5437	Tran.	0.4971	Vert.
StC15FS	0.5668	Long.	0.5005	Vert.
StC15FA	0.4970	Vert.	0.4873	Long.
StC15FH	0.4935	Vert.	0.4357	Long.
StC40FS	0.6278	Long.	0.6069	Tran.
StC40FA	0.5629	Tran.	0.5306	Long.
StC40FH	0.5375	Tran.	0.4946	Vert.

Unlike the three-span steel IAB, the three-span concrete IAB, whose modal data is provided in Table 7.4, does not experience any change in mode shape with variations in the foundation soil condition. Also unlike the three-span steel IAB, the three-span concrete IAB vertical mode is not present at all in the first two modes. This is due to the increased flexibility in the three-span concrete IABs causing the longitudinal and transverse periods to be much longer than the vertical period. The flexibility can be explained by observing that the stiffness from the abutments and pier columns are approximately equivalent to the steel IAB, but the mass of the concrete superstructure is much greater. The combination of these two factors leads to longer periods as demonstrated from Eq. (7.1) where k is the lateral stiffness from the piers and abutment,

m is the mass in the bridge superstructure, and *T* is the period. If mass, *m*, increases, the period, *T*, becomes longer.

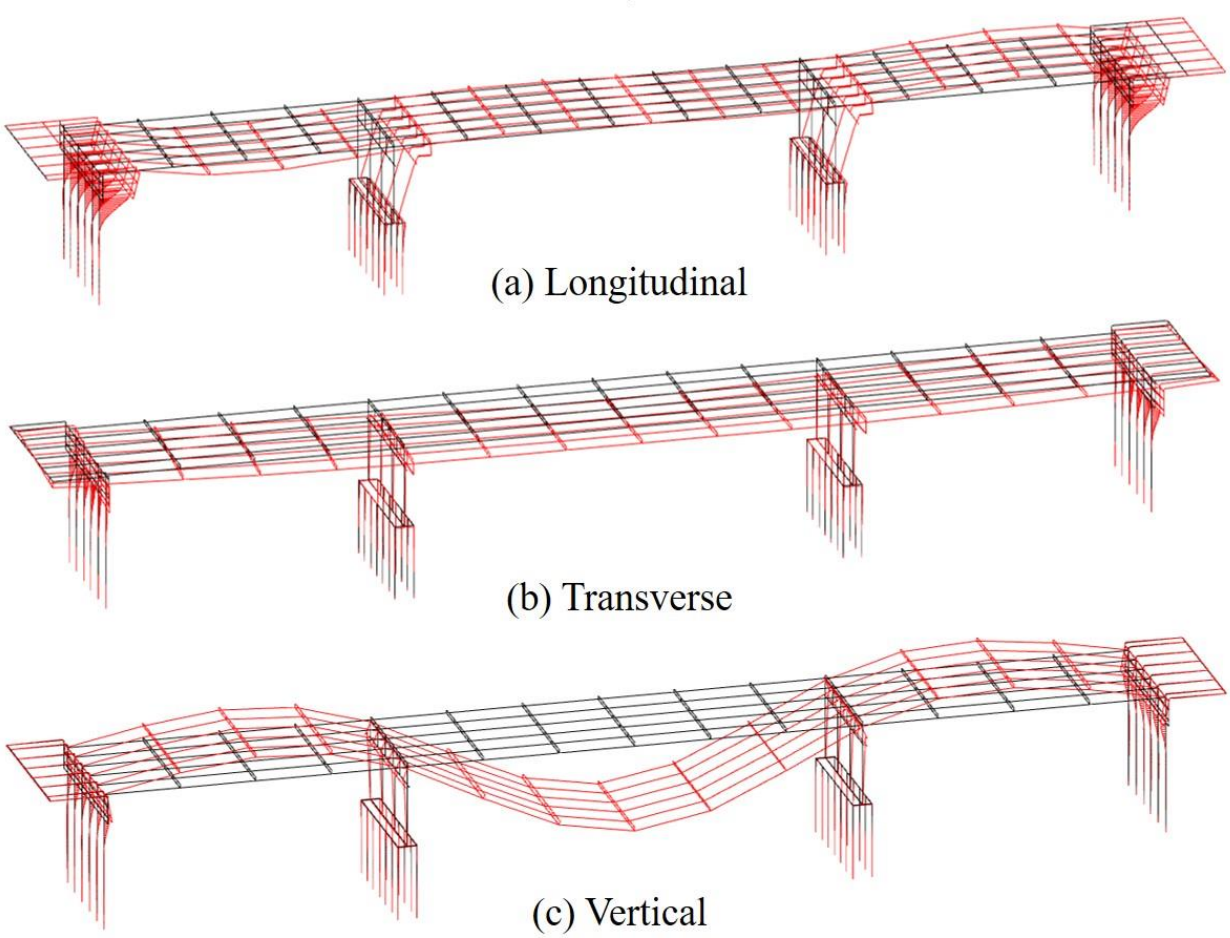

Figure 7.3: Mode shapes present in the first two modes of the three-span IABs.

$$T = 2\pi\sqrt{\frac{m}{k}} \tag{7.1}$$

The three-span concrete IABs do have similar trends as the three-span steel IABs with respect to pier height and foundation stiffness. With shorter pier heights the bridges become stiffer. Similarly, as the foundation soil becomes stiffer the bridges also become stiffer and have shorter periods. Another similarity which is easier to see in the three-span concrete results is the impact that bearing type has on the bridge. While there is little effect on the longitudinal mode period

depending on bearing type, there is a significant reduction in transverse mode period when fixed bearings are used. This decrease is demonstrated in in the CtC15__ bridges which switch first modes depending on bearing type due to the large decrease in the period of the transverse mode. The lack of change in the longitudinal mode period when different bearings are used is due to the large reliance on abutment and backfill stiffness in that direction while the transverse direction is heavily influenced by pier and bearing stiffness.

Table 7.4: Modal analysis data for three-span concrete IABs.

Bridge	1st Mode		2nd Mode	
	T1 (s)	Shape	T2 (s)	Shape
CtC15ES	0.7951	Tran.	0.6944	Long.
CtC15EA	0.7371	Tran.	0.5729	Long.
CtC15EH	0.7041	Tran.	0.4905	Long.
CtC40ES	0.8306	Tran.	0.7385	Long.
CtC40EA	0.7672	Tran.	0.6126	Long.
CtC40EH	0.7314	Tran.	0.5351	Long.
CtC15FS	0.6685	Long.	0.5281	Tran.
CtC15FA	0.5585	Long.	0.4934	Tran.
CtC15FH	0.4819	Long.	0.4750	Tran.
CtC40FS	0.7876	Tran.	0.7359	Long.
CtC40FA	0.7338	Tran.	0.6031	Long.
CtC40FH	0.7030	Tran.	0.5129	Long.

7.2.3 Four-Span IABs

The four-span steel IAB results presented in Table 7.5 demonstrate the increased flexibility of the four-span bridges in the transverse direction. While the longitudinal modes (Fig. 7.4c and 7.4d) are generally within the period ranges found in the three-span IABs, the transverse modes (Fig. 7.4a) are extremely long at around 1.1 to 1.4 s. This makes the transverse mode the predominant first mode for most of the four-span steel IABs. The exception to this is the four-span steel IAB with 15-ft tall piers and fixed bearings which reduce the transverse mode period so

significantly that it is no longer one of the first two modes. This is likely due to the effect that fixed bearings have on the transverse mode, as explained earlier, in conjunction with the stiffer 15-ft piers also shortening the period. A unique characteristic of the four-span steel IAB is the presence of a second longitudinal mode (Fig. 7.4d) and a torsional mode (Fig. 7.4e).

Table 7.5: Modal analysis data for four-span span IABs.

Bridge	1st Mode		2nd Mode	
	T1 (s)	Shape	T2 (s)	Shape
SlC15ES	1.2515	Tran.	0.7556	Long.
SlC15EA	1.2333	Tran.	0.7329	Long.
SlC15EH	1.2191	Tran.	0.7235	Long.
SlC40ES	1.4156	Tran.	0.7838	Long.
SlC40EA	1.3925	Tran.	0.7464	Long.
SlC40EH	1.3737	Tran.	0.7326	Long.
SlC15FS	0.7397	Long.	0.5943	Long. 2
SlC15FA	0.7241	Long.	0.5442	Tors.
SlC15FH	0.7172	Long.	0.5441	Tors.
SlC40FS	1.1480	Tran.	0.7816	Long.
SlC40FA	1.1320	Tran.	0.7451	Long.
SlC40FH	1.1203	Tran.	0.7315	Long.

The four-span concrete IAB results, presented in Table 7.6, also demonstrate the increased transverse flexibility while the longitudinal period remains much shorter. Due to the use of a heavier concrete superstructure the four-span concrete IABs are even more flexible in the transverse direction than the four-span steel IABs. This is demonstrated by the occurrence of two transverse modes (Fig. 7.4a and 7.4b) before any other modes are seen in 9 of the 12 four-span concrete IABs. The flexibility in the transverse direction as compared to the longitudinal direction is so large that even during a period shortening of around 1 s when fixed bearings are implemented in the ClC15__ bridges the transverse mode is still the first mode.

Table 7.6: Modal analysis data for four-span concrete IABs.

Bridge	1st Mode		2nd Mode	
	T1 (s)	Shape	T2 (s)	Shape
ClC15ES	1.7975	Tran.	1.0455	Tran. 2
ClC15EA	1.7780	Tran.	1.0284	Tran. 2
ClC15EH	1.7656	Tran.	1.0207	Tran. 2
ClC40ES	1.9995	Tran.	1.0860	Tran. 2
ClC40EA	1.9767	Tran.	1.0681	Tran. 2
ClC40EH	1.9614	Tran.	1.0599	Tran. 2
ClC15FS	0.8579	Long.	0.8175	Tran.
ClC15FA	0.7911	Tran.	0.7609	Long.
ClC15FH	0.7799	Tran.	0.7269	Long.
ClC40FS	1.5579	Tran.	1.0067	Tran. 2
ClC40FA	1.5411	Tran.	0.9905	Tran. 2
ClC40FH	1.5315	Tran.	0.9831	Tran. 2

In comparison with the three-span IABs, the four-span IABs do share many similarities. These include the bridges with shorter piers and stiffer foundation conditions being stiffer overall. As noted above, the use of fixed bearings also significantly impacts the transverse modes but not the longitudinal modes, and the concrete IABs are more flexible. The main difference between the three- and four-span bridges seems to be the increased flexibility of the four-span bridges in the transverse direction leading to an overall longer first period for the bridges.

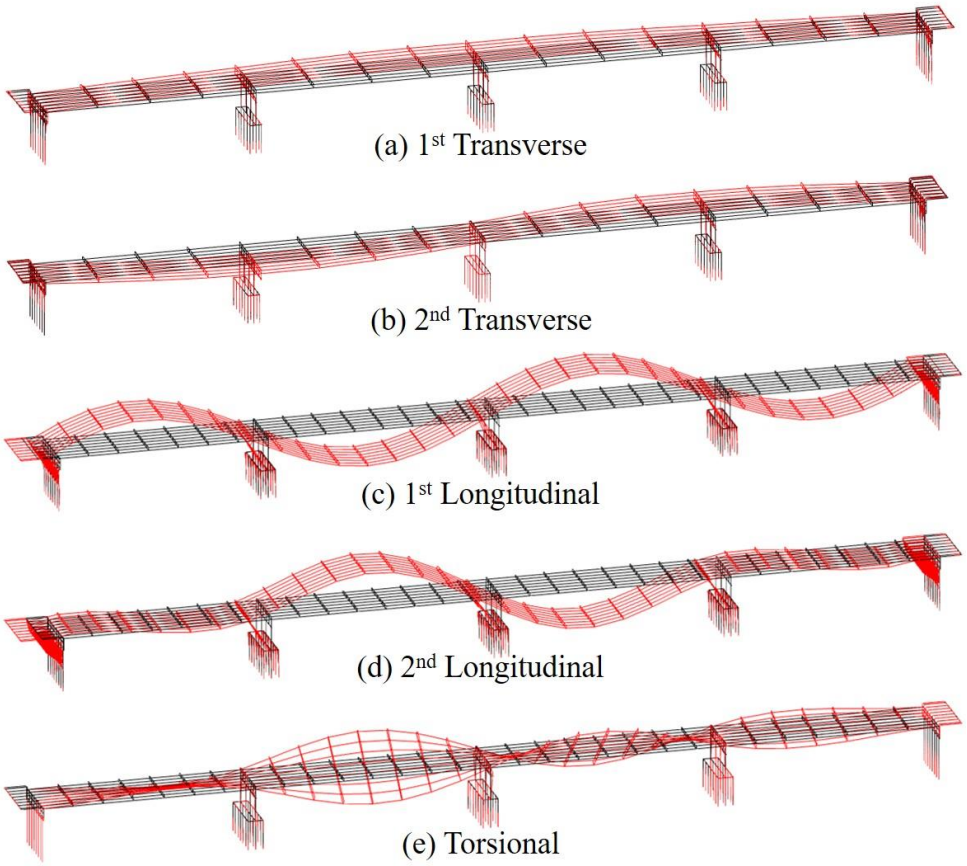

Figure 7.4: Mode shapes present in the first two modes of the four-span IABs.

7.2.4 General Observations from the Modal Analysis

Five general observations can be made from the modal analysis results. The observations tend to match well with the trends observed in the pushover analyses. The first observation concerns the pier height and concludes that shorter piers produce stiffer bridges. Similarly, the second observation finds that bridges with shorter spans tend to be stiffer and that long-span bridges are extremely flexible in the transverse directions leading to multiple transverse mode shapes in the first two modes. The third observation finds that stiffer soil produces stiffer IABs in all mode shapes due to the large influence of the abutment foundation behavior in all directions. The fourth observation concludes that the transverse mode is significantly stiffer when fixed bearings are used in comparison to elastomeric bearings. This observation is not true in the

longitudinal modes due to their heavy reliance on the abutment and backfill stiffness which is unchanged by bearing type selection. Finally, it was observed that concrete IABs are more flexible than steel IABs due to their larger superstructure weight. Overall, these observations help to identify potential issues in the IABs that could arise during earthquakes.

7.3 DESIGN-LEVEL DYNAMIC ANALYSIS RESULTS

The analysis of the 45 IAB models (recall that CtC15F_ and ClC15F_ did not yield results) at the 1000-year return period design-level earthquake hazard provides information concerning the frequency of occurrence of the various limit states within the bridges. By assessing which limit states occur and how often they occur the IABs may be deemed to be ideal, acceptable, or unacceptable designs for the current design-level. In order to illustrate the results, tables are presented which describe the frequency at which each limit state occurs for each IAB out of the 20 ground motions it is subjected to. Additionally, figures presenting typical behavior on an IAB with 15-ft tall piers, elastomeric bearings, and alluvial soil conditions during one of the ground motions is also provided to demonstrate key behavior. The behavior is presented using plots of the center node displacement time history, the center node displacement-base shear behavior, the overall backfill behavior at one abutment, the retainer behavior of all the retainers, the stress-strain behavior of the four extreme fibers at the top of one of the abutment piles, and the behavior of the top p-y spring in one of the abutment piles. The red dashed lines in the backfill behavior and top p-y spring behavior plots correspond to the load required to mobilize these components The bridge results are described in five sections based on their superstructure material and span configuration.

7.3.1 Single-Span Steel IABs

The design-level dynamic results for the three single-span steel IABs is presented in Table 7.7. Recall that due to the lack of piers there are only six limit states which could apply to these

bridges and the only variation is the foundation soil condition. A few general observations can be made from Table 7.7 which includes the observation that backfill mobilization and failure at the pile cap-abutment interface does not occur. This leaves the only limit states which occur being the yielding of the abutment piles (APY) and the mobilization of the soil surrounding the abutment piles (APS). Although the piles yield, the strain in the piles is not excessive as pile local buckling is never reached.

Table 7.7: Frequency of limit state occurrences for single-span steel IABs under design-level ground motion suite.

Bridge	Longitudinal Limit State Occurrence					
	Ideal	Acceptable				Unacceptable
	BF	APY	APB	APS	PA	APR
Ss____S	0%	65%	0%	30%	0%	0%
Ss____A	0%	80%	0%	0%	0%	0%
Ss____H	0%	30%	0%	0%	0%	0%
Bridge	**Transverse Limit State Occurrence**					
	Ideal	Acceptable				Unacceptable
	BF	APY	APB	APS	PA	APR
Ss____S	0%	80%	0%	65%	0%	0%
Ss____A	0%	10%	0%	5%	0%	0%
Ss____H	0%	0%	0%	0%	0%	0%

In the longitudinal direction there is more damage to the abutment foundation, both to the piles and the surrounding soil, under softer soil conditions. Due to the soft soil condition having the lowest ultimate capacity in the p-y springs the mobilization of the abutment soil (APS) only occurs in Ss____S. However, as shown in Fig. 7.5e for Ss____A, even when the APS limit state does not occur the top p-y springs in the piles are still very close to mobilizing (reaching the dashed red line in Fig. 7.5e). It can also be observed from Fig. 7.5d that the piles do not reach an extreme level of yielding, reaching a stress of less than 400 MPa and a strain of about 0.003 which is well short of the pile local buckling strain of 0.04 determined through estimates based on experimental

results (Frosch *et al.*, 2009). Although the backfill mobilization does not occur in the analyses, the backfill is still engaged during dynamic loading in the longitudinal direction. However, it is generally not close to mobilizing, as indicated in Fig. 7.5c where the dashed red line indicates backfill mobilization.

In the transverse direction there is once again less occurrence of abutment pile yielding (APY) and mobilization of the soil surrounding the abutment piles (APS) as the soil conditions become stiffer. In fact, APY and APS occur most of the time in the soft soil condition, rarely in the alluvial soil condition, and never in the stiff soil condition. Observations concerning the p-y spring behavior are also similar in both the longitudinal and transverse direction, as shown in Fig. 7.6e where the p-y spring almost reaches the ultimate capacity. It can be shown from Table 7.7 that APS occurs more often in the transverse direction with the soft and alluvial soil conditions when compared to the longitudinal direction. However, APS once again never occurs in the stiff soil condition. The increase in APS occurrence is due to the lack of backfill in the transverse direction (shown in Fig. 7.6c) requiring all the lateral force to be resisted by the abutment piles and the soil. Due to the arrangement of the piles, which has strong axis bending under transverse excitation, they do not yield as often (as shown in Fig. 7.6d) in the transverse direction allowing for more force to be taken within the soil.

Overall, the single-span steel IABs have acceptable designs due to the worst limit states being acceptable limit states. The lack of bearings and piers makes it impossible for the superstructure to unseat or piers to fail. While the APY and APS limit states are acceptable, they are still not as ideal as backfill mobilization, which does not occur in a single analysis. Improvements could be made by allowing for more backfill engagement and less damage to the abutment foundation.

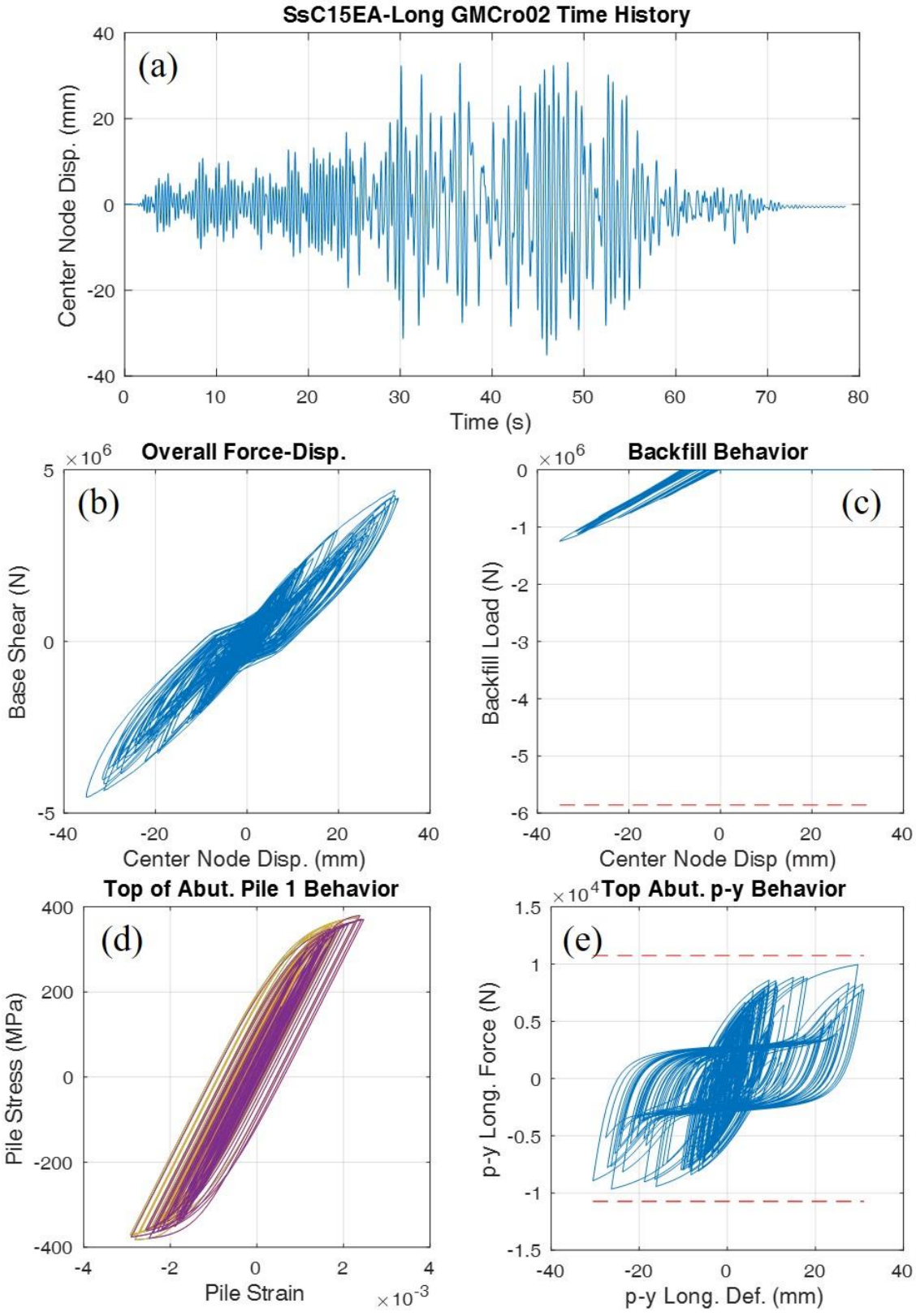

Figure 7.5: Dynamic analysis results for Ss____A subjected to a design-level ground motion in the longitudinal direction.

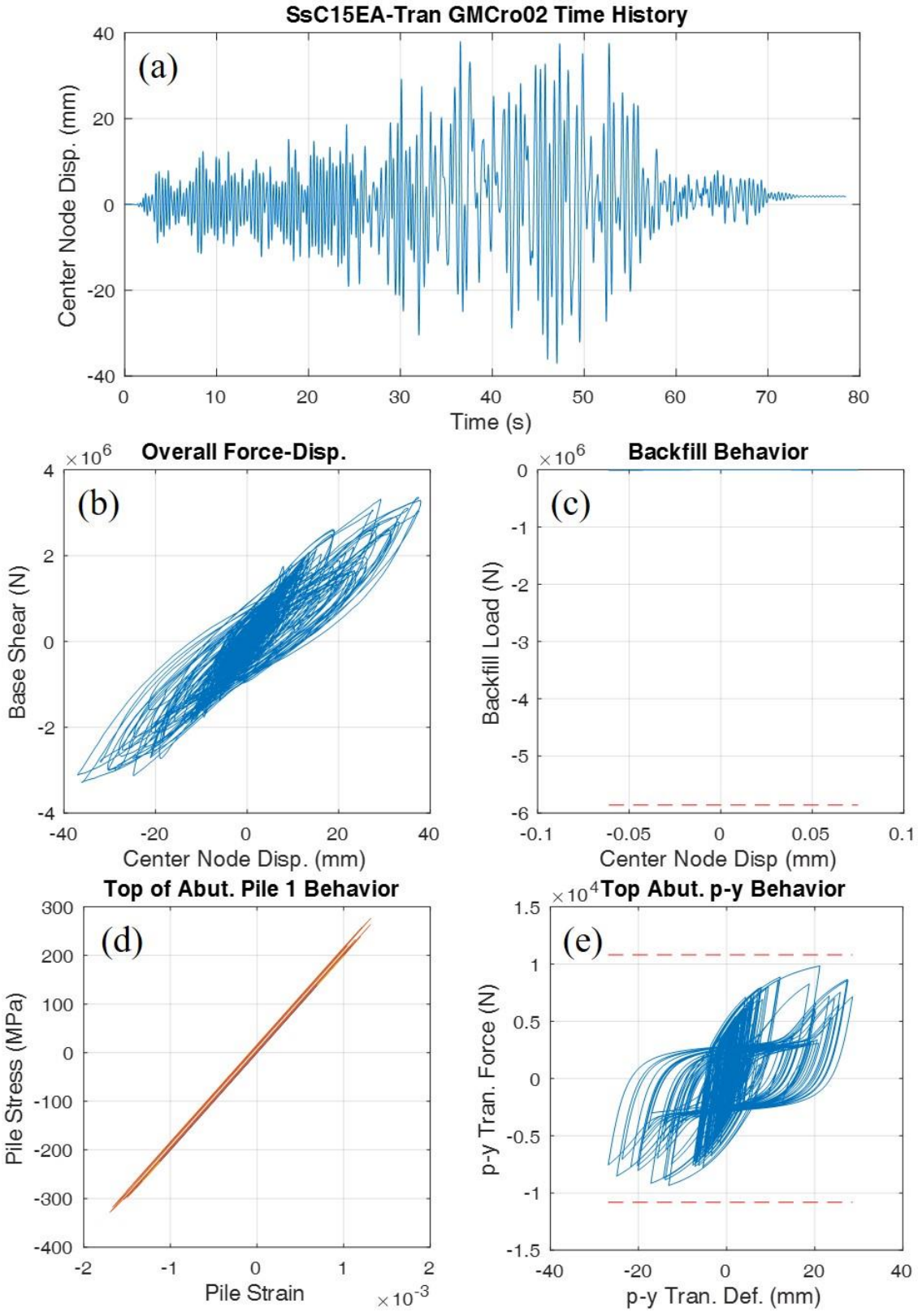

Figure 7.6: Dynamic analysis results for Ss____A subjected to a design-level ground motion in the transverse direction.

7.3.2 Three-Span Steel IABs

The three-span steel IAB dynamic analysis results are presented in Table 7.8 along with sample component behavior in Fig. 7.7 for longitudinal behavior and Fig. 7.8 for transverse behavior. The results from dynamic excitation in the longitudinal direction yield the occurrence of many limit states, however backfill mobilization (BF), retainer or fixed bearing damage (RE, RY, RF, FY, and FF), the failure of the pile cap-abutment interface (PA), or any of the unacceptable limit states do not occur. The lack of unacceptable limit states is encouraging, however in the longitudinal direction backfill mobilization is an ideal limit state. While mobilization of the backfill does not occur, it can be shown to be engaged (see Fig. 7.7c) and the engagement and compaction of the backfill is the reason for the pinching behavior in the center node displacement-base shear behavior of Fig. 7.7b.

The longitudinal results also yield important information concerning the abutment foundation which has its piles yield (APY) in every analysis of every bridge. The pile behavior is shown to reach nearly 5 times the yield strain in Fig 7.7d, nowhere near the 20 times yield strain value for pile local buckling (APB). The abutment foundation soil also mobilizes (APS) frequently, especially in soft soil conditions, where it always mobilizes, and in alluvial soil conditions, where it mobilizes most of the time. It can be observed from Table 7.8 that APB and APS occur more often in IABs with 40-ft tall piers as opposed to those with 15-ft tall piers. This is caused by the less stiff tall piers requiring the abutments to provide most of the stiffness for the bridge and therefore has larger demands in the abutments.

Table 7.8: Frequency of limit state occurrences for three-span steel IABs under design-level ground motion suite.

Bridge	Longitudinal Limit State Occurrence																			
	Ideal								Acceptable								Unacceptable			
	BF	SL	CL	RE	RY	RF	FY	FF	APY	APB	APS	PA	PPY	PPS	SM	CM	BU	SS	CS	APR
StC15ES	0%	100%	100%	0%	0%	0%	-	-	100%	0%	100%	0%	20%	45%	50%	65%	0%	0%	0%	0%
StC15EA	0%	60%	35%	0%	0%	0%	-	-	100%	0%	70%	0%	0%	0%	0%	0%	0%	0%	0%	0%
StC15EH	0%	20%	5%	0%	0%	0%	-	-	100%	0%	30%	0%	0%	0%	0%	0%	0%	0%	0%	0%
StC40ES	0%	80%	25%	0%	0%	0%	-	-	100%	30%	100%	0%	0%	70%	10%	5%	0%	0%	0%	0%
StC40EA	0%	15%	0%	0%	0%	0%	-	-	100%	15%	100%	0%	0%	5%	0%	0%	0%	0%	0%	0%
StC40EH	0%	0%	0%	0%	0%	0%	-	-	100%	0%	60%	0%	0%	0%	0%	0%	0%	0%	0%	0%
StC15FS	0%	100%	90%	-	-	-	0%	0%	100%	0%	95%	0%	5%	20%	50%	60%	0%	0%	0%	0%
StC15FA	0%	80%	60%	-	-	-	0%	0%	100%	0%	55%	0%	0%	0%	10%	20%	0%	0%	0%	0%
StC15FH	0%	35%	25%	-	-	-	0%	0%	100%	0%	30%	0%	0%	0%	0%	0%	0%	0%	0%	0%
StC40FS	0%	70%	35%	-	-	-	0%	0%	100%	30%	100%	0%	0%	35%	10%	10%	0%	0%	0%	0%
StC40FA	0%	15%	0%	-	-	-	0%	0%	100%	15%	100%	0%	0%	0%	0%	0%	0%	0%	0%	0%
StC40FH	0%	0%	0%	-	-	-	0%	0%	100%	0%	55%	0%	0%	0%	0%	0%	0%	0%	0%	0%

Bridge	Transverse Limit State Occurrence																			
	Ideal								Acceptable								Unacceptable			
	BF	SL	CL	RE	RY	RF	FY	FF	APY	APB	APS	PA	PPY	PPS	SM	CM	BU	SS	CS	APR
StC15ES	0%	80%	40%	100%	100%	0%	-	-	80%	0%	75%	0%	75%	35%	0%	0%	0%	0%	0%	0%
StC15EA	0%	40%	10%	100%	100%	0%	-	-	100%	0%	30%	0%	0%	0%	0%	0%	0%	0%	0%	0%
StC15EH	0%	40%	0%	100%	100%	0%	-	-	100%	0%	10%	0%	0%	0%	0%	0%	0%	0%	0%	0%
StC40ES	0%	100%	85%	100%	100%	0%	-	-	100%	50%	100%	0%	0%	20%	10%	10%	0%	0%	0%	0%
StC40EA	0%	65%	20%	100%	80%	0%	-	-	100%	5%	70%	0%	0%	0%	0%	0%	0%	0%	0%	0%
StC40EH	0%	25%	0%	100%	55%	0%	-	-	100%	0%	35%	0%	0%	0%	0%	0%	0%	0%	0%	0%
StC15FS	0%	70%	30%	-	-	-	100%	0%	75%	0%	35%	0%	50%	30%	0%	0%	0%	0%	0%	0%
StC15FA	0%	60%	5%	-	-	-	80%	0%	60%	0%	10%	0%	0%	0%	0%	0%	0%	0%	0%	0%
StC15FH	0%	80%	0%	-	-	-	100%	0%	60%	0%	0%	0%	0%	0%	0%	0%	0%	0%	0%	0%
StC40FS	0%	100%	95%	-	-	-	15%	0%	100%	45%	100%	0%	0%	0%	10%	15%	0%	0%	0%	0%
StC40FA	0%	65%	35%	-	-	-	0%	0%	100%	5%	75%	0%	0%	0%	0%	0%	0%	0%	0%	0%
StC40FH	0%	35%	0%	-	-	-	0%	0%	100%	0%	30%	0%	0%	0%	0%	0%	0%	0%	0%	0%

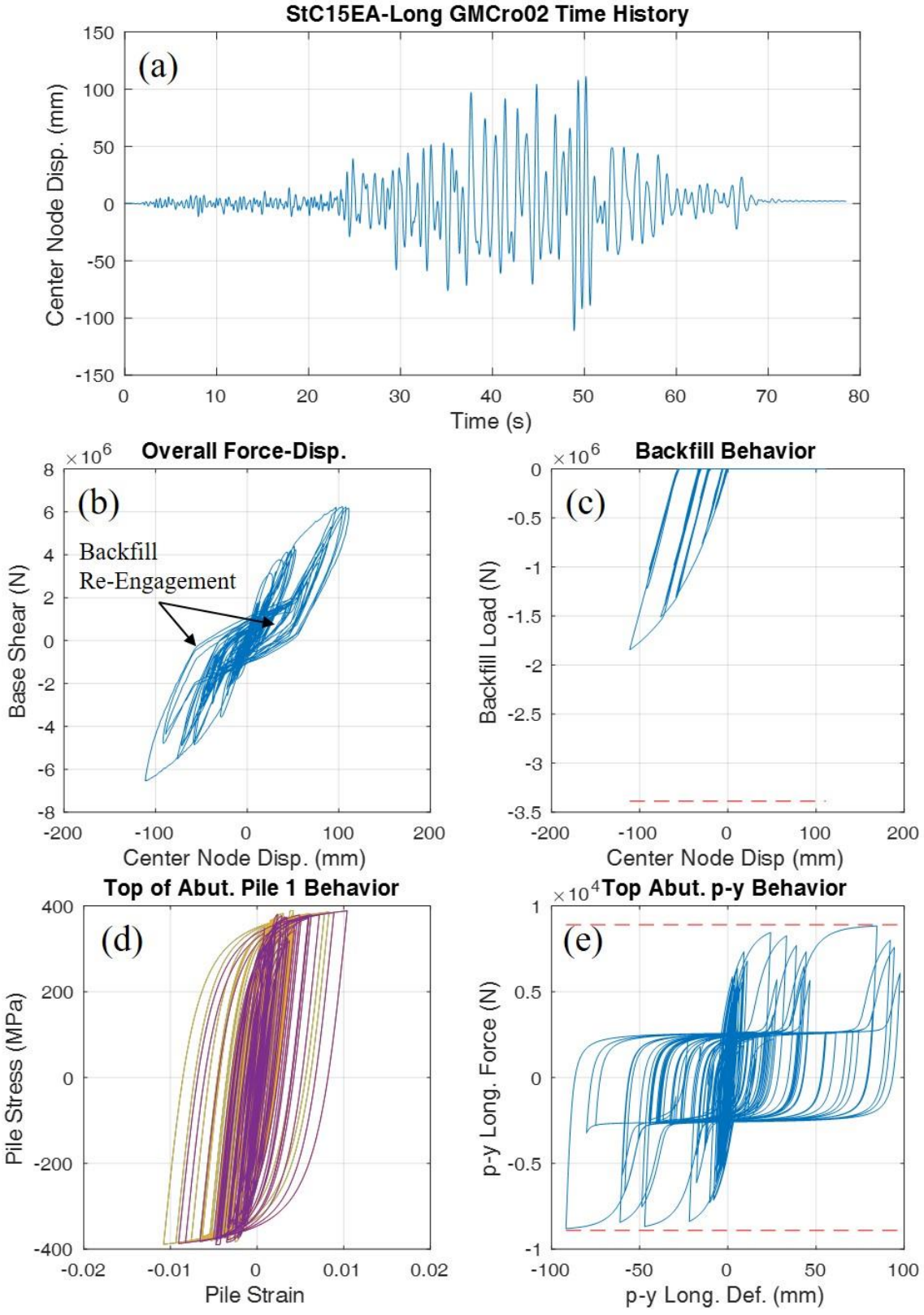

Figure 7.7: Dynamic analysis results for StC15EA subjected to a design-level ground motion in the longitudinal direction.

Pier column damage is another location of significant damage in the bridges under longitudinal excitation. Soft soil conditions consistently provide light (SL and CL) and moderate (SM and CM) damage. Moderate damage is rarely observed outside of the soft soil condition and the amount of light pier damage tends to decrease under stiffer soil conditions. It can also be noted that IABs with 15-ft tall piers experience more light pier damage due to their increased stiffness also increasing the force demand on the piers. Severe (SS and CS) pier column damage is never encountered.

The final set of limit states that commonly occurs under longitudinal excitation is the damage to the pier foundations – pier pile yielding (PPY) and mobilization of the soil (PPS). These limit states only tend to occur under the soft soil condition due to the decreased ultimate capacity of the soil. The only bridge where the majority of analyses experience PPY or PPS is StC40ES which has PPS occurring in 70% of the analyses.

The transverse dynamic results presented in Table 7.8 and Fig. 7.8 provide similar observations to the longitudinal results concerning initial abutment foundation damage (APY and APS). APY occurs most of the time with IABs with 40-ft tall piers having it occurring in all the analyses and APB also occurring due to the less stiff piers increasing the demand on the piles. In IABs with 15-ft tall piers, APY only occurs most of the time with strains reaching only about 3 times the yield strain, as seen in Fig. 7.8d. APS also tends to follow the trends identified in the longitudinal direction with the soft soil condition having more APS occurrences and the 40-ft tall pier IABs causing more demand in the abutments and therefore increasing the amount of APS occurrences. Despite StC15EA only having APS occur 30% of the time, Fig. 7.8e still shows that there is quite a lot of force on the p-y springs bringing it close to the ultimate capacity.

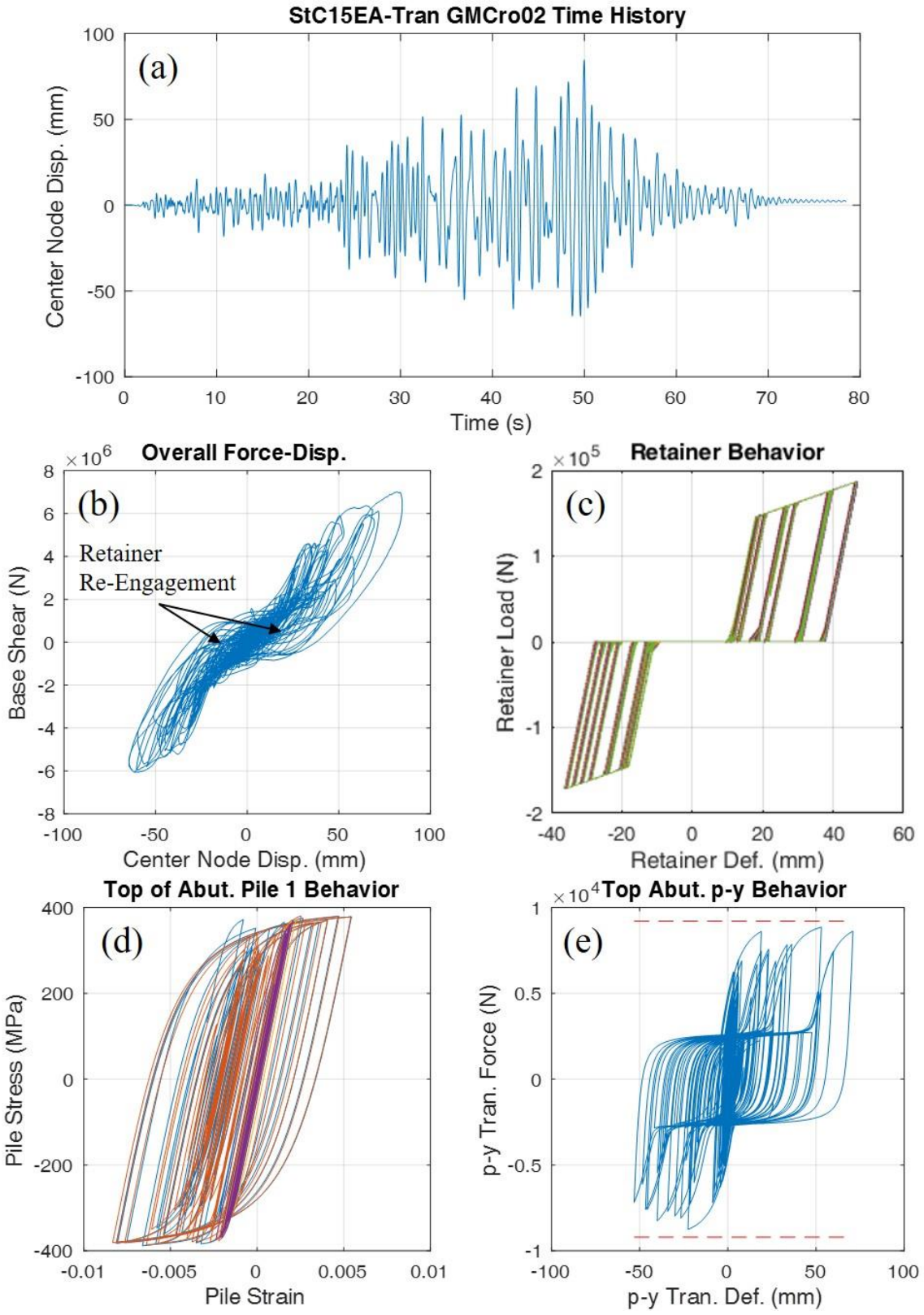

Figure 7.8: Dynamic analysis results for StC15EA subjected to a design-level ground motion in the transverse direction.

The transverse direction results also provide information concerning pier column damage. Once again, there is no severe damage to the piers (SS and CS). In terms of light and moderate damage there is less than in the longitudinal direction with moderate damage only occurring rarely in IABs with 40-ft piers and soft soil conditions. Light pier damage occurs frequently and is more common in bridges with soft soil and tall piers.

Other damage to the IABs includes damage to the pier foundations (PPY and PPS) in soft soil conditions and damage to the elastomeric bearing retainers and fixed bearings. Damage to the backfill is not expected in the transverse direction. The retainers experience significant damage in the form of anchor bolt yielding, as shown in Fig. 7.8c, which allows for the pinching behavior in Fig. 7.8b. While retainers yield all of the time in IABs with 15-ft tall piers and most of the time in IABs with 40-ft tall piers, they never fuse. Similarly, the fixed bearings yield almost all the time in IABs with 15-ft piers and sometimes in IABs with 40-ft piers, but never fuse. The reason for IABs with15-ft piers experiencing more retainer and fixed bearing damage is due to the shorter piers being stiffer and therefore not deforming as much and causing larger shear displacements and shear forces in the bearings between the superstructure and pier caps.

Overall, the three-span IAB designs are acceptable as there is no occurrence of unacceptable limit states in any analysis. However, the designs can be improved by engaging the backfill more as opposed to abutment foundation damage. Also, retainer and fixed bearing fusing should be increased, especially in IABs with 40-ft tall piers.

7.3.3 Four-Span Steel IABs

The four-span steel IAB dynamic analysis results are presented in Table 7.9 and accompanied by sample component behavior in the longitudinal direction (Fig. 7.9) and transverse direction (Fig. 7.10). The longitudinal direction results are very similar to the longitudinal direction

results for the three-span steel IABs. This is demonstrated through the APY limit state virtually always occurring with the piles reaching large strains around 5 times the yield strain, as shown in Fig. 7.9d. This leads to the APB limit state rarely occurring and the APR limit state never occurring. Similar trends are also observed in three-span steel IABs with APS always occurring in soft soil, almost always occurring in alluvial soil, and frequently occurring in stiff soil. It can also be observed that APS occurs more often in IABs with 40-ft tall piers.

The pier columns consistently encounter light damage (SL and CL) in the longitudinal direction, but less frequently encounter moderate damage (SM and CM) and encounter severe damage (SS and CS) in only a handful of analyses. It was found that pier column damage is more frequent in IABs with 15-ft tall piers. This is due to the stiff, short piers increasing the demand on the columns. The combination of the short piers and the soft soil conditions leads to frequent severe damage in the concrete of the pier columns (CS). Below the columns, in the pier foundation, the damage to the soil (PPS) is kept to the bridges with the soft soil condition.

Once again, there is no mobilization of the backfill (BF) in the longitudinal dynamic analyses, however backfill engagement is occurring as shown in Fig. 7.9c. As stated earlier, the backfill affects the overall bridge behavior due to its engagement and compaction behind each abutment which creates the pinching effect in the center node displacement-base shear plot of Fig. 7.9b. The similar behavior of the backfill and overall bridge in the longitudinal direction makes sense due to the reliance on backfill and abutment behavior when the bridge is subjected to longitudinal loads.

Table 7.9: Frequency of limit state occurrences for four-span steel IABs under design-level ground motion suite.

Bridge	Longitudinal Limit State Occurrence																			
	Ideal								Acceptable								Unacceptable			
	BF	SL	CL	RE	RY	RF	FY	FF	APY	APB	APS	PA	PPY	PPS	SM	CM	BU	SS	CS	APR
SlC15ES	0%	100%	100%	0%	0%	0%	-	-	100%	15%	100%	0%	0%	0%	85%	85%	0%	5%	45%	0%
SlC15EA	0%	100%	100%	0%	0%	0%	-	-	100%	0%	100%	0%	0%	5%	25%	35%	0%	0%	5%	0%
SlC15EH	0%	35%	25%	0%	0%	0%	-	-	100%	0%	30%	0%	0%	0%	0%	0%	0%	0%	0%	0%
SlC40ES	0%	80%	80%	0%	0%	0%	-	-	100%	35%	100%	0%	0%	25%	15%	20%	0%	0%	0%	0%
SlC40EA	0%	75%	50%	0%	0%	0%	-	-	100%	15%	100%	0%	0%	0%	0%	5%	0%	0%	0%	0%
SlC40EH	0%	5%	0%	0%	0%	0%	-	-	100%	0%	50%	0%	0%	0%	0%	0%	0%	0%	0%	0%
SlC15FS	0%	100%	100%	-	-	-	0%	0%	100%	15%	100%	0%	0%	0%	100%	100%	0%	5%	45%	0%
SlC15FA	0%	90%	85%	-	-	-	0%	0%	90%	0%	75%	0%	0%	0%	60%	80%	0%	0%	0%	0%
SlC15FH	0%	85%	80%	-	-	-	0%	0%	100%	0%	25%	0%	0%	0%	5%	25%	0%	0%	0%	0%
SlC40FS	0%	85%	80%	-	-	-	0%	0%	100%	35%	100%	0%	0%	35%	15%	20%	0%	0%	0%	0%
SlC40FA	0%	75%	50%	-	-	-	0%	0%	100%	15%	100%	0%	0%	5%	0%	0%	0%	0%	0%	0%
SlC40FH	0%	0%	0%	-	-	-	0%	0%	100%	0%	45%	0%	0%	0%	0%	0%	0%	0%	0%	0%

Bridge	Transverse Limit State Occurrence																			
	Ideal								Acceptable								Unacceptable			
	BF	SL	CL	RE	RY	RF	FY	FF	APY	APB	APS	PA	PPY	PPS	SM	CM	BU	SS	CS	APR
SlC15ES	0%	100%	100%	100%	0%	0%	-	-	15%	0%	0%	0%	0%	100%	100%	100%	0%	0%	50%	0%
SlC15EA	0%	100%	100%	100%	0%	0%	-	-	10%	0%	0%	0%	0%	0%	100%	100%	0%	0%	35%	0%
SlC15EH	0%	100%	100%	100%	0%	0%	-	-	20%	0%	0%	0%	0%	0%	100%	100%	0%	0%	35%	0%
SlC40ES	0%	100%	100%	100%	0%	0%	-	-	85%	15%	65%	0%	0%	0%	80%	85%	0%	0%	0%	0%
SlC40EA	0%	100%	100%	100%	0%	0%	-	-	100%	5%	80%	0%	0%	0%	85%	85%	0%	0%	0%	0%
SlC40EH	0%	100%	100%	100%	0%	0%	-	-	100%	0%	5%	0%	0%	0%	85%	90%	0%	0%	0%	0%
SlC15FS	0%	100%	100%	-	-	-	0%	0%	0%	0%	0%	0%	0%	100%	80%	85%	0%	0%	25%	0%
SlC15FA	0%	100%	100%	-	-	-	0%	0%	0%	0%	0%	0%	0%	0%	75%	90%	0%	0%	25%	0%
SlC15FH	0%	100%	100%	-	-	-	0%	0%	5%	0%	0%	0%	0%	0%	70%	90%	0%	0%	25%	0%
SlC40FS	0%	100%	100%	-	-	-	0%	0%	85%	15%	70%	0%	0%	0%	85%	90%	0%	0%	0%	0%
SlC40FA	0%	100%	100%	-	-	-	0%	0%	95%	0%	80%	0%	0%	0%	85%	95%	0%	0%	0%	0%
SlC40FH	0%	100%	100%	-	-	-	0%	0%	100%	0%	5%	0%	0%	0%	85%	95%	0%	0%	0%	0%

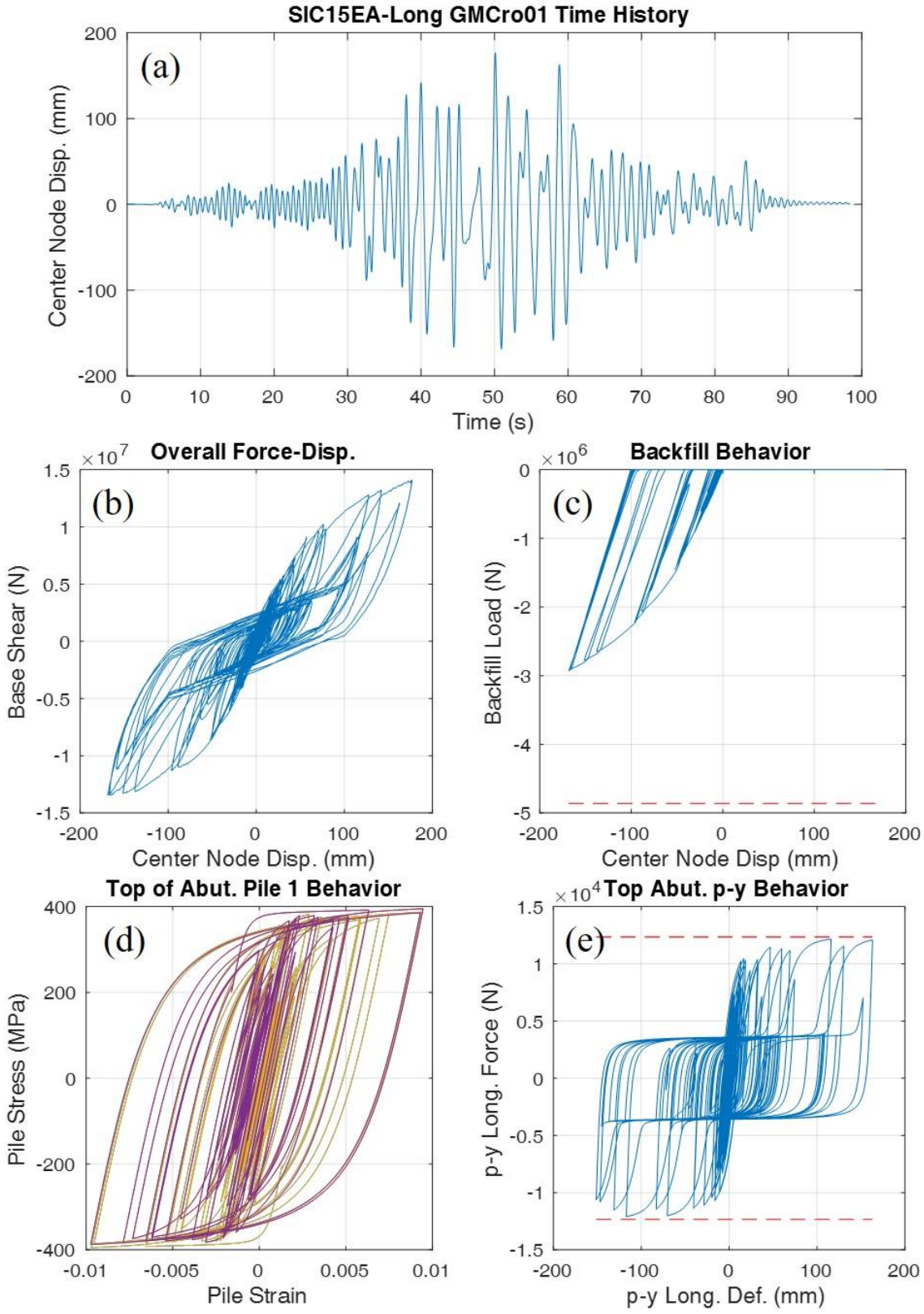

Figure 7.9: Dynamic analysis results for SlC15EA subjected to a design-level ground motion in the longitudinal direction.

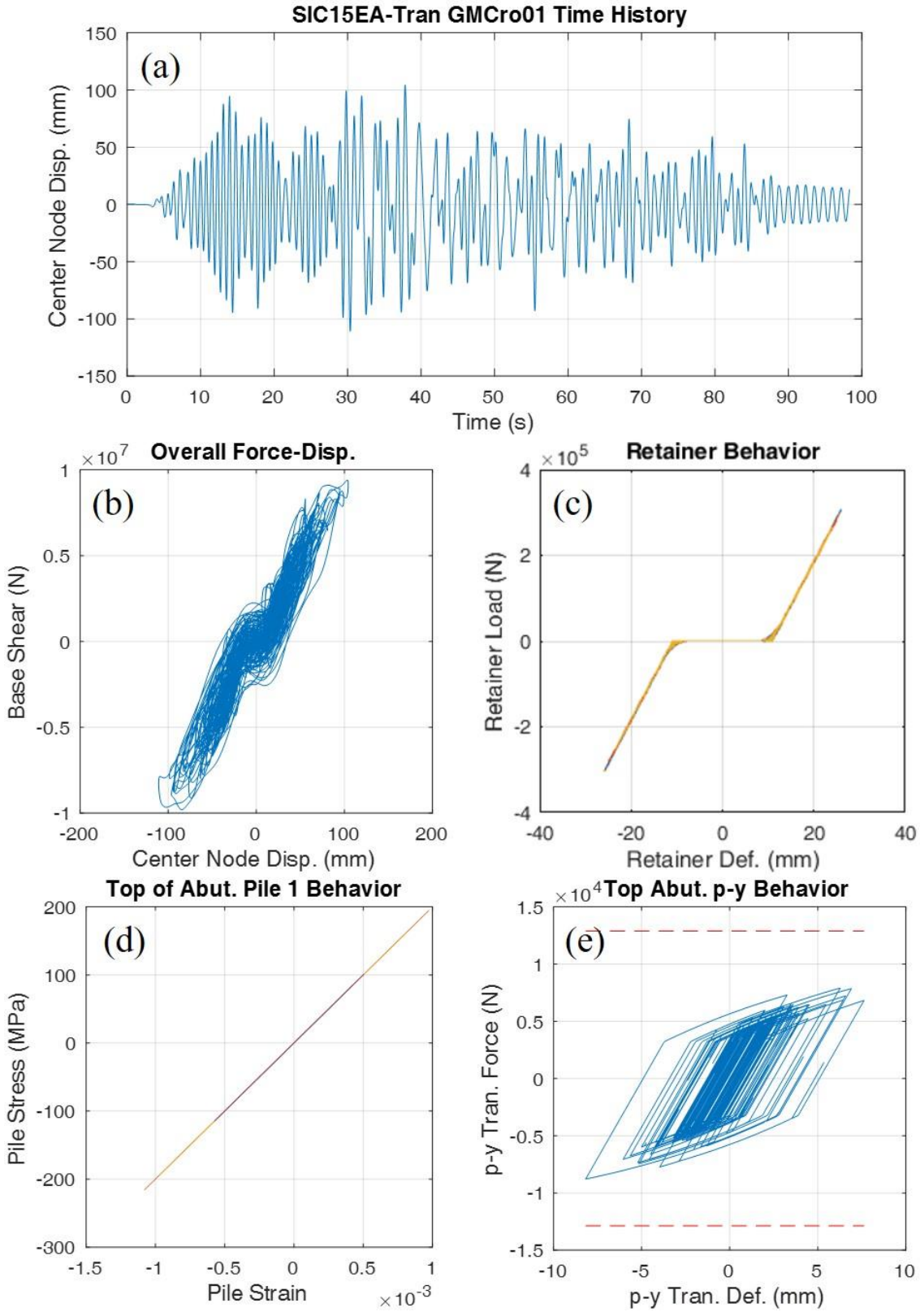

Figure 7.10: Dynamic analysis results for SlC15EA subjected to a design-level ground motion in the transverse direction.

As observed in the modal analyses, the four-span IABs in the transverse direction are extremely flexible. Following this, it can be observed that the transverse dynamic results for four-span steel IABs are different from the dynamic results for the three-span steel IABs. This is demonstrated immediately by observing that APY, APB and APS occur much less frequently than in the three-span IABs. The abutment piles rarely yield in 15-ft pier IABs and are quite far from yielding, as shown in Fig. 7.10d. On the other hand, due to the decreased pier stiffness in the 40-ft piers causing more demand in the abutments, the abutment piles in IABs with tall piers almost always yield, however the piles rarely reach strains associated with local buckling. For the same reason of the taller, less stiff, piers causing more demand in the abutments, it can be observed that APS is much more common in IABs with 40-ft tall piers. IABs with 15-ft tall piers are far from encountering APS as shown in Fig. 7.10e where the p-y behavior is not near mobilization.

The pier column damage in the transverse direction always encounters light damage (SL and CL) and almost always encounters moderate damage (SM and CM). The moderate damage is seen in IABs with both short and tall piers despite short piers being much stiffer and having an increased demand. Moderate damage is frequently encountered in IABs of both pier heights because the span is so long that the lateral force cannot be effectively redistributed to the abutments. The short pier IABs still have more force demand on them and frequently encounter severe damage to the pier column concrete (CS).

Retainer and fixed bearing damage in the transverse direction is minimal with retainer engagement (RE) occurring whenever possible, but no other limit states. The retainer engagement without yielding is demonstrated in Fig. 7.10c. The increased column damage and flexibility of the bridge in general creates a fuse which limits the amount of force transferred through the bearings. The increased pier damage and subsequent lack of damage to the retainers/fixed bearings

and abutment foundations in the transverse direction leads to the overall behavior of the bridge to be much more linear than in the longitudinal direction, as shown in Fig. 7.10b. Due to most components which would dissipate energy remaining linear, the overall behavior also largely remains linear with only a slight pinching behavior due to the retainer engagement.

Despite the increased flexibility and forces which come with the four-span bridges, the four-span steel IABs with 40-ft piers remain acceptable designs. The IABs with 15-ft piers are unacceptable due to the frequency of severe pier column damage (SS and CS) in the transverse direction results. The IABs with tall piers seem to avoid severe pier column damage by creating more damage to the abutment foundations, which is not an ideal solution but still better than the collapse of a pier. In the longitudinal cases, backfill mobilization never occurs and in the transverse directions retainer or fixed bearing yielding and fusing do not occur. These limit states would be more ideal ways to dissipate the seismic energy.

7.3.4 Three-Span Concrete IABs

The design-level dynamic analysis results are presented for three-span concrete IABs in Table 7.10 with sample component behavior for the longitudinal and transverse directions presented in Fig. 7.11 and Fig. 7.12, respectively. The larger mass present in the three-span concrete IAB superstructure (11.22 kips/ft) as opposed to the three-span steel IAB superstructure (7.019 kips/ft) is shown to have a significant effect by noting the more frequent occurrence of most limit states in Table 7.10 when compared to Table 7.8. The larger masses tend to increase the lateral inertia force produced by the superstructure during ground accelerations and results in unacceptable limit states beginning to occur under design-level shaking. Recall that the three-span concrete IABs with 15-ft tall piers and fixed bearings did not yield results, hence why they are omitted from Table 7.10.

Table 7.10: Frequency of limit state occurrences for three-span concrete IABs under design-level ground motion suite.

Bridge	Longitudinal Limit State Occurrence																			
	Ideal								Acceptable								Unacceptable			
	BF	SL	CL	RE	RY	RF	FY	FF	APY	APB	APS	PA	PPY	PPS	SM	CM	BU	SS	CS	APR
CtC15ES	0%	100%	100%	0%	0%	0%	-	-	100%	70%	100%	0%	0%	0%	85%	85%	0%	20%	75%	15%
CtC15EA	0%	100%	100%	0%	0%	0%	-	-	100%	75%	100%	0%	0%	0%	75%	85%	0%	5%	50%	20%
CtC15EH	0%	100%	80%	0%	0%	0%	-	-	100%	25%	100%	0%	0%	0%	25%	25%	0%	0%	0%	0%
CtC40ES	0%	75%	70%	0%	0%	0%	-	-	100%	65%	100%	0%	0%	10%	20%	30%	0%	0%	0%	15%
CtC40EA	0%	80%	75%	0%	0%	0%	-	-	100%	80%	100%	0%	0%	0%	20%	20%	0%	0%	0%	30%
CtC40EH	0%	55%	40%	0%	0%	0%	-	-	100%	75%	100%	0%	0%	10%	0%	5%	0%	0%	0%	20%
CtC40FS	0%	75%	70%	-	-	-	0%	0%	100%	70%	100%	0%	0%	15%	25%	30%	0%	0%	0%	15%
CtC40FA	0%	80%	65%	-	-	-	0%	0%	100%	80%	100%	0%	0%	15%	20%	20%	0%	0%	0%	30%
CtC40FH	0%	55%	35%	-	-	-	0%	0%	100%	75%	100%	0%	0%	0%	0%	5%	0%	0%	0%	20%

Bridge	Transverse Limit State Occurrence																			
	Ideal								Acceptable								Unacceptable			
	BF	SL	CL	RE	RY	RF	FY	FF	APY	APB	APS	PA	PPY	PPS	SM	CM	BU	SS	CS	APR
CtC15ES	0%	95%	80%	100%	100%	100%	-	-	100%	80%	100%	0%	0%	0%	65%	65%	0%	25%	50%	15%
CtC15EA	0%	100%	80%	100%	100%	100%	-	-	100%	90%	100%	0%	0%	0%	40%	40%	0%	5%	15%	10%
CtC15EH	0%	70%	45%	100%	100%	100%	-	-	100%	90%	90%	0%	0%	0%	0%	0%	0%	0%	0%	0%
CtC40ES	0%	85%	80%	100%	100%	60%	-	-	100%	75%	100%	0%	0%	0%	40%	50%	0%	0%	0%	15%
CtC40EA	0%	95%	80%	100%	100%	65%	-	-	100%	90%	100%	0%	0%	0%	25%	35%	0%	0%	0%	30%
CtC40EH	0%	90%	70%	100%	100%	20%	-	-	100%	100%	100%	0%	0%	0%	0%	5%	0%	0%	0%	45%
CtC40FS	0%	100%	100%	-	-	-	100%	0%	100%	80%	100%	0%	0%	0%	55%	60%	0%	0%	0%	15%
CtC40FA	0%	100%	95%	-	-	-	100%	0%	100%	90%	100%	0%	0%	0%	30%	55%	0%	0%	0%	25%
CtC40FH	0%	100%	100%	-	-	-	100%	0%	100%	100%	100%	0%	0%	0%	5%	10%	0%	0%	0%	20%

The longitudinal design-level dynamic analysis results show that abutment pile yielding (APY) and mobilization of the soil surrounding the abutment piles (APS) occurs in every analysis. As shown in Fig. 7.11d and 7.11e, these components tend to encounter large amounts of nonlinear behavior with the piles reaching strains over 50 times the yield strain and the p-y springs consistently reaching the ultimate capacity. The large strains correspond to frequent occurrences of the abutment pile local buckling (APB) and rupture (APR) limit states. The increased demand in the abutments is expected due to longitudinal loads typically being resisted primarily by the abutments and due to the increased lateral force in the concrete IABs. This point is further demonstrated through the large backfill contribution in Fig. 7.11c, which does not ever mobilize but does reach levels of backfill contribution larger than experienced in the steel IABs.

In terms of pier column damage in the longitudinal direction, there is frequent light damage (SL and CL) in IABs with 40-ft piers, but moderate damage (SM and CM) is rarer. This is not the case for IABs with 15-ft piers as they almost always have light damage, frequently have moderate damage, and have severe pier column damage (SS and CS) occurring most of the time in bridges with stiff and alluvial soil conditions. In general there is more pier column damage in softer soils. The increased occurrence of severe pier column damage in the IABs with 15-ft tall piers is due to the increased stiffness of the short piers causing more demand than on the tall piers. Once again, the increased mass of the superstructure increases the number of occurrences of pier damage.

The severe damage to the pier columns has an adverse effect on the overall bridge behavior. As observed in Fig. 7.11a, the column damage results in a permanent offset of the superstructure of around 400 mm. This offset is also observable in the center node displacement-base shear plot (Fig. 7.11b) through later cycles tending to center around the -400 mm mark. Despite, this damage the backfill engagement and compaction still provides pinching behavior in Fig. 7.11b.

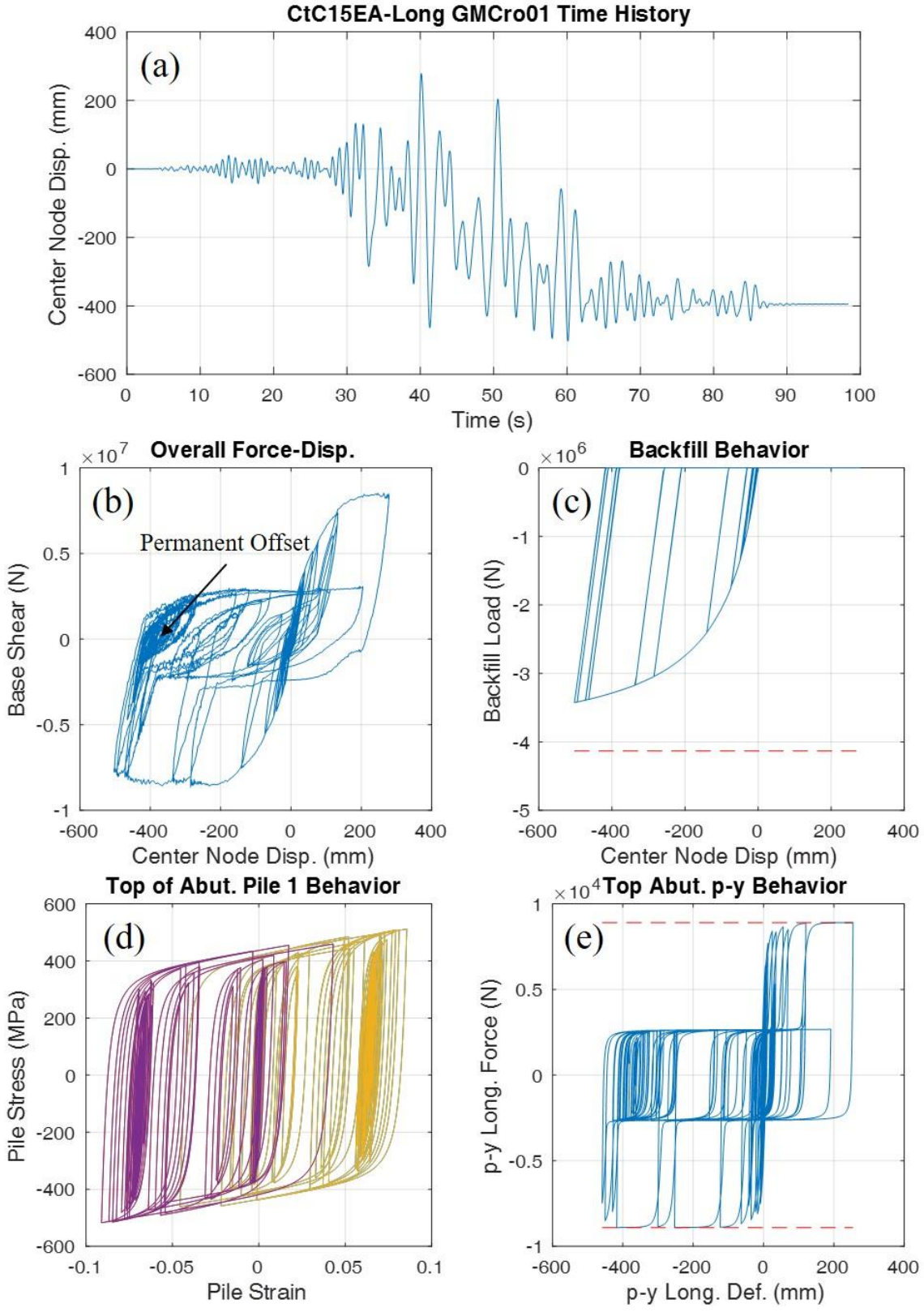

Figure 7.11: Dynamic analysis results for CtC15EA subjected to a design-level ground motion in the longitudinal direction.

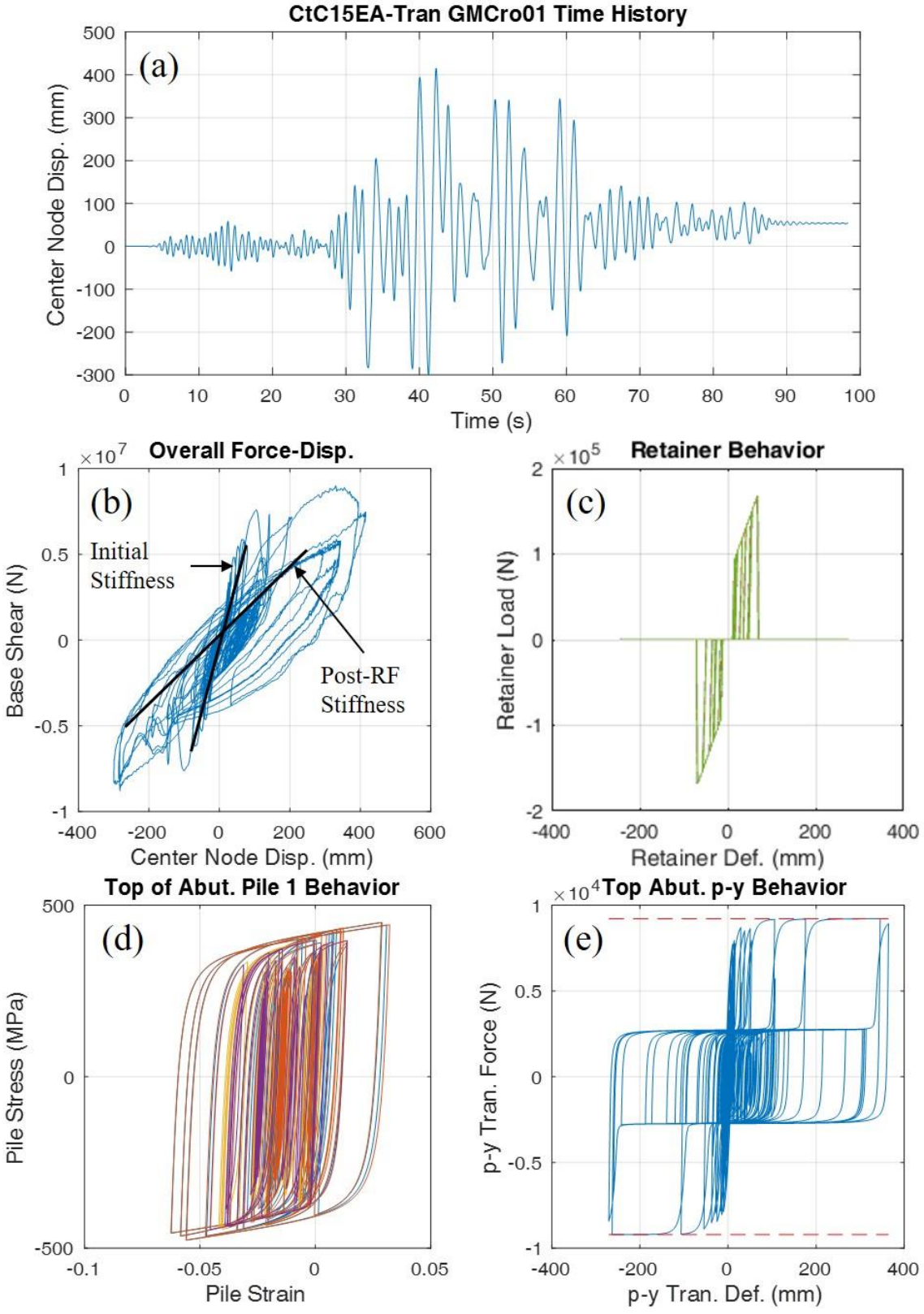

Figure 7.12: Dynamic analysis results for CtC15EA subjected to a design-level ground motion in the transverse direction.

The design-level dynamic results in the transverse direction also yield results which show the APY and APS limit states occurring almost all the time. The only exception is the APS limit state in CtC15EH which still reaches a high frequency with 90% occurrence. The piles reach a lesser state of nonlinear behavior than in the longitudinal direction by only having strains around 25 times the yield strain (see Fig. 7.12d), however that is still a significant amount of demand placed on the abutment piles and the APB and APR limit states often occur. Similarly, Fig. 7.12e shows the consistent reaching of the ultimate capacity in the p-y spring.

Pier column damage in the transverse direction is increased in most cases as compared to the longitudinal results. Light column damage is very frequent across all bridges while moderate damage is mainly observed in non-stiff soil conditions. Severe pier column damage (SS and CS) is only observed in IABs with 15-ft tall piers. Once again, these results follow the trend of having more pier column damage in bridges with shorter piers. This is due to the increased stiffness of the short piers causing more demand on the piers which leads to more damage.

Related to the stiffness of the piers is the retainer and fixed bearing behavior. The increased stiffness in the piers allows for more force to be transferred through the bearings from the superstructure to the pier cap. This is shown with CtC15E_ always encountering retainer fusing (RF) while CtC40E_ only encounter retainer fusing sometimes. This is also observed with the fixed bearings where the anchor bolts always yield (FY) yet never fuse (FF) due to the 40-ft tall piers limiting the amount of force transferred through the bearing. In general, the occurrences of retainer yielding (RY) and fusing (RF) are increased when compared to the three-span steel IABs due to the increased superstructure mass creating overall larger forces in the bridge. The fusing of the retainers, as shown in Fig. 7.12c, does have an interesting effect on the overall bridge behavior shown in Fig. 7.12b. Initially the behavior follows the pattern observed in other bridges which is

mostly linear with a bit of pinching due to retainer engagement, such as those shown in Fig. 7.8b and Fig. 7.10b. However, upon the fusing of the retainer the stiffness of the bridge decreases due to the lack of retainers resisting larger displacement. This post-retainer fusing behavior is shown in Fig. 7.12b.

The IABs with short piers are deemed unacceptable due to their consistent severe pier column damage. The exception to this is if the foundation soil is extremely stiff, in which case unacceptable limit states do not occur. The IABs with tall piers are generally unacceptable due to large amounts of abutment pile strain (frequent occurrences of APR) and no backfill mobilization (BF). Ideally, the amount of pile strain should be reduced while backfill contribution is increased.

7.3.5 Four-Span Concrete IABs

The design-level dynamic analysis results for four-span concrete IABs follows similar trends to the three-span concrete IABs in that they experience more damage than their steel counterparts. The additional occurrence of limit states, as presented in Table 7.11, is again due to the increased weight of the concrete superstructure (13.59 kips/ft) as opposed to the steel superstructure (8.204 kips/ft). Additionally, there is a lot of pier column and abutment damage in the transverse direction due to the four-span concrete IABs being extremely flexible in that direction, as discussed in the modal analysis section. Recall that ClC15F_ were unable to yield results at the design-level, so they are not included in Table 7.11. Accompanying Table 7.11 is Fig. 7.13 and Fig. 7.14 which plots the behavior of components in ClC15EA during excitation in the longitudinal and transverse directions, respectively.

Table 7.11: Frequency of limit state occurrences for four-span concrete IABs under design-level ground motion suite.

Bridge	Longitudinal Limit State Occurrence																			
	Ideal								Acceptable								Unacceptable			
	BF	SL	CL	RE	RY	RF	FY	FF	APY	APB	APS	PA	PPY	PPS	SM	CM	BU	SS	CS	APR
ClC15ES	0%	93%	93%	0%	0%	0%	-	-	100%	33%	100%	0%	0%	0%	67%	67%	0%	0%	67%	0%
ClC15EA	0%	94%	94%	0%	0%	0%	-	-	100%	59%	100%	0%	0%	0%	76%	76%	0%	6%	76%	6%
ClC15EH	0%	90%	90%	0%	0%	0%	-	-	100%	70%	100%	0%	0%	0%	75%	80%	0%	20%	70%	20%
ClC40ES	0%	75%	70%	0%	0%	0%	-	-	100%	60%	95%	0%	0%	0%	25%	35%	0%	0%	10%	15%
ClC40EA	0%	75%	70%	0%	0%	0%	-	-	100%	60%	100%	0%	0%	0%	20%	35%	0%	0%	0%	10%
ClC40EH	0%	80%	80%	0%	0%	0%	-	-	100%	80%	100%	0%	0%	0%	15%	25%	0%	0%	0%	20%
ClC40FS	0%	70%	70%	-	-	-	0%	0%	100%	60%	95%	0%	0%	0%	25%	45%	0%	0%	0%	15%
ClC40FA	0%	75%	70%	-	-	-	0%	0%	100%	65%	100%	0%	0%	0%	20%	35%	0%	0%	0%	10%
ClC40FH	0%	80%	70%	-	-	-	0%	0%	100%	80%	100%	0%	0%	0%	10%	20%	0%	0%	0%	25%

Bridge	Transverse Limit State Occurrence																			
	Ideal								Acceptable								Unacceptable			
	BF	SL	CL	RE	RY	RF	FY	FF	APY	APB	APS	PA	PPY	PPS	SM	CM	BU	SS	CS	APR
ClC15ES	0%	100%	100%	100%	100%	0%	-	-	75%	20%	40%	0%	0%	100%	100%	100%	0%	40%	95%	0%
ClC15EA	0%	100%	100%	100%	100%	0%	-	-	75%	15%	55%	0%	0%	0%	100%	100%	0%	35%	100%	0%
ClC15EH	0%	100%	100%	100%	100%	0%	-	-	80%	0%	25%	0%	0%	0%	100%	100%	0%	30%	95%	0%
ClC40ES	0%	100%	100%	100%	100%	0%	-	-	94%	22%	78%	0%	0%	0%	72%	89%	0%	6%	22%	11%
ClC40EA	0%	100%	100%	100%	100%	0%	-	-	100%	20%	85%	0%	0%	0%	75%	90%	0%	0%	25%	20%
ClC40EH	0%	100%	100%	100%	100%	0%	-	-	100%	20%	30%	0%	0%	0%	75%	90%	0%	0%	30%	20%
ClC40FS	0%	100%	100%	-	-	-	10%	0%	95%	25%	65%	0%	0%	0%	85%	100%	0%	10%	30%	20%
ClC40FA	0%	100%	100%	-	-	-	0%	0%	95%	20%	85%	0%	0%	0%	75%	100%	0%	0%	30%	15%
ClC40FH	0%	100%	100%	-	-	-	0%	0%	100%	20%	30%	0%	0%	0%	75%	100%	0%	0%	35%	10%

The dynamic results in the longitudinal direction indicate that damage to the abutment foundation through abutment pile yielding (APY) and mobilization of the soil surrounding the piles (APS) almost always occurs under design-level shaking. This can be confirmed by noting the high levels of nonlinearity experienced by the abutment piles and p-y behavior in Fig. 7.13d and 7.13e, respectively. The abutment piles reach a strain nearly 100 times the yield strain, often triggering the APR limit state, and the p-y springs are consistently reaching the ultimate capacity. Similar to the three-span concrete IABs, the large amount of lateral force caused by the inertia of the heavy superstructure is mainly resisted by the abutments in the longitudinal direction. This not only explains the frequent damage to the abutment foundation, but it also allows for large amounts of backfill contribution. This is indicated through Fig. 7.13c which comes close to mobilization and contributes a lot of resistance.

The pier column damage in the longitudinal direction indicates that there is common severe damage in IABs with 15-ft piers. In IABs with 40-ft tall piers there is common light pier damage and moderate pier damage occurs often, but severe damage is extremely rare. This discrepancy can once again be attributed to the shorter, stiffer piers distributing the lateral force such that they have a higher demand in the columns and therefore cause more damage. The taller, less stiff piers distribute the force such that there is more demand on the abutments and less on the columns leading to less pier column damage.

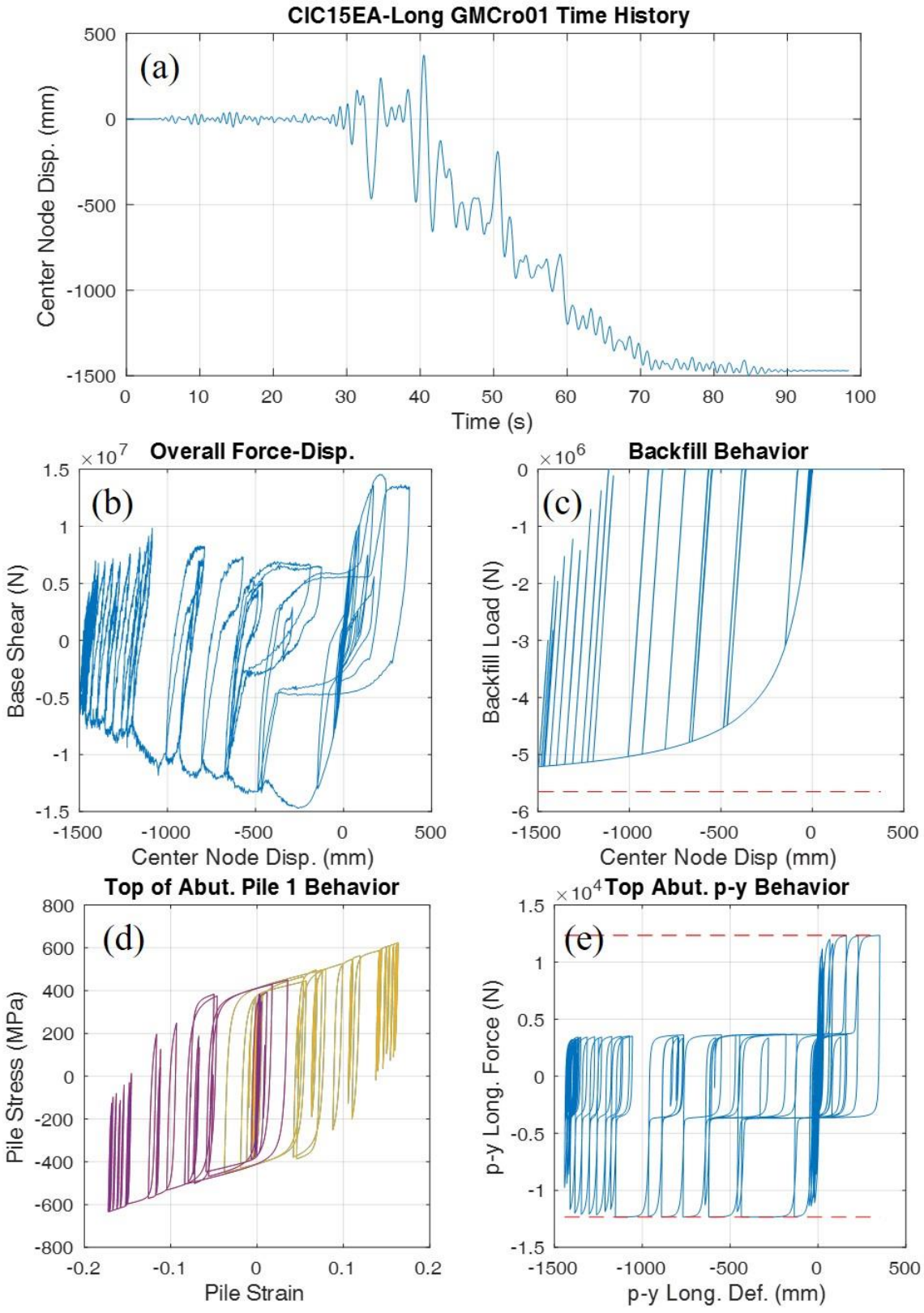

Figure 7.13: Dynamic analysis results for ClC15EA subjected to a design-level ground motion in the longitudinal direction.

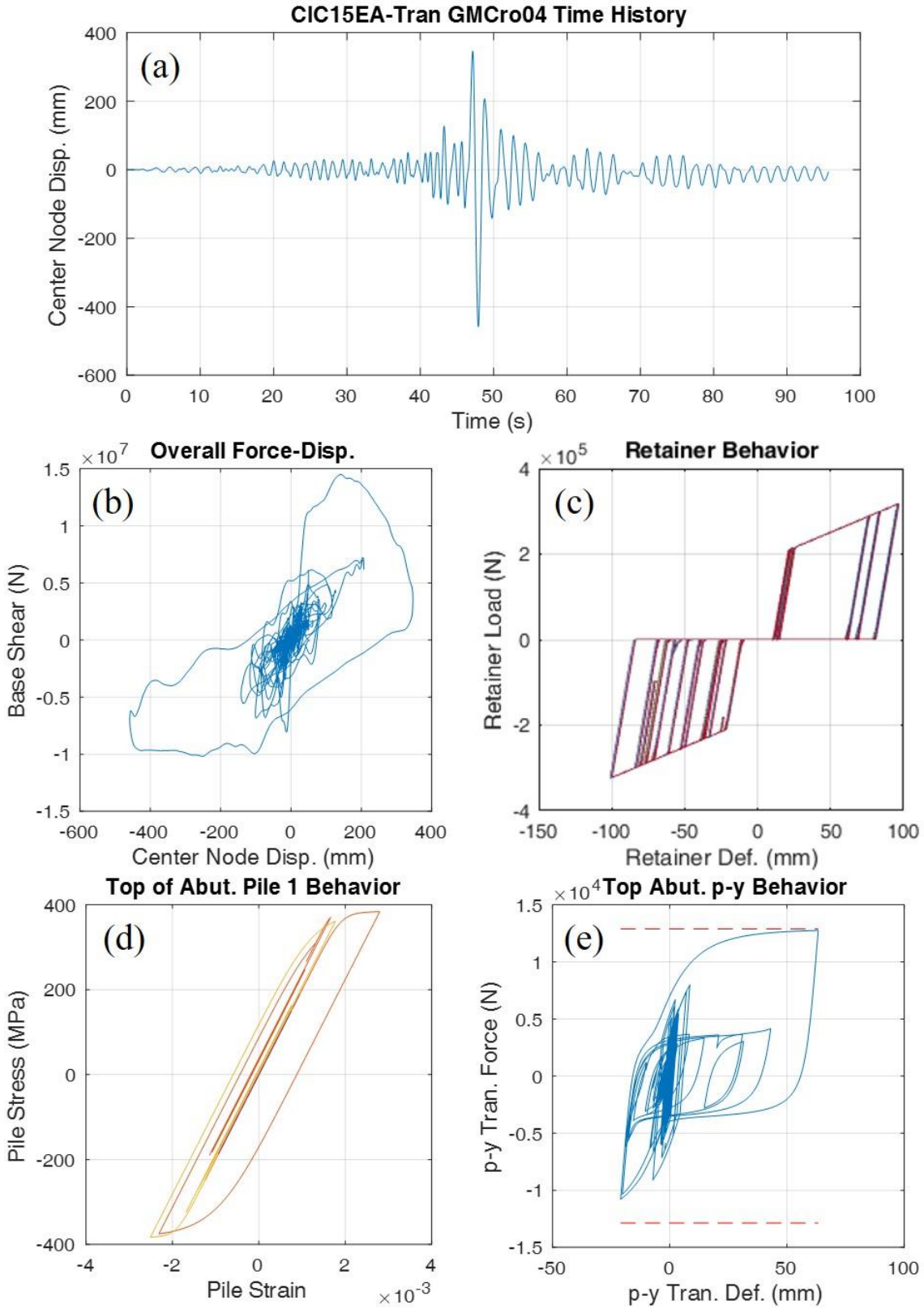

Figure 7.14: Dynamic analysis results for ClC15EA subjected to a design-level ground motion in the transverse direction.

The severe pier column damage observed in ClC15EA is shown to have an adverse effect on the overall bridge behavior. It is shown in Fig. 7.13a that the severe pier column damage causes a permanent offset in the IAB superstructure (represented by the center node) of close to 1500 mm. This offset is also observed in the center node displacement-base shear plot in Fig. 7.13b which shows the behavior re-centering at a displacement around -1500 mm. It should also be noted that there are other component behaviors involved in the poor overall behavior of the IAB presented in 7.13. Primarily, Fig. 7.13d presents stresses and strains in the piles are unrealistically large. This is a rare result and does not affect the conclusions of poor behavior in this IAB.

The transverse direction results provided in Table 7.11 demonstrate that although APY, APB, APR, and APS do occur frequently, it is less frequent than in the longitudinal direction. Another observation is that there is more APY, APB, APR and APS occurrences in IABs with 40-ft tall piers. This follows the trend that IABs with taller, less stiff piers redistribute the force such that there is less force on the piers and more on the abutments. The abutment pile and p-y behavior for ClC15EA is presented in Fig. 7.14d and 7.14e which shows that the piles barely yield and the p-y springs only reach the ultimate capacity briefly. This follows well with the Table 7.11 observations given the low frequency of APY and APS and the lack of APR occurrences.

Due to the very flexible nature of the four-span concrete IABs in the transverse direction there is always frequent severe damage to the piers. As expected, the IABs with shorter, stiffer piers experiences much more severe pier column damage than those with taller piers. Light pier column damage always occurs and moderate pier column damage is also very frequent, again with IABs with 15-ft tall piers experiencing more damage. Atop the piers are the elastomeric bearing retainers and fixed bearings. The retainers always engage and yield, but never fuse. Although they never fuse, they do yield more often than experienced in the four-span steel IAB due to the

increased superstructure mass causing more force to be transferred through the bearings. Similar to the retainers, the fixed bearings also never fuse. However, the fixed bearings also rarely yield with the only occurrences happening twice in ClC40FS.

The unacceptable limit state of either severe steel or concrete pier column damage consistently occurs in the four-span concrete IABs under design-level shaking. This leads to these bridge designs being unacceptable. The frequent occurrence of severe pier column damage is a major problem, however the lack of backfill mobilization (BF), retainer fusing (RF), or any fixed bearing damage (FY and FF) did not help the situation. Instead of having these ideal limit states occur and limit forces to components such as the piers and abutment foundation, they do not occur and those components frequently fail.

7.3.6 Overall Observations

The results presented in this subsection demonstrate that concrete superstructure IABs tend to perform worse than steel superstructure IABs. This is due to the increased mass of the superstructure introducing much larger lateral inertia forces during bridge shaking. Additionally, the results demonstrated that IABs with longer spans and shorter piers perform worse. Longer spans perform worse, especially in the transverse direction, due to the extreme flexibility of the bridge. Short piers perform worse due to the short, stiff piers increasing the demand on the pier columns often leading to more pier column damage.

While pier column damage is more prevalent in IABs with short piers, IABs with tall piers redistribute the force such that there is more demand on the abutments instead of the piers. The damage to the abutment piles is typically not significant enough to cause pile rupture (APR) and may not cause a loss of span such as when severe pier column damage occurs, but it is still difficult to identify and repair the damage in the abutments. While there is an observed trade-off between

damage to the abutment foundations and damage to the pier columns, it is important to notice that initial damage to the abutment foundations (APY and APS) occurs extremely frequently, even when significant pier column damage occurs.

The damage to the pier columns and abutment foundations is very common. However, backfill mobilization, elastomeric bearing retainer fusing, and fixed bearing fusing rarely occur. These ideal limit states would be helpful in mitigating damage to the pier columns and the abutment foundations. The lack of these limit states occurring is a location which could use improvement in future designs.

7.4 INCREMENTAL DYNAMIC ANALYSIS RESULTS

The IABs with alluvial soil conditions were also subjected to an incremental dynamic analysis (IDA) using the ground motion scale factor as the incremental intensity measure. This process involves subjecting the IABs to ground motions at scale factor increments of 0.25 between 0.5 and 1.75 with a scale factor of 1.0 representing the design-level hazard ground motions. Based on the scale factors required to transform the 1000-year return period (design-level earthquake) UHS to the 2500-year return period (maximum considered earthquake, MCE) UHS in southern Illinois, it can be assumed that a scale factor of 1.75 is comparable to the MCE-level. All IABs with alluvial soil conditions yielded results with the exception of CtC15FA, ClC15FA, and ClC40FA which failed to converge and are excluded from the IDA study.

The IDA results are presented in three fashions. The first is a table, similar to the tables for the design-level analysis results, which provides the percent of analyses at each scale factor that a limit state occurred. The second presentation is the IDA plots themselves which plot component and overall bridge response against ground motion scale factor. These plots help to identify the dispersion of the results by providing the maximum and minimum results from the 20 ground

motions at each scale factor along with the median. They also aid in determining how close components were to the limit states and can compare damage between bridges better than the frequency of limit state occurrence data The IDA plots are made for center node displacement, base shear, maximum abutment pile strain (normalized to pile yielding and including lines defining local buckling and rupture in yellow and red, respectively), maximum abutment p-y spring force (normalized to the p-y spring ultimate capacity), maximum backfill spring force (normalized to each backfill spring's ultimate capacity), maximum concrete and steel pier column strain (including lines defining the light, moderate, and severe limit states in green, yellow, and red, respectively), retainer force (including lines defining retainer engagement, yielding, and fusing in green, yellow, and red, respectively), and fixed bearing force (including lines defining anchor bolt yielding and fusing in yellow and red, respectively). The final presentation of the IDA results is through sequence of damage plots which are explained in more detail below.

7.4.1 Desired Sequence of Damage

IDA results are useful in determining at which scale factor each limit state begins to occur (*i.e.* the limit state's first occurrence). This data can be translated into the sequence of damage of the bridges which help identify vulnerable components whose limit states begin to occur at smaller scale factors than desired. Desired sequences of damage were produced for the bridges and include ideal, acceptable, discouraged, and unacceptable occurrences. Ideal occurrences happen when a limit state begins to occur in the desired sequence, acceptable is when a limit state begins to occur at larger scale factors than desired, discouraged is when a limit state begins to occur at smaller scale factors than desired, and unacceptable is when unacceptable limit states occur.

The desired sequence of damage for the single-span steel IAB includes having the backfill mobilization (BF) occur at scale factors of 1.0 or less and then initial damage to the abutment

foundation (APY and APS), failure of the pile cap-abutment connection (PA), and local buckling of the abutment piles (APB) occurs at scale factors of 1.0 or larger. The reason why the APY, APS, PA, and APB limit states are allowed at the design-level is due to the lack of other fuses in the single-span IAB.

The desired sequence of damage for the multi-span bridges are very similar to each other. Exceptions include that backfill mobilization (BF) only occurs in longitudinal sequences, retainer engagement (RE), yielding (RY), and fusing (RF) only occurs in transverse sequences, and fixed bearing damage (FY and FF) only occurs in IABs with fixed bearings. In terms of the actual sequence, RE is expected to occur first at the 0.5 scale factor when it is present. Following that, any ideal limit state is intended to begin to occur at scale factors of 1.0 or less. These ideal limit states include light pier column damage (SL/CL), backfill mobilization (BF), fixed bearing damage (FY and FF), and retainer damage (RY and RF). These are desired to occur early due to their fusing capabilities and their ease of access to repair after an event. Moderate pier column damage (SM/CM) is followed and is desired to be at a scale factor of 1.0 or larger. It is desired at a scale factor of 1.0 because of all the acceptable limit states, it is the easiest to identify and repair. All other acceptable limit states are desired to occur at a scale factor of 1.25 or larger. These limit states include initial abutment foundation damage (APY/APS), pier foundation damage (PPY/PPS), pier cap-abutment connection failure (PA), and abutment pile local buckling (APB). Finally, unacceptable limit states such as severe pier column damage (SS/CS), bearing unseating (BU), and abutment pile rupture (APR) are unacceptable at all scale factors. Note that some limit states are combined for the sequences of damage due to their close ties to each other. These limit states mostly comprise of the pier column damage (SL/CL, SM/CM, SS/CS) and pile and p-y spring damage (APY/APS, PPY/PPS).

7.4.2 Single-Span Steel IABs

As with the design-level response, abutment pile yielding (APY) and mobilization of the soil surrounding the piles (APS) occurs in single-span steel IABs at any scale factor. Additionally, at a scale factor of 1.75 under transverse excitation abutment pile local buckling (APB) also occurs. This result is shown in Table 7.12, which provides the frequency of limit state occurrences under ground motions at each scale factor. Table 7.12 demonstrates that the APY and APS limit states begin to occur in a majority of the analyses at scale factors of 1.0 and larger and they rarely occur at smaller scale factors. It can also be seen that in both directions APY occurs in all the analyses when subjected to ground motions with a scale factor of 1.5 and larger.

The IDA plots for the single-span steel IAB results indicate that backfill is not close to mobilizing at any scale factor. This is demonstrated in the longitudinal direction through Fig. 7.15e where the backfill force rarely exceeds 50% of the backfill capacity at the largest scale factor. Also in the longitudinal IDA plots presented in Fig. 7.15, a gradual increase in all variables as scale factors increase indicate there are no major events causing a fusing mechanism in this direction. In the transverse direction IDA plots, provided in Fig 7.16, we can confirm that there is no backfill force at all (see Fig. 7.16e) indicating all the force is taken by the abutment piles and soil. An interesting observation concerning the relationship of pile strain and maximum p-y force is that as APS occurs more frequently (*i.e.* the normalized maximum p-y force reaches 1) in Fig. 7.16d, pile strains begin to increase at a higher rate leading to APB occurring in Fig. 7.16a. This is especially noticeable at larger scale factors.

When observing the sequence of damage for the single-span steel IAB in Fig. 7.17 it can be determined that for the most part it is acceptable. The longitudinal sequence does have APY at a slightly smaller scale factor than ideal, but APS is within the ideal region at a scale factor of 1.25.

Although APY occurs at slightly smaller scale factors than ideal, there is limited energy dissipating components in the single-span IABs meaning it is better to have APY occur slightly too easily than have it not occur at all and the bridge be extremely stiff. The transverse sequence is ideal as both APY and APS occur at the design-level scale factor of 1.0 and APB occurs at a scale factor of 1.75. This leads to the conclusion that the single-span steel IAB designs are slightly discouraged to ideal. The lack of backfill mobilization at any level is concerning due to its potential help in allowing the APY to occur at a later scale factor and because backfill mobilization is ideal at low scale factors.

Table 7.12: Frequency of limit state occurrences for the IDA of single-span steel IABs where a scale factor of 1.00 represents the design-level.

Bridge	SF	Longitudinal Limit State Occurrence					
		Ideal	Acceptable				Unacc.
		BF	APY	APB	APS	PA	APR
Ss____A	0.50	0%	0%	0%	0%	0%	0%
	0.75	0%	5%	0%	0%	0%	0%
	1.00	0%	80%	0%	0%	0%	0%
	1.25	0%	80%	0%	10%	0%	0%
	1.50	0%	100%	0%	15%	0%	0%
	1.75	0%	100%	0%	45%	0%	0%
Bridge	**SF**	**Transverse Limit State Occurrence**					
		Ideal	Acceptable				Unacc.
		BF	APY	APB	APS	PA	APR
Ss____A	0.50	0%	0%	0%	0%	0%	0%
	0.75	0%	0%	0%	0%	0%	0%
	1.00	0%	10%	0%	5%	0%	0%
	1.25	0%	65%	0%	30%	0%	0%
	1.50	0%	100%	0%	65%	0%	0%
	1.75	0%	100%	45%	100%	0%	0%

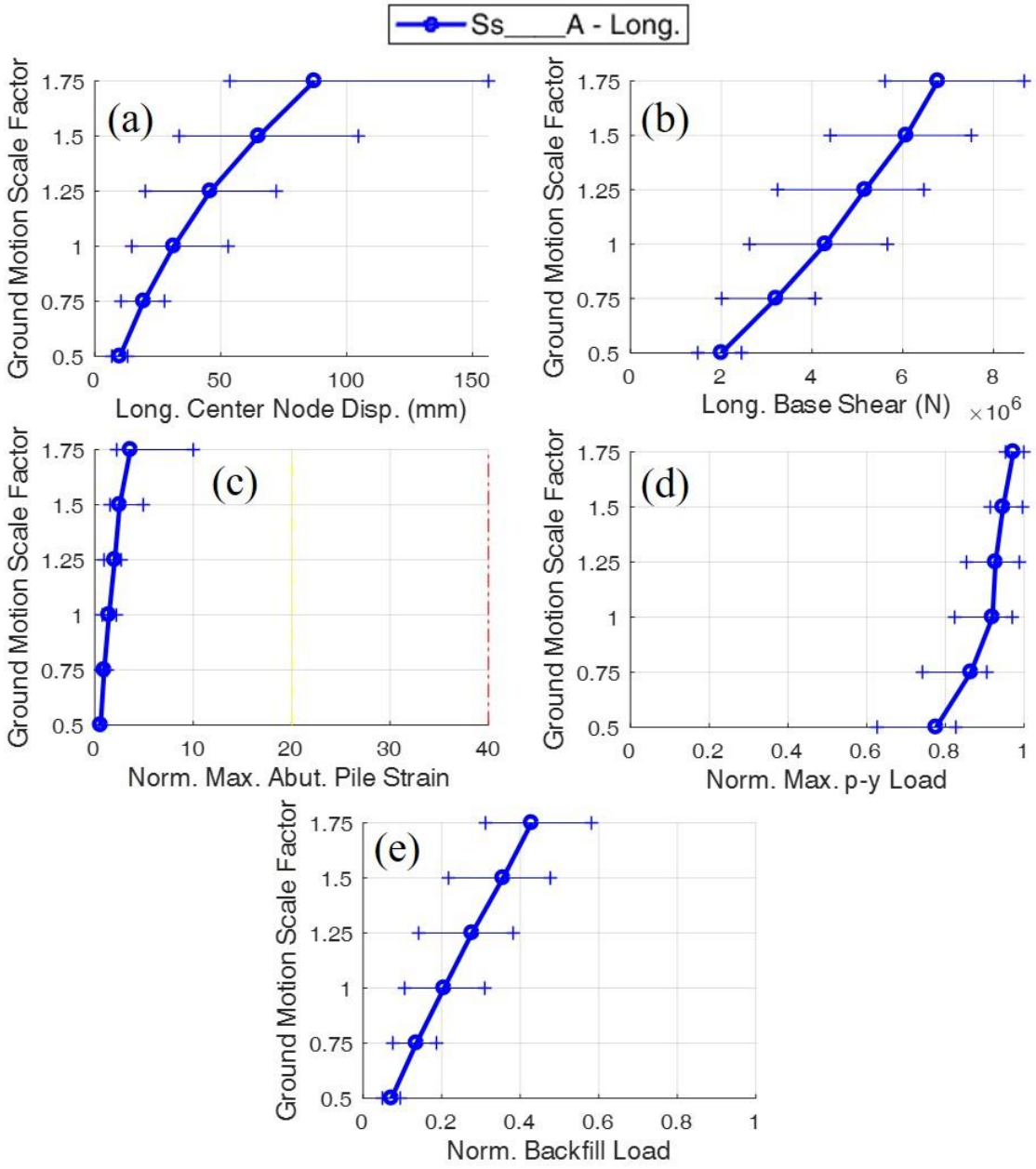

Figure 7.15: IDA plots for single-span steel IABs in the longitudinal direction where a scale factor of 1.00 represents the design-level.

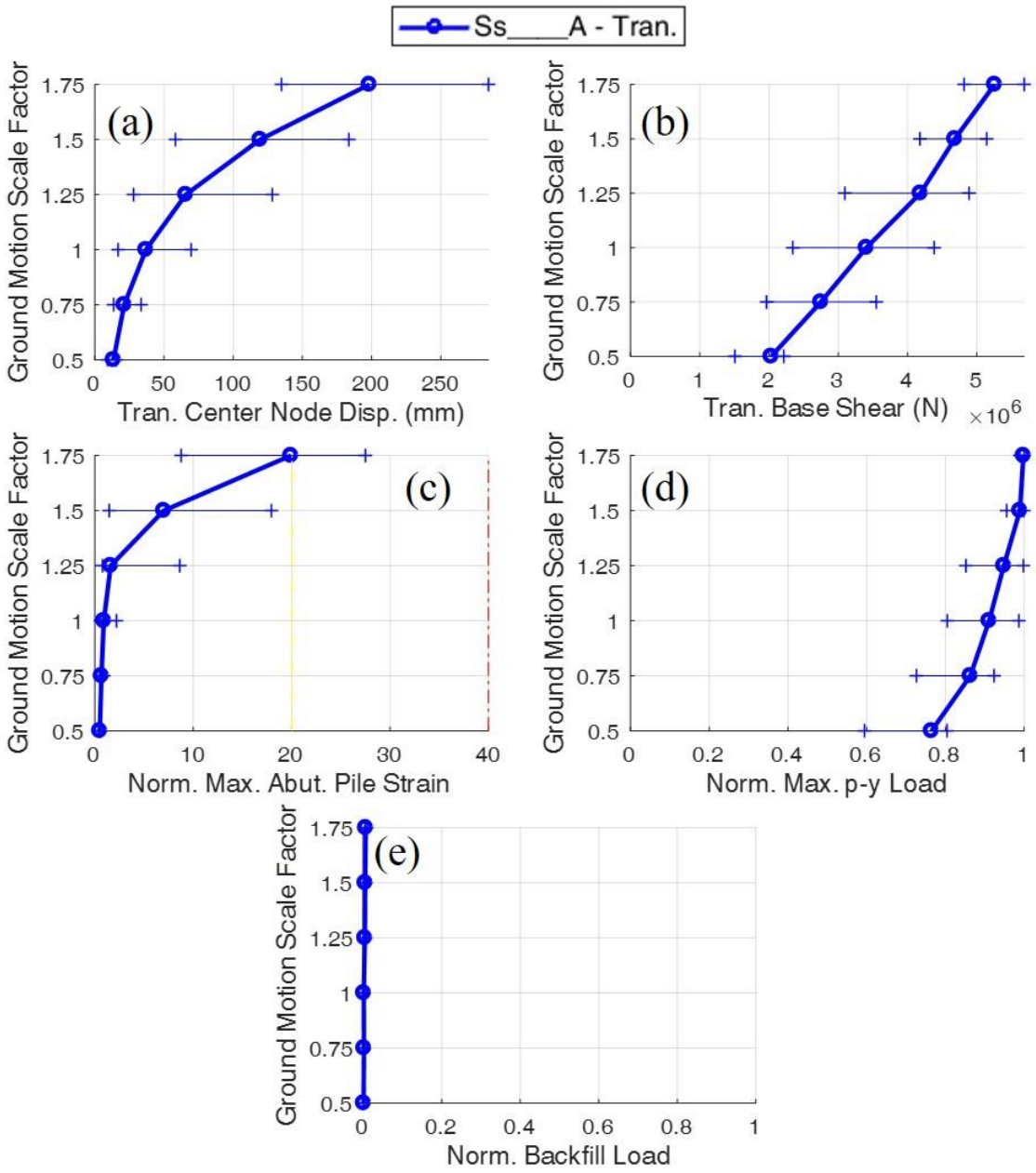

Figure 7.16: IDA plots for single-span steel IABs in the transverse direction where a scale factor of 1.00 represents the design-level.

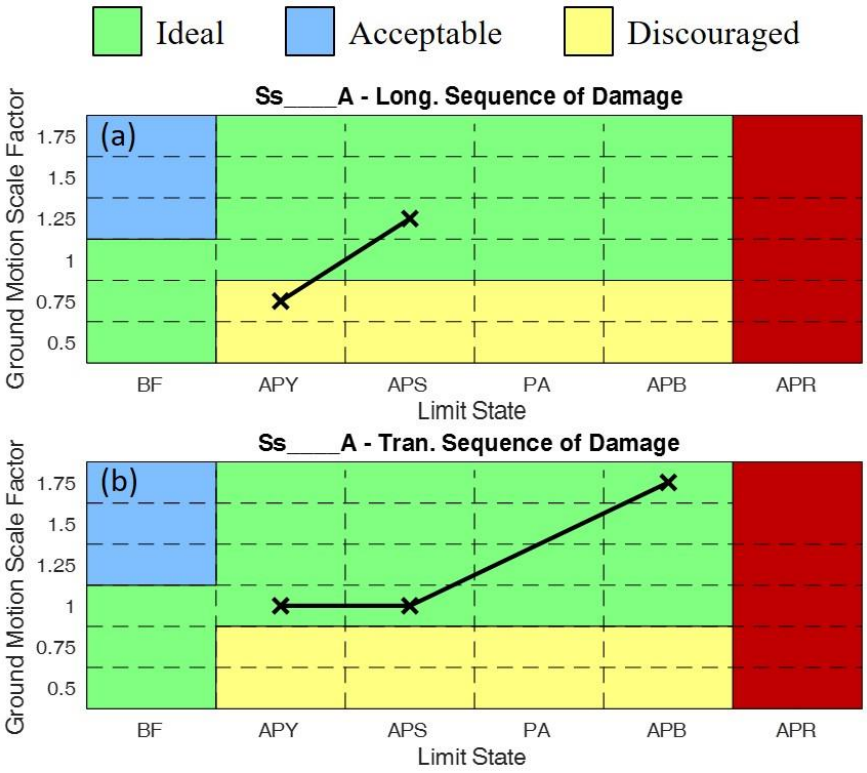

Figure 7.17: Sequences of damage for single-span steel IABs where a scale factor of 1.00 represents the design-level.

7.4.3 Three-Span Steel IABs

Table 7.13 presents the limit state occurrence results for the three-span steel IABs with 15-ft tall piers while Table 7.14 presents the results for the IABs with 40-ft tall piers. Throughout all the results it can be observed that there is no backfill mobilization in any bridge at any scale factor. Despite this, the other components in the abutment occur very frequently. APY occurs at high frequencies in most of the bridges and scale factors with the exception of the transverse 15-ft tall IABs. Aside from that situation, APY occurs in all of the analyses with a scale factor of 0.75 and larger but the piles do not tend to reach larger strain limit states such as APB and APR often. APS also occurs frequently and along with APB and APR provides an easier comparison across Table 7.13 and 7.14 to demonstrate that abutment foundation damage is more frequent in bridges with

40-ft piers due to the increased flexibility in the piers decreasing their demand and increasing it in the abutments.

At the pier columns, Table 7.13 and 7.14 indicate that damage to the pier foundation (PPY and PPS) does not begin to occur until scale factors of at least 1.25 with more damage occurring under longitudinal excitation. While light pier column damage (SL and CL) tends to occur at low scale factors, moderate column damage (SM and CM) typically doesn't occur in significant amounts until scale factors of at least 1.25 as well. Severe pier column damage (SS and CS) begins to occur much more frequently at scale factors of 1.5 and larger. It can be seen that there is more pier column damage in IABs with shorter piers. This is due to the shorter, stiffer piers increasing the demand on the piers and leading them to damage more often. This trend continues with the retainer engagement (RE) and yielding (RY) as well as the fixed bearing yielding (FY). These limit states also occur more often with shorter piers due to the increased forces being distributed to the piers through the bearings. In general, the retainer yielding is very common in both IABs using retainers. However, fixed bearing yielding rarely occur in IABs with 40-ft piers, even at large scale factors, while it commonly occurs at scale factors as low as 0.75 in IABs with 15-ft piers. Neither retainer fusing (RF) nor fixed bearing fusing (FF) occurs at any scale factor.

The IDA plots for the three-span steel IABs in the longitudinal and transverse directions are presented in Fig. 7.18 and 7.19, respectively. General observations in both directions demonstrate that IABs with 40-ft piers tend to have more deck displacement (center node displacement, Fig. 7.18a and 7.19a) despite having similar base shears (Fig. 7.18b and 7.19b). IABs with 40-ft piers also tend to have more abutment foundation damage in terms of the abutment pile strain (Fig. 7.18e and 7.19e) and p-y spring force (Fig. 7.18f and 7.19f). Both of these observations can be attributed to the increased flexibility of IABs with taller piers.

Table 7.13: Frequency of limit state occurrences for the IDA of three-span steel IABs with 15-ft tall piers where a scale factor of 1.00 represents the design-level.

Bridge	SF	Longitudinal Limit State Occurrence																			
		Ideal								Acceptable								Unacceptable			
		BF	SL	CL	RE	RY	RF	FY	FF	APY	APB	APS	PA	PPY	PPS	SM	CM	BU	SS	CS	APR
StC15EA	0.50	0%	0%	0%	0%	0%	0%	-	-	55%	0%	10%	0%	0%	0%	0%	0%	0%	0%	0%	0%
	0.75	0%	15%	0%	0%	0%	0%	-	-	100%	0%	30%	0%	0%	0%	0%	0%	0%	0%	0%	0%
	1.00	0%	60%	35%	0%	0%	0%	-	-	100%	0%	70%	0%	0%	0%	0%	0%	0%	0%	0%	0%
	1.25	0%	80%	80%	0%	0%	0%	-	-	100%	15%	95%	0%	0%	20%	40%	50%	0%	0%	5%	0%
	1.50	0%	100%	100%	0%	0%	0%	-	-	100%	80%	100%	0%	0%	70%	95%	100%	0%	0%	25%	0%
	1.75	0%	100%	100%	0%	0%	0%	-	-	100%	100%	100%	0%	0%	85%	100%	100%	0%	40%	80%	55%
StC15FA	0.50	0%	0%	0%	-	-	-	0%	0%	55%	0%	10%	0%	0%	0%	0%	0%	0%	0%	0%	0%
	0.75	0%	35%	15%	-	-	-	0%	0%	100%	0%	30%	0%	0%	0%	0%	0%	0%	0%	0%	0%
	1.00	0%	80%	60%	-	-	-	0%	0%	100%	0%	55%	0%	0%	0%	10%	20%	0%	0%	0%	0%
	1.25	0%	85%	80%	-	-	-	0%	0%	100%	5%	80%	0%	0%	10%	55%	65%	0%	0%	5%	0%
	1.50	0%	100%	100%	-	-	-	0%	0%	100%	55%	100%	0%	0%	65%	80%	80%	0%	0%	20%	0%
	1.75	0%	100%	100%	-	-	-	0%	0%	100%	100%	100%	0%	0%	90%	100%	100%	0%	20%	75%	25%
Bridge	**SF**	**Transverse Limit State Occurrence**																			
		Ideal								Acceptable								Unacceptable			
		BF	SL	CL	RE	RY	RF	FY	FF	APY	APB	APS	PA	PPY	PPS	SM	CM	BU	SS	CS	APR
StC15EA	0.50	0%	0%	0%	100%	25%	0%	-	-	10%	0%	0%	0%	0%	0%	0%	0%	0%	0%	0%	0%
	0.75	0%	10%	0%	100%	95%	0%	-	-	70%	0%	10%	0%	0%	0%	0%	0%	0%	0%	0%	0%
	1.00	0%	40%	10%	100%	100%	0%	-	-	100%	0%	30%	0%	0%	0%	0%	0%	0%	0%	0%	0%
	1.25	0%	80%	50%	100%	100%	0%	-	-	100%	0%	35%	0%	0%	0%	0%	10%	0%	0%	0%	0%
	1.50	0%	100%	80%	100%	100%	0%	-	-	100%	25%	80%	0%	10%	10%	40%	50%	0%	0%	0%	0%
	1.75	0%	100%	100%	100%	100%	0%	-	-	100%	60%	90%	0%	15%	0%	80%	80%	0%	5%	20%	0%
StC15FA	0.50	0%	0%	0%	-	-	-	0%	0%	0%	0%	0%	0%	0%	0%	0%	0%	0%	0%	0%	0%
	0.75	0%	5%	0%	-	-	-	80%	0%	5%	0%	0%	0%	0%	0%	0%	0%	0%	0%	0%	0%
	1.00	0%	60%	5%	-	-	-	80%	0%	60%	0%	10%	0%	0%	0%	0%	0%	0%	0%	0%	0%
	1.25	0%	100%	35%	-	-	-	100%	0%	100%	0%	15%	0%	0%	0%	0%	5%	0%	0%	0%	0%
	1.50	0%	100%	95%	-	-	-	100%	0%	100%	0%	55%	0%	0%	0%	15%	25%	0%	0%	0%	0%
	1.75	0%	100%	100%	-	-	-	100%	0%	100%	10%	80%	0%	0%	0%	35%	50%	0%	0%	0%	0%

Table 7.14: Frequency of limit state occurrences for the IDA of three-span steel IABs with 40-ft tall piers where a scale factor of 1.00 represents the design-level.

Bridge	SF	Longitudinal Limit State Occurrence																			
		Ideal								Acceptable								Unacceptable			
		BF	SL	CL	RE	RY	RF	FY	FF	APY	APB	APS	PA	PPY	PPS	SM	CM	BU	SS	CS	APR
StC40EA	0.50	0%	0%	0%	0%	0%	0%	-	-	65%	0%	30%	0%	0%	0%	0%	0%	0%	0%	0%	0%
	0.75	0%	0%	0%	0%	0%	0%	-	-	100%	0%	60%	0%	0%	0%	0%	0%	0%	0%	0%	0%
	1.00	0%	15%	0%	0%	0%	0%	-	-	100%	15%	100%	0%	0%	5%	0%	0%	0%	0%	0%	0%
	1.25	0%	75%	45%	0%	0%	0%	-	-	100%	75%	100%	0%	0%	55%	0%	5%	0%	0%	0%	10%
	1.50	0%	90%	80%	0%	0%	0%	-	-	100%	90%	100%	0%	0%	90%	20%	25%	0%	0%	0%	55%
	1.75	0%	100%	80%	0%	0%	0%	-	-	100%	95%	100%	0%	0%	95%	40%	55%	0%	0%	15%	80%
StC40FA	0.50	0%	0%	0%	-	-	-	0%	0%	70%	0%	30%	0%	0%	0%	0%	0%	0%	0%	0%	0%
	0.75	0%	0%	0%	-	-	-	0%	0%	100%	0%	60%	0%	0%	0%	0%	0%	0%	0%	0%	0%
	1.00	0%	15%	0%	-	-	-	0%	0%	100%	15%	100%	0%	0%	0%	0%	0%	0%	0%	0%	0%
	1.25	0%	75%	40%	-	-	-	0%	0%	100%	75%	100%	0%	0%	5%	0%	0%	0%	0%	0%	5%
	1.50	0%	85%	75%	-	-	-	0%	0%	100%	90%	100%	0%	0%	50%	20%	25%	0%	0%	0%	55%
	1.75	0%	95%	85%	-	-	-	0%	0%	100%	95%	100%	0%	0%	55%	40%	60%	0%	0%	15%	80%
Bridge	SF	Transverse Limit State Occurrence																			
		Ideal								Acceptable								Unacceptable			
		BF	SL	CL	RE	RY	RF	FY	FF	APY	APB	APS	PA	PPY	PPS	SM	CM	BU	SS	CS	APR
StC40EA	0.50	0%	0%	0%	80%	0%	0%	-	-	45%	0%	10%	0%	0%	0%	0%	0%	0%	0%	0%	0%
	0.75	0%	20%	0%	100%	40%	0%	-	-	100%	0%	35%	0%	0%	0%	0%	0%	0%	0%	0%	0%
	1.00	0%	65%	20%	100%	80%	0%	-	-	100%	5%	70%	0%	0%	0%	0%	0%	0%	0%	0%	0%
	1.25	0%	100%	100%	100%	100%	0%	-	-	100%	70%	100%	0%	0%	5%	0%	0%	0%	0%	0%	0%
	1.50	0%	100%	100%	100%	100%	0%	-	-	100%	100%	100%	0%	0%	10%	45%	55%	0%	0%	0%	20%
	1.75	0%	100%	100%	100%	100%	0%	-	-	100%	100%	100%	0%	0%	25%	70%	75%	0%	0%	15%	60%
StC40FA	0.50	0%	0%	0%	-	-	-	0%	0%	45%	0%	10%	0%	0%	0%	0%	0%	0%	0%	0%	0%
	0.75	0%	20%	0%	-	-	-	0%	0%	100%	0%	30%	0%	0%	0%	0%	0%	0%	0%	0%	0%
	1.00	0%	65%	35%	-	-	-	0%	0%	100%	5%	75%	0%	0%	0%	0%	0%	0%	0%	0%	0%
	1.25	0%	85%	80%	-	-	-	10%	0%	100%	55%	100%	0%	0%	0%	5%	0%	0%	0%	0%	0%
	1.50	0%	100%	100%	-	-	-	15%	0%	100%	100%	100%	0%	0%	5%	55%	55%	0%	0%	0%	15%
	1.75	0%	100%	100%	-	-	-	15%	0%	100%	100%	100%	0%	0%	25%	70%	85%	0%	0%	20%	55%

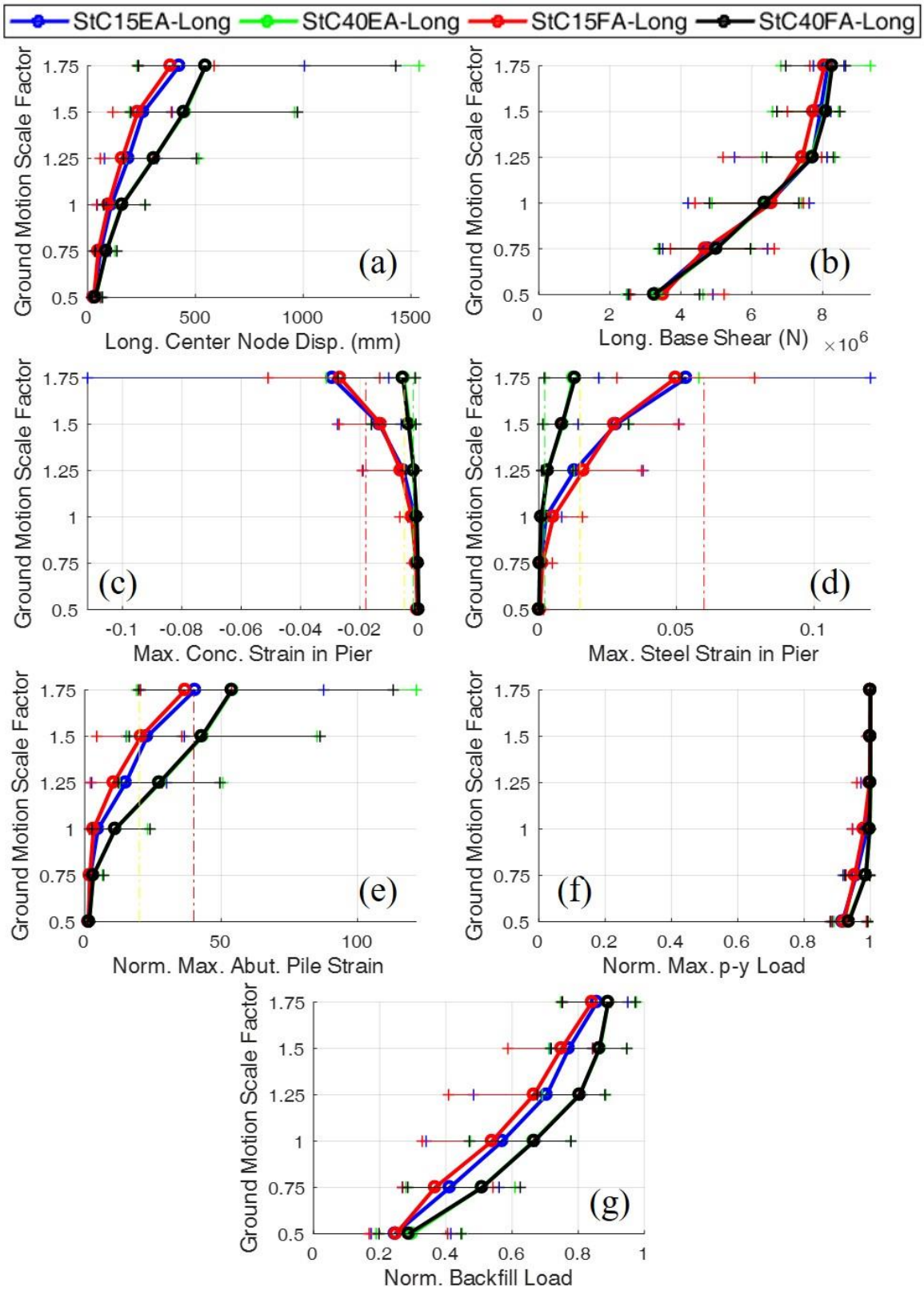

Figure 7.18: IDA plots for three-span steel IABs in the longitudinal direction where a scale factor of 1.00 represents the design-level.

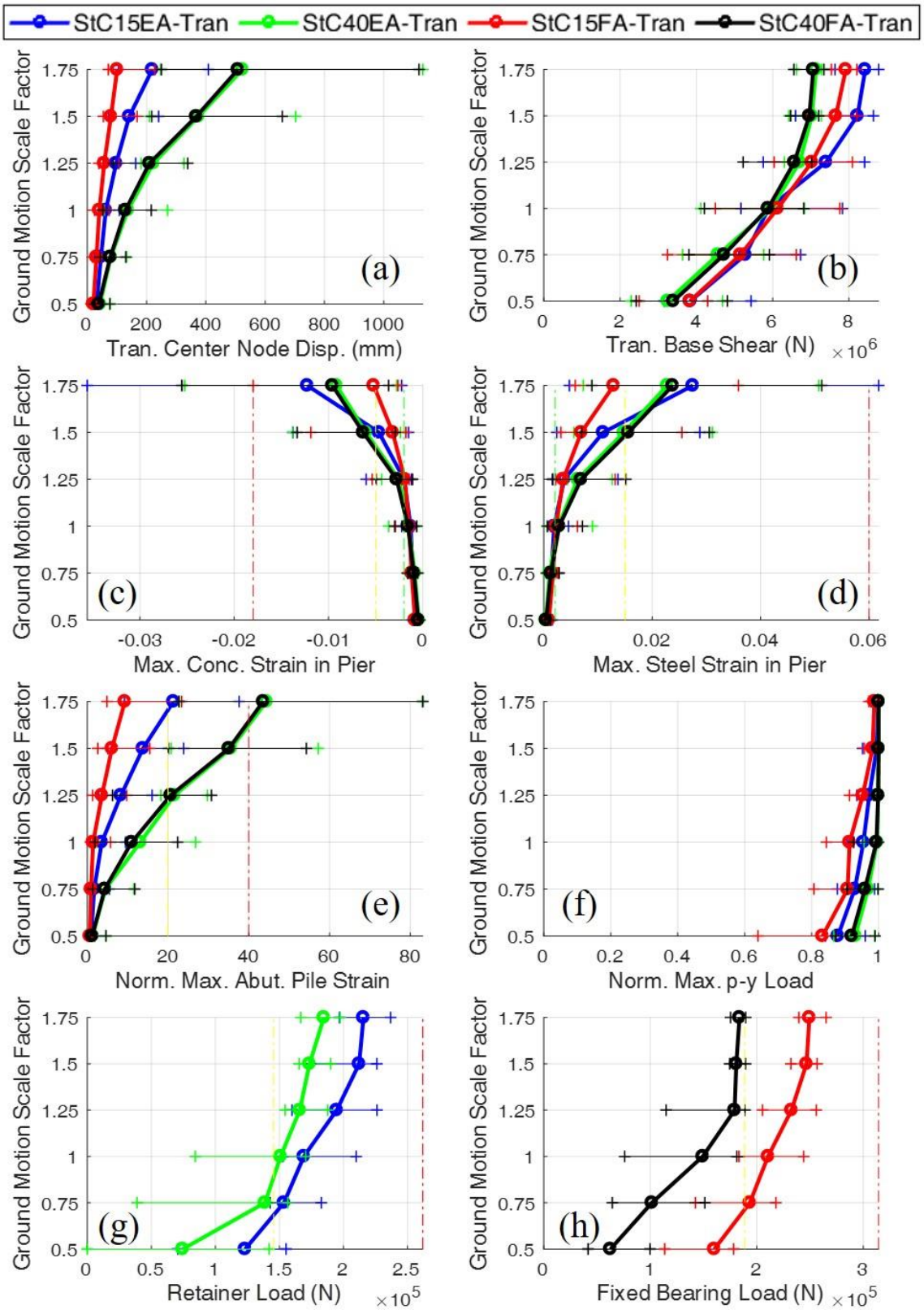

Figure 7.19: IDA plots for three-span steel IABs in the transverse direction where a scale factor of 1.00 represents the design-level.

Other interesting observations from the IDA plots involve the lack of fixed bearing yielding occurring in StC40FA. As demonstrated in Fig. 7.19f, the IDA curve for StC40FA fixed bearings reach forces close to the yellow dashed line representing fixed bearing yielding at scale factors around 1.25. However, at larger scale factors the fixed bearings seem unable to achieve yielding as it rarely occurs in the bridge. Another interesting observation concerns the strains in the piers. While it is clear in Fig. 7.18c and 7.18d that IABs with 15-ft piers experience more damage than those with 40-ft piers in the longitudinal direction, this trend does not hold in the transverse direction. Fig. 7.19c and 7.19d demonstrate that, while there is a lack of severe pier column damage (indicated by the red dashed line), the pier strains tend to be closer together.

The sequence of damage produced by the limit states encountered in the IDA of three-span steel IABs is provided in Fig. 7.20. The results show that the sequences tend to stay in the ideal range quite well for the ideal and acceptable limit states. The only slight variations are fixed bearing yielding occurring at a larger scale factor than ideal in the transverse direction of StC40FA, as well as a dip in each bridge at the abutment foundation damage limit states (APY/APS). This dip at APY/APS demonstrates that initial abutment foundation damage occurs too easily in the IABs such that they begin to occur at a scale factor half of the design-level, which is the minimum considered scale factor. However, the position of APB in the upper portion of the discouraged region indicates that the abutment pile strains only reach larger values around the design-level. While it is labeled as discouraged, this is a concerning result due to the difficulty to identify and repair damage to the abutment piles. Additionally, severe pier column damage (SS/CS) does occur in every bridge, which is unacceptable. However, SS/CS tends to occur at large scale factors, usually at 1.75, which is the most desirable scale factor for unacceptable limit states to occur at if they occur at all.

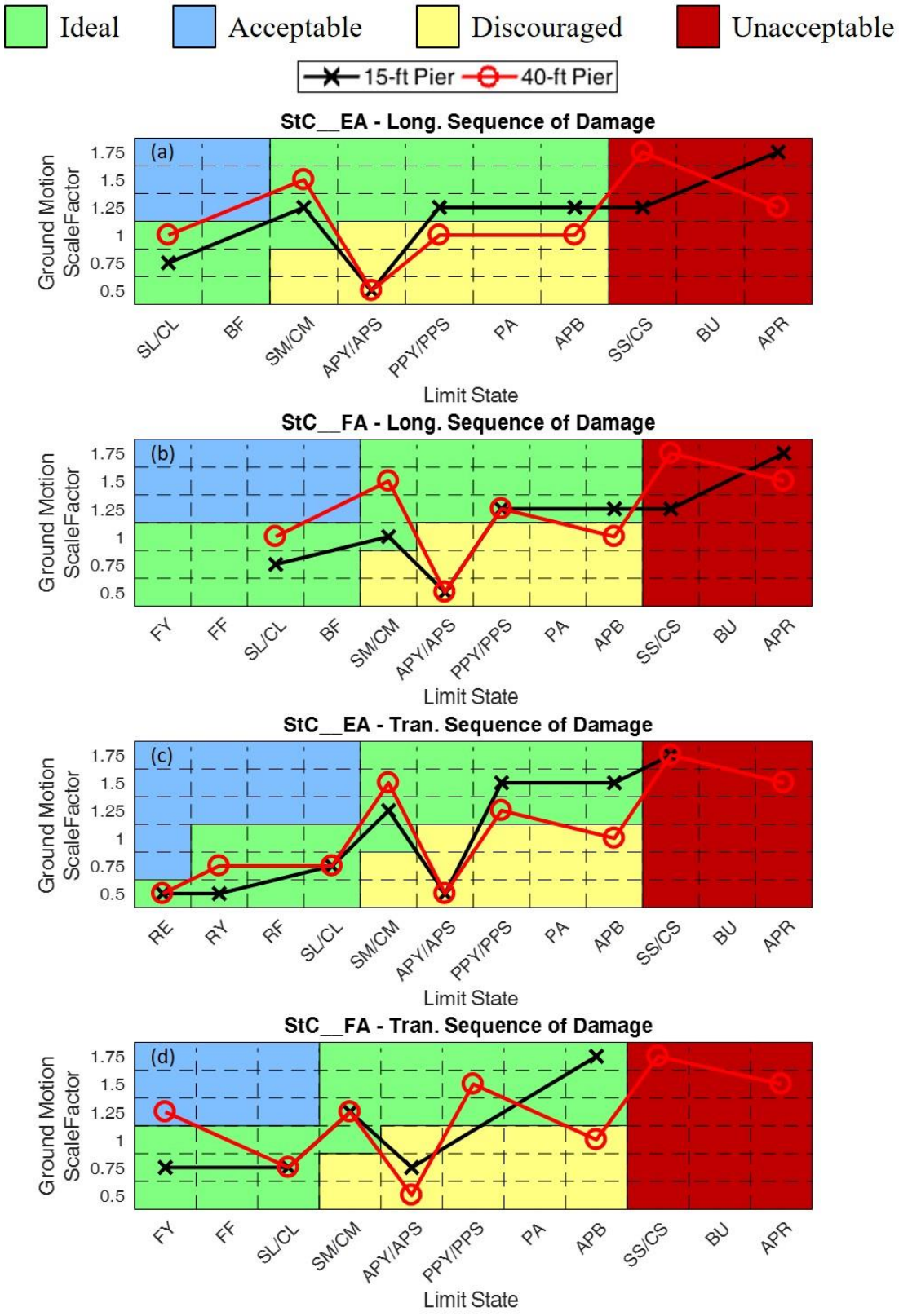

Figure 7.20: Sequences of damage for three-span steel IABs where a scale factor of 1.00 represents the design-level.

7.4.4 Four-Span Steel IABs

Table 7.15 describes the frequency of limit state occurrences in four-span steel IABs with 15-ft piers during the IDA. The results for the IABs with 40-ft piers are presented in Table 7.16. IABs with both pier heights demonstrate similar behavior concerning the initial abutment foundation damage limit states (APY and APS) in the longitudinal direction. While there are rare occurrences at the 0.5 scale factor, the APY and APS commonly occur in the analyses at scale factors of 0.75 and larger. They also quickly reach 100% occurrence in all the analyses at scale factors of 1.25 and larger. This corresponds to the onset of the APB and APR limit states at scale factors of 1.25 and 1.5, respectively. The APY, APB, APR, and APS occurrences in the transverse direction varies depending on the pier height. As shown in Table 7.15, the IABs with 15-ft piers do not begin to experience APY until the design-level and doesn't occur in 100% of the analyses until the MCE-level. APS occurs even less and never reaches 100% occurrence. APB and APR are rarely experienced and only at the largest scale factors. This changes for IABs with 40-ft piers in the transverse direction where damage occurs at much lower scale factors and APY and APS are very common and APB and APR begin occurring at smaller scale factors. The larger abutment foundation damage in IABs with tall piers can be attributed to the taller, more flexible piers distributing the force such that there is more demand on the abutment.

When using shorter piers the opposite is true with an increased demand being on the piers instead of the abutments. This can be seen when comparing the severe pier column damage limit states (SS and CS) in Table 7.15 and Table 7.16. It can be shown that there is much more pier column damage in IABs with 15-ft piers than there is in IABs with 40-ft piers. This culminates in IABs with 15-ft piers commonly having SS and CS occur at scale factors of 1.25 and larger while IABs with 40-ft piers experience less frequency of SS and CS and it begins to occur at larger scale

factors. In general across all the IABs it is shown that there is almost always light pier column damage (SL and CL) at scale factors of at least 1.0. Also, it can be shown that there is more damage at all scale factors in the transverse direction than the longitudinal direction.

The elastomeric bearing retainers and fixed bearings are shown to not encounter any yielding or fusing at any scale factor, as shown in Table 7.15 and 7.16. However, retainer engagement, which is expected to occur easily in the transverse direction, does occur in every bridge and at every scale factor that it is applicable to. Other limit states that occur include the mobilization of the soil surrounding the pier piles (PPS). PPS rarely occurs and when it does it is only present in the longitudinal direction at scale factors of at least 1.25.

Table 7.15: Frequency of limit state occurrences for the IDA of four-span steel IABs with 15-ft tall piers where a scale factor of 1.00 represents the design-level.

Bridge	SF	Longitudinal Limit State Occurrence																			
		Ideal								Acceptable								Unacceptable			
		BF	SL	CL	RE	RY	RF	FY	FF	APY	APB	APS	PA	PPY	PPS	SM	CM	BU	SS	CS	APR
SlC15EA	0.50	0%	0%	0%	0%	0%	0%	-	-	10%	0%	5%	0%	0%	0%	0%	0%	0%	0%	0%	0%
	0.75	0%	40%	10%	0%	0%	0%	-	-	80%	0%	40%	0%	0%	0%	0%	0%	0%	0%	0%	0%
	1.00	0%	100%	100%	0%	0%	0%	-	-	100%	0%	100%	0%	0%	5%	25%	35%	0%	0%	5%	0%
	1.25	0%	100%	100%	0%	0%	0%	-	-	100%	30%	100%	0%	0%	0%	85%	90%	0%	5%	60%	0%
	1.50	0%	100%	100%	0%	0%	0%	-	-	100%	60%	100%	0%	0%	0%	95%	100%	0%	35%	85%	20%
	1.75	0%	100%	100%	0%	0%	0%	-	-	100%	80%	100%	0%	0%	10%	100%	100%	0%	65%	90%	30%
SlC15FA	0.50	0%	20%	5%	-	-	-	0%	0%	5%	0%	0%	0%	0%	0%	0%	0%	0%	0%	0%	0%
	0.75	0%	80%	75%	-	-	-	0%	0%	75%	0%	30%	0%	0%	0%	0%	20%	0%	0%	0%	0%
	1.00	0%	90%	85%	-	-	-	0%	0%	90%	0%	75%	0%	0%	0%	60%	80%	0%	0%	0%	0%
	1.25	0%	100%	100%	-	-	-	0%	0%	100%	5%	100%	0%	0%	0%	100%	100%	0%	0%	55%	0%
	1.50	0%	100%	100%	-	-	-	0%	0%	100%	60%	100%	0%	0%	0%	100%	100%	0%	30%	85%	20%
	1.75	0%	100%	100%	-	-	-	0%	0%	100%	80%	100%	0%	0%	0%	100%	100%	0%	60%	95%	30%
Bridge	SF	Transverse Limit State Occurrence																			
		Ideal								Acceptable								Unacceptable			
		BF	SL	CL	RE	RY	RF	FY	FF	APY	APB	APS	PA	PPY	PPS	SM	CM	BU	SS	CS	APR
SlC15EA	0.50	0%	100%	100%	100%	0%	0%	-	-	0%	0%	0%	0%	0%	0%	30%	65%	0%	0%	0%	0%
	0.75	0%	100%	100%	100%	0%	0%	-	-	0%	0%	0%	0%	0%	0%	80%	85%	0%	0%	0%	0%
	1.00	0%	100%	100%	100%	0%	0%	-	-	10%	0%	0%	0%	0%	0%	100%	100%	0%	0%	35%	0%
	1.25	0%	100%	100%	100%	0%	0%	-	-	75%	0%	20%	0%	0%	0%	100%	100%	0%	30%	100%	0%
	1.50	0%	100%	100%	100%	0%	0%	-	-	90%	10%	50%	0%	0%	0%	100%	100%	0%	75%	100%	0%
	1.75	0%	100%	100%	100%	0%	0%	-	-	100%	20%	75%	0%	0%	0%	100%	100%	0%	85%	100%	15%
SlC15FA	0.50	0%	100%	100%	-	-	-	0%	0%	0%	0%	0%	0%	0%	0%	5%	10%	0%	0%	0%	0%
	0.75	0%	100%	100%	-	-	-	0%	0%	0%	0%	0%	0%	0%	0%	35%	75%	0%	0%	0%	0%
	1.00	0%	100%	100%	-	-	-	0%	0%	0%	0%	0%	0%	0%	0%	75%	90%	0%	0%	25%	0%
	1.25	0%	100%	100%	-	-	-	0%	0%	35%	0%	0%	0%	0%	0%	95%	100%	0%	10%	65%	0%
	1.50	0%	100%	100%	-	-	-	0%	0%	90%	0%	20%	0%	0%	0%	100%	100%	0%	60%	100%	0%
	1.75	0%	100%	100%	-	-	-	0%	0%	100%	15%	55%	0%	0%	0%	100%	100%	0%	85%	100%	5%

Table 7.16: Frequency of limit state occurrences for the IDA of four-span steel IABs with 40-ft tall piers where a scale factor of 1.00 represents the design-level.

Bridge	SF	Longitudinal Limit State Occurrence																			
		Ideal								Acceptable								Unacceptable			
		BF	SL	CL	RE	RY	RF	FY	FF	APY	APB	APS	PA	PPY	PPS	SM	CM	BU	SS	CS	APR
SlC40EA	0.50	0%	0%	0%	0%	0%	0%	-	-	35%	0%	10%	0%	0%	0%	0%	0%	0%	0%	0%	0%
	0.75	0%	15%	0%	0%	0%	0%	-	-	100%	0%	70%	0%	0%	0%	0%	0%	0%	0%	0%	0%
	1.00	0%	75%	50%	0%	0%	0%	-	-	100%	15%	100%	0%	0%	0%	0%	5%	0%	0%	0%	0%
	1.25	0%	85%	80%	0%	0%	0%	-	-	100%	50%	100%	0%	0%	10%	20%	30%	0%	0%	0%	15%
	1.50	0%	95%	85%	0%	0%	0%	-	-	100%	80%	100%	0%	0%	20%	55%	80%	0%	0%	10%	30%
	1.75	0%	100%	85%	0%	0%	0%	-	-	100%	80%	100%	0%	0%	30%	75%	80%	0%	0%	20%	50%
SlC40FA	0.50	0%	0%	0%	-	-	-	0%	0%	35%	0%	10%	0%	0%	0%	0%	0%	0%	0%	0%	0%
	0.75	0%	0%	0%	-	-	-	0%	0%	100%	0%	70%	0%	0%	0%	0%	0%	0%	0%	0%	0%
	1.00	0%	75%	50%	-	-	-	0%	0%	100%	15%	100%	0%	0%	5%	0%	0%	0%	0%	0%	0%
	1.25	0%	85%	80%	-	-	-	0%	0%	100%	50%	100%	0%	0%	25%	20%	25%	0%	0%	0%	15%
	1.50	0%	95%	85%	-	-	-	0%	0%	100%	80%	100%	0%	0%	35%	40%	65%	0%	0%	5%	30%
	1.75	0%	100%	85%	-	-	-	0%	0%	100%	80%	100%	0%	0%	40%	70%	75%	0%	0%	20%	50%
Bridge	SF	Transverse Limit State Occurrence																			
		Ideal								Acceptable								Unacceptable			
		BF	SL	CL	RE	RY	RF	FY	FF	APY	APB	APS	PA	PPY	PPS	SM	CM	BU	SS	CS	APR
SlC40EA	0.50	0%	100%	100%	100%	0%	0%	-	-	35%	0%	0%	0%	0%	0%	0%	10%	0%	0%	0%	0%
	0.75	0%	100%	100%	100%	0%	0%	-	-	90%	0%	15%	0%	0%	0%	70%	75%	0%	0%	0%	0%
	1.00	0%	100%	100%	100%	0%	0%	-	-	100%	5%	80%	0%	0%	0%	85%	85%	0%	0%	0%	0%
	1.25	0%	100%	100%	100%	0%	0%	-	-	100%	25%	75%	0%	0%	0%	85%	100%	0%	0%	20%	0%
	1.50	0%	100%	100%	100%	0%	0%	-	-	100%	45%	75%	0%	0%	0%	100%	100%	0%	15%	50%	20%
	1.75	0%	100%	100%	100%	0%	0%	-	-	100%	65%	75%	0%	0%	5%	95%	100%	0%	15%	55%	25%
SlC40FA	0.50	0%	100%	100%	-	-	-	0%	0%	20%	0%	0%	0%	0%	0%	0%	15%	0%	0%	0%	0%
	0.75	0%	100%	100%	-	-	-	0%	0%	85%	0%	10%	0%	0%	0%	65%	65%	0%	0%	0%	0%
	1.00	0%	100%	100%	-	-	-	0%	0%	95%	0%	80%	0%	0%	0%	85%	95%	0%	0%	0%	0%
	1.25	0%	100%	100%	-	-	-	0%	0%	100%	25%	75%	0%	0%	0%	95%	100%	0%	0%	30%	0%
	1.50	0%	100%	100%	-	-	-	0%	0%	100%	45%	75%	0%	0%	0%	95%	100%	0%	15%	50%	20%
	1.75	0%	100%	100%	-	-	-	0%	0%	100%	60%	75%	0%	0%	0%	95%	95%	0%	15%	60%	25%

The IDA plots for the longitudinal and transverse IDA results are presented in Fig. 7.21 and Fig. 7.22, respectively. General observations in both directions include that IABs with 40-ft piers encounter more deck displacement (as provided from center node displacement in Fig. 7.21a and 7.22a), IABs with 15-ft piers tend to have more pier strain leading to more pier damage (as shown in Fig. 7.21c, 7.21d, 7.22c, and 7.22d), and IABs with 40-ft piers have more abutment pile strain (Fig. 7.21e and 7.22e). These conclusions can be attributed to shorter, stiffer piers providing more pier column demand while taller, less stiff piers decrease the demand on the piers and increases it in the abutments.

As stated, IABs with 40-ft piers tend to have more damage to the abutment piles, however the effects on the soil surrounding the piles depends on the direction of excitation. In the longitudinal direction there is not much difference between IABs of different pier heights as they tend to reach the p-y spring ultimate capacity at low scale factors (see Fig. 7.21f). The transverse direction results in Fig. 7.22f demonstrate a clear distinction between the short and tall piers with the taller piers experiencing more damage at lower scale factors.

The retainer and fixed bearing behavior IDA plots provided in Fig. 7.22g and 7.22h, respectively, both demonstrate similar behavior. The observed behavior shows the force on the retainers and fixed bearing being consistent throughout the IDA. This is likely due to moderate pier damage occurring at low scale factors. Recall from the pushover analyses that the peak base shear is related to the onset of moderate pier damage, so the occurrence of these limit states would act as a fuse and limit the force being transferred across the bearings to the piers.

The sequence of damage plots, provided in Fig. 7.23, demonstrate that in the longitudinal direction the SM/CM and PPY/PPS limit states sometimes occur slightly too easily at scale factors just below ideal. However, a major issue in the longitudinal direction is the consistent onset of the

APY/APS limit states at the lowest scale factor and APB beginning to occur at the design level. Additionally, the unacceptable limit states SS/CS and APR begin to occur at scale factors between 1.0 and 1.5. The SS/CS limit state is unacceptable at any scale factor, having it begin to occur near the design-level is extremely undesirable.

As indicated in previous sections, the four-span IABs are extremely flexible in the transverse direction. This increased flexibility is shown to have negative effects on the sequences of damage presented in Fig. 7.23c and 7.23d. In the transverse directions most of the limit states begin to occur at the lowest scale factor of 0.5, well below the design-level. One of the only limit states not to begin to occur at a scale factor of 0.5 is the APY/APS limit state in IABs with 15-ft piers. This is one of the few times that APY/APS does not begin to occur at the 0.5 scale factor. The early moderate pier damage (SM/CM) may contribute to the later APY/APS onset due to the stiff piers taking most of the force until they reach their moderate damage limit. This would then redistribute additional force to the abutments which delays the onset of APY/APS. APB occurs within the acceptable range most of the time with the sole exception having it occur at the design level. The unacceptable limit states SS/CS begin to occur at scale factors larger than 0.5 as well. However, they occur at scale factors of 1.0 and 1.25 which is very low for an unacceptable limit state to occur.

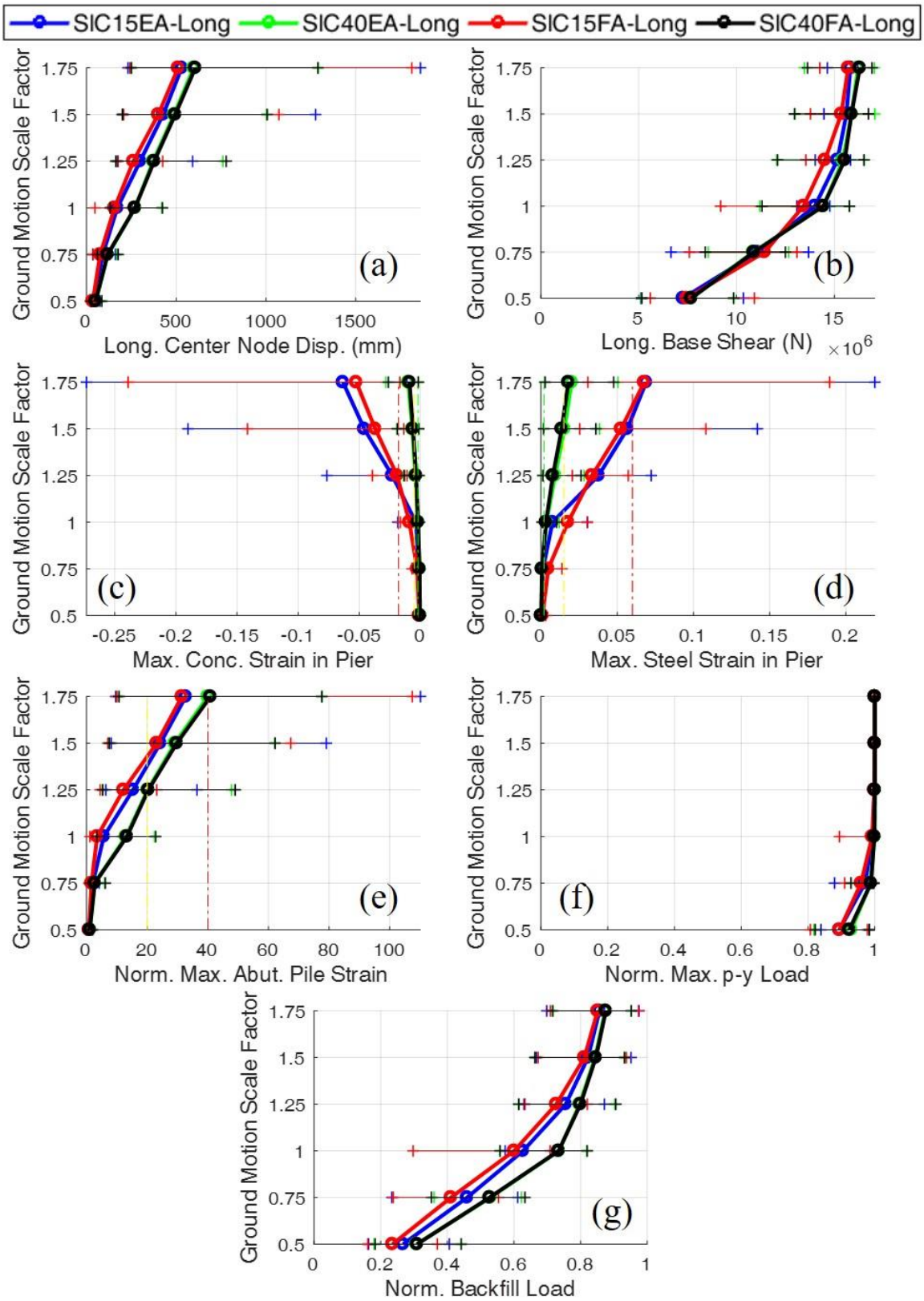

Figure 7.21: IDA plots for four-span steel IABs in the longitudinal direction where a scale factor of 1.00 represents the design-level.

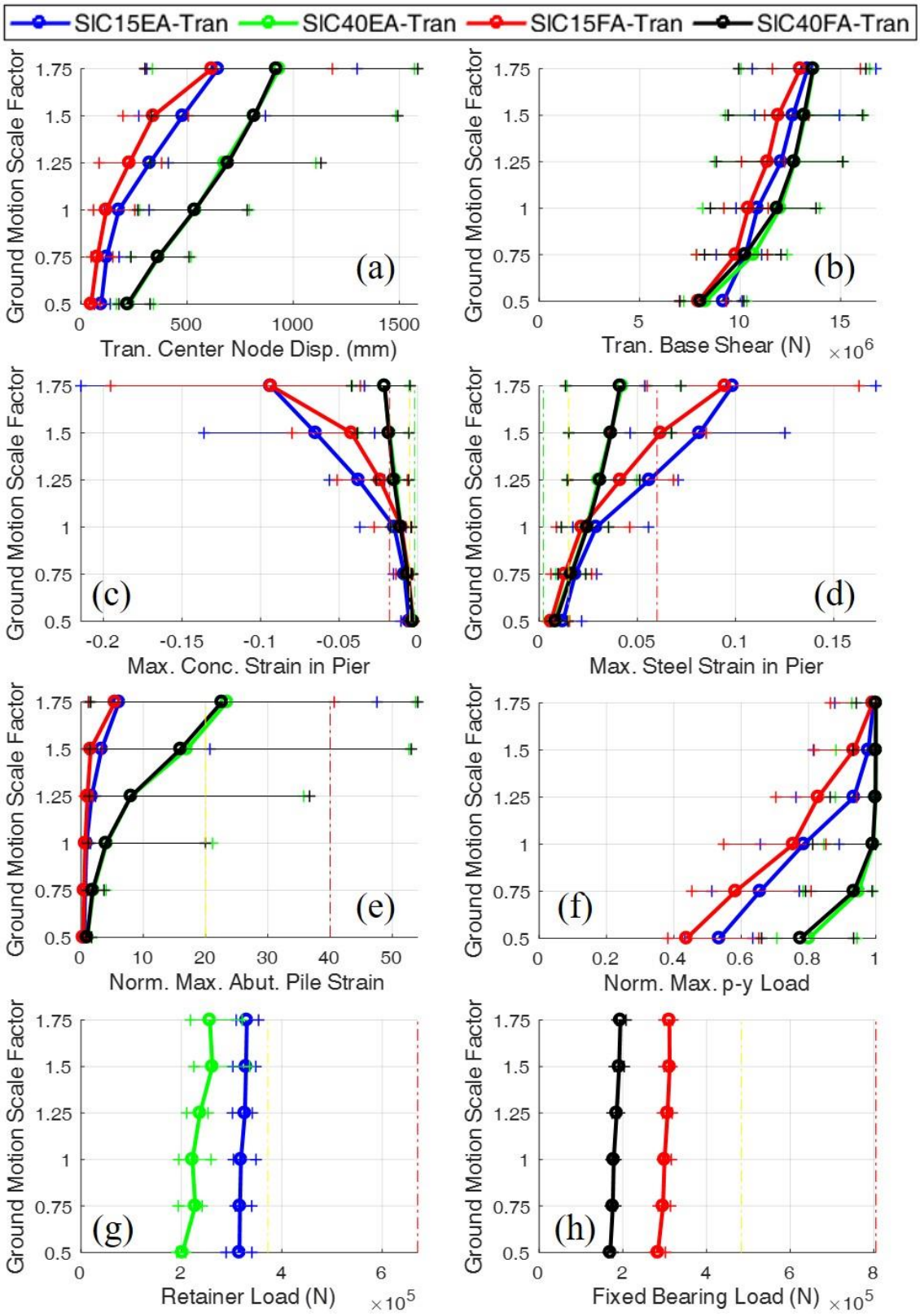

Figure 7.22: IDA plots for four-span steel IABs in the transverse direction where a scale factor of 1.00 represents the design-level.

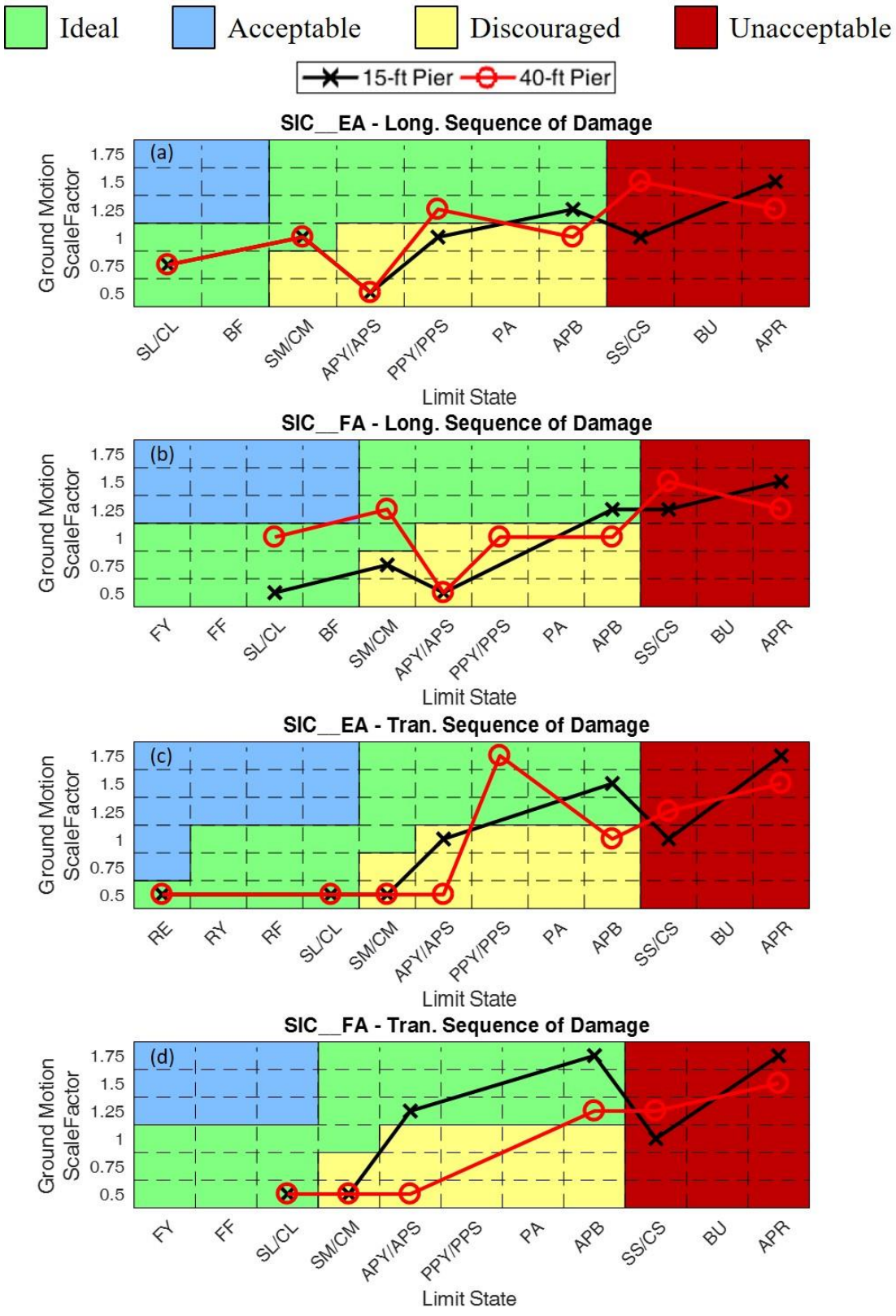

Figure 7.23: Sequences of damage for four-span steel IABs where a scale factor of 1.00 represents the design-level.

7.4.5 Three-Span Concrete IABs

The frequency of limit state occurrences during the IDA of the three-span concrete IABs is presented in Table 7.17 for IABs with 15-ft piers and Table 7.18 for IABs with 40-ft piers. The increased superstructure mass in the concrete IABs creates more damage in all the components of the IABs when compared to the steel IABs. This is exemplified in Tables 7.17 and 7.18 through APY always occurring in every bridge at every scale factor, APB occurring at scale factors of 0.75 and greater, APR occurring at the design level and greater, APS occurring in every bridge with scale factors of 0.75 or greater, and the increased light pier column damage which occurs most of the time in analyses with scale factors of 0.75 or greater. Backfill mobilization (BF), which is not encountered in any steel IAB begins to occur at larger scale factors.

The pier column damage results provided in Table 7.17 and Table 7.18 provide some other interesting observations. The first of which is that pier column damage of any level (light, moderate, severe) is rare at the 0.5 scale factor-level. Light pier column damage (SL and CL) occurs frequently at scale factors greater than and equal to the design-level. Similarly, the design-level scale factor of 1.0 is the beginning of significant amounts of moderate pier column damage (SM and CM) in all bridges and severe pier column damage (SS and CS) in IABs with 15-ft piers. The increased frequency of severe damage in IABs with short piers can once again be attributed to the increased stiffness of the piers leading to increased demands on the piers.

There is much more damage to the retainers and fixed bearings in the three-span concrete IABs as compared to the three-span steel IABs. This is shown by retainer yielding (RY) always occurring at every scale factor and retainer fusing (RF) always occurring at scale factors of 0.75 and larger in IABs with 15-ft piers. In IABs with 40-ft piers, RF frequently occurs at scale factors equal to and larger than 1.0 and always at the 1.5 scale factor and larger. The fixed bearings almost

always yield (FY) at every scale factor with the sole exception being the 80% occurrence frequency at a scale factor of 0.5 in Table 7.17. Despite this, fixed bearing fusing (FF) is still elusive as it only occurs in 20% of the analyses at the MCE-level scale factor of 1.75. These results once again show the ability for the shorter, stiffer piers to create more demand on the piers and the bearings.

The IDA plots for the results of the three-span concrete IABs in the longitudinal and transverse direction are provided in Fig. 7.24 and Fig. 7.25, respectively. These IDA plots demonstrate that there are similar deck displacements (via center node displacements, Fig. 7.24a and 101a) between IABs of varying pier heights. Common themes in both directions also include that IABs with 15-ft piers have larger pier strains (Fig. 7.24c, 7.24d, 7.25c, and 7.25d), especially after moderate pier column damage becomes more predominant in the longitudinal direction at a scale factor of 0.75 and in the transverse direction at a scale factor of 1.0. The abutment p-y springs are also shown to reach their ultimate capacity at very low scale factors, as shown in Fig. 7.24f and 7.25f. The abutment pile strains may seem to be consistent regardless of pier height in Fig. 7.24e and 7.25e, but due to the scale of the x-axis this is only true in the transverse direction. In the longitudinal direction the IABs with 40-ft piers consistently experience more pile strain. Some results of the backfill force at large scale factors are also shown to reach the ultimate capacity.

The behavior of the retainers and fixed bearings is also observed in the transverse direction through Fig. 7.25g and 7.25h, respectively. While IABs with 15-ft piers tend to have more force in the retainers, as expected due to the increased pier demand with short piers, this hardly matters as the retainers for all bridges fuse after scale factors of 1.0. The force in the fixed bearings are limited at scale factors of 0.75 and larger indicating a fuse is occurring elsewhere in the bridge. The fuse is likely the moderate damage of the pier columns which begins to occur at scale factors of 0.75 and typically signifies the maximum lateral force that the piers can resist.

Table 7.17: Frequency of limit state occurrences for the IDA of three-span concrete IABs with 15-ft tall piers where a scale factor of 1.00 represents the design-level.

Bridge	SF	Longitudinal Limit State Occurrence																		
		Ideal								Acceptable								Unacceptable			
		BF	SL	CL	RE	RY	RF	FY	FF	APY	APB	APS	PA	PPY	PPS	SM	CM	BU	SS	CS	APR
CtC15EA	0.50	0%	0%	0%	0%	0%	0%	-	-	100%	0%	55%	0%	0%	0%	0%	0%	0%	0%	0%	0%
	0.75	0%	95%	65%	0%	0%	0%	-	-	100%	5%	100%	0%	0%	0%	15%	20%	0%	0%	0%	0%
	1.00	0%	100%	100%	0%	0%	0%	-	-	100%	75%	100%	0%	0%	0%	75%	85%	0%	5%	50%	20%
	1.25	0%	100%	100%	0%	0%	0%	-	-	100%	85%	100%	0%	0%	0%	85%	90%	0%	35%	80%	60%
	1.50	10%	100%	100%	0%	0%	0%	-	-	100%	90%	100%	0%	10%	5%	90%	100%	0%	50%	75%	70%
	1.75	20%	100%	100%	5%	5%	0%	-	-	100%	100%	100%	0%	25%	15%	100%	100%	10%	70%	80%	70%

Bridge	SF	Transverse Limit State Occurrence																		
		Ideal								Acceptable								Unacceptable			
		BF	SL	CL	RE	RY	RF	FY	FF	APY	APB	APS	PA	PPY	PPS	SM	CM	BU	SS	CS	APR
CtC15EA	0.50	0%	0%	0%	100%	100%	5%	-	-	80%	0%	25%	0%	0%	0%	0%	0%	0%	0%	0%	0%
	0.75	0%	100%	25%	100%	100%	100%	-	-	100%	40%	100%	0%	0%	0%	0%	0%	0%	0%	0%	0%
	1.00	0%	100%	80%	100%	100%	100%	-	-	100%	90%	100%	0%	0%	0%	40%	40%	0%	5%	15%	10%
	1.25	0%	95%	85%	100%	100%	100%	-	-	100%	100%	100%	0%	0%	0%	80%	80%	0%	45%	65%	55%
	1.50	0%	95%	85%	100%	100%	100%	-	-	100%	100%	100%	0%	20%	20%	80%	80%	20%	75%	80%	80%
	1.75	0%	100%	95%	100%	100%	100%	-	-	100%	100%	100%	0%	20%	20%	80%	80%	20%	75%	80%	80%

Table 7.18: Frequency of limit state occurrences for the IDA of three-span concrete IABs with 40-ft tall piers where a scale factor of 1.00 represents the design-level.

Bridge	SF	Longitudinal Limit State Occurrence																			
		Ideal								Acceptable									Unacceptable			
		BF	SL	CL	RE	RY	RF	FY	FF	APY	APB	APS	PA	PPY	PPS	SM	CM	BU	SS	CS	APR
CtC40EA	0.50	0%	0%	0%	0%	0%	0%	-	-	100%	0%	75%	0%	0%	0%	0%	0%	0%	0%	0%	0%
	0.75	0%	55%	15%	0%	0%	0%	-	-	100%	45%	100%	0%	0%	5%	0%	0%	0%	0%	0%	0%
	1.00	0%	80%	75%	0%	0%	0%	-	-	100%	80%	100%	0%	0%	0%	20%	20%	0%	0%	0%	30%
	1.25	0%	85%	75%	0%	0%	0%	-	-	100%	85%	100%	0%	0%	20%	30%	50%	0%	0%	5%	70%
	1.50	10%	85%	75%	0%	0%	0%	-	-	100%	90%	100%	0%	5%	50%	50%	70%	0%	15%	20%	70%
	1.75	20%	90%	75%	0%	0%	0%	-	-	100%	90%	100%	0%	20%	30%	70%	70%	0%	20%	25%	70%
CtC40FA	0.50	0%	0%	0%	-	-	-	0%	0%	100%	0%	75%	0%	0%	0%	0%	0%	0%	0%	0%	0%
	0.75	0%	45%	20%	-	-	-	0%	0%	100%	45%	100%	0%	0%	0%	0%	0%	0%	0%	0%	0%
	1.00	0%	80%	65%	-	-	-	0%	0%	100%	80%	100%	0%	0%	15%	20%	20%	0%	0%	0%	30%
	1.25	0%	85%	75%	-	-	-	0%	0%	100%	85%	100%	0%	0%	5%	30%	45%	0%	0%	5%	70%
	1.50	10%	85%	75%	-	-	-	0%	0%	100%	90%	100%	0%	0%	20%	45%	70%	0%	10%	20%	70%
	1.75	20%	90%	85%	-	-	-	0%	0%	100%	90%	100%	0%	20%	15%	70%	70%	0%	20%	25%	70%

Bridge	SF	Transverse Limit State Occurrence																			
		Ideal								Acceptable									Unacceptable			
		BF	SL	CL	RE	RY	RF	FY	FF	APY	APB	APS	PA	PPY	PPS	SM	CM	BU	SS	CS	APR
CtC40EA	0.50	0%	5%	0%	100%	100%	0%	-	-	100%	5%	80%	0%	0%	0%	0%	0%	0%	0%	0%	0%
	0.75	0%	85%	60%	100%	100%	0%	-	-	100%	75%	100%	0%	0%	0%	0%	0%	0%	0%	0%	0%
	1.00	0%	95%	80%	100%	100%	65%	-	-	100%	90%	100%	0%	0%	0%	25%	35%	0%	0%	0%	30%
	1.25	0%	100%	85%	100%	100%	85%	-	-	100%	100%	100%	0%	0%	0%	55%	65%	0%	0%	10%	70%
	1.50	0%	100%	90%	100%	100%	100%	-	-	100%	100%	100%	0%	0%	0%	65%	70%	0%	20%	20%	70%
	1.75	0%	100%	95%	100%	100%	100%	-	-	100%	100%	100%	0%	0%	0%	70%	75%	0%	20%	30%	75%
CtC40FA	0.50	0%	15%	5%	-	-	-	80%	0%	100%	5%	70%	0%	0%	0%	0%	0%	0%	0%	0%	0%
	0.75	0%	100%	80%	-	-	-	100%	0%	100%	80%	100%	0%	0%	0%	0%	0%	0%	0%	0%	0%
	1.00	0%	100%	95%	-	-	-	100%	0%	100%	90%	100%	0%	0%	0%	30%	55%	0%	0%	0%	25%
	1.25	0%	100%	100%	-	-	-	100%	0%	100%	100%	100%	0%	0%	0%	70%	80%	0%	0%	15%	65%
	1.50	0%	100%	100%	-	-	-	100%	0%	100%	100%	100%	0%	0%	0%	75%	80%	0%	20%	20%	70%
	1.75	0%	100%	100%	-	-	-	100%	20%	100%	100%	100%	0%	0%	0%	80%	85%	5%	20%	30%	75%

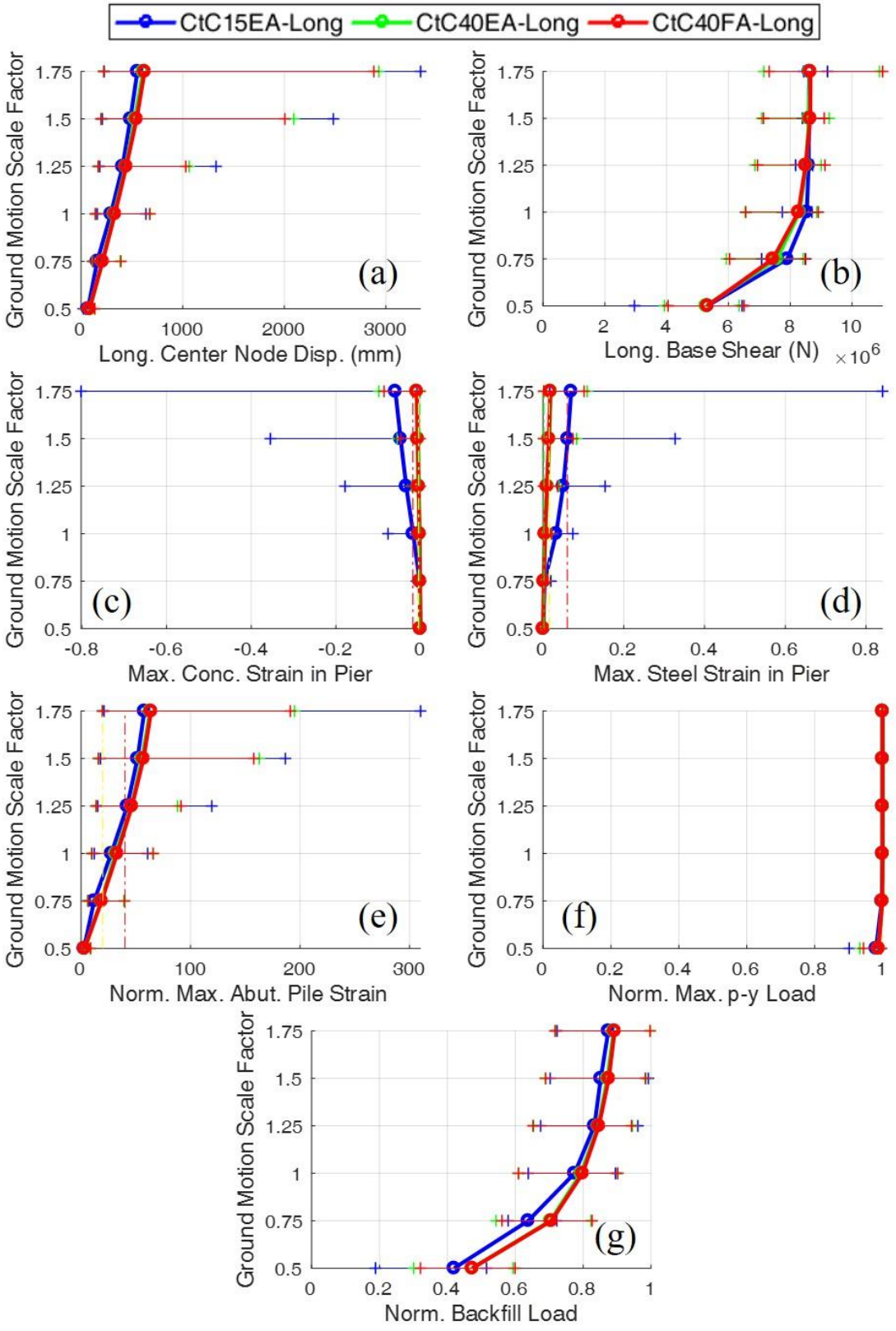

Figure 7.24: IDA plots for three-span concrete IABs in the longitudinal direction where a scale factor of 1.00 represents the design-level.

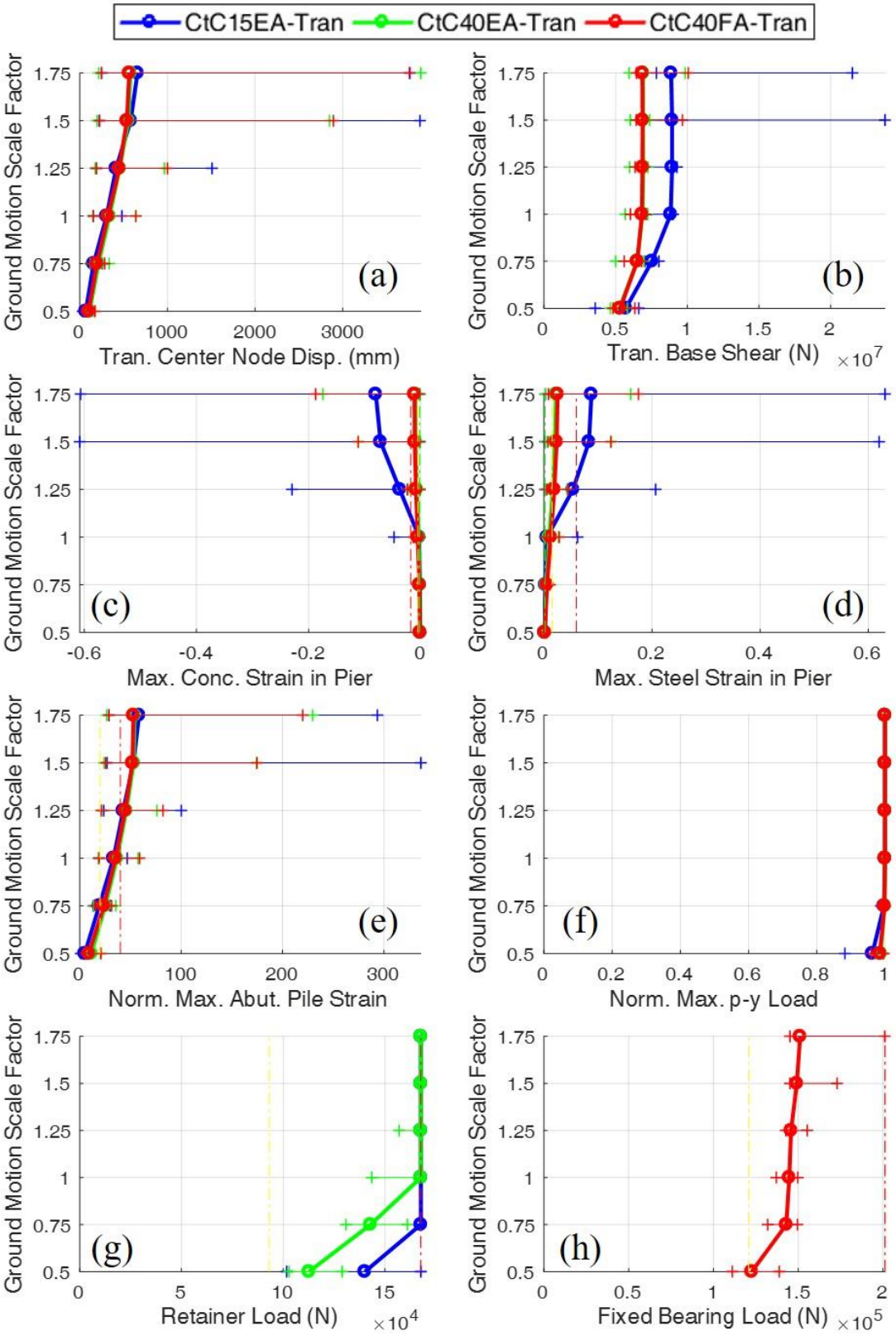

Figure 7.25: IDA plots for three-span concrete IABs in the transverse direction where a scale factor of 1.00 represents the design-level.

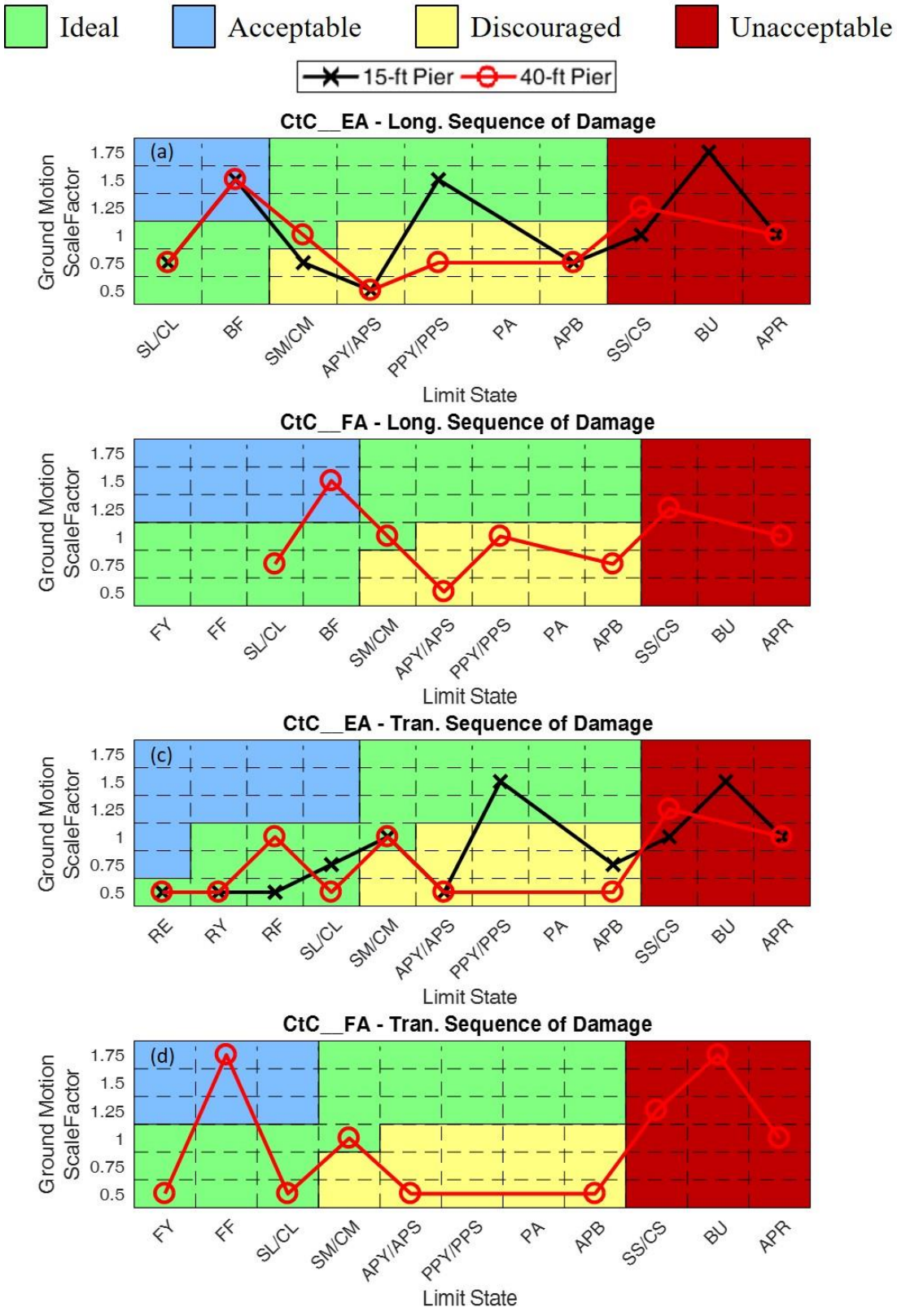

Figure 7.26: Sequences of damage for three-span concrete IABs where a scale factor of 1.00 represents the design-level.

The sequence of damage in the three-span concrete IABs is presented in Fig. 7.26. These sequences are generally unacceptable due to the onset of severe pier column damage (SS/CS) and abutment pile rupture (APR) occurring at limit states no greater than 1.25. The consistently low scale factor occurrence of SS/CS and APR can be attributed to the increased mass in the concrete superstructure as compared to the steel superstructure. This is far too close to having the unacceptable limit states occurring at the design-level. Aside from that issue, the PPY/PPS and SM/CM limit states begin to occur at slightly lower limit states than ideal in one bridge each and there is the common issue of APY/APS consistently occurring at the smallest limit state. Large abutment pile strains beyond yielding are also encountered at small scale factors as well, as shown by the location of first APB occurrences. The remaining limit states all occur in ideal or acceptable sequences.

7.4.6 Four-Span Concrete IABs

Table 7.19 and Table 7.20 provides the frequency of limit state occurrences during the IDA for four-span concrete IABs with 15-ft and 40-ft piers, respectively. The damage to the abutment foundation (APY, APB, APR and APS) is increased in this IAB as compared to its steel superstructure counterpart. This increase in damage is observed in the longitudinal direction by both abutment pile yielding (APY) and abutment soil mobilization (APS) occurring in almost all of the analyses at all the scale factors. The exceptions to this are the rare analyses where APS does not occur at a scale factor of 0.5. Larger levels of pile strain are also demonstrated by abutment pile local buckling (APB) occurring frequently at scale factors larger than 0.75, and abutment pile rupture (APR) occurring at scale factors of 1.0 and larger

In the transverse direction, the APY and APS damage does not occur at scale factors as low as those found in the longitudinal direction, but APY is still extremely frequent despite not

hitting 100% occurrence until a scale factor of 1.5 in IABs with 15-ft piers, and a scale factor of 1.0 in IABs with 40-ft piers. The amount of abutment pile strain achieved is also reduced when compared to the longitudinal direction, as demonstrated by the APB and APR limit states. The decreased abutment damage in the transverse direction is due to the extreme flexibility of the four-span IAB in that direction. This distributes more force to the piers and decreases the force in the abutments. Once again there is more abutment pile damage at the abutments in IABs with 40-ft piers due to their flexibility allowing for increased demand on the abutments when compared with the 15-ft pier IABs.

The pier column damage is also increased in the transverse direction when compared to the longitudinal direction due to the flexibility of the four-span bridge. Additionally, pier height also plays a part with IABs with 15-ft piers experiencing severe pier column damage (SS or CS) in the majority of analyses at scale factors of 0.75 and larger. The damage in the 40-ft piers is reduced with no severe damage occurring in the longitudinal direction at a scale factor of 1.0 and only 25% of analyses experiencing severe pier column damage at the 1.0 scale factor. However, these values increase to 30% in the longitudinal direction and 60% in the transverse direction at the 1.75 scale factor. The retainers atop the pier columns always yield (RY) at all scale factors, however they never fuse (RF).

The final limit state of interest is the ideal backfill mobilization limit state (BF). Despite being an ideal limit state it rarely occurs in other IABs. The maximum frequency of occurrence encountered in Table 7.20 is 15%, which is low, however BF does begin to occur at a scale factor of 1.75 for IABs with 15-ft piers and 1.25 for IABs with 40-ft piers. Once again, the increased occurrence of abutment limit states like BF in IABs with taller piers is observed.

The IDA plots for the four-span concrete IABs are presented in Fig. 7.27 for the longitudinal direction and Fig. 7.28 for the transverse direction. The deck displacements (via center node displacement) are shown to be very similar in the longitudinal direction (Fig. 7.27a) while the transverse displacements are more affected by the pier height with 40-ft pier IABs producing larger displacements (Fig. 7.28a). In terms of base shear (Fig. 7.27b and 7.28b), in both directions it can be seen that the base shear reaches a limit, and the point it goes vertical corresponds well to the occurrence of a significant amount of the analyses encountering severe pier column damage.

Table 7.19: Frequency of limit state occurrences for the IDA of four-span concrete IABs with 15-ft tall piers where a scale factor of 1.00 represents the design-level.

Bridge	SF	Longitudinal Limit State Occurrence																			
		Ideal								Acceptable								Unacceptable			
		BF	SL	CL	RE	RY	RF	FY	FF	APY	APB	APS	PA	PPY	PPS	SM	CM	BU	SS	CS	APR
ClC15EA	0.50	0%	50%	50%	0%	0%	0%	-	-	100%	0%	85%	0%	0%	0%	0%	0%	0%	0%	0%	0%
	0.75	0%	85%	85%	0%	0%	0%	-	-	100%	20%	100%	0%	0%	0%	70%	80%	0%	0%	50%	0%
	1.00	0%	95%	95%	0%	0%	0%	-	-	100%	65%	100%	0%	0%	0%	80%	80%	0%	5%	80%	5%
	1.25	0%	100%	100%	0%	0%	0%	-	-	100%	70%	100%	0%	0%	0%	85%	85%	0%	20%	75%	20%
	1.50	0%	100%	100%	0%	0%	0%	-	-	100%	70%	100%	0%	0%	0%	90%	95%	0%	20%	85%	25%
	1.75	5%	100%	100%	0%	0%	0%	-	-	100%	80%	100%	5%	0%	0%	95%	95%	0%	20%	95%	35%

Bridge	SF	Transverse Limit State Occurrence																			
		Ideal								Acceptable								Unacceptable			
		BF	SL	CL	RE	RY	RF	FY	FF	APY	APB	APS	PA	PPY	PPS	SM	CM	BU	SS	CS	APR
ClC15EA	0.50	0%	100%	100%	100%	100%	0%	-	-	5%	0%	0%	0%	0%	0%	95%	100%	0%	0%	45%	0%
	0.75	0%	100%	100%	100%	100%	0%	-	-	65%	0%	15%	0%	0%	0%	100%	100%	0%	5%	85%	0%
	1.00	0%	100%	100%	100%	100%	0%	-	-	75%	15%	55%	0%	0%	0%	100%	100%	0%	35%	100%	0%
	1.25	0%	100%	100%	100%	100%	0%	-	-	80%	15%	65%	0%	0%	0%	100%	100%	0%	30%	100%	5%
	1.50	0%	100%	100%	100%	100%	0%	-	-	100%	30%	75%	0%	0%	0%	100%	100%	0%	40%	100%	5%
	1.75	0%	100%	100%	100%	100%	0%	-	-	100%	35%	80%	0%	0%	0%	100%	100%	0%	45%	100%	5%

Table 7.20: Frequency of limit state occurrences for the IDA of four-span concrete IABs with 40-ft tall piers where a scale factor of 1.00 represents the design-level.

Bridge	SF	Longitudinal Limit State Occurrence																		
		Ideal								Acceptable								Unacceptable			
		BF	SL	CL	RE	RY	RF	FY	FF	APY	APB	APS	PA	PPY	PPS	SM	CM	BU	SS	CS	APR
ClC40EA	0.50	0%	5%	0%	0%	0%	0%	-	-	100%	0%	90%	0%	0%	0%	0%	0%	0%	0%	0%	0%
	0.75	0%	75%	60%	0%	0%	0%	-	-	100%	30%	100%	0%	0%	0%	10%	20%	0%	0%	0%	0%
	1.00	0%	75%	70%	0%	0%	0%	-	-	100%	60%	100%	0%	0%	0%	20%	35%	0%	0%	0%	10%
	1.25	10%	80%	75%	0%	0%	0%	-	-	100%	70%	100%	0%	0%	0%	35%	60%	0%	10%	20%	30%
	1.50	15%	85%	80%	0%	0%	0%	-	-	100%	70%	100%	0%	5%	5%	45%	70%	0%	15%	30%	35%
	1.75	15%	90%	90%	0%	0%	0%	-	-	100%	80%	100%	0%	5%	5%	50%	70%	0%	15%	30%	40%

Bridge	SF	Transverse Limit State Occurrence																		
		Ideal								Acceptable								Unacceptable			
		BF	SL	CL	RE	RY	RF	FY	FF	APY	APB	APS	PA	PPY	PPS	SM	CM	BU	SS	CS	APR
ClC40EA	0.50	0%	100%	90%	100%	100%	0%	-	-	55%	0%	20%	0%	0%	0%	40%	55%	0%	0%	5%	0%
	0.75	0%	100%	100%	100%	100%	0%	-	-	75%	20%	55%	0%	0%	0%	65%	75%	0%	0%	10%	0%
	1.00	0%	100%	100%	100%	100%	0%	-	-	100%	20%	85%	0%	0%	0%	75%	90%	0%	0%	25%	20%
	1.25	0%	100%	100%	100%	100%	0%	-	-	100%	30%	90%	0%	0%	0%	95%	100%	0%	20%	35%	20%
	1.50	0%	100%	100%	100%	100%	0%	-	-	100%	35%	95%	0%	0%	0%	100%	100%	0%	20%	50%	20%
	1.75	0%	100%	100%	100%	100%	0%	-	-	100%	50%	100%	0%	0%	0%	100%	100%	0%	20%	60%	30%

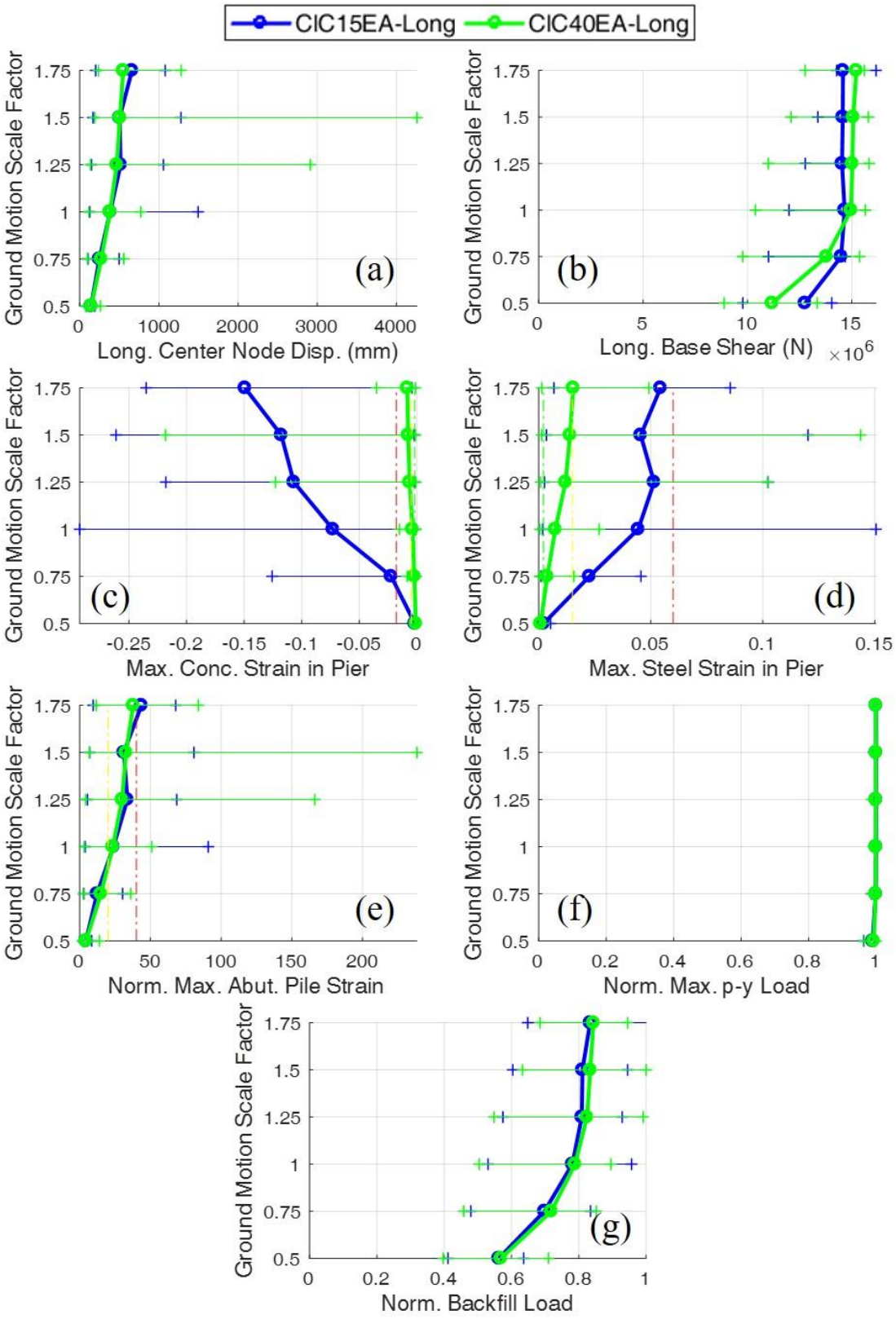

Figure 7.27: IDA plots for four-span concrete IABs in the longitudinal direction where a scale factor of 1.00 represents the design-level.

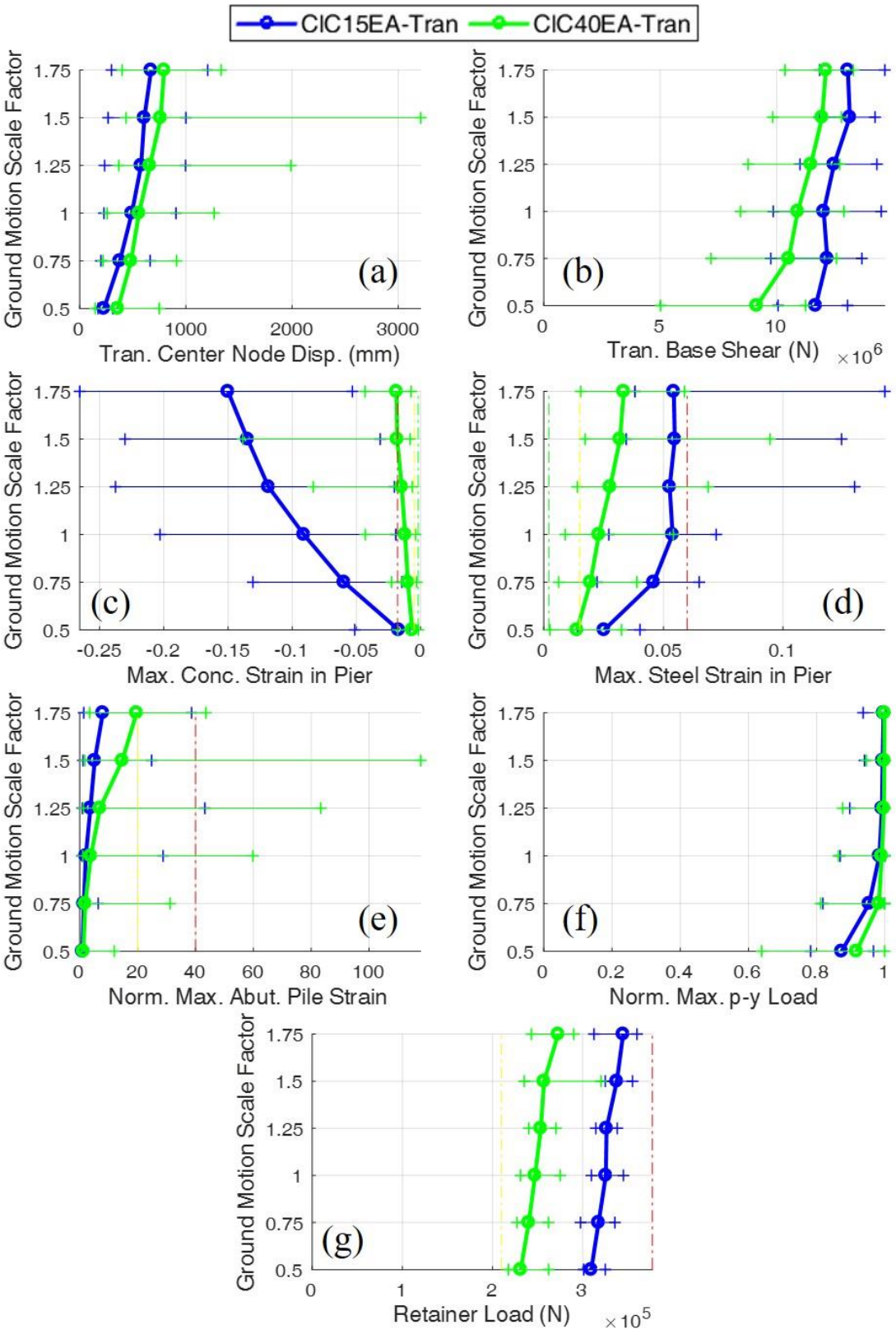

Figure 7.28: IDA plots for four-span concrete IABs in the transverse direction where a scale factor of 1.00 represents the design-level.

Other general observations from the IDA plots include the increased pier strain in IABs with 15-ft piers (Fig. 7.27c, 7.27d, 7.28c and 7.28d). The increased abutment pile strains in the transverse direction in IABs with 40-ft piers (Fig. 7.28e) while pile strain is about the same in the longitudinal direction regardless of pier height (Fig. 7.27e). These observations once again relate to stiffer piers causing more pier demand and more flexible piers leading to more abutment demand. The p-y spring behavior is difficult to differentiate due to the maximum p-y spring force consistently reaching the ultimate capacity at very low scale factors in both directions.

The increased abutment demand due to taller, more flexible piers is observed in the backfill behavior as well (Fig. 7.27g). It can be shown that there is more backfill engagement in IABs with 40-ft piers. Note that the backfill forces are large, however very few of the analyses produce backfill forces close to the ultimate backfill capacity indicated by a normalized force of 1.0. It is encouraging that some analyses at scale factors as low as 1.25 provide backfill so close to mobilizing. However, ideally the median (thick line) IDA curve would be closer to the normalized backfill force of 1.0.

As stated, the shorter piers produce more demand in the piers, this includes on the bearings and retainers. Fig. 7.28g demonstrates that IABs with 15-ft tall piers encounter more retainer force than IABs with 40-ft tall piers. It is also interesting to note that the retainer IDA curves for both IABs do not increase sharply, instead they minimally increase over the IDA analysis. This once again demonstrates that these retainers always yield (cross the yellow dashed line) but never fuse (cross the red dashed line) even at large scale factors.

The sequence of damage for the four-span concrete IABs in both directions is presented in Fig. 7.29. Similar to the three-span concrete IABs, the large superstructure mass causes the unacceptable severe column damage limit states (SS/CS) to begin at scale factors as low as 0.5 and

as high as 1.25. These scale factors are far too low for a limit state this damaging to occur at. In the longitudinal direction (Fig. 7.29a), aside from the SS/CS issue, moderate pier damage (SM/CM) occurs one scale factor too low and once again the initial abutment foundation damage (APY/APS) occurs at the lowest scale factor of 0.5. Abutment pile local buckling and rupture also occur at low scale factors indicating extremely large pile strains. Aside from these limit states, all others occur in the ideal or acceptable range in the longitudinal direction. The high flexibility of the four-span concrete IAB in the transverse direction leads to a terrible sequence of damage where every limit state that occurs begins at the lowest scale factor of 0.5. This result indicates that a four-span concrete IAB would not survive an earthquake even half the intensity of the design-level.

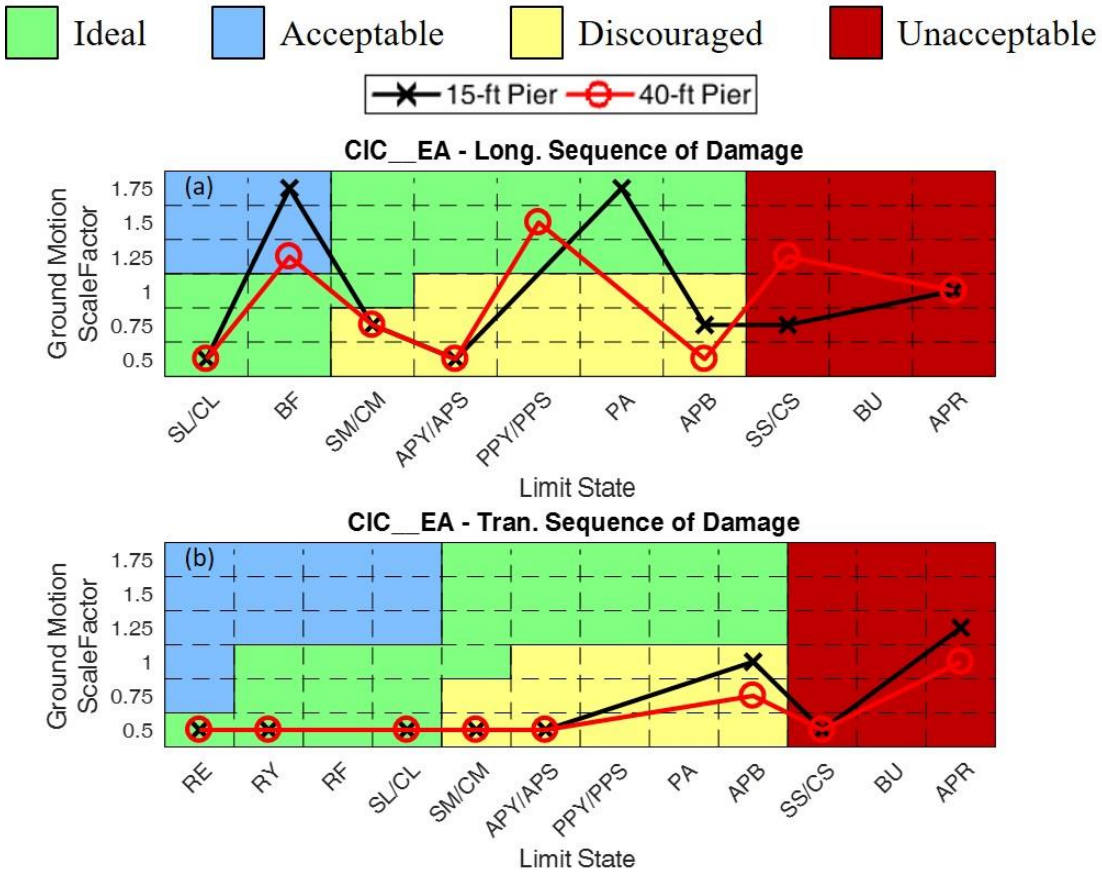

Figure 7.29: Sequences of damage for four-span concrete IABs where a scale factor of 1.00 represents the design-level.

7.4.7 Overall Observations

The general observations found through the IDA results tend to conclude that steel and three-span IAB designs are more effective at dealing with earthquakes than concrete and four-span IABs. Specifically, the four-span bridges are ineffective in the transverse direction and the additional mass from the concrete superstructure worsens the behavior. It is also found that at a variety of scale factors, the main areas of damage are located in the elastomeric bearing retainers, the fixed bearings, the pier columns, the abutment foundation piles, and the soil surrounding the piles.

Retainer fixed bearing yielding is found to consistently occur at lower scale factors in three-span IABs. Additionally, retainer damage is found to occur more frequently at lower scale factors in IABs with 15-ft piers. This demonstrates that an increased stiffness to the bridge through either a shorter deck or stiffer piers causes more retainer and fixed bearing damage under less ground motion intensity. Contrarily, the IABs with taller, more flexible piers have less demand on the piers and bearings, instead increasing the demand in the abutments. This last point is consistently observed throughout the IDA of the various IABs.

The sequences of damage provide useful insight into how the bridges will be damaged and in what order. Two consistent issues in the sequences of damage are the occurrences of initial abutment foundation damage (APY/APS) and severe pier column damage (SS/CS) at scale factors far too low. The APY/APS limit states consistently occur at the lowest scale factor of 0.5 when ideally it would occur at scale factors of 1.25 and larger so that other limit states such as backfill mobilization and moderate pier column damage can occur first. The SS/CS limit states do not usually occur at scale factors as low as the APY/APS, but they do often occur at scale factors at or below 1.25. This is far too close to the design-level scale factor of 1.0, and it is extremely

undesirable to encounter severe pier column damage during an earthquake slightly stronger than the design-level earthquake.

7.5 LIMIT STATE FRAGILITY CURVES

The IDA results are also used to develop fragility curves for the IAB limit states. Fragility curves are typically curves fitted through data points indicating the probability that a structure will collapse given a certain intensity measure (FEMA, 2012). In the case of this study, the intensity measure used is the ground motions scale factor (along the x-axis) and the probability (along the y-axis) represents the probability that a specific limit state will occur instead of structural failure. The y-axis scale goes from 0 to 1 where 0 never has the limit state occur and 1 always has the limit state occur. Fragility curves are useful in comparing bridges to each other as they present the data in a more visual manner. Additionally, the fragility curves are a good supplement to the IDA data previously presented by allowing factors such as how much the probability of a limit state occurring changes between scale factors to be shown. While not used for the purpose in this study, fragility curves are extremely useful in probabilistic analyses to determine how an IAB will behave given only an intensity measure.

This study developed limit state fragility curves for the 9 IABs which use elastomeric bearings and alluvial soils, as these are the most common bridges with the most realistic soil conditions. The fragility curves are developed by using the procedure provided in FEMA (2012) using the IDA responses of the bridges subjected to the 20 Cairo ground motions at various scale factors. The use of 20 ground motions is sufficiently large such that the curves should provide reliable estimates of fragility (FEMA, 2012). The data points are plotted first as stars followed by a curve fitted to the data using a lognormal distribution. While the lognormally fitted curves generally match well, there are some instances, especially with large amounts of occurrences at

low scale factors, where lognormal curves are unable to be plotted and the indicated fitted curves vary somewhat from the data.

7.5.1 Single-Span Steel IABs

The limit state fragility curves for Ss____A are provided in Fig. 7.30. These limit state fragility curves indicate that only abutment pile yielding (APY), abutment pile local buckling (APB), and mobilization of the soil surrounding the abutment piles (APS) occurs. In the longitudinal direction the APY seems to occur at a faster rate with respect to scale factor than the APS, as shown in Fig. 7.30 with the probability of APY occurrence rising from 0 to 1 between the scale factors of 0.5 to 1.25. APS does not even reach a probability of occurrence of 1. In the transverse direction it is shown that the APY curve is similar to the longitudinal APY curve, though it begins at larger scale factors, and the APS curve comes much closer to a probability of 1. APB increases steeply at the largest scale factor of 1.75.

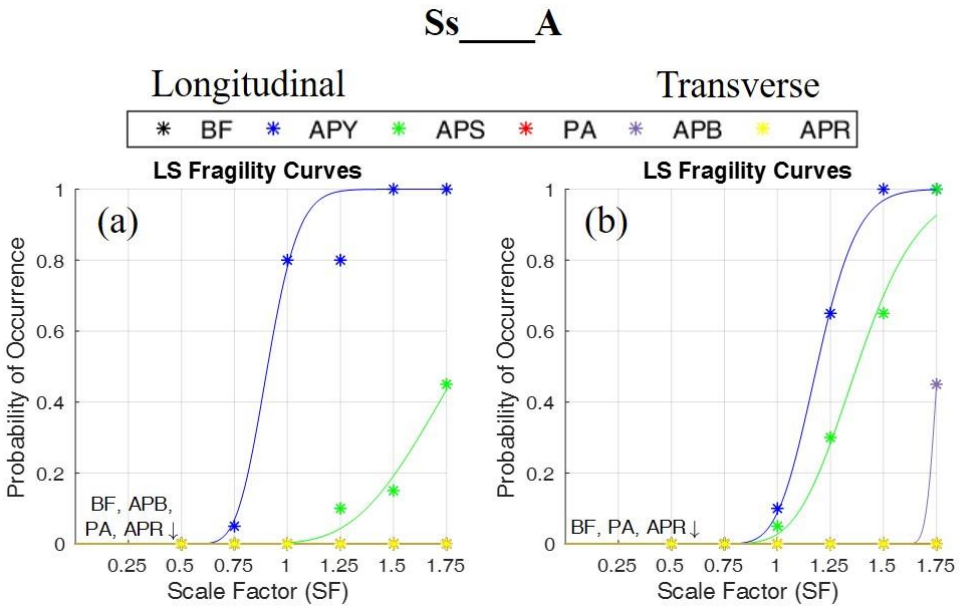

Figure 7.30: Limit state fragility curves for Ss____A in the (a) longitudinal and (b) transverse directions where a scale factor of 1.00 represents the design-level.

7.5.2 Three-Span Steel IABs

The limit state fragility curves for StC15EA is presented in Fig. 7.31. The limit states are divided into their respective categories of ideal, acceptable, and unacceptable. In the longitudinal direction it can be observed that light damage to the pier column steel (SL) and concrete (CL) are closely related as their fragility curves in Fig. 7.31a are very similar. The other ideal limit states do not occur at all. In Fig. 7.31c the abutment soil mobilization (APS) and moderate damage to the pier column steel (SM) limit states are observed to have a fairly gradual increase from a probability of occurrence of 0 to 1. On the other hand, the abutment pile yielding (APY) and moderate damage to the pier column concrete (CM) are shown to occur suddenly between the 0.5 and 1.25 scale factors, respectively. APS occurs at a rate similar to APY, however it is shifted to larger scale factors. Fig. 7.31e provides the curves for the unacceptable limit states and shows how much more often severe damage to the pier column concrete (CS) occurs over severe damage to the pier column steel (SS). However, CS never reaches a probability of occurrence of 1.

In the transverse direction plots of Fig. 7.31a it can once again be seen in the ideal limit states that SL and CL are closely related. Also in Fig. 7.31b, it can be shown that retainer yielding (RY) occurs at low scale factors and escalates quickly from a probability of 0 to 1. The acceptable limit state plot in Fig. 7.31d demonstrates how SM and CM are related in that direction and also how the probability of APY and APS occurring escalates more gradually between scale factors than when compared to the longitudinal direction results. APB also escalates gradually, but at larger scale factors than APY. Pier foundation damage through pile yielding (PPY) and soil mobilization (PPS) also makes an appearance with small probabilities of occurrence at large scale factors. There is not much occurring in Fig. 7.31f due to the lack of unacceptable limit states occurring until the 1.75 scale factor.

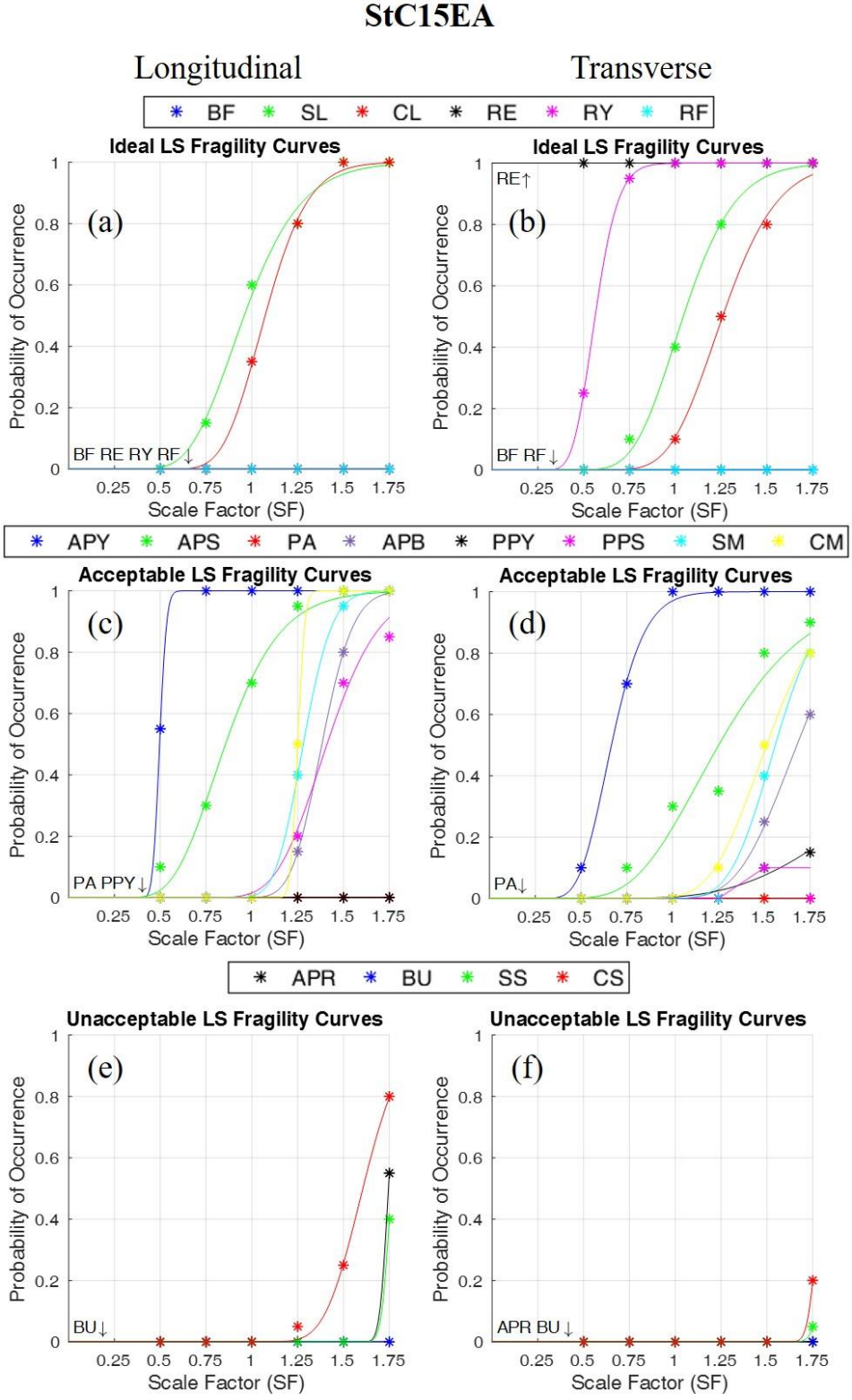

Figure 7.31: Ideal (a, b), acceptable (c, d), and unacceptable (e, f) limit state fragility curves for StC15EA in the longitudinal (left column) and transverse (right column) directions where a scale factor of 1.00 represents the design-level.

The limit state fragility curves for StC40EA are provided in Fig. 7.32. In the longitudinal direction, Fig. 7.32a demonstrates that there is a higher probability of SL occurring at a given scale factor than CL, especially since CL does not even reach a probability of occurrence of 1. The APY limit state escalates very quickly in Fig. 7.32c increasing in probability from 0 to 1 around the 0.5 scale factor. Once again, APB escalates at a similar rate to APY but at larger scale factors. APS is shown to reach a probability of occurrence as well, however its curve is much more gradual. As noted in other fragility plots, the SM and CM limit states are closely related due to their similarity in fitted curve shape. PPS also has a nice gradual curve in Fig. 7.32c where it does not begin occurring until a scale factor of 1.0 and reaches of probability of occurrence of 1 at the largest scale factor, this is an excellent trend for acceptable limit states. Fig. 7.32e demonstrates that there is minimal occurrences of unacceptable limit states outside of APR.

The transverse direction limit state fragility curves demonstrate an excellent fragility curve for ideal limit states to have in Fig. 7.32b with the RY curve. This curve leaves a probability of 0 at low scale factors and reaches a probability of occurrence of 1 just after the 1.0 scale factor. The SL and CL fragility curves also reach a probability of occurrence around the 1.0 scale factor with the SL curve being gradual and the CL curve being steep around the design-level scale factor. The acceptable limit state fragility curves provided in Fig. 7.32d indicate that APY occurs at low scale factors and develops quickly around the 0.5 scale factor. APB is similar to the APY curve but shifted about 0.75 scale factors to the right in the figure. Once again, APS is more gradual than the APY curve and still reaches a probability of occurrence of 1. It can also be observed that the curves for SM and CM are similar indicating that they are closely related. As in the longitudinal direction, there is minimal unacceptable limit states occurring in Fig. 7.32f outside of APR.

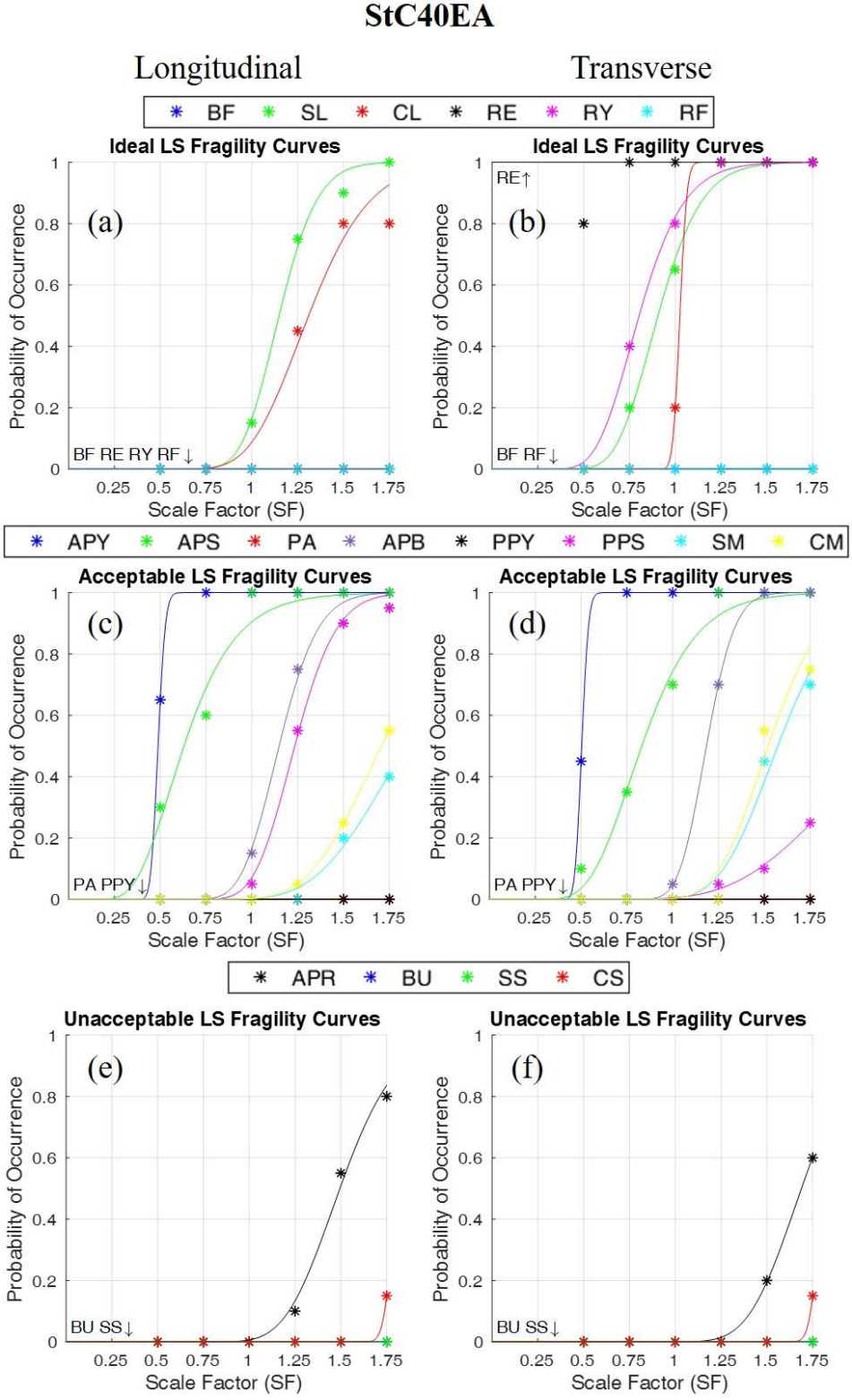

Figure 7.32: Ideal (a, b), acceptable (c, d), and unacceptable (e, f) limit state fragility curves for StC40EA in the longitudinal (left column) and transverse (right column) directions where a scale factor of 1.00 represents the design-level.

7.5.3 Four-Span Steel IABs

Fig. 7.33 presents the limit state fragility curves for SlC15EA. The longitudinal direction curves indicate that SL and CL are related due to their similar, steep curves around the 0.75 scale factor in Fig. 7.33a. In Fig. 7.33c it is shown that contrary to what was observed in the three-span steel fragility curves, the APY and APB curves are now more gradual than the APS curve which steeply changes from a probability of occurrence of 0 to 1 around the 0.75 scale factor. SM and CM are also shown to be related due to their similar fragility curves. The unacceptable limit state fragility curves provided in Fig. 7.33e demonstrate that CS begins to occur before the scale factor of 1.0 and has a large probability of occurrence at large scale factors.

The transverse limit state fragility curves in Fig. 7.33b, 7.33d, and 7.33f provide somewhat different observations than those in the longitudinal direction. To begin, the retainer engagement (RE), SL, and CL always occur and have a probability of occurrence of 1 regardless of the scale factor. This also applies to the CM curve, although the data points indicate it is actually closer to the SM curve. This error is produced due to the probability of occurrence of CM at the 0.5 scale factor being 0.65 and logically it must have a probability of occurrence of 0 at a scale factor of 0. This increase is too steep to determine a lognormal curve fit, so the curve is not ideally placed. Interestingly in this bridge, the APS curve never reaches a probability of 1, likely due to the short piers and long span of the IAB reducing the demand on the abutments. Similarly the delay in the onset of abutment damage leads to the APB curve remaining small in comparison to other curves. Unacceptable limit states are common in the transverse direction and CS escalates very quickly around the 1.0 scale factor while the SS curve is also concerning due to its size.

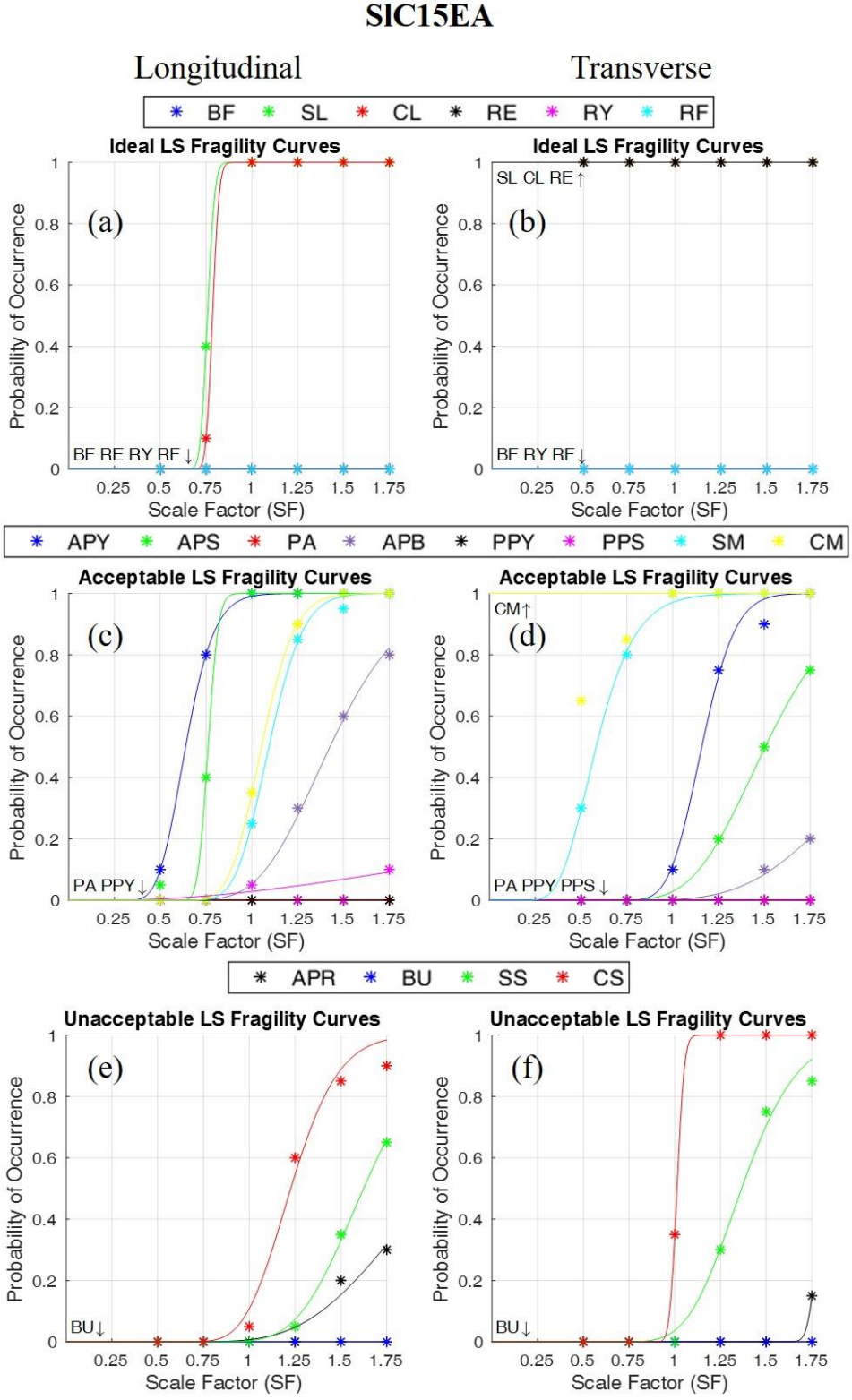

Figure 7.33: Ideal (a, b), acceptable (c, d), and unacceptable (e, f) limit state fragility curves for SlC15EA in the longitudinal (left column) and transverse (right column) directions where a scale factor of 1.00 represents the design-level.

Fig. 7.34a, 7.34c, and 7.34e provides the longitudinal limit state fragility curves for SlC40EA. These curves once again show that SL and CL are related due to their curve similarity, however the curves are much less steep than in the longitudinal direction. The fragility curves for APY and APS are also similar with APY being fairly steep around the 0.5 scale factor and APS being slightly more gradual. Despite APY being steep, the APS is gradual and demonstrates that the two are not necessarily related in this bridge. SM and CM are also observed to have similar fragility curves indicating, that they are related. There are some occurrences of CS, however the fragility curve is nowhere near the scale of the CS curve in SlC15EA. APR is also present at scale factors larger than 1.0.

The transverse limit state fragility curves for SlC40EA, presented in Fig. 7.34b, 7.34d, and 7.34f, demonstrate some similar behavior to SlC15EA curves in that RE, SL, and CL always have a probability of 1, and the SM and CM curves are very similar. The APY and APS fragility curves show that although they tend to begin at the same scale factor, APY occurs much more frequently at smaller scale factors given its steeper curve. The APB curve is much more gradual than the APY curve and does not reach a probability of 1 in the analyses. The CS limit state curve in Fig. 7.34f demonstrates that CS occurs often in the analyses. In fact, at larger scale factors such as 1.5 and 1.75 the probability of occurrence is above 0.5. While it is high in this bridge, the CS fragility curve is still more favorable than the CS curve for SlC15EA due to the taller, less stiff piers in SlC40EA decreasing the pier demand and increasing the abutment force demand.

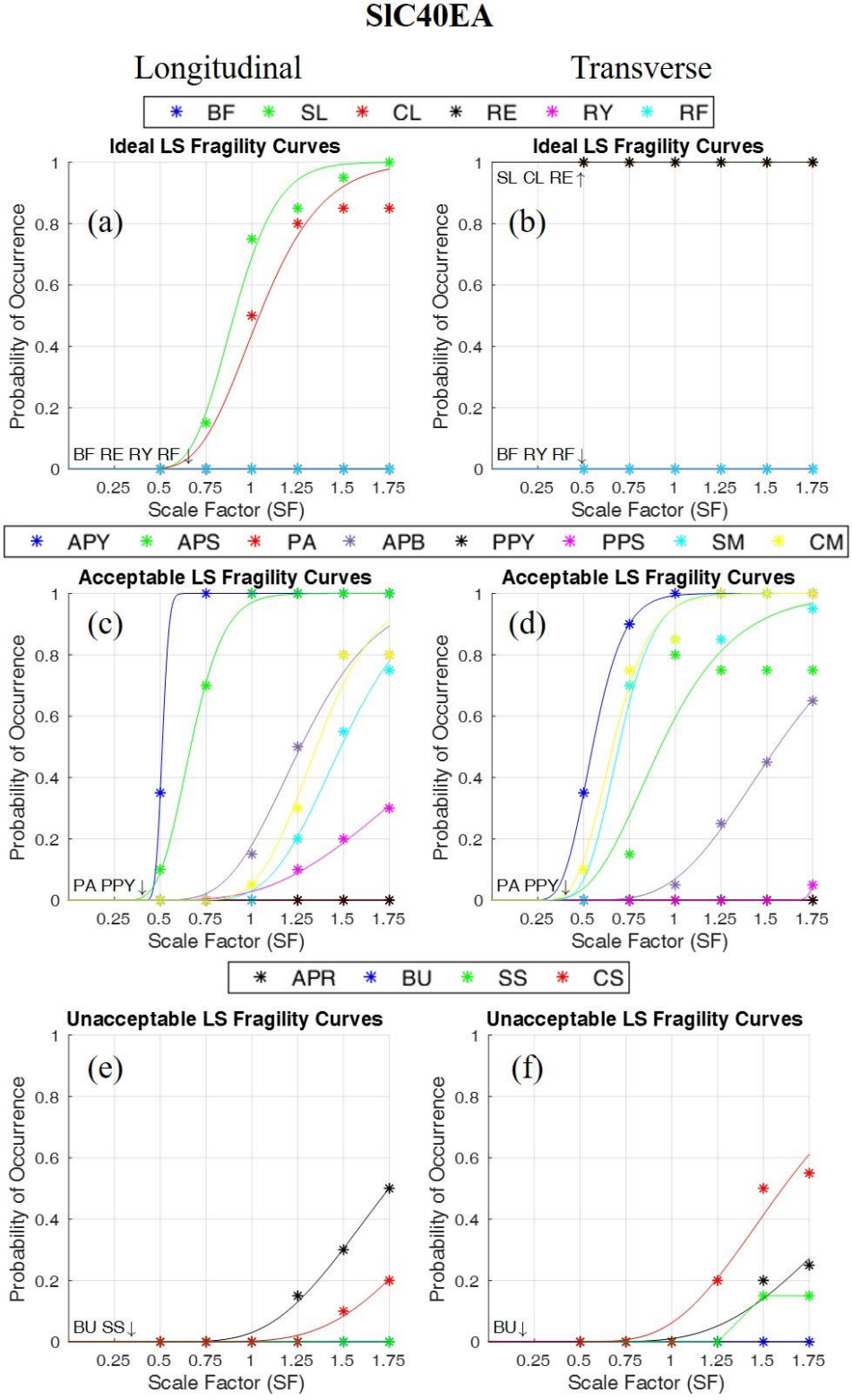

Figure 7.34: Ideal (a, b), acceptable (c, d), and unacceptable (e, f) limit state fragility curves for SlC40EA in the longitudinal (left column) and transverse (right column) directions where a scale factor of 1.00 represents the design-level.

7.5.4 Three-Span Concrete IABs

The longitudinal limit state fragility curves for CtC15EA are presented in Fig. 7.35a, 7.35c, and 7.35e. These fragility curves once again demonstrate that SL and CL are closely related, but also that backfill mobilization (BF) occurs at large scale factors, though the probability of occurrence is never large. In the acceptable limit state plot, APY has a probability of occurrence of 1 regardless of the scale factor. APS does not always have a probability of occurrence of 1, but does develop to a probability of 1 very quickly around the 0.5 scale factor. SM and CM once again have similar fragility curves indicating their close ties. Although APB is more closely related to APY, it's fragility curve is extremely similar to those from SM and CM. PPY and PPS also begin to occur at large scale factors and have similar curves. Although the fragility curves of the unacceptable limit states do not ever reach a probability of occurrence of 1, the curves still have probabilities of occurrence larger than zero at dangerously low scale factors such as around 0.5 for the CS curve.

The transverse limit state fragility curves, presented in Fig. 7.35b, 7.35d, and 7.35f, show that retainer engagement (RE) and yielding (RY) has a probability of occurrence of 1 regardless of the scale factor. Fusing of the retainer (RF) and SL does not always have a probability of 1, but does develop quickly around the 0.5 scale factor. The CL fragility curve is found to have a more gradual slope than the SL curve in this case. When moderate pier damage is analyzed, the fragility curves for SM and CM are once again found to be very similar. Although Fig. 7.35d describes APY as always having a probability of occurrence of 1, the data suggests that it should in fact be more similar to the APS curve which increases in probability steeply around the 0.5 scale factor. APB also occurs at small scale factors and develops quickly. Similar to the longitudinal direction, the CS curve begins to produce non-zero probabilities at dangerously low scale factors.

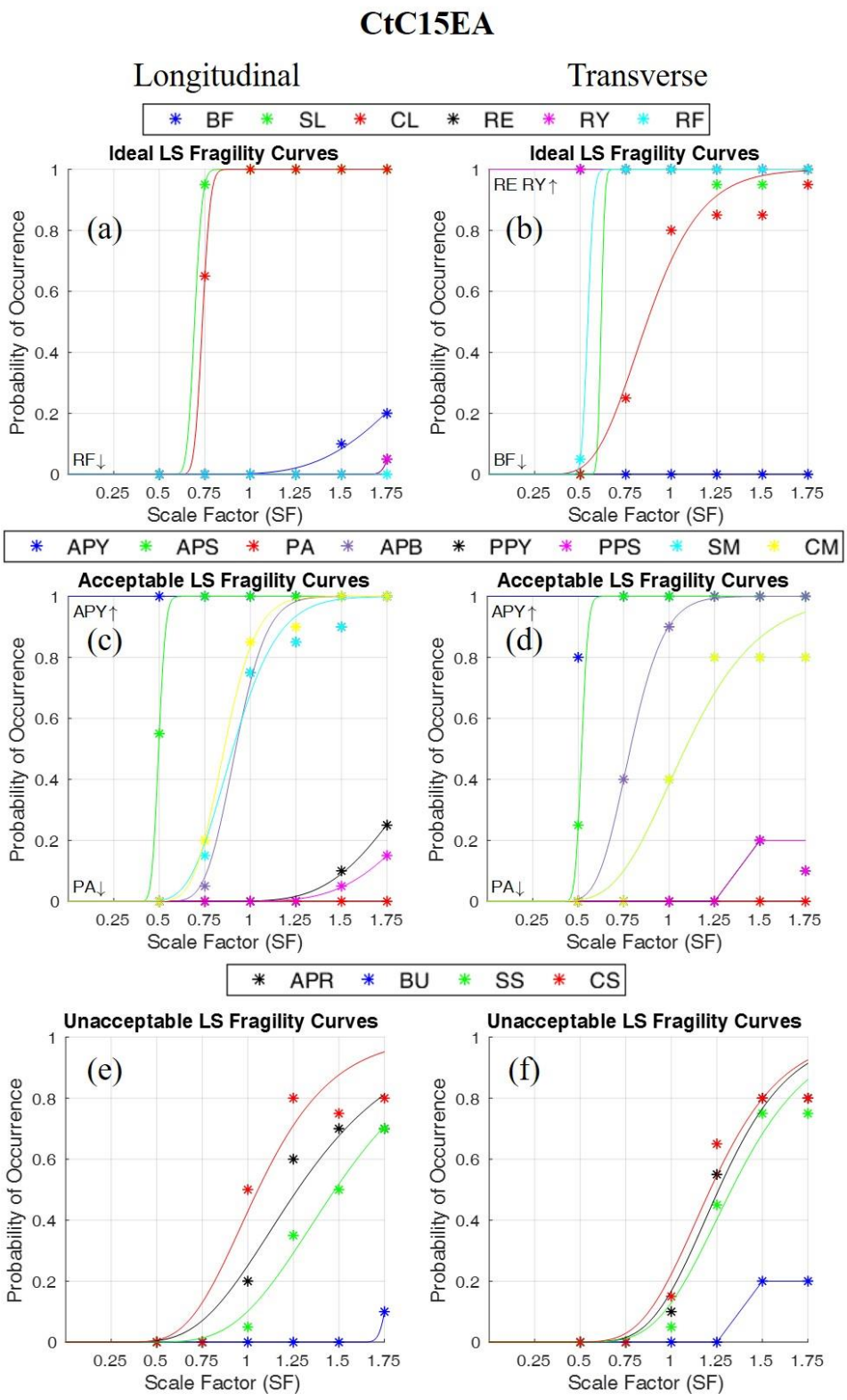

Figure 7.35: Ideal (a, b), acceptable (c, d), and unacceptable (e, f) limit state fragility curves for CtC15EA in the longitudinal (left column) and transverse (right column) directions where a scale factor of 1.00 represents the design-level.

Fig. 7.36a, 7.36c, and 7.36e provide the longitudinal limit state fragility curves for CtC40EA. These figures once again show that SL and CL have similar curves and that BF begins to occur at large scale factors, similar to CtC15EA curves. There is slightly more damage to the abutments as APY and APS always have a probability of occurrence of 1 in this bridge, this also leads to the APB curve beginning at small scale factors. Meanwhile, pier damage is decreased as indicated by the similar SM and CM curves not reaching a probability of occurrence of 1. PPS also has a similar curve to the SM and CM fragility curves. In terms of unacceptable limit states, CS and SS still occur and have similar curves, but the APR curve is much larger due to the increased abutment demands. However, these fragility curves are much more desirable than the unacceptable limit state fragility curves in CtC15EA.

The transverse fragility curves for CtC40EA are presented in Fig. 7.36b, 7.36d, and 7.36f. RE and RY are shown to always have a probability of occurrence of 1 while RF has a fragility curve that is gradual and generally encouraged for this limit state due to it reaching a probability of occurrence of 1 at just past the 1.25 scale factor. Unlike most bridges, the SL and CL fragility curves do not seem related, this changes when moderate damage to the piers occurs as the SM and CM curves are quite similar. Like in the longitudinal direction, APY and APS always have a probability of occurrence of 1 regardless of the scale factor and APB begins to occur at small scale factors and increases in probability quickly. This is due to the taller, less stiff piers in CtC40EA increasing the force demand on the abutments. Also, like the longitudinal results, unacceptable limit states occur, however their fragility curves are much more desirable than those presented for CtC15EA.

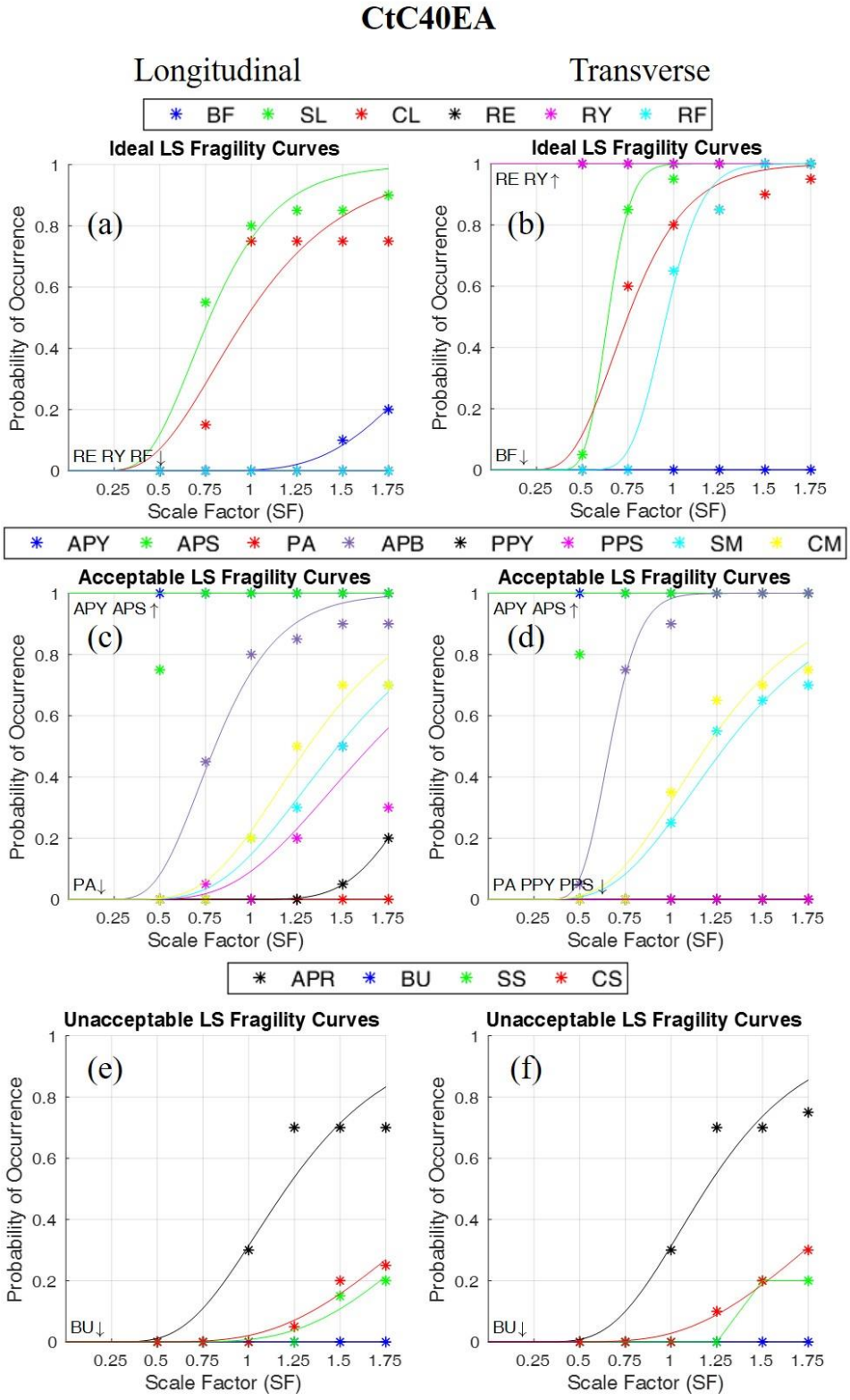

Figure 7.36: Ideal (a, b), acceptable (c, d), and unacceptable (e, f) limit state fragility curves for CtC40EA in the longitudinal (left column) and transverse (right column) directions where a scale factor of 1.00 represents the design-level.

7.5.5 Four-Span Concrete IABs

Fig. 7.37a, 7.37c, and 7.37e provide the longitudinal fragility curves for ClC15EA. The SL and CL curves are identical to each other indicating their close ties. The SM and CM curves are not identical, however they are very similar with CM being slightly steeper. APY and APS always have a probability of occurrence of 1 regardless of scale factor, however unlike in the Ct IABs the APB curve is not as steep as expected. As was shown for the other concrete IAB with 15-ft piers, the CS curve begins to have non-zero probabilities of occurrence at dangerously low scale factors and nearly reaches a probability of 1 at the 1.75 scale factor. This is due to the large mass of the concrete superstructure causing large amounts of damage to the piers.

In the transverse direction fragility curves (Fig. 7.37b, 7.37d, and 7.37f), RE, RY, SL, CL, SM, and CM always have a probability of occurrence of 1 at all scale factors. This is caused by the large superstructure mass and the inherent flexibility in the four-span bridges leading to more bearing and pier column damage. The reduced demand on the abutments creates APY and APS fragility curves which have gradual slopes instead of sharp, steep slopes. APB also has a very gradual slope which begins at low scale factors but does not even reach a probability of 0.4. Once again, severe damage to the pier column concrete is shown to occur at smaller scale factors in IABs with longer spans, concrete superstructures, and short piers. Fig. 7.37f demonstrates an extremely undesirable fragility curve for an unacceptable limit state in the CS curve which reaches a probability of 1 around the 1.0 scale factor mark.

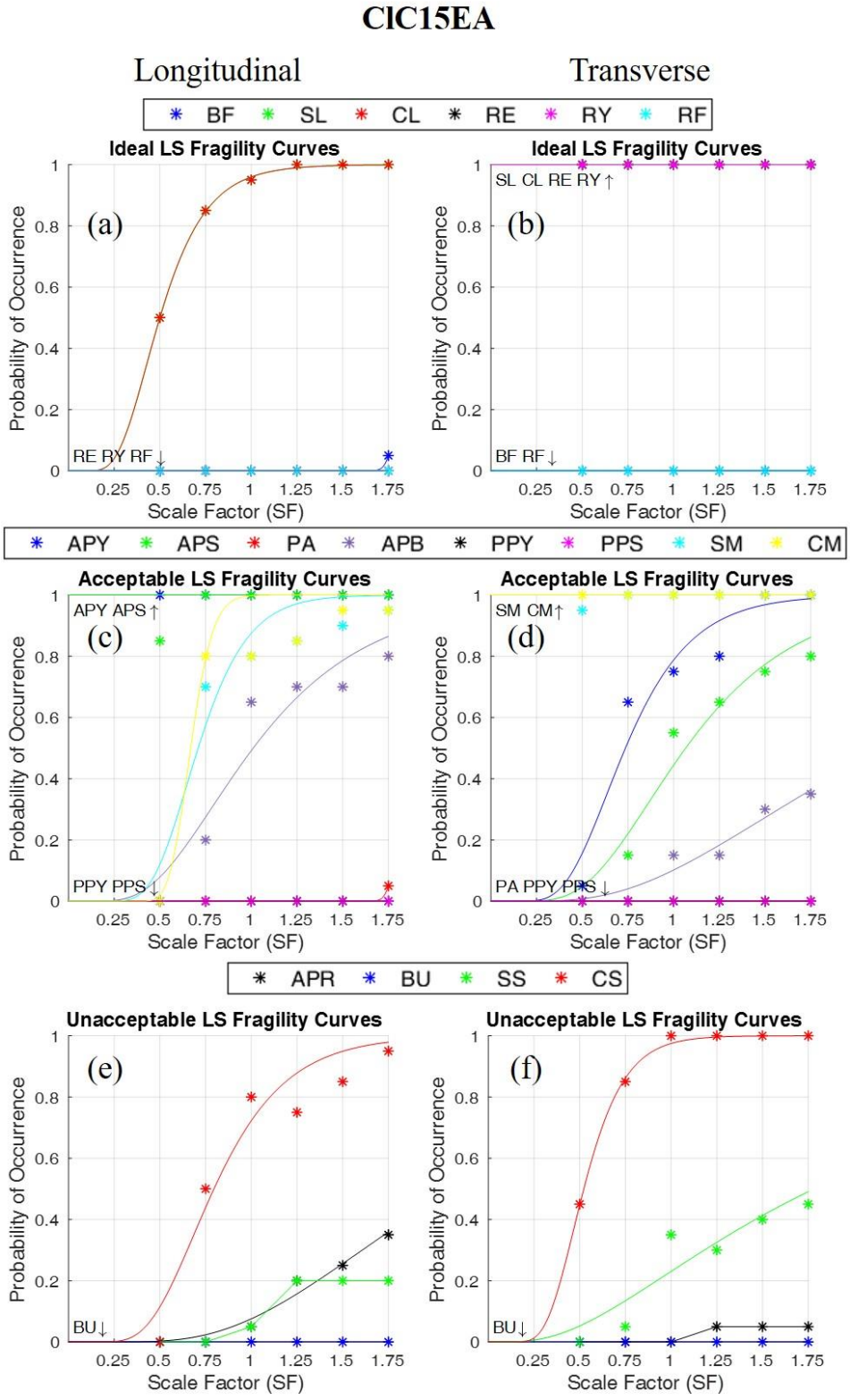

Figure 7.37: Ideal (a, b), acceptable (c, d), and unacceptable (e, f) limit state fragility curves for ClC15EA in the longitudinal (left column) and transverse (right column) directions where a scale factor of 1.00 represents the design-level.

ClC40EA also produces longitudinal limit state fragility curves (Fig. 7.38a, 7.38c, and 7.38e) which have SL and CL with similar curves. Also like in ClC15EA longitudinal fragility curves, APY and APS always have probabilities of occurrence of 1 and the SM and CM curves are similar though CM has a steeper slope. A difference is that neither the SM or CM fragility curves reaches a probability of occurrence of 1 at any scale factor provided. The APB curve is similar to the SM and CM curves and begins to occur at low scale factors due to the increased abutment demands. The unacceptable limit state fragility curves are also different from the ClC15EA curves. In ClC40EA there is less demand on the piers allowing for more desirable fragility curves. The worst unacceptable limit state fragility curve is the APR curve which produces a maximum probability of occurrence of about 0.4 and only begins to have non-zero probabilities at the 1.0 scale factor.

Fig. 7.38b, 7.38d, and 7.38f provide the fragility curves for ClC40EA in the transverse direction. In these fragility curves we can observe that RE, RY, SL, CL, CM, and APY always have a probability of occurrence of 1 across all scale factors. However, the data suggests that the CM curve should be more closely related to the SM curve. Despite APY always occurring, the APS curve is relatively gradual and has low probabilities of occurrence. The APS fragility curve is a nice gradual curve, however it can be improved given that the non-zero probability of occurrence values begin at small scale factors. The CS fragility curve does reach larger probabilities than in the longitudinal direction with a probability of occurrence of 0.6 at the 1.75 scale factor. However, this fragility curve is still more desirable than the transverse fragility curve for CtC40EA.

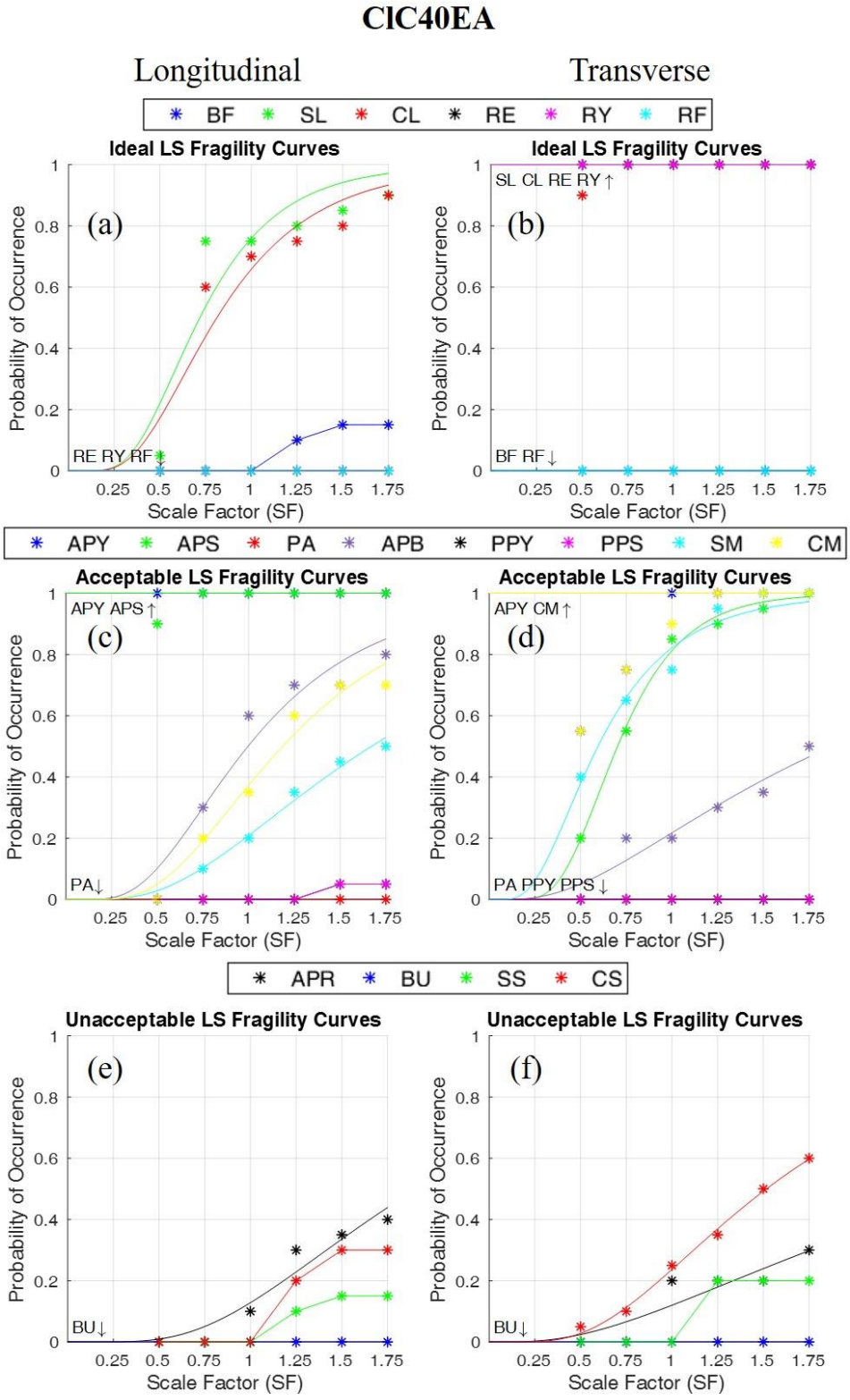

Figure 7.38: Ideal (a, b), acceptable (c, d), and unacceptable (e, f) limit state fragility curves for ClC40EA in the longitudinal (left column) and transverse (right column) directions where a scale factor of 1.00 represents the design-level.

7.6 GENERAL OBSERVATIONS

General observations and trends can be found through both the design-level and incremental dynamic analysis results. The first observation found across all the analyses is that in terms of span configuration, the three-span IABs are stiffer than the four-span IABs. In the longitudinal direction it can be shown that the abutment foundation damage (*i.e.* damage to the abutment piles and their surrounding soil) is about the same regardless of the span configuration. This is due to the entire bridge moving towards the abutments in both span configuration cases, leading to similar abutment demands. Additionally, the APY and APS limit states associated with the abutment foundation tend to occur frequently at low scale factors regardless, so the contributions are similar due to both the piles yielding and soil mobilizing early in the analyses. Large amounts of abutment pile strain (APB and APR) are generally infrequent in steel IABs though they are more frequent in concrete IABs. There is a difference between the frequencies of occurrence of pier column damage though, with four-span IABs producing more pier damage. This is due to the longer spans between piers leading to the piers being required to resist more lateral and axial force.

In the transverse direction it is shown that there is more abutment foundation damage and less pier column damage in three-span IABs. This is attributed to the shorter, stiffer bridge allowing for forces to be distributed more evenly with more force to the abutments and less to the piers than in the four-span bridge. Due to this, the opposite is true for four-span IABs which experience more pier column damage and less abutment foundation damage. The flexibility of the long-span bridges leads to large pier displacements and large amounts of damage. The four-span IABs perform poorly under transverse excitation with nearly all the damage limit states occurring under the smallest amount of excitation.

In both directions, damage to the abutment piles is found to be more significant than damage to the pier piles. The strains in the abutment piles frequently reach levels allowing for local buckling and rupture, however the maximum strains in the pier piles rarely causes yielding. In IABs where PPY does occur, the strains rarely become excessively large with typical maximum strains remaining below 7 times the yield strain. This indicates that local buckling and rupture of the pier piles is never encountered.

Trends are also observed when comparing bridges with short (15-ft tall) and tall (40-ft tall) piers. In general, short piers are stiffer then the tall piers and produce similar trends in both directions. With the stiffer short piers there is an increased demand on the piers leading to more damage. This increased pier demand decreases the demand on the abutments and slightly decreases the damage found in the abutment foundations and the strain in the abutment piles. The stiffer piers also lead to more retainer and fixed bearing damage due to the increased forces needing to be transferred through the bearings from the superstructure to the pier caps. The more flexible tall piers experience the opposite behavior as there is increased abutment foundation damage and decreased pier damage when they are used. This is attributed to the less stiff piers allowing for more force to be distributed to the much stiffer abutments which increases the demand in the abutments and decreases the demand in the piers.

This trade-off between abutment foundation damage and pier damage is observed numerous times in the analysis results. Ideal IAB seismic behavior would have them both occur under relatively large earthquakes only, so a balance point must be found where neither abutment foundation damage nor pier damage is too frequent. This solution is not ideal, however levels of strain in the abutment piles up to rupture will not lead to unacceptable limit states occurring as is the case with severe pier column damage. There is likely a point where columns are stiff enough

and robust enough to accommodate the increased demand while sufficiently reducing the abutment demand at the same time.

As mentioned earlier, there is increased retainer and fixed bearing damage in IABs with shorter piers. There is also a slight trend of having more retainer and fixed bearing damage in three-span IABs. However, the pier height is a much better predictor of retainer and fixed bearing behavior as some three-span IABs with taller piers do not experience much damage to the retainers and fixed bearings. Pier damage may also play a part as it has been observed in some cases that the occurrence of moderate pier column damage, which typically coincides with the force capacity of the piers, may act as a fuse and limit further force from being transferred through the bearings. Increased retainer and fixed bearing damage is also observed in concrete IABs over steel IABs due to the increased mass of the superstructure causing higher shear forces across the bearings.

Retainer and fixed bearing damage is not the only limit state affected by the superstructure material choice. Concrete IABs are found to produce more damage and/or force in many components such as the backfill, abutment foundation, and pier columns. The extra damage found in these components is attributed to the heavier superstructure, which causes more inertia (lateral) force during an earthquake and therefore leading to more force in most of the components. The added weight of the concrete superstructure also develops larger normal loads in the bearings which increases the friction force transferred between the superstructure and piers.

Given all these trends, it is found that there are serious seismic design concerns with four-span IABs, especially in the transverse direction and with concrete superstructures. The main components of concern in the IABs are the pier columns and abutment foundations due to the constant damage to them. The pier columns often reach severe damage which could cause failure of the pier and loss of span in the bridge. Severe pier damage usually occurs at earthquake

intensities larger than the design-level, but often not too much larger. The abutment foundation damage is a consistent occurrence at the lowest levels of earthquake shaking. Although damage to the abutment foundations may not cause immediate collapse, the amount of strain experienced in the abutment piles is significant enough to cause pile rupture and damage to these components is difficult to identify and repair. If left untreated they could have significant negative impacts to the bridge's behavior in future events. Additionally, many components which are desired to fail often do not. These components include the elastomeric bearing retainers and fixed bearings whose anchor bolt yielding and fracture could help mitigate the force and damage to other more vulnerable components such as the piers. Damage to the retainers and fixed bearings is easy to identify and replacement of the components is simple, making them ideal fuses in the IAB.

CHAPTER 8: EFFECT OF GROUND MOTION INTENSITY ON IAB BEHAVIOR

8.1 OVERVIEW

Bridge designs identical to those described above were also subjected to ground motions at locations in southern Illinois other than Cairo. The sites correspond to the ten sites around southern Illinois which ground motion time histories were developed for in Chapter 3. The IABs of interest for this portion of the study include only one IAB for each superstructure material and span configuration combination (single-span steel, three-span steel, four-span steel, three-span concrete, and four-span concrete). Each of the five IABs have 15-ft pier heights and realistic soil foundation conditions. Realistic soil foundation conditions consist of alluvial (models ending with A) and non-alluvial (models ending with N) soil conditions. The use of either alluvial or non-alluvial soil conditions varies from site to site depending on the soil conditions found to be most appropriate for the ten sites in Chapter 3. Recall that the sites with alluvial soil conditions are Benton, Cairo, East St. Louis, Mt. Carmel, Salem, and Sparta and the sites with non-alluvial soil conditions are Anna, Carbondale, Eldorado, and Elizabethtown. Table 3.1 and Fig. 3.1 in Chapter 3 provide more information concerning the location of the sites within the state of Illinois.

The five IABs at each of the ten sites in southern Illinois are subjected to dynamic analyses using 20 ground motions per site at the design-level 1000-year return period hazard. This allows for a direct comparison to the Cairo design-level results presented in section 7.3. The 20 ground motions used at each site were developed specifically for the site given the geographic hazard and soil conditions described in Chapter 3. The response spectra for the 20 ground motions used for the design-level dynamic analyses in this chapter can be found in Fig. 3.14 for the sites with alluvial soil conditions and in Fig. 3.15 for the sites with non-alluvial soil conditions. Additionally,

Table 8.1 describes the maximum, minimum, and median peak acceleration values for the 20 ground motions. This allows for comparisons to be made between the sites and the intensity of the ground motions that the IABs are subjected to. From Table 8.1 it can be seen that there is a difference in ground motion intensity between sites at the far south of the state (*i.e.* Cairo, Anna, Elizabethtown) which have relatively large peak accelerations, and more north in the southern Illinois region (*i.e.* Salem, East St. Louis, Mt. Carmel) which have relatively small peak accelerations.

Table 8.1: Statistics for the peak acceleration values, a_{max}, in the sets of 20 ground motions at each southern Illinois site.

Site	**Peak Acceleration, a_{max} (g)**		
	Minimum	**Maximum**	**Median**
Anna	0.1924	0.2421	0.2176
Benton	0.1410	0.2102	0.1709
Cairo	0.2601	0.3429	0.3049
Carbondale	0.1655	0.2099	0.1861
East St. Louis	0.0843	0.1650	0.1248
Eldorado	0.1295	0.1914	0.1732
Elizabethtown	0.1489	0.2047	0.1735
Mt. Carmel	0.0930	0.1732	0.1309
Salem	0.0900	0.1752	0.1281
Sparta	0.1203	0.1982	0.1499

The goal of this part of the study is to assess how much this drop in intensity of design-level ground motions affects the behavior of IABs during an earthquake. The results will help determine whether the vulnerabilities in the IABs assessed in Chapter 7 warrant enhancements to IAB designs throughout all of southern Illinois or perhaps just within the region surrounding Cairo. This is assessed by grouping the southern Illinois sites into their appropriate seismic performance zones (SPZs), which can be seen in Fig. 1.1, and making assessments based on the overall trends within each SPZ. Three SPZs are encountered in southern Illinois – SPZ 4, SPZ 3, and SPZ 2. SPZ

4 is the zone of largest earthquake intensity and encompasses the most southern portion of the state. Slightly further north is SPZ 3, followed by SPZ 2 even further north.

To make reading the tables in this chapter easier, the sites are arranged such that SPZ 4 sites are at the top followed by SPZ 3 and SPZ 2 sites. Within the SPZs themselves the sites are arranged based on latitude due to SPZ being strongly tied to latitude in southern Illinois. The only exception to the latitude sorting is Anna and Elizabethtown in SPZ 3. While Anna is further north, it is actually closer to the SPZ 3-4 border leading to it have larger ground motion intensities than Elizabethtown. The sorting of the ten sites is presented in Table 8.2 along with the SPZ, latitude and median peak acceleration of the ground motions appropriate for each site. SPZ 4 only comprises of Cairo, however Anna is extremely close to being in SPZ 4 despite being in SPZ 3 and is less than 50 miles to the north of Cairo. In addition to Anna, SPZ 3 also contains Elizabethtown, Carbondale, Eldorado, and Benton. SPZ 2 consists of Sparta, Mt. Carmel, East St. Louis, and Salem.

Table 8.2: Site, characteristics related to seismic performance zone, latitude, and median peak acceleration values.

Site	**Seismic Performance Zone**	**Latitude (º)**	**Median a_{max} (g)**
Cairo	4	37.013	0.3049
Anna	3	37.461	0.2176
Elizabethtown	3	37.449	0.1735
Carbondale	3	37.726	0.1861
Eldorado	3	37.814	0.1732
Benton	3	38.004	0.1709
Sparta	2	38.133	0.1499
Mt. Carmel	2	38.415	0.1309
East St. Louis	2	38.617	0.1248
Salem	2	38.628	0.1281

Describing the IAB seismic vulnerabilities based on SPZ is useful, however it should be noted that while SPZ 4 has the largest hazard in the state it also mainly consists of a sparsely

populated region in Illinois. This can be observed through noting that between 2005 and 2014 there were at least 114 IABs constructed in SPZs 2, 3, and 4 in Illinois, according to the online inventory of IDOT bridges (IDOT, 2016). Of these 114 IABs only 5 were in SPZ 4, 31 were in SPZ 3, and 78 were in SPZ 2. Given this information, it is important to recall while reviewing this chapter that although SPZ 4 produces the largest seismic hazard in Illinois, there are fewer IABs constructed in SPZ 4 than in other regions of Illinois.

8.2 DESIGN-LEVEL RESULTS

Results of the dynamic analyses at the 1000-year return period design-level hazard for the bridges at each of the ten southern Illinois sites are presented in Tables 8.3 through 8.7. As detailed in Chapter 7, these tables provide the percent of completed ground motion analyses which resulted in the specific limit state being achieved. The Cairo data presented is identical to the data presented for the Ss____A, StC15EA, SlC15EA, CtC15EA, and ClC15EA models presented in Tables 7.8 through 7.11.

8.2.1 Single-Span Steel IABs

The resulting limit state occurrences for the Ss____A and Ss____N models are presented in Table 8.3. The Cairo results show that only yielding of the abutment piles (APY) and mobilization of the soil surrounding the piles (APS) occurred at the design-level. At every other southern Illinois site there are no limit state occurrences in any analysis. Given that APY and APS rarely occurs in Cairo in the transverse direction, the drop to having no limit state occurrences in this direction at every other site is reasonable. The drop from APY being experienced 80% of the time in the longitudinal direction at Cairo to 0% of the time at Anna is mildly surprising given that Anna is nearly in SPZ 4 as well and less than 50 miles to the north of Cairo. This indicates that there is a steep drop off in seismic risk to single-span IABs just outside of Cairo. Given this and

the data in Table 8.3 it can be concluded that there is minimal to no seismic risk in SPZs lower than SPZ 4.

Table 8.3: Frequency of limit state occurrences during dynamic analyses at the design-level for single-span steel IABs across the southern Illinois sites.

SPZ	Site	Bridge	Longitudinal Limit State Occurrence					
			Ideal	Acceptable				Unacceptable
			BF	APY	APS	APB	PA	APR
4	Cairo	SsC15EA	0%	80%	0%	0%	0%	0%
3	Anna	SsC15EN	0%	0%	0%	0%	0%	0%
3	Elizabethtown	SsC15EN	0%	0%	0%	0%	0%	0%
3	Carbondale	SsC15EN	0%	0%	0%	0%	0%	0%
3	Eldorado	SsC15EN	0%	0%	0%	0%	0%	0%
3	Benton	SsC15EA	0%	0%	0%	0%	0%	0%
2	Sparta	SsC15EA	0%	0%	0%	0%	0%	0%
2	Mt. Carmel	SsC15EA	0%	0%	0%	0%	0%	0%
2	East St. Louis	SsC15EA	0%	0%	0%	0%	0%	0%
2	Salem	SsC15EA	0%	0%	0%	0%	0%	0%
SPZ	Site	Bridge	Transverse Limit State Occurrence					
			Ideal	Acceptable				Unacceptable
			BF	APY	APS	APB	PA	APR
4	Cairo	SsC15EA	0%	10%	5%	0%	0%	0%
3	Anna	SsC15EN	0%	0%	0%	0%	0%	0%
3	Elizabethtown	SsC15EN	0%	0%	0%	0%	0%	0%
3	Carbondale	SsC15EN	0%	0%	0%	0%	0%	0%
3	Eldorado	SsC15EN	0%	0%	0%	0%	0%	0%
3	Benton	SsC15EA	0%	0%	0%	0%	0%	0%
2	Sparta	SsC15EA	0%	0%	0%	0%	0%	0%
2	Mt. Carmel	SsC15EA	0%	0%	0%	0%	0%	0%
2	East St. Louis	SsC15EA	0%	0%	0%	0%	0%	0%
2	Salem	SsC15EA	0%	0%	0%	0%	0%	0%

8.2.2 Three-Span Steel IABs

The design-level limit state occurrence results for the three-span steel IABs with 15-ft tall piers is presented in Table 8.4. As previously discussed, the results at Cairo indicate that the design is acceptable under design-level hazard due to the majority of the damage in both directions being

confined to the abutment foundations (APY and APS only, limit states due to larger pile strains do not occur). Although this is not ideal, it will not cause collapse of the bridge. Light pier column damage (SL and CL) in both directions and retainer engagement (RE) and yielding (RY) in the transverse direction is also very common, though these limit states are ideal and desired to occur over less favorable limit states.

The longitudinal results indicate that the light pier column damage (SL and CL) ceases to be an issue in SPZ 2 and SPZ 3. This leaves only abutment pile yielding (APY) and mobilization of the soil surrounding the abutment piles (APS) occurring at sites outside of SPZ 4. While APY continues to occur for a majority of sites throughout SPZ 3 and SPZ 2, APS quickly ceases to become an issue. In SPZ 3, APS occurs very frequently at Anna, but rarely occurs at the other sites. APS does not occur at all in SPZ 2 sites. Anna having the largest frequency of APS occurrence outside SPZ 4 is logical considering that Anna is nearly in SPZ 4 and still experiences large earthquake accelerations. Abutment pile strain levels resulting in APB and APR do not occur at any site at the design level.

Salem is unique in the longitudinal direction in that it has absolutely no limit states occurring at all. This is likely due to Salem being the furthest north site considered and due to it being in the center of the state as opposed to near the Mississippi River to the west or the Wabash/Ohio River to the east. It is typically found that there is an increased amount of seismic hazard sources at sites closer to these rivers, such as East St. Louis and Mt. Carmel, which result in multiple hazard sources and different ground motion characteristics.

The transverse direction results show some similar characteristics to the longitudinal direction results. A good example of this is the disappearance of virtually all pier column damage at any level in SPZ 3 and SPZ 2. APS occurrences also decrease significantly in SPZ 3 and SPZ 2

when compared to SPZ 4. In the transverse direction there are actually no APS occurrences outside SPZ 4. A difference between the two directions is observed in the APY occurrences though. While APY persisted throughout SPZ 3 and SPZ 2 in the longitudinal direction, the frequency of APY occurrences steadily declines throughout SPZ 3 and there are no observed APY occurrences in SPZ 2. Instead, it appears that damage is consistently encountered in the retainers through engagement (RE) and yielding (RY) as opposed to damage to the abutment piles. RE consistently occurs at all sites in all SPZs and RY frequently occurs at most SPZ 3 and SPZ 2 sites. It can be shown that RY is much more common at the sites further south and closer to SPZ 4 with a 95% and 100% frequency of occurrence at Anna and Carbondale, respectively. This is a promising result as the ideal RY limit state remains frequent while the less favorable APY and APS decreases.

Overall, it is shown that the three-span steel IABs are acceptable designs at all SPZs. It is classified as acceptable and not ideal due to the consistent occurrence of the APY limit state in the longitudinal direction. The only site which demonstrates ideal behavior in both directions is Salem. This indicates that sites further north than Salem, which is still further south than midway through SPZ 2 in Illinois, likely do not need to implement any enhancements to the design. In general for southern Illinois, StC15EA or StC15EN at any SPZ would require enhancements to a lesser extent than the enhancements applied to unacceptable designs. Though it is not critical as amount of strain in the abutment piles is not large enough to cause APB or APR to occur, potential enhancements would reduce the number of APY occurrences.

Table 8.4: Frequency of limit state occurrences during dynamic analyses at the design-level for three-span steel IABs across the southern Illinois sites.

SPZ	Site	Bridge	Longitudinal Limit State Occurrence																	
			Ideal						Acceptable								Unacceptable			
			BF	SL	CL	RE	RY	RF	APY	APB	APS	PA	PPY	PPS	SM	CM	BU	SS	CS	APR
4	Cairo	StC15EA	0%	60%	35%	0%	0%	0%	100%	0%	70%	0%	0%	0%	0%	0%	0%	0%	0%	0%
3	Anna	StC15EN	0%	0%	0%	0%	0%	0%	100%	0%	80%	0%	0%	0%	0%	0%	0%	0%	0%	0%
3	Elizabethtown	StC15EN	0%	0%	0%	0%	0%	0%	90%	0%	0%	0%	0%	0%	0%	0%	0%	0%	0%	0%
3	Carbondale	StC15EN	0%	0%	0%	0%	0%	0%	100%	0%	15%	0%	0%	0%	0%	0%	0%	0%	0%	0%
3	Eldorado	StC15EN	0%	0%	0%	0%	0%	0%	100%	0%	5%	0%	0%	0%	0%	0%	0%	0%	0%	0%
3	Benton	StC15EA	0%	0%	0%	0%	0%	0%	45%	0%	0%	0%	0%	0%	0%	0%	0%	0%	0%	0%
2	Sparta	StC15EA	0%	0%	0%	0%	0%	0%	45%	0%	0%	0%	0%	0%	0%	0%	0%	0%	0%	0%
2	Mt. Carmel	StC15EA	0%	0%	0%	0%	0%	0%	55%	0%	0%	0%	0%	0%	0%	0%	0%	0%	0%	0%
2	East St. Louis	StC15EA	0%	0%	0%	0%	0%	0%	60%	0%	0%	0%	0%	0%	0%	0%	0%	0%	0%	0%
2	Salem	StC15EA	0%	0%	0%	0%	0%	0%	0%	0%	0%	0%	0%	0%	0%	0%	0%	0%	0%	0%

SPZ	Site	Bridge	Transverse Limit State Occurrence																	
			Ideal						Acceptable								Unacceptable			
			BF	SL	CL	RE	RY	RF	APY	APB	APS	PA	PPY	PPS	SM	CM	BU	SS	CS	APR
4	Cairo	StC15EA	0%	40%	10%	100%	100%	0%	100%	0%	30%	0%	0%	0%	0%	0%	0%	0%	0%	0%
3	Anna	StC15EN	0%	0%	0%	100%	95%	0%	75%	0%	0%	0%	0%	0%	0%	0%	0%	0%	0%	0%
3	Elizabethtown	StC15EN	0%	0%	0%	100%	40%	0%	20%	0%	0%	0%	0%	0%	0%	0%	0%	0%	0%	0%
3	Carbondale	StC15EN	0%	5%	0%	100%	100%	0%	75%	0%	0%	0%	0%	0%	0%	0%	0%	0%	0%	0%
3	Eldorado	StC15EN	0%	0%	0%	100%	90%	0%	45%	0%	0%	0%	0%	0%	0%	0%	0%	0%	0%	0%
3	Benton	StC15EA	0%	0%	0%	100%	30%	0%	10%	0%	0%	0%	0%	0%	0%	0%	0%	0%	0%	0%
2	Sparta	StC15EA	0%	0%	0%	100%	45%	0%	5%	0%	0%	0%	0%	0%	0%	0%	0%	0%	0%	0%
2	Mt. Carmel	StC15EA	0%	0%	0%	100%	20%	0%	5%	0%	0%	0%	0%	0%	0%	0%	0%	0%	0%	0%
2	East St. Louis	StC15EA	0%	0%	0%	100%	15%	0%	0%	0%	0%	0%	0%	0%	0%	0%	0%	0%	0%	0%
2	Salem	StC15EA	0%	0%	0%	65%	0%	0%	0%	0%	0%	0%	0%	0%	0%	0%	0%	0%	0%	0%

8.2.3 Four-Span Steel IABs

The four-span steel IAB with 15-ft piers and realistic soil foundation conditions provide an unacceptable design in Cairo under design-level shaking, as shown in Table 8.5. This unacceptable design is attributed to severe damage to the pier column concrete (CS) occurring in 35% of the analyses in the transverse direction. While CS only occurs in 5% of the analyses in the longitudinal direction in Cairo, yielding of the abutment piles (APY) and mobilization of the soil surrounding the abutment piles (APS) always occurs. However, despite the damage to the abutment piles causing yielding it is never so severe that local buckling occurs.

The occurrence of limit states in the longitudinal direction indicate that any pier column damage is virtually no longer applicable to SPZs beyond SPZ 4. The presence of pier column damage is not completely eliminated due to 10% of the analyses in Anna experiencing light damage to the steel in the pier columns (SL). However, this frequency of occurrence is minimal when compared to the 100% rate of SL occurrence in Cairo. APY and APS occur frequently in SPZ 3. However, the most northern site in SPZ 3, Benton, and all the sites in SPZ 2 experience no APY or APS occurrences at all. It can be shown that in the longitudinal direction of SPZ 2 sites there are no limit states occurring at all.

The limit state occurrence results in the transverse direction also show a decrease in pier column damage, though not as much as observed in the longitudinal direction. While severe pier column damage (SS and CS) does not occur in SPZs outside of SPZ 4, the four-span bridges are still very flexible in the transverse direction, leading to moderate pier damage (SM and CM) continuing to be frequent in SPZ 3. The occurrence of SM and CM does disappear as sites become further north, the ground motion intensity decreases, and the SPZ decreases from SPZ 3 to SPZ 2. Similar to how the frequency of APY occurrences dissipated to nothing in the northern part of SPZ

3 (*i.e.*, in Benton), SM and CM no longer have any occurrences at locations of Benton and further north, this includes all of the sites in SPZ 2. Light pier columns damage (SL and CL) continues to be frequent in all sites except for the furthest north site of Salem. SL and CL are ideal limit states and do not pose significant threats to the safety of the IAB. Retainer engagement (RE), another ideal limit state, always occurs at every site in the transverse direction. This limit state indicates that the elastomeric bearing simply contacts the side retainer, so no negative effects are produced from this limit state. Further damage to the retainer through yielding or fusing does not occur at any site. Abutment foundation initial damage through APY and APS rarely occurs at Cairo due to the flexibility of the bridge placing more demand on the piers. The occurrence of APY and APS drops from rarely occurring in SPZ 4 to never occurring outside SPZ 4.

Overall, the designs for the four-span steel IABs are more favorable at other sites than observed at Cairo. A reduction in severe pier column damage from SPZ 4 to SPZ 3 allows for the four-span steel IAB design to be acceptable in SPZ 3. While there is significant amounts of abutment foundation damage and moderate pier column damage at the furthest south sites in SPZ 3, these limit states are acceptable, though not necessarily desired. Enhancements to the design could be implemented to a lesser extent than enhancements for Cairo bridges in order to reduce the occurrence of acceptable limit states at SPZ 3 sites. All SPZ 2 sites require no enhancements as the only limit states applying to the four-span steel IABs at these sites are ideal. Light pier column damage and retainer engagement are the only limit states experienced. At the furthest north site of Salem, even light pier column damage (SL and CL) virtually never occurs indicating that only retainer engagement, which is expected to occur under even the smallest amounts of shaking, consistently occurs. This last point demonstrates that sites further north than Salem would likely encounter no damage at all to key IAB components.

Table 8.5: Frequency of limit state occurrences during dynamic analyses at the design-level for four-span steel IABs across the southern Illinois sites.

SPZ	Site	Bridge	Longitudinal Limit State Occurrence																	
			Ideal						Acceptable								Unacceptable			
			BF	SL	CL	RE	RY	RF	APY	APB	APS	PA	PPY	PPS	SM	CM	BU	SS	CS	APR
4	Cairo	SlC15EA	0%	100%	100%	0%	0%	0%	100%	0%	100%	0%	0%	5%	25%	35%	0%	0%	5%	0%
3	Anna	SlC15EN	0%	10%	0%	0%	0%	0%	95%	0%	30%	0%	0%	0%	0%	0%	0%	0%	0%	0%
3	Elizabethtown	SlC15EN	0%	0%	0%	0%	0%	0%	70%	0%	10%	0%	0%	0%	0%	0%	0%	0%	0%	0%
3	Carbondale	SlC15EN	0%	0%	0%	0%	0%	0%	40%	0%	0%	0%	0%	0%	0%	0%	0%	0%	0%	0%
3	Eldorado	SlC15EN	0%	0%	0%	0%	0%	0%	10%	0%	0%	0%	0%	0%	0%	0%	0%	0%	0%	0%
3	Benton	SlC15EA	0%	0%	0%	0%	0%	0%	0%	0%	0%	0%	0%	0%	0%	0%	0%	0%	0%	0%
2	Sparta	SlC15EA	0%	0%	0%	0%	0%	0%	0%	0%	0%	0%	0%	0%	0%	0%	0%	0%	0%	0%
2	Mt. Carmel	SlC15EA	0%	0%	0%	0%	0%	0%	0%	0%	0%	0%	0%	0%	0%	0%	0%	0%	0%	0%
2	East St. Louis	SlC15EA	0%	0%	0%	0%	0%	0%	0%	0%	0%	0%	0%	0%	0%	0%	0%	0%	0%	0%
2	Salem	SlC15EA	0%	0%	0%	0%	0%	0%	0%	0%	0%	0%	0%	0%	0%	0%	0%	0%	0%	0%
SPZ	Site	Bridge	Transverse Limit State Occurrence																	
			Ideal						Acceptable								Unacceptable			
			BF	SL	CL	RE	RY	RF	APY	APB	APS	PA	PPY	PPS	SM	CM	BU	SS	CS	APR
4	Cairo	SlC15EA	0%	100%	100%	100%	0%	0%	10%	0%	0%	0%	0%	0%	100%	100%	0%	0%	35%	0%
3	Anna	SlC15EN	0%	100%	100%	100%	0%	0%	0%	0%	0%	0%	0%	10%	85%	100%	0%	0%	0%	0%
3	Elizabethtown	SlC15EN	0%	100%	100%	100%	0%	0%	0%	0%	0%	0%	0%	0%	70%	90%	0%	0%	0%	0%
3	Carbondale	SlC15EN	0%	95%	90%	100%	0%	0%	0%	0%	0%	0%	0%	0%	35%	65%	0%	0%	0%	0%
3	Eldorado	SlC15EN	0%	70%	65%	100%	0%	0%	0%	0%	0%	0%	0%	0%	0%	20%	0%	0%	0%	0%
3	Benton	SlC15EA	0%	65%	50%	100%	0%	0%	0%	0%	0%	0%	0%	0%	0%	0%	0%	0%	0%	0%
2	Sparta	SlC15EA	0%	45%	30%	100%	0%	0%	0%	0%	0%	0%	0%	0%	0%	0%	0%	0%	0%	0%
2	Mt. Carmel	SlC15EA	0%	60%	60%	100%	0%	0%	0%	0%	0%	0%	0%	0%	0%	0%	0%	0%	0%	0%
2	East St. Louis	SlC15EA	0%	60%	60%	100%	0%	0%	0%	0%	0%	0%	0%	0%	0%	5%	0%	0%	0%	0%
2	Salem	SlC15EA	0%	5%	0%	100%	0%	0%	0%	0%	0%	0%	0%	0%	0%	0%	0%	0%	0%	0%

8.2.4 Three-Span Concrete IABs

The design-level dynamic analysis results for the three-span concrete IAB with 15-ft tall piers and realistic soil conditions indicate that the designs are unacceptable in Cairo due to severe pier column damage (SS and CS) frequently occurring and rupture of the abutment piles (APR) also being present. The results for other sites in southern Illinois, provided in Table 8.6, indicate that in both directions all the unacceptable limit states (*i.e.*, SS and CS) do not affect IABs at locations outside of SPZ 4 in Illinois. This is especially notable in the longitudinal direction where CS occurs in 50% of the analyses at Cairo, and does not occur at all at Anna, which is less than 50 miles north of Cairo.

Pier column damage in general decreases as sites further north and at lower SPZs are considered. Moderate pier column damage (SM and CM) is essentially non-existent at SPZs outside of SPZ 4 leaving only light pier column damage (SL and CL) occurring. Even SL and CL occur only at Anna, the site closest to SPZ 4 in SPZ 3. While the pier columns experience little damage outside of SPZ 4 in the longitudinal direction, APY continues to occur in SPZ 3 and SPZ 2, though APB and APR dissipates beyond SPZ 4. The mobilization of the soil surrounding the abutment piles (APS) is frequent in southern sites within SPZ 3, but the frequency of occurrence of APS fades to nothing within the SPZ 2 sites. The yielding of the abutment piles continues to be frequent throughout SPZ 3 and SPZ 2 with frequencies of occurrence exceeding 60% at all sites except the most northern site of Salem.

The transverse direction results, also presented in Table 8.6, show steep drops in the occurrence of pier column damage when leaving SPZ 4. The only occurrence of pier column damage outside of SPZ 4 is in Anna, which is very close to the SPZ 3-4 border, for light pier column steel damage (SL) and only occurs in 45% of the analyses. APY and APS continue to

occur in SPZ 3 and SPZ 2, however APS once again fails to be a concern at the northern SPZ 3 sites and in any SPZ 2 sites. APY is still extremely common at the southern SPZ 3 sites of Anna, Elizabethtown, and Carbondale, but the frequency of occurrence begins to decrease at sites further north. Additionally, beyond Anna the level of damage in the abutment piles is limited to yielding as local buckling (APB) and rupture (APR) dissipates quickly. While some SPZ 2 sites indicate APY occurring fairly frequently when subjected to design-level ground motions, other SPZ 2 sites like Sparta and Salem, as well as the SPZ 3 site of Benton, rarely have occurrences of APY. Benton, Salem, and Sparta are all similar in that they are within the middle of the state away from the rivers which border Illinois on either side, unlike East St. Louis and Mt. Carmel which are directly adjacent to the rivers. This indicates a correlation between proximity to the rivers and increased risk. The final limit states indicated to occur in the transverse direction are those associated with the retainers. As expected, retainer engagement (RE) almost always occurs and with the exception of Salem, retainer yielding is also very frequent. Retainer fusing (RF) does occur in some SPZ 3 sites, however it is only in the furthest south sites of Anna and Elizabethtown.

In general, the design of the three-span concrete IABs with 15-ft tall piers and realistic soil conditions is unacceptable in SPZ 4 but acceptable in SPZ 3 and SPZ 2. This indicates that any enhancements discussed in Chapter 9 may be applied to a lesser extent to the IABs in SPZ 3 and SPZ 2 where the current bridge designs do not encounter any unacceptable limit states. It can be noted that the IAB at Salem has ideal results indicating that three-span concrete IAB designs at sites further north than Salem likely require no enhancements.

Table 8.6: Frequency of limit state occurrences during dynamic analyses at the design-level for three-span concrete IABs across the southern Illinois sites.

SPZ	Site	Bridge	Longitudinal Limit State Occurrence																	
			Ideal						Acceptable								Unacceptable			
			BF	SL	CL	RE	RY	RF	APY	APB	APS	PA	PPY	PPS	SM	CM	BU	SS	CS	APR
4	Cairo	CtC15EA	0%	100%	100%	0%	0%	0%	100%	75%	100%	0%	0%	0%	75%	85%	0%	5%	50%	20%
3	Anna	CtC15EN	0%	35%	20%	0%	0%	0%	100%	0%	80%	0%	0%	0%	0%	5%	0%	0%	0%	0%
3	Elizabethtown	CtC15EN	0%	0%	0%	0%	0%	0%	100%	0%	45%	0%	0%	0%	0%	0%	0%	0%	0%	0%
3	Carbondale	CtC15EN	0%	0%	0%	0%	0%	0%	100%	0%	25%	0%	0%	0%	0%	0%	0%	0%	0%	0%
3	Eldorado	CtC15EN	0%	0%	0%	0%	0%	0%	90%	0%	15%	0%	0%	0%	0%	0%	0%	0%	0%	0%
3	Benton	CtC15EA	0%	0%	0%	0%	0%	0%	60%	0%	0%	0%	0%	0%	0%	0%	0%	0%	0%	0%
2	Sparta	CtC15EA	0%	0%	0%	0%	0%	0%	60%	0%	0%	0%	0%	0%	0%	0%	0%	0%	0%	0%
2	Mt. Carmel	CtC15EA	0%	0%	0%	0%	0%	0%	80%	0%	10%	0%	0%	0%	0%	0%	0%	0%	0%	0%
2	East St. Louis	CtC15EA	0%	0%	0%	0%	0%	0%	75%	0%	0%	0%	0%	0%	0%	0%	0%	0%	0%	0%
2	Salem	CtC15EA	0%	0%	0%	0%	0%	0%	0%	0%	0%	0%	0%	0%	0%	0%	0%	0%	0%	0%
SPZ	Site	Bridge	Transverse Limit State Occurrence																	
			Ideal						Acceptable								Unacceptable			
			BF	SL	CL	RE	RY	RF	APY	APB	APS	PA	PPY	PPS	SM	CM	BU	SS	CS	APR
4	Cairo	CtC15EA	0%	100%	80%	100%	100%	100%	100%	90%	100%	0%	0%	0%	40%	40%	0%	5%	15%	10%
3	Anna	CtC15EN	0%	45%	0%	100%	100%	70%	100%	15%	65%	0%	0%	0%	0%	0%	0%	0%	0%	0%
3	Elizabethtown	CtC15EN	0%	0%	0%	100%	100%	20%	100%	0%	30%	0%	0%	0%	0%	0%	0%	0%	0%	0%
3	Carbondale	CtC15EN	0%	0%	0%	100%	100%	0%	85%	0%	10%	0%	0%	0%	0%	0%	0%	0%	0%	0%
3	Eldorado	CtC15EN	0%	0%	0%	100%	100%	0%	40%	0%	0%	0%	0%	0%	0%	0%	0%	0%	0%	0%
3	Benton	CtC15EA	0%	0%	0%	100%	75%	0%	10%	0%	0%	0%	0%	0%	0%	0%	0%	0%	0%	0%
2	Sparta	CtC15EA	0%	0%	0%	100%	85%	0%	0%	0%	0%	0%	0%	0%	0%	0%	0%	0%	0%	0%
2	Mt. Carmel	CtC15EA	0%	0%	0%	100%	85%	0%	35%	0%	0%	0%	0%	0%	0%	0%	0%	0%	0%	0%
2	East St. Louis	CtC15EA	0%	0%	0%	100%	80%	0%	25%	0%	0%	0%	0%	0%	0%	0%	0%	0%	0%	0%
2	Salem	CtC15EA	0%	0%	0%	65%	5%	0%	0%	0%	0%	0%	0%	0%	0%	0%	0%	0%	0%	0%

8.2.5 Four-Span Concrete IABs

The design-level dynamic analysis results for the four-span concrete IAB with 15-ft tall piers and realistic soil conditions are provided in Table 8.7. These results demonstrate the high frequency of damage to the abutment piles leading to yielding (APY), local buckling (APB), and mobilization of the soil (APS), as well as severe damage to the pier columns (SS and CS) at Cairo. These large frequencies are products of the concrete superstructure being much heavier than steel superstructures leading to increased lateral inertia forces during excitation, as well as from the increased flexibility of the bridge in the transverse direction. Recall and observe in Table 8.7 that severe pier column concrete damage (CS) occurs in all of the analyses for Cairo in the transverse direction and leads to an extremely unacceptable design.

The longitudinal direction results also contain significant amounts of CS occurrences at the SPZ 4 site of Cairo. The damage to the piers decreases in Anna, which is very close to the SPZ 3-4 border, but still contains some CS occurrences. Beyond Anna, all pier column damage (SL, CL, SM, CM, SS, and CS) does not occur at any other site in the longitudinal direction. This signifies a significant drop off in potential pier damage in the longitudinal direction beyond SPZ 4. In the longitudinal direction the majority of the damage occurs in the abutment foundations with abutment pile yielding (APY) occurring extremely frequently at the southern SPZ 3 sites. However, APY occurrences dissipate to having no APY occurrences at the northern SPZ 3 site of Benton and any SPZ 2 site. APB and APR are frequent in SPZ 4 but disappears in SPZ 3. Mobilization of the soil surrounding the abutment piles (APS) is also common in southern SPZ 3 sites but reduces to having no occurrences at northern SPZ 3 sites or SPZ 2 sites. In general, for the longitudinal direction, SPZ 2 sites experience essentially no damage to any components.

Table 8.7: Frequency of limit state occurrences during dynamic analyses at the design-level for four-span concrete IABs across the southern Illinois sites.

SPZ	Site	Bridge	Longitudinal Limit State Occurrence																	
			Ideal						Acceptable								Unacceptable			
			BF	SL	CL	RE	RY	RF	APY	APB	APS	PA	PPY	PPS	SM	CM	BU	SS	CS	APR
4	Cairo	ClC15EA	0%	94%	94%	0%	0%	0%	100%	65%	100%	0%	0%	0%	76%	76%	0%	6%	76%	5%
3	Anna	ClC15EN	0%	25%	25%	0%	0%	0%	100%	0%	80%	0%	0%	0%	10%	15%	0%	0%	10%	0%
3	Elizabethtown	ClC15EN	0%	0%	0%	0%	0%	0%	100%	0%	25%	0%	0%	0%	0%	0%	0%	0%	0%	0%
3	Carbondale	ClC15EN	0%	0%	0%	0%	0%	0%	80%	0%	0%	0%	0%	0%	0%	0%	0%	0%	0%	0%
3	Eldorado	ClC15EN	0%	0%	0%	0%	0%	0%	15%	0%	0%	0%	0%	0%	0%	0%	0%	0%	0%	0%
3	Benton	ClC15EA	0%	0%	0%	0%	0%	0%	0%	0%	0%	0%	0%	0%	0%	0%	0%	0%	0%	0%
2	Sparta	ClC15EA	0%	0%	0%	0%	0%	0%	0%	0%	0%	0%	0%	0%	0%	0%	0%	0%	0%	0%
2	Mt. Carmel	ClC15EA	0%	0%	0%	0%	0%	0%	0%	0%	0%	0%	0%	0%	0%	0%	0%	0%	0%	0%
2	East St. Louis	ClC15EA	0%	0%	0%	0%	0%	0%	5%	0%	0%	0%	0%	0%	0%	0%	0%	0%	0%	0%
2	Salem	ClC15EA	0%	0%	0%	0%	0%	0%	0%	0%	0%	0%	0%	0%	0%	0%	0%	0%	0%	0%
SPZ	Site	Bridge	Transverse Limit State Occurrence																	
			Ideal						Acceptable								Unacceptable			
			BF	SL	CL	RE	RY	RF	APY	APB	APS	PA	PPY	PPS	SM	CM	BU	SS	CS	APR
4	Cairo	ClC15EA	0%	100%	100%	100%	100%	0%	75%	15%	55%	0%	0%	0%	100%	100%	0%	35%	100%	0%
3	Anna	ClC15EN	0%	100%	100%	100%	100%	0%	10%	0%	0%	0%	0%	0%	70%	90%	0%	0%	45%	0%
3	Elizabethtown	ClC15EN	0%	100%	100%	100%	100%	0%	0%	0%	0%	0%	0%	0%	5%	35%	0%	0%	0%	0%
3	Carbondale	ClC15EN	0%	80%	80%	100%	100%	0%	0%	0%	0%	0%	0%	0%	0%	0%	0%	0%	0%	0%
3	Eldorado	ClC15EN	0%	35%	40%	100%	90%	0%	0%	0%	0%	0%	0%	0%	0%	0%	0%	0%	0%	0%
3	Benton	ClC15EA	0%	20%	20%	100%	85%	0%	0%	0%	0%	0%	0%	0%	0%	0%	0%	0%	0%	0%
2	Sparta	ClC15EA	0%	0%	0%	100%	70%	0%	0%	0%	0%	0%	0%	0%	0%	0%	0%	0%	0%	0%
2	Mt. Carmel	ClC15EA	0%	5%	10%	100%	75%	0%	0%	0%	0%	0%	0%	0%	0%	0%	0%	0%	0%	0%
2	East St. Louis	ClC15EA	0%	15%	15%	100%	70%	0%	0%	0%	0%	0%	0%	0%	0%	0%	0%	0%	0%	0%
2	Salem	ClC15EA	0%	5%	5%	100%	35%	0%	0%	0%	0%	0%	0%	0%	0%	0%	0%	0%	0%	0%

The transverse direction results, also presented in Table 8.7, shows a reduction in pier column damage outside of SPZ 4, however not as large of a reduction as observed in the longitudinal direction. Once again, Anna, which is close to the SPZ 4 border, still experiences significant amounts of severe pier column concrete damage (CS). Additionally, Elizabethtown in SPZ 3 experiences some moderate pier column damage (SM and CM). Beyond these two exceptions moderate and sever pier column damage is not found at any other sites. Light pier column damage (SL and CL) is present throughout SPZ 3 sites with the most southern sites experiencing high frequencies of occurrence. In SPZ 2 sites the light pier column damage rarely occurs. The increased amount of pier damage in the transverse direction as compared to the longitudinal direction can be attributed to the increased flexibility of the IAB in this direction. APY and APS experiences significant amounts of occurrences in SPZ 4, but this quickly reduces to no occurrences in SPZ 3 where it is extremely rare even at Anna. Limit states describing larger abutment pile strains (APB and APR) are rare in SPZ 4 and disappear in SPZ 3. Retainer fusing (RF) does not occur at any site, however retainer yielding (RY) is frequent throughout all sites with the frequency of occurrence ranging between 35% and 75% in SPZ 2. As expected, retainer engagement (RE) always occurs due to it ideally occurring under even the smallest amounts of lateral excitation.

By evaluating the limit states reached at the sites in each of the SPZs it can be determined that in SPZ 2 the four-span concrete IAB designs are ideal. Further north SPZ 3 sites also tend to have ideal designs, however as a whole SPZ 3 is generally acceptable. An exception to this is Anna where the designs are unacceptable. Given that the designs are unacceptable in SPZ 4 and Anna's close proximity to SPZ 4 this behavior makes sense.

8.2.6 Overall Observations

The results from the design-level dynamic analyses at different sites around southern Illinois with varying ground motion intensity levels indicates that although there are consistent unacceptable designs for IABs at Cairo in SPZ 4, the IABs are at least acceptable outside of SPZ 4. The only major exception to this is at Anna where unacceptable designs for four-span concrete IABs are present. However, Anna is extremely close to SPZ 4 further showing that IAB designs are generally unacceptable in SPZ 4. IAB designs in SPZ 3 sites are generally acceptable and designs at SPZ 2 sites are frequently ideal with only light pier damage and retainer damage. Recall that while the largest seismic hazard and amount of limit state occurrences occurs in SPZ 4, the amount of IABs in SPZ4 is relatively sparse in comparison to SPZ 2 and 3. This sparsity of IABs in SPZ 4 reduces the potential risk to the overall inventory of IABs in southern Illinois, though their increased demands should not be ignored in design.

As the sites become further north and change SPZ certain trends seem to emerge throughout the IABs analyzed. The first observed trend is the relatively small effect that location has on the occurrence of retainer engagement, yielding, and fusing. Retainer engagement tends to always occur while there is a slight decrease in retainer yielding and fusing occurrences as the sites become further away from Cairo and the ground motion intensity decreases. However, this decrease in retainer damage is relatively gradual when compared to abutment foundation and pier column damage changes which decreases rapidly once the site is not in SPZ 4. Across all the IABs analyzed above, the change in limit state occurrences between SPZ 4 and SPZ 3 drops to occurring 0% of the time in SPZ 3 if the frequency of occurrence is less than 60% in SPZ 4 (*i.e.*, Cairo) The decrease in pier column damage is especially noticeable in four-span IABs where the designs typically change from unacceptable due to severe pier column damage in SPZ 4 to acceptable

outside of SPZ 4. The reason why the four-span IABs significantly benefit is due to their large spans which lead to larger superstructure masses when compared to the three-span IABs. The reduction in ground motion accelerations across the sites, as shown in Table 8.1 and Table 8.2, causes a greater reduction in lateral inertia forces in the long-span bridges. The four-span concrete IAB especially benefits from this severe decrease in lateral force due to it being the heaviest bridge analyzed.

The results for the limit state occurrence frequencies at various sites impacts the potential IAB designs by ensuring that unnecessary enhancements are not made to designs which already behave ideally during design-level seismic events. The enhancements addressing the vulnerabilities identified in Chapter 7 are applicable to sites within SPZ 4, such as Cairo. Sites in SPZ 3 are usually acceptable, indicating that they potentially require enhancements using similar theories, but to a lesser extent, as those utilized for SPZ 4 sites. This is to ensure the IABs in SPZ 3 have closer to ideal seismic performance. The ideal designs, typically in SPZ 2, require no enhancements as their current designs already yield ideal seismic performance. These results may vary slightly with different soil conditions as liquefaction and significant clay softening due to shaking is not accounted for in these analyses.

CHAPTER 9: PROPOSED ENHANCEMENTS TO ILLINOIS IAB SEISMIC DESIGN

9.1 OVERVIEW

The seismic assessment of current IAB designs in Illinois, which was performed in Chapter 7, demonstrated consistent vulnerabilities in the pier columns and abutment foundations. Additionally, the fusing of ideal components, such as the side retainers and fixed bearings, does not occur in many analyses, leading to increased load in the pier columns. The analyses revealed four areas of concern: the lack of elastomeric bearing side retainer fusing, the lack of fixed bearings fusing, the abundance of pier column damage, and the abundance of abutment foundation damage. This chapter aims to address the concerns identified in Chapter 7 by enhancing IABs with the objective of increasing retainer and fixed bearing fusing and reducing damage in the pier columns and in the abutment foundations. This objective is accomplished by reducing the number of retainers in the IAB, reducing the size of the fixed bearing anchor bolts, increasing the size of the pier columns, and increasing the backfill contribution at the abutments. The effectiveness of these enhancements is discussed.

Enhancements are made to address the four areas of concern separately. The enhanced IAB designs are analyzed using both pushover analyses, as described in Chapter 6, and incremental dynamic analyses (IDA) using the ground motion scale factor as the intensity measure, as described in Chapter 7. The enhanced IABs are analyzed for the site of Cairo since it has the highest seismic hazard in the state of Illinois, seismic performance zone (SPZ) 4. As discussed in Chapter 8, recommendations that are developed in this chapter may not apply or may only partially apply to sites in SPZs 2 or 3. Many sites in SPZ 3 demonstrate IAB damage to a lesser extent and may benefit from the recommendations presented, but may not require the full spectrum of design

enhancements proposed for IABs in SPZ 4. IABs in SPZ 2 typically already exhibit ideal seismic behavior and would likely not require any enhancements described in this chapter.

9.2 REDUCTION IN RETAINER USE

Reducing the number of elastomeric bearing side retainers to two retainers per pier (one at each exterior beam) should enhance retainer yielding and fusing. Currently there is a retainer around every elastomeric bearing at every beam. As retainers fuse there is a significant drop in the amount of load transferred from the superstructure to the piers. In quasi-isolated bridge design, fracture of retainers is a key fusing event that limits damage in the pier columns when subjected to transverse earthquake loads. While lack of retainer fusing does not necessarily indicate poor performance, the fusing of these components is more desirable than severe pier column damage.

The two IABs with enhanced designs are StC40EA and SlC15EA. These IABs were selected since steel superstructure IABs consistently experienced less retainer fusing than concrete superstructure IABs, owing to the lighter steel superstructures that generate smaller inertial forces that must be transferred through the bearings during an earthquake. These IABs were also selected because they provide a good range of pier force demands: larger force demands (long-span IABs with short piers) and smaller force demands (taller piers).

For the IDA reported in Chapter 7, StC40EA experiences no retainer fusing, however it does encounter frequent retainer yielding at large ground motion scale factors in the transverse direction. The lack of retainer fusing is a likely cause of the severe pier column concrete damage which occurs in 15% of the analyses at a scale factor of 1.75. The original designs for this IAB have 6 retainers per pier, so by reducing the number of retainers per pier to two, the total lateral load resisted by the retainers in a single pier reduces by a factor of three, from 1,572 kN to 524 kN.

The IDA for SlC15EA in Chapter 7 also indicated that no retainer fusing occurred at any scale factor. However, this IAB also showed that no retainer yielding occurs either. The lack of both retainer yielding and fusing, along with the increased load demands on the pier due to the four-span condition and the short and stiff piers, leads to severe pier column damage in every analysis at a scale factor of 1.25 and larger. Once again, to induce more retainer fusing, the number of retainers used per pier was reduced to two, this time from 8. This dropped the total lateral resistance from the retainers at each pier from 5,366 kN to 1,342 kN.

Additionally, SlC15EA is modified further by weakening the anchor bolts of the retainers in a separate subset of the study. This second enhanced design also includes only two retainers per pier, but the anchor bolts are reduced from 2-in diameter bolts to 1.25-in diameter bolts to further encourage retainer fusing.

9.2.1 Pushover Results

The pushover analysis results for the two bridges with and without enhancements are presented in Fig. 9.1. As expected, there is no difference in longitudinal behavior when the enhancements are made due to retainers only resisting forces in the transverse direction.

In the transverse direction for StC40EA (Fig. 9.1b) there is minimal difference between the IAB with and without the enhancement. Retainer fusing (RF) still never occurs and retainer engagement (RE) and yielding (RY) occur at similar displacements despite using less retainers. The only distinguishable difference is a slight decrease in stiffness of the IAB after retainer yielding occurs in the enhanced design.

The transverse results for SlC15EA (Fig. 9.1d) clearly demonstrate that the IAB is less stiff when fewer retainers are used and even less stiff once the anchor bolts of the two retainers per pier are reduced in size. In the bridge with only the reduced number of retainers it can be observed that

retainer fusing once again does not occur. However, the decreased stiffness does allow for severe pier column concrete damage (CS) to occur at larger force and displacement when compared to the original design. In the IAB which also has reduced anchor bolt sizes, it is shown that retainer fusing (RF) does occur and is followed by some bearing slipping, but the friction between the bearing and pier cap remains strong enough to allow for forces to transfer and pier column damage to continue. The fusing of the retainer does allow for severe pier column concrete damage to occur at much larger displacements and loads than the other two designs though.

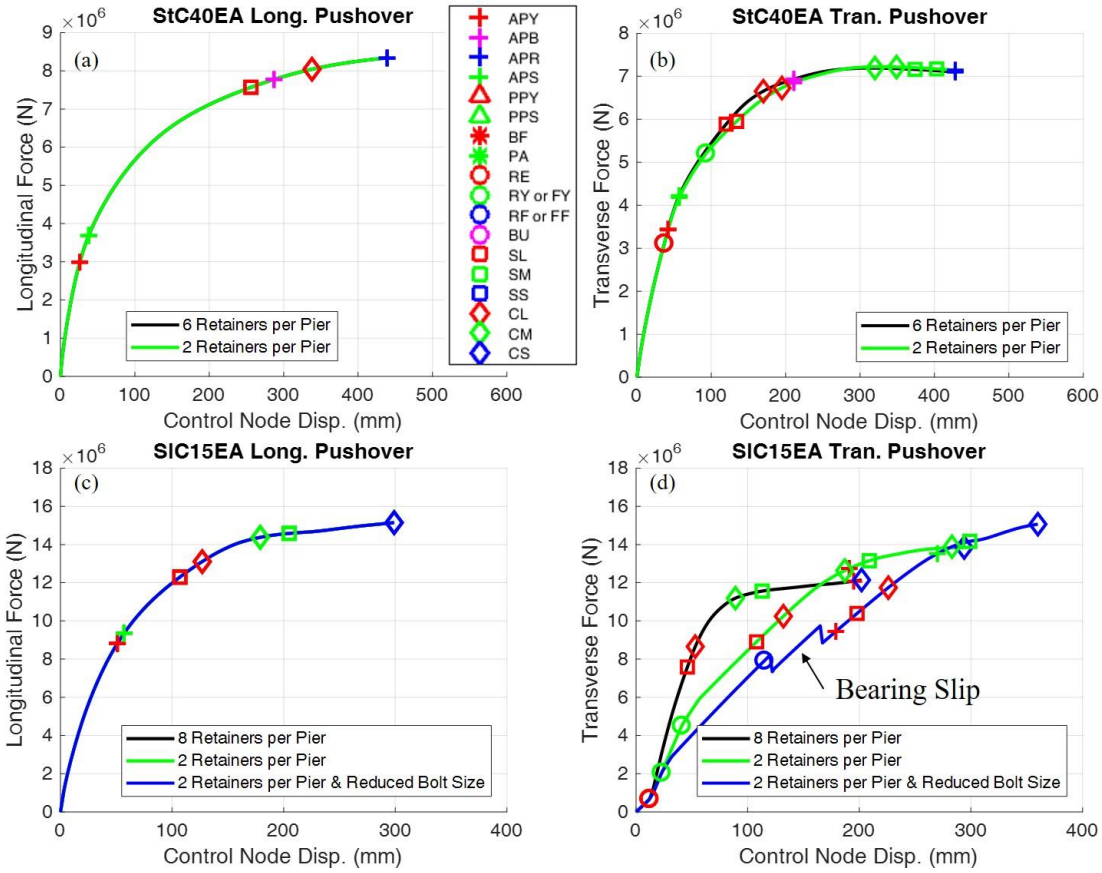

Figure 9.1: Pushover analysis results for IABs with various retainer configurations.

9.2.2 IDA Results

The limit state occurrence results during the IDA for StC40EA are presented in Table 9.1. Once again, no difference can be found between the two designs in the longitudinal direction, as

expected. In the transverse direction it is found that there is still no retainer fusing (RF) occurring when the number of retainers is decreased, however there is an increase in the frequency of retainer yielding (RY). There is also a general increase in the force magnitude resisted by the retainers, as presented in the IDA curve of Fig. 9.2g. In both bridges, Fig. 9.2g indicates that the retainer force reaches a maximum value, due to some other component acting as a fuse. This fusing component is the pier columns, whose peak resistance corresponds to the moderate pier column damage limit states (SM and CM). SM and CM begin to occur at scale factors of 1.5 and larger, as shown in Fig. 9.2c and 9.2d, corresponding to the vertical turn of the retainer behavior at a scale factor of 1.5 in Fig. 9.2g.

Aside from the difference in retainer force, there are minimal differences between StC40EA in terms of the frequency of limit state occurrences in Table 9.1 and IDA curves in Fig. 9.2 for other components. There are small decreases in the frequency of pier column damage limit state occurrences as fewer retainers are used. However, the largest difference in frequency of limit state occurrence is a drop in light pier column steel damage by 20% at a scale factor of 0.75, most others are only drops of 5-10%.

Table 9.1: Frequency of limit state occurrences for the StC40EA IDA with various retainer configurations where a scale factor of 1.00 represents the design-level.

Bridge	Revision	SF	Longitudinal Limit State Occurrence																	
			Ideal						Acceptable								Unacceptable			
			BF	SL	CL	RE	RY	RF	APY	APB	APS	PA	PPY	PPS	SM	CM	BU	SS	CS	APR
StC40EA	6 Retainers per Pier	0.50	0%	0%	0%	0%	0%	0%	65%	0%	30%	0%	0%	0%	0%	0%	0%	0%	0%	0%
		0.75	0%	0%	0%	0%	0%	0%	100%	0%	60%	0%	0%	0%	0%	0%	0%	0%	0%	0%
		1.00	0%	15%	0%	0%	0%	0%	100%	15%	100%	0%	0%	5%	0%	0%	0%	0%	0%	0%
		1.25	0%	75%	45%	0%	0%	0%	100%	75%	100%	0%	0%	55%	0%	5%	0%	0%	0%	10%
		1.50	0%	90%	80%	0%	0%	0%	100%	90%	100%	0%	0%	90%	20%	25%	0%	0%	0%	55%
		1.75	0%	100%	80%	0%	0%	0%	100%	95%	100%	0%	0%	95%	40%	55%	0%	0%	15%	80%
	2 Retainers per Pier	0.50	0%	0%	0%	0%	0%	0%	65%	0%	30%	0%	0%	0%	0%	0%	0%	0%	0%	0%
		0.75	0%	0%	0%	0%	0%	0%	100%	0%	60%	0%	0%	0%	0%	0%	0%	0%	0%	0%
		1.00	0%	15%	0%	0%	0%	0%	100%	15%	100%	0%	0%	5%	0%	0%	0%	0%	0%	0%
		1.25	0%	75%	45%	0%	0%	0%	100%	75%	100%	0%	0%	55%	0%	5%	0%	0%	0%	10%
		1.50	0%	90%	80%	0%	0%	0%	100%	90%	100%	0%	0%	90%	20%	25%	0%	0%	0%	55%
		1.75	0%	100%	80%	0%	0%	0%	100%	95%	100%	0%	0%	95%	40%	55%	0%	0%	15%	80%

Bridge	Revision	SF	Transverse Limit State Occurrence																	
			Ideal						Acceptable								Unacceptable			
			BF	SL	CL	RE	RY	RF	APY	APB	APS	PA	PPY	PPS	SM	CM	BU	SS	CS	APR
StC40EA	6 Retainers per Pier	0.50	0%	0%	0%	80%	0%	0%	45%	0%	10%	0%	0%	0%	0%	0%	0%	0%	0%	0%
		0.75	0%	20%	0%	100%	40%	0%	100%	0%	35%	0%	0%	0%	0%	0%	0%	0%	0%	0%
		1.00	0%	65%	20%	100%	80%	0%	100%	5%	70%	0%	0%	0%	0%	0%	0%	0%	0%	0%
		1.25	0%	100%	100%	100%	100%	0%	100%	70%	100%	0%	0%	5%	0%	0%	0%	0%	0%	0%
		1.50	0%	100%	100%	100%	100%	0%	100%	100%	100%	0%	0%	10%	45%	55%	0%	0%	0%	20%
		1.75	0%	100%	100%	100%	100%	0%	100%	100%	100%	0%	0%	25%	70%	75%	0%	0%	15%	60%
	2 Retainers per Pier	0.50	0%	0%	0%	80%	35%	0%	45%	0%	15%	0%	0%	0%	0%	0%	0%	0%	0%	0%
		0.75	0%	0%	0%	100%	85%	0%	100%	0%	40%	0%	0%	0%	0%	0%	0%	0%	0%	0%
		1.00	0%	60%	5%	100%	95%	0%	100%	5%	80%	0%	0%	0%	0%	0%	0%	0%	0%	0%
		1.25	0%	100%	85%	100%	100%	0%	100%	80%	100%	0%	0%	0%	0%	0%	0%	0%	0%	0%
		1.50	0%	100%	100%	100%	100%	0%	100%	100%	100%	0%	0%	5%	45%	50%	0%	0%	0%	25%
		1.75	0%	100%	100%	100%	100%	0%	100%	100%	100%	0%	0%	5%	70%	75%	0%	0%	10%	60%

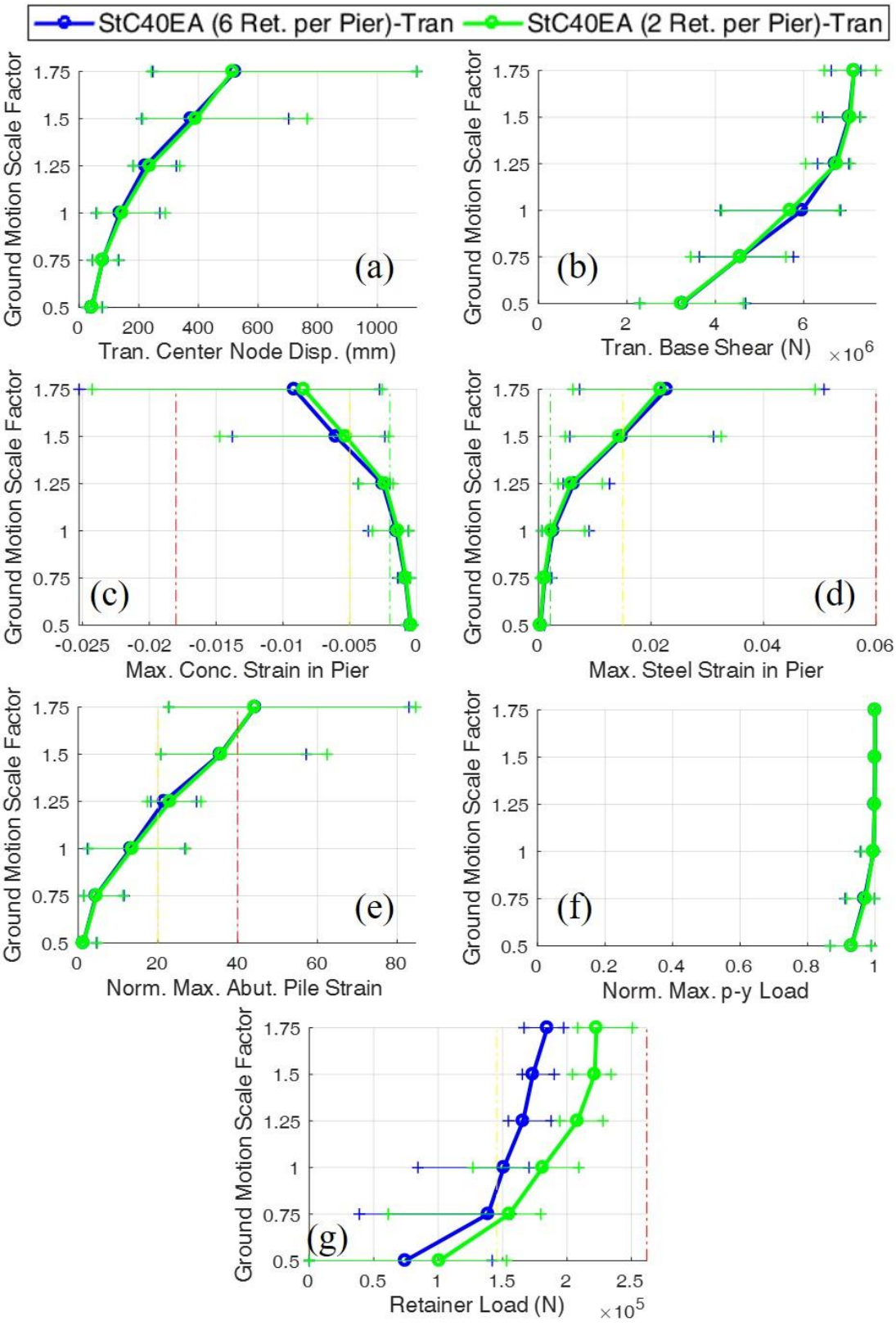

Figure 9.2: IDA plots for the original and enhanced StC40EA in the transverse direction where a scale factor of 1.00 represents the design-level.

The frequency of limit state occurrences for SlC15EA with 8 retainers per pier and two retainers per pier is presented in Table 9.2. The transverse results indicate that retainer yielding (RY) always occurs and retainer fusing (RF) never occurs when the number of retainers is reduced. This occurs despite significantly larger forces developing in the retainers, as shown in Fig. 9.3g. It can also be noted from Fig. 9.3g that the retainer forces do not vary significantly from scale factor to scale factor. This is attributed to moderate pier column damage (SM and CM) occurring at the 0.5 scale factor, as shown in Fig. 9.3c and 9.3d, which allows the piers to limit the force transferred through the bearings and retainers. The occurrence of SM and CM at low scale factors is due to the high demand placed on stiff piers in long span IABs.

Additionally, using fewer retainers allows for the bridge to be more flexible and causes larger displacements in the superstructure, as shown in Fig. 9.3a. The lack of retainer fusing also means that the displacement of the superstructure is still related to the pier displacement. This increased drift due to increased bridge flexibility explains why severe pier column damage (SS and CS) actually occurs more often in the IAB with two retainers per pier.

The lack of retainer fusing in SlC15EA is the motivation behind weakening the retainers further by decreasing the anchor bolt size. The resulting limit state occurrences for SlC15EA with two retainers per pier and smaller anchor bolts is presented in Table 9.3. From Table 9.3 and Fig. 9.3g it can be seen that the goal of having the retainers fuse is accomplished with smaller anchor bolts. However, the demand on the piers is still so large that the retainer fusing provides only mild relief for the pier column damage observed in SlC15EA with only two retainers per pier. Nevertheless, it is an improvement. For the most part, the component behavior provided in Fig. 9.3, aside from retainer behavior, is similar between the IAB with only two retainers per pier and the IAB with two retainers per pier and smaller anchor bolts.

Table 9.2: Frequency of limit state occurrences for the SlC15EA IDA with various retainer configurations where a scale factor of 1.00 represents the design-level.

Bridge	Revision	SF	Longitudinal Limit State Occurrence																	
			Ideal						Acceptable								Unacceptable			
			BF	SL	CL	RE	RY	RF	APY	APB	APS	PA	PPY	PPS	SM	CM	BU	SS	CS	APR
SlC15EA	8 Retainers per Pier	0.50	0%	0%	0%	0%	0%	0%	10%	0%	5%	0%	0%	0%	0%	0%	0%	0%	0%	0%
		0.75	0%	40%	10%	0%	0%	0%	80%	0%	40%	0%	0%	0%	0%	0%	0%	0%	0%	0%
		1.00	0%	100%	100%	0%	0%	0%	100%	0%	100%	0%	0%	5%	25%	35%	0%	0%	5%	0%
		1.25	0%	100%	100%	0%	0%	0%	100%	30%	100%	0%	0%	0%	85%	90%	0%	5%	60%	0%
		1.50	0%	100%	100%	0%	0%	0%	100%	60%	100%	0%	0%	0%	95%	100%	0%	35%	85%	20%
		1.75	0%	100%	100%	0%	0%	0%	100%	80%	100%	0%	0%	10%	100%	100%	0%	65%	90%	30%
	2 Retainers per Pier	0.50	0%	0%	0%	0%	0%	0%	10%	0%	5%	0%	0%	0%	0%	0%	0%	0%	0%	0%
		0.75	0%	40%	10%	0%	0%	0%	80%	0%	40%	0%	0%	0%	0%	0%	0%	0%	0%	0%
		1.00	0%	100%	100%	0%	0%	0%	100%	0%	100%	0%	0%	5%	25%	35%	0%	0%	5%	0%
		1.25	0%	100%	100%	0%	0%	0%	100%	30%	100%	0%	0%	0%	85%	90%	0%	5%	60%	0%
		1.50	0%	100%	100%	0%	0%	0%	100%	60%	100%	0%	0%	0%	95%	100%	0%	35%	85%	20%
		1.75	0%	100%	100%	0%	0%	0%	100%	80%	100%	0%	0%	10%	100%	100%	0%	65%	90%	30%

Bridge	Revision	SF	Transverse Limit State Occurrence																	
			Ideal						Acceptable								Unacceptable			
			BF	SL	CL	RE	RY	RF	APY	APB	APS	PA	PPY	PPS	SM	CM	BU	SS	CS	APR
SlC15EA	8 Retainers per Pier	0.50	0%	100%	100%	100%	0%	0%	0%	0%	0%	0%	0%	0%	30%	65%	0%	0%	0%	0%
		0.75	0%	100%	100%	100%	0%	0%	0%	0%	0%	0%	0%	0%	80%	85%	0%	0%	0%	0%
		1.00	0%	100%	100%	100%	0%	0%	10%	0%	0%	0%	0%	0%	100%	100%	0%	0%	35%	0%
		1.25	0%	100%	100%	100%	0%	0%	75%	0%	20%	0%	0%	0%	100%	100%	0%	30%	100%	0%
		1.50	0%	100%	100%	100%	0%	0%	90%	10%	50%	0%	0%	0%	100%	100%	0%	75%	100%	0%
		1.75	0%	100%	100%	100%	0%	0%	100%	20%	75%	0%	0%	0%	100%	100%	0%	85%	100%	15%
	2 Retainers per Pier	0.50	0%	100%	100%	100%	100%	0%	10%	0%	0%	0%	0%	0%	85%	90%	0%	0%	5%	0%
		0.75	0%	100%	100%	100%	100%	0%	75%	0%	0%	0%	0%	0%	100%	100%	0%	0%	65%	0%
		1.00	0%	100%	100%	100%	100%	0%	95%	0%	20%	0%	0%	0%	100%	100%	0%	20%	90%	0%
		1.25	0%	100%	100%	100%	100%	0%	100%	0%	50%	0%	0%	0%	100%	100%	0%	70%	100%	0%
		1.50	0%	100%	100%	100%	100%	0%	100%	15%	80%	0%	0%	0%	100%	100%	0%	80%	100%	0%
		1.75	0%	100%	100%	100%	100%	0%	100%	35%	85%	0%	0%	0%	100%	100%	0%	95%	100%	10%

Table 9.3: Frequency of limit state occurrences for the SlC15EA IDA with 8 retainers per pier and 2 weakened retainers per pier where a scale factor of 1.00 represents the design-level.

Bridge	Revision	SF	Longitudinal Limit State Occurrence																	
			Ideal						Acceptable								Unacceptable			
			BF	SL	CL	RE	RY	RF	APY	APB	APS	PA	PPY	PPS	SM	CM	BU	SS	CS	APR
SlC15EA	8 Retainers per Pier	0.50	0%	0%	0%	0%	0%	0%	10%	0%	5%	0%	0%	0%	0%	0%	0%	0%	0%	0%
		0.75	0%	40%	10%	0%	0%	0%	80%	0%	40%	0%	0%	0%	0%	0%	0%	0%	0%	0%
		1.00	0%	100%	100%	0%	0%	0%	100%	0%	100%	0%	0%	5%	25%	35%	0%	0%	5%	0%
		1.25	0%	100%	100%	0%	0%	0%	100%	30%	100%	0%	0%	0%	85%	90%	0%	5%	60%	0%
		1.50	0%	100%	100%	0%	0%	0%	100%	60%	100%	0%	0%	0%	95%	100%	0%	35%	85%	20%
		1.75	0%	100%	100%	0%	0%	0%	100%	80%	100%	0%	0%	10%	100%	100%	0%	65%	90%	30%
	2 Retainers per Pier & Smaller Bolts	0.50	0%	0%	0%	0%	0%	0%	10%	0%	5%	0%	0%	0%	0%	0%	0%	0%	0%	0%
		0.75	0%	40%	10%	0%	0%	0%	80%	0%	40%	0%	0%	0%	0%	0%	0%	0%	0%	0%
		1.00	0%	100%	100%	0%	0%	0%	100%	0%	100%	0%	0%	5%	25%	35%	0%	0%	5%	0%
		1.25	0%	100%	100%	0%	0%	0%	100%	30%	100%	0%	0%	0%	85%	90%	0%	5%	60%	0%
		1.50	0%	100%	100%	0%	0%	0%	100%	60%	100%	0%	0%	0%	95%	100%	0%	35%	85%	20%
		1.75	0%	100%	100%	0%	0%	0%	100%	80%	100%	0%	0%	10%	100%	100%	0%	65%	90%	30%

Bridge	Revision	SF	Transverse Limit State Occurrence																	
			Ideal						Acceptable								Unacceptable			
			BF	SL	CL	RE	RY	RF	APY	APB	APS	PA	PPY	PPS	SM	CM	BU	SS	CS	APR
SlC15EA	8 Retainers per Pier	0.50	0%	100%	100%	100%	0%	0%	0%	0%	0%	0%	0%	0%	30%	65%	0%	0%	0%	0%
		0.75	0%	100%	100%	100%	0%	0%	0%	0%	0%	0%	0%	0%	80%	85%	0%	0%	0%	0%
		1.00	0%	100%	100%	100%	0%	0%	10%	0%	0%	0%	0%	0%	100%	100%	0%	0%	35%	0%
		1.25	0%	100%	100%	100%	0%	0%	75%	0%	20%	0%	0%	0%	100%	100%	0%	30%	100%	0%
		1.50	0%	100%	100%	100%	0%	0%	90%	10%	50%	0%	0%	0%	100%	100%	0%	75%	100%	0%
		1.75	0%	100%	100%	100%	0%	0%	100%	20%	75%	0%	0%	0%	100%	100%	0%	85%	100%	15%
	2 Retainers per Pier & Smaller Bolts	0.50	0%	100%	90%	100%	100%	100%	50%	0%	0%	0%	0%	0%	20%	35%	0%	0%	5%	0%
		0.75	0%	100%	100%	100%	100%	100%	95%	0%	15%	0%	0%	0%	85%	90%	0%	15%	35%	0%
		1.00	0%	100%	100%	100%	100%	100%	100%	0%	25%	0%	0%	0%	100%	100%	0%	40%	90%	0%
		1.25	0%	100%	100%	100%	100%	100%	100%	0%	75%	0%	0%	0%	100%	100%	0%	70%	100%	0%
		1.50	0%	100%	100%	100%	100%	100%	100%	25%	85%	0%	0%	0%	100%	100%	0%	95%	100%	0%
		1.75	0%	100%	100%	100%	100%	100%	100%	50%	95%	0%	0%	0%	100%	100%	0%	100%	100%	5%

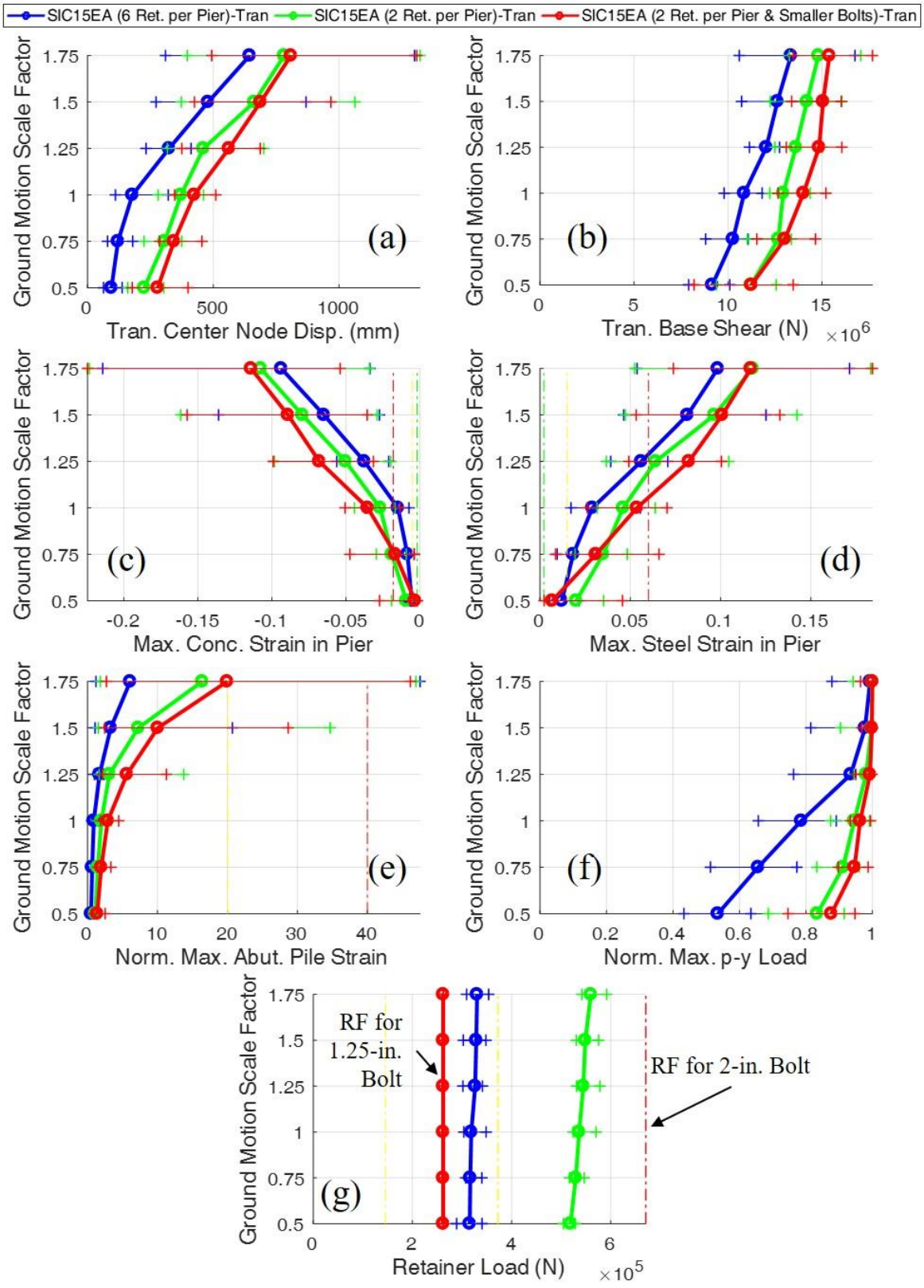

Figure 9.3: IDA plots for the original and enhanced SlC15EA in the transverse direction where a scale factor of 1.00 represents the design-level.

9.2.3 Overall Observations

The sequence of damage for both the original and enhanced designs of StC40EA and SlC15EA is presented in Fig. 9.4. Only the transverse results are presented as changes in the retainers have no effect on the longitudinal direction results. The general observations concerning inducing more retainer damage and less pier column damage by using the minimum number of two retainers per pier to reduce pier column damage is that the three-span bridges with tall piers see minimal benefits while the four-span bridges with short piers have no benefit.

In both IABs, moderate pier column damage is the predominant fuse mechanism in the system. This is especially true in bridges with large pier column demands, like SlC15EA, due to the larger demands leading to the very early occurrence of moderate pier column damage. Even with weakened and reduced retainers in the bridge, SlC15EA encounters high lateral force demand in the piers and moderate pier column damage occurs at low scale factors, as shown in Fig. 9.4b. This indicates that reducing the number of retainers alone is not a viable recommendation for limiting pier column damage in IABs with large pier demands such as IABs with four-spans or short piers. However, if the demand on the pier columns was reduced or the piers could accommodate the demand more effectively and not reach moderate damage, then a smaller number of retainers may have a positive effect on the bridge behavior.

The SlC15EA IABs were flexible in their original designs, so increasing the flexibility by using fewer retainers led to more pier column damage. However, reducing the number of retainers in StC40EA, which has less pier column demand, does show some decreases in pier column damage. Additionally, weakening the retainer anchor bolts was shown to have small positive impacts on pier column behavior in SlC15EA. Weakening the retainer anchor bolts in StC40EA could be even more beneficial by inducing retainer fusing, which does not occur under a reduced

number of retainers alone. This leads to the conclusion that for IABs with taller piers, reducing the number of retainers per pier to the minimum value of two slightly helps pier column behavior, however it does not lead to retainer fusing. Weakening the retainers further may improve pier column behavior by allowing for retainers to fuse.

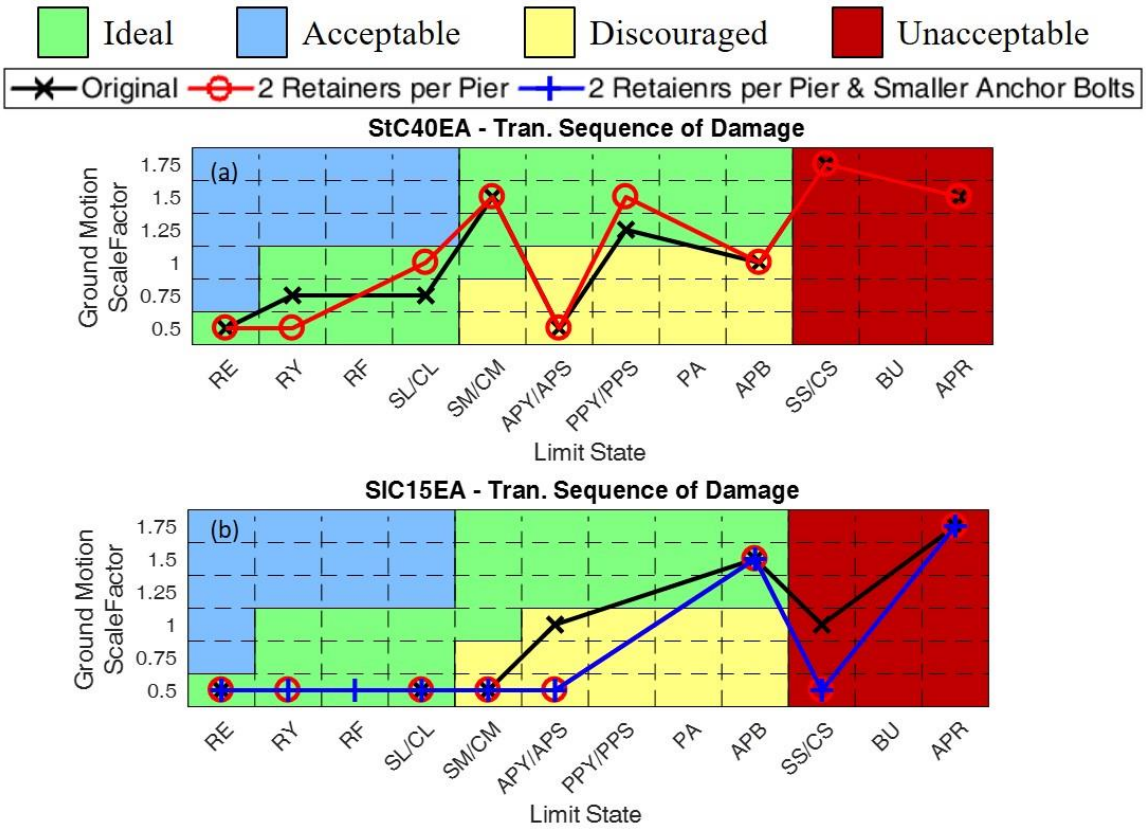

Figure 9.4: Sequences of damage for the IABs with various retainer configurations where a scale factor of 1.00 represents the design-level.

9.3 REDUCTION IN FIXED BEARING RESISTANCE

The fixed bearings also do not fuse in many analyses. By reducing the size of the anchor bolts in the fixed bearings they will become weaker. The goal in doing this is to weaken the fixed bearings such that they fracture and act as fuses, limiting the force transferred to the piers and limiting pier column damage. Similar to the enhanced designs provided in section 9.2, the IABs with revised fixed bearing designs were also selected to represent IABs which rarely encounter

fixed bearing yielding or fusing under Cairo ground motions. The two IABs selected both have steel superstructures due to the decreased load being transferred through the bearings when compared to the concrete superstructure bridges. The two IABs with enhanced designs are StC40FA and SlC15FA.

In the IDA of Chapter 7 it was found that StC40FA in the transverse direction encounters some fixed bearing yielding, but only at low rates of occurrence and at large scale factors. In general, there is little pier damage beyond light pier column damage with severe pier column concrete damage only occurring when the scale factor is 1.75. The original design of the fixed bearings has two 1.25-in diameter anchor bolts. The enhanced design weakened the anchor bolts as much as allowed by IDOT by reducing the diameter to 0.625 in. This reduces the ultimate resistance of each fixed bearing from 314 kN to 79 kN.

SlC15FA in the transverse direction experiences no fixed bearing yielding or fusing in the IDA of Chapter 7. Additionally, the flexible nature of the bridge and short piers increases the pier column demands such that severe pier column concrete damage is experienced in every analysis at scale factors of 1.5 and larger. The original IAB design has fixed bearings with two 2-in diameter anchor bolts. The anchor bolt diameter is not reduced all the way to the minimum allowed by IDOT (0.625 in) as this would likely cause the fixed bearings to fuse too easily and encourage bearing unseating. Instead the enhanced design had the fixed bearing anchor bolts be 1.625 in in diameter. This reduces the ultimate resistance of each fixed bearing from 805 kN to 531 kN.

9.3.1 Pushover Results

The pushover results for StC40FA and SlC15FA is presented in Fig. 9.5. As expected, there is no difference in the longitudinal direction behavior as the majority of the fixed bearing impact comes during transverse excitation. The transverse direction results are also extremely similar to

each other regardless of if the design is the original or enhanced version. The StC40FA transverse pushover curve (Fig. 9.5b) does indicate that fixed bearing fusing does occur, however this has a minimal effect on the behavior. It does allow for any pier damage after the fixed bearing fusing to occur at larger displacements though. There is no difference at all in the transverse direction behavior of SlC15FA (Fig. 9.5d). This is likely due to the large demand in the piers still leading to moderate pier column damage before any fixed bearing effects take place.

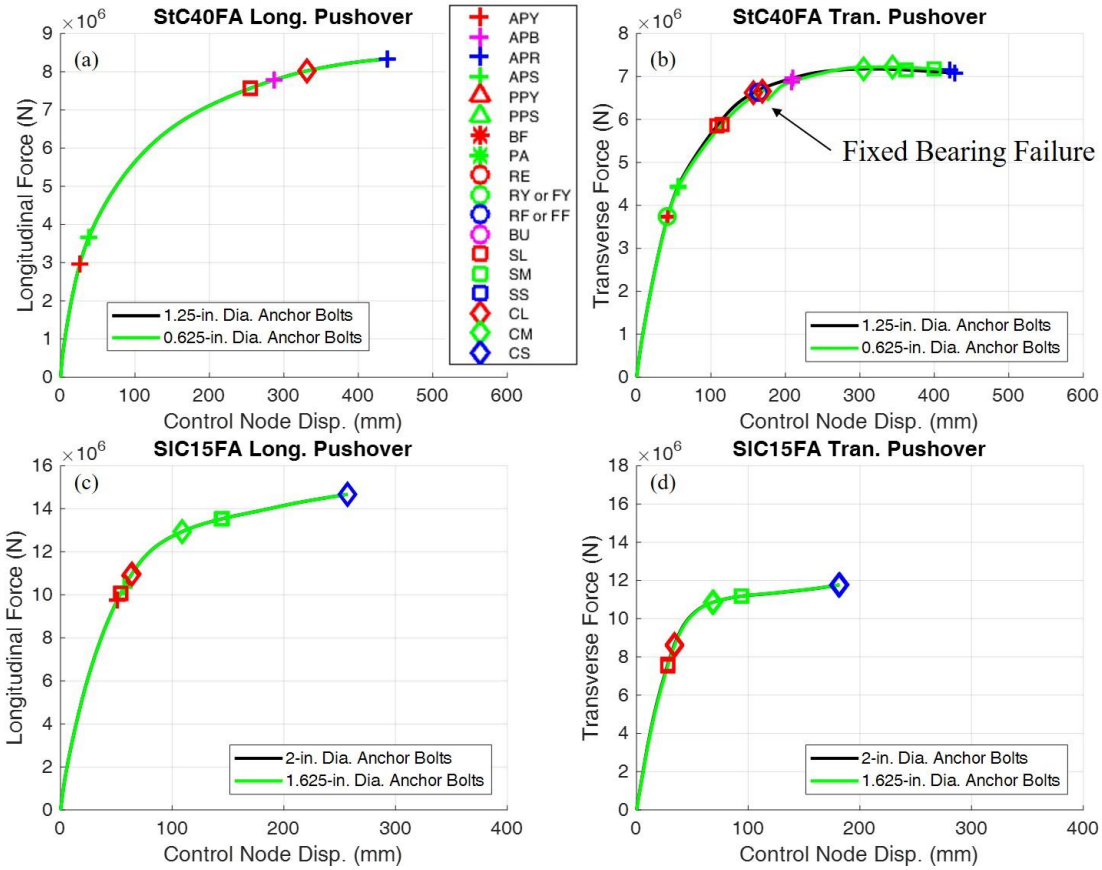

Figure 9.5: Pushover analysis results for IABs with various fixed bearing anchor bolt sizes.

9.3.2 IDA Results

A comparison of the frequency of limit state occurrences between the original and enhanced designs for StC40EA is provided in Table 9.4. As with the pushover results, there is no difference between the longitudinal results. The enhanced designs provide an increase in fixed

bearing yielding (FY) and fusing (FF). This is reflected in the fixed bearing forces encountered in the IDA in Fig. 9.6g. Also reflected in Fig. 9.6g is that the fixed bearings in both cases are limited at scale factors of 1.25 and larger. In the original design this is due to moderate pier column damage occurring around this scale factor, as shown in Fig. 9.6c and 9.6d. In the enhanced design, this limit is reached due to fixed bearing fusing. Having the fixed bearing fusing occur before moderate pier damage does allow for the piers to experience slightly less strain and limit state occurrences, as shown in Fig. 9.6c and 9.6d as well as in Table 9.4 where the occurrence rate of pier column damage drops by about 10-15% in most cases. Aside from these differences there are no other changes to the behavior, as indicated in Fig. 9.6.

The IDA results and the frequency of limit state occurrence of the original and enhanced design of SlC15FA is presented in Fig. 9.7 and Table 9.5. Similar to the behavior in the pushover analysis, there are extremely minor to no changes in the results despite the fixed bearings being 275 kN weaker and having anchor bolts 0.375-in smaller in diameter. The IDA results presented in Fig. 9.7 also show very little to no difference. In Table 9.5 it is shown that the only pier column damage differences are drops of 5% at CM with a scale factor of 0.75 and 5% at SS with a scale factor of 1.75. Table 9.5 also demonstrates that the fixed bearings in both designs do not yield or fuse despite the reduction in bearing strength. Fig. 9.7g shows that the forces in the fixed bearings are very similar and do not vary from scale factor to scale factor leaving the fixed bearings well short of yielding in both designs. This lack of variation in fixed bearing load is due to the forces in the piers, and therefore the forces transferred through the bearings, being limited by moderate pier column damage which occurs at scale factors as low as 0.5. This is caused by the large load demand in the piers from the short pier and long span characteristics of the IAB.

Table 9.4: Frequency of limit state occurrences for the StC40FA IDA with original and weakened fixed bearing anchor bolts where a scale factor of 1.00 represents the design-level.

Bridge	Revision	SF	Longitudinal Limit State Occurrence																
			Ideal					Acceptable								Unacceptable			
			BF	SL	CL	FY	FF	APY	APB	APS	PA	PPY	PPS	SM	CM	BU	SS	CS	APR
StC40FA	1.25-inch Diameter Anchor Bolts	0.50	0%	0%	0%	0%	0%	70%	0%	30%	0%	0%	0%	0%	0%	0%	0%	0%	0%
		0.75	0%	0%	0%	0%	0%	100%	0%	60%	0%	0%	0%	0%	0%	0%	0%	0%	0%
		1.00	0%	15%	0%	0%	0%	100%	15%	100%	0%	0%	0%	0%	0%	0%	0%	0%	0%
		1.25	0%	75%	40%	0%	0%	100%	75%	100%	0%	0%	5%	0%	0%	0%	0%	0%	5%
		1.50	0%	85%	75%	0%	0%	100%	90%	100%	0%	0%	50%	20%	25%	0%	0%	0%	55%
		1.75	0%	95%	85%	0%	0%	100%	95%	100%	0%	0%	55%	40%	60%	0%	0%	15%	80%
	0.625-inch Diameter Anchor Bolts	0.50	0%	0%	0%	0%	0%	70%	0%	30%	0%	0%	0%	0%	0%	0%	0%	0%	0%
		0.75	0%	0%	0%	0%	0%	100%	0%	60%	0%	0%	0%	0%	0%	0%	0%	0%	0%
		1.00	0%	15%	0%	0%	0%	100%	15%	100%	0%	0%	0%	0%	0%	0%	0%	0%	0%
		1.25	0%	75%	40%	0%	0%	100%	75%	100%	0%	0%	15%	0%	0%	0%	0%	0%	5%
		1.50	0%	85%	75%	0%	0%	100%	90%	100%	0%	0%	45%	20%	25%	0%	0%	0%	55%
		1.75	0%	95%	85%	0%	0%	100%	95%	100%	0%	0%	55%	40%	60%	0%	0%	15%	80%

Bridge	Revision	SF	Transverse Limit State Occurrence																
			Ideal					Acceptable								Unacceptable			
			BF	SL	CL	FY	FF	APY		APS	PA	PPY	PPS	SM	CM	BU	SS	CS	APR
StC40FA	1.25-inch Diameter Anchor Bolts	0.50	0%	0%	0%	0%	0%	45%	0%	10%	0%	0%	0%	0%	0%	0%	0%	0%	0%
		0.75	0%	20%	0%	0%	0%	100%	0%	30%	0%	0%	0%	0%	0%	0%	0%	0%	0%
		1.00	0%	65%	35%	0%	0%	100%	5%	75%	0%	0%	0%	0%	0%	0%	0%	0%	0%
		1.25	0%	85%	80%	10%	0%	100%	55%	100%	0%	0%	0%	5%	0%	0%	0%	0%	0%
		1.50	0%	100%	100%	15%	0%	100%	100%	100%	0%	0%	5%	55%	55%	0%	0%	0%	15%
		1.75	0%	100%	100%	15%	0%	100%	100%	100%	0%	0%	25%	70%	85%	0%	0%	20%	55%
	0.625-inch Diameter Anchor Bolts	0.50	0%	0%	0%	50%	0%	45%	0%	10%	0%	0%	0%	0%	0%	0%	0%	0%	0%
		0.75	0%	20%	0%	100%	0%	100%	0%	30%	0%	0%	0%	0%	0%	0%	0%	0%	0%
		1.00	0%	60%	20%	100%	20%	100%	5%	70%	0%	0%	0%	0%	0%	0%	0%	0%	0%
		1.25	0%	95%	70%	100%	75%	100%	55%	100%	0%	0%	0%	0%	0%	0%	0%	0%	0%
		1.50	0%	100%	100%	100%	85%	100%	100%	100%	0%	0%	5%	40%	45%	0%	0%	0%	20%
		1.75	0%	100%	100%	100%	100%	100%	100%	100%	0%	0%	5%	70%	70%	0%	0%	10%	55%

Table 9.5: Frequency of limit state occurrences for the SlC15FA IDA with original and weakened fixed bearing anchor bolts where a scale factor of 1.00 represents the design-level.

Bridge	Revision	SF	Longitudinal Limit State Occurrence																
			Ideal					Acceptable								Unacceptable			
			BF	SL	CL	FY	FF	APY	APB	APS	PA	PPY	PPS	SM	CM	BU	SS	CS	APR
SlC15FA	2-inch Diameter Anchor Bolts	0.50	0%	20%	5%	0%	0%	5%	0%	0%	0%	0%	0%	0%	0%	0%	0%	0%	0%
		0.75	0%	80%	75%	0%	0%	75%	0%	30%	0%	0%	0%	0%	20%	0%	0%	0%	0%
		1.00	0%	90%	85%	0%	0%	90%	0%	75%	0%	0%	0%	60%	80%	0%	0%	0%	0%
		1.25	0%	100%	100%	0%	0%	100%	5%	100%	0%	0%	0%	100%	100%	0%	0%	55%	0%
		1.50	0%	100%	100%	0%	0%	100%	60%	100%	0%	0%	0%	100%	100%	0%	30%	85%	20%
		1.75	0%	100%	100%	0%	0%	100%	80%	100%	0%	0%	0%	100%	100%	0%	60%	95%	30%
	1.625-inch Diameter Anchor Bolts	0.50	0%	20%	5%	0%	0%	5%	0%	0%	0%	0%	0%	0%	0%	0%	0%	0%	0%
		0.75	0%	80%	75%	0%	0%	75%	0%	30%	0%	0%	0%	0%	20%	0%	0%	0%	0%
		1.00	0%	90%	85%	0%	0%	95%	0%	75%	0%	0%	0%	60%	80%	0%	0%	0%	0%
		1.25	0%	100%	100%	0%	0%	100%	5%	100%	0%	0%	0%	100%	100%	0%	0%	55%	0%
		1.50	0%	100%	100%	0%	0%	100%	60%	100%	0%	0%	0%	100%	100%	0%	30%	85%	20%
		1.75	0%	100%	100%	0%	0%	100%	80%	100%	0%	0%	0%	100%	100%	0%	60%	95%	30%

Bridge	Revision	SF	Transverse Limit State Occurrence																
			Ideal					Acceptable								Unacceptable			
			BF	SL	CL	FY	FF	APY	APB	APS	PA	PPY	PPS	SM	CM	BU	SS	CS	APR
SlC15FA	2-inch Diameter Anchor Bolts	0.50	0%	100%	100%	0%	0%	0%	0%	0%	0%	0%	0%	5%	10%	0%	0%	0%	0%
		0.75	0%	100%	100%	0%	0%	0%	0%	0%	0%	0%	0%	35%	75%	0%	0%	0%	0%
		1.00	0%	100%	100%	0%	0%	0%	0%	0%	0%	0%	0%	75%	90%	0%	0%	25%	0%
		1.25	0%	100%	100%	0%	0%	35%	0%	0%	0%	0%	0%	95%	100%	0%	10%	65%	0%
		1.50	0%	100%	100%	0%	0%	90%	0%	20%	0%	0%	0%	100%	100%	0%	60%	100%	0%
		1.75	0%	100%	100%	0%	0%	100%	15%	55%	0%	0%	0%	100%	100%	0%	85%	100%	5%
	1.625-inch Diameter Anchor Bolts	0.50	0%	100%	100%	0%	0%	0%	0%	0%	0%	0%	0%	5%	10%	0%	0%	0%	0%
		0.75	0%	100%	100%	0%	0%	0%	0%	0%	0%	0%	0%	35%	70%	0%	0%	0%	0%
		1.00	0%	100%	100%	0%	0%	0%	0%	0%	0%	0%	0%	75%	90%	0%	0%	25%	0%
		1.25	0%	100%	100%	0%	0%	35%	0%	0%	0%	0%	0%	95%	100%	0%	10%	65%	0%
		1.50	0%	100%	100%	0%	0%	90%	0%	25%	0%	0%	0%	100%	100%	0%	60%	100%	0%
		1.75	0%	100%	100%	0%	0%	100%	20%	60%	0%	0%	0%	100%	100%	0%	90%	100%	5%

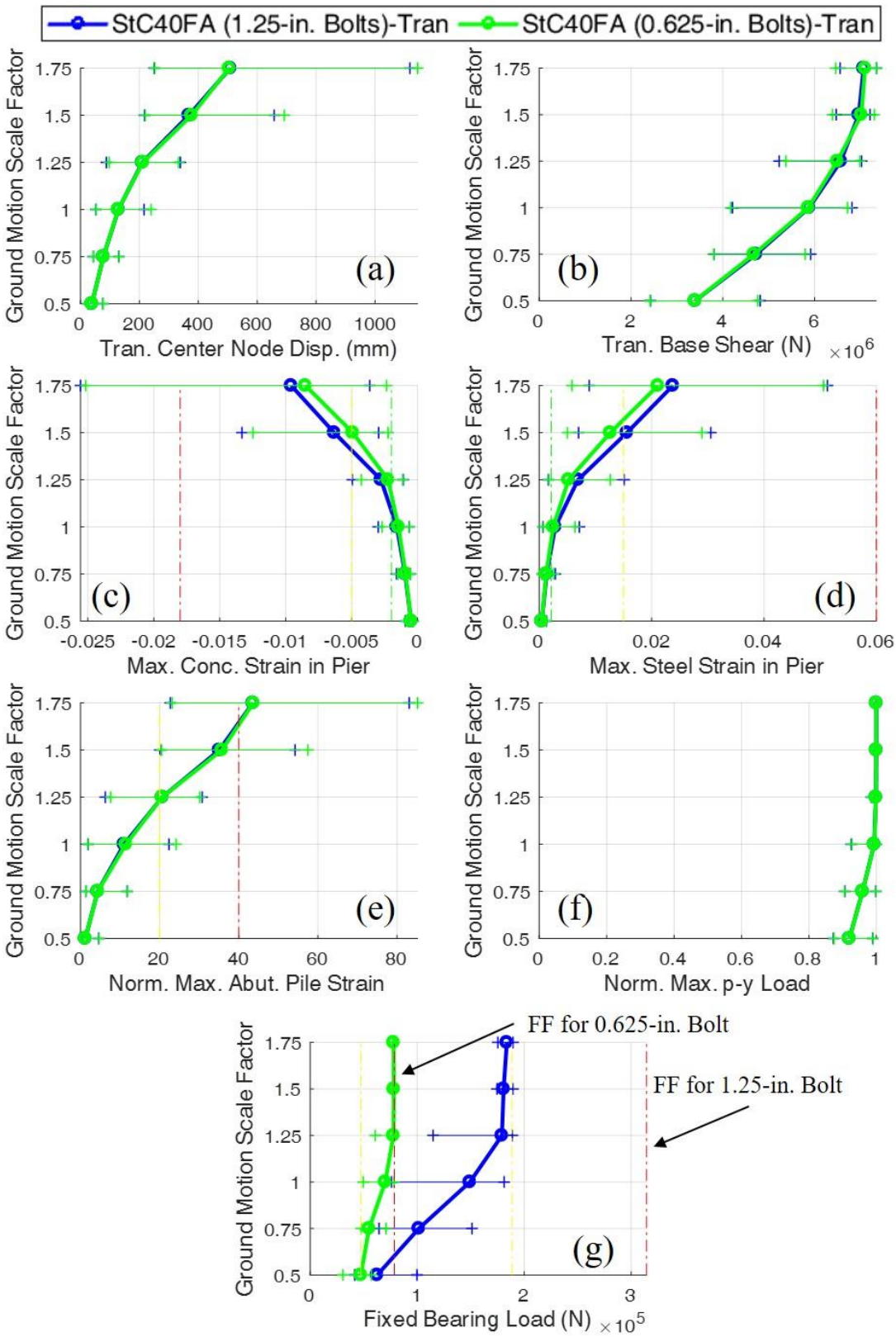

Figure 9.6: IDA plots for the original and enhanced StC40FA in the transverse direction where a scale factor of 1.00 represents the design-level.

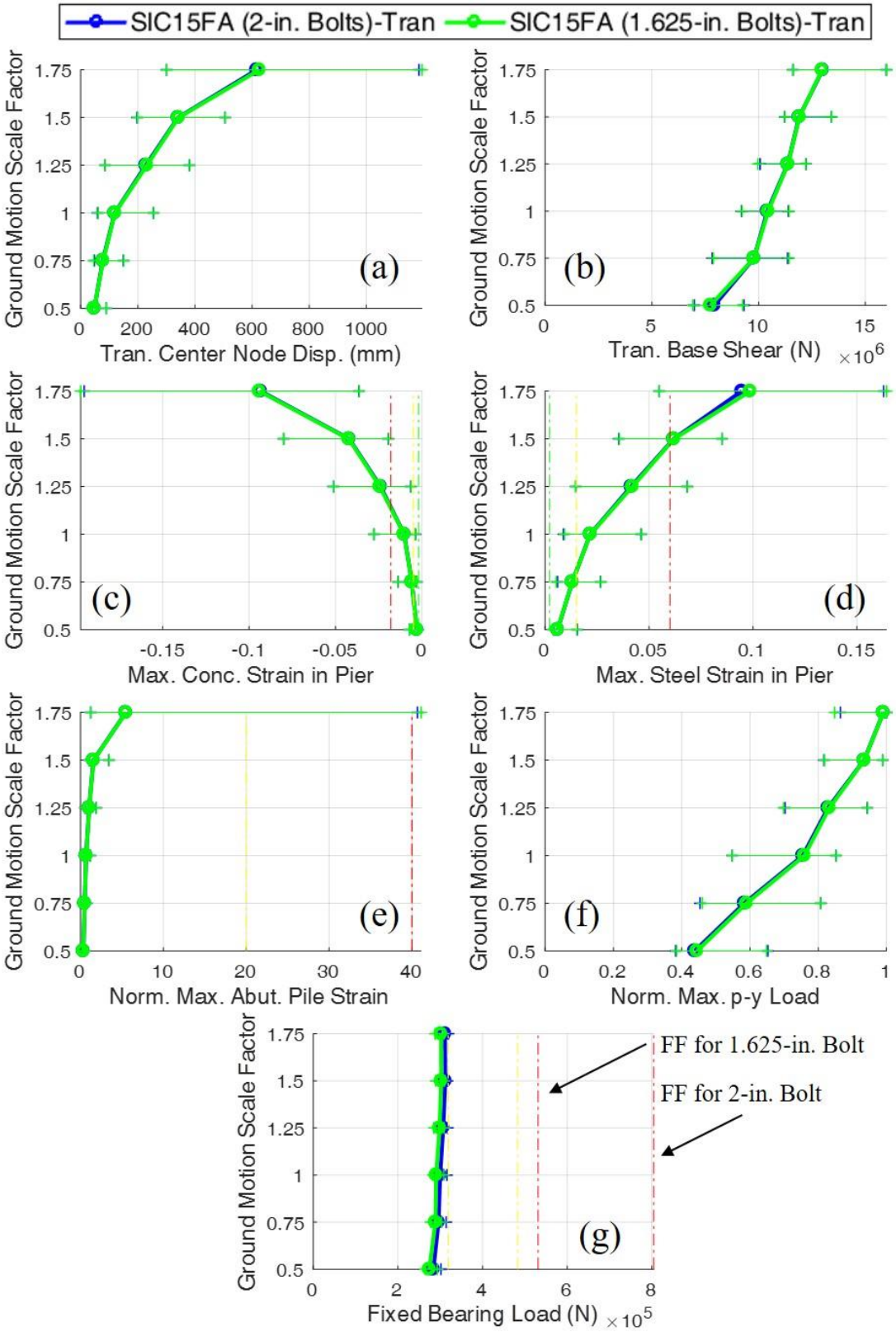

Figure 9.7: IDA plots for the original and enhanced SlC15FA in the transverse direction where a scale factor of 1.00 represents the design-level.

9.3.3 Overall Observations

The sequences of damage for StC40FA and SlC15FA in the transverse direction are presented in Fig. 9.8. The StC40FA results indicate that there are minimal changes despite the inclusion of fixed bearing fusing (FF). Fixed bearing yielding (FY) occurs at smaller scale factors and severe pier column damage (SS/CS) occurs at slightly large scale factors. From this and the IDA results it can be shown that IABs with lesser pier demands, such as IABs with taller piers, do show some improvement when the fixed bearing anchor bolt sizes are reduced. This happens by allowing the fixed bearing to fuse first and limit the forces in the columns. However, the minimum diameter of 0.625-in is still too large to encounter any significant improvement in the seismic performance.

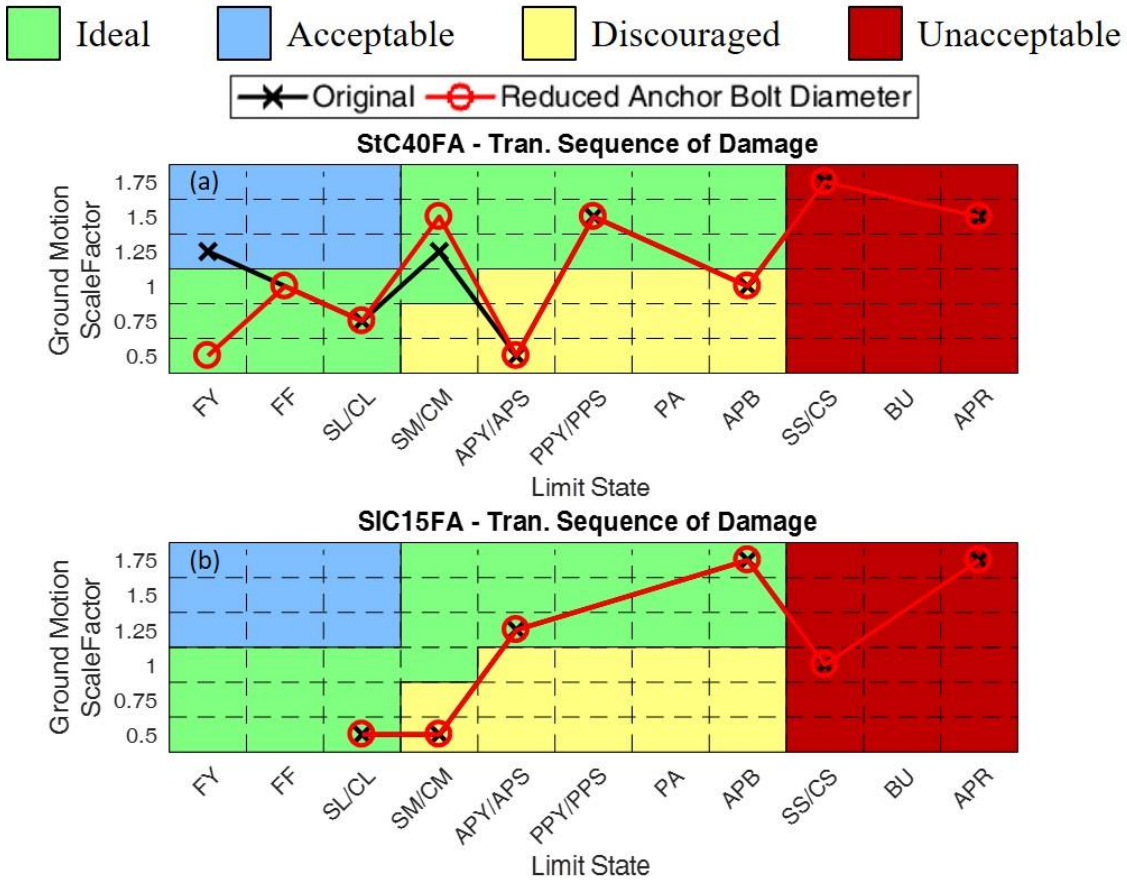

Figure 9.8: Sequences of damage for the IABs with various fixed bearing anchor bolt sizes where a scale factor of 1.00 represents the design-level.

The SlC15FA results indicate that there is no benefit to reducing the fixed bearing anchor bolt diameter by 0.375 in. The issue in this IAB is the extreme demand placed on the piers due to the short columns and long spans having moderate pier column damage (SM/CM) occur at low scale factors. Once moderate damage occurs the load through the fixed bearing is limited. If the longer span bridges had more robust columns which delay the onset of moderate pier column damage, the fixed bearings would potentially fuse first leading to limited forces in the pier columns and less damage. As the pier column designs currently stand, decreasing the fixed bearing anchor bolt diameters is not a viable solution.

9.4 STRENGTHENING OF THE PIER COLUMNS

The frequent severe damage to the pier columns at moderate ground shaking intensity is of concern in IABs. The greatest damage to the pier columns is observed in the concrete IABs with 15-ft tall piers. This is due to the shorter, stiffer piers creating more demand in the pier columns and the concrete superstructure creating more lateral inertia load in the bridge. A potential solution to this concern is to increase the size of the pier columns. By doing this the pier columns will be strengthened and be capable of accommodating the large demands without experiencing moderate or severe pier column damage. The original pier column designs for the IABs with 15-ft piers were 2.5-ft diameter concrete columns with (12) #10 reinforcing bars (grade 60). The enhanced designs assessed in this section use 3-ft diameter concrete columns with (14) #10 bars (grade 60). Although this reduces the reinforcement ratio in the columns from 2.1% to 1.7%, the overall strength is increased such that it is about twice as strong as required for the Extreme Event I load combination (AASHTO, 2011).

Both IABs whose designs are enhanced are concrete IABs with 15-ft tall piers. The first enhanced IAB is CtC15EA. In this bridge's original design severe pier column concrete damage

occurs under design-level shaking. The second enhanced IAB is ClC15EA. Due to the extreme flexibility of ClC15EA in the transverse direction, severe pier column concrete damage occurs at the lowest scale factor of 0.5 in the original design.

9.4.1 Pushover Results

The pushover curves for the original and enhanced CtC15EA and ClC15EA are presented in Fig. 9.9. Overall the enhanced designs have a larger load capacity, as is logical given the increased size of the revised columns. In the longitudinal pushover curves of both IABs it can be seen that aside from the magnitude of the load there is little difference in the shape of the curve or the sequence of limit state occurrences. The one main difference is that the moderate pier column steel damage limit state (SM) occurs sooner after its concrete counterpart occurs. This is attributed to the smaller reinforcement ratio of the revised designs.

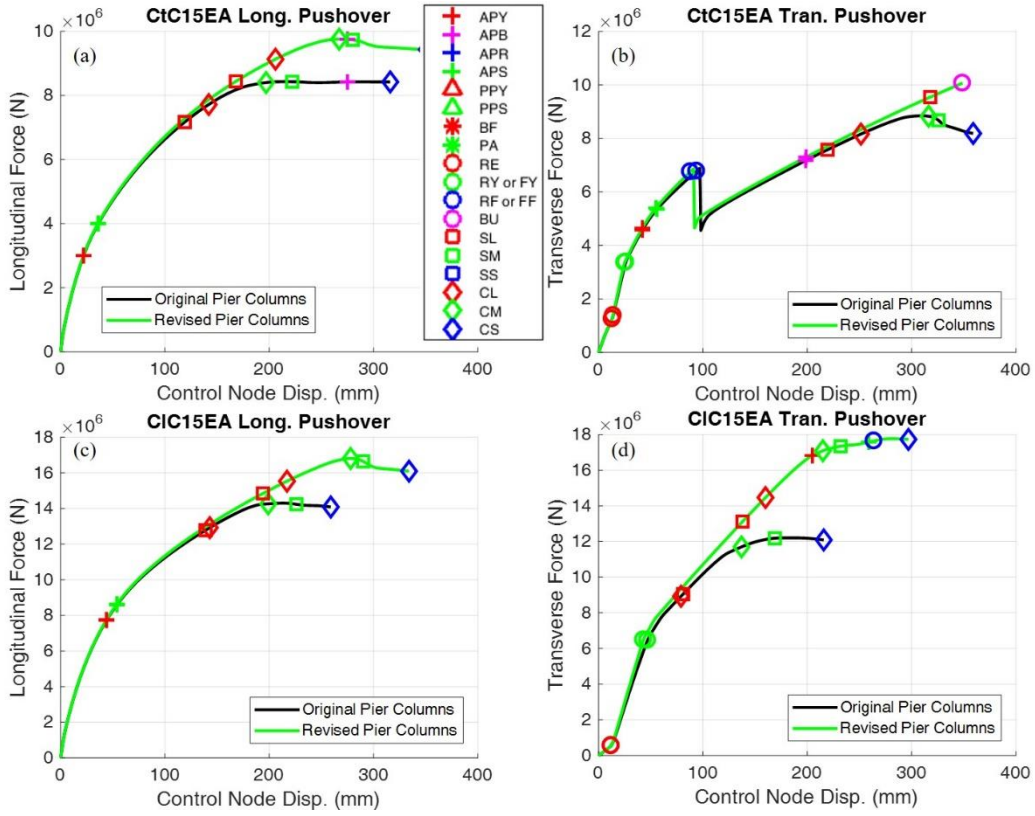

Figure 9.9: Pushover analysis results for IABs with various pier column designs.

The transverse results for CtC15EA (Fig. 9.9b) shows retainer fusing (RF) in both designs. However, the original designs begin to encounter pier column damage shortly after. The revised columns withstand larger forces and therefore does not begin to experience even light pier column damage (SL) until around the same displacement that the original design experiences moderate pier column damage (SM and CM), as shown in Fig. 9.9b. This extra displacement allows for bearing unseating to occur and the analysis to fail to converge shortly beyond that.

The enhanced designs in the transverse direction of ClC15EA also allows the pier columns to experience damage at larger displacements and forces, as shown in Fig. 9.9d. The enhanced design also allows for the retainer to fuse, which coincides with the peak load capacity of the bridge. This differs from most other bridges where moderate pier column damage occurs first and limits the IAB's load capacity. Severe pier column damage is followed shortly after retainer fusing in the enhanced design.

9.4.2 IDA Results

The frequency of limit state occurrences in the IDA for CtC15EA is presented in Table 9.6. The longitudinal results indicate that there is a moderate decrease in pier column damage limit state occurrences, although severe pier column limit states (SS and CS) are still very frequent at larger scale factors. Despite less pier column damage occurrences there is no increase in abutment foundation damage (APY, APB, APR, and APS). However, the number of APY, APB, APR, and APS occurrences is already quite large in the original design. In the IDA results presented in Fig. 9.10 for the longitudinal direction, it can be observed that for the most part there is no significant difference in the behavior of the individual components across the ground motion scale factors. The primary difference is in the total load on the IAB in Fig. 9.10b which shows that both designs

reach a limit when the pier columns begin to experience moderate pier column damage around the design-level scale factor of 1.0.

The transverse ClC15EA results presented in Fig. 9.11 and Table 9.6 demonstrate that there is much less pier column strain (Fig. 9.11c and 9.11d) and occurrence of pier column damage when the enhanced design is used. Severe pier column damage (SS and CS) as well as moderate pier column damage (SM and CM) is essentially eliminated in the enhanced designs. However, the stiffer piers of the enhanced design and the frequent occurrence of retainer fusing (RF) does lead to increased occurrences of bearing unseating (BU) despite the bridge not encountering any larger deck displacements than in the original design (see Fig. 9.11a). The loads in the enhanced design bridge is once again larger, as seen in Fig. 9.11b, though a hard limit is not encountered due to the lack of moderate pier column damage as experienced in the original design.

Table 9.6: Frequency of limit state occurrences for the CtC15EA IDA with original and revised pier column designs where a scale factor of 1.00 represents the design-level.

Bridge	Revision	SF	Longitudinal Limit State Occurrence																
			Ideal						Acceptable								Unacceptable			
			BF	SL	CL	RE	RY	RF	APY	APB	APS	PA	PPY	PPS	SM	CM	BU	SS	CS	APR
CtC15EA	Original Pier Columns	0.50	0%	0%	0%	0%	0%	0%	100%	0%	55%	0%	0%	0%	0%	0%	0%	0%	0%	0%
		0.75	0%	95%	65%	0%	0%	0%	100%	5%	100%	0%	0%	0%	15%	20%	0%	0%	0%	0%
		1.00	0%	100%	100%	0%	0%	0%	100%	75%	100%	0%	0%	0%	75%	85%	0%	5%	50%	20%
		1.25	0%	100%	100%	0%	0%	0%	100%	85%	100%	0%	0%	0%	85%	90%	0%	35%	80%	60%
		1.50	10%	100%	100%	0%	0%	0%	100%	90%	100%	0%	10%	5%	90%	100%	0%	50%	75%	70%
		1.75	20%	100%	100%	5%	5%	0%	100%	100%	100%	0%	25%	15%	100%	100%	10%	70%	80%	70%
	Revised Pier Columns	0.50	0%	0%	0%	0%	0%	0%	100%	0%	55%	0%	0%	0%	0%	0%	0%	0%	0%	0%
		0.75	0%	40%	15%	0%	0%	0%	100%	5%	100%	0%	0%	0%	0%	0%	0%	0%	0%	0%
		1.00	0%	95%	80%	0%	0%	0%	100%	75%	100%	0%	0%	15%	55%	55%	0%	5%	35%	15%
		1.25	0%	100%	90%	0%	0%	0%	100%	85%	100%	0%	0%	40%	80%	80%	0%	45%	75%	55%
		1.50	0%	100%	100%	0%	0%	0%	100%	95%	100%	0%	10%	35%	85%	85%	0%	75%	80%	75%
		1.75	20%	100%	100%	0%	0%	0%	100%	100%	100%	0%	20%	20%	85%	90%	0%	70%	80%	70%

Bridge	Revision	SF	Transverse Limit State Occurrence																	
			Ideal						Acceptable								Unacceptable			
			BF	SL	CL	RE	RY	RF	APY	APB	APS	PA	PPY	PPS	SM	CM	BU	SS	CS	APR
CtC15EA	Original Pier Columns	0.50	0%	0%	0%	100%	100%	5%	80%	0%	25%	0%	0%	0%	0%	0%	0%	0%	0%	0%
		0.75	0%	100%	25%	100%	100%	100%	100%	40%	100%	0%	0%	0%	0%	0%	0%	0%	0%	0%
		1.00	0%	100%	80%	100%	100%	100%	100%	90%	100%	0%	0%	0%	40%	40%	0%	5%	15%	10%
		1.25	0%	95%	85%	100%	100%	100%	100%	100%	100%	0%	0%	0%	80%	80%	0%	45%	65%	55%
		1.50	0%	95%	85%	100%	100%	100%	100%	100%	100%	0%	20%	20%	80%	80%	20%	75%	80%	80%
		1.75	0%	100%	95%	100%	100%	100%	100%	100%	100%	0%	20%	20%	80%	80%	20%	75%	80%	80%
	Revised Pier Columns	0.50	0%	0%	0%	100%	100%	20%	85%	0%	25%	0%	0%	0%	0%	0%	0%	0%	0%	0%
		0.75	0%	0%	0%	100%	100%	100%	100%	35%	100%	0%	0%	0%	0%	0%	0%	0%	0%	0%
		1.00	0%	40%	0%	100%	100%	100%	100%	90%	100%	0%	0%	0%	0%	0%	0%	0%	0%	15%
		1.25	0%	80%	30%	100%	100%	100%	100%	100%	100%	0%	0%	0%	0%	0%	15%	0%	0%	55%
		1.50	0%	80%	45%	100%	100%	100%	100%	100%	100%	0%	0%	0%	0%	0%	55%	0%	0%	80%
		1.75	0%	85%	55%	100%	100%	100%	100%	100%	100%	0%	0%	0%	5%	5%	60%	5%	5%	80%

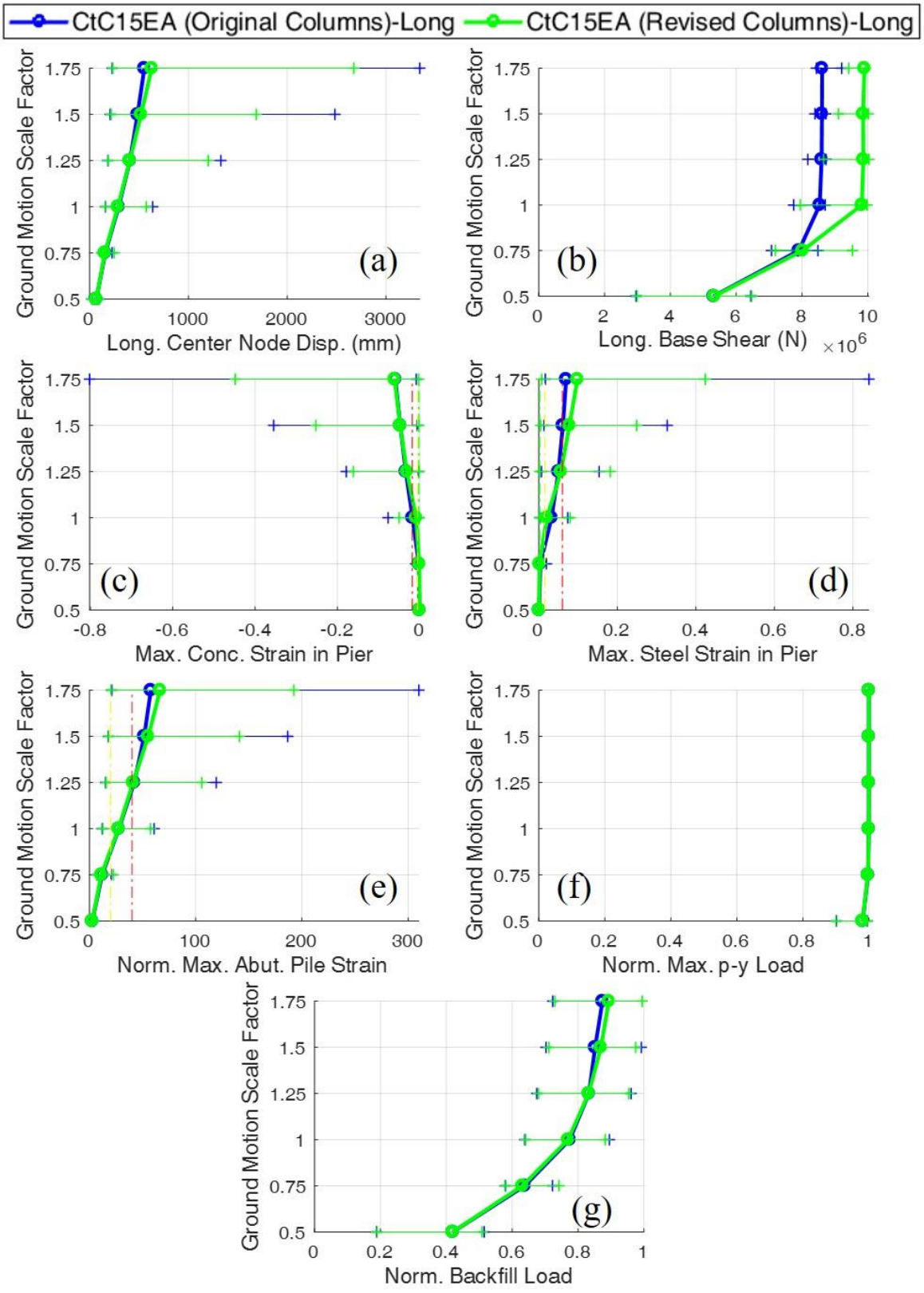

Figure 9.10: IDA plots for the original and enhanced CtC15EA in the longitudinal direction where a scale factor of 1.00 represents the design-level.

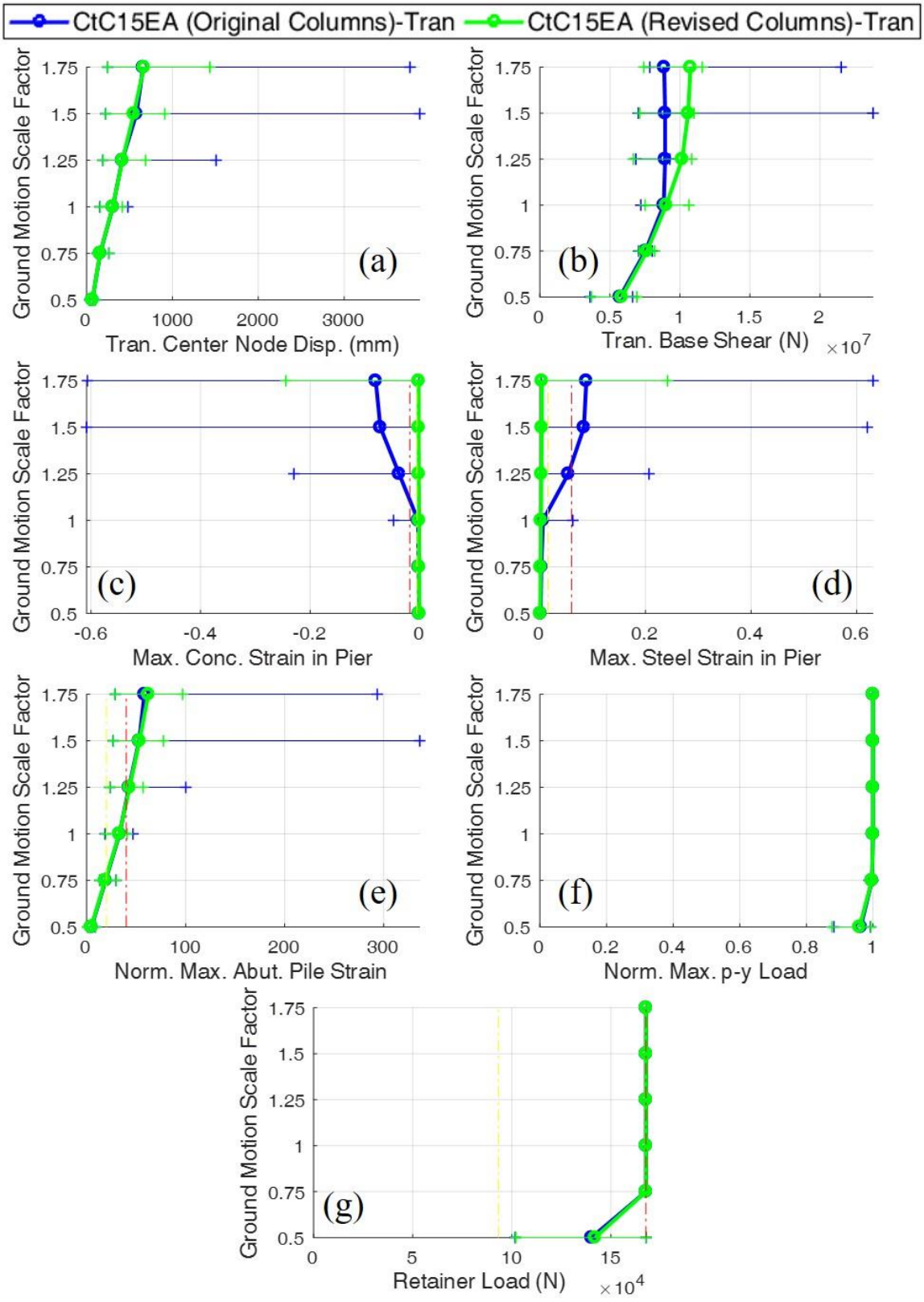

Figure 9.11: IDA plots for the original and enhanced CtC15EA in the transverse direction where a scale factor of 1.00 represents the design-level.

The frequency of limit state occurrences for ClC15EA is presented in Table 9.7. The longitudinal IDA results presented in Table 9.7 and in Fig. 9.12 indicate similar results to the CtC15EA longitudinal results. These results indicate moderate decreases in all three levels of pier column damage. APY and APS are once again consistently large as most of the longitudinal load is resisted by the abutments. APB and APR are also frequent at moderate to large scale factors but do increase slightly as the pier damage limit state occurrences decrease. This indicates a decrease in the abutment demand as pier demand increases. The enhanced design IAB is also capable of obtaining larger loads in Fig. 9.12b, but both designs reach caps set by moderate pier column damage.

The transverse IDA results, presented in Fig. 9.13 and Table 9.7, show that the stiffer revised pier columns lead to much more frequent occurrences of retainer fusing (RF). This in turn leads to larger deck displacements in the enhanced bridge. Unlike the three-span bridge observed above, the four-span ClC15EA does not experience a large drop in pier column damage. There are still significant amounts of moderate (SM and CM) and severe (SS and CS) limit state occurrences in the enhanced design and any decrease in pier column damage is increased in abutment pile damage with larger APB and APR frequencies. This can be attributed to the long span bridge with short piers creating a demand too large for even the enhanced design's columns to accommodate. This can be observed in Fig. 9.13c where the enhanced design produces smaller pier concrete strains at the 0.75 scale factor, however the demand is so large that these smaller strains still exceed the severe damage limit state (dashed red line). The larger revised columns may even hinder in this situation as the columns cannot accommodate the extra force they demand, so there is an increase in abutment foundation damage as well, as seen in Fig. 9.13e.

Table 9.7: Frequency of limit state occurrences for the ClC15EA IDA with original and revised pier column designs where a scale factor of 1.00 represents the design-level.

Bridge	Revision	SF	Longitudinal Limit State Occurrence																	
			Ideal						Acceptable								Unacceptable			
			BF	SL	CL	RE	RY	RF	APY	APB	APS	PA	PPY	PPS	SM	CM	BU	SS	CS	APR
ClC15EA	Original Pier Columns	0.50	0%	50%	50%	0%	0%	0%	100%	0%	85%	0%	0%	0%	0%	0%	0%	0%	0%	0%
		0.75	0%	85%	85%	0%	0%	0%	100%	20%	100%	0%	0%	0%	70%	80%	0%	0%	50%	0%
		1.00	0%	95%	95%	0%	0%	0%	100%	65%	100%	0%	0%	0%	80%	80%	0%	5%	80%	5%
		1.25	0%	100%	100%	0%	0%	0%	100%	70%	100%	0%	0%	0%	85%	85%	0%	20%	75%	20%
		1.50	0%	100%	100%	0%	0%	0%	100%	70%	100%	0%	0%	0%	90%	95%	0%	20%	85%	25%
		1.75	5%	100%	100%	0%	0%	0%	100%	80%	100%	5%	0%	0%	95%	95%	0%	20%	95%	35%
	Revised Pier Columns	0.50	0%	0%	0%	0%	0%	0%	100%	0%	85%	0%	0%	0%	0%	0%	0%	0%	0%	0%
		0.75	0%	80%	70%	0%	0%	0%	100%	20%	100%	0%	0%	10%	35%	40%	0%	10%	25%	0%
		1.00	0%	85%	80%	0%	0%	0%	100%	65%	100%	0%	0%	30%	70%	70%	0%	40%	70%	15%
		1.25	0%	85%	85%	0%	0%	0%	100%	70%	100%	0%	0%	25%	75%	75%	0%	70%	70%	30%
		1.50	0%	95%	95%	0%	0%	0%	100%	75%	100%	0%	0%	45%	75%	80%	0%	70%	75%	45%
		1.75	0%	95%	95%	0%	0%	0%	100%	80%	100%	0%	0%	45%	85%	90%	0%	70%	80%	50%

Bridge	Revision	SF	Transverse Limit State Occurrence																	
			Ideal						Acceptable								Unacceptable			
			BF	SL	CL	RE	RY	RF	APY	APB	APS	PA	PPY	PPS	SM	CM	BU	SS	CS	APR
ClC15EA	Original Pier Columns	0.50	0%	100%	100%	100%	100%	0%	5%	0%	0%	0%	0%	0%	95%	100%	0%	0%	45%	0%
		0.75	0%	100%	100%	100%	100%	0%	65%	0%	15%	0%	0%	0%	100%	100%	0%	5%	85%	0%
		1.00	0%	100%	100%	100%	100%	0%	75%	15%	55%	0%	0%	0%	100%	100%	0%	35%	100%	0%
		1.25	0%	100%	100%	100%	100%	0%	80%	15%	65%	0%	0%	0%	100%	100%	0%	30%	100%	5%
		1.50	0%	100%	100%	100%	100%	0%	100%	30%	75%	0%	0%	0%	100%	100%	0%	40%	100%	5%
		1.75	0%	100%	100%	100%	100%	0%	100%	35%	80%	0%	0%	0%	100%	100%	0%	45%	100%	5%
	Revised Pier Columns	0.50	0%	100%	100%	100%	100%	95%	65%	0%	35%	0%	0%	0%	5%	10%	0%	0%	0%	0%
		0.75	0%	100%	100%	100%	100%	100%	85%	20%	65%	0%	0%	0%	55%	60%	0%	40%	55%	0%
		1.00	0%	100%	100%	100%	100%	100%	85%	35%	75%	0%	0%	0%	80%	90%	0%	60%	60%	10%
		1.25	0%	100%	100%	100%	100%	100%	90%	50%	80%	0%	0%	0%	90%	100%	0%	70%	80%	10%
		1.50	0%	100%	100%	100%	100%	100%	100%	45%	90%	0%	0%	0%	95%	100%	0%	75%	85%	15%
		1.75	0%	100%	100%	100%	100%	100%	100%	65%	100%	0%	0%	0%	85%	95%	0%	80%	85%	20%

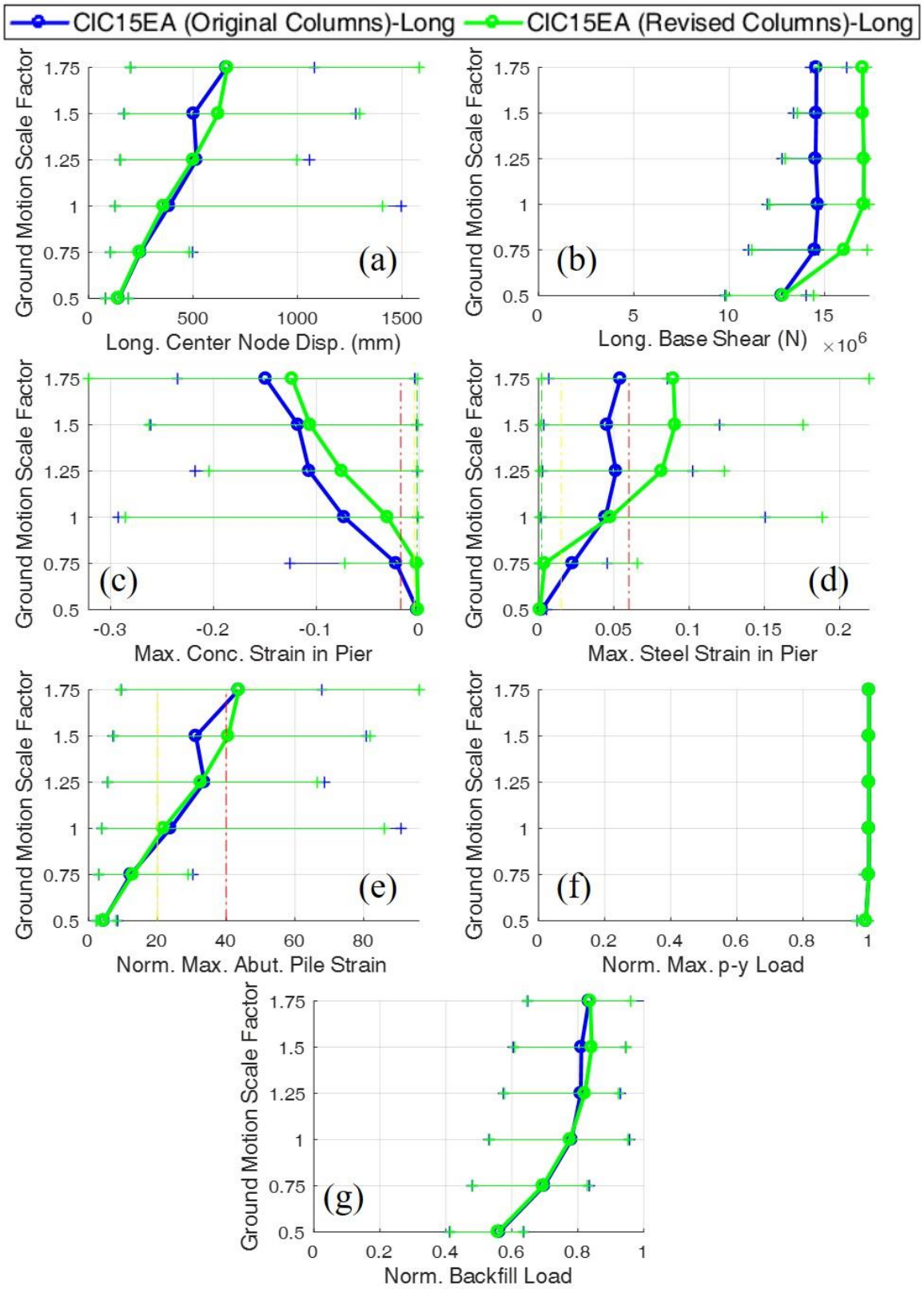

Figure 9.12: IDA plots for the original and enhanced ClC15EA in the longitudinal direction where a scale factor of 1.00 represents the design-level.

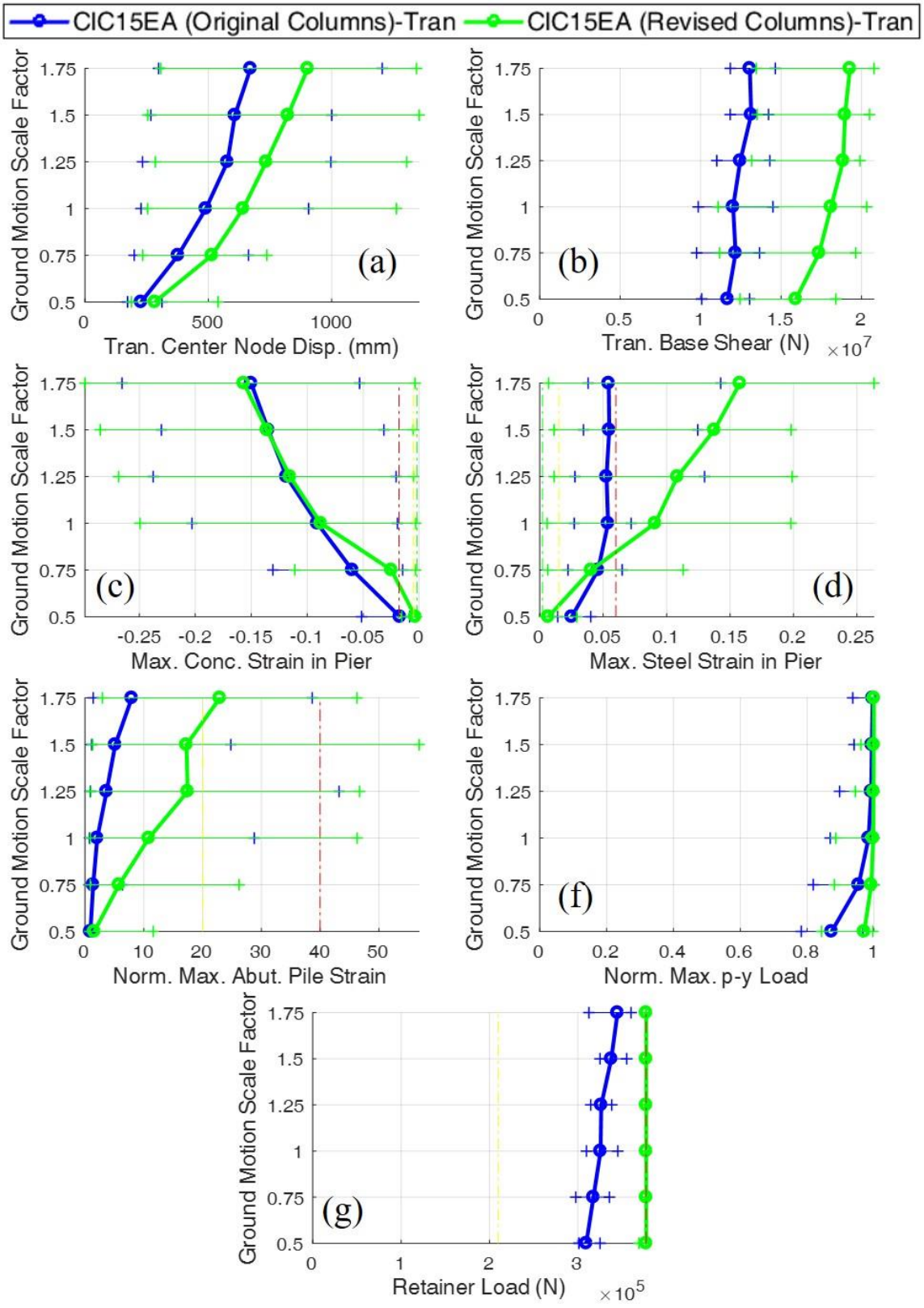

Figure 9.13: IDA plots for the original and enhanced ClC15EA in the transverse direction where a scale factor of 1.00 represents the design-level.

9.4.3 Overall Observations

The sequence of damage of CtC15EA and ClC15EA in both directions is presented in Fig. 9.14. In general the CtC15EA enhanced designs perform better than the original designs, though the issue with occurrences of APY/APS at low scale factors persists. There is more benefit to the CtC15EA IAB in the transverse direction (Fig. 9.14c) where moderate (SM/CM) and severe (SS/CS) pier column damage is relegated to the largest scale factor. This is better than having SS/CS occur at the design-level scale factor of 1.0 as it does in the original design. Bearing unseating (BU) does occur at a scale factor of 1.25 in the enhanced design, but this is still an improvement on having an unacceptable limit state occur at a scale factor of 1.0

Conversely, there is no major benefit to increasing the pier column size for ClC15EA in either direction. This is largely due to the increased flexibility of the four-span IAB, especially in the transverse direction, leading to pier column load demands still too large for the enhanced design to accommodate. The sequences of damage are nearly identical with the exception of BF and PA not occurring in the enhanced design in the longitudinal direction in Fig. 9.14b, and the APB, SS/CS and APR limit states differing in the transverse direction in Fig. 9.14d.

Overall, the larger piers do seem to help decrease pier column damage in both directions. However, a main stipulation to this is that they only help if they are strong enough to accommodate the demand in the pier columns. As shown in the ClC15EA enhanced design, when the columns are not strong enough to accommodate the design then there is no benefit. As such, longer span IABs will require more robust pier columns due to the increased demand on the piers. Additionally, if the pier columns can accommodate the demand, then retainer damage is likely to increase and the chance of bearing unseating increases as well.

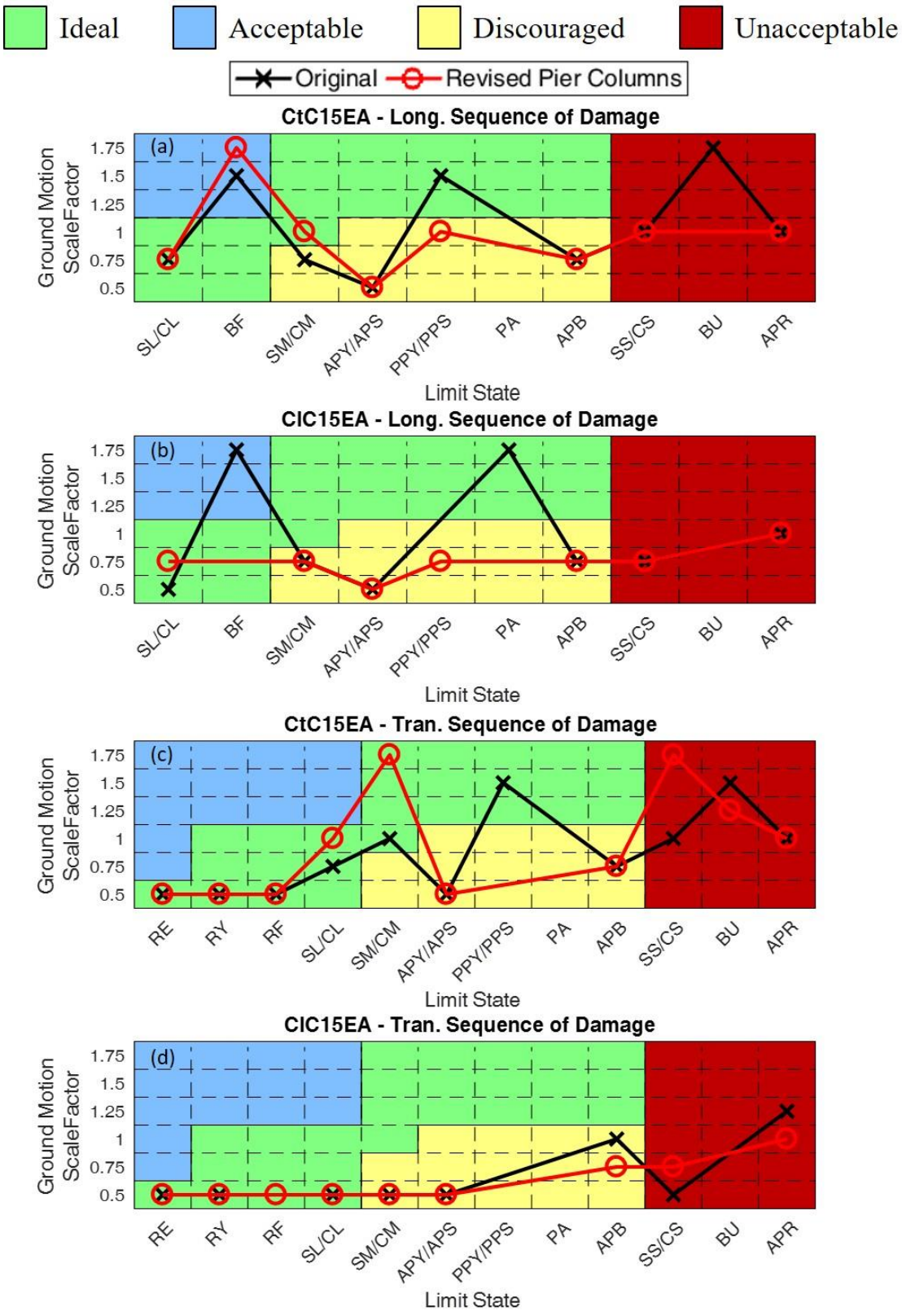

Figure 9.14: Sequences of damage for the IABs with various pier column designs where a scale factor of 1.00 represents the design-level.

9.5 INCREASING BACKFILL CONTRIBUTION

A common concern in many of the IAB analyses performed in Chapter 7 is the consistent yielding, local buckling, and rupture of the abutment piles and mobilization of the soil surrounding the abutment piles at low intensities of shaking. While not unacceptable, these limit states are not desired since they are difficult to identify and repair. The worst abutment foundation damage (either pile damage or mobilization of the soil surrounding the piles) occurs in IABs with concrete superstructures and tall piers. The concrete superstructures are heavier than the steel superstructures, which increases total lateral force in the system during earthquakes. The use of tall piers creates larger abutment foundation damage due to the relative flexibility of the piers decreasing the force in the piers and increasing the force demand that is resisted by the abutments.

Additionally, although abutment foundation damage frequently occurs, backfill mobilization rarely occurs in the longitudinal direction. The enhanced designs in this section look to increase the backfill contribution to force resistance in order to decrease the amount of force resisted by the abutment foundation. This is accomplished by increasing the height of the pile cap-backfill contact surface from 42 in to 84 in, as shown in Fig. 9.15. The entire pile cap height is not increased due to the desire not to increase the stiffness of the abutment piles.

The revised abutment pile cap design is applied to CtC40EA and ClC40EA, both of which have concrete superstructures and 40-ft tall piers. CtC40EA experiences significant amounts of abutment pile yielding (APY), local buckling (APB), rupture (APR), and soil mobilization (APS) with APY occurring in all of the analyses at all scale factors and APS occurring nearly all the time with a minimum rate of occurrence of 75%. Increasing the height of the backfill contact surface increases the total ultimate capacity for the backfill soil at each abutment from 6.147 MN to 11.75 MN. Similarly, ClC40EA experiences large amounts of APY and APS with APY always occurring

and the lowest frequency of APS occurrences is 90%. However, the occurrence of limit states describing further damage to the abutment piles (APB and APR) decreases from CtC40EA. The increased backfill contact surface height leads to an ultimate backfill soil capacity of 14.75 MN in the enhanced design as compared to 8.269 MN from the original design.

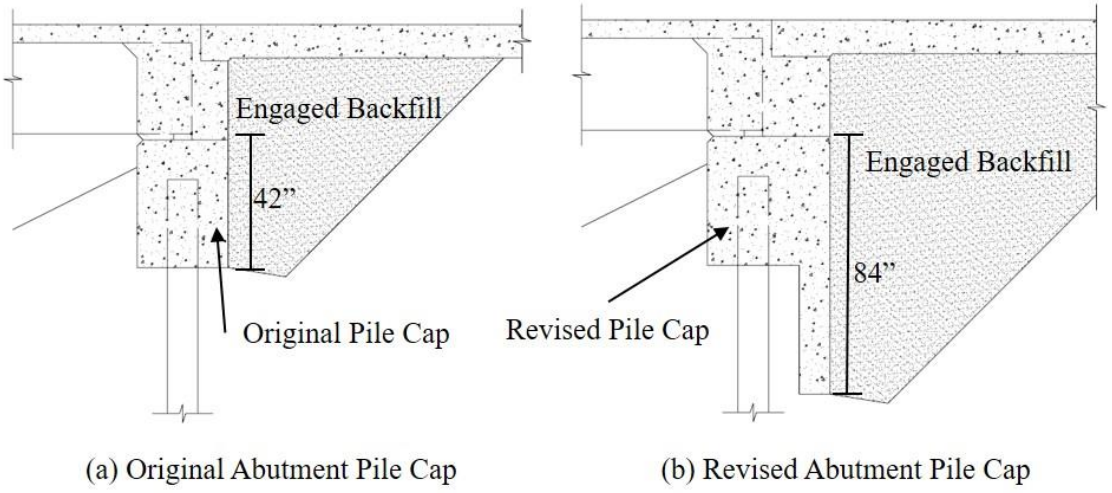

(a) Original Abutment Pile Cap (b) Revised Abutment Pile Cap

Figure 9.15: Original and revised abutment pile cap designs.

The implementation of the revised abutment pile cap design presented in Fig. 9.15 is purely conceptual given the increased difficulty to constructability that it would pose. However, the concept of increasing backfill engagement by increasing the backfill-pile cap contact area is plausible. So, despite the unlikeliness of the revised design being used in actual IABs, the analyses will yield results which are important in understanding whether increasing the pile cap size aids in increasing backfill engagement.

It should be noted that the lack of backfill mobilization may be less of a concern if temperature effects are considered prior to an earthquake occurring. Temperature changes will produce a ratcheting effect in the abutments by causing a gap behind the abutment which will be filled by loose backfill during cold temperatures. When temperatures rise the backfill will already be engaged and the loads in the backfill at a normal operating temperature will be larger than those

determined in this study. This means that the backfill will be more likely to mobilize should the effects of temperature cycles be considered.

9.5.1 Pushover Results

As expected, in Fig. 9.16b and 9.16d there is shown to be no difference in the transverse direction behavior of the designs. This is due to backfill mainly contributing to behavior in the longitudinal direction. The longitudinal results for both IABs (Fig. 9.16a and 9.16c) have similar responses between the original and enhanced designs. The enhanced designs tend to have larger force capacities, as is expected due to the increased backfill force capacity. The longitudinal results also demonstrate that the order of limit state occurrences between the original and enhanced designs are identical with limit states occurring at approximately the same center node displacements. Note that although there are larger forces resisted by the backfill, the increased ultimate capacity of the backfill leads to backfill mobilization (BF) continuing to not occur in the revised designs.

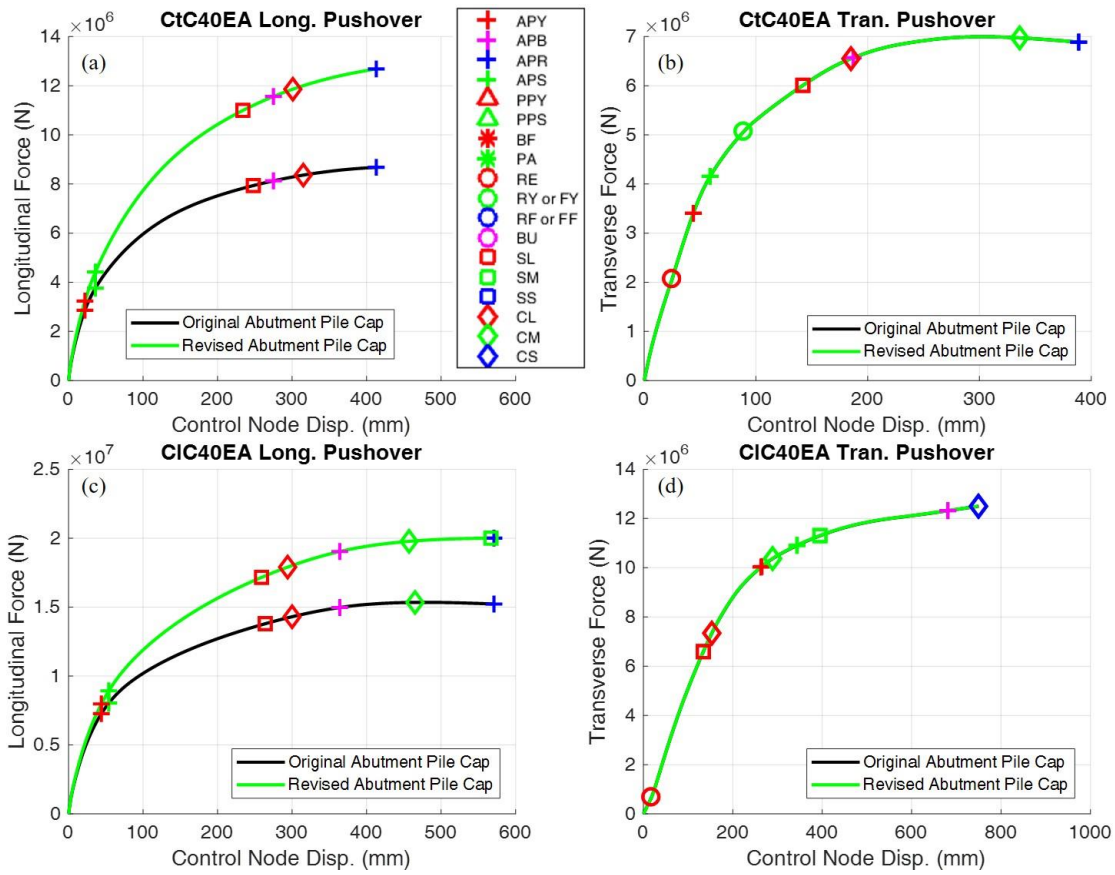

Figure 9.16: Pushover analysis results for IABs with various abutment pile cap designs.

9.5.2 IDA Results

The frequency of limit state occurrence for the original and enhanced design of CtC40EA is presented in Table 9.8 where it shows that there is no difference in the transverse behavior. The component behavior during the longitudinal IDA are also presented in Fig. 9.17. From Fig. 9.17e it can be observed that there is slightly less strain in the abutment piles in the enhanced design leading to less occurrences of APB and APR. Similarly, in Fig. 9.17f a very slight reduction in abutment soil p-y spring load at low scale factors can be observed in the enhanced designs. Unfortunately, the forces in the abutment foundations are still extremely large, leading to only a reduction in the occurrence of the APS limit states at the 0.5 scale factor when the enhanced design is used.

The increased backfill contribution does allow for more load in the bridge, as shown in Fig. 9.17b. The increased backfill contribution also increases the demand on the abutment and reduces the demand on the piers leading to less occurrences of pier damage in Table 9.8. Finally, Table 9.8 shows that the enhanced CtC40EA actually has less backfill mobilization (BF) occurrences. This is due to the increased backfill ultimate capacity. While the amount of force resisted by the backfill actually increases, the load-to-capacity ratio of the backfill (Fig. 9.17g) demonstrates that the enhanced design actually has the backfill further from mobilization than the original design.

The ClC40EA results and frequency of limit state occurrence (Fig. 9.18 and Table 9.9, respectively) also show a very slight decrease in pier damage (SL, CL, SM, CM, SS, and CS) in the longitudinal direction due to the increased stiffness of the abutments. Also, despite the increased force contribution from the backfill, the frequency of APY, APB, APR, and APS occurrences remain largely unchanged with the exception of APS at the 0.5 scale factor and some minor differences in APB and APR. In the IDA results plots for the abutment piles and abutment pile soil p-y load (Fig. 9.18e and 9.18f) there is very little difference between the behavior of the two designs. This is true for most of the component behaviors presented in Fig. 9.18. The main exceptions being the increased load in the bridge due to increased backfill capacity (Fig. 9.18b), and a change in backfill behavior values also due to the increased backfill capacity (Fig. 9.18g).

Table 9.8: Frequency of limit state occurrences for the CtC40EA IDA with original and revised abutment pile cap designs where a scale factor of 1.00 represents the design-level.

Bridge	Revision	SF	Longitudinal Limit State Occurrence																	
			Ideal						Acceptable								Unacceptable			
			BF	SL	CL	RE	RY	RF	APY	APB	APS	PA	PPY	PPS	SM	CM	BU	SS	CS	APR
CtC40EA	Original Abutment Pile Cap	0.50	0%	0%	0%	0%	0%	0%	100%	0%	75%	0%	0%	0%	0%	0%	0%	0%	0%	0%
		0.75	0%	55%	15%	0%	0%	0%	100%	45%	100%	0%	0%	5%	0%	0%	0%	0%	0%	0%
		1.00	0%	80%	75%	0%	0%	0%	100%	80%	100%	0%	0%	0%	20%	20%	0%	0%	0%	30%
		1.25	0%	85%	75%	0%	0%	0%	100%	85%	100%	0%	0%	20%	30%	50%	0%	0%	5%	70%
		1.50	10%	85%	75%	0%	0%	0%	100%	90%	100%	0%	5%	50%	50%	70%	0%	15%	20%	70%
		1.75	20%	90%	75%	0%	0%	0%	100%	90%	100%	0%	20%	30%	70%	70%	0%	20%	25%	70%
	Revised Abutment Pile Cap	0.50	0%	0%	0%	0%	0%	0%	100%	0%	45%	0%	0%	0%	0%	0%	0%	0%	0%	0%
		0.75	0%	20%	15%	0%	0%	0%	100%	0%	100%	0%	0%	0%	0%	0%	0%	0%	0%	0%
		1.00	0%	80%	55%	0%	0%	0%	100%	70%	100%	0%	0%	10%	0%	0%	0%	0%	0%	10%
		1.25	0%	95%	85%	0%	0%	0%	100%	90%	100%	0%	0%	35%	20%	35%	0%	0%	0%	35%
		1.50	0%	100%	85%	0%	0%	0%	100%	95%	100%	0%	0%	45%	65%	75%	0%	0%	15%	80%
		1.75	0%	100%	95%	0%	0%	0%	100%	100%	100%	0%	0%	60%	75%	80%	0%	5%	15%	80%

Bridge	Revision	SF	Transverse Limit State Occurrence																	
			Ideal						Acceptable								Unacceptable			
			BF	SL	CL	RE	RY	RF	APY	APB	APS	PA	PPY	PPS	SM	CM	BU	SS	CS	APR
CtC40EA	Original Abutment Pile Cap	0.50	0%	5%	0%	100%	100%	0%	100%	5%	80%	0%	0%	0%	0%	0%	0%	0%	0%	0%
		0.75	0%	85%	60%	100%	100%	0%	100%	75%	100%	0%	0%	0%	0%	0%	0%	0%	0%	0%
		1.00	0%	95%	80%	100%	100%	65%	100%	90%	100%	0%	0%	0%	25%	35%	0%	0%	0%	30%
		1.25	0%	100%	85%	100%	100%	85%	100%	100%	100%	0%	0%	0%	55%	65%	0%	0%	10%	70%
		1.50	0%	100%	90%	100%	100%	100%	100%	100%	100%	0%	0%	0%	65%	70%	0%	20%	20%	70%
		1.75	0%	100%	95%	100%	100%	100%	100%	100%	100%	0%	0%	0%	70%	75%	0%	20%	30%	75%
	Revised Abutment Pile Cap	0.50	0%	5%	0%	100%	100%	0%	100%	5%	80%	0%	0%	0%	0%	0%	0%	0%	0%	0%
		0.75	0%	85%	60%	100%	100%	0%	100%	75%	100%	0%	0%	0%	0%	0%	0%	0%	0%	0%
		1.00	0%	95%	80%	100%	100%	65%	100%	90%	100%	0%	0%	0%	25%	35%	0%	0%	0%	30%
		1.25	0%	100%	85%	100%	100%	85%	100%	100%	100%	0%	0%	0%	55%	65%	0%	0%	10%	70%
		1.50	0%	100%	90%	100%	100%	100%	100%	100%	100%	0%	0%	0%	65%	70%	0%	20%	20%	70%
		1.75	0%	100%	95%	100%	100%	100%	100%	100%	100%	0%	0%	0%	75%	75%	0%	20%	30%	75%

Table 9.9: Frequency of limit state occurrences for the ClC40EA IDA with original and revised abutment pile cap designs where a scale factor of 1.00 represents the design-level.

Bridge	Revision	SF	Longitudinal Limit State Occurrence																	
			Ideal						Acceptable								Unacceptable			
			BF	SL	CL	RE	RY	RF	APY	APB	APS	PA	PPY	PPS	SM	CM	BU	SS	CS	APR
ClC40EA	Original Abutment Pile Cap	0.50	0%	5%	0%	0%	0%	0%	100%	0%	90%	0%	0%	0%	0%	0%	0%	0%	0%	0%
		0.75	0%	75%	60%	0%	0%	0%	100%	30%	100%	0%	0%	0%	10%	20%	0%	0%	0%	0%
		1.00	0%	75%	70%	0%	0%	0%	100%	60%	100%	0%	0%	0%	20%	35%	0%	0%	0%	10%
		1.25	10%	80%	75%	0%	0%	0%	100%	70%	100%	0%	0%	0%	35%	60%	0%	10%	20%	30%
		1.50	15%	85%	80%	0%	0%	0%	100%	70%	100%	0%	5%	5%	45%	70%	0%	15%	30%	35%
		1.75	15%	90%	90%	0%	0%	0%	100%	80%	100%	0%	5%	5%	50%	70%	0%	15%	30%	40%
	Revised Abutment Pile Cap	0.50	0%	0%	0%	0%	0%	0%	100%	0%	80%	0%	0%	0%	0%	0%	0%	0%	0%	0%
		0.75	0%	65%	50%	0%	0%	0%	100%	25%	100%	0%	0%	0%	0%	15%	0%	0%	0%	0%
		1.00	0%	80%	80%	0%	0%	0%	100%	70%	100%	0%	0%	0%	30%	40%	0%	0%	0%	15%
		1.25	0%	80%	80%	0%	0%	0%	100%	70%	100%	0%	0%	0%	45%	70%	0%	0%	5%	30%
		1.50	0%	90%	80%	0%	0%	0%	100%	70%	100%	0%	0%	0%	60%	70%	0%	10%	25%	50%
		1.75	10%	90%	90%	0%	0%	0%	100%	80%	100%	10%	10%	5%	70%	70%	0%	20%	35%	60%

Bridge	Revision	SF	Transverse Limit State Occurrence																	
			Ideal						Acceptable								Unacceptable			
			BF	SL	CL	RE	RY	RF	APY	APB	APS	PA	PPY	PPS	SM	CM	BU	SS	CS	APR
ClC40EA	Original Abutment Pile Cap	0.50	0%	100%	90%	100%	100%	0%	55%	0%	20%	0%	0%	0%	40%	55%	0%	0%	5%	0%
		0.75	0%	100%	100%	100%	100%	0%	75%	20%	55%	0%	0%	0%	65%	75%	0%	0%	10%	0%
		1.00	0%	100%	100%	100%	100%	0%	100%	20%	85%	0%	0%	0%	75%	90%	0%	0%	25%	20%
		1.25	0%	100%	100%	100%	100%	0%	100%	30%	90%	0%	0%	0%	95%	100%	0%	20%	35%	20%
		1.50	0%	100%	100%	100%	100%	0%	100%	35%	95%	0%	0%	0%	100%	100%	0%	20%	50%	20%
		1.75	0%	100%	100%	100%	100%	0%	100%	50%	100%	0%	0%	0%	100%	100%	0%	20%	60%	30%
	Revised Abutment Pile Cap	0.50	0%	100%	90%	100%	100%	0%	55%	0%	20%	0%	0%	0%	40%	55%	0%	0%	5%	0%
		0.75	0%	100%	100%	100%	100%	0%	75%	20%	55%	0%	0%	0%	65%	75%	0%	0%	10%	0%
		1.00	0%	100%	100%	100%	100%	0%	95%	20%	85%	0%	0%	0%	75%	90%	0%	0%	25%	20%
		1.25	0%	100%	100%	100%	100%	0%	100%	30%	90%	0%	0%	0%	95%	100%	0%	20%	40%	20%
		1.50	0%	100%	100%	100%	100%	0%	100%	35%	95%	0%	0%	0%	100%	100%	0%	20%	50%	20%
		1.75	0%	100%	100%	100%	100%	0%	100%	50%	100%	0%	0%	0%	100%	100%	0%	20%	60%	30%

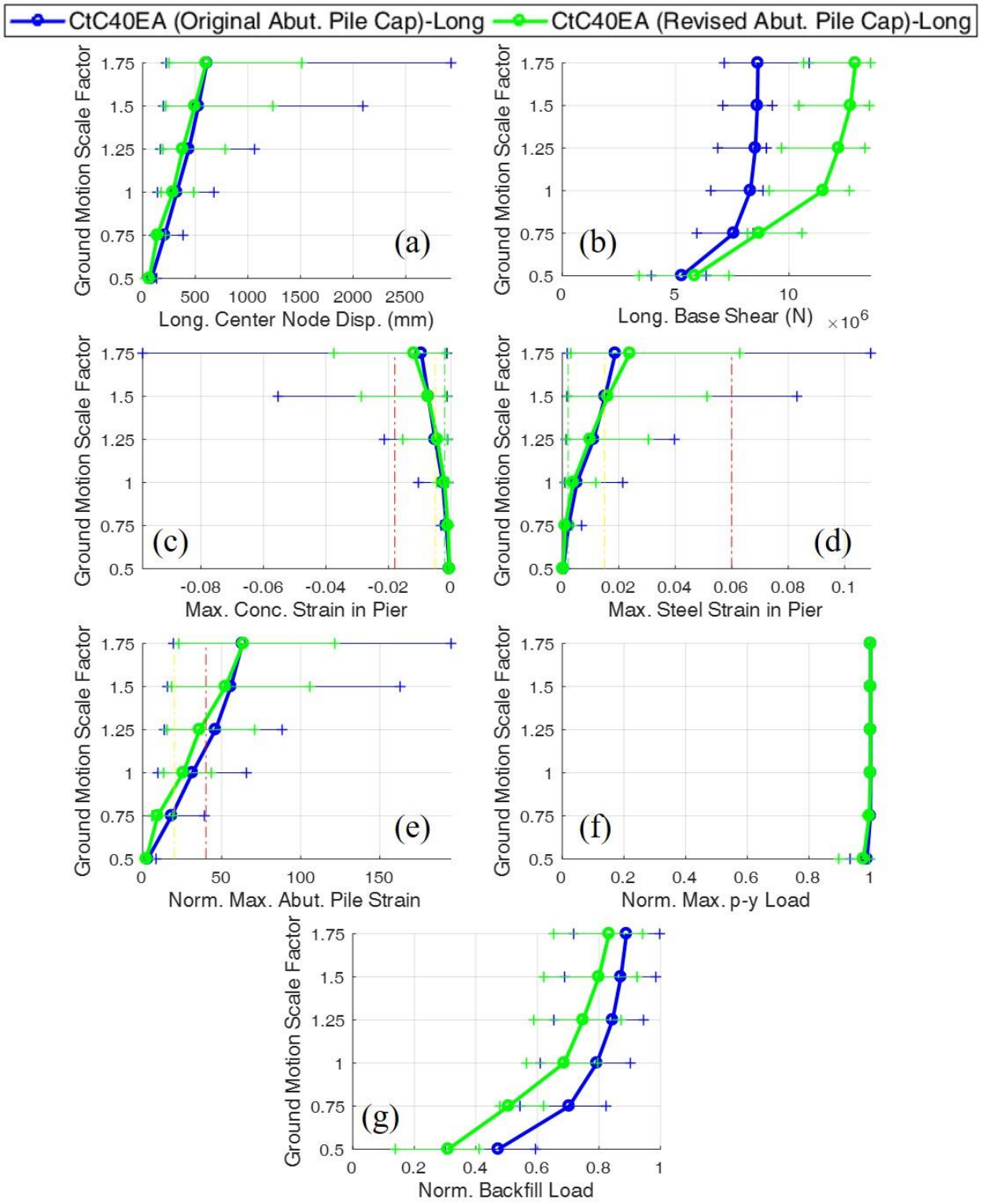

Figure 9.17: IDA plots for the original and enhanced CtC40EA in the longitudinal direction where a scale factor of 1.00 represents the design-level.

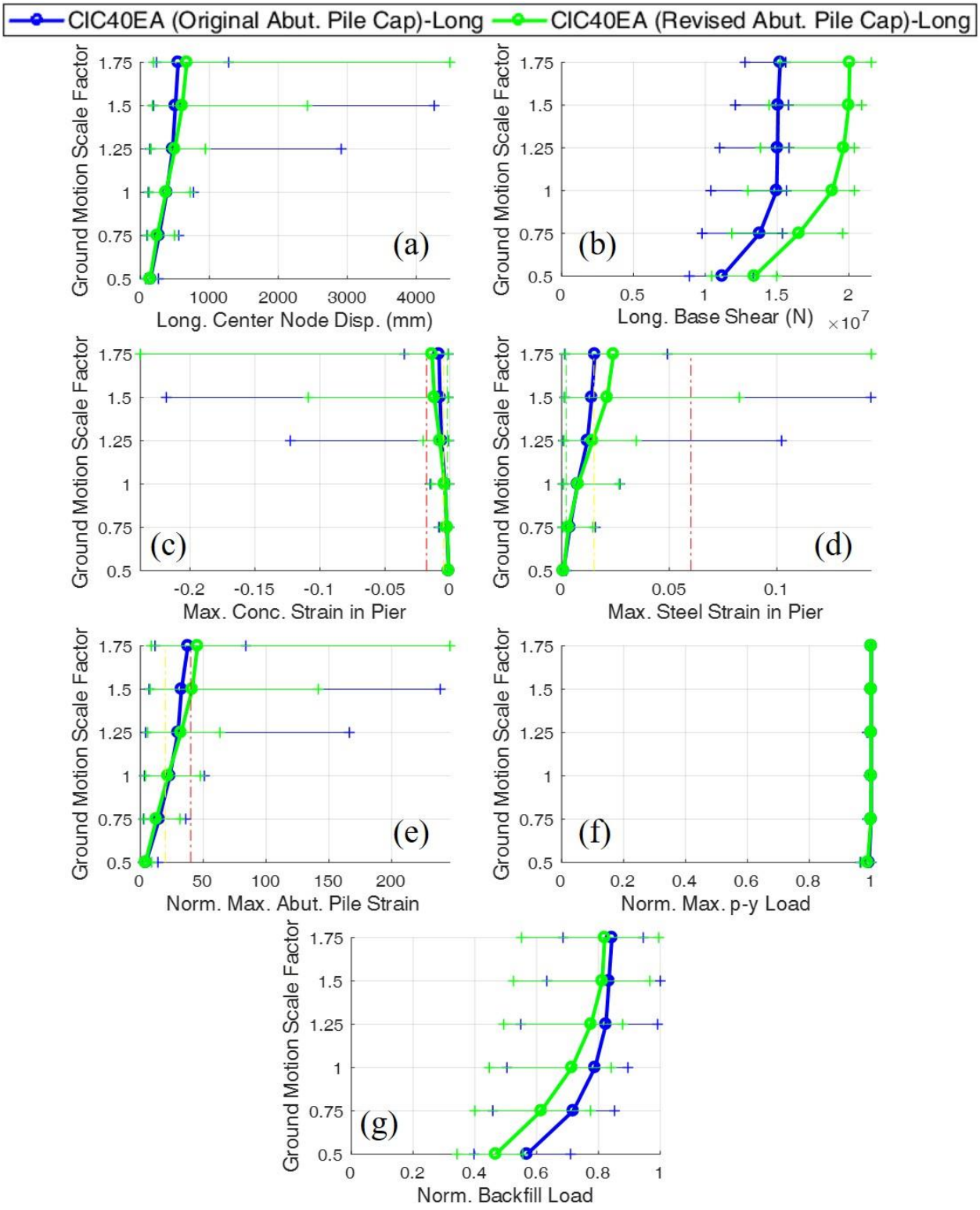

Figure 9.18: IDA plots for the original and enhanced ClC40EA in the longitudinal direction where a scale factor of 1.00 represents the design-level.

9.5.3 Overall Observations

The sequences of damage in the longitudinal direction for CtC40EA and ClC40EA with various abutment pile cap designs is presented in Fig. 9.19. The enhanced designs do provide better results than the original designs in both cases. However, the occurrence of APY/APS at a scale factor of 0.5 still occurs as well as APB and APR occurring at small scale factors. This is very concerning as increasing the backfill contribution was intended to reduce the damage in the abutment foundations. This slightly occurred, as indicated by the change in location of APB in Fig. 9.19a, but the forces in the abutment foundation were too large to be counteracted by redesigning the pile cap alone.

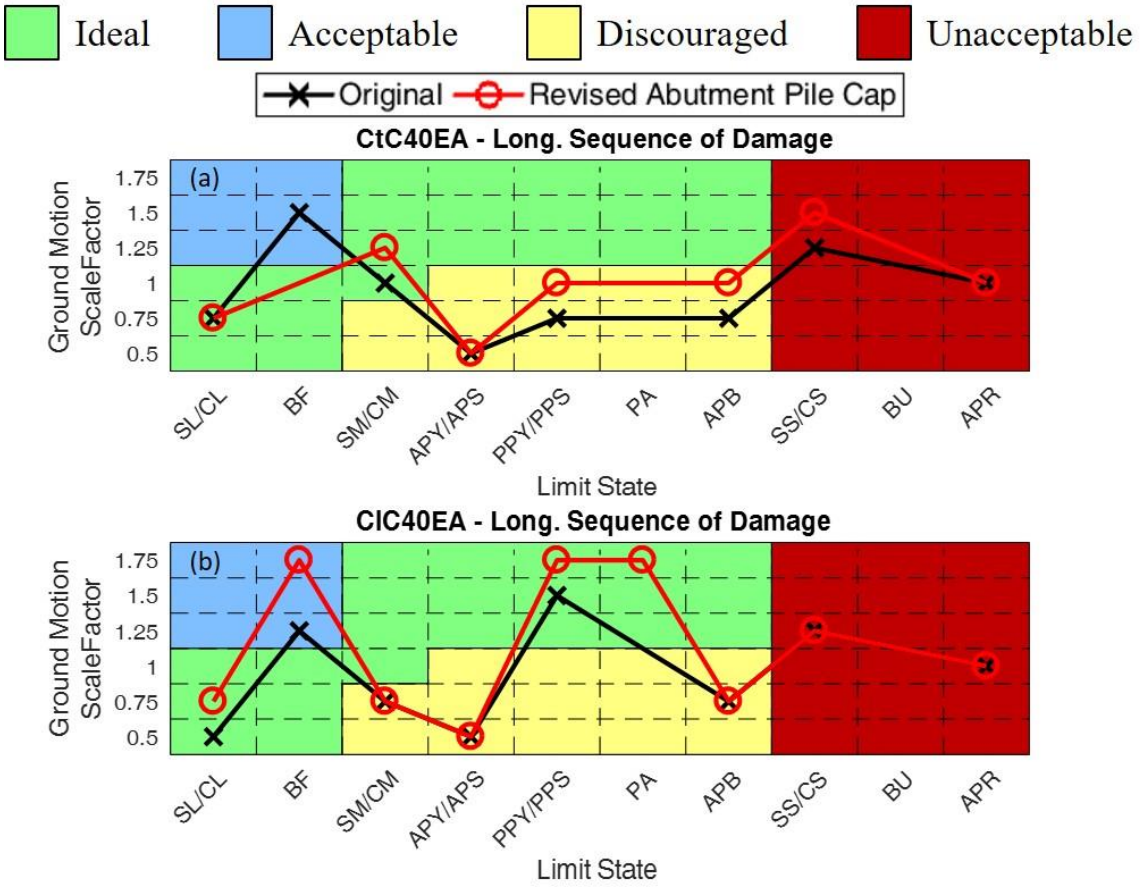

Figure 9.19: Sequences of damage for the IABs with various abutment pile cap designs where a scale factor of 1.00 represents the design-level.

The increased backfill contribution did have an effect on pier behavior by increasing the stiffness and force demand in the abutments and consequently reducing the force demand in the pier columns slightly. This effect is much more pronounced in the three-span IAB due to the already low demand in those piers. Overall, this effect is helpful, by increasing the stiffness in the abutments further, pier column damage can be reduced.

9.6 FINAL DESIGN ENHANCEMENT RECOMMENDATIONS

The potential design enhancements discussed in this chapter lead to recommendations on ameliorating the seismic performance of IABs. Recall that the design enhancements explored in this chapter applied only for the site of Cairo, IL and the immediate vicinity in seismic performance zone (SPZ) 4. SPZ 3 and SPZ 2 may require enhancements of the same manner, but to a lesser extent to those presented.

The first enhancement explored concerned the reduction of number of elastomeric bearing side retainers used in each pier. It was found that in three-span IABs with tall bridges there is a slight benefit to reducing the number of retainers, Unfortunately, even reducing the number of retainers to the minimum of two is not a viable method of ensuring the retainers fuse before pier column concrete spalling. The retainers may additionally be weakened by reducing the size of the anchor bolts, which further decreases the amount of damage in the piers, however in some scenarios even this is insufficient in weakening the retainers such that they fuse before the columns. The main trend in these analyses revealed that the current pier column designs were too weak to allow for any retainer design changes to cause retainer fusing to occur before pier column concrete spalling (moderate pier column damage). This means that retainer design change alone is not sufficient to mitigate damage in the piers.

Similar conclusions are reached when the fixed bearings are weakened by reducing anchor bolt sizes. It is found that the current pier column designs are once again too weak to allow for IAB behavior to be significantly affected by changes to the fixed bearing design. It is shown that under ideal circumstances when an IAB with low pier column load demands (three-span, tall pier) and the smallest allowable anchor bolts (5/8-in diameter), fixed bearing fusing occurs slightly before concrete spalling in the columns occurs. An improvement in pier column behavior is observed in this scenario, however it is not substantial. This leads to the conclusion that reducing the fixed bearing anchor bolt size alone is not sufficient to ensure the protection of the columns.

As noted in the scenarios involving retainers and fixed bearings, the weak columns are consistently an issue. Analyses on IABs with different pier column designs led to some useful conclusions. The first is that strengthening the columns does help the pier columns avoid moderate and severe damage. However, the damage is now in the retainers, which fracture easily and cause an increase in bearing unseating occurrences. Additionally, the piers are shown to require much stronger columns in longer-span bridges. This last point helps to address the increased flexibility in the transverse direction of four-span IABs.

Recommendations based on the first three enhancements (retainers, fixed bearings, and pier columns) go beyond ensuring larger pier columns for longer span bridges in the future. It was shown that reducing the retainer or fixed bearing strength alone does not provide a viable solution, however used in conjunction with strengthened pier columns may help. A recommendation for the future would be to design the retainers/fixed bearings in conjunction with the pier columns. This would allow a compromise to be achieved such that the retainers are sufficiently weak enough to fuse before concrete spalling occurs, yet strong enough to not fuse early and allow for bearing unseating to occur. Additionally, bearing size could be modified to discourage bearing unseating.

Finally, increasing the backfill contribution by increasing the size of the backfill-abutment contact area is shown to reduce forces in the abutment piles in three-span bridges. Unfortunately, the increase of the pile cap height by a factor of two is still insufficient to reduce abutment foundation damage substantially. A recommendation for future designs would be to increase backfill contribution in another way to further reduce abutment foundation damage. This could be achieved through greater compaction of the backfill causing it to be stiffer or continuing to increase the backfill-abutment contact area through other means.

CHAPTER 10: CONCLUSIONS AND FUTURE WORK

10.1 SUMMARY OF OBJECTIVES AND SCOPE OF THE RESEARCH

The research presented in this dissertation accomplishes the research objectives and tasks associated with seismic assessments of integral abutment bridges in southern Illinois. These objectives and tasks advanced the research associated with the ICT-R27-133 project, *Calibration and Refinement of Illinois' Earthquake Resisting System Bridge Design Methodology: Phase II*. The research expands the number of bridge types investigated in the ICT-R27-133 project by providing information concerning IAB seismic behavior while previous iterations of the project had focused solely on stub abutment bridges. The inclusion of IABs in the scope of bridges investigated in the ICT-R27-133 project is essential in accurately representing the inventory of bridges in Illinois due to the popularity of IABs. The conclusions from this research are used to provide seismic assessments and seismic design enhancements to fulfill the goal of the ICT-R27-133 project of calibrating and refining the seismic design methodology of bridges in Illinois.

The research presented in this dissertation focused on developing ground motion records for southern Illinois, developing a framework for modeling Illinois IABs in *OpenSees*, identifying critical limit states of components within IABs during earthquakes, contributing to a more comprehensive and complete understanding of IAB seismic behavior, and developing insight and recommendations for current Illinois IAB designs to improve seismic behavior.

Ground motion records were developed for ten sites within southern Illinois with a 1000-year return period hazard level. The ground motions were developed by modifying existing recorded and synthetic ground motion time histories for central North America such that they match appropriate spectral properties of the conditional mean spectra (CMS) in southern Illinois.

The existing time histories were matched to the CMS at the bedrock level then propagated through soil profiles representative of two common soil conditions in southern Illinois. The soil profiles were developed using exiting boring log data from previous bridge construction details. The surface-level ground motions are useful in the assessment of IABs and other bridges in southern Illinois since they have accurate intensity measures for the AASHTO design-level hazard of a 1000-year return period, and since they excite bridges of various fundamental periods. The developed ground motions expand the limited collection of ground motion time histories available for the area and provides resources for researchers and designers to conduct dynamic analyses of structures in southern Illinois.

The ground motions developed for southern Illinois are an important contribution of this study, however the primary focus of this research dealt with the seismic assessment of and design enhancement for IABs. These assessments and the subsequent recommendations for design enhancement were achieved using nonlinear IAB models in *OpenSees*, which accurately represent IAB components through models that are based on experimentation and literature. The modeled components within the IABs included piles in the pier and abutment foundations, the pile-soil interaction in the pier and abutment foundations (through p-y and t-z springs), the abutment backfill soil, the elastomeric bearings, side retainers, and fixed bearings between the superstructure and piers, and the pier columns. Key limit states were monitored within the modeled components throughout the analyses such that representative levels of damage within the IABs were identified. The damage and limit state classification were used to assess whether the IAB design is ideal, acceptable, or unacceptable under the subjected ground motions.

The IABs in this research were developed and designed in consultation with IDOT to achieve realistic IAB designs for southern Illinois. Five main types of IABs were studied; single-

span steel superstructure (Ss), three-span steel superstructure (St), four-span steel superstructure (Sl), three-span prestressed precast concrete (PPC, often referred to simply as concrete) superstructure (Ct) and four-span PPC superstructure (Cl). Along with these variations, additional variations were introduced to the pier height (15-ft or 40-ft tall), bearing layout (all type I elastomeric or all fixed), and foundation soil type (soft, stiff, or alluvial/non-alluvial). These variations were used to create a parametric study that involved 51 bridge variations.

The 51 IABs of the parametric study were analyzed using both static pushover analyses and dynamic analyses. These analyses allowed for trends within the bridge variations to be identified. The dynamic analyses also facilitated observations concerning critical components during design-level earthquakes at Cairo, IL where there is the largest seismic hazard in the state. These observations are important in achieving the objective of contributing to a more comprehensive and complete understanding of IAB seismic behavior. Subjecting entire IAB models to dynamic loads allowed for interactions between components to be observed. This interaction behavior has often been neglected in previous IAB studies. Incremental dynamic analyses (IDA) were also performed to determine the areas of concern in the IABs at intensity levels other than the design-level earthquake.

Recommendations were developed based on the static pushover and dynamic analysis results. These recommendations sought to minimize any potentially catastrophic damage which could occur during earthquakes in Cairo. Additionally, IABs at sites other than Cairo were analyzed to evaluate the applicability of the recommendations developed for Cairo to other regions of Illinois. These recommendations and observations increase the understanding of IAB seismic behavior not only in Illinois but in other locations as well due to the relative scarcity of IAB seismic research.

10.2 OVERALL CONCLUSIONS

The conclusions from the pushover analyses of Chapter 6 and dynamic analyses, including incremental dynamic analyses, of Chapter 7 are important contributions towards better understanding the seismic behavior of IABs. Unlike most past seismic IAB studies, the models in this study accounted for numerous components throughout the IAB and allowed for interactions between the components. In general, it was determined that the piers, abutment foundations, and bearings/retainers were the most important components with respect to seismic behavior. More detailed observations and conclusions are presented below:

- Moderate pier column damage, typically initiated by the onset of concrete spalling in the pier column concrete, usually corresponds to the peak load capacity of the bridge. This is shown to often occur before the fusing of retainers or fixed bearings leading to the pier columns becoming the fusing elements in the IAB. Ideally, the fracture of the retainers or fixed bearing anchor bolts would be the fusing elements by limiting the force transferred to the piers and saving the pier columns from severe damage. Retainers and fixed bearings are much easier and more economical to replace than entire piers. However, as indicated, current designs often have weak piers which allow for concrete spalling to occur before retainer or fixed bearing fusing. Even in analyses where retainer or fixed bearing fusing occurs, it is often accompanied by appreciable pier damage.
- Abutment foundations almost always experience significant damage through pile yielding and mobilization of the soil surrounding the piles. Damage to these components occurs in almost all the analyses, including the analyses with ground motion intensities half the magnitude of the design-level ground motions (scale factor of 0.5). The consistent occurrence of these limit

states is not ideal due to the difficulty in identifying and repairing or replacing the abutment piles.

- There is a small trade-off between abutment foundation damage and pier column damage. This is indicated through decreases in damage to abutment piles and soil when there is an increase in pier column damage and vice versa. These changes are evident between IABs with different pier heights and different span configurations. Shorter piers are stiffer than taller piers, and this increased stiffness in the shorter piers increases the force demand in the pier columns and leads to more damage. The increased proportion of the lateral force that is carried by the piers decreases the force resisted by the abutments, which usually leads to small decreases in the frequency of damage. Similarly, four-span IABs excited in the transverse direction experience greater pier force demands than three-span IABs excited in the transverse direction. This is due to the flexibility of the four-span IABs in the transverse direction, which limits load redistribution to the abutments. Load redistribution is easier in the three-span IABs as they are stiffer and have a shorter overall span, leading to less demand on the piers. The increased pier forces in four-span IABs leads to decreases in abutment force demands while three-span IABs see more abutment force demand and less pier force demand. Increases in the force demand typically correspond to increases in component damage, though this is often not observed in abutment foundation components since they frequently incur damage regardless of other parameter variations.
- Concrete superstructure IABs experience more damage than steel superstructure IABs. PPC girders weigh considerably more than the steel plate girders leading the overall deck weight to be 60% larger in the concrete three-span IABs and 66% larger in the concrete four-span IABs. The increased mass of the concrete superstructures leads to larger lateral loads under the same

ground accelerations. The increased lateral loads during seismic events means that there is increased forces and damage in most of the components. This leads to the conclusion that components in concrete IABs need to be more robust to accommodate the increased forces in the bridge.

10.3 OVERVIEW OF RECOMMENDATIONS

The conclusions described above led to further analyses concerning potential design enhancements to ameliorate the seismic behavior of IABs. Additionally, Chapter 8 investigated various sites within southern Illinois to determine how applicable any design revisions would be at sites other than Cairo. Design recommendations and comments concerning the applicability of the recommendations are listed below.

10.3.1 Design Recommendations

The design recommendations are based on the conclusions from the pushover and dynamic analyses of existing Illinois IAB designs in Chapters 6 and 7 along with the assessment of potential revisions to the current Illinois IAB designs explored in Chapter 9. Three main design recommendations, which were formed based on the conclusions from these chapters, are listed below:

- *Recommendation 1:* Longer span IABs require more robust columns than those with shorter spans.

  The current IAB designs adopted from IDOT details had identical pier columns for both the three- and four-span IABs with matching pier heights. This was shown to be a concern as the increased flexibility in the transverse direction of four-span IABs causes an increase in forces, and therefore damage, within the piers. It was also shown that by increasing the pier column size by identical amounts in both three-span and four-span IABs, the damage

to the three-span IABs is significantly reduced while damage to the four-span IAB is still frequent. While it is not ideal to have oversized columns in light of economy and unnecessary increases in bridge stiffness, the columns should accommodate the forces such that severe pier column damage is minimized. By this reasoning, increased pier forces in the longer span IABs requires more robust columns to resist the increased forces.

- *Recommendation 2:* Design the bearings, retainers, and piers as a system.

  Chapter 9 investigates the effects that individual design revisions have on the overall IAB seismic behavior. It was shown that reducing the number of side retainers per pier as well as reducing the size of the retainer and fixed bearing anchor bolts may allow for these components to fuse before pier column concrete spalling occurs. However, none of these revisions alone eliminate unacceptable limit state occurrences and sometimes the revisions have insignificant effects. Similarly, strengthening the pier columns allows for severe pier column damage to be reduced, however these changes alone are often not enough to completely eliminate unacceptable limit states. Two major issues that occur when pier columns are strengthened are the occurrence of pier column concrete spalling before retainer fusing, and bearing unseating after the retainers fuse. These issues can be remedied by either decreasing the retainer strength such that the retainers fuse before column concrete spalling occurs or increasing the retainer strength or bearing size such that bearing unseating is less likely. This formulates the recommendation that the piers, fixed bearings, elastomeric bearings, and retainers should be designed together such that the retainers/fixed bearings are weak enough to fuse before concrete spalling in the columns, yet strong enough to minimize bearing unseating.

- *Recommendation 3:* Increase the backfill contribution to limit abutment foundation damage.

  It was shown that increasing the backfill contribution, both strength and stiffness, increased the force resisted by the backfill and decreased the demand in the abutment foundation components. However, the studied method of achieving increased backfill contribution involved increasing the backfill-abutment contact area and demonstrated that this method alone is not sufficient to significantly reduce abutment foundation damage. In order to significantly decrease the amount of damage in the abutment foundations, increasing the strength and stiffness of the backfill through other means must be achieved. In addition to further increasing the backfill-abutment contact area, increasing the compaction of the backfill soil or ensuring a backfill soil which is stronger and stiffer should also be implemented.

10.3.2 Recommendation Applicability

The recommendations provided above are not necessarily needed for IABs in all regions of Illinois. Chapter 8 explored the seismic behavior of IABs in different seismic performance zones (SPZs) across southern Illinois and determined that recommendations formed for Cairo, which is in SPZ 4 and has the largest seismic hazard. Sites in SPZ 3 or SPZ 2, further to the north of SPZ 4, do not necessarily need revisions as severe as those for SPZ 4. However, while the recommendations are based on analyses at Cairo, it is reasonable to apply the recommendations to other similar sites within SPZ 4 as well.

Outside of SPZ 4, the recommendations are either needed to a lesser extent or not needed at all. In SPZ 3, which is just north of SPZ 4, it was shown that there are similar seismic behavior concerns in IABs to those in SPZ 4, yet the concerns are not as severe as those found in SPZ 4. For this reason it is suggested that the recommendations provided above are applicable to a lesser

extent. For example, the pier columns do need to be strengthened in SPZ 3 but not to the extent that they were strengthened for SPZ 4 IABs.

SPZ 2 is further north than SPZ 3 and IABs are found to have little unacceptable behavior during seismic events. This indicates that there is no need to apply any recommendations to SPZ 2 IABs due to their designs already being acceptable. Taking these recommendation applicability suggestions into account is an economic method of ensuring IAB seismic performance while not overdesigning bridges in any SPZ.

10.4 LIMITATIONS OF THE STUDY

The main limitation of this study stem from the lack of IAB experimental seismic studies and real-world case studies of seismic response to validate the overall IAB seismic behavior against. The lack of monitored IABs and the relative infrequency of earthquakes in southern Illinois contribute to this scarcity of data. There is some qualitative information concerning the behavior and damage found in IABs after earthquakes in New Zealand (Waldin *et al.*, 2012; Wood, 2015) and the observed damage to the piers and the abutment piles corresponds well with the damage occurring in the IAB models of this study. The model developed in this study does incorporate individual component experimental behavior when available.

10.5 FUTURE WORK

The research described in this dissertation expands the scope of knowledge concerning the seismic behavior of IABs and provides useful assessments of current Illinois IAB designs. Looking beyond the progress made as part of ICT-R27-133 project, *Calibration and Refinement of Illinois' Earthquake Resisting System Bridge Design Methodology: Phase II*, future directions of research based on the results of the study presented in this dissertation are provided below:

- As mentioned, the majority of this study entailed the assessment of current Illinois IAB designs to design-level ground motions. While some recommendations were proposed and analyzed, a much more detailed analysis of potential solutions to identified IAB seismic vulnerabilities is recommended for work in the future. This will allow for more detailed guidelines on how to design the bearings, retainers, and piers as a system. Further study of the recommended solutions and other damage mitigation techniques should also look into methods for increasing the backfill contribution in a feasible manner.
- An expansion of the parametric study is also suggested as a topic for future work. While many parameters were evaluated in the study discussed in this dissertation, there are still parameters which have not been investigated. Given the importance of the piers and abutment foundations, future parametric studies should include more options in terms of the pier configuration (wall or columns, number of columns) as well as the number of abutment piles and their orientation. The inclusion of various bridge skew angles and earthquake incident angles should also be included in future studies as IABs are often skewed and only ground motions occurring in two orthogonal directions (bridge transverse and longitudinal) were explored in this study. Design modifications such as including the potential nonlinear behavior of the superstructure elements should be included in the future parametric studies.
- Vertical ground motions should also be considered along with horizontal ground motions with varying incident angles in future parametric studies. The inclusion of vertical ground motions will allow for more realistic component behavior to be observed. The potential effects of vertical ground motions includes the t-z springs of the piles being engaged more and the decrease or increase in normal force in the bearings changing the fiction force between the bearings and pier caps during analyses.

- The seismic assessment of highway bridges in Illinois should also be expanded to include more types of bridges. Stub abutment bridges have been extensively studied by the ICT-R27-133 project and preceding projects (Steelman *et al.*, 2013; Filipov *et al.*, 2013a; Filipov *et al.*, 2013b; Steelman *et al.*, 2014; Steelman *et al.*, 2016; LaFave *et al.*, 2013a; LaFave *et al.*, 2013b; Luo *et al.*, 2016; Luo *et al.*, 2017), however there are other bridge types that have not been considered. Chief among these unconsidered bridge types is the semi-integral abutment bridge. Semi-integral abutment bridges are similar to IABs in that the abutment and superstructure are cast in a single pour, but they differ in that semi-integral abutments have a defined joint between the abutment and pile cap, which can accommodate different movements of the abutment and its foundation. Given the concerns in IABs related to the abutment foundation, having the ability to separate the abutment foundation from the behavior of the rest of the abutment and superstructure is worth exploring further.
- Beyond seismic assessments, the thermal effects of IABs should also be considered along with seismic effects in future studies. IAB thermal behavior has been studied extensively in Illinois, however the resulting damage from thermal effects has not been applied to IABs before an earthquake analysis takes place. This study considers the IABs studied to be without damage before an earthquake occurs. This is not always the case as temperature changes could have significant effects on bridge components leaving the bridge already damaged before an earthquake. IAB component effects of special interest when considering thermal effects before earthquake analysis is the yielding of the abutment piles and the engagement of the backfill. The latter is interesting due to a ratcheting effect from the contraction of IABs in colder temperatures allowing the backfill to fill the gaps created behind the abutment and increase the

stress in the backfill when temperatures rise again. This would cause the backfill to be significantly closer to mobilization before an earthquake strikes.

REFERENCES

AASHTO (2011) *Guide Specifications for LRFD Seismic Bridge Design*, American Association of State Highway and Transportation Officials, Washington, DC, USA.

AISC (2017) *Steel Construction Manual, 15th Edition*. American Institute of Steel Construction, Chicago, IL, USA.

Al Atik, L. and Abrahamson, N. (2010) "An improved method for nonstationary spectral matching," *Earthquake Spectra* **26**(3), 601-617.

Ambraseys, N.N., Douglas, J., Rinaldis, D., Berge-Thierry, C., Suhadolc, P., Costa, G., Sigbjornsson, R. and Smit, P. (2004) *Dissemination of European Strong-Motion Data, Col. 2. CD-ROM Collection*, Engineering and Physical Sciences Research Council, Swindon, UK.

API (2002) *Recommended Practice for Planning, Designing and Constructing Fixed Offshore Platforms – Working Stress Design*, American Petroleum Institute, Washington, DC, USA.

ASCE (2016) *ASCE 7-16: Minimum Design Loads for Buildings and Other Structures*, American Society of Civil Engineers, Reston, VA, USA.

Atkinson, G.M. and Boore, D.M. (2006) "Earthquake ground-motion prediction equations for Eastern North America," *Bulletin of the Seismological Society of America* **96**(6), 2181-2205.

Baker, J.W. (2011) "Conditional mean spectrum: Tool for ground motion selection," *Journal of Structural Engineering* **137**(3), 322-331.

Baker, J.W. and Cornell, C.A. (2006) "Spectral shape, epsilon and record selection," *Earthquake Engineering and Structural Dynamics* **35**(9), 1077-1095.

Baker, J.W. and Jayaram, N. (2008) "Correlation of spectral acceleration values from NGA ground motions models," *Earthquake Spectra* **24**(1), 299-317.

Banerjee A.K., Pramanik, D. and Roy, R. (2016) "Seismic structural fragilities: Proposals for improved methodology per spectral matching of accelerogram," *Engineering Structures* **111**, 538-551.

Berry, M.P., Lehman, D.E. and Lowes, L.N. (2008) "Lumped-Plasticity Models for Performance Simulation of Bridge Columns," *ACI Structural Journal* **105**(3), 270-279.

Boulanger, R.W., Curras, C.J., Kutter, B.L., Wilson, D.W. and Abghari, A. (1999) "Seismic Soil-Pile-Structure Interaction Experiments and Analyses," *Journal of Geotechnical and Geoenvironmental Engineering* **125**(9), 750-759.

Cimellaro, G.P. (2013) "Correlation in spectral accelerations for earthquakes in Europe," *Earthquake Engineering and Structural Dynamics* **42**(4), 623-633.

Coduto, D.P., Yeung, M.R. and Kitch, W.A. (2011) *Geotechnical Engineering: Principles and Practices*. Pearson Higher Education, Upper Saddle River, NJ, USA.

Daneshvar, P. Bouaanani, N. and Leger, P. (2014) "Application of conditional mean spectra for evaluation of a building's seismic response in Eastern Canada," *Canadian Journal of Civil Engineering* **41**(8), 7669-773.

Darendeli, M. (2001) "Development of a new family of normalized modulus reduction and material damping curves," Ph.D. Dissertation, University of Texas, Austin, TX, USA.

FEMA (2003) *FEMA 450-2: NEHRP Recommended Provisions for Seismic Regulations for New Buildings and Other Structures, Part 2: Commentary*, Federal Emergency Management Agency, Washington, DC, USA.

FEMA (2012) *FEMA P-58-1: Seismic Performance Assessment of Buildings, Volume 1 – Methodology*, Federal Emergency Management Agency, Washington, DC, USA.

Fernandez, J.A. and Rix, G.J. (2006) "Soil attenuation relationships and seismic hazard analyses in the upper Mississippi embayment," *Eighth U.S. National Conference on Earthquake Engineering*, San Francisco, CA, April.

Filipov, E.T., Fahnestock, L.A., Steelman, J.S., Hajjar, J.F., LaFave, J.M. and Foutch, D.A. (2013a) "Evaluation of quasi-isolated seismic bridge behavior using nonlinear bearing models," *Engineering Structures* **49**, 168-181.

Filipov, E.T., Revell, J.R., Fahnestock, L.A., LaFave, J.M., Hajjar, J.F., Foutch, D.A. and Steelman, J.S. (2013b) "Seismic performance of highway bridges with fusing bearing components for quasi-isolation," *Earthquake Engineering and Structural Dynamics* **42**, 1375-1394.

Franchin, P. and Pinto, P.E. (2014) "Performance-based seismic design of integral abutment bridges," *Bulletin of Earthquake Engineering* **12** 939-960.

Frosch, R.J., Kreger, M.E. and Talbott, A.M. (2009) *Earthquake Resistance of Integral Abutment Bridges*, Indiana Department of Transportation, West Lafayette, IN, USA.

Goulet, C.A., Kishida, T., Ancheta, T.D., Cramer, C.H., Darragh, R.B., Silva, W.J., Hashash, Y.M.A., Harmon, J., Stewart, J.P., Wooddell, K.E. and Youngs, R.R. (2014) *PEER Report No. 2014-17: PEER NGA-East Database*, Pacific Earthquake Engineering Research Center, University of California, Berkeley, CA, USA.

Groholski, D.R., Hashash, Y.M.A., Kim, B. and Musgrove, M. (2016) "Simplified model for small-strain nonlinearity and strength in 1D seismic site response analysis," *Journal of Geotechnical and Geoenvironmental Engineering* **142**(9), 04016042-1-14.

Hancock, J. Bommer, J.J. and Stafford, P.J. (2008) "Numbers of scaled and matched acceleragrams required for inelastic dynamic analyses," *Earthquake Engineering and Structural Dynamics* **37**(14), 1585-1607.

Hashash, Y. and Moon, S. (2011) *Site Amplification Factors for Deep Deposits and Their Application in Seismic Hazard Analysis for Central U.S.*, United States Geological Survey, Reston, VA, USA.

Hashash, Y.M.A., Kottke, A.R., Stewart, J.P., Campbell, K.W., Kim, B., Rathje, E.M., Silva, W.J., Nikolaou, S. and Moss, C. (2014) *PEER Report No, 2013-08: Reference Rock Site Condition for Central and Eastern North America, Part I – Velocity Definition*, Pacific Earthquake Engineering Research Center, University of California, Berkeley, CA, USA.

Hashash, Y.M.A., Abrahamson, N.A., Olson, S.M., Hague, S. and Kim, B. (2015a) "Conditional mean spectra in site-specific seismic hazard evaluation for a major river crossing in the Central United States," *Earthquake Spectra* **31**(1), 47-69.

Hashash, Y.M.A., Musgrove, M.I., Harmon, J.A., Groholski, D.R., Phillips, C.A. and Park, D. (2015b) *DEEPSOIL 6.0, User Manual*, University of Illinois, Urbana, IL, USA.

Herzog, B.L., Stiff, B.J., Chenoweth, C.A., Warner, K.L., Sievering, J.B. and Avery, C. (1994) *Buried Bedrock Surface of Illinois: ISGS GIS Database GISDB_BEDGEO. IL_Bedrock_Topography_1994_Ln*, Illinois State Geological Survey, Champaign, IL, USA.

Hettiarachchi, H. and Brown, T. (2009) "Use of SPT blow count to estimate shear strength properties of soils: Energy balance approach," *Journal of Geotechnical and Geoenvironmental Engineering* **135**(6), 830-834.

Holloway, K. (2012) "Illinois Integral Abutment Bridges: Behavior under Extreme Thermal Loading and Design Recommendations," M.S. Dissertation, University of Illinois, Urbana, IL, USA.

IDOT (2008) *Design Guides: 3.15 – Seismic Design*, Illinois Department of Transportation, Springfield, IL, USA.

IDOT (2012a) *Bridge Manual*, Illinois Department of Transportation, Springfield, IL, USA.

IDOT (2012b) *All Bridge Designers Memo 12.3: 2012 Integral Abutment Bridge Policies and Details*, Illinois Department of Transportation, Springfield, IL, USA.

IDOT (2014) *E-mail Communication 3/6/2014 to 6/13/2014*.

IDOT (2015a) *All Bridge Designers Memo 15.2: New Precast Prestressed Concrete IL-Beam Section and Revisions to the I-Beams and Bulb T-Beams*, Illinois Department of Transportation, Springfield, IL, USA.

IDOT (2015b) *All Bridge Designers Memo 15.6: New Elastomeric Bearing Sizes*, Illinois Department of Transportation, Springfield, IL, USA.

IDOT (2016) *IDOT Bridge Information System*, Illinois Department of Transportation, Springfield, IL, USA. Retrieved in 2016 from https://apps.dot.illinois.gov/bridgesinfosystem/search.aspx.

ISGS (2015) *Quaternary (Ice Age) Deposits Map*, Illinois State Geological Survey, Champaign, IL, USA.

Itani, A.M. and Pekcan, G. (2011) *Seismic Performance of Steel Plate Girder Bridges with Integral Abutments*, Federal Highway Administration, Washington, DC, USA.

Katsanos, E.I., Sextos, A.G. and Manolis, G.D. (2010) "Selection of earthquake ground motion records: A state-of-the-art review from a structural engineering perspective," *Soil Dynamics and Earthquake Engineering* **30**(4), 157-169.

Kim, W. and Laman, J.A. (2012) "Seven-Year Field Monitoring of Four Integral Abutment Bridges," *Journal of Performance of Constructed Facilities* **26**(1), 54-64.

Kong, B., Cai, C.S. and Kong, X. (2015) "Field monitoring study of an integral abutment bridge supported by prestressed precast concrete piles on soft soils," *Engineering Structures* **104**, 18-31.

Kotsoglou, A.N. and Pantazopoulou, S.J. (2009) "Assessment and modeling of embankment participation in the seismic response of integral abutment bridges," *Bulletin of Earthquake Engineering* **7**, 343-361.

Kowalsky, M.J. (2000) "Deformation limit states for circular reinforced concrete bridge columns," *Journal of Structural Engineering* **126**(8), 869-878.

Kowalsky, M.J., Priestly, M.J.N. and Seible, F. (1999) "Shear and flexural behavior of lightweight concrete bridge columns in seismic regions," *ACI Structural Journal* **96**, 135-148.

Kozak, D.L., Luo, J., Olson, S.M., LaFave, J.M. and Fahnestock, L.A. (2017a) "Modification of Ground Motions for Use in Central North America," *Journal of Earthquake Engineering*, dx.doi.org/10.1080/13632469.2017.1387190.

Kozak, D.L., Luo, J., Olson, S.M., LaFave, J.M. and Fahnestock, L.A. (2017b) *Report No. NSEL-048: Modification of ground motions for use in Central North America: southern Illinois surface ground motions for structural analysis*, Newmark Structural Engineering Laboratory Report Series, University of Illinois, Urbana, IL, USA. hdl.handle.net/2142/98456.

Kunin, J. and Alampalli, S. (1999) *Integral Abutment Bridges: Current practice in the United States and Canada*, New York State Department of Transportation, Albany, NY, USA.

LaFave, J.M., Riddle, J.K., Jarrett, M.W., Wright, B.A., Svatora, J.S., An, H. and Fahnestock, L.A. (2016) "Numerical Simulations of Steel Integral Abutment Bridges under Thermal Loading," *Journal of Bridge Engineering*, 04016061.

LaFave, J., Fahnestock, L., Foutch, D., Steelman, J., Revell, J., Filipov, E. and Hajjar, J. (2013a) *Seismic Performance of Quasi-Isolated Highway Bridges in Illinois*, Illinois Department of Transportation, Springfield, IL, USA.

LaFave, J., Fahnestock, L., Foutch, D., Steelman, J., Revell, J., Filipov, E. and Hajjar, J. (2013b) *Experimental Investigation of the Seismic Response of Bridge Bearings*, Illinois Department of Transportation, Springfield, IL, USA.

LaFave, J.M., Fahnestock, L.A., Brambila, G., Riddle, J.K., Jarrett, M.W., Svatora, J.S., Wright, B.A. and An, H. (2017) *Research Report No. FHWA-ICT-17-017: Integral Abutment Bridges under Thermal Loading: Field Monitoring and Analysis*, Illinois Center for Transportation, Rantoul, IL, USA.

Luo, J., Fahnestock, L.A., Kozak, D.L. and LaFave, J.M. (2016) "Seismic analysis incorporating detailed structure-abutment-foundation interaction for quasi-isolated highway bridges," *Structure and Infrastructure Engineering* **13**(5), 581-603.

Luo, J., Fahnestock, L.A. and LaFave, J.M. (2017) "Nonlinear static pushover and eigenvalue modal analyses of quasi-isolated highway bridges with seat-type abutments," *Structures* **12**, 145-167.

Matlock, H. (1970) "Correlation for Design of Laterally Loaded Piles in Soft Clay," *Offshore Technology Conference*, Houston, TX, April.

McGuire, R.K., Silva, W.J. and Costantino, C. (2001) *Report NUREG/CR-6728: Technical Basis for Revision of Regulatory Guidance on Design Ground Motions: Hazards- and Risk-Consistent Ground Motion Spectra Guidelines*, US Nuclear Regulatory Commission, Washington, DC, USA.

McKenna, F., Mazonni, S. and Fenves, G.L. (2006) *Open system for earthquake engineering simulation (OpenSees)*, Pacific Earthquake Engineering Research Center, University of California, Berkeley, CA, USA.

Naeim, F., Alimoradi, A. and Pezeshk, S. (2004) "Selection and scaling of ground motion time histories for structural design using genetic algorithms," *Earthquake Spectra* **20**(2), 413-426.

Olson, S.M., Long, J.H., Hansen, J.R., Renekis, D. and LaFave, J.M. (2009) *Modification of IDOT Integral Abutment Design Limitations and Details*, Illinois Department of Transportation, Springfield, IL, USA.

Olson, S.M., Holloway, K.P., Buenker, J.M., Long, J.H. and LaFave, J.M. (2013) *Thermal Behavior of IDOT Integral Abutment Bridges and Proposed Design Modifications*, Illinois Department of Transportation, Springfield, IL, USA.

Paraschos, A. and Made, A.M. (2011) "A survey on the status of use, problems, and costs associated with Integral Abutment Bridges," *Better Roads*, 1-20.

Peck, R.B., Hanson, W.E. and Thornburn, T.H. (1974) *Foundation Engineering*, John Wiley & Sons, New York, NY, USA.

Petersen, M.D., Frankel, A.D., Harmsen, S.C., Mueller, C.S., Haller, K.M., Wheeler, R.L., Wesson, R.L., Zeng, Y., Boyd, O.S., Perkins, D.M., Luco, N., Field, E.H., Wills, C.J. and Rukstales, K.S. (2008) *Documentation for the 2008 Update of the United States National Seismic Hazard Maps: U.S. Geological Survey Open-File Report 2008-1128*, U.S. Geological Survey, Reston, VA, USA.

Phillips, C. and Hashash, Y. (2009) "Damping formulation for non-linear 1D site response analyses," *Soil Dynamics and Earthquake Engineering* **29**, 1143-1158.

Revell, J. (2013) "Quasi-isolated highway bridges: Influence of bearing anchorage strength on seismic performance," M.S. Dissertation, University of Illinois, Urbana, IL, USA.

Roy, R., Thakur, P. and Chakroborty, S. (2014) "Spectral Matching of Real Ground Motions: Applications to Horizontally Irregular Systems in Elastic Range," *Advances in Structural Engineering* **17**(11), 1623-1638.

Scott, M.H. and Fenves, G.L. (2006) "Plastic Hinge Integration Methods for Force-Based Beam-Column Elements," *Journal of Structural Engineering* **132**(2), 244-252.

Shamsabadi, A., Ashour, M. and Norris, G. (2005) "Bridge Abutment Nonlinear Force-Displacement-Capacity Prediction for Seismic Design," *Journal of Geotechnical and Geoenvironmental Engineering* **131**(2), 151-161.

Shamsabadi, A., Rollins, K.M. and Kapuskar, M. (2007) "Nonlinear Soil-Abutment-Bridge Structure Interaction for Seismic Performance-Based Design," *Journal of Geotechnical and Geoenvironmental Engineering* **133**(6), 707-720.

Silva, W. and Costantino, C. (2002) "Development of site-specific design ground motions in Western and Eastern North America," *Soil Dynamics and Earthquake Engineering* **22**(9), 755-764.

Sizemore, J.G. (2017) "Inelastic Behavior and Seismic Collapse Prevention Performance of Low-Ductility Steel Braced Frames," Ph.D. Dissertation, University of Illinois, Urbana, IL, USA.

Somerville, P., Smith, N., Punyamurthula, S. and Sun, J. (1997) *Development of Ground Motion Time Histories for Phase 2 of the FEMA/SAC Steel Project*, SAC Joint Venture, Sacramento, CA, USA.

Spyrakos, C. and Ioannidis, G. (2003) "Seismic behavior of a post-tensioned integral bridge including soil-structure interaction (SSI)," *Soil Dynamics and Earthquake Engineering* **23**, 53-63.

Steelman, J.S., Fahnestock, L.A., Filipov, E.T., LaFave, J.M., Hajjar, J.F. and Foutch, D.A. (2013) "Shear and Friction Response of Non-Seismic Laminated Elastomeric Bridge Bearings Subject to Seismic Demands," *Journal of Bridge Engineering* **18**(7), 612-623.

Steelman, J.S., Filipov, E.T., Fahnestock, L.A., Revell, J.R., LaFave, J.M., Hajjar, J.F. and Foutch, D.A. (2014) "Experimental Behavior of Steel Fixed Bearings and Implications for Seismic Bridge Response," *Journal of Bridge Engineering* **19**(8), A4014007.

Steelman, J.S., Fahnestock, L.A., Hajjar, J.F. and LaFave, J.M. (2016) "Performance of Non-Seismic PTFE Sliding Bearings when Subjected to Seismic Demands," *Journal of Bridge Engineering* **21**(1), 04015028.

Steelman, J.S., Fahnestock, L.A., Hajjar, J.F. and LaFave, J.M. (2018) "Cyclic Experimental Behavior of Nonseismic Elastomeric Bearings with Stiffened Angle Side Retainer Fuses for Quasi-Isolated Seismic Bridge Response," *Journa" of Bridge Engineering* **23**(1), 04017120.

Tassios, T.P. (1983) "Physical and mathematical models for re-design of damaged structures," *Introductory Report, IABSE Symposium*, Venice, 29-77.

Teguh, M. Duffield, C.F., Mendis, P.A. and Hutchinson, G.L. (2006) "Seismic performance of pile-to-pile cap connections: An investigation of design issues," *Electronic Journal of Structural Engineering* **6**, 8-18.

Terzaghi, K., Peck, R.B. and Mesri, G. (1996) *Soil Mechanics in Engineering Practice, Third Edition*. John Wiley & Sons, New York, NY, USA.

Toro, G.R., Abrahamson, N.A. and Schneider, J.F. (1997) "Model of strong ground motions from earthquakes in central and eastern North America: Best estimates and uncertainties," *Seismological Research Letters* **68**(1), 41-57.

USGS (2008) *2008 Interactive Deaggregation*, United States Geological Survey, Reston, VA, USA. Retrieved from http://geohazards.usgs.gov/deaggint/2008/.

USGS (2014) *Hazard Curve Application*, United States Geological Survey, Reston, VA, USA. Retrieved from http://geohazards.usgs.gov/hazardtool/.

Vacareanu, R., Iancovici, M. and Pavel, F. (2014) "Conditional mean spectrum for Bucharest," *Earthquakes and Structures, an International Journal* **7**(2), 147-157.

Vasheghani-Farahani, R., Zhao, Q. and Burdette, E.G. (2010) "Seismic Analysis of Integral Abutment Bridge in Tennessee, Including Soil-Structure Interaction," *Transportation Resource Records: Journal of the Transportation Research Board* **2201**, 70-79.

Vintzeleou, E.N. and Tassios, T.P. (1986) "Mathematical models for dowel action under monolithic and cyclic conditions," *Magazine of Concrete Research* **38**(134), 13-22.

Wair, B.R., DeJong, J.T. and Shantz, T. (2012) *PEER Report No. 2012/08: Guidelines for Estimation of Shear Wave Velocity Profiles*, Pacific Earthquake Engineering Research Center, University of California, Berkeley, CA, USA.

Waldin, J., Jennings, J. and Routledge, P. (2012) "Critically, damaged bridges & concepts for earthquake recovery," *2012 New Zealand Society for Earthquake Engineering Conference*, Christchurch, NZ, January.

Watson-Lamprey, J. and Abrahamson, N. (2006) "Selection of ground motion time series and limits on scaling," *Soil Dynamics and Earthquake Engineering* **26**, 477-482.

Wen, Y.K. and Wu, C.L. (2001) "Uniform hazard ground motions for Mid-America cities," *Earthquake Spectra* **17**(2), 359-384.

White, H. (2007) *Integral Abutment Bridges: Comparison of Current Practice Between European Countries and the United States of America*, New York State Department of Transportation, New York, NY, USA.

Wilson, D.W. (1998) "Soil-Pile-Superstructure Interaction in Liquefying Sand and Soft Clay," Ph.D. Dissertation, University of California, Davis, CA, USA.

Wolff, T.E. (1989) "Pile capacity prediction using parameter functions," *ASCE Geotechnical Special Publication* **23**, 96-107.

Wood, J.H. (2015) "Earthquake Design of Bridges With Integral Abutments," *6th International Conference on Earthquake Geotechnical Engineering*, Christchurch, NZ, November.

Zhao, Q., Vashghani-Farahani, R. and Burdette, E.G. (2011) "Seismic Analysis of Integral Abutment Bridges Including Soil-Structure Interaction," *Structures Congress 2011*, Las Vegas, NV, April.